ISSN 1948-5204 (online)

World Journal of *Gastrointestinal Oncology*

World J Gastrointest Oncol 2022 April 15; 14(4): 748-946

Published by Baishideng Publishing Group Inc

World Journal of Gastrointestinal Oncology

Contents

Monthly Volume 14 Number 4 April 15, 2022

World Journal of Gastrointestinal Oncology

Monthly Volume 14 Number 4 April 15, 2022

Contents

ABOUT COVER

Editorial Board Member of *World Journal of Gastrointestinal Oncology*, Hanlin L Wang, MD, PhD, Professor, Department of Pathology and Laboratory Medicine, University of California Los Angeles, David Geffen School of Medicine and Ronald Reagan UCLA Medical Center, Los Angeles, CA 90095, United States. hanlinwang@mednet.ucla.edu

AIMS AND SCOPE

The primary aim of *World Journal of Gastrointestinal Oncology* (*WJGO*, *World J Gastrointest Oncol*) is to provide scholars and readers from various fields of gastrointestinal oncology with a platform to publish high-quality basic and clinical research articles and communicate their research findings online.

WJGO mainly publishes articles reporting research results and findings obtained in the field of gastrointestinal oncology and covering a wide range of topics including liver cell adenoma, gastric neoplasms, appendiceal neoplasms, biliary tract neoplasms, hepatocellular carcinoma, pancreatic carcinoma, cecal neoplasms, colonic neoplasms, colorectal neoplasms, duodenal neoplasms, esophageal neoplasms, gallbladder neoplasms, *etc*.

INDEXING/ABSTRACTING

The *WJGO* is now indexed in Science Citation Index Expanded (also known as SciSearch®), PubMed, PubMed Central, and Scopus. The 2021 edition of Journal Citation Reports® cites the 2020 impact factor (IF) for *WJGO* as 3.393; IF without journal self cites: 3.333; 5-year IF: 3.519; Journal Citation Indicator: 0.5; Ranking: 163 among 242 journals in oncology; Quartile category: Q3; Ranking: 60 among 92 journals in gastroenterology and hepatology; and Quartile category: Q3. The *WJGO*'s CiteScore for 2020 is 3.3 and Scopus CiteScore rank 2020: Gastroenterology is 70/136.

RESPONSIBLE EDITORS FOR THIS ISSUE

Production Editor: *Ying-Yi Yuan*; **Production Department Director:** *Xiang Li*; **Editorial Office Director:** *Ya-Juan Ma*.

NAME OF JOURNAL
World Journal of Gastrointestinal Oncology

ISSN
ISSN 1948-5204 (online)

LAUNCH DATE
February 15, 2009

FREQUENCY
Monthly

EDITORS-IN-CHIEF
Monjur Ahmed, Florin Burada

EDITORIAL BOARD MEMBERS
https://www.wjgnet.com/1948-5204/editorialboard.htm

PUBLICATION DATE
April 15, 2022

INSTRUCTIONS TO AUTHORS
https://www.wjgnet.com/bpg/gerinfo/204

GUIDELINES FOR ETHICS DOCUMENTS
https://www.wjgnet.com/bpg/GerInfo/287

GUIDELINES FOR NON-NATIVE SPEAKERS OF ENGLISH
https://www.wjgnet.com/bpg/gerinfo/240

PUBLICATION ETHICS
https://www.wjgnet.com/bpg/GerInfo/288

PUBLICATION MISCONDUCT
https://www.wjgnet.com/bpg/gerinfo/208

ARTICLE PROCESSING CHARGE
https://www.wjgnet.com/bpg/gerinfo/242

STEPS FOR SUBMITTING MANUSCRIPTS
https://www.wjgnet.com/bpg/GerInfo/239

ONLINE SUBMISSION
https://www.f6publishing.com

World Journal of Gastrointestinal Oncology

Submit a Manuscript: https://www.f6publishing.com

World J Gastrointest Oncol 2022 April 15; 14(4): 748-764

DOI: 10.4251/wjgo.v14.i4.748

ISSN 1948-5204 (online)

REVIEW

Regulatory RNAs, microRNA, long-non coding RNA and circular RNA roles in colorectal cancer stem cells

Hsiao-Mei Chao, Teh-Wei Wang, Edward Chern, Shan-hui Hsu

Specialty type: Oncology

Provenance and peer review: Invited article; Externally peer reviewed.

Peer-review model: Single blind

Peer-review report's scientific quality classification
Grade A (Excellent): 0
Grade B (Very good): B
Grade C (Good): C
Grade D (Fair): 0
Grade E (Poor): 0

P-Reviewer: Hou L, China; Luo ZW, China

Received: February 22, 2021
Peer-review started: February 22, 2021
First decision: July 29, 2021
Revised: August 18, 2021
Accepted: March 25, 2022
Article in press: March 25, 2022
Published online: April 15, 2022

Hsiao-Mei Chao, Department of Pathology, Wan Fang Hospital, Taipei Medical University, Taipei 11696, Taiwan

Hsiao-Mei Chao, Department of Pathology, School of Medicine, College of Medicine, Taipei Medical University, Taipei 110, Taiwan

Teh-Wei Wang, Edward Chern, niChe Lab for Stem Cell and Regenerative Medicine, Department of Biochemical Science and Technology, National Taiwan University, Taipei 10617, Taiwan

Shan-hui Hsu, Institute of Polymer Science and Engineering, National Taiwan University, Taipei 10617, Taiwan

Corresponding author: Shan-hui Hsu, PhD, Professor, Institute of Polymer Science and Engineering, National Taiwan University, No. 1, Sec. 4, Roosevelt Rd., Taipei 10617, Taiwan. shhsu@ntu.edu.tw

Abstract

The properties of cancer stem cells (CSCs), such as self-renewal, drug resistance, and metastasis, have been indicated to be responsible for the poor prognosis of patients with colon cancers. The epigenetic regulatory network plays a crucial role in CSC properties. Regulatory non-coding RNA (ncRNA), including microRNAs, long noncoding RNAs, and circular RNAs, have an important influence on cell physiopathology. They modulate cells by regulating gene expression in different ways. This review discusses the basic characteristics and the physiological functions of colorectal cancer (CRC) stem cells. Elucidation of these ncRNAs will help us understand the pathological mechanism of CRC progression, and they could become a new target for cancer treatment.

Key Words: Regulatory RNAs; MicroRNA; Long-non coding RNA; Circular RNA; Colorectal cancer; Cancer stem cell; Stemness

Core Tip: Cancer stemness is one of the key reasons to contribute to the tumor aggressiveness, disease progression and cancer recurrence. Some reports have suggested the essential roles of regulatory RNAs in the modulation of the colorectal cancer (CRC) stemness. Here, we focus on the findings of microRNAs, long noncoding RNAs, and circular RNAs in CRC stem cells. We not only introduce the basic concepts of these non-coding RNA but address their pathologic roles in the stemness related signals and molecules to realize their functions in CRC stem cells and CRC progression.

Citation: Chao HM, Wang TW, Chern E, Hsu SH. Regulatory RNAs, microRNA, long-non coding RNA and circular RNA roles in colorectal cancer stem cells. *World J Gastrointest Oncol* 2022; 14(4): 748-764
URL: https://www.wjgnet.com/1948-5204/full/v14/i4/748.htm
DOI: https://dx.doi.org/10.4251/wjgo.v14.i4.748

INTRODUCTION

Colorectal adenocarcinoma is the most common colorectal cancer (CRC), resulting from the abnormal proliferation of colon epithelial cells. According to statistics from the American Cancer Society, the risk factors of CRC include obesity, physical inactivity, high consumption of red or processed meat, alcohol uptake, and very low intake of fruit and vegetables[1]. Other factors include inflammatory bowel diseases such as Crohn's disease and ulcerative colitis. Based on TNM classification for CRC, which includes the invasive depth of primary tumor, the status of lymph nodes, and distant metastasis, CRC can be categorized into four stages: I, II, III, and IV. Typical treatments for CRC are surgical resection, neoadjuvant/adjuvant radiation therapy, and chemotherapy. Advanced CRC has high potential for metastasis and recurrence. Therefore, clarifying the mechanisms of drug-resistance and the metastasis of cancer cells is an important issue in cancer treatment. According to previous research, RNA plays important roles in physiology and pathology. Non-coding RNA (ncRNA) such as microRNA (miRNA), long non-coding RNA (lncRNA), and circular RNA (circRNA) have functional roles in physiopathological processes. These RNA molecules are involved in the pathobiology of cancer and have become targets for the diagnosis, prognosis, and treatment of various cancers. At present, in CRC, ncRNA regulates CRC metastasis, drug resistance, and stemness characteristics through various signal networks. Therefore, understanding the role of ncRNA in the CRC signaling pathway can help develop new strategies for the prognosis and treatment of CRC. In this review, we analyzed the latest findings about ncRNA, particularly miRNA and lncRNA, which are involved in the pathological mechanism of CRC.

CANCER STEM CELL

The existence of cancer stem cells (CSCs) is considered to account for cancer recurrence and metastasis. Tumor heterogeneity exists, which means that there are different cancer cell clones within tumors including different cancer cell clones, cancer progenitor cells, and CSCs[2]. Two competing theories have been proposed to explain the development of heterogeneous tumors: Clonal evolution theory and CSC theory[3,4]. The first postulates that each cell within a tumor is considered to have equal potential to promote tumorigenesis. In contrast to the clonal evolution theory, CSC theory claims that CSC is a small group of cancer cell population located at the highest level in the hierarchy of solid tumor tissues [5]. Only CSCs have the potential to form new tumors on serial transplantation. *In vivo* research studies also provide evidence to support this theory by the xenograft model[6,7]. On the other hand, CSCs have been reported to exist in many different types of cancer. For instance, many studies show that CSCs dominate the tumorigenic potential in CRC[8,9]. Based on CSC theory, eliminating the CSC population would be an efficient way to prevent tumor relapse and can be expected to achieve a complete clinical therapeutic response[10].

Self-renewal is the process by which a stem cell divides to generate daughter cells that have similar developmental potential to the mother cell[11]. In normal stem cells, self-renewal is essential for expanding their population pool during development. When tissue injury occurs, stem cells differentiate into somatic cells to restore damage. In hematopoietic stem cells, defects in self-renewal reduce the potential of repopulation capacity upon serial transplantation[12,13]. On the other hand, CSCs also possess the ability to self-renew and differentiate[14,15]. CSCs are injected into immunodeficient mice and only the CSCs with self-renewal and tumor-initiating potential could generate tumors successfully in xenograft models compared to non-CSC[16]. Due to self-renewal, stem cells can overcome anoikis (a kind of programmed cell death induced when cells detach from the surrounding extracellular matrix). Therefore, stem cells can form spheres in suspension culture[17]. As a result, the sphere-forming frequency can be used to estimate CSC frequency in cancers[18].

CSCs are believed to have higher drug resistance ability and could escape from chemotherapy, leading to tumor relapse. Most cytotoxic drugs used for cancer therapy damage DNA to induce the cell death of proliferative tumor cells. However, CSCs have three different pathways to avoid death. First, CSCs can repair DNA damage more efficiently than non-stem cancer cells through ataxia telangiectasia mutated and the activation of the checkpoint kinases Chk1 and Chk2[19]. This characteristic also helps CSCs overcome the effect of radiation therapy[20]. Second, CSCs could remain at a quiescent stage to slow the cell cycle[21], which would protect CSCs from most chemotherapeutic drugs that target rapidly proliferating cells[22]. The last is that the up-regulated expression of ATP-binding cassette transporters (ABC transporters) is observed in CSCs[23]. The ABC transporter is a membrane protein that could extrude toxins out of the cell[24].

Most cancer-related deaths are attributed to recurrence and metastasis. However, metastasis initiating cells (MICs) have not yet been well-defined to date. Evidence from many previous studies implies that a subpopulation of MICs is probably comprised of CSCs[25]. For example, in CRC patients, tumors with higher expressions of CSC markers CD133 and CD44 are correlated to metastasis[26]. In the "seed and soil" hypothesis[27], metastatic cancer cells have to float in the circulatory system as seeds and find appropriate organs as "soil" in which to settle down. Consequently, the self-renewal capacity that resists anoikis might explain why CSCs are related to metastasis. On the other hand, the beginning of metastasis includes two irreplaceable steps, invasion and migration[28]. As mentioned above, repressing self-renewal or migration abilities, or even restricting the CSC population directly may reduce cancer metastasis.

Regulatory signals of CRC stem cells

Many molecular networks are related to the stemness of CRC, and several have been found to be important and crucial in the growth and functional maintenance of CSCs, such as Wnt, bone morphogenetic protein (BMP), Hedgehog (Hh), and Notch signals. The Wnt signaling pathway has been recognized as a stemness-related pathway in CSCs[29,30]. Wnt is involved in the maintenance, proliferation, apoptosis, and differentiation of intestinal tract stem cells and CSCs. In the intestine, after Wnt signal activation, the downstream β-catenin translocates into the nucleus and turns on the transcriptional activity of important developmental-related genes such as c-Myc, Axin2, and Lgr5. These downstream factors are also involved in colorectal CSCs' characteristics[31-33]. In CRC cells, this is often accompanied by abnormal Wnt signals. For example, adenomatous polyposis coli (APC) mutation leading to the excessive activation of Wnt signals has been considered the first step in tumor formation with CRC. In addition, in the population of colorectal CSCs, it has been found to have a high degree of Wnt activity. All these suggest that Wnt signaling is closely related to the origin of CRC.

Notch signaling is also enhanced in colorectal CSCs; its interaction with Wnt signaling is also considered to be an important message affecting tumor proliferation[34]. In addition, if the Notch signal were inhibited by the deletion or inhibition of γ-secretase inhibitors, this will lead to an increase in the level of Math1 that promotes stem cell differentiation and undermines the maintenance of stem cell populations[35]. On the other hand, BMP and Hh signals are more present in differentiated intestinal cells. Studies have pointed out that the Hh signal also antagonizes the Wnt signal and helps Gli-dependent tumor cell differentiation[36].

The transforming growth factor (TGF)-β/BMP pathway has multiple roles in colorectal CSCs[30]. It inhibits Wnt messages to promote cancer stem cell differentiation and promotes Wnt messages to help tumor formation[37]. BMP signaling inhibits the stemness of Lgr5+ stem cells through Smad-mediated transcriptional repression[38]. In addition, it was found that knocking out GATA6-α zinc finger transcription factor that helps maintain Lgr5+ CSCs in adenomas - can up-regulate BMP signaling, thereby inhibiting the development of CRC. Knocking out GATA6 *in vivo* can up-regulate BMP signaling, thereby inhibiting the development of CRC[39]. Therefore, these signaling pathways are multiple mechanisms of stem cell regulation during the origin and development of CRC, which contributes to the development of therapeutic strategies required to treat CRC.

MIRNA

MiRNA is a small non-coding RNA molecule with 20-22 nucleotides (nt)[40]. After primary miRNA is initially transcribed, two splicing processes sequentially occur by Drosha and Dicer to generate precursor miRNA and mature miRNA. One of the two major functions of miRNA is translational repression, causing mRNA degradation through hybridization between the target mRNA and miRNA. In recent decades, numerous studies have reported that the expression of miRNA is dysregulated in malignancies as an oncogene or tumor-suppressor gene. For example, miR-21 as oncomir has been shown to be associated with poor prognosis and metastasis in patients with breast cancers[41,42]. In breast CSCs, diminished miRNA let-7 is required to maintain self-renewal ability and inhibit differentiation[43]. In pancreatic cancer, miR-34a suppresses the expression of BCL2, Notch1, and Notch2, which are implicated in anti-apoptosis to maintain the tumor-initiating cell population[44]. Furthermore, MRX34, a liposomal miR-34 mimic, has already been evaluated in phase I clinical trials

against liver cancer[45]. Most studies about miRNA have focused on the regulation of transcription factors or abnormal copy numbers. However, the epigenetic regulation of miRNA in cancers has attracted more attention in the last decade[46]. Unraveling the regulatory mechanisms of cancer-associated miRNA may provide a novel therapeutic strategy for cancers.

In the progression of CRC, regulatory miRNAs are also involved in the CRC stem cell population and many studies have also described the regulation of miRNA, which is involved in the network of the origin of CRC. Many current studies have found that certain miRNAs related to CRC stem cells mostly target certain important signaling pathways and molecules that maintain colorectal CSCs or cell surface markers, showing the cancer-inhibition function. Such miRNAs are often found in cancer. The amount of expression in the cells decreases. In contrast, some miRNAs that target tumor-suppressor genes will play an important role in the cancer process.

In previous studies, under the deficiency of Dicer - an important protein involved in the miRNA process - the expression of CD44 and Lgr5 will increase, as will the stem cell transcription factors Sox2 and Nanog. This shows that some miRNAs are inhibitory molecules for CRC. Meanwhile, it will also affect the stem cell population in CRC cells and enhance the ability to initiate tumors and metastasis [47]. At present, many studies have reported that miRNAs have been targeting stem cell genes or genes involved in the regulation of stem cell properties, which have led to the development of different CSC populations.

CRC stem cell surface markers

CRC stem cell markers such as CD44, CD133, and Lgr5 also participate in the physiological network regulation of many CSCs as the surface antigens of colorectal CSCs. For example, CD44 can participate in the Wnt/β-catenin signal to induce stem cell properties whether in breast cancer or CRC[33]. Lgr5 belongs to the GPCR family and can identify stem cells in colonic epithelial cells. It is considered a negative modulator of the Wnt signal. A group found that miR-23b can distinguish malignant CRC from normal intestinal epithelium and the miR-23b added in CRC is expected to target the Lgr5 gene. In CRC, miR-23b promotes cell proliferation and the cell cycle and improves the self-renewal ability, thus affecting metastasis and drug resistance, which are closely related to the characteristics of CSCs. Furthermore, this also increased the aldehyde dehydrogenase (ALDH) + CSC population group[48]. CD24, a glycosylphosphatidylinositol-anchor protein, is considered a CRC stem cell marker and has been shown to increase cancer stem cell properties. Wang *et al*[49] reported that miR-1185-1 suppresses the expression of CD24 by targeting its 3′ untranslated region (3′UTR) and could be inhibited by SIRT1 *via* histone deacetylation. Targeting SIRT1 by RNAi could increase the expression of miR-1185-1 and further repress CD24 translation and CRC stemness. Transmembrane-4-L-six-family-1 (TM4SF1), a cell surface antigen, is increased in various human epithelial carcinomas[50]. In CRC tumor tissues and cell lines, miR-30a is downregulated. Overexpression of miR-30a reduces migration and invasion in CRC cell lines. miR-30a could target TM4SF1, and it inhibits vascular endothelial-derived growth factor expression and enhances E-cadherin expression[51]. LRIG1, leucine-rich repeats and immunoglobulin-like domains protein 1, is a type I single-transmembrane protein and an intestinal stem cell marker that functions as a tumor suppressor[52]. Viswanathan *et al*[53] found that miR-92a can target LRIG1 and promote the proliferation of HT29 CRC cells. miR-92a also promotes the tumorigenesis of CRC.

CRC stemness-related intracellular regulatory and transcription factors

Some miRNAs regulate important stemness transcription factors in CRC progress. SOX2 plays an important role in embryonic development and the formation of induced pluripotent stem cells[54]. SOX2 is also necessary to maintain CSC. A study found that miR-450a-5p can target the 3′UTR region to inhibit SOX2 expression in CRC. Therefore, SOX2-induced CSC properties and angiogenesis are inhibited. On the contrary, overexpression of SOX2 can rescue the inhibition brought by miR-450a-5p *in vivo* and *in vitro*. Kruppel-like factor 5 (KLF5) is a zinc-finger transcription factor of the KLF family. KLF family proteins play various roles in homeostasis and stem cell regulation[55]. The transcription factor YAP1 affects multiple signaling pathways in CRC cells. Ou's[56] group has pointed out that miR-590-5p directly inhibits YAP1 in CRC cells and inhibits tumorigenesis. The miR-590-5p-YAP1 axis in CRC specimens is dysregulated and affects the survival of patients. GATA transcription factors comprise a family of zinc-finger proteins and play an essential role in embryo development[57]. In CRC cells, GATA6 is the direct target of miR-203. miR-203-overexpressing HCT-116 and HT-29 cells decrease self-renewal ability and cancer stemness[58]. Spalt-like (SALL) transcription factor is an important transcription factor for self-renewal and pluripotency. A study showed that miR-3622a-3p is downregulated in CRC tissues and cells. miR-3362a-3p inhibits the malignant biological characteristics of CRC. miR-3622a-3p also inhibits the stemness and epithelial to mesenchymal transition (EMT) of CRC cells through SALL4 targeting. In tumor xenograft models and *in vivo* metastasis models, miR-3622a-3p can also inhibit the tumorigenesis and metastasis of CRC cells *in vivo*[59].

EMT is related to tumor metastasis and is considered one of the properties of CSCs. The EMT-related ZEB2 gene was verified as the binding target of miR-377. The expression of miR-377 was downregulated in colon cancer tissues and cell lines. Knockdown of miR-377 increases the number of ALDH+ cells and promotes the ability to form cancer spheres. Overexpression of ZEB2 could prevent the inhibition of miR-377 in cancer stem cell phenotypes, EMT, migration, and invasion[60]. Regulation of cytoskeleton

remodeling is a crucial process in cellular migration. Recently, miR-210-3p has been shown to target stathmin1, a microtubule destabilization regulator, to reduce cell elasticity without affecting EMT and upregulate the invasion ability of CRC stem cells[61]. Quaking (QKI) is a member of the signal transduction and activation of RNA protein family. QKI is highly conserved over different species and is important for normal development[62]. Studies have pointed out that miR-221 has high expression in EpCAM+/(CD44 + CRC stem cells). When miR-221 is overexpressed, it can promote the tumorigenesis of CRC by targeting the most abundant splicing isoform of the human QKI gene, QKI-5, in the CRC patient-derived xenograft model. In addition, overexpression of QKI-5 in CRC could inhibit the formation of cancer[63].

Hypoxia

Rapid cell division and abnormal blood vessel formation can be observed in tumor hypoxic areas. Hypoxia-inducible factors are also activated due to hypoxia, and they stimulate many transcription factors that control stem cell self-renewal and pluripotency, such as CSCs, which are also considered to play an important role[64]. Under hypoxic conditions, miR-34a targets and reduces the expression of PPP1R11, E3 ubiquitin-protein ligase, which activates signal transducer and activator of transcription 3 (STAT3) by phosphorylation and inhibits metastasis to the liver[65]. Hypoxia can also upregulate miR-215. miR-215 can target Lgr5 and affect the stemness of CRC stem cells[66].

Notch signaling

Transfer RNA-derived RNA fragments (tRFs) belong to a family of short noncoding RNAs and can be produced by multiple RNA enzymes and ribonuclease to regulate translation, similar to miRNAs[67]. A study found that a fragment derived from tRF/miR-1280, a 17-bp fragment derived from tRNALeu and pre-miRNA, affects Notch signaling. tRF/miR-1280 targets Notch ligand JAG2, which reduces the stem cell properties of CRC and inhibits the transcription of Gata1/3 and miR-200b genes[68]. Moreover, some tumor suppressor miRNAs are inhibited and promote the tumorigenesis of CRC. Cullin 4B (CUL4B) is considered an oncogene that promotes the development of many solid tumors. CUL4B drives the development and metastasis of colon cancer by maintaining cancer stem-like characteristics. The CUL4B and PRC2 complex synergistically inhibits the expression of miR-34a, a tumor suppressor miR that targets oncogenic MYCN and NOTCH1, to promote stem cell properties[69].

Wnt/β-catenin signaling

Wnt/β-catenin signaling is involved in the regulation of stem cells and tumorigenesis in several kinds of cancers[29,70]. Some positive regulatory miRs of Wnt/β-catenin signaling have also been addressed. The current study reported that miR-501-3p is overexpressed in colorectal tumor tissues. miR-501-3p targeted APC, a negative regulator of Wnt/β-catenin signaling. The downregulation of miR-501-3p in CRC cells inhibited tumor proliferation and sphere formation and induced cell cycle arrest at the G1 phase. miR-501-3p promotes cancer stem cell properties through Wnt/β-catenin[71]. Many studies have also found that inflammation is related to tumor formation. Interleukin (IL)-6/STAT3 signaling is one of the important pathways induced by inflammation. Zhang *et al*[72] found that the activation of IL-6/STAT3 can induce miR-92a expression in chemical-resistant CRC and tissues. miR-92a targets the negative factors KLF4, glycogen synthase kinase-3β, and Dickkopf 3 to upregulate Wnt/β-catenin signaling activity in CRC. Decreased levels of the miR-30-5p family have been reported in CRC patients and human CD133 + CRC cells. Overexpression of miR-30-5p inhibits the expression of stem cell markers CD133 and SOX2, spheroid formation, and cell proliferation by suppressing USP22/Wnt/β-catenin signals[73]. CD133+ and Lgr5+ stem cells in the colon cancer cell lines HCT-116 and SW-480 show high levels of miR-3120-5p. Overexpression of miR-3120-5p increases the CSC population and promotes the stemness and invasiveness of colon cancer cells by directly targeting Axin2[74]. Inhibition of the RCN2/Wnt/β-catenin pathway by miR-183-5p also inhibits the proliferation and invasion of CRC [75]. On the other hand, negative regulator miRs of Wnt/β-catenin signaling play tumor suppressor roles in CRC. In SW1116 and SW480 CRC cells, overexpression of miR-302c weakens the proliferation, invasion, and migration capabilities of CRC stem cells. miR-302c binds to CARF and inhibits its expression. CARF has been shown to maintain the stemness of CSCs of CRC and to be a positive regulator of Wnt/β-catenin signaling[76,77].

TGF-β/Smad signaling

TGF-β/Smad signaling is involved in the regulation of many physiological processes in the body, including the regulation of CSCs. Through bioinformatics analysis and research, it was also found that miR-4666-3p and miR-329 target TGF-βR1 to prevent the activation of the TGF-β1/Smad pathway and act as tumor suppressor genes in quiescent CSCs, identified as a subgroup of colon cancer cells that are in a dormant state and have strong stem cell-like properties[78]. Recently, decreased levels of miR-147 were found in colon cancer. Overexpressed miR-147 decreases the CRC stem cell markers such as OCT4, SOX2, and NANOG and inhibits EMT and the TGF-β/Smand pathway in HCT116 and SW480 colon cancer cells. Moreover, miR-147 downregulates the expression of β-catenin, c-myc, and survivin related to Wnt/β-catenin signaling[79].

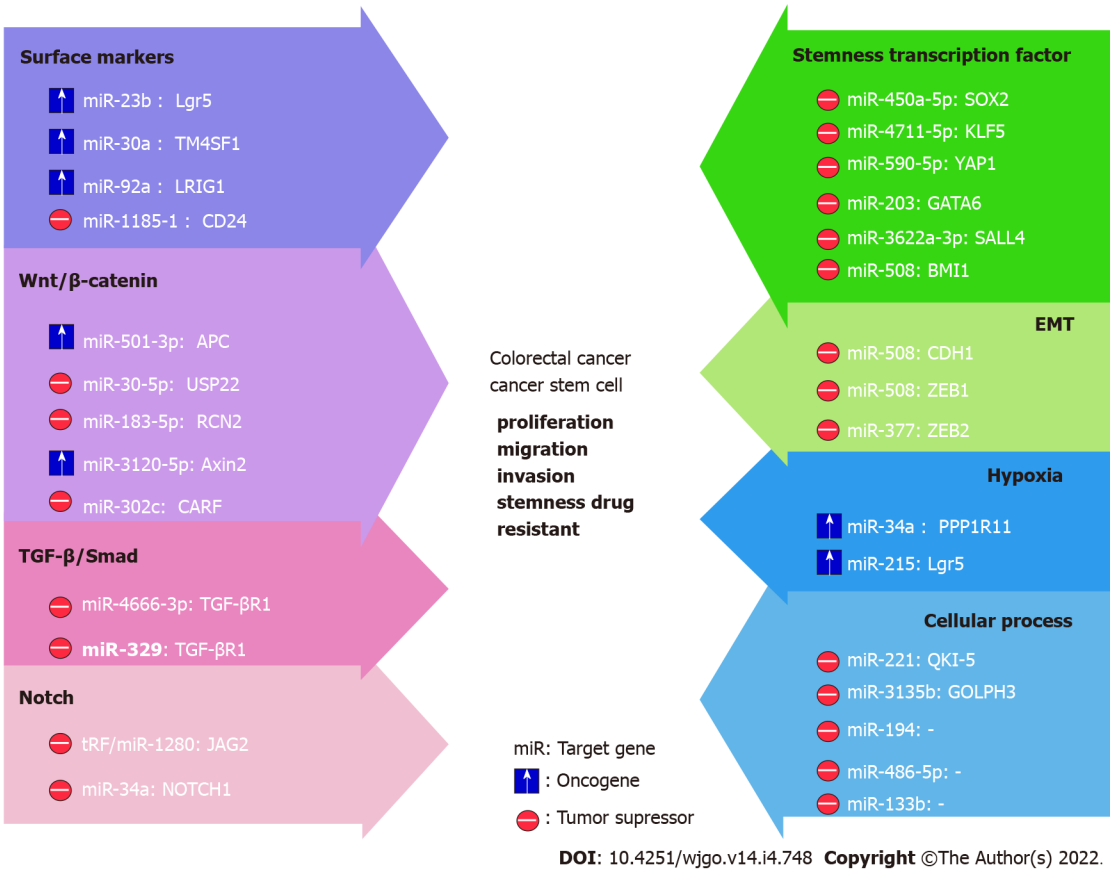

Figure 1 The role of regulatory micro RNAs of colorectal cancer stem cells in this article. TGF: Transforming growth factor; QKI: Quaking; EMT: Epithelial to mesenchymal transition; KLF: Kruppel-like factor; SALL: Spalt-like; tRF: Transfer RNA-derived RNA fragments.

Cellular response and process

Golgi fragmentation of cancer cells is one of the new chemotherapy strategies. This phenomenon is affected by the Golgi phosphoprotein-3 (GOLPH3)/Myo18A/F-actin axis. Núñez-Olvera *et al*[80] found that miR-3135b overexpression attenuates Golgi fragmentation induced by chemotherapy drugs in CRC cells and that miR-3135b targets the 3′UTR of the GOLPH3 proto-oncogene. Moreover, they noted that overexpression of miR-3135b in HCT-15 cancer cells can significantly inhibit cell proliferation, increase sensitivity to 5-fluorouracil lysis, and promote late cell degradation and necrosis. They also indicated that miR-3135b reduces the phosphorylation level of p-AKT1 (Ser473) and p-mTOR (Ser2448) and activates the autophagy and stemness of CRC. Many studies have indicated that the expression of some miRs in CSCs decreases, and the forced expression of these miRs can inhibit the characteristics of CSCs. For example, the expression of miR-194 in CRC stem cells decreases. Overexpression of miR-194 can cause G1/S transition, induce cell apoptosis, and inhibit the malignant behavior of CRC stem cells[81]. Pisano *et al*[82] found that miR-486-5p was downregulated in CRC stem cells. Overexpression of miR-486-5p can also inhibit stem cell characteristics. miR-133b was found to be downregulated in the colorectal spheroids, a model to enrich CSCs. Overexpression of miR-133b inhibits the stemness and chemoresistance of CRC. This study also found that miR-133b affected the DOT1L-mediated modification of H3K79me2 and the transcription of stem cell-related genes (Figure 1)[83].

Many miRs are involved in the regulation of the fate of CRC stem cells and affect the prognosis of CRC. At present, high-throughput next-generation sequencing is used to screen these miRs. In addition, it can also be predicted by miR-targeting sequences of genes that regulate CSC-related genes and signaling pathways. The information of the tumor suppressor miR may be used to develop a nucleic acid biosimilar drug for the treatment of CRC. These findings are quite helpful for the development of new drugs.

LNCRNAS

LncRNAs comprise various RNA species longer than 200 nt, lack protein-coding ability, and are involved in regulation of genes expression and regulate diverse functions. There are many different structure forms of lncRNA, such as mRNA-like gene transcripts (lincRNA), covalently closed circular

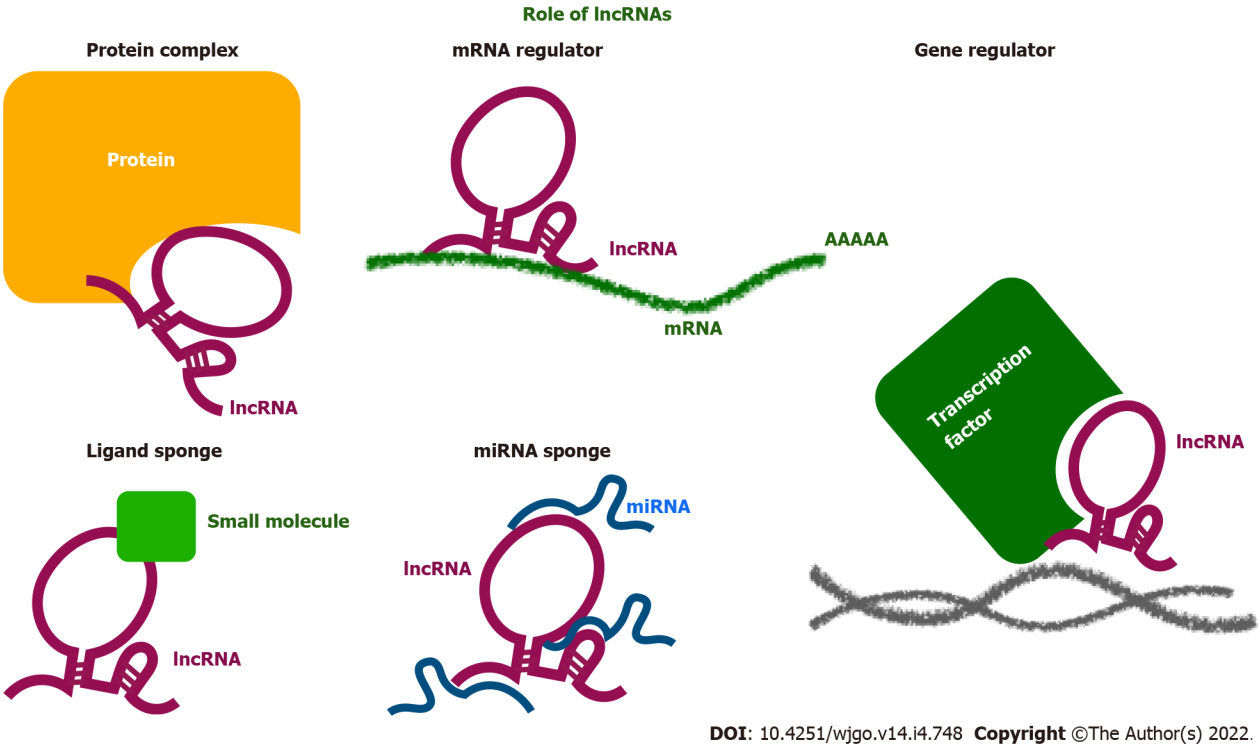

DOI: 10.4251/wjgo.v14.i4.748 **Copyright** ©The Author(s) 2022.

Figure 2 The functions of long non-coding RNAs. lncRNAs: Long-non coding RNAs; miRNA: MicroRNA.

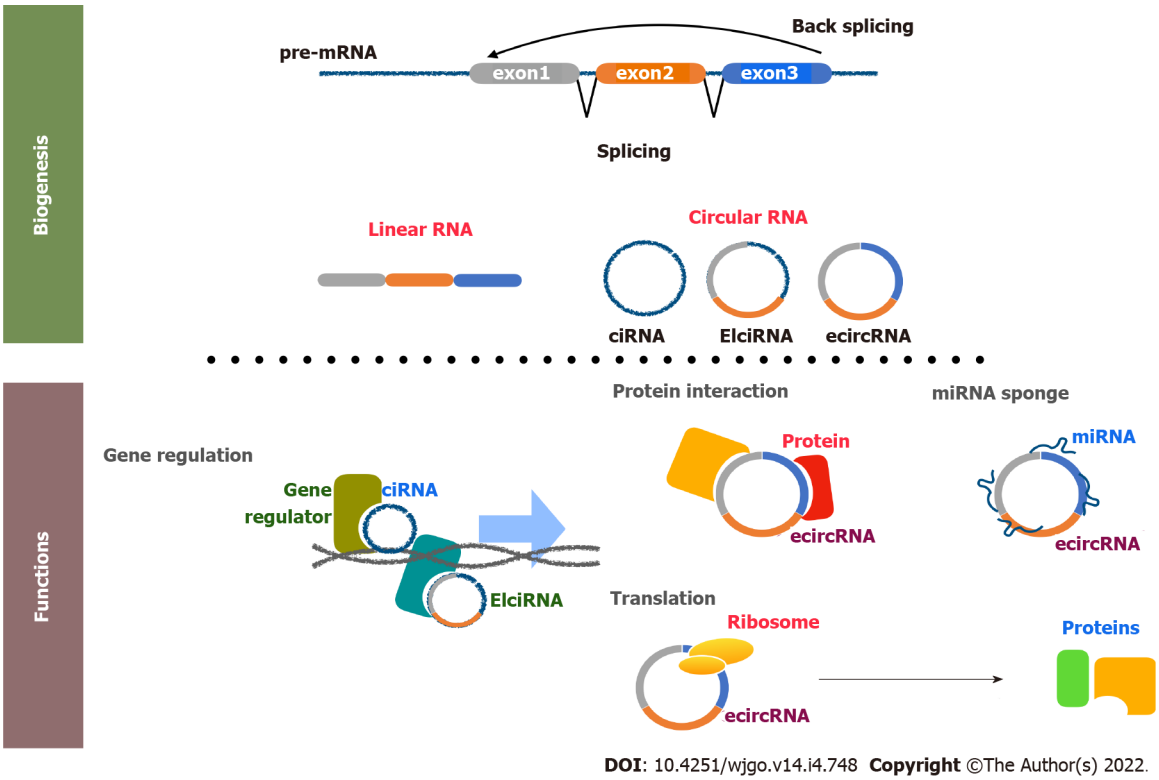

DOI: 10.4251/wjgo.v14.i4.748 **Copyright** ©The Author(s) 2022.

Figure 3 The functions of circular RNAs. miRNA: MicroRNA; ciRNA: Circular intronic RNA; EIciRNA: Exon-intron circular RNA; ecircRNA: Exonic circular RNA.

structures, antisense transcripts that inhibit gene expression, and A-U triple-helix structure of unconventional lincRNA modified by RNase P[84], which participate in global cellular behavior through different modifications and complexes with different molecules to control cell death and cell growth. LncRNAs control nuclear architecture and transcription in the nucleus. On the other hand, cytoplasmic lncRNAs regulate mRNA stability, affect translation, and act as miRNA sponges,

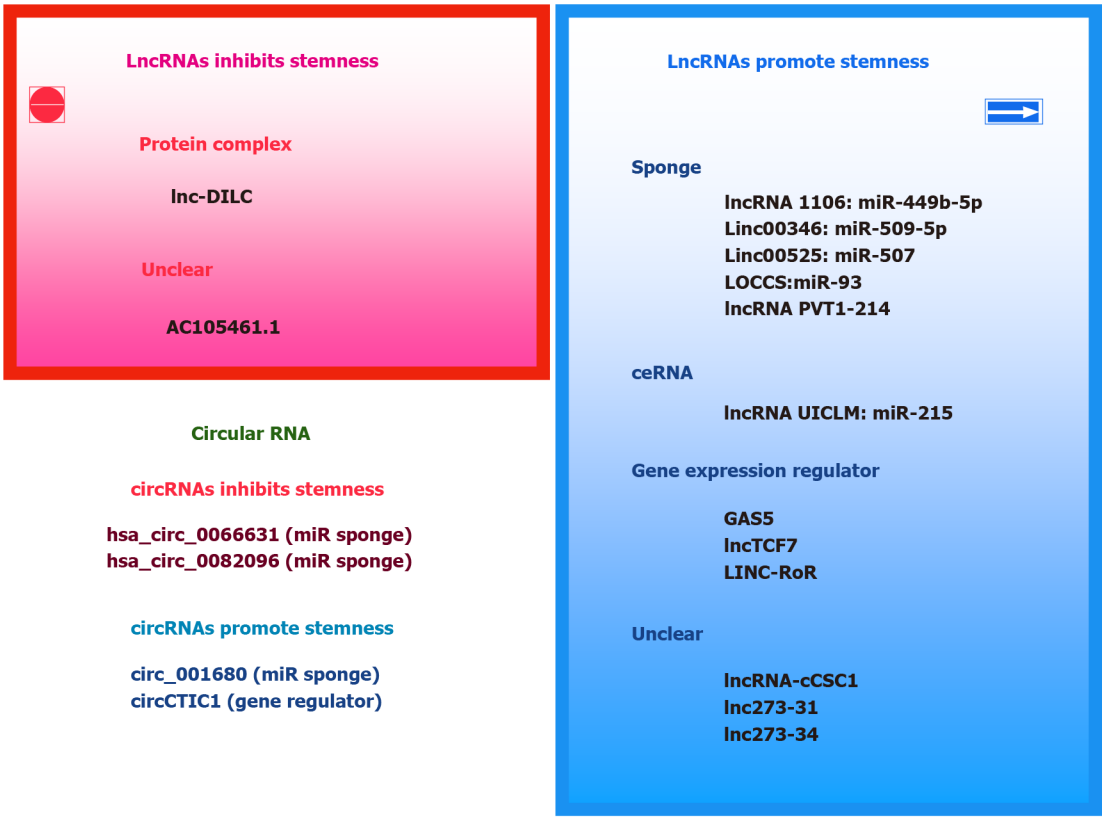

DOI: 10.4251/wjgo.v14.i4.748

Figure 4 The role of regulatory long-non coding RNAs and circular RNAs of colorectal cancer stem cells in this article. lncRNA: Long-non coding RNAs; circRNA: Circular RNA; lnc-DILC: LncRNA downregulation in liver cancer stem cells; CSC: Cancer stem cell.

translation, and post-translational modifications[85]. Nowadays, over 170000 human lncRNA transcripts have already been identified; however, the mechanisms and the functions of most lncRNA are still unclear[86].

In nuclei, lncRNAs can regulate chromosome architecture and regulate genome organization at different statuses, such as imprinting. In females, X-chromosome inactivation (XCI) occurs to silence an X chromosome during embryonic development. XCI-induced gene silencing is initiated by the Xist lncRNA[87]. LncRNAs play an important role in gene regulation. They regulate gene expression in *cis* proximal transcription sites or *trans* distant transcription sites. LncRNA can form an R loop structure with transcription factors to form a complex and regulate transcription at the target gene locus[88]. Some lncRNAs serve as scaffold-like structure of RNA-protein interaction in nuclear bodies[89].

In cytoplasm, lncRNAs can control the stability of mRNA by regulating miRNA through competitive endogenous RNA that functions like a miRNA sponge. In addition, it has recently been reported that lncRNAs related to ribosomes can regulate translation. For example, MALAT1 interacts with ribosomes to regulate translation[90]. LncRNA also regulates post-translational modifications, such as regulating the phosphorylation of STAT3 and controlling the differentiation of human dendritic cells[91]. At present, many lncRNAs have been reported to be involved in tumor formation or to play a role in tumor suppression. C9orf139 is highly expressed in pancreatic cancer and serves as a prognostic marker for pancreatic cancer[92], HOXD-AS2 and LINC00511 promote gastric cancer[93,94]. In addition, LINC02532 promotes gastric cancer progression, migration, and invasion in Figure 2[95].

LncRNAs in CRC

Recent studies have pointed out that in CRC stem cells, lncRNA is also involved in many regulatory functions in transcription, translation, and signaling transductions. LncRNAs can play positive or negative roles for stem cell properties in CRC. Therefore, the lncRNA in CRC stem cells has the potential to become a target for CRC diagnosis and treatment.

Positive regulator of stem cell properties in CRC

Recently, many studies have found many lncRNAs that promote CSCs properties. These lncRNAs also relate to CRC prognosis. Guo *et al*[96] found that lncRNA1106 is highly expressed in colon adenocarcinoma and induces the proliferation, migration, and stem cell properties of CRC cells. Cytoplasmic lncRNA1106 can be used as miR-449b-5p sponge. The gene lncRNA1106 positively regulates Gli4 in CRC cells. In addition, Gli2 also induces lncRNA1106 expression up-regulation. The lncRNA1106-Gli

network plays an important role in CRC stem cells. LINC-RoR can induce many stem cell properties in many tumors. Li *et al*[97] found that LINC-RoR was up-regulated in CRC cell lines. Overexpression of LINC-RoR promotes cell proliferation, and its inhibition can reverse this effect *in vitro*. Fuortes *et al*[98] reported that GAS5 was associated with malignant features in HCT116-derived CSCs. Knockdown GAS5 significantly suppressed CSC self-renewal capacity, proliferation, drug resistant, stemness, and migration. Methyltransferase WBSCR22 is considered as a tumor promoter in CRC. WBSCR22 was negatively regulated by miR-509-5p. Zhao *et al*[99] reported that Linc00346 promotes the expression of WBSCR22 by adsorbing miR-509-5p, a WBSCR22 negative regulator. The Linc00346/miR-509-5p/WBSCR22 signal axis promotes the stemness of colon cancer.

Using bioinformatic analysis, Zhou *et al*[100] identified a novel lncRNA (lncRNA-cCSC1) that is highly expressed in CRC and colorectal CSCs. LncRNA-cCSC1 promotes the self-renewal capacity of the CRCSCs. Their study indicates that lncRNA-cCSC1 may regulate CSC-like properties *via* the Hh signaling pathway. Besides, lnc273-31 or lnc273-34 depletion inhibits CRC migration, invasion, cancer stem cell self-renewal and chemoresistance in p53-R273H mutation cells[101]. In addition, high expressions of LINC00525 are observed in CRC patients with poor prognosis. Wang *et al*[102] found that LINC00525 knockdown decreased stemness properties and tumorigenesis *via* miR-507, which is the direct target of LINC00525. LncRNA portal vein thrombosis (PVT)1-214 is a key regulator of CRC development and progression. Overexpression of PVT1-214 can upregulate Lin28 protein in CRC cells and serves as a critical role of CRC pathogenesis[103]. LncTCF7 can activate the Wnt/β-catenin signaling pathway. Knocking down lncTCF7 in CRC cells decreased cancer cell progression[104]. Chen *et al*[105]'s study shows that lncRNA up-regulated in CRC liver metastasis (UICLM) was significantly up-regulated in liver metastasis-CRC. UICLM acted as a ceRNA for miR-215 to regulate ZEB2 expression and promote metastasis. Yu *et al*[106] also found an lncRNA: LOCCS was obviously upregulated in colon CD133+/CD166+/CD44+ CSCs. Knockdown of LOCCS reduced cell proliferation, invasion, migration, and tumorigenesis *in vivo*. Recently, lncRNA KLK8 has been reported that was upregulated and positively correlated with the stemness gene in CRC[107]. Wu *et al*[108] found that lncRNA SLCO4A1-AS1 could bind with miR-150-3p to elevate the expression of SLCO4A1 and the stemness of CRC.

Negative regulator of stem cell properties in CRC

Some lncRNAs that inhibit the properties of stem cells tend to have lower expression in CRC than normal colorectal cells. Overexpression of these lncRNAs can also inhibit tumor progression. LncRNA downregulation in liver CSCs (lnc-DILC) is a tumor suppressor in CRC. Li *et al*[109] found that lnc-DILC expression was downregulated in CRC tissues of human patients. Down-regulation of lnc-DILC increase aggressive of clinical characteristics. According their clinical study, lnc-DILC could be a diagnostic and prognostic marker in CRC. Besides, Liu *et al*[110] found an lncRNA (AC105461.1) is related to cancer stem cell properties. AC105461.1 overexpression reduced the percentage of CD133+CD44+ CRC stem cells, whereas its knockdown increased the population of CD133+CD44+ CRC stem cells (Figure 2).

CIRCRNAS

CircRNAs are circular noncoding RNAs (ncRNAs). This type of ncRNA was discovered in early 1990. Recently, using RNA-sequencing technology, researchers have found a large number of novel circRNAs in mammalian cells; however, the function of circRNAs is still unclear. Regarding the biogenesis, circRNA can be formed in the following ways: Exon reverse splicing into loops (exonic circRNA, ecircRNA), intron-preserving transcript reverse splicing (exon-intron circRNA, eIcircRNA), and intron reverse complementary pairing (circular intronic RNA, ciRNA). According to a report, the precursor tRNA can be cut into a ring to form tricRNA (tRNA intronic circRNA)[111]. CircRNA can regulate many biological functions. CircRNA can act as an antagonist of miRNA sponge to regulate miRNA. Therefore, it is possible to control gene expression by competing miRNA. CircRNA has also been found to form complexes with proteins to regulate physiological functions together. Although circRNA is considered to be ncRNA, a previous study found that ribosome binding to the stop codon of circMBL was identified in the brain tissue of *Drosophila*, and the circRNA translation protein products were obtained by protein profiling. This result also confirms that circRNA may be like mRNA, which can translate protein functions[112]. (Figure 3)

In a study of PML/RARα in leukemia, two fusion circRNAs (f-circRNA) were found in its chromosomal translocation. Further *in vivo* experiments showed that the f-circRNA can promote tumor growth. Several recent studies have shown that abnormal expression of circRNA occurs in almost all types of cancer. CircRNA can be an oncogene or a tumor suppressor gene, and it is involved in tumorigenesis of cancer[113].

CircRNAs in CRC stem cells

Currently, many scientists are interested in circRNAs involved in CRC stem cells. Understanding the

Table 1 Non-coding RNAs in colorectal cancer

Gene	Molucular mechanism in CRC	Molecular targets and interacts in CRC	Ref.
MicroRNAs			
		CRC stemness-related intracellular regulatory and transcription factors	
MiR-1185-1	Inhibits tumor suppressor	CD24	[49]
MiR-30a	Reduces migration and invasion	Transmembrane-4-L-six-family-1	[51]
MiR-92a	Promotes the proliferation	Leucine-rich repeats and immunoglobulin-like domains protein 1	[53]
MiR-450a-5p	Inhibits CSC properties and angiogenesis	SOX2	[55]
MiR-590-5p	Inhibits tumorigenesis	YAP1	[56]
MiR-203	Inhibits self-renewal ability and cancer stemness	GATA6	[58]
MiR-3622a-3p	Inhibits the stemness and epithelial to mesenchymal transition	SALL4	[59]
MiR-210-3p	Upregulates the invasion ability	Stathmin1	[61]
MiR-221	Promotes the tumorigenesis	Quaking	[63]
		Hypoxia signaling	
MiR-34a	Promotes metastasis	PPP1R11	[65]
MiR-215	Inhibit stemness	Lgr-5	[66]
		Notch signaling	
MiR-1280	Reduces stemness	JAG2	[68]
		Wnt/β-catenin signaling	
MiR-501-3p	Promotes tumor proliferation and stemness	APC	[71]
MiR-92a	Increases chPPemical-resistant	KLF4, GSK3β, and DKK3	[72]
MiR-30-5p	Reduces stemness	CD133 and SOX2	[73]
MiR-3120-5p	Increases the CSC population and promotes the stemness and invasiveness	Axin2	[74]
MiR-302c	Reduces stemness	CARF	[77]
		TGF-β/Smad pathway	
MiR-4666-3p	Tumor suppressor genes in quiescent CSCs	TGF-βR1	[78]
MiR-329	Tumor suppressor genes in quiescent CSCs	TGF-βR1	[78]
		Cellular response and process	
MiR-3135b	Inhibits cell proliferation, increase sensitivity to 5-fluorouracil lysis, and promote late cell degradation and necrosis	GOLPH3	[80]
MiR-194	Induces cell apoptosis	NA	[81]
MiR-486-5p	Inhibits stem cell characteristics	NA	[82]
MiR-133b	Inhibits the stemness and chemoresistance of CRC	NA	[83]
Long noncoding RNAs			
		Positive regulator	
LncRNA1106	Induces the proliferation, migration, and stem cell properties	MiR-449b-5p sponge, Gli4	[96]
LINC-RoR	Induces stem cell properties	NA	[97]
GAS5	Promotes CSC self-renewal capacity, proliferation, drug resistant, stemness, and migration	NA	[98]
Linc00346	Promotes the stemness	MiR-509-5p sponge, WBSCR22	[99]
LncRNA-cCSC1	Promotes the self-renewal capacity	Hh signaling pathway	[100]

Lnc273-31	Promotes migration, invasion, cancer stem cell self-renewal and chemoresistanc	NA	[101]
Lnc273-34	Promotes migration, invasion, cancer stem cell self-renewal and chemoresistanc	NA	[101]
LINC00525	Increase stemness properties and tumorigenesis	MiR-507	[102]
LncRNA PVT1-214	Promotes CRC progression	Lin28	[103]
LncTCF7	Promotes CRC progression	Wnt signaling	[104]
LncRNA UICLM	Promotes metastasis	ceRNA for miR-215	[105]
LncRNA: LOCCS	Promotes cell proliferation, invasion, migration, and tumorigenesis	NA	[106]
LncRNA KLK8	Increases stemness	NA	[107]
LncRNA SLCO4A1-AS1	Promote stemness	MiR-150-3p sponge	[108]
		Negative regulator	
Lnc-DILC	Reduces aggressive of clinical characteristics	NA	[109]
LncRNA (AC105461.1)	Reduces stemness	NA	[110]
Circular RNAs			
Hsa_circ_0066631	High expression in CRC spheroid cells, associated with the stemness-associated signaling pathway network	MiRNA sponge: MiR-140-3p, miR-224, miR-382, miR-548c-3p, and miR-579	[114]
Hsa_circ_0082096	High expression in CRC spheroid cells, associated with the stemness-associated signaling pathway network	MiRNA sponge: MiR-140-3p, miR-224, miR-382, miR-548c-3p, and miR-579	[114]
Circ_001680	Enhances the proliferation and migration capacity	MiR-340	[115]
Circular RNA (circCTIC1)	Promotes stemness and triggers the transcriptional initiation of c-Myc	Nuclear remodeling factor complex	[116]

TGF: Transforming growth factor; KLF: Kruppel-like factor; SALL: Spalt-like; Lnc-DILC: LncRNA downregulation in liver cancer stem cells; CRC: Colorectal cancer; miRNA: MicroRNA; LncRNA: Long-non coding RNA; CSC: Cancer stem cell; UICLM: Up-regulated in colorectal cancer liver metastasis; PVT: Portal vein thrombosis; Hh: Hedgehog; GSK: Glycogen synthase kinase; TGF: Transforming growth factor; APC: Adenomatous polyposis coli; KLF: Krüppel-like factor; DKK: Dickkopf.

roles of these circRNAs can help to elucidate CRC tumorigenesis. High-throughput next-generation sequencing and bioinformatics methods can be good tools to find novel circRNAs. Recently, Rengganaten *et al*[114] used genome-wide sequencing to identify 1503 and 636 circRNAs specific to the CRC parental and spheroid cells (enriched CSCs), respectively. They found that the expression levels of circRNAs, has_circ_0066631 and hsa_circ_0082096, in a circRNA-miRNA-mRNA axis associated with the stemness-associated signaling pathway network, were significantly upregulated in the spheroid cells. The two circRNAs, as miRNA sponge, were found to target and downregulate CRC stemness miRs, miR-140-3p, miR-224, miR-382, miR-548c-3p, and miR-579. Moreover, circ_001680 was observed to enhance the proliferation and migration capacity of CRC cells. Bioinformatics analysis data from Jian *et al*[115] also reveals that circ_001680 affects the expression of stemness gene BMI1 by targeting miR-340. From the results of *in vivo* and *in vitro* experiments, circ_001680 could promote the CSC population in CRC.

CircRNA also affects CRC stemness *via* circRNA-mediated genome modeling to regulate gene transcription. Zhan *et al*[116] found that circular RNA (circCTIC1) was highly expressed in colon tumor and CRC stem cells and promoted the self-renewal of CRC stem cells. CircCTIC1 interacted with the nuclear remodeling factor complex on the c-Myc promoter and triggered the transcriptional initiation of c-Myc (Figure 4).

CLINICAL CHALLENGES AND PROSPECTION

CSCs are considered to be the origin of cancer and are also related to cancer progression. Recently, CSCs have become the therapeutic target cells for cancer. According to the clinicaltrials.gov database, CRC stem cells were also clinically evaluated (NCT01577511) to identify their invasive capacity in CRC. Reducing the stemness of cancer to increase the sensitivity of chemotherapy could be a useful strategy for cancer treatment. For example, inducing CSCs to differentiate and then combining treatment with

traditional chemotherapeutics will also help eliminate cancer tissues. Therefore, elucidating the molecular mechanisms that regulate cell stemness in CSCs is an important issue. In recent years, many reports have shown that ncRNA plays various roles in CRC stem cells and affects the fate of CSCs. These ncRNAs affect the functions of CRC stem cells and further affect the progress of CRC. Thus, characterizing the regulatory mechanism of ncRNA will provide new strategies for cancer treatment. Among ncRNAs, miRNA is the most widely used clinically. MiRNA profiles of different cancer types may be used as diagnostic biomarkers. Tumor suppressor miRNAs have the potential to become RNA biosimilar drugs. So far, in the clinicaltrials.gov database, clinical research has begun on a number of miRNA biomarkers. Some of this research focuses on assessing the progress of diseases, including diabetes, breast cancer, *etc.* In the case of NCT03362684, the performance of miRNA's miR-31-3p and miR-31-5p was used for the diagnosis and prognosis evaluation of anti-EGFR therapy in stage III Colon Cancer.

For treatment using RNA, the first small interfering RNA (siRNA), patisiran, was approved by the Food and Drug Administration (FDA) in 2018. This drug is used for rare polyneuropathy mediated by hereditary transthyretin (hATTR) caused by amyloidosis. Later, givosiran and lumasiran were approved by the FDA as siRNA drugs to treat hATTR-mediated amyloidosis and primary hyperoxaluria type 1, respectively. However, there are no approved drugs for miRNA.

Nevertheless, in different cancers, there are still many pharmaceutical companies that are developing miRNA mimics or anti-miRNA drugs and starting clinical testing. For example, miRagen Therapeutics Inc. developed MRG-106 (an inhibitor of miRNA-155), MRG-201 (a synthetic miRNA mimic to miRNA-29b), and MRG-110 (a synthetic miRNA inhibitor of miRNA-92). The MRX34 developed by Mirna Therapeutics Inc. for liver cancer has entered a phase 1 clinical trial. SantarisPharma's inhibitor, miravirsen (SPC3649), which was developed for miR-122, has also entered clinical testing. These tests all show that miRNA has the opportunity to become a potential drug for cancer treatment. In addition, in the current clinical trials' cases, lncRNA and circRNA still only serve as biomarkers of diseases. For example, in the report of clinical test NCT042697462, lncRNA CCAT1 was also used as a biomarker for the diagnosis and stage determination of CRC.

At present, ncRNAs are used as a biomarker for diagnosing diseases in most clinical trials. ncRNAs have multi-target genes and widely regulate cellular function, which are their advantages as a therapeutic drug. However, these complex and unclear functions also become challenges in the drug development. For carcinogenic ncRNA, the delivery of anti-ncRNA or siRNA may be a good strategy for cancer treatment, but the side effect issues of off-targeting and the effects on the expression of other genes must also be considered. In addition, a safe, high efficiency and highly specific gene delivery system of tumor suppressor ncRNA to target cancer cells is also a challenge for ncRNA drug applications. Despite these challenges, the understanding of the function of ncRNA in the cancer could provide new treatment targets and strategies for cancer treatment.

CONCLUSION

CRC is a common disease with high morbidity and fatality rates worldwide. Cancer targeted therapies have become an emerging and urgent topic in cancer research. CSCs are considered the new targets of cancer therapies. CRC stem cells are involved in the malignancy of CRC, such as proliferation, drug resistance, and metastasis; ncRNA research on CRC stem cells is also a current focus. With the advancement of bioinformatics and high-throughput RNA-sequencing technology, the role of ncRNAs in CRC stem cells has been revealed. These ncRNAs are involved in the fate of CSCs and affect tumor development (Table 1). Understanding the role of ncRNAs in oncogenes or tumor suppressors in CRC stem cells will improve CRC diagnosis, treatment, and new drug development.

FOOTNOTES

Author contributions: Chao HM, Wang TW, Chern E and Hsu Sh reviewed the papers and wrote the manuscript; and all authors have read and approve the final manuscript.

Conflict-of-interest statement: Authors declare no conflict of interests for this article.

Country/Territory of origin: Taiwan

ORCID number: Hsiao-Mei Chao 0000-0003-1211-0234; Teh-Wei Wang 0000-0001-9874-2392; Edward Chern 0000-0002-9317-5410; Shan-hui Hsu 0000-0003-3399-055X.

S-Editor: Wang JJ
L-Editor: A
P-Editor: Wang JJ

REFERENCES

1 **American Cancer Society**. In: Siegel R, Miller K, Jemal A. Descriptive Epidemiology. New York: Wiley, 2017 [DOI: 10.1002/9781119468868.ch1]
2 **Reya T**, Morrison SJ, Clarke MF, Weissman IL. Stem cells, cancer, and cancer stem cells. *Nature* 2001; **414**: 105-111 [PMID: 11689955 DOI: 10.1038/35102167]
3 **Nowell PC**. The clonal evolution of tumor cell populations. *Science* 1976; **194**: 23-28 [PMID: 959840 DOI: 10.1126/science.959840]
4 **Kreso A**, Dick JE. Evolution of the cancer stem cell model. *Cell Stem Cell* 2014; **14**: 275-291 [PMID: 24607403 DOI: 10.1016/j.stem.2014.02.006]
5 **Vlashi E**, Pajonk F. Cancer stem cells, cancer cell plasticity and radiation therapy. *Semin Cancer Biol* 2015; **31**: 28-35 [PMID: 25025713 DOI: 10.1016/j.semcancer.2014.07.001]
6 **Kelly PN**, Dakic A, Adams JM, Nutt SL, Strasser A. Tumor growth need not be driven by rare cancer stem cells. *Science* 2007; **317**: 337 [PMID: 17641192 DOI: 10.1126/science.1142596]
7 **Quintana E**, Shackleton M, Sabel MS, Fullen DR, Johnson TM, Morrison SJ. Efficient tumour formation by single human melanoma cells. *Nature* 2008; **456**: 593-598 [PMID: 19052619 DOI: 10.1038/nature07567]
8 **Dalerba P**, Dylla SJ, Park IK, Liu R, Wang X, Cho RW, Hoey T, Gurney A, Huang EH, Simeone DM, Shelton AA, Parmiani G, Castelli C, Clarke MF. Phenotypic characterization of human colorectal cancer stem cells. *Proc Natl Acad Sci U S A* 2007; **104**: 10158-10163 [PMID: 17548814 DOI: 10.1073/pnas.0703478104]
9 **Ricci-Vitiani L**, Lombardi DG, Pilozzi E, Biffoni M, Todaro M, Peschle C, De Maria R. Identification and expansion of human colon-cancer-initiating cells. *Nature* 2007; **445**: 111-115 [PMID: 17122771 DOI: 10.1038/nature05384]
10 **Lee G**, Hall RR 3rd, Ahmed AU. Cancer Stem Cells: Cellular Plasticity, Niche, and its Clinical Relevance. *J Stem Cell Res Ther* 2016; **6** [PMID: 27891292 DOI: 10.4172/2157-7633.1000363]
11 **He S**, Nakada D, Morrison SJ. Mechanisms of stem cell self-renewal. *Annu Rev Cell Dev Biol* 2009; **25**: 377-406 [PMID: 19575646 DOI: 10.1146/annurev.cellbio.042308.113248]
12 **Allsopp RC**, Morin GB, DePinho R, Harley CB, Weissman IL. Telomerase is required to slow telomere shortening and extend replicative lifespan of HSCs during serial transplantation. *Blood* 2003; **102**: 517-520 [PMID: 12663456 DOI: 10.1182/blood-2002-07-2334]
13 **Yuan Y**, Shen H, Franklin DS, Scadden DT, Cheng T. In vivo self-renewing divisions of haematopoietic stem cells are increased in the absence of the early G1-phase inhibitor, p18INK4C. *Nat Cell Biol* 2004; **6**: 436-442 [PMID: 15122268 DOI: 10.1038/ncb1126]
14 **Tan BT**, Park CY, Ailles LE, Weissman IL. The cancer stem cell hypothesis: a work in progress. *Lab Invest* 2006; **86**: 1203-1207 [PMID: 17075578 DOI: 10.1038/Labinvest.3700488]
15 **Clevers H**. The cancer stem cell: premises, promises and challenges. *Nat Med* 2011; **17**: 313-319 [PMID: 21386835 DOI: 10.1038/nm.2304]
16 **O'Brien CA**, Kreso A, Jamieson CH. Cancer stem cells and self-renewal. *Clin Cancer Res* 2010; **16**: 3113-3120 [PMID: 20530701 DOI: 10.1158/1078-0432.CCR-09-2824]
17 **Reynolds BA**, Tetzlaff W, Weiss S. A multipotent EGF-responsive striatal embryonic progenitor cell produces neurons and astrocytes. *J Neurosci* 1992; **12**: 4565-4574 [PMID: 1432110 DOI: 10.1523/JNEUROSCI.12-11-04565.1992]
18 **Pastrana E**, Silva-Vargas V, Doetsch F. Eyes wide open: a critical review of sphere-formation as an assay for stem cells. *Cell Stem Cell* 2011; **8**: 486-498 [PMID: 21549325 DOI: 10.1016/j.stem.2011.04.007]
19 **Eyler CE**, Rich JN. Survival of the fittest: cancer stem cells in therapeutic resistance and angiogenesis. *J Clin Oncol* 2008; **26**: 2839-2845 [PMID: 18539962 DOI: 10.1200/JCO.2007.15.1829]
20 **Bao S**, Wu Q, McLendon RE, Hao Y, Shi Q, Hjelmeland AB, Dewhirst MW, Bigner DD, Rich JN. Glioma stem cells promote radioresistance by preferential activation of the DNA damage response. *Nature* 2006; **444**: 756-760 [PMID: 17051156 DOI: 10.1038/nature05236]
21 **Holyoake T**, Jiang X, Eaves C, Eaves A. Isolation of a highly quiescent subpopulation of primitive leukemic cells in chronic myeloid leukemia. *Blood* 1999; **94**: 2056-2064 [PMID: 10477735]
22 **Chen W**, Dong J, Haiech J, Kilhoffer MC, Zeniou M. Cancer Stem Cell Quiescence and Plasticity as Major Challenges in Cancer Therapy. *Stem Cells Int* 2016; **2016**: 1740936 [PMID: 27418931 DOI: 10.1155/2016/1740936]
23 **Dean M**, Fojo T, Bates S. Tumour stem cells and drug resistance. *Nat Rev Cancer* 2005; **5**: 275-284 [PMID: 15803154 DOI: 10.1038/nrc1590]
24 **Shi GM**, Xu Y, Fan J, Zhou J, Yang XR, Qiu SJ, Liao Y, Wu WZ, Ji Y, Ke AW, Ding ZB, He YZ, Wu B, Yang GH, Qin WZ, Zhang W, Zhu J, Min ZH, Wu ZQ. Identification of side population cells in human hepatocellular carcinoma cell lines with stepwise metastatic potentials. *J Cancer Res Clin Oncol* 2008; **134**: 1155-1163 [PMID: 18470535 DOI: 10.1007/s00432-008-0407-1]
25 **Baccelli I**, Trumpp A. The evolving concept of cancer and metastasis stem cells. *J Cell Biol* 2012; **198**: 281-293 [PMID: 22869594 DOI: 10.1083/jcb.201202014]
26 **Pitule P**, Cedikova M, Daum O, Vojtisek J, Vycital O, Hosek P, Treska V, Hes O, Kralickova M, Liska V.

Immunohistochemical detection of cancer stem cell related markers CD44 and CD133 in metastatic colorectal cancer patients. *Biomed Res Int* 2014; **2014**: 432139 [PMID: 24864242 DOI: 10.1155/2014/432139]

27 **Langley RR**, Fidler IJ. The seed and soil hypothesis revisited--the role of tumor-stroma interactions in metastasis to different organs. *Int J Cancer* 2011; **128**: 2527-2535 [PMID: 21365651 DOI: 10.1002/ijc.26031]

28 **Bravo-Cordero JJ**, Hodgson L, Condeelis J. Directed cell invasion and migration during metastasis. *Curr Opin Cell Biol* 2012; **24**: 277-283 [PMID: 22209238 DOI: 10.1016/j.ceb.2011.12.004]

29 **Chao HM**, Huang HX, Chang PH, Tseng KC, Miyajima A, Chern E. Y-box binding protein-1 promotes hepatocellular carcinoma-initiating cell progression and tumorigenesis *via* Wnt/β-catenin pathway. *Oncotarget* 2017; **8**: 2604-2616 [PMID: 27911878 DOI: 10.18632/oncotarget.13733]

30 **Pandurangan AK**, Divya T, Kumar K, Dineshbabu V, Velavan B, Sudhandiran G. Colorectal carcinogenesis: Insights into the cell death and signal transduction pathways: A review. *World J Gastrointest Oncol* 2018; **10**: 244-259 [PMID: 30254720 DOI: 10.4251/wjgo.v10.i9.244]

31 **Jubb AM**, Chalasani S, Frantz GD, Smits R, Grabsch HI, Kavi V, Maughan NJ, Hillan KJ, Quirke P, Koeppen H. Achaete-scute like 2 (ascl2) is a target of Wnt signalling and is upregulated in intestinal neoplasia. *Oncogene* 2006; **25**: 3445-3457 [PMID: 16568095 DOI: 10.1038/sj.onc.1209382]

32 **Tanabe S**, Aoyagi K, Yokozaki H, Sasaki H. Regulation of CTNNB1 signaling in gastric cancer and stem cells. *World J Gastrointest Oncol* 2016; **8**: 592-598 [PMID: 27574551 DOI: 10.4251/wjgo.v8.i8.592]

33 **Chang PH**, Sekine K, Chao HM, Hsu SH, Chern E. Chitosan promotes cancer progression and stem cell properties in association with Wnt signaling in colon and hepatocellular carcinoma cells. *Sci Rep* 2017; **8**: 45751 [PMID: 28367998 DOI: 10.1038/srep45751]

34 **Rauff B**, Malik A, Bhatti YA, Chudhary SA, Qadri I, Rafiq S. Notch signalling pathway in development of cholangiocarcinoma. *World J Gastrointest Oncol* 2020; **12**: 957-974 [PMID: 33005291 DOI: 10.4251/wjgo.v12.i9.957]

35 **Yang Q**, Bermingham NA, Finegold MJ, Zoghbi HY. Requirement of Math1 for secretory cell lineage commitment in the mouse intestine. *Science* 2001; **294**: 2155-2158 [PMID: 11739954 DOI: 10.1126/science.1065718]

36 **van Dop WA**, Uhmann A, Wijgerde M, Sleddens-Linkels E, Heijmans J, Offerhaus GJ, van den Bergh Weerman MA, Boeckxstaens GE, Hommes DW, Hardwick JC, Hahn H, van den Brink GR. Depletion of the colonic epithelial precursor cell compartment upon conditional activation of the hedgehog pathway. *Gastroenterology* 2009; **136**: 2195-2203.e1 [PMID: 19272384 DOI: 10.1053/j.gastro.2009.02.068]

37 **He XC**, Zhang J, Tong WG, Tawfik O, Ross J, Scoville DH, Tian Q, Zeng X, He X, Wiedemann LM, Mishina Y, Li L. BMP signaling inhibits intestinal stem cell self-renewal through suppression of Wnt-beta-catenin signaling. *Nat Genet* 2004; **36**: 1117-1121 [PMID: 15378062 DOI: 10.1038/ng1430]

38 **Qi Z**, Li Y, Zhao B, Xu C, Liu Y, Li H, Zhang B, Wang X, Yang X, Xie W, Li B, Han JJ, Chen YG. BMP restricts stemness of intestinal $Lgr5^+$ stem cells by directly suppressing their signature genes. *Nat Commun* 2017; **8**: 13824 [PMID: 28059064 DOI: 10.1038/ncomms13824]

39 **Whissell G**, Montagni E, Martinelli P, Hernando-Momblona X, Sevillano M, Jung P, Cortina C, Calon A, Abuli A, Castells A, Castellvi-Bel S, Nacht AS, Sancho E, Stephan-Otto Attolini C, Vicent GP, Real FX, Batlle E. The transcription factor GATA6 enables self-renewal of colon adenoma stem cells by repressing BMP gene expression. *Nat Cell Biol* 2014; **16**: 695-707 [PMID: 24952462 DOI: 10.1038/ncb2992]

40 **Zhang Q**, Xu HF, Song WY, Zhang PJ, Song YB. Potential microRNA panel for the diagnosis and prediction of overall survival of hepatocellular carcinoma with hepatitis B virus infection. *World J Gastrointest Oncol* 2020; **12**: 383-393 [PMID: 32368317 DOI: 10.4251/wjgo.v12.i4.383]

41 **Yan LX**, Huang XF, Shao Q, Huang MY, Deng L, Wu QL, Zeng YX, Shao JY. MicroRNA miR-21 overexpression in human breast cancer is associated with advanced clinical stage, lymph node metastasis and patient poor prognosis. *RNA* 2008; **14**: 2348-2360 [PMID: 18812439 DOI: 10.1261/rna.1034808]

42 **Hernandez YG**, Lucas AL. MicroRNA in pancreatic ductal adenocarcinoma and its precursor lesions. *World J Gastrointest Oncol* 2016; **8**: 18-29 [PMID: 26798434 DOI: 10.4251/wjgo.v8.i1.18]

43 **Yu F**, Yao H, Zhu P, Zhang X, Pan Q, Gong C, Huang Y, Hu X, Su F, Lieberman J, Song E. let-7 regulates self renewal and tumorigenicity of breast cancer cells. *Cell* 2007; **131**: 1109-1123 [PMID: 18083101 DOI: 10.1016/j.cell.2007.10.054]

44 **Ji Q**, Hao X, Zhang M, Tang W, Yang M, Li L, Xiang D, Desano JT, Bommer GT, Fan D, Fearon ER, Lawrence TS, Xu L. MicroRNA miR-34 inhibits human pancreatic cancer tumor-initiating cells. *PLoS One* 2009; **4**: e6816 [PMID: 19714243 DOI: 10.1371/journal.pone.0006816]

45 **Bader AG**, Brown D, Stoudemire J, Lammers P. Developing therapeutic microRNAs for cancer. *Gene Ther* 2011; **18**: 1121-1126 [PMID: 21633392 DOI: 10.1038/gt.2011.79]

46 **Dai E**, Yu X, Zhang Y, Meng F, Wang S, Liu X, Liu D, Wang J, Li X, Jiang W. EpimiR: a database of curated mutual regulation between miRNAs and epigenetic modifications. *Database (Oxford)* 2014; **2014**: bau023 [PMID: 24682734 DOI: 10.1093/database/bau023]

47 **Iliou MS**, da Silva-Diz V, Carmona FJ, Ramalho-Carvalho J, Heyn H, Villanueva A, Muñoz P, Esteller M. Impaired DICER1 function promotes stemness and metastasis in colon cancer. *Oncogene* 2014; **33**: 4003-4015 [PMID: 24096488 DOI: 10.1038/onc.2013.398]

48 **Viswanathan V**, Damle S, Zhang T, Opdenaker L, Modarai S, Accerbi M, Schmidt S, Green P, Galileo D, Palazzo J, Fields J, Haghighat S, Rigoutsos I, Gonye G, Boman BM. An miRNA Expression Signature for the Human Colonic Stem Cell Niche Distinguishes Malignant from Normal Epithelia. *Cancer Res* 2017; **77**: 3778-3790 [PMID: 28487386 DOI: 10.1158/0008-5472.CAN-16-2388]

49 **Wang TW**, Chern E, Hsu CW, Tseng KC, Chao HM. SIRT1-Mediated Expression of CD24 and Epigenetic Suppression of Novel Tumor Suppressor miR-1185-1 Increases Colorectal Cancer Stemness. *Cancer Res* 2020; **80**: 5257-5269 [PMID: 33046442 DOI: 10.1158/0008-5472.CAN-19-3188]

50 **Fu F**, Yang X, Zheng M, Zhao Q, Zhang K, Li Z, Zhang H, Zhang S. Role of Transmembrane 4 L Six Family 1 in the Development and Progression of Cancer. *Front Mol Biosci* 2020; **7**: 202 [PMID: 33015133 DOI:

10.3389/fmolb.2020.00202]
51 **Park YR**, Kim SL, Lee MR, Seo SY, Lee JH, Kim SH, Kim IH, Lee SO, Lee ST, Kim SW. MicroRNA-30a-5p (miR-30a) regulates cell motility and EMT by directly targeting oncogenic TM4SF1 in colorectal cancer. *J Cancer Res Clin Oncol* 2017; **143**: 1915-1927 [PMID: 28528497 DOI: 10.1007/s00432-017-2440-4]
52 **Powell AE**, Wang Y, Li Y, Poulin EJ, Means AL, Washington MK, Higginbotham JN, Juchheim A, Prasad N, Levy SE, Guo Y, Shyr Y, Aronow BJ, Haigis KM, Franklin JL, Coffey RJ. The pan-ErbB negative regulator Lrig1 is an intestinal stem cell marker that functions as a tumor suppressor. *Cell* 2012; **149**: 146-158 [PMID: 22464327 DOI: 10.1016/j.cell.2012.02.042]
53 **Viswanathan V**, Opdenaker L, Modarai S, Fields JZ, Gonye G, Boman BM. MicroRNA Expression Profiling of Normal and Malignant Human Colonic Stem Cells Identifies *miRNA92a* as a Regulator of the *LRIG1* Stem Cell Gene. *Int J Mol Sci* 2020; **21** [PMID: 32316543 DOI: 10.3390/ijms21082804]
54 **Chang PH**, Chao HM, Chern E, Hsu SH. Chitosan 3D cell culture system promotes naïve-like features of human induced pluripotent stem cells: A novel tool to sustain pluripotency and facilitate differentiation. *Biomaterials* 2021; **268**: 120575 [PMID: 33341735 DOI: 10.1016/j.biomaterials.2020.120575]
55 **Bialkowska AB**, Yang VW, Mallipattu SK. Krüppel-like factors in mammalian stem cells and development. *Development* 2017; **144**: 737-754 [PMID: 28246209 DOI: 10.1242/dev.145441]
56 **Ou C**, Sun Z, Li X, Ren W, Qin Z, Zhang X, Yuan W, Wang J, Yu W, Zhang S, Peng Q, Yan Q, Xiong W, Li G, Ma J. Corrigendum to "MiR-590-5p, a density-sensitive microRNA, inhibits tumorigenesis by targeting YAP1 in colorectal cancer", [Canc. Lett. 399 (2017) 53-63]. *Cancer Lett* 2018; **420**: 260 [PMID: 29429755 DOI: 10.1016/j.canlet.2018.01.073]
57 **Tremblay M**, Sanchez-Ferras O, Bouchard M. GATA transcription factors in development and disease. *Development* 2018; **145** [PMID: 30348673 DOI: 10.1242/dev.164384]
58 **Lai HT**, Tseng WK, Huang SW, Chao TC, Su Y. MicroRNA-203 diminishes the stemness of human colon cancer cells by suppressing GATA6 expression. *J Cell Physiol* 2020; **235**: 2866-2880 [PMID: 31544978 DOI: 10.1002/jcp.29192]
59 **Chang S**, Sun G, Zhang D, Li Q, Qian H. MiR-3622a-3p acts as a tumor suppressor in colorectal cancer by reducing stemness features and EMT through targeting spalt-like transcription factor 4. *Cell Death Dis* 2020; **11**: 592 [PMID: 32719361 DOI: 10.1038/s41419-020-02789-z]
60 **Shayimu P**, Yusufu A, Rehemutula A, Redati D, Jiapaer R, Tuerdi R. MicroRNA-377 Counteracts With Cancer Stem Cell Phenotypes and Epithelial Mesenchymal Transformation by Targeting ZEB2 in Colon Cancer. *Technol Cancer Res Treat* 2020; **19**: 1533033820967475 [PMID: 33084522 DOI: 10.1177/1533033820967475]
61 **Liao TT**, Cheng WC, Yang CY, Chen YQ, Su SH, Yeh TY, Lan HY, Lee CC, Lin HH, Lin CC, Lu RH, Chiou AE, Jiang JK, Hwang WL. The microRNA-210-Stathmin1 Axis Decreases Cell Stiffness to Facilitate the Invasiveness of Colorectal Cancer Stem Cells. *Cancers (Basel)* 2021; **13** [PMID: 33921319 DOI: 10.3390/cancers13081833]
62 **Chen T**, Richard S. Structure-function analysis of Qk1: a lethal point mutation in mouse quaking prevents homodimerization. *Mol Cell Biol* 1998; **18**: 4863-4871 [PMID: 9671495 DOI: 10.1128/MCB.18.8.4863]
63 **Mukohyama J**, Isobe T, Hu Q, Hayashi T, Watanabe T, Maeda M, Yanagi H, Qian X, Yamashita K, Minami H, Mimori K, Sahoo D, Kakeji Y, Suzuki A, Dalerba P, Shimono Y. miR-221 Targets QKI to Enhance the Tumorigenic Capacity of Human Colorectal Cancer Stem Cells. *Cancer Res* 2019; **79**: 5151-5158 [PMID: 31416845 DOI: 10.1158/0008-5472.CAN-18-3544]
64 **Keith B**, Simon MC. Hypoxia-inducible factors, stem cells, and cancer. *Cell* 2007; **129**: 465-472 [PMID: 17482542 DOI: 10.1016/j.cell.2007.04.019]
65 **Li H**, Rokavec M, Jiang L, Horst D, Hermeking H. Antagonistic Effects of p53 and HIF1A on microRNA-34a Regulation of PPP1R11 and STAT3 and Hypoxia-induced Epithelial to Mesenchymal Transition in Colorectal Cancer Cells. *Gastroenterology* 2017; **153**: 505-520 [PMID: 28435028 DOI: 10.1053/j.gastro.2017.04.017]
66 **Ullmann P**, Nurmik M, Schmitz M, Rodriguez F, Weiler J, Qureshi-Baig K, Felten P, Nazarov PV, Nicot N, Zuegel N, Haan S, Letellier E. Tumor suppressor miR-215 counteracts hypoxia-induced colon cancer stem cell activity. *Cancer Lett* 2019; **450**: 32-41 [PMID: 30790680 DOI: 10.1016/j.canlet.2019.02.030]
67 **Kumar P**, Anaya J, Mudunuri SB, Dutta A. Meta-analysis of tRNA derived RNA fragments reveals that they are evolutionarily conserved and associate with AGO proteins to recognize specific RNA targets. *BMC Biol* 2014; **12**: 78 [PMID: 25270025 DOI: 10.1186/s12915-014-0078-0]
68 **Huang B**, Yang H, Cheng X, Wang D, Fu S, Shen W, Zhang Q, Zhang L, Xue Z, Li Y, Da Y, Yang Q, Li Z, Liu L, Qiao L, Kong Y, Yao Z, Zhao P, Li M, Zhang R. tRF/miR-1280 Suppresses Stem Cell-like Cells and Metastasis in Colorectal Cancer. *Cancer Res* 2017; **77**: 3194-3206 [PMID: 28446464 DOI: 10.1158/0008-5472.CAN-16-3146]
69 **Li Y**, Hu H, Wang Y, Fan Y, Yang Y, Guo B, Xie X, Lian J, Jiang B, Han B, Shao C, Gong Y. CUL4B contributes to cancer stemness by repressing tumor suppressor miR34a in colorectal cancer. *Oncogenesis* 2020; **9**: 20 [PMID: 32054830 DOI: 10.1038/s41389-020-0206-3]
70 **Hsu SH**, Huang GS. Substrate-dependent Wnt signaling in MSC differentiation within biomaterial-derived 3D spheroids. *Biomaterials* 2013; **34**: 4725-4738 [PMID: 23562051 DOI: 10.1016/j.biomaterials.2013.03.031]
71 **Wu F**, Xing T, Gao X, Liu F. miR5013p promotes colorectal cancer progression *via* activation of Wnt/βcatenin signaling. *Int J Oncol* 2019; **55**: 671-683 [PMID: 31364752 DOI: 10.3892/ijo.2019.4852]
72 **Zhang GJ**, Li LF, Yang GD, Xia SS, Wang R, Leng ZW, Liu ZL, Tian HP, He Y, Meng CY, Liu DZ, Hou SL, Tang XG, Zhou T. MiR-92a promotes stem cell-like properties by activating Wnt/β-catenin signaling in colorectal cancer. *Oncotarget* 2017; **8**: 101760-101770 [PMID: 29254202 DOI: 10.18632/oncotarget.21667]
73 **Jiang S**, Miao D, Wang M, Lv J, Wang Y, Tong J. MiR-30-5p suppresses cell chemoresistance and stemness in colorectal cancer through USP22/Wnt/β-catenin signaling axis. *J Cell Mol Med* 2019; **23**: 630-640 [PMID: 30338942 DOI: 10.1111/jcmm.13968]
74 **Hongdan L**, Feng L. miR-3120-5p promotes colon cancer stem cell stemness and invasiveness through targeting Axin2. *Biochem Biophys Res Commun* 2018; **496**: 302-308 [PMID: 29307822 DOI: 10.1016/j.bbrc.2018.01.021]
75 **Wang G**, Zhou J, Lu F, Qiu L, Xu L, Yang X, Miao Y. Downregulation of microRNA1835p inhibits the proliferation and

invasion of colorectal cancer cells by inactivating the reticulocalbin2/Wnt/βcatenin signaling pathway. *Mol Med Rep* 2019; **19**: 4475-4483 [PMID: 30896885 DOI: 10.3892/mmr.2019.10059]

76 **Dong W**, Cao Z, Pang Y, Feng T, Tian H. CARF, As An Oncogene, Promotes Colorectal Cancer Stemness By Activating ERBB Signaling Pathway. *Onco Targets Ther* 2019; **12**: 9041-9051 [PMID: 31802911 DOI: 10.2147/OTT.S225733]

77 **Zhang Y**, Meng H, Guo K. Inhibition of MicroRNA-302c on Stemness of Colon Cancer Stem Cells *via* the CARF/Wnt/β-Catenin Axis. *Dig Dis Sci* 2021; **66**: 1906-1915 [PMID: 32617772 DOI: 10.1007/s10620-020-06435-8]

78 **Ye J**, Lei J, Fang Q, Shen Y, Xia W, Hu X, Xu Q, Yuan H, Huang J, Ni C. miR-4666-3p and miR-329 Synergistically Suppress the Stemness of Colorectal Cancer Cells *via* Targeting TGF-β/Smad Pathway. *Front Oncol* 2019; **9**: 1251 [PMID: 31824844 DOI: 10.3389/fonc.2019.01251]

79 **Ning X**, Wang C, Zhang M, Wang K. Ectopic Expression of miR-147 Inhibits Stem Cell Marker and Epithelial-Mesenchymal Transition (EMT)-Related Protein Expression in Colon Cancer Cells. *Oncol Res* 2019; **27**: 399-406 [PMID: 29426374 DOI: 10.3727/096504018X15179675206495]

80 **Núñez-Olvera SI**, Chávez-Munguía B, Del Rocío Terrones-Gurrola MC, Marchat LA, Puente-Rivera J, Ruíz-García E, Campos-Parra AD, Vázquez-Calzada C, Lizárraga-Verdugo ER, Ramos-Payán R, Salinas-Vera YM, López-Camarillo C. A novel protective role for microRNA-3135b in Golgi apparatus fragmentation induced by chemotherapy *via* GOLPH3/AKT1/mTOR axis in colorectal cancer cells. *Sci Rep* 2020; **10**: 10555 [PMID: 32601379 DOI: 10.1038/s41598-020-67550-0]

81 **Sun B**, Fang YT, Jin DJ, Chen ZY, Li ZY, Gu XD, Xiang JB. miR-194 Inhibits the Proliferation of SW620 Colon Cancer Stem Cells Through Downregulation of SSH2 Expression. *Cancer Manag Res* 2019; **11**: 10229-10238 [PMID: 31824193 DOI: 10.2147/CMAR.S221150]

82 **Pisano A**, Griñan-Lison C, Farace C, Fiorito G, Fenu G, Jiménez G, Scognamillo F, Peña-Martin J, Naccarati A, Pröll J, Atzmüller S, Pardini B, Attene F, Ibba G, Solinas MG, Bernhard D, Marchal JA, Madeddu R. The Inhibitory Role of miR-486-5p on CSC Phenotype Has Diagnostic and Prognostic Potential in Colorectal Cancer. *Cancers (Basel)* 2020; **12** [PMID: 33227890 DOI: 10.3390/cancers12113432]

83 **Lv L**, Li Q, Chen S, Zhang X, Tao X, Tang X, Wang S, Che G, Yu Y, He L. miR-133b suppresses colorectal cancer cell stemness and chemoresistance by targeting methyltransferase DOT1L. *Exp Cell Res* 2019; **385**: 111597 [PMID: 31525340 DOI: 10.1016/j.yexcr.2019.111597]

84 **Yao RW**, Wang Y, Chen LL. Cellular functions of long noncoding RNAs. *Nat Cell Biol* 2019; **21**: 542-551 [PMID: 31048766 DOI: 10.1038/s41556-019-0311-8]

85 **Wilusz JE**, Sunwoo H, Spector DL. Long noncoding RNAs: functional surprises from the RNA world. *Genes Dev* 2009; **23**: 1494-1504 [PMID: 19571179 DOI: 10.1101/gad.1800909]

86 **Gao F**, Cai Y, Kapranov P, Xu D. Reverse-genetics studies of lncRNAs-what we have learnt and paths forward. *Genome Biol* 2020; **21**: 93 [PMID: 32290841 DOI: 10.1186/s13059-020-01994-5]

87 **Tjalsma SJD**, Hori M, Sato Y, Bousard A, Ohi A, Raposo AC, Roensch J, Le Saux A, Nogami J, Maehara K, Kujirai T, Handa T, Bagés-Arnal S, Ohkawa Y, Kurumizaka H, da Rocha ST, Żylicz JJ, Kimura H, Heard E. H4K20me1 and H3K27me3 are concurrently loaded onto the inactive X chromosome but dispensable for inducing gene silencing. *EMBO Rep* 2021; **22**: e51989 [PMID: 33605056 DOI: 10.15252/embr.202051989]

88 **Vydzhak O**, Luke B, Schindler N. Non-coding RNAs at the Eukaryotic rDNA Locus: RNA-DNA Hybrids and Beyond. *J Mol Biol* 2020; **432**: 4287-4304 [PMID: 32446803 DOI: 10.1016/j.jmb.2020.05.011]

89 **Thakur J**, Henikoff S. Architectural RNA in chromatin organization. *Biochem Soc Trans* 2020; **48**: 1967-1978 [PMID: 32897323 DOI: 10.1042/BST20191226]

90 **Malakar P**, Stein I, Saragovi A, Winkler R, Stern-Ginossar N, Berger M, Pikarsky E, Karni R. Long Noncoding RNA MALAT1 Regulates Cancer Glucose Metabolism by Enhancing mTOR-Mediated Translation of TCF7L2. *Cancer Res* 2019; **79**: 2480-2493 [PMID: 30914432 DOI: 10.1158/0008-5472.CAN-18-1432]

91 **Ding H**, Liu J, Zou R, Cheng P, Su Y. Long non-coding RNA TPTEP1 inhibits hepatocellular carcinoma progression by suppressing STAT3 phosphorylation. *J Exp Clin Cancer Res* 2019; **38**: 189 [PMID: 31072375 DOI: 10.1186/s13046-019-1193-0]

92 **Ge JN**, Yan D, Ge CL, Wei MJ. LncRNA C9orf139 can regulate the growth of pancreatic cancer by mediating the miR-663a/Sox12 axis. *World J Gastrointest Oncol* 2020; **12**: 1272-1287 [PMID: 33250960 DOI: 10.4251/wjgo.v12.i11.1272]

93 **Sun CB**, Wang HY, Han XQ, Liu YN, Wang MC, Zhang HX, Gu YF, Leng XG. LINC00511 promotes gastric cancer cell growth by acting as a ceRNA. *World J Gastrointest Oncol* 2020; **12**: 394-404 [PMID: 32368318 DOI: 10.4251/wjgo.v12.i4.394]

94 **Yao L**, Ye PC, Tan W, Luo YJ, Xiang WP, Liu ZL, Fu ZM, Lu F, Tang LH, Xiao JW. Decreased expression of the long non-coding RNA *HOXD-AS2* promotes gastric cancer progression by targeting HOXD8 and activating PI3K/Akt signaling pathway. *World J Gastrointest Oncol* 2020; **12**: 1237-1254 [PMID: 33250958 DOI: 10.4251/wjgo.v12.i11.1237]

95 **Zhang C**, Ma MH, Liang Y, Wu KZ, Dai DQ. Novel long non-coding RNA LINC02532 promotes gastric cancer cell proliferation, migration, and invasion *in vitro*. *World J Gastrointest Oncol* 2019; **11**: 91-101 [PMID: 30788037 DOI: 10.4251/wjgo.v11.i2.91]

96 **Guo K**, Gong W, Wang Q, Gu G, Zheng T, Li Y, Li W, Fang M, Xie H, Yue C, Yang J, Zhu Z. LINC01106 drives colorectal cancer growth and stemness through a positive feedback loop to regulate the Gli family factors. *Cell Death Dis* 2020; **11**: 869 [PMID: 33067422 DOI: 10.1038/s41419-020-03026-3]

97 **Li X**, Chen W, Jia J, You Z, Hu C, Zhuang Y, Lin Z, Liu Y, Yang C, Xu R. The Long Non-Coding RNA-RoR Promotes the Tumorigenesis of Human Colorectal Cancer by Targeting miR-6833-3p Through SMC4. *Onco Targets Ther* 2020; **13**: 2573-2581 [PMID: 32273727 DOI: 10.2147/OTT.S238947]

98 **Fuortes L**, Phillips K, Muldoon J. Traumatic head and spinal cord injury in Iowa. *Iowa Med* 1990; **80**: 560-562 [PMID: 2269616]

99 **Zhao H**, Su W, Sun Y, Wu Z. WBSCR22 Competes with Long Non-coding RNA Linc00346 for miR-509-5p Binding Site to Regulate Cancer Stem Cell Phenotypes of Colorectal Cancer. *Biochem Genet* 2020; **58**: 384-398 [PMID: 32008219 DOI: 10.1007/s10528-020-09949-y]

100 **Zhou H**, Xiong Y, Peng L, Wang R, Zhang H, Fu Z. LncRNA-cCSC1 modulates cancer stem cell properties in colorectal cancer *via* activation of the Hedgehog signaling pathway. *J Cell Biochem* 2020; **121**: 2510-2524 [PMID: 31680315 DOI: 10.1002/jcb.29473]

101 **Zhao Y**, Li Y, Sheng J, Wu F, Li K, Huang R, Wang X, Jiao T, Guan X, Lu Y, Chen X, Luo Z, Zhou Y, Hu H, Liu W, Du B, Miao S, Cai J, Wang L, Zhao H, Ying J, Bi X, Song W. P53-R273H mutation enhances colorectal cancer stemness through regulating specific lncRNAs. *J Exp Clin Cancer Res* 2019; **38**: 379 [PMID: 31455383 DOI: 10.1186/s13046-019-1375-9]

102 **Wang S**, Li J, Yang X. Long Non-Coding RNA LINC00525 Promotes the Stemness and Chemoresistance of Colorectal Cancer by Targeting miR-507/ELK3 Axis. *Int J Stem Cells* 2019; **12**: 347-359 [PMID: 31242722 DOI: 10.15283/ijsc19041]

103 **He F**, Song Z, Chen H, Chen Z, Yang P, Li W, Yang Z, Zhang T, Wang F, Wei J, Wei F, Wang Q, Cao J. Long noncoding RNA PVT1-214 promotes proliferation and invasion of colorectal cancer by stabilizing Lin28 and interacting with miR-128. *Oncogene* 2019; **38**: 164-179 [PMID: 30076414 DOI: 10.1038/s41388-018-0432-8]

104 **Li T**, Zhu J, Wang X, Chen G, Sun L, Zuo S, Zhang J, Chen S, Ma J, Yao Z, Zheng Y, Chen Z, Liu Y, Wang P. Long non-coding RNA lncTCF7 activates the Wnt/β-catenin pathway to promote metastasis and invasion in colorectal cancer. *Oncol Lett* 2017; **14**: 7384-7390 [PMID: 29344178 DOI: 10.3892/ol.2017.7154]

105 **Chen DL**, Lu YX, Zhang JX, Wei XL, Wang F, Zeng ZL, Pan ZZ, Yuan YF, Wang FH, Pelicano H, Chiao PJ, Huang P, Xie D, Li YH, Ju HQ, Xu RH. Long non-coding RNA UICLM promotes colorectal cancer liver metastasis by acting as a ceRNA for microRNA-215 to regulate ZEB2 expression. *Theranostics* 2017; **7**: 4836-4849 [PMID: 29187907 DOI: 10.7150/thno.20942]

106 **Yu X**, Mi L, Dong J, Zou J. Long intergenic non-protein-coding RNA 1567 (LINC01567) acts as a "sponge" against microRNA-93 in regulating the proliferation and tumorigenesis of human colon cancer stem cells. *BMC Cancer* 2017; **17**: 716 [PMID: 29110645 DOI: 10.1186/s12885-017-3731-5]

107 **Wang K**, Song W, Shen Y, Wang H, Fan Z. LncRNA KLK8 modulates stem cell characteristics in colon cancer. *Pathol Res Pract* 2021; **224**: 153437 [PMID: 34271345 DOI: 10.1016/j.prp.2021.153437]

108 **Wu K**, Xu T, Song X, Shen J, Zheng S, Zhang L, Tao G, Jiang B. LncRNA SLCO4A1-AS1 modulates colon cancer stem cell properties by binding to miR-150-3p and positively regulating SLCO4A1. *Lab Invest* 2021; **101**: 908-920 [PMID: 33958701 DOI: 10.1038/s41374-021-00577-7]

109 **Li QG**, Xu XQ, Zhou DY, Jia ZB, Yu BF, Xu FG, Zhang L. Long non-coding RNA DILC as a potentially useful biomarker for the diagnosis and prognosis of colorectal cancer. *Eur Rev Med Pharmacol Sci* 2019; **23**: 3320-3325 [PMID: 31081085 DOI: 10.26355/eurrev_201904_17694]

110 **Liu W**, Yu Q, Ma J, Cheng Y, Zhang H, Luo W, Yao J. Knockdown of a DIS3L2 promoter upstream long noncoding RNA (AC105461.1) enhances colorectal cancer stem cell properties *in vitro* by down-regulating DIS3L2. *Onco Targets Ther* 2017; **10**: 2367-2376 [PMID: 28496335 DOI: 10.2147/OTT.S132708]

111 **Schmidt CA**, Giusto JD, Bao A, Hopper AK, Matera AG. Molecular determinants of metazoan tricRNA biogenesis. *Nucleic Acids Res* 2019; **47**: 6452-6465 [PMID: 31032518 DOI: 10.1093/nar/gkz311]

112 **Pamudurti NR**, Bartok O, Jens M, Ashwal-Fluss R, Stottmeister C, Ruhe L, Hanan M, Wyler E, Perez-Hernandez D, Ramberger E, Shenzis S, Samson M, Dittmar G, Landthaler M, Chekulaeva M, Rajewsky N, Kadener S. Translation of CircRNAs. *Mol Cell* 2017; **66**: 9-21.e7 [PMID: 28344080 DOI: 10.1016/j.molcel.2017.02.021]

113 **Guarnerio J**, Bezzi M, Jeong JC, Paffenholz SV, Berry K, Naldini MM, Lo-Coco F, Tay Y, Beck AH, Pandolfi PP. Oncogenic Role of Fusion-circRNAs Derived from Cancer-Associated Chromosomal Translocations. *Cell* 2016; **165**: 289-302 [PMID: 27040497 DOI: 10.1016/j.cell.2016.03.020]

114 **Rengganaten V**, Huang CJ, Tsai PH, Wang ML, Yang YP, Lan YT, Fang WL, Soo S, Ong HT, Cheong SK, Choo KB, Chiou SH. Mapping a Circular RNA-microRNA-mRNA-Signaling Regulatory Axis That Modulates Stemness Properties of Cancer Stem Cell Populations in Colorectal Cancer Spheroid Cells. *Int J Mol Sci* 2020; **21** [PMID: 33114016 DOI: 10.3390/ijms21217864]

115 **Jian X**, He H, Zhu J, Zhang Q, Zheng Z, Liang X, Chen L, Yang M, Peng K, Zhang Z, Liu T, Ye Y, Jiao H, Wang S, Zhou W, Ding Y, Li T. Hsa_circ_001680 affects the proliferation and migration of CRC and mediates its chemoresistance by regulating BMI1 through miR-340. *Mol Cancer* 2020; **19**: 20 [PMID: 32005118 DOI: 10.1186/s12943-020-1134-8]

116 **Zhan W**, Liao X, Wang Y, Li L, Li J, Chen Z, Tian T, He J. circCTIC1 promotes the self-renewal of colon TICs through BPTF-dependent c-Myc expression. *Carcinogenesis* 2019; **40**: 560-568 [PMID: 30403769 DOI: 10.1093/carcin/bgy144]

World Journal of Gastrointestinal Oncology

Submit a Manuscript: https://www.f6publishing.com

World J Gastrointest Oncol 2022 April 15; 14(4): 765-793

DOI: 10.4251/wjgo.v14.i4.765

ISSN 1948-5204 (online)

REVIEW

Role of three-dimensional printing and artificial intelligence in the management of hepatocellular carcinoma: Challenges and opportunities

Chrysanthos D Christou, Georgios Tsoulfas

Specialty type: Oncology

Provenance and peer review: Invited article; Externally peer reviewed.

Peer-review model: Single blind

Peer-review report's scientific quality classification

Grade A (Excellent): 0
Grade B (Very good): B
Grade C (Good): 0
Grade D (Fair): 0
Grade E (Poor): 0

P-Reviewer: Casaca W, Brazil

Received: April 15, 2021
Peer-review started: April 15, 2021
First decision: June 4, 2021
Revised: August 24, 2021
Accepted: March 25, 2022
Article in press: March 25, 2022
Published online: April 15, 2022

Chrysanthos D Christou, Georgios Tsoulfas, Department of Transplantation Surgery, Hippokration General Hospital, School of Medicine, Aristotle University of Thessaloniki, Thessaloniki 54622, Greece

Corresponding author: Georgios Tsoulfas, MD, PhD, Associate Professor, Surgeon, Department of Transplantation Surgery, Hippokration General Hospital, School of Medicine, Aristotle University of Thessaloniki, 49 Konstantinoupoleos Street, Thessaloniki 54622, Greece. tsoulfasg@gmail.com

Abstract

Hepatocellular carcinoma (HCC) constitutes the fifth most frequent malignancy worldwide and the third most frequent cause of cancer-related deaths. Currently, treatment selection is based on the stage of the disease. Emerging fields such as three-dimensional (3D) printing, 3D bioprinting, artificial intelligence (AI), and machine learning (ML) could lead to evidence-based, individualized management of HCC. In this review, we comprehensively report the current applications of 3D printing, 3D bioprinting, and AI/ML-based models in HCC management; we outline the significant challenges to the broad use of these novel technologies in the clinical setting with the goal of identifying means to overcome them, and finally, we discuss the opportunities that arise from these applications. Notably, regarding 3D printing and bioprinting-related challenges, we elaborate on cost and cost-effectiveness, cell sourcing, cell viability, safety, accessibility, regulation, and legal and ethical concerns. Similarly, regarding AI/ML-related challenges, we elaborate on intellectual property, liability, intrinsic biases, data protection, cybersecurity, ethical challenges, and transparency. Our findings show that AI and 3D printing applications in HCC management and healthcare, in general, are steadily expanding; thus, these technologies will be integrated into the clinical setting sooner or later. Therefore, we believe that physicians need to become familiar with these technologies and prepare to engage with them constructively.

Key Words: Artificial intelligence; Machine learning; Three-dimensional printing; Bioprinting; Hepatocellular carcinoma; Liver cancer

Core Tip: The opportunities that arise from the application of three-dimensional (3D) printing and 3D bioprinting in the management of hepatocellular carcinoma (HCC) include resident education, patient education, preoperative planning, fabrication of custom-made medical tools, liver models for antitumor drug development, and patient-derived HCC models for targeted treatment selection. Similarly, the opportunities that arise from the application of artificial intelligence/machine learning in the management of HCC include targeted screening for patients with chronic hepatitis B and C infections, non-invasive early detection of HCC, increased diagnostic accuracy, frameworks for evidence-based, individualized treatment allocation, and prognostic models for the prediction of patient outcomes including overall survival, disease-free survival, and recurrence that could be used for patient and family counseling.

Citation: Christou CD, Tsoulfas G. Role of three-dimensional printing and artificial intelligence in the management of hepatocellular carcinoma: Challenges and opportunities. *World J Gastrointest Oncol* 2022; 14(4): 765-793
URL: https://www.wjgnet.com/1948-5204/full/v14/i4/765.htm
DOI: https://dx.doi.org/10.4251/wjgo.v14.i4.765

INTRODUCTION

Hepatocellular carcinoma (HCC) constitutes the fifth most frequent malignancy worldwide and the third most frequent cause of cancer-related deaths[1]. The factors that predispose to HCC development include chronic infection with hepatitis B virus (HBV) and hepatitis C virus (HCV), alcohol, metabolic liver disease, and exposure to different toxins[2]. Currently, the diagnosis of HCC is mainly based on multiphasic computed tomography (CT) and magnetic resonance imaging (MRI), whose findings are standardized based on the Liver Reporting and Data System (LI-RADS) developed by the American College of Radiology[3,4]. The cornerstone of treatment selection for HCC patients is the stage of the disease. The most prominent staging system acknowledged in United States and EU guidelines is the Barcelona Clinic Liver Cancer (BCLC) classification system[3,5]. Liver transplantation, hepatic resection, and ablative techniques are recommended for the very early and early stages of the disease, while transarterial chemoembolization (TACE) and oral sorafenib are recommended for the intermediate and advanced stages of the disease, respectively[5,6]. While the BCLC classification is generally accepted, teams report the need for an individualized approach in HCC management[7,8]. Emerging fields such as three-dimensional (3D) printing, artificial intelligence (AI), machine learning (ML), and novel biomarkers that allow the classification of HCC at a molecular level could facilitate our efforts to reach individualized treatment in HCC management.

3D printing is defined as the "translation" of a computer-generated image into a 3D solid object. It involves the use of materials, which are printed into consecutive thin layers[9]. Despite originally emerging from non-medical disciplines to serve the demand of rapid engineering of design prototypes, 3D printing has, since then, found extensive applications in medicine, including education and training, simulation, anatomical comprehension, surgical planning, surgical tools, and patient counseling[9,10]. From the combination of 3D printing and tissue engineering the field of bioprinting has emerged[11]. Bioprinting uses 3D printing-based methods to utilize biomaterials, growth factors, and cells for fabricating biomedical parts with a complex and precise internal and external structure that ultimately imitates natural tissue characteristics[12,13]. Notably, the concept of bioprinting functional organs and tissues could ameliorate the consequences of the current imbalance between the supply and demand of organs for transplantation.

AI is an umbrella term that describes any application where tasks typically associated with human intelligence are conducted by computer systems instead[14,15]. AI is a cluster of interrelated fields with a core aspect in common; they are all driven by computing power and Big Data advancements. In healthcare, the field of AI and ML, has profound applications. ML models could be described as models educated from past data to predict future data[16]. In the past decade, the healthcare industry has been established as a data-rich science, with a profound increase in the amount of generated data each year, with data becoming an omnipresent concept[17]. These extensive repositories of data could not be managed by traditional software. AI promises to analyze them and turn them into meaningful insights. The management of HCC is a fruitful field for AI application since it generates enormous amounts of data, including clinical data, histopathologic images, gene sequencing, long-non coding RNA and microRNA expression profiling, ultrasound (US) imaging, CT imaging, and MRI.

In this study, we aim to comprehensively review the applications of 3D printing and AI in HCC management, present the opportunities that arise from these applications, and finally identify the current challenges of integrating these technologies into the healthcare system to identify means to overcome them.

SEARCH STRATEGY

We conducted a literature review of the Scopus, Cochrane, and Medline databases using the following algorithms or queries: (1) [(3D printing OR 3D printing OR three-dimensional printing OR rapid prototyping OR additive manufacturing) AND (hepatocellular carcinoma OR liver cancer OR hepatic cancer OR HCC)]; and (2) [(machine learning OR artificial intelligence OR support vector machine OR neural networks OR deep learning OR computer-aided OR computer-assisted) AND (hepatocellular carcinoma OR liver cancer OR hepatic cancer OR HCC)]. The two authors (Christou CD, Tsoulfas G) reviewed the articles for eligibility independently, and any disagreements were resolved through discussion between them. Finally, the authors similarly reviewed the reference lists of eligible articles to identify further eligible articles, books, and other forms of publication. Publications written in any other language other than English were excluded. Publications of abstracts were also excluded. In addition, animal studies and studies conducted with animal cells were also excluded. The literature review was completed on March 30, 2021.

APPLICATIONS OF 3D PRINTING AND BIOPRINTING IN HCC MANAGEMENT

3D printing

In liver surgery, 3D printing could be used for educational purposes and preoperative planning. Regarding education, 3D printed models enhance physicians' knowledge base at all levels of expertise. New residents can become familiar with the complex liver anatomy, build confidence, and thus be more efficient surgical team members[18-20]. Specifically, in a study where forty-five residents were trained by: (1) Images from multi-detector CT; (2) A virtual 3D reconstruction model; and (3) A 3D printed model, residents in the latter group assessed and assigned tumor location faster and more precisely[21]. 3D printed models have been employed for educational purposes in choledochal and hepatobiliary laparoscopic operations[22,23]. Also, 3D printed models could be used in patient education to help the patients reach a higher understanding of their disease and the proposed procedure, thus enhancing communication and trust, increasing cooperation, and facilitating obtaining informed consent[20]. In liver transplantation, 3D printed models could be used from living donors to facilitate the donors' understanding of the procedure and its risks. Focusing on educational use for HCC, Streba *et al*[24] developed ten personalized 3D liver models of patients with HCC, which were given to a group of medical students and residents to interact with. The vast majority of the participants agreed that the models were easy to interact with and valuable in gaining further knowledge about specific aspects of tumor morphology[24]. However, a significant number of the participants did not find the models' weight as expected, and the majority agreed that the models' texture was different to their expectation [24].

Regarding preoperative planning, in 2013, Zein *et al*[25] in a study investigating the role of 3D printing in liver transplantation, produced six 3D printed liver models, three of living donors and three of their respective recipients. The study aimed to produce models of volumetric accuracy and anatomical precision that could unveil any unsuitable anatomy between the donors and the recipients, particularly regarding the vascular and biliary tract of the liver[25]. The authors reported a mean dimensional error for the entire model of less than 4 mm and less than 1.3 cm for the vascular diameters [25]. Similarly, other studies have used 3D printed liver models as part of the preoperative planning of major or complex hepatic resections[26-30].

Focusing on HCC preoperative planning, Xiang *et al*[31] reported the case of a patient with HCC and rare variations of the abdominal blood vessels, particularly the portal vein, for whom 3D printed models were constructed to aid the preoperative planning. Notably, the model helped the physicians decide between two different surgical plans, performing, consequently, a hepatectomy with the highest residual volume[31]. In a different study, Perica *et al*[32] developed a four-stage production process (CT data acquisition, image segmentation, image data editing, and 3D printing) to construct a scaled-down 3D printed liver model of a patient with HCC. In a questionnaire given to radiologists, the 3D models were perceived as having a minimal value in diagnostic radiology, while for surgeons, the 3D models were found to be valuable in preoperative surgical planning[32]. Kuroda *et al*[33] reported two patients with HCC for whom 3D printed models were used to delineate intrahepatic vessels to facilitate preoperative planning. In the first case, the 3D printed model was used to identify the regional Glissonian pedicle, while in the second, to reveal the diverging pattern of the dorsal and ventral branches of the intrahepatic vessels of the anterior section[33]. Regarding laparoscopic liver resections, Witowski *et al*[34] proposed in a recent study a 3D printing-based decision-making system for preoperative planning of laparoscopic hepatic resection performed with intraoperative US guidance. The protocol was implemented in nineteen patients, including four patients with HCC[34]. Information from the 3D printed models changed the initially planned surgical approach in 26% of cases[34].

Besides educational purposes and preoperative planning, 3D printed models have applications in the diagnosis and treatment of HCC. Regarding diagnosis, Damiati *et al*[35] developed a hybrid 3D printed electrochemical biosensor that could detect liver cancer using immunochemistry. 3D printed capillary

Table 1 Artificial intelligence applications in the prevention of hepatocellular carcinoma

	First author	Parameters employed	AI classifier	Sizes of the training/validation sets	Outcomes	Performance	Ref.
1	Wang J	Genetic and epigenetic biomarkers	Several	137 HCC and 431 non-HCC patients	HCC screening	0.910-0.950[1,2], 0.897-0.938[1,3], 75.0-91.5[2,4], 66.4-90.6[3,4], 1.0-88.8[2,5], 0.5-87.9[3,5]	[47]
2	Nam JY	Laboratory results, clinicopathological parameters	DNN	424/316[3] patients	HCC development in HBV cirrhosis	0.719[1,2], 0.782[1,3]	[48]
3	Xia Q	Long non-coding RNAs	Several	38 healthy samples, 45 chronic HBV patients, 46 liver cirrhosis, and 46 HCC patients	HCC development in HBV cirrhosis	71.1-89.5[3,6]	[49]
4	Chen S	HBV reverse transcriptase gene sequencing	RF, SVM, KNN	307 chronic HBV patients (202/105), 237 HCC patients (159/78)	HCC development in HBV cirrhosis	RF: 0.902-0.903[1,2], 0.903-0.943[1,3], SVM: 0.879-0.924[1,2], 0.727-0.858[1,3], KNN: 0.680-0.737[1,2], 0.734-0.747[1,3]	[50]
5	Hashem S	Laboratory results, clinicopathological parameters	Several	3099 chronic HCV patients1324 HCC patients	HCC development in HCV cirrhosis	93.2-95.6[3,6], 0.955-0.990[1,3], 86.3-91.8[3,4], 93.9-97.3[3,5]	[51]
6	Audureau E	Laboratory results, clinicopathological parameters	Several	836/668[7]	HCC development in HCV cirrhosis	0.633-0.807[1,2], 0.623-0.715[1,7]	[52]
7	Ioannou GN	Clinical/laboratory data extracted directly from electronic health records	DNN	48151 patients with HCV-related cirrhosis (training:test = 9:1)	HCC development in HCV cirrhosis	0.759-0.806[1,3]	[53]
8	Singal AG	Laboratory results, clinicopathological parameters	RF	442/1050[7]	HCC development in cirrhosis	0.71[1,2], 0.64[1,7]	[54]

[1]Area under the receiver operating curve or c-index.
[2]Training.
[3]Internal validation.
[4]Sensitivity (%).
[5]Specificity (%).
[6]Accuracy (%).
[7]External validation/testing.
CCA: Cholangiocarcinoma; CNN: Convolutional neural network; CT: Computed tomography; DNN: Deep neural network; HBV: Hepatitis B virus; HCC: Hepatocellular carcinoma; HCV: Hepatitis C virus; KNN: K-nearest neighbor; RF: Random forest; SVM: Support vector machine; WSI: Whole-slide image.

channels were used to efficiently guide and constrain the sample containing cells of a human HCC cell line (HepG2)[35]. This study demonstrates how the combination of traditionally fabricated parts and 3D printed parts could enable the use of optimal materials for the model's various components. In a different study, Joo *et al*[36] used enhanced MRI scans of twenty patients with multiple focal liver lesions, including patients with HCC. Twenty transparent 3D printed liver models were constructed with color-coded anatomical structures that included 98 focal liver lesions[36]. The authors evaluated these models' role in increasing the detection rate of focal liver lesions by pathologists and radiologists [36]. Notably, during the gross pathologic examination, the per focal lesion detection rate significantly improved when utilizing the 3D model[36]. A sub-analysis revealed that these models' positive impact was more remarkable for smaller focal liver lesions[36]. Following hepatic resection, Trout *et al*[37] have proposed a 3D printing-based protocol for anatomically oriented, uniform sectioning of resected hepatic specimens to facilitate accurate tumor mapping and a precise radiological-pathological correlation. The protocol was applied in thirteen patients (including HCC patients), achieving a close correlation between imaging and gross pathology[37]. Regarding non-operative treatment, Han *et al*[38] investigated the therapeutic value of 3D printing template-assisted radioactive ^{125}I seed implantation for the treatment of malignant liver tumors. In their study, fifteen patients (six with HCC) received the 3D-assisted treatment, and twenty-five (ten with HCC) did not[38]. Notably, the 3D printed template-assisted treatment significantly shortened the operation time and optimized the radiation-dose distribution[38]. TACE is the prominent treatment choice for intermediate HCC. 3D visualization and 3D printed models could be used to clearly display the tumor's blood supply and facilitate the super-selective embolization of all the feeding arteries[39,40].

Bioprinting

3D bioprinted scaffolds have several advantages compared with other tissue engineering methods, such

as greater accuracy, fast reconstruction, and good integration[41]. Unlike traditional scaffold fabrication methods, 3D bioprinting skips the cell-seeding process since, during the fabrication process, the cells are dispersed at the desired locations[42]. Xie *et al*[43] expanding their department's work on mice, recently published a study where they constructed patient-specific 3D bioprinted HCC models. Primary HCC cells were isolated from six operated patients' liver specimens and were mixed with gelatin and sodium alginate to form the bio-ink[43]. The models were printed in a layer-by-layer manner and demonstrated cell viability at days 7 and 28 after the printing of 95% and 80%, respectively[43]. In addition, the resulting models retained compared to their patient-derived HCC: (1) The expression pattern of the biomarker a-fetoprotein; (2) A high level of concordance of the single nucleotide variants; and (3) The mutational pattern of key HCC gene mutations[43]. Finally, the models were used to assess the efficacy of four commonly used targeted drugs for HCC to reveal correlations between drug sensitivity and key HCC mutations[43]. Therefore, 3D bioprinted liver models could be used to develop patient-specific drugs for HCC patients. 3D bioprinted organoids could revolutionize the current drug development process by substituting early phases of clinical trials.

Other studies have used human HCC cell lines to construct 3D bioprinted liver models. Zhang *et al*[44] combined alginate with cellulose nanofibril hydrogels and colloidal lignin particles to fabricate precise nano-composite scaffolds. Consequently, HepG2 cells were used to conduct cell viability tests that demonstrated the proliferation of the cells at the scaffold's surface and within the scaffolding structure and a steady increase in density of HepG2 cells from day one up to day five in all the scaffolds. In a recent study, Sun *et al*[45] using HepG2 cells, formed a bio-ink to develop 3D bioprinted models to evaluate the effect of antitumor drugs. During the *in vitro* culture, the models preserved cell viability above 90%[45]. Compared to 2D-HepG2 cultures, the 3D bioprinted models retained higher expression levels of HCC-related biomarkers and mRNAs over the culture time[45]. Finally, the 2D and 3D models were compared based on their response to antitumor drugs[45]. The 3D models demonstrated higher drug resistance due to their higher expression of drug-resistance-related genes[45]. In another study, Ma *et al*[46] constructed a 3D bioprinted liver decellularized extracellular matrix model that was consequently used to compare the *in vitro* cultures of the HepG2 cell line in 3D-based scaffolds with conventional tissue-engineered liver constructs. The 3D bioprinted model demonstrated improved cell viability and gene expression. In addition, the authors investigated how the stiffness of the scaffolds impacted the growth of the cultures[46]. Their results support that stiff scaffolds, which better represent a cirrhotic liver, demonstrate a slower growth rate of HepG2 cells and lower cell viability[46]. In a different study, a different human HCC cell line (SMMC-7721) was used to develop 3D bioprinted models with and without microfluidic chips to pharmacodynamically test the effect of a chimeric IgG1 anti-CD147 monoclonal antibody[44]. During cell culture, the models maintained a cell survival rate of 96.21%[44]. The 3D models with microfluidic chips were found to be less vulnerable to the increase in drug dosage[44]. The authors concluded that these results are more consistent with animal studies due to the model's microenvironment and biomimetic drug transport efficiency[44].

APPLICATIONS OF AI IN HCC MANAGEMENT

AI/ML-based tools have been developed to prevent, diagnose, and treat HCC and for HCC prognosis. Tables 1-4 summarize the studies we identified that developed AI/ML-based models for the management of HCC.

Prevention

Regarding HCC screening, genetic and epigenetic biomarkers have been utilized to develop several AI/ML-based models aiming for a urine test to screen for HCC[47]. AI/ML tools based on data automatically mined from patients' hospital records could be used to stratify the risk of HCC development and for HCC early detection in patients with chronic HBV and HCV infection. These models could be used to reliably identify patients who are more susceptible to developing HCC and who would greatly benefit from a sustained virological response (SVR). Specifically for HBV cirrhosis, a recent study developed a deep neural network (DNN) employing only non-invasive parameters to predict the development of HCC[48]. Other studies have employed data from gene sequencing and expression patterns. Specifically, in a study, data from circulating long non-coding RNAs were employed to develop an AI/ML model that isolated distinctive signatures of expression of 171 different long non-coding RNAs that distinguish the healthy control group from patients with chronic HBV, liver cirrhosis, and HCC[49]. Another study developed four different models that used data from reverse transcriptase gene sequencing to predict the patients with HBV who would develop HCC[50]. A random forest (RF)-based model outperformed the rest with an area under the receiver operating curve (AUROC) in the independent validation of 0.96[50].

Regarding the development of HCC in HCV cirrhosis, several AI/ML-based tools were developed in a new study using routinely collected data to predict HCC development in patients with HCV infection [51]. In the same spirit, in a recent study, several AI/ML-based models were developed that employ laboratory results and clinicopathological parameters that predict HCC development in patients with

HCV before and after achieving SVR[52]. A recent study investigated whether a DNN could surpass the performance of conventional logistic regression (LR) models in predicting HCC development in patients with chronic HCV infection[53]. Notably, the DNN had outperformed the LR model with longitudinal inputs[53]. Finally, a study utilizing laboratory results and clinicopathological parameters developed a RF model to predict HCC development in a cohort of patients with Child-Pugh A and B cirrhosis, which was externally validated in a cohort of patients with HCV cirrhosis[54].

Diagnostics

Following prevention, several studies have focused on developing AI/ML-based models for the early detection of HCC. In a study, clinicopathological and laboratory data were employed to develop several AI/ML-based models for the early detection of HCC[55]. Notably, a gradient boosting-based model achieved the highest predictive value[55]. In another study, data from the expression profiles of microRNAs of patients with HCC were analyzed, and the five microRNAs with the optimal predictive value were used to develop several AI/ML models for the non-invasive, early diagnosis of HCC[56]. In a different study focusing on early detection, data from gene expression profiles were used to develop a support vector machine (SVM) model that outstandingly identifies patients with HCC[57]. In a recent study, data from somatic copy number abbreviations acquired from circulating tumor DNA was employed to develop an RF-based model for the early detection of HCC in a cohort of patients with chronic HBV infection[58]. Finally, several AI/ML-based models were developed in a different study using data from biomarkers (long non-coding RNA and microRNA expression) to identify patients with HCC[59].

Several studies have developed AI/ML-based models to distinguish between the various focal liver lesions (having a non-binary output). US imaging has been used to develop a convolutional neural network (CNN) that initially distinguishes focal lesions between benign and malignant and then classifies them into five different types of focal liver lesions (angioma, HCC, metastasis, cyst, focal nodular hyperplasia)[60]. In a recent, multi-center study, US imaging along with clinical parameters were used to develop a CNN model that classifies 16 different focal liver lesions[61]. Interestingly, the model's accuracy was comparable with that of contrast-enhanced CT but inferior to MRI[61]. B-mode has been used in a study to develop a neural network ensemble-based computer-aided diagnosis (CAD) model that classifies normal liver and four different focal liver lesions, including HCC[62]. Similarly, a different artificial neural network (ANN)-based CAD model was developed using contrast-enhanced US microflow imaging that differentiates HCC from metastasis and hemangioma, and classifies the HCC lesions into well, moderately, and poorly differentiated[63].

In a recent study, a CNN was developed, employing images from multi-phasing CT scans, to classify focal liver lesions as benign or malignant automatically and then distinguish between HCC, intrahepatic cholangiocarcinoma (CCA), metastasis, cyst, hemangioma, and focal nodular hyperplasia[64]. A different CNN was developed using dynamic contrast-enhanced CT scans to classify focal liver lesions into five different lesion types[65]. In another study, different multiphasic CT scan models (four-phase, three-phase without portal-venous phase, and three-phase without pre-contrast phase) were used to develop multiphase convolutional dense networks to distinguish between HCCs and other focal liver lesions[66]. Similarly, multiphasic CT imaging was used to develop a CNN to classify five different focal liver lesions[67]. An ANN was developed in a different study employing 33 features (24 radiological and nine clinical) to differentiate among several lesions (hemangioma, metastasis, intrahepatic peripheral CCA, and HCC)[68]. Regarding the radiologists' performance, when the ANN's output was taken into account, their performance improved significantly (AUROC = 0.888-0.934)[68]. In a different study, data from CT and MRI radiomics were used to develop an RF model to differentiate between HCC, hepatic epithelioid angiomyolipoma, and focal nodular hyperplasia[69]. Multi-phasic MRI imaging was used in another study to develop a CNN that classifies six different focal liver lesions and distinguishes between the LI-RADS classes 1 and 5[70,71]. MRI was employed in a different study to develop an extremely randomized trees classifier-based model that differentiates five different focal liver lesion types[72]. Finally, in a recent study, MRI images were employed to develop a CNN that could distinguish seven different focal liver lesions (cyst, hemangioma, focal nodular hyperplasia, benign nodules, HCC, metastasis, and other than HCC primary malignancy)[73].

Histopathologic data could also be employed to develop AI/ML models for HCC diagnosis. A recent study developed a CNN employing hematoxylin and eosin-stained whole slide imaging (WSI) to distinguish patients with HCC and CCA[74]. The model was used prospectively to evaluate the impact of AI-assisted diagnosis on diagnostic accuracy[74]. Interestingly, the model did not benefit the mean diagnostic accuracy of all 11 pathologists in a statistically significant manner[74]. However, it managed to significantly increase diagnostic accuracy in a sub-cohort of 9 pathologists with well-defined expertise [74]. In a similar study, the CNN employing hematoxylin and eosin-stained WSI was used to distinguish between healthy liver from HCC, classify HCC based on the grade of differentiation, and predict the presence of HCC-related gene mutations[75]. Another study used multiphoton microscopy images to develop a CNN that classifies images as well, moderately and poorly differentiated HCC[76]. A different study developed two CNNs, a model to detect HCC lesions in hematoxylin and eosin-stained WSI, and another model to predict recurrence following surgical resection[77]. In a different study, supervised and unsupervised ML methods were combined to develop a convolutional autoencoder

Table 2 Artificial intelligence application in hepatocellular carcinoma diagnosis

	First author	Diagnostic modality	AI classifier	Sizes of the training/validation sets	Outcomes	Performance	Ref.
1	Sato M	Laboratory results, clinicopathological parameters	Several	1582 patients	HCC early detection	81.65-87.36[1,2], 0.870-0.940[3,2]	[55]
2	Zhao X	MicroRNA expression profiles	Several	392 patients	HCC early detection	RF: 0.982[3], SVM: 0.970[3], DT: 0.831[3]	[56]
3	Zhang ZM	Gene expression profiles	SVM	1333/336 HCC samples	HCC early detection	100[1,2], 100[2,4], 100[2,5], 0.9597[3,6], 91.93[4,6], 100[5,6]	[57]
4	Tao K	Circulating tumor DNA	RF-based	209/76[6]/99[6]	HCC early detection	0.874-0.933[1,2], 0.812-0.920[3,6]	[58]
5	Li G	MicroRNA and long non-coding RNA expression profiles	SVM, RF, DT	361 patients	HCC early detection	RF: 0.992[1,2], 95.6[2,4], 100[2,5]; SVM: 0.992[2,3], 97.2[2,4], 98.0[2,5]; DT: 0.927[2,3], 98.3[2,4], 92.0[2,5]	[59]
6	Schmauch B	US imaging	CNN	109 images with focal liver lesions	Classification of benign from malignant focal liver lesions; classification among five focal liver lesions	0.916-0.942[2,3]; 0.886-0.954[2,3]	[60]
7	Yang Q	US imaging, clinical parameters	CNN	16500/4125[2]/3718[6] US images	Classification among 16 different focal liver lesions	0.859-0.966[3,7], 0.765-0.925[2,3], 0.750-0.924[3,6]	[61]
8	Virmani J	B-mode US imaging	NNE	108 images	Classification among normal liver and four focal liver lesions	95.0[1,2]	[62]
9	Shiraishi J	Microflow imaging of contrast-enhanced US	ANN	103 focal liver lesions	Classification among HCC, metastasis, and hemangioma; histopathological grade	86.9-93.8[1,2]; 50.0-79.2[1,2]	[63]
10	Zhou J	Multiphasic CT scans	CNN	616 liver lesions	Classification of benign and malignant lesions. Classification of 6 types of focal liver lesions	76.6-88.4[2,4,5], 82.5[1,2], 0.921[2,3], 46.4-93.1[2,4], 91.9-98.6[2,5], 73.4[1,2], 0.766-0.983[2,3]	[64]
11	Yasaka K	Contrast-enhancedCT imaging	CNN	460/100[6] patients	Classification among five types of focal liver lesions	95[1,7], 84[1,6], 33-100[4,6]	[65]
12	Shi W	Multiphasic CT scans	MP-CDN	449 focal lesions. Training:validation ratio = 8:2	Classification between HCC and non-HCC focal lesions	0.811-0.856[1,2], 0.862-0.925[2,3], 0.744-0.923[2,4], 0.725-0.941[2,5]	[66]
13	Todoroki Y	Multiphasic CT imaging	CNN	89 patients	Classification among five focal liver lesions	79-100[2,4]	[67]
14	Matake K	Clinicopathological parameters, CT imaging	ANN	120 patients	Classification among four types of focal liver lesions	0.961[2,3]	[68]
15	Liang W	CT and MRI radiomics	RF	170 CT scans; 137 MRI scans	Classification of three types of focal liver lesions	CT model: 0.996[3,7], 0.879[2,3]. MRI model: 0.999[3,7], 0.925[2,3]	[69]
16	Hamm CA	Multiphasic MRI imaging	CNN	434/60 lesions	Classification among six types of focal liver lesions; identify HCC; classification of LI-RADS	92[2,4], 98[2,5]; 0.992[2,3]; 94[4,6], 97[2,5]	[70,71]
17	Jansen MJA	MRI imaging	Extremely randomized trees classifier	95 patients	Classification among five different focal liver lesions	85-92[1,2], 62-93[2,4], 56-93[2,5]	[72]
18	Zhen SH	MRI scans	CNN	1210/201[6]	Classification among seven different focal liver lesions	0.841-0.987[3,6], 40.5-100[4,6], 86.4-99.5[5,6]	[73]
19	Kiani A	Hematoxylin and eosin-stained WSI	CNN	20[7]/26[2]/80[6] WSIs	Classification of HCC and CCA	88.5[1,2], 84.2[1,6]	[74]

20	Chen M	Hematoxylin and eosin-stained WSI	CNN	491 WSIs (402 HCC, 89 normal liver tissue)	Classification of HCC and normal liver tissue; histopathological grade	0.960[1,2], 0.961[2,3]; 89.6[1,2]	[75]
21	Lin H	Multiphoton microscopy	CNN	217 images	Histopathological grade	0.812-0.941[1,2], 0.891-0.917[2,3]	[76]
22	Yamashita R	Hematoxylin and eosin-stained WSI	CNN	28/4[2]/30[6] WSIs	HCC lesion detection	0.952[2,3], 0.956[3,6]	[77]
23	Roy M	Hematoxylin and eosin-stained WSI	CAE	50 WSIs	Segmentation of viable tumors	91-95[1,2]	[78]
24	Giordano S	PESI-MS	SVM, RF	117 HCCs, 50 CCA, 151 non-tumor group	Classification of HCC, CCA, and non-tumor groups	SVM: 95.1-98.5[1,6]; RF: 94-94.9[1,6]	[79]
25	Guo LH	Contrast-enhanced ultrasound imaging	MKL	93 lesions	Classification of benign from malignant focal liver lesions	90.41[1,2], 93.56[2,4], 86.89[2,5]	[80]
26	Bharti P	US imaging	Several	189 images	Classify among normal liver, chronic liver disease, cirrhosis, and HCC	96.6[1,2], 95.5-96.9[2,4], 98.0-99.8[2,5]	[81]
27	Brehar R	US imaging	CNN	268 patients	Classification between HCC and cirrhotic parenchyma	84.84-91[1,2], 0.91-0.95[2,3], 86.79-94.37[2,4], 82.95%-88.38%[2,5]	[82]
28	Mao B	Ultrasound radiomics	Several	114 patients	Classify primary from metastatic liver cancer	0.729-0.808[1,2], 0.737-0.793[2,3], 0.775-0.868[2,4], 0.667-0.880[2,5]	[83]
29	Almotairi S	CT imaging	CNN	20 CT scans	Tumor segmentation	98.8[1,7]	[84]
30	Budak Ü	CT imaging	CNN	20 CT scans	Tumor segmentation	Volumetric overlap error: 9.05%[2]	[85]
31	Nayak A	Multiphasic CT imaging	SVM	40 patients	Classification between HCC and cirrhotic parenchyma	80-86.9[1,2], 0.93[2,3]	[86]
32	Krishan A	CT scans	Several	1638 CT scans	Identification of liver lesions; classification between HCC and metastasis	98.39-100[1,2], 0.99-1.00[2,3]; 76.38-87.01[1,2], 0.77-0.99[2,3]	[87]
33	Chen WF	CT scans	SED	300 CT scans	Tumor segmentation	0.992[1], 0.95[2,3]	[88]
34	Khan AA	CT scans	Several	179 patients	Classification between HCC and hemangioma	96.6-98.3[1,6], 0.94-0.97[3,6], 94.23-97.03[5,6]	[88]
35	Mokrane FZ	Multiphasic CT radiomics	Several	106/36[2]/36[6]	Classification between HCC and non-HCC lesions	0.81[3,7], 0.81[4,7], 0.72[5,7], 0.72[2,3], 0.66[3,6]	[90]
36	Mao B	CT radiomics, clinical parameters	Gradient boosting	237/60[6] patients	Histopathological grade	61.18-97.05[1,6], 0.7071-0.9964[3,7], 60.67-95.51[4,7], 51.35-80.41[5,7], 48.33-70.00[1,6], 0.6128-0.8014[3,6], 43.48-65.22[4,6], 37.84-81.08[5,6]	[91]
37	Preis O	PET/CT imaging	ANN	98 patients	Classification between benign and malignant liver lesions	0.896-0.905[2,3]	[92]
38	Trivizakis E	Diffusion-weighted MRI	CNN, SVM	134 patients	Classification between primary liver cancer and metastasis	85.5[1,7], 83[1,2], 0.80[2,3], 93[2,4], 67[2,5]	[93]
39	Oestmann PM	Multiphasic MRI scans	CNN	150/10[2]	Classification of HCC and non-HCC lesions	94.1[1,7], 87.3[1,2], 0.912[2,3]. For HCC: 92.7[2,4], 82.0[2,5]. For non-HCC: 82.0[2,4], 92.7[2,5]	[94]
40	Bousabarah K	MRI scans	CNN, RF	174 patients/ 231 lesions	HCC detection	0.66-0.75[2,4], 0.55-0.73[4,6]	[95]
41	Kim J	MRI scans	CNN	455[2,7]/54[6]	HCC detection	0.97[2,3], 94[2,4], 99[2,5], 0.90[3,6], 87[4,6], 93[5,6]	[96]
42	Jian W	Non-enhanced MRI	CNN	75/40[6] HCCs	HCC detection	65.00-77.00[1,6], 0.70-0.82[3]	[97]

		scans				[,6], 64.55-78.18[4,6], 65.56-75.56[5,6]	
43	Wu Y	Multiphasic MRI imaging	CNN	89 HCCs	Classification between LI-RADS 3 and LI-RADS 4/5	0.767-0.900[1,6], 0.90-0.95[3] [,6], 0.76-1.00[4,6], 0.633-0.807[5,6]	[98]

[1]Accuracy (%).
[2]Internal validation.
[3]Area under the receiver operating curve or c-index.
[4]Sensitivity (%).
[5]Specificity (%).
[6]External validation/testing.
[7]Training.
ANN: Artificial neural network; CAE: Convolutional autoencoder; CCA: Cholangiocarcinoma; CNN: Convolutional neural network; CT: Computed tomography; DNN: Deep neural network; DT: Decision tree; HCC: Hepatocellular carcinoma; LI-RADS: Liver imaging reporting and data system; MKL: Multiple kernel learning; MP-CDN: Multiphase convolutional dense networks; MRI: Magnetic resonance imaging; NGS: Next-generation sequencing; NNE: Neural network ensemble; PESI-MS: Probe electrospray ionization mass spectrometry; PET: Positron emission tomography; RF: Random forest; SED: Successive Encoder-Decoder; SVM: Support vector machine; US: Ultrasound; WSI: Whole-slide image.

(CAE) that employs WSI images for the automated segmentation of viable tumors[78]. Finally, in a recent study, probe electrospray ionization mass spectrometry was used on specimens from patients with HCC and mass-forming CCA to develop two AI/ML-based models to distinguish these primary liver malignancies[79].

US imaging has also been used to develop models that aid in HCC diagnosis. A multiple-kernel learning-based model was developed using contrast-enhanced US imaging to distinguish between benign and malignant liver tumors[80]. Several AI/ML-based models were developed using US images to classify normal liver, chronic liver disease, cirrhosis, and HCC[81]. A recently developed CNN model managed to outperform other conventional ML methods in distinguishing between HCC and surrounding cirrhotic parenchyma in US images[82]. Data from US radiomics were employed in a recent study to develop multiple AI/ML-based models to distinguish between primary liver cancer and metastasis[83]. Interestingly a conventional LR model outperformed all the AI models[83].

CT imaging could be used to develop AI/ML-based models that aid HCC diagnosis. In a study, segmentation of the liver tumors was achieved using a CNN developed using CT scans[84]. Similarly, two encoder-decoder CNNs were developed in another study to cascade segments of both the liver and lesions in CT images[85]. An SVM-based CAD model was developed in another study from multiphasic CT scans to distinguish between cirrhosis and HCC[86]. CT scans were employed in a different study to develop several AI/ML-based models to distinguish between HCC and secondary liver lesions[87]. In a different study, a Successive Encoder-Decoder model was developed to automatically interpret liver tumor segmentation through CT images for patients with HCC[88]. Another study developed several AI/ML-based models employing CT images to distinguish between HCC and hemangioma[89]. Multiphasic CT radiomics were used in a different study to develop several AI/ML-based models to distinguish between HCC and non-HCC liver lesions[90]. CT radiomics and clinical data were combined in another study to develop gradient boosting-based models to classify the histopathological grade of HCC[91]. Finally, positron emission tomographic (PET)/CT imaging was employed in a different study to distinguish between benign and malignant liver lesions[92].

Regarding MRI imaging, diffusion-weighted MRI was used to develop a CNN-based model to distinguish between primary liver cancer and metastasis[93]. A recent retrospective study developed a CNN that employed multiphasic MRI scans of patients with HCC. The model was trained with a combination of images that met the LI-RADS criteria (typical) and with images that did not (atypical) and aimed to distinguish between HCC and non-HCC lesions[94]. In a recent study, MRI scans were employed to develop a CNN-based model for the automatic detection and delineation of HCC[95]. In a multicenter, retrospective study, a CNN was developed that employed MRI scans to identify HCC lesions[96]. Notably, the model surpassed less experienced radiologists' performance in the diagnosis of small HCC lesions[96]. In just 3.4 s, the model was able to assess 100 photos[96]. Non-enhanced MRI scans have been used to develop a CNN that identifies HCC lesions[97]. Finally, in a recent study, multiphasic MRI scans were used to develop a CNN that distinguishes between LI-RADS 3 and LI-RADS 4/5 HCC[98].

Treatment

Data generated from clinicopathological parameters, serum biomarkers, gene and RNA profiles, and imaging could be combined to train AI/ML-based models to develop frameworks for the evidence-based, individualized treatment of patients with HCC, including targeted radiotherapy, chemotherapy, and immunotherapy. In an international, multi-institutional study, a CART model was developed that aimed to create a framework for treatment allocation beyond the BCLC staging system[99]. Based on predicting parameters of overall survival, the model generated six distinct prognostic groups of patients

Table 3 Artificial intelligence application in hepatocellular carcinoma treatment

	First author	Parameters employed	AI classifier	Sizes of the training/validation sets	Outcomes	Performance	Ref.
1	Tsilimigras DI	Laboratory results, clinicopathological parameters, tumor characteristics	CART	976	Determining factors of prognostic weight preoperatively within the BCLC staging system	-	[99]
2	Liu F	Contrast-enhanced US radiomics, laboratory tests, and clinicopathological parameters	CNN	293/126 patients	2-yr progression-free survival of patients following RFA or surgical resection	0.754-0.784[1,2], 0.726-0.741[1,3]	[100]
3	Choi GH	Demographics, laboratory results, tumor characteristics, clinicopathological parameters	RF	813/208 patients	Treatment recommendation. Survival prediction	76.6-88.4[3,4], 53.0-82.3[3,5], 69.3-95.8[3,6]. 0.676-0.959[1,3]	[101]
4	Chen M	Hematoxylin and eosin-stained WSI	CNN	377 (training:validation = 3:1)/ 67[7] patients	Mutation prediction	89.6-94.0[3,4], 0.720-0.805[1,7]	[75]
5	Liao H	Hematoxylin and eosin-stained WSI	CNN	309/65[3]/78[7]	Mutation prediction	0.519-0.903[1,3], 0.605-0.797[1,7]	[103]
6	Gu J	Multiphasic CT scans	CNN	14 patients	Mutation prediction	67.7-77.3[3,4]	[104]
7	Chen G	Laboratory results	LIME	1007/1085[7] patients	MVI	0.918[1,2], 0.832[1,3], 0.905[1,7]	[105]
8	Zhang Y	MRI scans	CNN	158/79 patients	MVI	0.81[1,2], 69[2,5], 79[2,6], 0.72[1,3], 55[3,5], 81[3,6]	[106]
9	Wang G	DWI	CNN	60/40[2] HCCs	MVI	66.81-77.50[2,3,4], 68.65-79.69[1,2,3], 56.56-76.47[2,3,5], 64.35-79.13[2,3,6]	[107]
10	Liu QP	CT radiomics	RF, SVM	494 patients	MVI	0.84[1,2], 0.79[1,3]	[108]
11	Jiang YQ	CT radiomics, clinical/laboratory parameters	Gradient boosting, CNN	405 patients [220 MVI (+)/185 MVI (-)]	MVI	Gradient boosting: 0.900-0.952[1,2], 0.873-0.887[1,3]. CNN: 80.2-85.2[3,4], 0.900-0.980[1,2], 0.875-0.906[1,3], 0.659-0.932[3,5], 0.757-0.973[3,6]	[109]
12	Cucchetti A	Laboratory results, clinicopathological parameters, radiological data, histological data	ANN	175/75[3]	MVI. Histopathological grade	0.92[1,2], 91.0[3,4]. 0.94[1,2], 93.3[3,4]	[110]
13	Mai RY	Laboratory results, clinicopathological parameters, liver volumetry	ANN	265/88 patients	Posthemihepatectomy liver failure	0.880[1,2], 0.876[1,3]	[111]
14	Shi HY	Laboratory results, clinicopathological parameters, surgery parameters	ANN	22926 hepatectomies	In-hospital mortality following surgical resection	97.28[3,4], 0.84[1,3], 95.93[4,7], 0.82[1,7], 78.40[5,7], 94.57[6,7]	[112]
15	Liu D	US radiomics	CNN	89/41 patients	Classify full/partial response from stable disease/ progression in patients treated with TACE	78-98[2,4], 0.82-0.98[1,2], 78.6-98.2[2,5], 74.2-96.7[2,6], 0.80-0.90[3,4], 0.80-0.93[1,3], 82.1-89.3[3,5], 73.3-92.3[3,6]	[113]
16	Morshid A	Multiphasic CT scans, BCLC stage	CNN, RF	105 patients	Classify TACE-susceptible from TACE-refractory HCC	62.9-74.2[3,4], 0.733[1,3]	[114]
17	Peng J	CT imaging	CNN	562/89[7]/138[7]	Classification of complete response, partial response, stable disease, and progressive disease following TACE	84.0[3,4], 0.95-0.97[1,2], 82.8-85.1[4,7], 0.94-0.98[1,7]	[115]
18	Abajian A	MRI imaging, clinical data	RF	36 patients	Classification of responders and non-responders following TACE	66[3,4], 62.5[3,5], 67.9[3,6]	[116]

19	Zhu Y	FF-OCT	SVM	285 en face images	Cancerous hepatic cell identification	0.9378[1,7]	[117]
20	Liang Z	X-ray imaging	CNN	2943/1542[3]/1442[7] images	Localization of fiducial markers	98.6[4,7]	[118]
21	Liu Y	CT/MRI imaging	Dense-cycle GAN	21 patients	Identify differences between synthetic CT and CT, and compare their dose distribution	-	[119]
22	Taebi A	Computational fluid dynamics	CNN	3804 samples	Yttrium-90 distribution in radioembolization	Mean square error: 0.54 ± 0.14	[120]
23	Tong Z	DNA profiling	SVM	43 patients	Drug target prediction	0.8827-0.8849[1,3], 53-65.44[3,5], 88.76-93.63[3,6]	[121]

[1]Area under the receiver operating curve or c-index.
[2]Training.
[3]Internal validation.
[4]Accuracy (%).
[5]Sensitivity (%).
[6]Specificity (%).
[7]External validation/ testing.
ANN: Artificial neural network; BCLC: Barcelona clinic liver cancer; CART: Classification and regression tree; CNN: Convolutional neural network; CT: Computed tomography; DWI: Diffusion-weighted imaging; FF-OCT: Full-field optical coherence tomography; GAN: Generative adversarial network; HCC: Hepatocellular carcinoma; LIME: Local Interpretable Model-agnostic Explanations; MRI: Magnetic resonance imaging; MVI: Microvascular invasion; RF: Random forest; RFA: Radiofrequency ablation; TACE: Transarterial chemoembolization; US: Ultrasound; WSI: Whole-slide image.

that could be utilized as a framework for treatment allocation[99]. Interestingly, the radiologic tumor burden score that is not part of the BCLC staging system was identified as the optimal predictor of outcomes for staged B patients[99]. In a different study, data from contrast-enhanced US radiomics, laboratory tests, clinicopathological parameters, and course of treatment were employed to develop a CNN that could be used to select between radiofrequency ablation (RFA) and surgical resection[100]. Specifically, in their cohort of patients, the authors concluded that if 17.3% of the RFA group and 27.3% of the operated patients swapped treatment, they would benefit from a 12% and 15% increase in the probability of 2-year progression-free survival, respectively[100]. Finally, an AI/ML-based clinical decision support system for patients with HCC was developed using several RF-based classifiers in a large cohort of patients[101]. The model was designed to offer treatment recommendations and predict the overall survival of patients with HCC. The conclusions of these studies could aid the re-evaluation of our current HCC management practices to an individualized, multimodal strategy[102].

Models that reliably predict the presence of particular mutations in HCC patients could be used as a tool for the early administration of appropriate treatment such as immunotherapy or multi-targeted tyrosine kinase inhibitors. In a recent study, a CNN was developed that employs images from hematoxylin and eosin-stained WSIs to predict the presence of specific mutations in patients with HCC [75]. A similar study developed a CNN that classifies HCC and then predicts the presence of specific mutations[103]. Finally, a CNN model was developed in a recent study based on multiphasic CT scans as a non-invasive prediction tool of particular mutations[104].

Several studies designed AI/ML-based models that preoperatively predict microvascular invasion (MVI) as reliable treatment allocation tools. In a recent study, an AI/ML-based model was developed as a non-invasive tool, employing only presurgical blood parameters to predict MVI in patients with HCC [105]. In a different study, a CNN was developed employing presurgical MRI scans in an effort to predict MVI[106]. Finally, another study developed a CNN, employing diffusion-weighted imaging from patients with HCC to predict MVI preoperatively[107]. Another study used CT radiomics data to develop an RF/SVM-based model that predicts MVI in patients with HCC[108]. Similarly, in a recent study, CT radiomics were combined with laboratory and clinical data to develop two models, a gradient boosting-based and a CNN-based, to predict MVI preoperatively[109]. Finally, an ANN was developed in a different study to predict MVI that notably outperformed a conventional LR model[110].

Several studies have investigated how AI/ML-based models could determine the response to treatment in patients with HCC. Focusing on hepatic resection, an ANN model was developed that predicts liver failure following hemihepatectomy, which could be used as the basis of a triage tool for intensive care[111]. Similarly, in a different study, an ANN model was developed to predict in-hospital mortality risk following hepatic resection[112]. The model outperformed conventional LR models. Interestingly, the study reported that the best single predictor of in-hospital mortality was the surgeon volume[112].

Besides hepatic resection, several studies have developed models to predict the response to TACE treatment. Particularly for response prediction in patients treated with TACE, US radiomics were used in a study to develop a CNN to classify patients with HCC who fully/partially respond to TACE from

patients who either remain stable or progress[113]. In a different study, multiphasic CT scans and the BCLC staging system were used to develop an AI/ML-based model to classify TACE-susceptible from TACE-refractory HCC[114]. CT imaging was also used in a different study to develop a CNN as a multi-class tool for complete response, partial response, stable disease, and progressive disease following TACE[115]. Another study used MRI to classify patients with HCC as responders and non-responders to TACE treatment[116].

In a recent study, images from full-field optical coherence tomography were used to develop an SVM model that recognizes hepatic cancerous cells as a tool to detect tumor boundaries for resection intraoperatively[117]. A different study used X-ray imaging to develop a CNN model as the basis of a framework that automatically detects fiducial markers, performs 3D position reconstruction, and evaluates intrafraction motion during stereotactic body radiation therapy for liver malignancies[118]. In another study, MRI and CT imaging were employed to develop a novel dense-cycle-generative adversarial network for the generation of synthetic CT scans that could be used to optimize treatment planning for liver stereotactic body therapy[119]. Data from computational fluid dynamics were used in another study to develop a CNN to estimate Yttrium-90 distribution during radioembolization[120]. Finally, in a study conducted in silico, an SVM model was used to identify potential drug targets for HCC treatment[121].

Prognosis

Several studies have focused on constructing AI/ML-based tools able to consistently predict patient outcomes (progression and disease-free survival, overall survival, and recurrence) in the context of HCC prognosis. Several ML algorithms were combined in a study to develop an AI model that employs data from DNA methylation and RNA and microRNA profiling to predict overall survival for patients with HCC[122]. Several AI/ML-based models were developed in a recent study, employing non-invasive parameters to predict survival in operated patients with HCC[123]. Another study developed a 20-features gradient-boosting survival classifier to stratify an HCC-related death risk into three distinct categories[124]. In a different nationwide study, an ANN model was developed to predict the 5-year survival of patients with HCC following hepatic resection[125]. Interestingly, the independent predictor with the strongest correlation to survival was the surgical volume of the surgeon[125]. The performance of the ANN was found to be superior to the LR's performance[125]. Likewise, in another study, the ANN model surpassed the performance of the LR model in predicting overall survival following surgical resection[126]. The ANN model was also able to identify more independent predictors of survival than the LR model[126]. In a prospective study, the ANN model's ability to predict the survival of operated patients with early staged HCC was compared with the performance of traditionally used staging systems; the ANN model outperformed all staging systems in all training and validation cohorts [127]. Data from RNA sequencing were employed, in a recent study, to develop an RF-based model that uses five biomarkers to predict patients' overall survival[128]. Finally, hematoxylin and eosin-stained WSIs were used in a different study to develop a CNN that predicts survival following resection[129].

Focusing on the survival of non-operated patients, in a recent study, an ANN was developed that employed albumin/bilirubin grade and Child-Turcotte-Pugh (CTP) grade to predict survival in patients with HCC who received as initial treatment a monotherapy with TACE[130]. In a similar study, albumin/bilirubin grade and CTP grade were used to develop an ANN to predict survival in patients who received as initial treatment the combination of TACE and sorafenib[131]. A different study, also considering patients treated with TACE and sorafenib, used CT scans instead to develop a CNN to predict survival[132]. Another study focusing on patients treated with TACE developed a DNN model to predict overall survival in patients with HCC[108]. Finally, an ANN-based model was developed employing routinely collected data to predict 1-year survival in HCC patients treated with TACE[133].

Different models have focused on predicting progression-free or disease-free survival. Such models could be used to design personalized follow-up schedules. A recent study employed routine laboratory results and clinicopathological data to develop an ANN that predicts progression-free survival and overall survival[134]. Notably, the model outperformed traditionally used classification systems. Similarly, in a retrospective study, data from operated patients were employed to develop an ANN, a decision tree, and an LR model for predicting the 1-, 3-, and 5-year disease-free survival[135]. The ANN model managed to outperform the other two models[135]. A recent study developed an RF model based on 34 epigenetic features of DNA methylation profiles to predict the 6-mo progression-free survival [136]. In another recent study, an RF model was developed employing routinely collected data to predict the disease-free survival of patients with HCC following surgical resection[137]. Finally, an ANN was developed in a different study to predict disease-free survival for patients with HCC treated with CT-guided RFA[138].

Besides survival, AI/ML-based tools have been used for predicting HCC recurrence following curative treatment. Specifically, several AI/ML-based tools were developed in a study, including an RF model, an SVM model, and an Artificial Plant Optimization model for predicting HCC recurrence following RFA[139]. In a recent study, a gradient boosting algorithm-based model was developed employing clinical parameters to predict patients' recurrence following surgical resection, as well as survival[140]. In a different study, gene sequencing data were used to develop AI/ML models to predict recurrence in patients with HCC following surgery[141]. Early recurrence has been the focus of a study

that combined different AI/ML classifiers to develop a model that predicts recurrence in operated patients with HCC[142]. In a different, multi-center study, several ML algorithms were used to develop AI/ML-based models to predict HCC recurrence following hepatic resection[143]. Notably, the models that employed CT radiomics outperformed the models that used clinical data[143]. A Bayesian network-based model was developed in another study aiming to classify patients according to the recurrence time (early, late) following hepatic resection[144]. Finally, a study focusing on patients with cancer recurrence following surgical resection developed an SVM model employing several clinical indicators to predict the time and location of HCC recurrence[145].

Hematoxylin and eosin-stained WSIs have been used to develop AI/ML-based models to predict recurrence in operated patients with HCC. A CNN was constructed in a recent study utilizing histopathologic images for predicting recurrence in HCC operated patients[77]. The model outperformed the conventional TNM classification system[77]. A different study developed an RF-based model to predict overall survival that notably performed comparably with the TNM classification system[146]. Finally, a study focusing on recurrence timing used hematoxylin and eosin-stained WSIs to develop an SVM model that predicts the early recurrence of HCC patients following resection[147].

Other studies have focused on predicting the recurrence of patients treated with ablative techniques. An SVM model was developed in a study using clinical data to predict recurrence in a group of patients with HCC who were treated with RFA[148]. In another study, an unsupervised landmark-constrained CNN-based deformable image registration technique was used to predict local tumor progression in patients with HCC treated with microwave ablation based on the ablative margin[149].

Focusing on liver transplantation, a team developed a DNN model that employs routinely collected data to predict HCC recurrence in patients receiving a living donor graft[150]. Notably, the model significantly outperformed all the conventionally used staging systems. An ANN model was developed employing data from genotyping for microsatellite mutations/deletion to predict post-transplant HCC recurrence[151]. Clinical data and CT radiomics were employed in a different study to develop a least absolute shrinkage and selection operator model to predict recurrence-free survival in transplanted HCC patients[152]. Several other studies have developed AI/ML-based tools for predicting liver graft survival following liver transplantation[153,154]. Specifically, in a multi-center study, an ANN model was developed for predicting the 3-mo graft loss and survival[154]. Notably, the model surpassed all the currently used scores, including the Donor Risk Index, the Model for End-stage Liver Disease, the Balance of Risk, and the Survival Outcome Following Liver Transplantation; their performance was found to be significantly lower with an AUROC range of 0.42-0.67[154]. An ANN and an RF model were developed in another study for predicting 30-d and 3-mo graft failure following transplantation[153]. Notably, these models outperformed the Model for End-stage Liver Disease and the Donor Risk Index [153]. Finally, in a study using data from the United Network for Organ Sharing, a DNN was developed to predict 90-d post-liver transplant survival[155]. Similarly, this model outperformed traditionally used classification systems[155].

CURRENT CHALLENGES

Challenges of 3D printing application in HCC management

Even though the cost related to 3D printing is steadily decreasing, it still remains the main challenge for the widespread application of 3D printing in healthcare facilities. The 3D printing-related cost consists of hardware, software, printing materials, and labor. Among the seven families of additive manufacturing as per the American Society for Testing And Materials International, those more frequently applied in the medical field are selective laser sintering, stereo lithography, laminated object manufacturing, fused deposition modeling, and inkjet printing[156]. Each of these 3D printing types has its characteristics regarding accuracy/precision, availability, printing speed, required materials, color capabilities, transparency, sterilization capability, biocompatibility, and cost[9]. The characteristics of each printing type define its cost. For example, while selective laser sintering printers are highly productive, with the ability to print complex structures with quick printing times, their cost is significantly higher, and their availability is limited compared with fused deposition modeling printers, which, although cheap, have low processing times and low accuracy[41,157].

The cost is also dependent on the size and complexity of the targeted structure. The liver is a large organ with complex anatomy; thus, the cost and time required to construct a 3D liver model are higher than other organs. A valid solution is scaling down the 3D models[26]. Studies usually overlook the costs associated with labor; however, they should be considered, particularly when evaluating cost-effectiveness ratios. Focusing on cost-effectiveness, it is essential to highlight that the additional cost/resources related to 3D printing should be evaluated in conjunction with the magnitude of the improvement in medical outcome. Unfortunately, based on a systematic review, only 7% of published studies related to 3D printing mention cost-effectiveness, and no study has evaluated cost-effectiveness in a quantitative manner[158].

In addition to cost, other challenges/limitations include the reliance of the 3D printed models' accuracy on the underlying 2D imaging data that makes them prone to imaging errors[41]. Therefore, high-accuracy imaging is a precondition of highly accurate 3D models. In addition, due to long printing times, 3D printing currently has no application in the emergency clinical setting, such as the rupture of an HCC tumor[18]. However, printing times are becoming shorter, with reports of 3D models printed within a single day. Another challenge is the limited availability of software for 3D printing in medicine and the absence of many visual aids and manipulation tools for postprocessing[9]. The shortcoming of limited software further deteriorates by the notable absence of specialists in 3D printing software and technologies in most healthcare facilities[34].

Bioprinting of 3D models faces its own challenges and limitations. High-resolution is particularly important in 3D bioprinting to facilitate proper interactions of the biomaterials, which are crucial for tissue development[42]. Particularly for the liver, a metabolically active tissue, the appropriate microenvironment should be created inside the 3D bioprinted model to retain its hepatocyte-like phenotype. The development of large-scale liver tissues with hepatocytes retaining viability and longer-term functionality following sequential differentiation is clearly a challenge[42]. Even though 3D bioprinted liver models are reported as superior to other tissue engineering methods in that regard, scaling up these models to a substantial volume to provide a significant *in vivo* liver function could prove to be a herculean task. The evolution and increased complexity of 3D bioprinting could reach a saturation point where the functional outcomes do not improve further[159]. Current 3D bioprinted tissues lack any vascular network and rely on diffusion for nutrient supply. The integration of a vascular network, particularly for the liver, which has a complex vascular network, could prove particularly challenging. Potential solutions include embedding angiogenic growth factors into the bio-ink, direct bioprinting of the vasculature, and sacrificial templates for fabricating perfusable microchannel networks[160-163]. Another challenge of 3D bioprinting is cell availability. Expanding the current applications of 3D bioprinted models would require reliable sources of human cell lines[164]. Current sources include specimens from hepatic resections and transplantations and fetal liver cells from abortion; these cell sources are all in limited supply, which could restrain research progress[164]. A potential solution could be the use of liver stem cells, immortalized hepatic cell lines, and minimally invasive cell harvesting[42, 165,166]. Compared to stem cells, adult hepatocytes propagate poorly and lose functionality more rapidly *in vitro*[167]. In summary, further research is required to investigate how these 3D bioprinted models behave *in vivo* in terms of viability, stability, retaining functionality, compatibility, and degradation rate of the polymer hydrogels before they could be implanted in a clinical setting. Finally, the logistics of healthcare facilities maintaining production chains for patient-specific tissues, given the biomaterials' environmental and time sensitivity, could prove impractical, creating the need for a centralized logistical model[159].

3D printing and mainly 3D bioprinting face regulatory, legal, and ethical challenges. 3D printable products should comply with existing control and manufacturing standards for medical devices and products. The Food and Drug Administration (FDA) published in 2017 the Technical Considerations for Additive Manufactured Medical Devices, which provides a framework for manufacturers and guidance regarding the main aspects of 3D printing, including hardware, software, validation procedures, and quality control[168]. As acknowledged by the guidelines, there is significant variability among the different types of additive manufacturing to the extent that each printing methodology requires different regulatory standards[168]. A genuine concern for 3D bioprintable organoids is safety. Even though "absolute" safety could not be guaranteed in any biomedical novelty, a comprehensive evaluation of benefits and risks is required to decide if it reaches a safety threshold[169]. However, bioprintable organoids significantly differ from novel drugs and could not be assessed by our current drug development evaluation processes. Due to the interindividual differences among patients, extrapolating on the safety of patient-tailored organoids is challenging. However, accumulated results and experience over a series of cases could serve as a basis to gain regulatory approval. The precautionary principle dictates that in applying novel technologies where our knowledge is limited and the uncertainty is high, a higher and stricter standard should be adopted compared with known biomedical products[170]. Another concern is obtaining genuine informed consent. For the patients donating, before consenting, the patients' autonomy and control over their biological condition should be established, and concerns regarding anonymity, data protection, future claims on their donated tissues, as well as these tissues intended short-term and long-term use should be addressed[169,171]. Similarly, before giving informed consent, transplanted patients' concerns regarding safety, short-term and long-term risks, the uncertainty involved, and potential unknown consequences should be addressed. Unlike with clinical trials where a drug is tested, the patient's withdrawal is impeded due to the irreversible nature of transplantation[172].

3D bioprinting faces several ethical challenges. An ethical advantage of 3D bioprinted organoids could be used in pre-clinical drug testing and significantly minimize the need for animals in the laboratory. An ethical concern is the potential use of donated biomaterials in the development of embryonic cell lines. Donors should be informed of this perspective before providing informed consent [169]. Generally, there are ethical concerns about whether all possible cell sources, including embryonic cell lines, pluripotent stem cells, or even animal cells, could be used for bioink fabrication[173]. Another ethically challenging point is the accessibility of 3D bioprinted materials. Since healthcare facilities may

be unable to be reimbursed for 3D bioprinted-related treatments, there is a justifiable concern that these treatments will be accessible only to those who can afford them[169]. To add to this concern, when 3D bioprinting is advanced enough to produce organs that are superior in certain aspects compared to human organs, 3D bioprinting technologies could be used for eugenic purposes[172]. With steadily decreasing prices and steadily increasing availability, there is an actual concern about unregulated 3D bioprinting research that could be used for malignant purposes, including bioterrorism[171]. Evidently, there is a need for a robust regulatory framework to address all these emerging concerns, which could be obtained by elaborating on our existing ethical and regulatory standards as encompassed in the Helsinki Declaration, the Oviedo Convention system, and UN's Declaration on Human Rights. However, the real challenge will not be to develop these regulatory frameworks but to ensure that they evolve in conjunction with the evolution of these technologies and are not outpaced by them.

Challenges of AI application in HCC management

The application of AI in HCC management, and healthcare in general, faces a plethora of challenges that include intellectual property concerns, liability, intrinsic bias, data protection and cybersecurity threats, ethical concerns, and lack of transparency. Regarding intellectual property, the first step for regulation is determining whether an AI/ML-based model should be classified as a medical device, a service, or a product. Assessing the intended usage of the developed model is critical. Tools designed to assist in diagnosing and treating diseases could be considered as medical devices and therefore should adhere to the respective regulations[174]. FDA receives an increasingly high number of submissions with regard to the marketing of AI/ML-based software and has recently published the Artificial Intelligence/Machine Learning (AI/ML) – Based Software as a Medical Device (SaMD) Action Plan[175-177]. The action plan regards AI/ML-based software classified as medical devices and sets five pillars to facilitate the innovation and advancement of AI/ML-based software[175]. A different point of concern is the significant divergence of the original licensed product years after the approval[178]. These concerns regard both intellectual property and the safety of the tool. What are the rights of developers over their evolving products? Are the original product and the deviated model two entirely different products? While the original product is clearly protected under copyright law, it is unclear if the healthcare facility could have intellectual property demands over the final product that now encompasses data generated in the clinical setting[179]. In addition, there are concerns over the product's safety as it evolves and significantly deviates from its initial form. A regulatory framework should be established for AI/ML-based software that monitors these models throughout their lifecycle[180]. When it comes to regulation, rigid regulation suppresses and strangles innovation and creativity, while little regulation could have devastating and unintended ramifications. Therefore, the real challenge is finding the optimal balance between the two.

A different concern regarding AI/ML-based software applications relates to liability issues. As AI/ML-based models advance, they will eventually perform specific tasks better than physicians. How could physicians then legally justify their decision to ignore the recommendations presented by AI models? Could the AI models' recommendations become legally binding in the foreseeable future? And most importantly, who is liable, when during the AI-assisted management of a patient, an injury occurs? Currently, no legal precedent exists concerning the liability of AI-assisted case management, where a patient injury occurred[181]. In a recent legal analysis, the authors insightfully analyzed the various scenarios regarding liability when an AI model is involved in medical care. Based on the analysis, current law protects from liability when physicians follow the standard treatment care[181]. Unfortunately, that could lead to AI/ML-based tools having an affirmative role in patient management and not actually contributing to a higher level of care.

Lack of accuracy due to intrinsic biases is another primary concern when AI/ML-based models are applied. A primary reason for the lack of accuracy is the unavailability of volume, high-quality, high-variety, standardized datasets for the model's training. A secondary reason is that weaknesses in the datasets, such as incorrectly labeled cases and discrepancies in the data collection process, are inadvertently integrated into the model, limiting its accuracy[182]. Two significant types of bias encountered in AI/ML-based models are overfitting and spectrum bias. During the training of the models' algorithms, overfitting occurs when a model is customized for the training data (with outstanding evaluation metrics in the training data) but performs significantly poorer in the validation set[183]. CNNs, which, as demonstrated, are extensively used in the models for the management of HCC, are particularly vulnerable to overfitting[184]. On the other hand, spectrum bias occurs when the training dataset consists of samples not representative of the target population; thus, the model's performance is significantly reduced when applied in the intended clinical setting[183]. Another limitation of actual accuracy is the in silico nature of most studies, which should lower the expectations of similar performances when these models are applied in actual clinical settings.

Several measures could be taken to alleviate the impact of biases on AI/ML models' accuracy. First, a consistent way of reporting performance should be used to allow benchmarking and the drawing of meaningful comparisons among the plethora of studies[185]. Second, standardized data collection methods and evaluation systems for bias detection should be established to avoid the impact of low-quality data on the models' accuracy[186,187]. Finally, when these models are implemented in actual clinical settings, an approach similar to the clinical trial phases should be adopted[188].

Integrating AI into the clinical setting requires an entirely digital tracking of healthcare records. That could pose a significant concern and a justified reason to resist AI integration into healthcare since it will expand the amount of sensitive data to massive disclosures[189]. An example of such disclosure was the transfer of healthcare data from 1.6 million patients in the United Kingdom, which was ruled illegal [190]. Due to the nature of the data that it generates, the healthcare industry is particularly attractive as a potential target for cyberattacks. Steps have been taken under the Health Insurance Portability and Accountability Act to shield healthcare facilities from potential breaches of sensitive data[191]. However, AI introduces new dangers and vulnerabilities beyond traditional cybersecurity concerns. Cyberattacks could target AI models and introduce malignant data into the algorithms to manipulate the AI models' output. These vulnerabilities could significantly undermine the trust in AI software. Further steps are required to strengthen the information technology infrastructure in order to ensure the integrity of AI systems before they could be integrated into the healthcare system.

Several ethical challenges emerge from the inclusion of AI models into the patient's management. First, data sharing concerns could undermine the physician and the patient's trust and lead patients to conceal information[192]. Second, AI software is incapable of understanding non-quantifiable aspects of physicians' lives, such as understanding the patients' needs, sympathizing with their beliefs, and respecting their wishes. Finally, there are fears that prejudices relating to racism, sexism, and socioeconomic inequality included in the training datasets would be mistakenly included in the AI model. An infamous example is the COMPAS algorithm, which erroneously flagged black people as usual re-offenders[193]. To make things worse, the developers argued that their algorithm was not open to scrutiny since it was protected by intellectual property law[193]. It is, therefore, no surprise that around two-thirds of the population oppose AI/ML-based models to perform tasks, which physicians typically perform[194].

Finally, a last but also significant concern of integrating AI/ML-based software in the healthcare system is the lack of transparency. AI models are often described as black-boxes since there are non-interpretable, and their inner logic is hidden, which creates an intriguing ethical dilemma[195]. On the one hand, we could argue that applying technologies that we barely comprehend violates a fundamental tenet of medical ethics[196]. However, on the other hand, we could argue that withholding the application of AI models that could significantly benefit the patient's well-being is unethical[194]. To overcome this conundrum, regulators, developers, and physicians should cooperate to create a robust regulatory framework that increases transparency and addresses biases. A trustworthy AI/ML-based model should be built around the principles of credibility, transparency, reliability, auditability, and recoverability[197].

LIMITATIONS

This review has several limitations. First, despite our efforts to follow a tight search strategy, as a narrative review, this study is prone to selection bias. Second, we did not systematically evaluate each study's risk of bias using a risk assessment tool. Therefore, we advise the readers to keep in mind that each study has its own biases and limitations that are not elaborated in this review. Another point is that the majority of studies included were conducted in silico, and their models' reported performance could substantially deviate when applied in an actual clinical setting. Finally, our review is prone to publication bias, similar to every narrative review, since studies that developed AI models with poor performance are less likely to be published.

CONCLUSION

In this review, we have comprehensively presented the applications of 3D printing and AI in the management of HCC and summarized the current obstacles that hinder the general use of these technologies in the healthcare industry, and identified several means to overcome them. Several opportunities arise from the application of these technologies in the management of HCC. Particularly for 3D printing, these opportunities include educational purposes, both regarding the medical staff and the patients, preoperative planning, and the development of custom-made medical tools. Specifically, cheap patient-specific 3D printed hepatic models developed from radiology images could be used to aid surgical residents in becoming familiar with the complex liver anatomy[19]. In addition, 3D models have been developed to familiarize surgical residents with laparoscopic operations[22,23]. The work of Yang *et al* [20] demonstrated how 3D printed liver models could be used for patient education to reach a higher understanding of their disease, understand the potential risk of an operation, and facilitate obtaining informed consent.

3D printed models also facilitate the preoperative planning of patients operated for HCC. Several teams have demonstrated how 3D printed models could significantly improve the surgical outcome specifically for patients with rare variations of the abdominal blood vessels[31-33]. Optimizing preoperative planning could substantially reduce the operation time and improve surgical outcomes. In

Table 4 Artificial intelligence application in hepatocellular carcinoma prognosis

	First author	Parameters employed	AI classifier	Sizes of the training/validation sets	Outcomes	Performance	Ref.
1	Chaudhary K	DNA methylation, RNA, and microRNA profiling	Several	360 patients (training:validation = 6:4)	Overall survival	0.70[1,2], 0.66-0.70[1,3], 0.67-0.82[1,4]	[122]
2	Chicco D	50 laboratory and clinical parameters	Several	165 patients with HCC	Overall survival	RF: 77.2[1], 0.766[5]; Linear SVM: 77.1[5], 0.763[1]; MLP: 72.7[5], 0.695[1]; Radial SVM: 68.0[5], 0.663[1]; DT: 65.9[5], 0.650[1]	[123]
3	Liu X	Laboratory results, data from immunochemistry of peripheral blood mononuclear cells, tumor characteristics	GBA classifier	136/56[3]/105[4]	Risk of HCC-related death	0.844[1,2], 0.827[1,3], 0.806[1,4]	[124]
4	Shi HY	Laboratory results, clinicopathological parameters, tumor characteristics	ANN	22926 patients	5-yr survival following surgical resection	96.57[3,5], 0.885[1,3], 97.43[4,5], 0.871[1,4], 74.23[4,6]	[125]
5	Chiu HC	Laboratory results, clinicopathological parameters, tumor characteristics	ANN	434, 341, and 264 patients for 1-, 3-, and 5-year survival(training:validation = 8:2)	1-, 3-, and 5-yr overall survivalfollowing surgical resection	98.5-99.5[2,5], 0.980-0.993[1,2], 99.7-100[2,6], 96.2-99.2[2,7], 72.1-85.1[3,5], 0.798-0.875[1,3], 71.4-88.6[3,6], 50.0-82.1[3,7]	[126]
6	Qiao G	Laboratory results, clinicopathological parameters, tumor characteristics	ANN	362/181[3]/104[4] patients	Survival following surgical resection	0.855[1,2], 80.00[2,6], 73.40[2,7], 0.832[1,3], 78.67[3,6], 75.70[3,7], 0.829[1,4], 77.42[4,6], 78.08[4,7]	[127]
7	Guo L	RNA sequencing	RF	239/130 patients	Overall survival	89[3,5]	[128]
8	Saillard C	Hematoxylin and eosin-stained WSI	CNN	309/342[4] WSIs	Survival following surgical resection	0.75-0.78[1,2], 0.68-0.70[1,4]	[129]
9	Zhong BY	ALBI/CTP stage	ANN	548/115[4]/175[4]	Survival of patients treated with chemoembolization as monotherapy	ALBI-based: 0.799[1,4], 0.700[1,4]; CTP-based: 0.729[1,4], 0.802[1,4]	[130]
10	Zhong BY	ALBI/CTP stage	ANN	319/61[4]/124[4]	Survival of patients treated with chemoembolization and sorafenib	ALBI-based: 0.716[1,4], 0.823[1,4]; CTP-based: 0.779[1,4], 0.693[1,4]	[131]
11	Zhang L	CT scans, clinical features	CNN	120/81[3] patients	Survival of patients treated with chemoembolization and sorafenib	0.717[1,2], 0.714[1,3]	[132]
12	Liu QP	CT radiomics, clinical parameters	DNN-DAE	243 patients	Overall survival following TACE	0.87-0.93[1,3]	[108]
13	Mähringer-Kunz A	Routine laboratory tests and clinicopathological parameters	ANN	125/57 patients	1-yr overall survival following TACE	0.77[1,2], 0.83[1,3], 77.8[3,6], 81.0[3,7]	[133]
14	Liu X	Routine laboratory tests and clinicopathological parameters	ANN	1480/637 patients	Progression-free survival. Overall survival	0.866[1,2], 0.730[1,3]. 0.877[1,2], 0.804[1,3]	[134]
15	Ho WH	Laboratory results, clinicopathological parameters, surgery parameters	ANN, DT	427, 354, and 297 patients for 1-, 3-, and 5-yr survival (training:validation = 8:2)	1-, 3-, and 5-yr disease-free survival following surgical resection	ANN: 0.963-0.989[1,2], 93.5-96.3[2,6], 91.6-97.9[2,7], 0.774-0.864[1,3], 70.0-78.7[3,6], 54.2-92.7[3,7]. DT: 0.675-0.825[1,2], 19.6-94.8[2,6], 45.8-97.9[2,7], 0.561-0.718[1,3], 0-88.5[3,6], 37.5-96.4[3,7]	[135]
16	Bedon L	DNA methylation profiling	RF-based	300/74 specimens	6-mo progression-free survival	67.1-80.6[2,5], 64.8-80.2[4,5]	[136]
17	Schoenberg MB	Routine laboratory tests and clinicopathological parameters	RFS	127/53 patients	Disease-free survival following resection	0.766-0.788[1,3]	[137]

18	Wu CF	Laboratory tests and clinicopathological parameters, treatment data	ANN	252 patients(training:validation = 8:2)	1-yr and 2-yr disease-free survival following RFA	0.72-0.77[1,3], 56.3-63.6[3,6], 70.0-71.8[3,7]	[138]
19	Divya R	Laboratory results, clinicopathological parameters, tumor characteristics	APO, SVM, RF	152 patients	Recurrence following RFA	95.5[3,5], 95.1[3,6], 95.8[3,7]	[139]
20	Huang Y	Demographics, laboratory tests, tumor characteristics	GBS classifier	5928/1483 patients	Recurrence following surgical resection. Overall survival	0.704[1,2], 0.697-0.713[1,3]. 0.565-0.736[1,2], 0.551-0.751[1,3]	[140]
21	Shen J	Disease-free related genes sequencing	DT, SVM	315 HCC patients	Recurrence following surgical resection	DT: 74.19[5], 0.75[1], 70.41[4,5]. SVM: 80.65[5], 0.595[1]	[141]
22	Wang W	CT radiomics, clinical data	CNN, SVM, RF	167 patients	Early recurrence following surgical resection	0.723-0.825[1,3]	[142]
23	Ji GW	CT radiomics, laboratory results, clinicopathological parameters	Several	210/107[3]/153[4] patients	Recurrence time following surgical resection	Radiomics model: 0.748-0.752[1,2], 0.781-0.801[1,3], 0.733-0.741[1,4]. Clinical model: 0.716-0.727[1,2], 0.707-0.739[1,3], 0.696-0.716[1,4]	[143]
24	Xu D	Routine laboratory tests and clinicopathological parameters, intra-operative parameters	BN-based	995 patients	Recurrence time following surgical resection	0.57[3,5], 0.57[3,6]	[144]
25	Jianzhu B	Several including immune, tumor, nutrition, and indicators	CS-SVM	776 liver cancer recurrences	Recurrence time. Recurrence location	Mean square error = 9.2101, 95.7[5], 0.95[1]	[145]
26	Yamashita R	Hematoxylin and eosin-stained WSI	CNN	299/53[3]/198[4] WSIs	Recurrence following surgical resection	0.724[1,3], 0.683[1,4]	[77]
27	Liao H	Hematoxylin and eosin-stained WSI	RF	491 WSIs	Overall survival	0.563-0.706[1,3], 0.565-0.621[1,4]	[146]
28	Saito A	Hematoxylin and eosin-stained WSI	SVM	69/89[4]	Recurrence time following surgical resection	99.8[2,5], 68.1-80.6[4,5]	[147]
29	Liang JD	Laboratory results, clinicopathological parameters	SVM	83 patients	Recurrence following RFA	73-82[3,5], 0.60-0.69[1,3], 77-86[3,6], 73-82[3,7]	[148]
30	An C	MRI scans	CNN	141 HCC lesions	Local tumor progression following MWA	0.728[1]	[149]
31	Nam JY	Routine laboratory tests and clinicopathological parameters	DNN	349/214 patients	Post-transplant HCC recurrence	0.62-0.75[1,3], 0.63-0.76[3,6], 0.46-0.62[3,7]	[150]
32	Nam JY	Laboratory results, clinicopathological parameters, tumor characteristics	DNN	349/214 transplanted patients	Post-transplant HCC recurrence	0.75[1,3], 76[3,6], 46[3,7]	[150]
33	Rodriguez-Luna H	Genotyping data from microsatellite mutations/deletions	ANN	19 transplanted patients	Post-transplant HCC recurrence	89.5[3,5]	[151]
34	Guo D	Laboratory results, clinicopathological parameters CT radiomics	LASSO	93/40 transplanted patients	Recurrence free-survival following liver transplantation	0.675-0.785[1,2], 0.705-0.789[1,3]	[152]
35	Lau L	Laboratory results, clinicopathological parameters, donor characteristics	ANN, RF	90/90 transplants	Graft failure/primary nonfunction. 3-mo graft failure	ANN: 0.734-0.835[1,3]; RF: 0.787-0.818[1,3]. ANN: 0.559[1,3], RF: 0.715[1,3]	[153]
36	Briceño J	Laboratory results, clinicopathological parameters, surgical parameters, donor characteristics	ANN	1003 liver transplants	3-mo graft failure	0.806-0.821[1,3]	[154]

37	Ershoff BD	Laboratory results, clinicopathological parameters, donor characteristics	DNN	46035/11509	90-d post-transplant survival	0.695-0.708[1,3], 30.9-35.8[3,6], 88.1-90.8[3,7]	[155]

[1]Area under the receiver operating curve or c-index.
[2]Training.
[3]Internal validation.
[4]External validation/testing.
[5]Accuracy (%).
[6]Sensitivity (%).
[7]Specificity (%).
ALBI: Albumin-bilirubin; ANN: Artificial neural network; APO: Artificial plant optimization; BN: Bayesian network; CNN: Convolutional neural network; CS: Cuckoo-search; CT: Computed tomography; CTP: Child-Turcotte-Pugh; DNN: Deep neural network; DAE: Deep auto-encoder; DT: Decision tree; GBS: Gradient boosting survival; HCC: Hepatocellular carcinoma; LASSO: Least absolute shrinkage and selection operator; MLP: Multi-layer perceptron neural network; MRI: Magnetic resonance imaging; MWA: Microwave ablation; RF: Random forest; RFA: Radiofrequency ablation; SVM: Support vector machine; TACE: Transarterial chemoembolization; US: Ultrasound; WSI: Whole-slide image.

liver transplantation, the work of Zein *et al*[25] demonstrated how 3D printed models of high anatomical precision could be used to optimize the recipient-donor matching in graft allocation by unveiling any unsuitable anatomy between the donor and the recipient. In recently published consensus recommendations, it is strongly recommended that for complicated cases of HCC, 3D visualization is carried out to comprehend the course/variation of the portal vein and understand how it is related to the tumor[198]. In addition, 3D visualization is recommended as part of preoperative planning for centrally located HCC and/or complex vascular anatomy[198]. Finally, the works of Damiati *et al*[35] and Han *et al*[38] highlight the opportunity that arises from 3D printing in the fabrication of custom-made medical tools for the diagnosis and treatment of HCC.

3D printing is an evolving field in the medical disciplines, evident by the increasing number of publications each year[10]. It is pretty impressive that even though the majority of the studies regarding 3D printing report a significant improvement of the investigated medical outcome, only 14% of those studies support their findings in a quantitative manner, rendering their conclusions rather subjective [158]. This lack of consistency on how to report results precludes any meaningful comparison between studies. With the costs related to 3D printed models steadily decreasing, it is expected that 3D printing applications will significantly expand[199].

Bioprinting could potentially have a profound impact on liver surgery. Currently, the opportunities that arise from its application in HCC management include the development of 3D bioprinted hepatic scaffolds that could be used to develop antitumor drugs since 3D bioprinted models more precisely represent the microenvironment of HCC compared to other tissue engineering methods. Specifically, the work of Sun *et al*[45], who used HepG2, and the work of Xie *et al*[45], who used patient-derived HCC cells, demonstrate how 3D bioprinting could aid the individualized treatment of patients with HCC.

Liver transplantation is the only definitive treatment of liver failure. However, it is currently being restricted by the limited number of liver grafts. Promising results from animal studies demonstrate how 3D bioprinted liver organoids could be transplanted to prolong the survival of mice with liver failure [200]. These results raise the expectations that bioprintable liver grafts could be used in the future in regenerative medicine to ameliorate the burden of the liver graft shortage. However, despite a promising field, we should highlight that bioprinting is currently in its infancy.

The application of AI/ML-based models offers a plethora of opportunities in the management of HCC. First, in prevention, AI/ML models could be integrated into the healthcare system and analyze data directly from patients' healthcare records in real-time to flag patients at high risk of developing HCC. Current efforts include predicting HCC development in patients with chronic HBV infection[48] and chronic HCV infection[51-54]. Other studies focusing on prevention have developed AI/ML models employing genetic and epigenetic markers such as long-coding RNAs to screen for HCC[47,49,50]. These models demonstrate how AI could facilitate tailoring individualized follow-up schedules and identifying patients at a greater need to achieve a SVR. Following prevention, early detection is equivalently crucial in the management of HCC. Current efforts for early detection include studies that employ biomarkers to develop AI/ML models to detect HCC development[55-59].

In diagnostics, AI/ML models could enhance diagnostic accuracy in different diagnostic modalities. Specifically, current efforts include CAD models for detecting HCC either among a plethora of focal hepatic lesions or between HCC and non-HCC lesions. These models employ different diagnostic modalities, including US imaging[60-62,80,81], CT imaging[64-66,90,91], MRI[69-73], and PET/CT imaging[92]. Other studies employed hematoxylin and eosin-stained WSI to detect HCC lesions and classify the level of differentiation[74-79].

Regarding treatment, AI/ML models provide several opportunities to reduce the morbidity and mortality associated with HCC. These opportunities include the development of frameworks for

individualized, evidence-based treatment allocation[99,101], the prediction of the presence of certain mutations as a base for appropriate drug selection[75,103,104], the prediction of MVI presence to facilitate the appropriate treatment selection[105-110], and finally the prediction of the response to treatment, and particularly TACE, as a tool to identify patients who would benefit more from treatment [113-116].

Finally, regarding prognosis, AI/ML models could be used to predict patient outcomes. Such models could be used as the basis to counsel the patient and the patient's family. Recent initiatives include the prediction of overall survival[123-127], the prediction of progression-free survival[134-138], the prediction of survival of non-operated patients treated with TACE[130-133], and HCC recurrence following therapeutic treatment[77,139-142]. In liver transplantation, current efforts include models to predict post-transplant HCC recurrence and individual liver graft survival as tools to optimize the graft allocation procedure[150-155].

As demonstrated by our findings, there is a lack of consistency regarding the validation strategies employed by each study and the different metrics used to assess the models' performance. This lack of consistency significantly limits our ability to draw any meaningful comparisons among the models. A challenge for the future would be to develop a robust tool for presenting the performance of these models that would allow benchmarking.

Even though AI has been on the frontline for several decades, AI has not yet been integrated into the healthcare system. AI in medicine could be seen as a field that overpromises but invariably underdelivers. This is evident during AI winters, where the funding for AI research is halted due to the investors' dissatisfaction that AI does not progress at a rate at which they are comfortable investing[14]. Overcoming the current challenges of AI applications is a vital part of integrating AI in the healthcare industry.

Physicians should keep in mind that AI/ML-based models are simply medical tools that, similar to all medical tools, have weaknesses, biases, and limitations. Overelining on AI could exclude non-quantifiable information from decision-making, with unknown ramifications[194]. AI should not subsume out critical thinking and reasoning. The aim should therefore be an AI-assisted rather than an AI-driven clinical practice[201]. Furthermore, the integration of AI in healthcare must occur in conjunction with integrating sophisticated and robust evaluation tools that monitor the consequences of AI application in the clinical setting, and more importantly, the impact of these tools on patient outcomes[202]. A notable example is the Digital Health Innovation Action Plan supported by the FDA to facilitate the evaluation of developing medical software. It is based on the following five excellence criteria: Patient safety, product quality, proactive culture, cybersecurity responsibility, and clinical responsibility[203].

Finally, an intriguing challenge for the future is to combine emerging technologies, including 3D printing and 3D bioprinting, AI and ML, augmented reality, novel biomarkers, and robotics, into a unified, interrelated framework[204-208]. In this new, complex, and sophisticated clinical setting, physicians would reject oversimplifying an inherently complex field but rather embrace the complexity. Finally, are shown by our findings, AI and 3D printing applications in healthcare are steadily expanding; thus, these technologies will be integrated into the clinical setting sooner or later. Therefore, we believe that physicians need to become familiar with these technologies and prepare to engage with them constructively.

ACKNOWLEDGEMENTS

The authors declare no conflict of interest for this article. The authors received no specific funding for this work.

FOOTNOTES

Author contributions: Christou CD performed the screening of articles for eligibility and drafted the manuscript; Tsoulfas G performed the screening of articles for eligibility and edited the manuscript.

Conflict-of-interest statement: The authors declare no conflict of interest for this article. The authors received no specific funding for this work.

Country/Territory of origin: Greece

ORCID number: Chrysanthos D Christou 0000-0002-5417-8686; Georgios Tsoulfas 0000-0001-5043-7962.

Corresponding Author's Membership in Professional Societies: American Association of Transplant Surgeons; American Gastroenterological Association; American Society of Transplantation; American Hepatico Pancreatico Biliary Association (AHPBA); International Liver Transplantation Society; American College of Surgeons.

S-Editor: Wang JJ
L-Editor: Webster JR
P-Editor: Wang JJ

REFERENCES

1 **Ferlay J**, Soerjomataram I, Dikshit R, Eser S, Mathers C, Rebelo M, Parkin DM, Forman D, Bray F. Cancer incidence and mortality worldwide: sources, methods and major patterns in GLOBOCAN 2012. *Int J Cancer* 2015; **136**: E359-E386 [PMID: 25220842 DOI: 10.1002/ijc.29210]
2 **Yang JD**, Hainaut P, Gores GJ, Amadou A, Plymoth A, Roberts LR. A global view of hepatocellular carcinoma: trends, risk, prevention and management. *Nat Rev Gastroenterol Hepatol* 2019; **16**: 589-604 [PMID: 31439937 DOI: 10.1038/s41575-019-0186-y]
3 **Heimbach JK**, Kulik LM, Finn RS, Sirlin CB, Abecassis MM, Roberts LR, Zhu AX, Murad MH, Marrero JA. AASLD guidelines for the treatment of hepatocellular carcinoma. *Hepatology* 2018; **67**: 358-380 [PMID: 28130846 DOI: 10.1002/hep.29086]
4 **Mitchell DG**, Bruix J, Sherman M, Sirlin CB. LI-RADS (Liver Imaging Reporting and Data System): summary, discussion, and consensus of the LI-RADS Management Working Group and future directions. *Hepatology* 2015; **61**: 1056-1065 [PMID: 25041904 DOI: 10.1002/hep.27304]
5 **European Association for the Study of the Liver**. EASL Clinical Practice Guidelines: Management of hepatocellular carcinoma. *J Hepatol* 2018; **69**: 182-236 [PMID: 29628281 DOI: 10.1016/j.jhep.2018.03.019]
6 **Cillo U**, Vitale A, Grigoletto F, Farinati F, Brolese A, Zanus G, Neri D, Boccagni P, Srsen N, D'Amico F, Ciarleglio FA, Bridda A, D'Amico DF. Prospective validation of the Barcelona Clinic Liver Cancer staging system. *J Hepatol* 2006; **44**: 723-731 [PMID: 16488051 DOI: 10.1016/j.jhep.2005.12.015]
7 **Reig M**, Darnell A, Forner A, Rimola J, Ayuso C, Bruix J. Systemic therapy for hepatocellular carcinoma: the issue of treatment stage migration and registration of progression using the BCLC-refined RECIST. *Semin Liver Dis* 2014; **34**: 444-455 [PMID: 25369306 DOI: 10.1055/s-0034-1394143]
8 **Roberts SK**, Gazzola A, Lubel J, Gow P, Bell S, Nicoll A, Dev A, Fink MA, Sood S, Knight V, Hong T, Paul E, Mishra G, Majeed A, Kemp W; Melbourne Liver Group. Treatment choice for early-stage hepatocellular carcinoma in real-world practice: impact of treatment stage migration to transarterial chemoembolization and treatment response on survival. *Scand J Gastroenterol* 2018; **53**: 1368-1375 [PMID: 30394145 DOI: 10.1080/00365521.2018.1517277]
9 **Mitsouras D**, Liacouras P, Imanzadeh A, Giannopoulos AA, Cai T, Kumamaru KK, George E, Wake N, Caterson EJ, Pomahac B, Ho VB, Grant GT, Rybicki FJ. Medical 3D Printing for the Radiologist. *Radiographics* 2015; **35**: 1965-1988 [PMID: 26562233 DOI: 10.1148/rg.2015140320]
10 **Pietrabissa A**, Marconi S, Negrello E, Mauri V, Peri A, Pugliese L, Marone EM, Auricchio F. An overview on 3D printing for abdominal surgery. *Surg Endosc* 2020; **34**: 1-13 [PMID: 31605218 DOI: 10.1007/s00464-019-07155-5]
11 **Mironov V**, Boland T, Trusk T, Forgacs G, Markwald RR. Organ printing: computer-aided jet-based 3D tissue engineering. *Trends Biotechnol* 2003; **21**: 157-161 [PMID: 12679063 DOI: 10.1016/S0167-7799(03)00033-7]
12 **Zadpoor AA**, Malda J. Additive Manufacturing of Biomaterials, Tissues, and Organs. *Ann Biomed Eng* 2017; **45**: 1-11 [PMID: 27632024 DOI: 10.1007/s10439-016-1719-y]
13 **Melchels FPW**, Domingos MAN, Klein TJ, Malda J, Bartolo PJ, Hutmacher DW. Additive manufacturing of tissues and organs. *Prog Polym Sci* 2012; **37**: 1079-1104 [DOI: 10.1016/j.progpolymsci.2011.11.007]
14 **Trends in China, Europe, and the United States**. Artificial Intelligence: How knowledge is created, transferred, and used. In: Artificial Intelligence: a multifaceted field. Amsterdam: Elsevier. 2018: 24-27
15 **Russell SJ**, Norvig P. Artificial intelligence: a modern approach. 2021
16 **Cruz JA**, Wishart DS. Applications of machine learning in cancer prediction and prognosis. *Cancer Inform* 2007; **2**: 59-77 [PMID: 19458758]
17 **Statista**. Total amount of global healthcare data generated in 2013 and a projection for 2020. [cited 1 April 2021]. Available from: https://www.statista.com/statistics/1037970/global-healthcare-data-volume/
18 **Tsoulfas G**, Bangeas PI, Suri JS. 3D Printing: Applications in Medicine and Surgery. In: Ziogas IA, Zein NN, Quintini C, Miller CM, Tsoulfas G. Three-dimensional (3D) printing and liver transplantation. Amsterdam: Elsevier. 2020: 97-116 [DOI: 10.1016/B978-0-323-66164-5.00007-6]
19 **Watson RA**. A low-cost surgical application of additive fabrication. *J Surg Educ* 2014; **71**: 14-17 [PMID: 24411417 DOI: 10.1016/j.jsurg.2013.10.012]
20 **Yang T**, Tan T, Yang J, Pan J, Hu C, Li J, Zou Y. The impact of using three-dimensional printed liver models for patient education. *J Int Med Res* 2018; **46**: 1570-1578 [PMID: 29436243 DOI: 10.1177/0300060518755267]
21 **Yang T**, Lin S, Xie Q, Ouyang W, Tan T, Li J, Chen Z, Yang J, Wu H, Pan J, Hu C, Zou Y. Impact of 3D printing technology on the comprehension of surgical liver anatomy. *Surg Endosc* 2019; **33**: 411-417 [PMID: 29943060 DOI: 10.1007/s00464-018-6308-8]
22 **Tang R**, Ma L, Li A, Yu L, Rong Z, Zhang X, Xiang C, Liao H, Dong J. Choledochoscopic Examination of a 3-Dimensional Printing Model Using Augmented Reality Techniques: A Preliminary Proof of Concept Study. *Surg Innov*

2018; **25**: 492-498 [PMID: 29909727 DOI: 10.1177/1553350618781622]
23 **Burdall OC**, Makin E, Davenport M, Ade-Ajayi N. 3D printing to simulate laparoscopic choledochal surgery. *J Pediatr Surg* 2016; **51**: 828-831 [PMID: 27085850 DOI: 10.1016/j.jpedsurg.2016.02.093]
24 **Streba CT**, Popescu S, Pirici D, Gheonea IA, Vlădaia M, Ungureanu BS, Gheonea DI, Ţenea-Cojan TŞ. Three-dimensional printing of liver tumors using CT data: proof of concept morphological study. *Rom J Morphol Embryol* 2018; **59**: 885-893 [PMID: 30534830]
25 **Zein NN**, Hanouneh IA, Bishop PD, Samaan M, Eghtesad B, Quintini C, Miller C, Yerian L, Klatte R. Three-dimensional print of a liver for preoperative planning in living donor liver transplantation. *Liver Transpl* 2013; **19**: 1304-1310 [PMID: 23959637 DOI: 10.1002/lt.23729]
26 **Oshiro Y**, Mitani J, Okada T, Ohkohchi N. A novel three-dimensional print of liver vessels and tumors in hepatectomy. *Surg Today* 2017; **47**: 521-524 [PMID: 27456277 DOI: 10.1007/s00595-016-1383-8]
27 **Igami T**, Nakamura Y, Hirose T, Ebata T, Yokoyama Y, Sugawara G, Mizuno T, Mori K, Nagino M. Application of a three-dimensional print of a liver in hepatectomy for small tumors invisible by intraoperative ultrasonography: preliminary experience. *World J Surg* 2014; **38**: 3163-3166 [PMID: 25145821 DOI: 10.1007/s00268-014-2740-7]
28 **Javan R**, Zeman MN. A Prototype Educational Model for Hepatobiliary Interventions: Unveiling the Role of Graphic Designers in Medical 3D Printing. *J Digit Imaging* 2018; **31**: 133-143 [PMID: 28808803 DOI: 10.1007/s10278-017-0012-4]
29 **Baimakhanov Z**, Soyama A, Takatsuki M, Hidaka M, Hirayama T, Kinoshita A, Natsuda K, Kuroki T, Eguchi S. Preoperative simulation with a 3-dimensional printed solid model for one-step reconstruction of multiple hepatic veins during living donor liver transplantation. *Liver Transpl* 2015; **21**: 266-268 [PMID: 25302632 DOI: 10.1002/lt.24019]
30 **Madurska MJ**, Poyade M, Eason D, Rea P, Watson AJ. Development of a Patient-Specific 3D-Printed Liver Model for Preoperative Planning. *Surg Innov* 2017; **24**: 145-150 [PMID: 28134003 DOI: 10.1177/1553350616689414]
31 **Xiang N**, Fang C, Fan Y, Yang J, Zeng N, Liu J, Zhu W. Application of liver three-dimensional printing in hepatectomy for complex massive hepatocarcinoma with rare variations of portal vein: preliminary experience. *Int J Clin Exp Med* 2015; **8**: 18873-18878 [PMID: 26770510]
32 **Perica E**, Sun Z. Patient-specific three-dimensional printing for pre-surgical planning in hepatocellular carcinoma treatment. *Quant Imaging Med Surg* 2017; **7**: 668-677 [PMID: 29312871 DOI: 10.21037/qims.2017.11.02]
33 **Kuroda S**, Kobayashi T, Ohdan H. 3D printing model of the intrahepatic vessels for navigation during anatomical resection of hepatocellular carcinoma. *Int J Surg Case Rep* 2017; **41**: 219-222 [PMID: 29096348 DOI: 10.1016/j.ijscr.2017.10.015]
34 **Witowski J**, Budzyński A, Grochowska A, Ballard DH, Major P, Rubinkiewicz M, Złahoda-Huzior A, Popiela TJ, Wierdak M, Pędziwiatr M. Decision-making based on 3D printed models in laparoscopic liver resections with intraoperative ultrasound: a prospective observational study. *Eur Radiol* 2020; **30**: 1306-1312 [PMID: 31773294 DOI: 10.1007/s00330-019-06511-2]
35 **Damiati S**, Küpcü S, Peacock M, Eilenberger C, Zamzami M, Qadri I, Choudhry H, Sleytr UB, Schuster B. Acoustic and hybrid 3D-printed electrochemical biosensors for the real-time immunodetection of liver cancer cells (HepG2). *Biosens Bioelectron* 2017; **94**: 500-506 [PMID: 28343102 DOI: 10.1016/j.bios.2017.03.045]
36 **Joo I**, Kim JH, Park SJ, Lee K, Yi NJ, Han JK. Personalized 3D-Printed Transparent Liver Model Using the Hepatobiliary Phase MRI: Usefulness in the Lesion-by-Lesion Imaging-Pathologic Matching of Focal Liver Lesions-Preliminary Results. *Invest Radiol* 2019; **54**: 138-145 [PMID: 30379728 DOI: 10.1097/RLI.0000000000000521]
37 **Trout AT**, Batie MR, Gupta A, Sheridan RM, Tiao GM, Towbin AJ. 3D printed pathological sectioning boxes to facilitate radiological-pathological correlation in hepatectomy cases. *J Clin Pathol* 2017; **70**: 984-987 [PMID: 28596154 DOI: 10.1136/jclinpath-2016-204293]
38 **Han T**, Yang X, Xu Y, Zheng Z, Yan Y, Wang N. Therapeutic value of 3-D printing template-assisted ^{125}I-seed implantation in the treatment of malignant liver tumors. *Onco Targets Ther* 2017; **10**: 3277-3283 [PMID: 28740402 DOI: 10.2147/OTT.S134290]
39 **Wang Z**, Chapiro J, Schernthaner R, Duran R, Chen R, Geschwind JF, Lin M. Multimodality 3D Tumor Segmentation in HCC Patients Treated with TACE. *Acad Radiol* 2015; **22**: 840-845 [PMID: 25863795 DOI: 10.1016/j.acra.2015.03.001]
40 **Liapi E**, Hong K, Georgiades CS, Geschwind JF. Three-dimensional rotational angiography: introduction of an adjunctive tool for successful transarterial chemoembolization. *J Vasc Interv Radiol* 2005; **16**: 1241-1245 [PMID: 16151066 DOI: 10.1097/01.RVI.0000174283.03032.8E]
41 **Yao R**, Xu G, Mao SS, Yang HY, Sang XT, Sun W, Mao YL. Three-dimensional printing: review of application in medicine and hepatic surgery. *Cancer Biol Med* 2016; **13**: 443-451 [PMID: 28154775 DOI: 10.20892/j.issn.2095-3941.2016.0075]
42 **Datta P**, Barui A, Wu Y, Ozbolat V, Moncal KK, Ozbolat IT. Essential steps in bioprinting: From pre- to post-bioprinting. *Biotechnol Adv* 2018; **36**: 1481-1504 [PMID: 29909085 DOI: 10.1016/j.biotechadv.2018.06.003]
43 **Xie F**, Sun L, Pang Y, Xu G, Jin B, Xu H, Lu X, Xu Y, Du S, Wang Y, Feng S, Sang X, Zhong S, Wang X, Sun W, Zhao H, Zhang H, Yang H, Huang P, Mao Y. Three-dimensional bio-printing of primary human hepatocellular carcinoma for personalized medicine. *Biomaterials* 2021; **265**: 120416 [PMID: 33007612 DOI: 10.1016/j.biomaterials.2020.120416]
44 **Zhang X**, Morits M, Jonkergouw C, Ora A, Valle-Delgado JJ, Farooq M, Ajdary R, Huan S, Linder M, Rojas O, Sipponen MH, Österberg M. Three-Dimensional Printed Cell Culture Model Based on Spherical Colloidal Lignin Particles and Cellulose Nanofibril-Alginate Hydrogel. *Biomacromolecules* 2020; **21**: 1875-1885 [PMID: 31992046 DOI: 10.1021/acs.biomac.9b01745]
45 **Sun L**, Yang H, Wang Y, Zhang X, Jin B, Xie F, Jin Y, Pang Y, Zhao H, Lu X, Sang X, Zhang H, Lin F, Sun W, Huang P, Mao Y. Application of a 3D Bioprinted Hepatocellular Carcinoma Cell Model in Antitumor Drug Research. *Front Oncol* 2020; **10**: 878 [PMID: 32582546 DOI: 10.3389/fonc.2020.00878]
46 **Ma X**, Yu C, Wang P, Xu W, Wan X, Lai CSE, Liu J, Koroleva-Maharajh A, Chen S. Rapid 3D bioprinting of decellularized extracellular matrix with regionally varied mechanical properties and biomimetic microarchitecture. *Biomaterials* 2018; **185**: 310-321 [PMID: 30265900 DOI: 10.1016/j.biomaterials.2018.09.026]

47 **Wang J**, Jain S, Chen D, Song W, Hu CT, Su YH. Development and Evaluation of Novel Statistical Methods in Urine Biomarker-Based Hepatocellular Carcinoma Screening. *Sci Rep* 2018; **8**: 3799 [PMID: 29491388 DOI: 10.1038/s41598-018-21922-9]

48 **Nam JY**, Sinn DH, Bae J, Jang ES, Kim JW, Jeong SH. Deep learning model for prediction of hepatocellular carcinoma in patients with HBV-related cirrhosis on antiviral therapy. *JHEP Rep* 2020; **2**: 100175 [PMID: 33117971 DOI: 10.1016/j.jhepr.2020.100175]

49 **Xia Q**, Shu Z, Ye T, Zhang M. Identification and Analysis of the Blood lncRNA Signature for Liver Cirrhosis and Hepatocellular Carcinoma. *Front Genet* 2020; **11**: 595699 [PMID: 33365048 DOI: 10.3389/fgene.2020.595699]

50 **Chen S**, Zhang Z, Wang Y, Fang M, Zhou J, Li Y, Dai E, Feng Z, Wang H, Yang Z, Huang X, Jia J, Li S, Huang C, Tong L, Xiao X, He Y, Duan Y, Zhu S, Gao C. Using Quasispecies Patterns of Hepatitis B Virus to Predict Hepatocellular Carcinoma With Deep Sequencing and Machine Learning. *J Infect Dis* 2021; **223**: 1887-1896 [PMID: 33049037 DOI: 10.1093/infdis/jiaa647]

51 **Hashem S**, ElHefnawi M, Habashy S, El-Adawy M, Esmat G, Elakel W, Abdelazziz AO, Nabeel MM, Abdelmaksoud AH, Elbaz TM, Shousha HI. Machine Learning Prediction Models for Diagnosing Hepatocellular Carcinoma with HCV-related Chronic Liver Disease. *Comput Methods Programs Biomed* 2020; **196**: 105551 [PMID: 32580053 DOI: 10.1016/j.cmpb.2020.105551]

52 **Audureau E**, Carrat F, Layese R, Cagnot C, Asselah T, Guyader D, Larrey D, De Lédinghen V, Ouzan D, Zoulim F, Roulot D, Tran A, Bronowicki JP, Zarski JP, Riachi G, Calès P, Péron JM, Alric L, Bourlière M, Mathurin P, Blanc JF, Abergel A, Chazouillères O, Mallat A, Grangé JD, Attali P, d'Alteroche L, Wartelle C, Dao T, Thabut D, Pilette C, Silvain C, Christidis C, Nguyen-Khac E, Bernard-Chabert B, Zucman D, Di Martino V, Sutton A, Pol S, Nahon P; ANRS CO12 CirVir group. Personalized surveillance for hepatocellular carcinoma in cirrhosis - using machine learning adapted to HCV status. *J Hepatol* 2020; **73**: 1434-1445 [PMID: 32615276 DOI: 10.1016/j.jhep.2020.05.052]

53 **Ioannou GN**, Tang W, Beste LA, Tincopa MA, Su GL, Van T, Tapper EB, Singal AG, Zhu J, Waljee AK. Assessment of a Deep Learning Model to Predict Hepatocellular Carcinoma in Patients With Hepatitis C Cirrhosis. *JAMA Netw Open* 2020; **3**: e2015626 [PMID: 32870314 DOI: 10.1001/jamanetworkopen.2020.15626]

54 **Singal AG**, Mukherjee A, Elmunzer BJ, Higgins PD, Lok AS, Zhu J, Marrero JA, Waljee AK. Machine learning algorithms outperform conventional regression models in predicting development of hepatocellular carcinoma. *Am J Gastroenterol* 2013; **108**: 1723-1730 [PMID: 24169273 DOI: 10.1038/ajg.2013.332]

55 **Sato M**, Morimoto K, Kajihara S, Tateishi R, Shiina S, Koike K, Yatomi Y. Machine-learning Approach for the Development of a Novel Predictive Model for the Diagnosis of Hepatocellular Carcinoma. *Sci Rep* 2019; **9**: 7704 [PMID: 31147560 DOI: 10.1038/s41598-019-44022-8]

56 **Zhao X**, Dou J, Cao J, Wang Y, Gao Q, Zeng Q, Liu W, Liu B, Cui Z, Teng L, Zhang J, Zhao C. Uncovering the potential differentially expressed miRNAs as diagnostic biomarkers for hepatocellular carcinoma based on machine learning in The Cancer Genome Atlas database. *Oncol Rep* 2020; **43**: 1771-1784 [PMID: 32236623 DOI: 10.3892/or.2020.7551]

57 **Zhang ZM**, Tan JX, Wang F, Dao FY, Zhang ZY, Lin H. Early Diagnosis of Hepatocellular Carcinoma Using Machine Learning Method. *Front Bioeng Biotechnol* 2020; **8**: 254 [PMID: 32292778 DOI: 10.3389/fbioe.2020.00254]

58 **Tao K**, Bian Z, Zhang Q, Guo X, Yin C, Wang Y, Zhou K, Wan S, Shi M, Bao D, Yang C, Xing J. Machine learning-based genome-wide interrogation of somatic copy number aberrations in circulating tumor DNA for early detection of hepatocellular carcinoma. *EBioMedicine* 2020; **56**: 102811 [PMID: 32512514 DOI: 10.1016/j.ebiom.2020.102811]

59 **Li G**, Shi H, Wang X, Wang B, Qu Q, Geng H, Sun H. Identification of diagnostic long noncoding RNA biomarkers in patients with hepatocellular carcinoma. *Mol Med Rep* 2019; **20**: 1121-1130 [PMID: 31173205 DOI: 10.3892/mmr.2019.10307]

60 **Schmauch B**, Herent P, Jehanno P, Dehaene O, Saillard C, Aubé C, Luciani A, Lassau N, Jégou S. Diagnosis of focal liver lesions from ultrasound using deep learning. *Diagn Interv Imaging* 2019; **100**: 227-233 [PMID: 30926443 DOI: 10.1016/j.diii.2019.02.009]

61 **Yang Q**, Wei J, Hao X, Kong D, Yu X, Jiang T, Xi J, Cai W, Luo Y, Jing X, Yang Y, Cheng Z, Wu J, Zhang H, Liao J, Zhou P, Song Y, Zhang Y, Han Z, Cheng W, Tang L, Liu F, Dou J, Zheng R, Yu J, Tian J, Liang P. Improving B-mode ultrasound diagnostic performance for focal liver lesions using deep learning: A multicentre study. *EBioMedicine* 2020; **56**: 102777 [PMID: 32485640 DOI: 10.1016/j.ebiom.2020.102777]

62 **Virmani J**, Kumar V, Kalra N, Khandelwal N. Neural network ensemble based CAD system for focal liver lesions from B-mode ultrasound. *J Digit Imaging* 2014; **27**: 520-537 [PMID: 24687642 DOI: 10.1007/s10278-014-9685-0]

63 **Shiraishi J**, Sugimoto K, Moriyasu F, Kamiyama N, Doi K. Computer-aided diagnosis for the classification of focal liver lesions by use of contrast-enhanced ultrasonography. *Med Phys* 2008; **35**: 1734-1746 [PMID: 18561648 DOI: 10.1118/1.2900109]

64 **Zhou J**, Wang W, Lei B, Ge W, Huang Y, Zhang L, Yan Y, Zhou D, Ding Y, Wu J. Automatic Detection and Classification of Focal Liver Lesions Based on Deep Convolutional Neural Networks: A Preliminary Study. *Front Oncol* 2020; **10**: 581210 [PMID: 33585197 DOI: 10.3389/fonc.2020.581210]

65 **Yasaka K**, Akai H, Abe O, Kiryu S. Deep Learning with Convolutional Neural Network for Differentiation of Liver Masses at Dynamic Contrast-enhanced CT: A Preliminary Study. *Radiology* 2018; **286**: 887-896 [PMID: 29059036 DOI: 10.1148/radiol.2017170706]

66 **Shi W**, Kuang S, Cao S, Hu B, Xie S, Chen S, Chen Y, Gao D, Zhu Y, Zhang H, Liu H, Ye M, Sirlin CB, Wang J. Deep learning assisted differentiation of hepatocellular carcinoma from focal liver lesions: choice of four-phase and three-phase CT imaging protocol. *Abdom Radiol (NY)* 2020; **45**: 2688-2697 [PMID: 32232524 DOI: 10.1007/s00261-020-02485-8]

67 **Todoroki Y**, Iwamoto Y, Lin L, Hu H, Chen YW. Automatic Detection of Focal Liver Lesions in Multi-phase CT Images Using A Multi-channel & Multi-scale CNN. *Annu Int Conf IEEE Eng Med Biol Soc* 2019; **2019**: 872-875 [PMID: 31946033 DOI: 10.1109/EMBC.2019.8857292]

68 **Matake K**, Yoshimitsu K, Kumazawa S, Higashida Y, Irie H, Asayama Y, Nakayama T, Kakihara D, Katsuragawa S, Doi K, Honda H. Usefulness of artificial neural network for differential diagnosis of hepatic masses on CT images. *Acad Radiol* 2006; **13**: 951-962 [PMID: 16843847 DOI: 10.1016/j.acra.2006.04.009]

69 **Liang W**, Shao J, Liu W, Ruan S, Tian W, Zhang X, Wan D, Huang Q, Ding Y, Xiao W. Differentiating Hepatic Epithelioid Angiomyolipoma From Hepatocellular Carcinoma and Focal Nodular Hyperplasia *via* Radiomics Models. *Front Oncol* 2020; **10**: 564307 [PMID: 33123475 DOI: 10.3389/fonc.2020.564307]

70 **Hamm CA**, Wang CJ, Savic LJ, Ferrante M, Schobert I, Schlachter T, Lin M, Duncan JS, Weinreb JC, Chapiro J, Letzen B. Deep learning for liver tumor diagnosis part I: development of a convolutional neural network classifier for multi-phasic MRI. *Eur Radiol* 2019; **29**: 3338-3347 [PMID: 31016442 DOI: 10.1007/s00330-019-06205-9]

71 **Wang CJ**, Hamm CA, Savic LJ, Ferrante M, Schobert I, Schlachter T, Lin M, Weinreb JC, Duncan JS, Chapiro J, Letzen B. Deep learning for liver tumor diagnosis part II: convolutional neural network interpretation using radiologic imaging features. *Eur Radiol* 2019; **29**: 3348-3357 [PMID: 31093705 DOI: 10.1007/s00330-019-06214-8]

72 **Jansen MJA**, Kuijf HJ, Veldhuis WB, Wessels FJ, Viergever MA, Pluim JPW. Automatic classification of focal liver lesions based on MRI and risk factors. *PLoS One* 2019; **14**: e0217053 [PMID: 31095624 DOI: 10.1371/journal.pone.0217053]

73 **Zhen SH**, Cheng M, Tao YB, Wang YF, Juengpanich S, Jiang ZY, Jiang YK, Yan YY, Lu W, Lue JM, Qian JH, Wu ZY, Sun JH, Lin H, Cai XJ. Deep Learning for Accurate Diagnosis of Liver Tumor Based on Magnetic Resonance Imaging and Clinical Data. *Front Oncol* 2020; **10**: 680 [PMID: 32547939 DOI: 10.3389/fonc.2020.00680]

74 **Kiani A**, Uyumazturk B, Rajpurkar P, Wang A, Gao R, Jones E, Yu Y, Langlotz CP, Ball RL, Montine TJ, Martin BA, Berry GJ, Ozawa MG, Hazard FK, Brown RA, Chen SB, Wood M, Allard LS, Ylagan L, Ng AY, Shen J. Impact of a deep learning assistant on the histopathologic classification of liver cancer. *NPJ Digit Med* 2020; **3**: 23 [PMID: 32140566 DOI: 10.1038/s41746-020-0232-8]

75 **Chen M**, Zhang B, Topatana W, Cao J, Zhu H, Juengpanich S, Mao Q, Yu H, Cai X. Classification and mutation prediction based on histopathology H&E images in liver cancer using deep learning. *NPJ Precis Oncol* 2020; **4**: 14 [PMID: 32550270 DOI: 10.1038/s41698-020-0120-3]

76 **Lin H**, Wei C, Wang G, Chen H, Lin L, Ni M, Chen J, Zhuo S. Automated classification of hepatocellular carcinoma differentiation using multiphoton microscopy and deep learning. *J Biophotonics* 2019; **12**: e201800435 [PMID: 30868728 DOI: 10.1002/jbio.201800435]

77 **Yamashita R**, Long J, Saleem A, Rubin DL, Shen J. Deep learning predicts postsurgical recurrence of hepatocellular carcinoma from digital histopathologic images. *Sci Rep* 2021; **11**: 2047 [PMID: 33479370 DOI: 10.1038/s41598-021-81506-y]

78 **Roy M**, Kong J, Kashyap S, Pastore VP, Wang F, Wong KCL, Mukherjee V. Convolutional autoencoder based model HistoCAE for segmentation of viable tumor regions in liver whole-slide images. *Sci Rep* 2021; **11**: 139 [PMID: 33420322 DOI: 10.1038/s41598-020-80610-9]

79 **Giordano S**, Takeda S, Donadon M, Saiki H, Brunelli L, Pastorelli R, Cimino M, Soldani C, Franceschini B, Di Tommaso L, Lleo A, Yoshimura K, Nakajima H, Torzilli G, Davoli E. Rapid automated diagnosis of primary hepatic tumour by mass spectrometry and artificial intelligence. *Liver Int* 2020; **40**: 3117-3124 [PMID: 32662575 DOI: 10.1111/liv.14604]

80 **Guo LH**, Wang D, Qian YY, Zheng X, Zhao CK, Li XL, Bo XW, Yue WW, Zhang Q, Shi J, Xu HX. A two-stage multi-view learning framework based computer-aided diagnosis of liver tumors with contrast enhanced ultrasound images. *Clin Hemorheol Microcirc* 2018; **69**: 343-354 [PMID: 29630528 DOI: 10.3233/CH-170275]

81 **Bharti P**, Mittal D, Ananthasivan R. Preliminary Study of Chronic Liver Classification on Ultrasound Images Using an Ensemble Model. *Ultrason Imaging* 2018; **40**: 357-379 [PMID: 30015593 DOI: 10.1177/0161734618787447]

82 **Brehar R**, Mitrea DA, Vancea F, Marita T, Nedevschi S, Lupsor-Platon M, Rotaru M, Badea RI. Comparison of Deep-Learning and Conventional Machine-Learning Methods for the Automatic Recognition of the Hepatocellular Carcinoma Areas from Ultrasound Images. *Sensors (Basel)* 2020; **20** [PMID: 32485986 DOI: 10.3390/s20113085]

83 **Mao B**, Ma J, Duan S, Xia Y, Tao Y, Zhang L. Preoperative classification of primary and metastatic liver cancer *via* machine learning-based ultrasound radiomics. *Eur Radiol* 2021; **31**: 4576-4586 [PMID: 33447862 DOI: 10.1007/s00330-020-07562-6]

84 **Almotairi S**, Kareem G, Aouf M, Almutairi B, Salem MA. Liver Tumor Segmentation in CT Scans Using Modified SegNet. *Sensors (Basel)* 2020; **20** [PMID: 32164153 DOI: 10.3390/s20051516]

85 **Budak Ü**, Guo Y, Tanyildizi E, Şengür A. Cascaded deep convolutional encoder-decoder neural networks for efficient liver tumor segmentation. *Med Hypotheses* 2020; **134**: 109431 [PMID: 31669758 DOI: 10.1016/j.mehy.2019.109431]

86 **Nayak A**, Baidya Kayal E, Arya M, Culli J, Krishan S, Agarwal S, Mehndiratta A. Computer-aided diagnosis of cirrhosis and hepatocellular carcinoma using multi-phase abdomen CT. *Int J Comput Assist Radiol Surg* 2019; **14**: 1341-1352 [PMID: 31062266 DOI: 10.1007/s11548-019-01991-5]

87 **Krishan A**, Mittal D. Ensembled liver cancer detection and classification using CT images. *Proc Inst Mech Eng H* 2021; **235**: 232-244 [PMID: 33183141 DOI: 10.1177/0954411920971888]

88 **Chen WF**, Ou HY, Liu KH, Li ZY, Liao CC, Wang SY, Huang W, Cheng YF, Pan CT. In-Series U-Net Network to 3D Tumor Image Reconstruction for Liver Hepatocellular Carcinoma Recognition. *Diagnostics (Basel)* 2020; **11** [PMID: 33374672 DOI: 10.3390/diagnostics11010011]

89 **Khan AA**, Narejo GB. Analysis of Abdominal Computed Tomography Images for Automatic Liver Cancer Diagnosis Using Image Processing Algorithm. *Curr Med Imaging Rev* 2019; **15**: 972-982 [PMID: 32008524 DOI: 10.2174/1573405615666190716122040]

90 **Mokrane FZ**, Lu L, Vavasseur A, Otal P, Peron JM, Luk L, Yang H, Ammari S, Saenger Y, Rousseau H, Zhao B, Schwartz LH, Dercle L. Radiomics machine-learning signature for diagnosis of hepatocellular carcinoma in cirrhotic patients with indeterminate liver nodules. *Eur Radiol* 2020; **30**: 558-570 [PMID: 31444598 DOI: 10.1007/s00330-019-06347-w]

91 **Mao B**, Zhang L, Ning P, Ding F, Wu F, Lu G, Geng Y, Ma J. Preoperative prediction for pathological grade of hepatocellular carcinoma *via* machine learning-based radiomics. *Eur Radiol* 2020; **30**: 6924-6932 [PMID: 32696256 DOI: 10.1007/s00330-020-07056-5]

92 **Preis O**, Blake MA, Scott JA. Neural network evaluation of PET scans of the liver: a potentially useful adjunct in clinical interpretation. *Radiology* 2011; **258**: 714-721 [PMID: 21339347 DOI: 10.1148/radiol.10100547]

93 **Trivizakis E**, Manikis GC, Nikiforaki K, Drevelegas K, Constantinides M, Drevelegas A, Marias K. Extending 2-D Convolutional Neural Networks to 3-D for Advancing Deep Learning Cancer Classification With Application to MRI Liver Tumor Differentiation. *IEEE J Biomed Health Inform* 2019; **23**: 923-930 [PMID: 30561355 DOI: 10.1109/JBHI.2018.2886276]

94 **Oestmann PM**, Wang CJ, Savic LJ, Hamm CA, Stark S, Schobert I, Gebauer B, Schlachter T, Lin M, Weinreb JC, Batra R, Mulligan D, Zhang X, Duncan JS, Chapiro J. Deep learning-assisted differentiation of pathologically proven atypical and typical hepatocellular carcinoma (HCC) versus non-HCC on contrast-enhanced MRI of the liver. *Eur Radiol* 2021; **31**: 4981-4990 [PMID: 33409782 DOI: 10.1007/s00330-020-07559-1]

95 **Bousabarah K**, Letzen B, Tefera J, Savic L, Schobert I, Schlachter T, Staib LH, Kocher M, Chapiro J, Lin M. Automated detection and delineation of hepatocellular carcinoma on multiphasic contrast-enhanced MRI using deep learning. *Abdom Radiol (NY)* 2021; **46**: 216-225 [PMID: 32500237 DOI: 10.1007/s00261-020-02604-5]

96 **Kim J**, Min JH, Kim SK, Shin SY, Lee MW. Detection of Hepatocellular Carcinoma in Contrast-Enhanced Magnetic Resonance Imaging Using Deep Learning Classifier: A Multi-Center Retrospective Study. *Sci Rep* 2020; **10**: 9458 [PMID: 32527998 DOI: 10.1038/s41598-020-65875-4]

97 **Jian W**, Ju H, Cen X, Cui M, Zhang H, Zhang L, Wang G, Gu L, Zhou W. Improving the malignancy characterization of hepatocellular carcinoma using deeply supervised cross modal transfer learning for non-enhanced MR. *Annu Int Conf IEEE Eng Med Biol Soc* 2019; **2019**: 853-856 [PMID: 31946029 DOI: 10.1109/EMBC.2019.8857467]

98 **Wu Y**, White GM, Cornelius T, Gowdar I, Ansari MH, Supanich MP, Deng J. Deep learning LI-RADS grading system based on contrast enhanced multiphase MRI for differentiation between LR-3 and LR-4/LR-5 liver tumors. *Ann Transl Med* 2020; **8**: 701 [PMID: 32617321 DOI: 10.21037/atm.2019.12.151]

99 **Tsilimigras DI**, Mehta R, Moris D, Sahara K, Bagante F, Paredes AZ, Farooq A, Ratti F, Marques HP, Silva S, Soubrane O, Lam V, Poultsides GA, Popescu I, Grigorie R, Alexandrescu S, Martel G, Workneh A, Guglielmi A, Hugh T, Aldrighetti L, Endo I, Pawlik TM. Utilizing Machine Learning for Pre- and Postoperative Assessment of Patients Undergoing Resection for BCLC-0, A and B Hepatocellular Carcinoma: Implications for Resection Beyond the BCLC Guidelines. *Ann Surg Oncol* 2020; **27**: 866-874 [PMID: 31696396 DOI: 10.1245/s10434-019-08025-z]

100 **Liu F**, Liu D, Wang K, Xie X, Su L, Kuang M, Huang G, Peng B, Wang Y, Lin M, Tian J. Deep Learning Radiomics Based on Contrast-Enhanced Ultrasound Might Optimize Curative Treatments for Very-Early or Early-Stage Hepatocellular Carcinoma Patients. *Liver Cancer* 2020; **9**: 397-413 [PMID: 32999867 DOI: 10.1159/000505694]

101 **Choi GH**, Yun J, Choi J, Lee D, Shim JH, Lee HC, Chung YH, Lee YS, Park B, Kim N, Kim KM. Development of machine learning-based clinical decision support system for hepatocellular carcinoma. *Sci Rep* 2020; **10**: 14855 [PMID: 32908183 DOI: 10.1038/s41598-020-71796-z]

102 **Christou CD**, Tooulias A, Tsolakidis A, Papayiannis V, Pianetcki-Tsiantzi B, Tsoulfas G, Papadopoulos VN. Management of Hepatocellular Carcinoma in the Era of Individualized Therapy: The Experience of a Greek Tertiary Center. *Ochsner J* 2020; **20**: 272-278 [PMID: 33071659 DOI: 10.31486/toj.19.0092]

103 **Liao H**, Long Y, Han R, Wang W, Xu L, Liao M, Zhang Z, Wu Z, Shang X, Li X, Peng J, Yuan K, Zeng Y. Deep learning-based classification and mutation prediction from histopathological images of hepatocellular carcinoma. *Clin Transl Med* 2020; **10**: e102 [PMID: 32536036 DOI: 10.1002/ctm2.102]

104 **Gu J**, Zhao Z, Zeng Z, Wang Y, Qiu Z, Veeravalli B, Poh Goh BK, Kunnath Bonney G, Madhavan K, Ying CW, Kheng Choon L, Hua TC, Chow PKH. Multi-Phase Cross-modal Learning for Noninvasive Gene Mutation Prediction in Hepatocellular Carcinoma. *Annu Int Conf IEEE Eng Med Biol Soc* 2020; **2020**: 5814-5817 [PMID: 33019296 DOI: 10.1109/EMBC44109.2020.9176677]

105 **Chen G**, Wang R, Zhang C, Gui L, Xue Y, Ren X, Li Z, Wang S, Zhang Z, Zhao J, Zhang H, Yao C, Wang J, Liu J. Integration of pre-surgical blood test results predict microvascular invasion risk in hepatocellular carcinoma. *Comput Struct Biotechnol J* 2021; **19**: 826-834 [PMID: 33598098 DOI: 10.1016/j.csbj.2021.01.014]

106 **Zhang Y**, Lv X, Qiu J, Zhang B, Zhang L, Fang J, Li M, Chen L, Wang F, Liu S, Zhang S. Deep Learning With 3D Convolutional Neural Network for Noninvasive Prediction of Microvascular Invasion in Hepatocellular Carcinoma. *J Magn Reson Imaging* 2021; **54**: 134-143 [PMID: 33559293 DOI: 10.1002/jmri.27538]

107 **Wang G**, Jian W, Cen X, Zhang L, Guo H, Liu Z, Liang C, Zhou W. Prediction of Microvascular Invasion of Hepatocellular Carcinoma Based on Preoperative Diffusion-Weighted MR Using Deep Learning. *Acad Radiol* 2021; **28** Suppl 1: S118-S127 [PMID: 33303346 DOI: 10.1016/j.acra.2020.11.014]

108 **Liu QP**, Xu X, Zhu FP, Zhang YD, Liu XS. Prediction of prognostic risk factors in hepatocellular carcinoma with transarterial chemoembolization using multi-modal multi-task deep learning. *EClinicalMedicine* 2020; **23**: 100379 [PMID: 32548574 DOI: 10.1016/j.eclinm.2020.100379]

109 **Jiang YQ**, Cao SE, Cao S, Chen JN, Wang GY, Shi WQ, Deng YN, Cheng N, Ma K, Zeng KN, Yan XJ, Yang HZ, Huan WJ, Tang WM, Zheng Y, Shao CK, Wang J, Yang Y, Chen GH. Preoperative identification of microvascular invasion in hepatocellular carcinoma by XGBoost and deep learning. *J Cancer Res Clin Oncol* 2021; **147**: 821-833 [PMID: 32852634 DOI: 10.1007/s00432-020-03366-9]

110 **Cucchetti A**, Piscaglia F, Grigioni AD, Ravaioli M, Cescon M, Zanello M, Grazi GL, Golfieri R, Grigioni WF, Pinna AD. Preoperative prediction of hepatocellular carcinoma tumour grade and micro-vascular invasion by means of artificial neural network: a pilot study. *J Hepatol* 2010; **52**: 880-888 [PMID: 20409605 DOI: 10.1016/j.jhep.2009.12.037]

111 **Mai RY**, Lu HZ, Bai T, Liang R, Lin Y, Ma L, Xiang BD, Wu GB, Li LQ, Ye JZ. Artificial neural network model for preoperative prediction of severe liver failure after hemihepatectomy in patients with hepatocellular carcinoma. *Surgery* 2020; **168**: 643-652 [PMID: 32792098 DOI: 10.1016/j.surg.2020.06.031]

112 **Shi HY**, Lee KT, Lee HH, Ho WH, Sun DP, Wang JJ, Chiu CC. Comparison of artificial neural network and logistic regression models for predicting in-hospital mortality after primary liver cancer surgery. *PLoS One* 2012; **7**: e35781 [PMID: 22563399 DOI: 10.1371/journal.pone.0035781]

113 **Liu D**, Liu F, Xie X, Su L, Liu M, Kuang M, Huang G, Wang Y, Zhou H, Wang K, Lin M, Tian J. Accurate prediction of responses to transarterial chemoembolization for patients with hepatocellular carcinoma by using artificial intelligence in contrast-enhanced ultrasound. *Eur Radiol* 2020; **30**: 2365-2376 [PMID: 31900703 DOI: 10.1007/s00330-019-06553-6]

114 **Morshid A**, Elsayes KM, Khalaf AM, Elmohr MM, Yu J, Kaseb AO, Hassan M, Mahvash A, Wang Z, Hazle JD, Fuentes D. A machine learning model to predict hepatocellular carcinoma response to transcatheter arterial chemoembolization. *Radiol Artif Intell* 2019; **1** [PMID: 31858078 DOI: 10.1148/ryai.2019180021]

115 **Peng J**, Kang S, Ning Z, Deng H, Shen J, Xu Y, Zhang J, Zhao W, Li X, Gong W, Huang J, Liu L. Residual convolutional neural network for predicting response of transarterial chemoembolization in hepatocellular carcinoma from CT imaging. *Eur Radiol* 2020; **30**: 413-424 [PMID: 31332558 DOI: 10.1007/s00330-019-06318-1]

116 **Abajian A**, Murali N, Savic LJ, Laage-Gaupp FM, Nezami N, Duncan JS, Schlachter T, Lin M, Geschwind JF, Chapiro J. Predicting Treatment Response to Intra-arterial Therapies for Hepatocellular Carcinoma with the Use of Supervised Machine Learning-An Artificial Intelligence Concept. *J Vasc Interv Radiol* 2018; **29**: 850-857.e1 [PMID: 29548875 DOI: 10.1016/j.jvir.2018.01.769]

117 **Zhu Y**, Gao W, Guo Z, Zhou Y. Liver tissue classification of en face images by fractal dimension-based support vector machine. *J Biophotonics* 2020; **13**: e201960154 [PMID: 31909553 DOI: 10.1002/jbio.201960154]

118 **Liang Z**, Zhou Q, Yang J, Zhang L, Liu D, Tu B, Zhang S. Artificial intelligence-based framework in evaluating intrafraction motion for liver cancer robotic stereotactic body radiation therapy with fiducial tracking. *Med Phys* 2020; **47**: 5482-5489 [PMID: 32996131 DOI: 10.1002/mp.14501]

119 **Liu Y**, Lei Y, Wang T, Kayode O, Tian S, Liu T, Patel P, Curran WJ, Ren L, Yang X. MRI-based treatment planning for liver stereotactic body radiotherapy: validation of a deep learning-based synthetic CT generation method. *Br J Radiol* 2019; **92**: 20190067 [PMID: 31192695 DOI: 10.1259/bjr.20190067]

120 **Taebi A**, Vu CT, Roncali E. Estimation of Yttrium-90 Distribution in Liver Radioembolization using Computational Fluid Dynamics and Deep Neural Networks. *Annu Int Conf IEEE Eng Med Biol Soc* 2020; **2020**: 4974-4977 [PMID: 33019103 DOI: 10.1109/EMBC44109.2020.9176328]

121 **Tong Z**, Zhou Y, Wang J. Identifying potential drug targets in hepatocellular carcinoma based on network analysis and one-class support vector machine. *Sci Rep* 2019; **9**: 10442 [PMID: 31320657 DOI: 10.1038/s41598-019-46540-x]

122 **Chaudhary K**, Poirion OB, Lu L, Garmire LX. Deep Learning-Based Multi-Omics Integration Robustly Predicts Survival in Liver Cancer. *Clin Cancer Res* 2018; **24**: 1248-1259 [PMID: 28982688 DOI: 10.1158/1078-0432.CCR-17-0853]

123 **Chicco D**, Oneto L. Computational intelligence identifies alkaline phosphatase (ALP), alpha-fetoprotein (AFP), and hemoglobin levels as most predictive survival factors for hepatocellular carcinoma. *Health Informatics J* 2021; **27**: 1460458220984205 [PMID: 33504243 DOI: 10.1177/1460458220984205]

124 **Liu X**, Lu J, Zhang G, Han J, Zhou W, Chen H, Zhang H, Yang Z. A Machine Learning Approach Yields a Multiparameter Prognostic Marker in Liver Cancer. *Cancer Immunol Res* 2021; **9**: 337-347 [PMID: 33431375 DOI: 10.1158/2326-6066.CIR-20-0616]

125 **Shi HY**, Lee KT, Wang JJ, Sun DP, Lee HH, Chiu CC. Artificial neural network model for predicting 5-year mortality after surgery for hepatocellular carcinoma: a nationwide study. *J Gastrointest Surg* 2012; **16**: 2126-2131 [PMID: 22878787 DOI: 10.1007/s11605-012-1986-3]

126 **Chiu HC**, Ho TW, Lee KT, Chen HY, Ho WH. Mortality predicted accuracy for hepatocellular carcinoma patients with hepatic resection using artificial neural network. *ScientificWorldJournal* 2013; **2013**: 201976 [PMID: 23737707 DOI: 10.1155/2013/201976]

127 **Qiao G**, Li J, Huang A, Yan Z, Lau WY, Shen F. Artificial neural networking model for the prediction of post-hepatectomy survival of patients with early hepatocellular carcinoma. *J Gastroenterol Hepatol* 2014; **29**: 2014-2020 [PMID: 24989634 DOI: 10.1111/jgh.12672]

128 **Guo L**, Wang Z, Du Y, Mao J, Zhang J, Yu Z, Guo J, Zhao J, Zhou H, Wang H, Gu Y, Li Y. Random-forest algorithm based biomarkers in predicting prognosis in the patients with hepatocellular carcinoma. *Cancer Cell Int* 2020; **20**: 251 [PMID: 32565735 DOI: 10.1186/s12935-020-01274-z]

129 **Saillard C**, Schmauch B, Laifa O, Moarii M, Toldo S, Zaslavskiy M, Pronier E, Laurent A, Amaddeo G, Regnault H, Sommacale D, Ziol M, Pawlotsky JM, Mulé S, Luciani A, Wainrib G, Clozel T, Courtiol P, Calderaro J. Predicting Survival After Hepatocellular Carcinoma Resection Using Deep Learning on Histological Slides. *Hepatology* 2020; **72**: 2000-2013 [PMID: 32108950 DOI: 10.1002/hep.31207]

130 **Zhong BY**, Ni CF, Ji JS, Yin GW, Chen L, Zhu HD, Guo JH, He SC, Deng G, Zhang Q, Li PC, Yu H, Song JJ, Teng GJ. Nomogram and Artificial Neural Network for Prognostic Performance on the Albumin-Bilirubin Grade for Hepatocellular Carcinoma Undergoing Transarterial Chemoembolization. *J Vasc Interv Radiol* 2019; **30**: 330-338 [PMID: 30819473 DOI: 10.1016/j.jvir.2018.08.026]

131 **Zhong BY**, Yan ZP, Sun JH, Zhang L, Hou ZH, Yang MJ, Zhou GH, Wang WS, Li Z, Huang P, Zhang S, Zhu XL, Ni CF. Prognostic Performance of Albumin-Bilirubin Grade With Artificial Intelligence for Hepatocellular Carcinoma Treated With Transarterial Chemoembolization Combined With Sorafenib. *Front Oncol* 2020; **10**: 525461 [PMID: 33392064 DOI: 10.3389/fonc.2020.525461]

132 **Zhang L**, Xia W, Yan ZP, Sun JH, Zhong BY, Hou ZH, Yang MJ, Zhou GH, Wang WS, Zhao XY, Jian JM, Huang P, Zhang R, Zhang S, Zhang JY, Li Z, Zhu XL, Gao X, Ni CF. Deep Learning Predicts Overall Survival of Patients With Unresectable Hepatocellular Carcinoma Treated by Transarterial Chemoembolization Plus Sorafenib. *Front Oncol* 2020; **10**: 593292 [PMID: 33102242 DOI: 10.3389/fonc.2020.593292]

133 **Mähringer-Kunz A**, Wagner F, Hahn F, Weinmann A, Brodehl S, Schotten S, Hinrichs JB, Düber C, Galle PR, Pinto Dos Santos D, Kloeckner R. Predicting survival after transarterial chemoembolization for hepatocellular carcinoma using a neural network: A Pilot Study. *Liver Int* 2020; **40**: 694-703 [PMID: 31943703 DOI: 10.1111/liv.14380]

134 **Liu X**, Hou Y, Wang X, Yu L, Jiang L, Yang Z. Machine learning-based development and validation of a scoring system for progression-free survival in liver cancer. *Hepatol Int* 2020; **14**: 567-576 [PMID: 32556865 DOI: 10.1007/s12072-020-10046-w]

135 **Ho WH**, Lee KT, Chen HY, Ho TW, Chiu HC. Disease-free survival after hepatic resection in hepatocellular carcinoma patients: a prediction approach using artificial neural network. *PLoS One* 2012; **7**: e29179 [PMID: 22235270 DOI: 10.1371/journal.pone.0029179]

136 **Bedon L**, Dal Bo M, Mossenta M, Busato D, Toffoli G, Polano M. A Novel Epigenetic Machine Learning Model to

Define Risk of Progression for Hepatocellular Carcinoma Patients. *Int J Mol Sci* 2021; **22** [PMID: 33499054 DOI: 10.3390/ijms22031075]

137 **Schoenberg MB**, Bucher JN, Koch D, Börner N, Hesse S, De Toni EN, Seidensticker M, Angele MK, Klein C, Bazhin AV, Werner J, Guba MO. A novel machine learning algorithm to predict disease free survival after resection of hepatocellular carcinoma. *Ann Transl Med* 2020; **8**: 434 [PMID: 32395478 DOI: 10.21037/atm.2020.04.16]

138 **Wu CF**, Wu YJ, Liang PC, Wu CH, Peng SF, Chiu HW. Disease-free survival assessment by artificial neural networks for hepatocellular carcinoma patients after radiofrequency ablation. *J Formos Med Assoc* 2017; **116**: 765-773 [PMID: 28117199 DOI: 10.1016/j.jfma.2016.12.006]

139 **Divya R**, Radha P. An Optimized HCC Recurrence Prediction Using APO Algorithm Multiple Time Series Clinical Liver Cancer Dataset. *J Med Syst* 2019; **43**: 193 [PMID: 31115780 DOI: 10.1007/s10916-019-1265-x]

140 **Huang Y**, Chen H, Zeng Y, Liu Z, Ma H, Liu J. Development and Validation of a Machine Learning Prognostic Model for Hepatocellular Carcinoma Recurrence After Surgical Resection. *Front Oncol* 2020; **10**: 593741 [PMID: 33598425 DOI: 10.3389/fonc.2020.593741]

141 **Shen J**, Qi L, Zou Z, Du J, Kong W, Zhao L, Wei J, Lin L, Ren M, Liu B. Identification of a novel gene signature for the prediction of recurrence in HCC patients by machine learning of genome-wide databases. *Sci Rep* 2020; **10**: 4435 [PMID: 32157118 DOI: 10.1038/s41598-020-61298-3]

142 **Wang W**, Chen Q, Iwamoto Y, Han X, Zhang Q, Hu H, Lin L, Chen YW. Deep Learning-Based Radiomics Models for Early Recurrence Prediction of Hepatocellular Carcinoma with Multi-phase CT Images and Clinical Data. *Annu Int Conf IEEE Eng Med Biol Soc* 2019; **2019**: 4881-4884 [PMID: 31946954 DOI: 10.1109/EMBC.2019.8856356]

143 **Ji GW**, Zhu FP, Xu Q, Wang K, Wu MY, Tang WW, Li XC, Wang XH. Machine-learning analysis of contrast-enhanced CT radiomics predicts recurrence of hepatocellular carcinoma after resection: A multi-institutional study. *EBioMedicine* 2019; **50**: 156-165 [PMID: 31735556 DOI: 10.1016/j.ebiom.2019.10.057]

144 **Xu D**, Sheng JQ, Hu PJ, Huang TS, Lee WC. Predicting hepatocellular carcinoma recurrences: A data-driven multiclass classification method incorporating latent variables. *J Biomed Inform* 2019; **96**: 103237 [PMID: 31238108 DOI: 10.1016/j.jbi.2019.103237]

145 **Jianzhu B**, Shuang L, Pengfei M, Yi Z, Yanshu Z. Research on Early Warning Mechanism and Model of Liver Cancer Rehabilitation Based on CS-SVM. *J Healthc Eng* 2021; **2021**: 6658776 [PMID: 33520150 DOI: 10.1155/2021/6658776]

146 **Liao H**, Xiong T, Peng J, Xu L, Liao M, Zhang Z, Wu Z, Yuan K, Zeng Y. Classification and Prognosis Prediction from Histopathological Images of Hepatocellular Carcinoma by a Fully Automated Pipeline Based on Machine Learning. *Ann Surg Oncol* 2020; **27**: 2359-2369 [PMID: 31916093 DOI: 10.1245/s10434-019-08190-1]

147 **Saito A**, Toyoda H, Kobayashi M, Koiwa Y, Fujii H, Fujita K, Maeda A, Kaneoka Y, Hazama S, Nagano H, Mirza AH, Graf HP, Cosatto E, Murakami Y, Kuroda M. Prediction of early recurrence of hepatocellular carcinoma after resection using digital pathology images assessed by machine learning. *Mod Pathol* 2021; **34**: 417-425 [PMID: 32948835 DOI: 10.1038/s41379-020-00671-z]

148 **Liang JD**, Ping XO, Tseng YJ, Huang GT, Lai F, Yang PM. Recurrence predictive models for patients with hepatocellular carcinoma after radiofrequency ablation using support vector machines with feature selection methods. *Comput Methods Programs Biomed* 2014; **117**: 425-434 [PMID: 25278224 DOI: 10.1016/j.cmpb.2014.09.001]

149 **An C**, Jiang Y, Huang Z, Gu Y, Zhang T, Ma L, Huang J. Assessment of Ablative Margin After Microwave Ablation for Hepatocellular Carcinoma Using Deep Learning-Based Deformable Image Registration. *Front Oncol* 2020; **10**: 573316 [PMID: 33102233 DOI: 10.3389/fonc.2020.573316]

150 **Nam JY**, Lee JH, Bae J, Chang Y, Cho Y, Sinn DH, Kim BH, Kim SH, Yi NJ, Lee KW, Kim JM, Park JW, Kim YJ, Yoon JH, Joh JW, Suh KS. Novel Model to Predict HCC Recurrence after Liver Transplantation Obtained Using Deep Learning: A Multicenter Study. *Cancers (Basel)* 2020; **12** [PMID: 33003306 DOI: 10.3390/cancers12102791]

151 **Rodriguez-Luna H**, Vargas HE, Byrne T, Rakela J. Artificial neural network and tissue genotyping of hepatocellular carcinoma in liver-transplant recipients: prediction of recurrence. *Transplantation* 2005; **79**: 1737-1740 [PMID: 15973178 DOI: 10.1097/01.tp.0000161794.32007.d1]

152 **Guo D**, Gu D, Wang H, Wei J, Wang Z, Hao X, Ji Q, Cao S, Song Z, Jiang J, Shen Z, Tian J, Zheng H. Radiomics analysis enables recurrence prediction for hepatocellular carcinoma after liver transplantation. *Eur J Radiol* 2019; **117**: 33-40 [PMID: 31307650 DOI: 10.1016/j.ejrad.2019.05.010]

153 **Lau L**, Kankanige Y, Rubinstein B, Jones R, Christophi C, Muralidharan V, Bailey J. Machine-Learning Algorithms Predict Graft Failure After Liver Transplantation. *Transplantation* 2017; **101**: e125-e132 [PMID: 27941428 DOI: 10.1097/TP.0000000000001600]

154 **Briceño J**, Cruz-Ramírez M, Prieto M, Navasa M, Ortiz de Urbina J, Orti R, Gómez-Bravo MÁ, Otero A, Varo E, Tomé S, Clemente G, Bañares R, Bárcena R, Cuervas-Mons V, Solórzano G, Vinaixa C, Rubín A, Colmenero J, Valdivieso A, Ciria R, Hervás-Martínez C, de la Mata M. Use of artificial intelligence as an innovative donor-recipient matching model for liver transplantation: results from a multicenter Spanish study. *J Hepatol* 2014; **61**: 1020-1028 [PMID: 24905493 DOI: 10.1016/j.jhep.2014.05.039]

155 **Ershoff BD**, Lee CK, Wray CL, Agopian VG, Urban G, Baldi P, Cannesson M. Training and Validation of Deep Neural Networks for the Prediction of 90-Day Post-Liver Transplant Mortality Using UNOS Registry Data. *Transplant Proc* 2020; **52**: 246-258 [PMID: 31926745 DOI: 10.1016/j.transproceed.2019.10.019]

156 **AlAli AB**, Griffin MF, Butler PE. Three-Dimensional Printing Surgical Applications. *Eplasty* 2015; **15**: e37 [PMID: 26301002]

157 **Witowski JS**, Coles-Black J, Zuzak TZ, Pędziwiatr M, Chuen J, Major P, Budzyński A. 3D Printing in Liver Surgery: A Systematic Review. *Telemed J E Health* 2017; **23**: 943-947 [PMID: 28530492 DOI: 10.1089/tmj.2017.0049]

158 **Tack P**, Victor J, Gemmel P, Annemans L. 3D-printing techniques in a medical setting: a systematic literature review. *Biomed Eng Online* 2016; **15**: 115 [PMID: 27769304 DOI: 10.1186/s12938-016-0236-4]

159 **Murphy SV**, De Coppi P, Atala A. Opportunities and challenges of translational 3D bioprinting. *Nat Biomed Eng* 2020; **4**: 370-380 [PMID: 31695178 DOI: 10.1038/s41551-019-0471-7]

160 **Lee W**, Debasitis JC, Lee VK, Lee JH, Fischer K, Edminster K, Park JK, Yoo SS. Multi-layered culture of human skin

fibroblasts and keratinocytes through three-dimensional freeform fabrication. *Biomaterials* 2009; **30**: 1587-1595 [PMID: 19108884 DOI: 10.1016/j.biomaterials.2008.12.009]

161 **Poldervaart MT**, Gremmels H, van Deventer K, Fledderus JO, Oner FC, Verhaar MC, Dhert WJ, Alblas J. Prolonged presence of VEGF promotes vascularization in 3D bioprinted scaffolds with defined architecture. *J Control Release* 2014; **184**: 58-66 [PMID: 24727077 DOI: 10.1016/j.jconrel.2014.04.007]

162 **Norotte C**, Marga FS, Niklason LE, Forgacs G. Scaffold-free vascular tissue engineering using bioprinting. *Biomaterials* 2009; **30**: 5910-5917 [PMID: 19664819 DOI: 10.1016/j.biomaterials.2009.06.034]

163 **Pattanaik S**, Arbra C, Bainbridge H, Dennis SG, Fann SA, Yost MJ. Vascular Tissue Engineering Using Scaffold-Free Prevascular Endothelial-Fibroblast Constructs. *Biores Open Access* 2019; **8**: 1-15 [PMID: 30637179 DOI: 10.1089/biores.2018.0039]

164 **Yoon No D**, Lee KH, Lee J, Lee SH. 3D liver models on a microplatform: well-defined culture, engineering of liver tissue and liver-on-a-chip. *Lab Chip* 2015; **15**: 3822-3837 [PMID: 26279012 DOI: 10.1039/c5lc00611b]

165 **Chang R**, Emami K, Wu H, Sun W. Biofabrication of a three-dimensional liver micro-organ as an in vitro drug metabolism model. *Biofabrication* 2010; **2**: 045004 [PMID: 21079286 DOI: 10.1088/1758-5082/2/4/045004]

166 **Faulkner-Jones A**, Fyfe C, Cornelissen DJ, Gardner J, King J, Courtney A, Shu W. Bioprinting of human pluripotent stem cells and their directed differentiation into hepatocyte-like cells for the generation of mini-livers in 3D. *Biofabrication* 2015; **7**: 044102 [PMID: 26486521 DOI: 10.1088/1758-5090/7/4/044102]

167 **Lee SY**, Kim HJ, Choi D. Cell sources, liver support systems and liver tissue engineering: alternatives to liver transplantation. *Int J Stem Cells* 2015; **8**: 36-47 [PMID: 26019753 DOI: 10.15283/ijsc.2015.8.1.36]

168 **US Department of Health and Human Services Food and Drug Administration**. Technical Considerations for Additive Manufactured Medical Devices: Guidance for Industry and Food and Drug Administration Staff Document. [cited 1 April 2021]. Available from: https://www.fda.gov/files/medical%20devices/published/Technical-Considerations-for-Additive-Manufactured-Medical-Devices---Guidance-for-Industry-and-Food-and-Drug-Administration-Staff.pdf

169 **Tsoulfas G**, Bangeas PI, Suri JS. 3D Printing: Applications in Medicine and Surgery. In: Vidalis T. 3D printing and bioprinting: ethical and legal issues. Amsterdam: Elsevier. 2020: 51-68 [DOI: 10.1016/B978-0-323-66164-5.00004-0]

170 **Andorno R**. The Precautionary Principle: A New Legal Standard for a Technological Age. *J Int Biotechnol Law* 2004; **1**: 11 [DOI: 10.1515/jibl.2004.1.1.11]

171 **Rinaldi T**, Colotti G. Use of organoids in medicinal chemistry: challenges on ethics and biosecurity. *Future Med Chem* 2019; **11**: 1087-1090 [PMID: 31280671 DOI: 10.4155/fmc-2018-0341]

172 **Pashkov V**, Harkusha A. 3-D bioprinting law regulation perspectives. *Wiad Lek* 2017; **70**: 480-482 [PMID: 28711892]

173 **Gilbert F**, O'Connell CD, Mladenovska T, Dodds S. Print Me an Organ? *Sci Eng Ethics* 2018; **24**: 73-91 [PMID: 28185142 DOI: 10.1007/s11948-017-9874-6]

174 **Sugawara E**, Nikaido H. Properties of AdeABC and AdeIJK efflux systems of Acinetobacter baumannii compared with those of the AcrAB-TolC system of Escherichia coli. *Antimicrob Agents Chemother* 2014; **58**: 7250-7257 [PMID: 25246403 DOI: 10.1128/AAC.03728-14]

175 **FDA**. Artificial Intelligence and Machine Learning in Software as a Medical Device. [cited 1 April 2021]. Available from: https://www.fda.gov/medical-devices/software-medical-device-samd/artificial-intelligence-and-machine-learning-software-medical-device

176 **FDA**. Proposed Regulatory Framework for Modifications to Artificial Intelligence/Machine Learning (AI/ML)-Based Software as a Medical Device (SaMD) - Discussion Paper and Request for Feedback. [cited 1 April 2021]. Available from: https://www.fda.gov/files/medical%20devices/published/US-FDA-Artificial-Intelligence-andMachine-Learning-Discussion-Paper.pdf

177 **Topol EJ**. High-performance medicine: the convergence of human and artificial intelligence. *Nat Med* 2019; **25**: 44-56 [PMID: 30617339 DOI: 10.1038/s41591-018-0300-7]

178 **Institute of Medicine**. Medical devices and the public's health: The FDA 510(k) clearance process at 35 years. *The National Academies Press* 2011 [DOI: 10.17226/13150]

179 Artificial Intelligence and Machine Learning to Accelerate Translational Research: Proceedings of a Workshop-in Brief. Washington (DC): National Academies Press (US); 2018-Jul-24 [PMID: 30048078]

180 **Hwang TJ**, Kesselheim AS, Vokinger KN. Lifecycle Regulation of Artificial Intelligence- and Machine Learning-Based Software Devices in Medicine. *JAMA* 2019; **322**: 2285-2286 [PMID: 31755907 DOI: 10.1001/jama.2019.16842]

181 **Price WN 2nd**, Gerke S, Cohen IG. Potential Liability for Physicians Using Artificial Intelligence. *JAMA* 2019; **322**: 1765-1766 [PMID: 31584609 DOI: 10.1001/jama.2019.15064]

182 **Crawford K**, Calo R. There is a blind spot in AI research. *Nature* 2016; **538**: 311-313 [PMID: 27762391 DOI: 10.1038/538311a]

183 **Park SH**, Han K. Methodologic Guide for Evaluating Clinical Performance and Effect of Artificial Intelligence Technology for Medical Diagnosis and Prediction. *Radiology* 2018; **286**: 800-809 [PMID: 29309734 DOI: 10.1148/radiol.2017171920]

184 **Anwar SM**, Majid M, Qayyum A, Awais M, Alnowami M, Khan MK. Medical Image Analysis using Convolutional Neural Networks: A Review. *J Med Syst* 2018; **42**: 226 [PMID: 30298337 DOI: 10.1007/s10916-018-1088-1]

185 **Le Berre C**, Sandborn WJ, Aridhi S, Devignes MD, Fournier L, Smaïl-Tabbone M, Danese S, Peyrin-Biroulet L. Application of Artificial Intelligence to Gastroenterology and Hepatology. *Gastroenterology* 2020; **158**: 76-94.e2 [PMID: 31593701 DOI: 10.1053/j.gastro.2019.08.058]

186 **Parikh RB**, Teeple S, Navathe AS. Addressing Bias in Artificial Intelligence in Health Care. *JAMA* 2019; **322**: 2377-2378 [PMID: 31755905 DOI: 10.1001/jama.2019.18058]

187 **Loftus TJ**, Tighe PJ, Filiberto AC, Efron PA, Brakenridge SC, Mohr AM, Rashidi P, Upchurch GR Jr, Bihorac A. Artificial Intelligence and Surgical Decision-making. *JAMA Surg* 2020; **155**: 148-158 [PMID: 31825465 DOI: 10.1001/jamasurg.2019.4917]

188 **Shortliffe EH**, Sepúlveda MJ. Clinical Decision Support in the Era of Artificial Intelligence. *JAMA* 2018; **320**: 2199-2200

[PMID: 30398550 DOI: 10.1001/jama.2018.17163]
189 **National Research Council**. For the Record: Protecting Electronic Health Information. *The National Academies Press* 1997 [DOI: 10.17226/5595]
190 **Hern A**. Royal Free breached UK data law in 1.6 m patient deal with Google's DeepMind. The Guardian. [cited 1 April 2021]. Available from: https://scholar.google.com/scholar?hl=en&as_sdt=0%2C5&q=Royal+Free+breached+UK+data+law+in+1.6m+patient+deal+with+Google%27s+DeepMind&btnG=
191 **U.S. Department OF Labor**. Employee Benefits Security Administration. [cited 1 April 2021]. Available from: https://www.dol.gov/agencies/ebsa
192 **Nundy S**, Montgomery T, Wachter RM. Promoting Trust Between Patients and Physicians in the Era of Artificial Intelligence. *JAMA* 2019; **322**: 497-498 [PMID: 31305873 DOI: 10.1001/jama.2018.20563]
193 Machine Bias-ProPublica. [cited 1 April 2021]. Available from: https://www.propublica.org/article/machine-bias-risk-assessments-in-criminal-sentencing
194 Ethical, social, and political challenges of artificial intelligence in health. [cited 1 April 2021]. Available from: https://ge2p2-center.net/2018/05/06/ethical-social-and-political-challenges-of-artificial-intelligence-in-health/
195 **Yang YJ**, Bang CS. Application of artificial intelligence in gastroenterology. *World J Gastroenterol* 2019; **25**: 1666-1683 [PMID: 31011253 DOI: 10.3748/wjg.v25.i14.1666]
196 **Vayena E**, Blasimme A, Cohen IG. Machine learning in medicine: Addressing ethical challenges. *PLoS Med* 2018; **15**: e1002689 [PMID: 30399149 DOI: 10.1371/journal.pmed.1002689]
197 **Al'Aref SJ**, Singh G, Baskaran L, Metaxas D. Machine Learning in Cardiovascular Medicine. [cited 1 April 2021]. Available from: http://public.eblib.com/choice/PublicFullRecord.aspx?p=6404325
198 **Fang C**, An J, Bruno A, Cai X, Fan J, Fujimoto J, Golfieri R, Hao X, Jiang H, Jiao LR, Kulkarni AV, Lang H, Lesmana CRA, Li Q, Liu L, Liu Y, Lau W, Lu Q, Man K, Maruyama H, Mosconi C, Örmeci N, Pavlides M, Rezende G, Sohn JH, Treeprasertsuk S, Vilgrain V, Wen H, Wen S, Quan X, Ximenes R, Yang Y, Zhang B, Zhang W, Zhang P, Zhang S, Qi X. Consensus recommendations of three-dimensional visualization for diagnosis and management of liver diseases. *Hepatol Int* 2020; **14**: 437-453 [PMID: 32638296 DOI: 10.1007/s12072-020-10052-y]
199 **Witowski JS**, Pędziwiatr M, Major P, Budzyński A. Cost-effective, personalized, 3D-printed liver model for preoperative planning before laparoscopic liver hemihepatectomy for colorectal cancer metastases. *Int J Comput Assist Radiol Surg* 2017; **12**: 2047-2054 [PMID: 28144830 DOI: 10.1007/s11548-017-1527-3]
200 **Yang H**, Sun L, Pang Y, Hu D, Xu H, Mao S, Peng W, Wang Y, Xu Y, Zheng YC, Du S, Zhao H, Chi T, Lu X, Sang X, Zhong S, Wang X, Zhang H, Huang P, Sun W, Mao Y. Three-dimensional bioprinted hepatorganoids prolong survival of mice with liver failure. *Gut* 2021; **70**: 567-574 [PMID: 32434830 DOI: 10.1136/gutjnl-2019-319960]
201 **Ruffle JK**, Farmer AD, Aziz Q. Artificial Intelligence-Assisted Gastroenterology- Promises and Pitfalls. *Am J Gastroenterol* 2019; **114**: 422-428 [PMID: 30315284 DOI: 10.1038/s41395-018-0268-4]
202 **Patel VL**, Shortliffe EH, Stefanelli M, Szolovits P, Berthold MR, Bellazzi R, Abu-Hanna A. The coming of age of artificial intelligence in medicine. *Artif Intell Med* 2009; **46**: 5-17 [PMID: 18790621 DOI: 10.1016/j.artmed.2008.07.017]
203 **US Food and Drug Administration**. Developing a Software Precertification Program: A Working Model. [cited 1 April 2021]. Available from: https://www.fda.gov/media/113802/download
204 **Christou CD**, Tsoulfas G. The Role of microRNA in Hepatic Ischemia/Reperfusion Injury. *Microrna* 2020; **9**: 248-254 [PMID: 31995027 DOI: 10.2174/2211536609666200129162531]
205 **Panesar S**, Cagle Y, Chander D, Morey J, Fernandez-Miranda J, Kliot M. Artificial Intelligence and the Future of Surgical Robotics. *Ann Surg* 2019; **270**: 223-226 [PMID: 30907754 DOI: 10.1097/SLA.0000000000003262]
206 **Kassahun Y**, Yu B, Tibebu AT, Stoyanov D, Giannarou S, Metzen JH, Vander Poorten E. Surgical robotics beyond enhanced dexterity instrumentation: a survey of machine learning techniques and their role in intelligent and autonomous surgical actions. *Int J Comput Assist Radiol Surg* 2016; **11**: 553-568 [PMID: 26450107 DOI: 10.1007/s11548-015-1305-z]
207 **Wang DD**, Qian Z, Vukicevic M, Engelhardt S, Kheradvar A, Zhang C, Little SH, Verjans J, Comaniciu D, O'Neill WW, Vannan MA. 3D Printing, Computational Modeling, and Artificial Intelligence for Structural Heart Disease. *JACC Cardiovasc Imaging* 2021; **14**: 41-60 [PMID: 32861647 DOI: 10.1016/j.jcmg.2019.12.022]
208 **Volonté F**, Pugin F, Bucher P, Sugimoto M, Ratib O, Morel P. Augmented reality and image overlay navigation with OsiriX in laparoscopic and robotic surgery: not only a matter of fashion. *J Hepatobiliary Pancreat Sci* 2011; **18**: 506-509 [PMID: 21487758 DOI: 10.1007/s00534-011-0385-6]

World Journal of Gastrointestinal Oncology

Submit a Manuscript: https://www.f6publishing.com

World J Gastrointest Oncol 2022 April 15; 14(4): 794-807

DOI: 10.4251/wjgo.v14.i4.794

ISSN 1948-5204 (online)

REVIEW

Role of sirtuins in esophageal cancer: Current status and future prospects

Ryota Otsuka, Koichi Hayano, Hisahiro Matsubara

Specialty type: Oncology

Provenance and peer review: Invited article; Externally peer reviewed.

Peer-review model: Single blind

Peer-review report's scientific quality classification

Grade A (Excellent): 0
Grade B (Very good): B
Grade C (Good): C
Grade D (Fair): D
Grade E (Poor): 0

P-Reviewer: Kalayarasan R, India; Yang X, China; Zhuge YZ, China

Received: December 17, 2021
Peer-review started: December 17, 2021
First decision: January 27, 2022
Revised: February 2, 2022
Accepted: March 17, 2022
Article in press: March 17, 2022
Published online: April 15, 2022

Ryota Otsuka, Koichi Hayano, Hisahiro Matsubara, Department of Frontier Surgery, Graduate School of Medicine, Chiba University, Chiba 260-8670, Japan

Corresponding author: Koichi Hayano, FACS, MD, PhD, Associate Professor, Department of Frontier Surgery, Graduate School of Medicine, Chiba University, 1-8-1, Inohana, Chuo-ku, Chiba 260-8670, Japan. hayatin1973@gmail.com

Abstract

Esophageal cancer (EC) is a malignant cancer that still has a poor prognosis, although its prognosis has been improving with the development of multidisciplinary treatment modalities such as surgery, chemotherapy and radiotherapy. Therefore, identifying specific molecular markers that can be served as biomarkers for the prognosis and treatment response of EC is highly desirable to aid in the personalization and improvement of the precision of medical treatment. Sirtuins are a family of nicotinamide adenine dinucleotide (NAD+)-dependent proteins consisting of seven members (SIRT1-7). These proteins have been reported to be involved in the regulation of a variety of biological functions including apoptosis, metabolism, stress response, senescence, differentiation and cell cycle progression. Given the variety of functions of sirtuins, they are speculated to be associated in some manner with cancer progression. However, while the role of sirtuins in cancer progression has been investigated over the past few years, their precise role remains difficult to characterize, as they have both cancer-promoting and cancer-suppressing properties, depending on the type of cancer. These conflicting characteristics make research into the nature of sirtuins all the more fascinating. However, the role of sirtuins in EC remains unclear due to the limited number of reports concerning sirtuins in EC. We herein review the current findings and future prospects of sirtuins in EC.

Key Words: Esophageal cancer; Sirtuin; Esophageal squamous cell carcinoma; Esophageal adenocarcinoma; Biomarker; Treatment

Core Tip: Although there have been several reports on the function of sirtuins in cancer progression, the biological roles and clinical implications of sirtuins in esophageal cancer (EC) remain controversial. This is the first review to focus on sirtuins in the field of EC. In this review, we will briefly summarize the role of sirtuins in cancer and discuss the current findings and future prospects of sirtuins in EC.

Citation: Otsuka R, Hayano K, Matsubara H. Role of sirtuins in esophageal cancer: Current status and future prospects. *World J Gastrointest Oncol* 2022; 14(4): 794-807
URL: https://www.wjgnet.com/1948-5204/full/v14/i4/794.htm
DOI: https://dx.doi.org/10.4251/wjgo.v14.i4.794

INTRODUCTION

Esophageal cancer (EC) is the seventh leading cause of morbidity and the sixth leading cause of mortality worldwide[1], and the prognosis of advanced EC patients is extremely poor[2]. Therefore, identifying specific molecular markers that can be used as prognostic markers or therapeutic targets for EC is highly desirable to aid in the personalization and improvement of the precision of medical treatment, which can prevent side effects and extra expenses, thereby leading to a more effective multidisciplinary treatment.

Sirtuins are a highly conserved family of proteins that exist in a wide range of prokaryotic and eukaryotic organisms, and their functional activity is dependent on the cofactor nicotinamide adenine dinucleotide (NAD+)[3]. The mammalian sirtuin family is a homolog of the yeast silent information regulator 2 (Sir2) protein and consists of seven members: SIRT1-7. Sirtuins are distinguished by their subcellular localization: SIRT1, SIRT6 and SIRT7 are mainly found in the nucleus; SIRT3, SIRT4 and SIRT5 are mainly located in the mitochondria; and SIRT2 is mainly found in the cytoplasm. Furthermore, the SIRT family proteins have conserved domains in their core catalytic activities, with SIRT1, SIRT2 and SIRT3 designated as class I; SIRT4 designated as class II; SIRT5 designated as class III; and SIRT6 and SIRT7 designated as class IV (Figure 1)[4]. Sirtuins are involved in the regulation of various biological functions, such as apoptosis, metabolism, stress response, aging, differentiation and cell cycle progression[5]. However, while the role of sirtuins in cancer progression has been investigated over the past few years, their precise role remains difficult to characterize, as they have both cancer-promoting and cancer-suppressing properties, depending on the type of cancer[6]. These conflicting characteristics make research into the nature of sirtuins all the more fascinating.

In EC, the clinical impact of sirtuins remains unclear due to the limited number of reports concerning sirtuins in EC. Therefore, this is the first review to focus on sirtuins in the field of EC. In this review, we will briefly summarize the role of sirtuins in cancer and discuss the current findings and future prospects of sirtuins in EC.

LITERATURE SEARCH

PubMed was searched to identify studies on sirtuins and cancer from inception until January 2022. The following search terms were applied: “Sirtuin” or “Silent mating type information regulation 2 homolog” or “SIRT” and “carcinoma” or “cancer”. The reference lists of all related articles were screened for other potentially relevant studies.

SIRT1

The role of SIRT1 in cancer progression is contradictory. This is because SIRT1 can both promote and inhibit tumorigenesis (Table 1 and Figure 2)[7].

Several mechanisms that are responsible for the tumor-promoting nature of SIRT1 have been uncovered as follows: (1) SIRT1 contributes to cell proliferation by epigenetically suppressing the expression and activity of many tumor suppressor genes and proteins with DNA damage repair functions such as protein 53 (p53)[8], forkhead class O transcription factor (FOXO) family members[9], E2F transcription factor 1 (E2F1)[10], protein 73 (p73)[11], retinoblastoma protein (RB)[12], Ku70[13], secreted Frizzled-related protein 1(SFRP1), SFRP2, GATA4, GATA5 and mutL homolog 1 (MLH1)[14]; (2) SIRT1 acts as a regulator of apoptosis by deacetylating key apoptosis-related proteins and cell signaling molecules such as p53, nuclear factor kappa B subunit 1 (NF-κB), FOXO3, Ku70, protein kinase B (AKT), mitogen-activated protein kinase (MAPK), and nuclear factor erythroid 2-related factor 2 (NRF2), in response to DNA damage and oxidative stress[6]; and (3) SIRT1 induces epithelial-

Table 1 Roles of sirtuins in cancer control

	Role	Effect	Involved pathway or mechanism
SIRT1	Promotor	Promote proliferation	p53, FOXO family member, E2F1, p73, RB, Ku70, SFRP1, SFRP2, GATA4, GATA5, MLH1
		Inhibit apoptosis	p53, NF-κβ, FOXO3, Ku70, AKT, MAPK, NRF2
		Induce EMT, promote migration and metastasis	ZEB1
	Suppressor	Inhibit tumor formation and proliferation	β-catenin
		Induce apoptosis	survivin
		Inhibit EMT	SMAD4, TGF-β signaling on MMP7
SIRT2	Promotor	Promote proliferation	Mediating immune evasion, altering the alkaline environment
		Inhibit apoptosis	cMYC
		Promote invasion and migration	Stimulating mitochondrial metabolism, mediating EMT
	Suppressor	Inhibit proliferation	Inhibiting fibroblast activity and tumor angiogenesis
		Inhibit invasion and migration	MMP9, E-cadherin
SIRT3	Promotor	Inhibit apoptosis and promote proliferation	p53, SHMT2, IDH2
		Promote invasion and metastasis	Reprogramming fatty acid metabolism
	Suppressor	Induce cell arrest and apoptosis	Bcl-2, p53, HIF1α, PDC, SOD2, GOT2
		Inhibit EMT and migration	FOXO3A, Wnt / β-catenin pathway
		Inhibit tumorigenesis	PDH
SIRT4	Promotor	Promote proliferation	PTEN
	Suppressor	Inhibit glutamine metabolism and proliferation	mTORC1 pathway
		Inhibit EMT, invasion and migration	E-cadherin
		Induce G1 cell cycle arrest	Cyclin D, cyclin E
SIRT5	Promotor	Promote proliferation	GLUD1, SHMT2, NRF2, PKM2, SUN2
		Inhibit mitochondrial apoptosis	Cyt c
		Promote autophagy	AMPK–mTOR pathway
		Promote invasion and migration	E2F1
		Promote resistance to chemotherapy	SDHA
	Suppressor	Inhibit carcinoma development	ACOX1
		Inhibit proliferation	SOD1
		Represent protective mechanism for tumor cells	Inhibiting ammonia-induced autophagy
SIRT6	Promotor	Promote proliferation and inhibit apoptosis	ERK1/2 pathway, AKT
		Promote invasion and migration	ERK1/2/MMP9 signaling
		Contribute to cancer development and progression	Regulating autophagy
	Suppressor	Inhibit proliferation	PCBP2, ERK1/2
		Inhibit Warburg effect	HIF-1α
		Induce apoptosis	NF-κβ, Bax, survivin

		Inhibit proliferation, invasion and migration	PKM2
SIRT7	Promotor	Promote proliferation	ERK1/2, H3K18ac
		Inhibit apoptosis	miR34a, NF-κβ family subunits, mTOR/IGF2 pathway
		Promote invasion	Vimentin, fibronectin, E-cadherin, β-catenin
	Suppressor	Inhibit proliferation and invasion	SMAD4
		Inhibit EMT	TGF-β signaling

ACOX1: Acyl-CoA oxidase 1; AKT: Protein kinase B; Bax: BCL2 associated X; β-catenin: Catenin beta; Cyt c: Cytochrome C; E2F1: E2F transcription factor 1; E-cadherin: Cadherin 1; ERK1/2: Extracellular signal-regulated kinases 1/2; FOXO: Forkhead class O transcription factor; GLUD1: Glutamate dehydrogenase 1; GOT2: Glutamic-oxaloacetic transaminase 2; H3K18ac: Histone H3 lysine 18 acetylation; HIF1α: Hypoxia inducible factor 1 subunit alpha; IDH2: Isocitrate dehydrogenase 2; IGF2: Insulin like growth factor 2; MAPK: Mitogen-activated protein kinase; MLH1: MutL homolog 1; MMP7: Matrix metallopeptidase 7; MMP9: Matrix metallopeptidase 9; mTOR: Mammalian target of rapamycin; mTORC1: Mammalian target of rapamycin complex 1; NF-κB: Nuclear factor kappa B; NRF2: Nuclear factor erythroid 2-related factor 2; p53: Protein 53; p73: Protein 73; PCBP2: Poly(rC) binding protein 2; PDH: Pyruvate dehydrogenase; PKM2: Pyruvate kinase M2; PTEN: Phosphatase and tensin homolog; RB: Retinoblastoma protein; SDHA: Succinate dehydrogenase complex flavoprotein subunit A; SFRP: Secreted Frizzled-related protein; SHMT2: Serine hydroxymethyl transferase 2; SIRT: Sirtuin; SMAD4: SMAD family member 4; SOD1: Superoxide dismutase 1; SOD2: Superoxide dismutase 2; SUN2: Sad1 and UNC84 domain containing 2; TGF-β: Transforming growth factor beta; ZEB1: Zinc finger E-box binding homeobox 1.

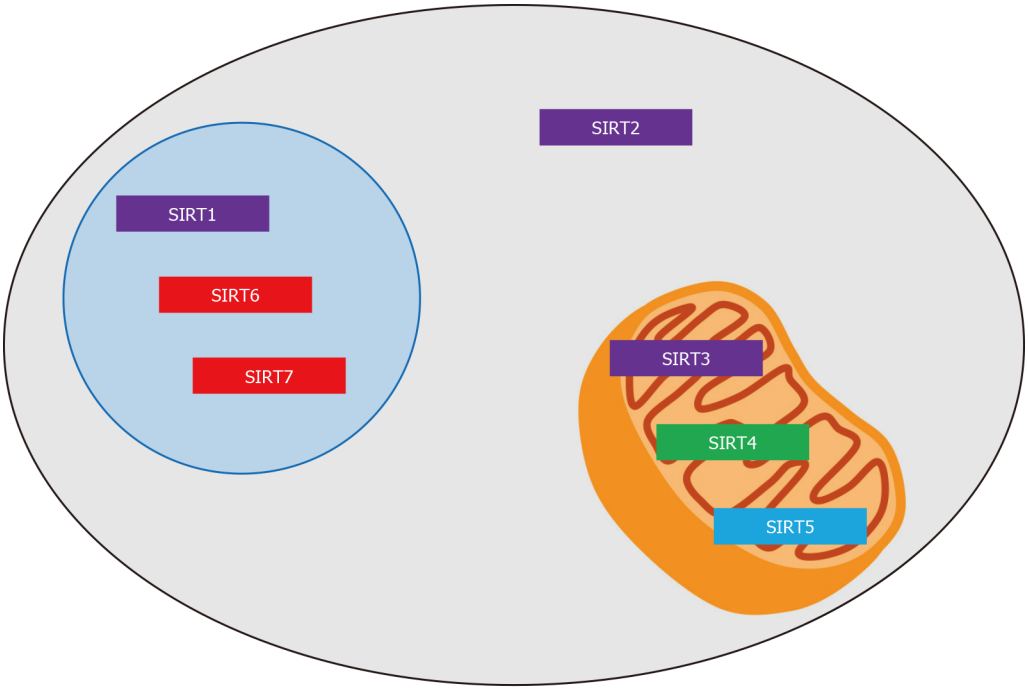

DOI: 10.4251/wjgo.v14.i4.794

Figure 1 Schematic representation of the subcellular localization of sirtuins. Catalyst domains reflecting sirtuin classes are shown in purple (Class I), green (Class II), blue (Class III) and red (Class IV). SIRT: Sirtuin.

mesenchymal transition (EMT) and promotes cell migration and metastasis by cooperating with EMT transcription factors such as zinc finger E-box binding homeobox 1 (ZEB1) in prostate cancer[15]. It has also been reported that the high expression of SIRT1 is associated with an advanced stage and poor prognosis in certain types of cancer such as gastric cancer[16], lung adenocarcinoma[17] and colorectal cancer[18].

However, SIRT1 has also been reported to function as a tumor suppressor through the following mechanisms: (1) SIRT1 inhibits tumor formation and proliferation by deacetylating catenin beta (β-catenin) in colon cancer[19]; (2) SIRT1 induces apoptosis in breast cancer 1 (BRCA1)-related breast cancer by suppressing survivin, an inhibitor of apoptosis[20]; and (3) SIRT1 suppresses EMT in cancer by deacetylating SMAD family member 4 (SMAD4) and inhibiting the effect of transforming growth factor beta (TGF-β) signaling on matrix metallopeptidase 7 (MMP7), a target gene of SMAD4[21].

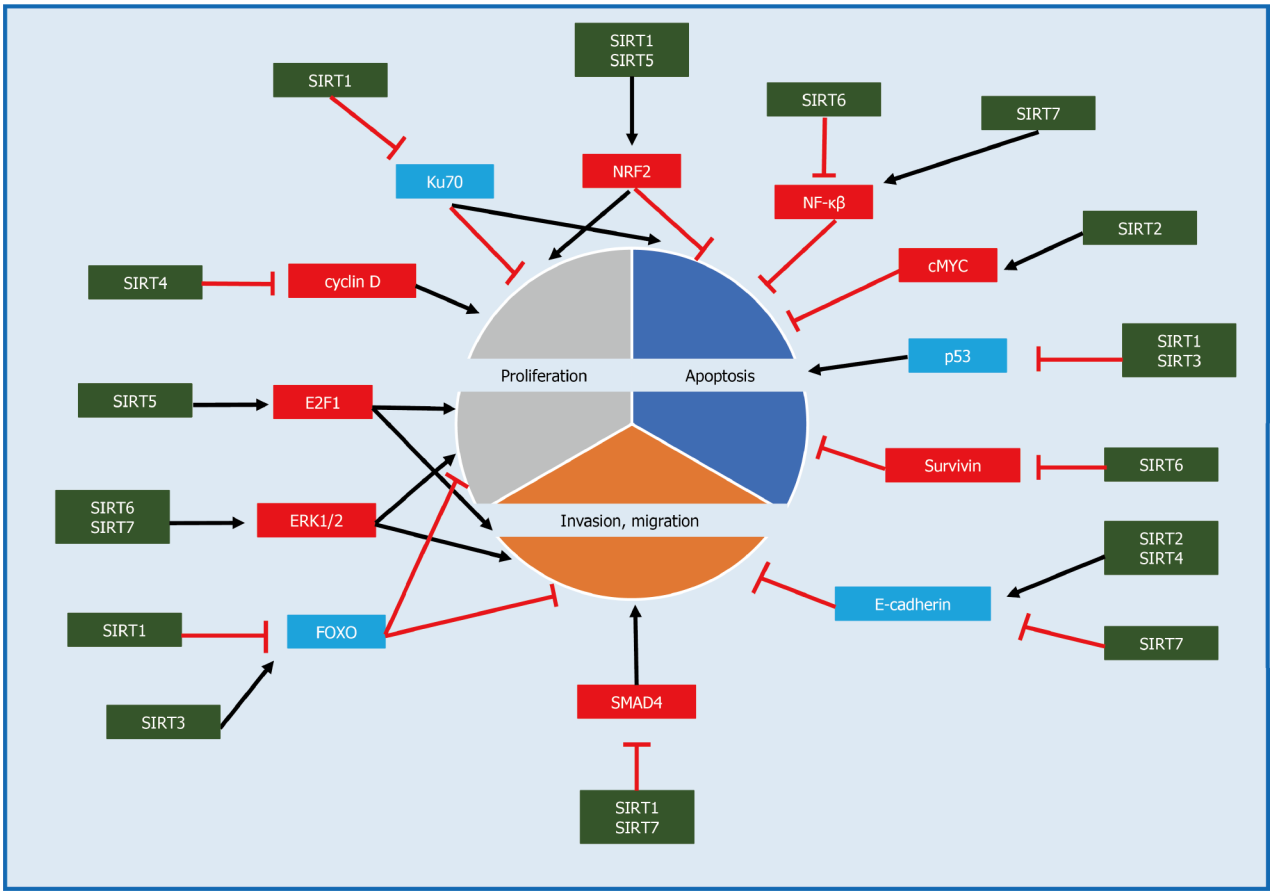

DOI: 10.4251/wjgo.v14.i4.794

Figure 2 Roles of sirtuins in cell proliferation, apoptosis, invasion and migration. E2F1: E2F transcription factor 1; E-cadherin: Cadherin 1; ERK1/2: Extracellular signal-regulated kinases 1/2; FOXO: Forkhead class O transcription factor; NF-κB: Nuclear factor kappa B; NRF2: Nuclear factor erythroid 2-related factor 2; IRT: Sirtuin; SMAD4: SMAD family member 4.

In EC, SIRT1 has been reported as a tumor-promoting factor (Table 2). Suppression of SIRT1 inhibits cell proliferation, cell migration and EMT in esophageal squamous cell carcinoma (ESCC) cell line[22,23]. SIRT1 has been suggested to be useful as a biomarker in EC as follows: (1) It has been reported that SIRT1 expression is associated with a poor prognosis in both ESCC and esophageal adenocarcinoma (EAC)[23-28]; (2) SIRT1 has also been demonstrated to be related to chemotherapy and chemoradiotherapy resistance in several ESCC studies[29-32]; and (3) SIRT1 has been described to be a useful biomarker for high-grade dysplasia and cancer of Barrett's esophagus[33]. Furthermore, we conducted a meta-analysis of these articles and demonstrated that a high expression of SIRT1 was correlated with a poor overall survival (OS), deeper tumors and a more advanced TNM stage in patients with ESCC[34]. In addition, recent studies have reported the potential utility of SIRT1 as a therapeutic target in EC. Liu *et al*[35] reported that rapamycin suppressed cell viability, migration, invasion and the phosphoinositide 3-kinase (PI3K)/AKT/mammalian target of rapamycin (mTOR) signaling pathways in EC by negatively regulating SIRT1. Jiang *et al*[36] reported that sirtinol inhibited cell viability in EAC in a dose-dependent manner, affected proliferation in the long term and potentially suppressed resistant and recurrent tumors under hypoxic conditions. Taken together, these reports suggest that SIRT1 inhibition may play an important role in the therapeutic field of EC.

SIRT2

Similar to SIRT1, SIRT2 has been reported to have both tumor-promoting and tumor-suppressing effects depending on the cancer type (Table 1 and Figure 2).

SIRT2 has been reported to promote cell proliferation in hepatocellular carcinoma (HCC), pancreatic cancer and neuroblastoma[37,38]. SIRT2 also promotes cell growth by interacting with the tumor microenvironment, such as mediating immune evasion and altering the alkaline environment[39]. In cholangiocarcinoma, SIRT2 inhibits apoptosis *via* the peroxidation reaction through metabolic reprogramming by activating cMYC[40]. In addition, SIRT2 promotes invasion and migration in HCC by stimulating mitochondrial metabolism and mediating EMT[41,42].

Table 2 Roles of sirtuins in esophageal cancer

	Type	Role	Effect	Ref.
SIRT1	ESCC	Promotor	Suppression of SIRT1 inhibits cell proliferation, cell migration, and EMT in ESCC cell line	[22,23]
			SIRT1 expression is associated with poor prognosis	[23-27, 34]
			SIRT1 enhances chemotherapy and chemoradiotherapy resistance	[29-32]
			Rapamycin suppresses cell viability, migration, invasion by negatively regulating SIRT1	[35]
	EAC		SIRT1 is associated with poor overall survival	[28]
			SIRT1 is a useful biomarker for high-grade dysplasia and cancer of Barrett's esophagus	[33]
			Sirtinol, SIRT1 inhibitor, inhibits cell viability, affects proliferation in the long term, and potentially suppresses resistant and recurrent tumors under hypoxic conditions	[36]
SIRT2	ESCC	Promotor	SIRT2 expression was associated with tumor invasion, lymph node metastasis, advanced clinical stage, poor progression-free survival, and overall survival	[47]
	EAC	Suppressor	Dysregulation of SIRT2 is associated with poor prognosis	[48,49]
SIRT3	ESCC	Promotor	Serum SIRT3 levels are higher in ESCC patients compared to those in the control subjects	[63]
			SIRT3 induces the proliferation inhibition and apoptosis	[64]
			High SIRT3 expression is associated with poor survival outcome	[65,66]
	EAC		No report	
SIRT4	ESCC	Suppressor	SIRT4 rescues the promoting effect of miR-424-5p on ESCC cell proliferation and migration	[76]
			Low SIRT4 expression is associated with a high distant recurrence rate and poor prognosis, and in vitro, knockdown of SIRT4 promotes cell proliferation and migration	[77]
	EAC		No report	
SIRT5	ESCC		No report	
	EAC			
SIRT6	ESCC	Promotor	SIRT 6 is overexpressed in ESCC tissues and that it also promotes cell proliferation and induces the expression of Bcl2, an important anti-apoptotic factor, and autophagy in ESCC cells	[102]
	EAC		No report	
SIRT7	ESCC		No report	
	EAC			

EAC: Esophageal adenocarcinoma; EMT: Epithelial-mesenchymal transition; ESCC: Esophageal squamous cell carcinoma; SIRT: Sirtuin.

Conversely, SIRT2 has been reported as a tumor suppressor that inhibits the growth of tumor cells through interaction with the tumor microenvironment, such as by inhibiting fibroblast activity and tumor angiogenesis[39]. In addition, the increased expression of matrix metalloproteinase 9 (MMP9) and decreased expression of cadherin 1 (E-cadherin) were shown to promote cell migration and invasion in SIRT2-deficient mouse embryonic fibroblasts[43]. In addition, a low expression of SIRT2 is reportedly associated with a poor prognosis in prostate cancer[44], cervical cancer[45] and colorectal cancer[46].

In EC, Yan *et al*[47] reported that SIRT2 expression was associated with tumor invasion, lymph node metastasis, advanced clinical stage, a poor progression-free survival and the OS in ESCC patients (Table 2). In contrast, SIRT2 has been reported to be a tumor suppressor in EAC. Ong *et al*[48] revealed that dysregulation of SIRT2 significantly increased the hazard ratio of death. Peters *et al*[49] also demonstrated that the dysregulation of SIRT2 was significantly associated with a poor prognosis in esophageal and junctional adenocarcinoma.

SIRT3

Whether SIRT3, a major mitochondrial deacetylase, functions as a tumor promoter or suppressor remains controversial (Table 1 and Figure 2).

SIRT3 regulates deacetylation to a variety of substrates, including p53, serine hydroxymethyltransferase 2 (SHMT2) and isocitrate dehydrogenase 2 (IDH2), preventing apoptosis and promoting cell proliferation[50-52]. In addition, Li *et al*[53] showed that SIRT3 promotes infiltration and metastasis of cervical cancer cells by reprogramming fatty acid metabolism.

In contrast, many studies have suggested the role of SIRT3 as a tumor suppressor. It has been reported that SIRT3 induces tumor-suppressing effects such as cell arrest and apoptosis by controlling Bcl-2, p53, hypoxia inducible factor 1 subunit alpha (HIF1α), pyruvate dehydrogenase complex (PDC), superoxide dismutase 2 (SOD2) and glutamic-oxaloacetic transaminase 2 (GOT2)[54-59]. Regarding metastasis, Li *et al*[60] revealed that SIRT3 promoted FOXO3A expression by weakening the Wnt/β-catenin pathway thereby inhibiting EMT and prostate cancer cell migration. Furthermore, Ozden *et al*[61] reported that activation of pyruvate dehydrogenase (PDH) by SIRT3 increased oxidative phosphorylation and reactive oxygen species production and reduced glycolysis which contributed to reduced tumorigenesis in cancer cells.

The relationship between SIRT3 expression and the clinical prognosis reportedly differs depending on the type of cancer and no clear consensus has yet been reached[62].

Regarding EC, several reports showed SIRT3 was a tumor promotor in ESCC (Table 2). Cobanoğlu *et al*[63] reported that serum SIRT3 Levels were significantly higher in ESCC patients than in the control subjects. Yang *et al*[64] showed that downregulation of SIRT3 induced the proliferation inhibition and apoptosis in ESCC cells. In addition, two articles demonstrated that a high SIRT3 expression was significantly associated with a poor survival outcome[65,66]. There have been no reports yet on the relationship between EAC and SIRT3.

SIRT4

SIRT4 has been reported primarily as a tumor suppressor (Table 1 and Figure 2). Wang *et al*[67] revealed that SIRT4 was downregulated in 30 cancers according to an analysis using data from The Cancer Genome Atlas (TCGA) database. SIRT4 is an important component of the DNA damage response pathway that inhibits glutamine metabolism, arrests the cell cycle and suppresses tumors. When SIRT4 is deficient, glutamine-dependent proliferation and stress-induced genomic instability increase resulting in a tumorigenic phenotype[68]. Csibi *et al*[69] also reported that the mammalian target of rapamycin complex 1 (mTORC1) pathway inhibited SIRT4 and stimulated glutamine metabolism and cell proliferation. In addition, SIRT4 has been reported to enhance E-cadherin and inhibit EMT, thereby decreasing migration and the invasion ability in gastric and colorectal cancer cells[70,71]. Furthermore, Hu *et al*[72] showed that overexpression of SIRT4 induced G1 cell cycle arrest through the inhibition of the phosphorylated extracellular signal-regulated kinases cyclin D and cyclin E. In addition, several studies have revealed that a low SIRT4 expression was significantly correlated with a poor prognosis in patients with various cancers[73].

In contrast, a small number of studies have reported the function of SIRT4 as a tumor-promoting factor (Table 1). Jeong *et al*[74] demonstrated that the overexpression of SIRT4 protected cancer cells from DNA damage or endoplasmic reticulum stress, and conversely, the loss of SIRT4 sensitized cells after drug treatment. Furthermore, when cells are starved of nutrients, SIRT4 cooperates with insulin-degrading enzymes to degrade phosphatase and tensin homolog (PTEN), a tumor-suppressing factor, and promote the survival of cancer cells[75].

In EC, SIRT4 has been reported as a tumor suppressor (Table 2). Cui *et al*[76] revealed that SRT4 was negatively regulated by miR-424-5p, and overexpression of SIRT4 strongly rescued the promoting effect of miR-424-5p on ESCC cell proliferation and migration capacity. In addition, Nakahara *et al*[77] reported that a low SIRT4 expression was significantly associated with a high distant recurrence rate and poor prognosis, and *in vitro*, knockdown of SIRT4 promoted glutamine dehydrogenase activity and stimulated cell proliferation and migration.

SIRT5

As with other sirtuins, the role of SIRT5 in cancer is highly controversial with some reports emphasizing the cancer-promoting function of SIRT5. (Table 1 and Figure 2). SIRT5 functionally activates glutamate dehydrogenase 1 (GLUD1), an important regulator of intracellular glutaminolysis, and is involved in cell proliferation[78]. In addition, Yang reported that SIRT5 mediated the desuccinylation of SHMT2 and enhanced its activity, which in turn promotes serine metabolism in tumor cells thereby promoting cancer cell growth[79]. Furthermore, studies have shown that SIRT3 promotes cell proliferation by targeting NRF2, pyruvate kinase M2 (PKM2), and Sad1 and UNC84 domain containing 2 (SUN2)[80-82]. Regarding apoptosis, SIRT5 has been reported to deacetylate cytochrome C (Cyt c) and induce mitochondrial apoptosis[83]. Gu *et al*[84] demonstrated that SIRT5 enhances autophagy and exerts tumor-promoting functions in gastric cancer cells. Moreover, SIRT5 promotes cancer cell invasion and migration by targeting E2F1[85]. Du *et al*[86] revealed that SIRT5 demalonylated and inactivated

succinate dehydrogenase complex flavoprotein subunit A (SDHA) and accumulated its metabolite succinate resulting in resistance to chemotherapy.

In contrast, SIRT5 has also been reported to have tumor-suppressive effects (Table 1). Chen *et al*[87] revealed that SIRT5-mediated desuccinylation inhibited the activity of acyl-CoA oxidase 1 (ACOX1) and played an important role in the suppression of oxidative stress, protection of the liver and inhibition of HCC development. SIRT5 has been suggested to have a tumor-suppressor function *via* desuccinylation of superoxide dismutase 1 (SOD1)[88]. Furthermore, Polletta *et al*[89] demonstrated that SIRT5 inhibited ammonia-induced autophagy which is regarded as a protective mechanism for tumor cells. Therefore, activation of SIRT5 is thought to reduce the survival of tumor cells in response to stresses, such as chemotherapy, hypoxia and nutrient starvation.

The relationship between the SIRT5 expression and clinical prognosis has also been reported to vary by cancer type[78,90].

In EC, there have been no reports on the role of SIRT5, and there is much room for further investigation of the association between SIRT5 and EC.

SIRT6

SIRT6, like other sirtuins, functions as a double-edged sword in cancer (Table 1 and Figure 2). SIRT6 inhibits tumor growth by targeting poly(rC) binding protein 2 (PCBP2) and extracellular signal-regulated kinases 1/2 (ERK1/2)[91,92]. SIRT6 represses HIF-1α and regulates the expression of multiple glycolytic genes[93]. This indicates that SIRT6 plays a role in tumor suppression by inhibiting the Warburg effect. In addition, SIRT6 induces apoptosis in cancer cells by acting on NF-κB, BCL2 associated X (Bax) and survivin[94,95]. Bhardwaj *et al*[96] found that SIRT6 inhibited the oncogenic activity of PKM2, which has a non-metabolic nuclear carcinogenic function, resulting in a reduced cell proliferation, migration ability and invasiveness. One meta-analysis revealed that a high SIRT6 expression was associated with a longer OS in gastrointestinal cancers and a favorable TNM stage[97].

However, the role of SIRT6 as a tumor-promoting factor has also been reported. SIRT6 enhances HCC cell proliferation and inhibits apoptosis through the regulation of the ERK1/2 pathway[98]. In addition, Zhou *et al*[99] revealed that SIRT6 inhibited the acetylation of AKT and promoted its activation thereby preventing apoptosis and inducing cell proliferation. Bai *et al*[100] reported that the overexpression of SIRT6 in non-small-cell lung cancer cell lines promoted migration and invasion *via* ERK1/2/MMP9 signaling. SIRT6 has also been reported to positively regulate autophagy in melanoma cells and to exhibit tumor-promoting effects[101].

In EC, SIRT6 has been reported as a tumor-promoting factor (Table 2). Huang *et al*[102] demonstrated that SIRT6 was markedly overexpressed in ESCC tissues and that it also promoted cell proliferation and induced the expression of Bcl2, an important anti-apoptotic factor and autophagy in ESCC cells.

SIRT7

Like other sirtuins, SIRT7 has also been reported to have both tumor-promoting and tumor-suppressing roles (Table 1 and Figure 2). SIRT7 promotes cell proliferation by regulating ERK1/2 and histone H3 Lysine 18 acetylation (H3K18ac)[103,104]. In addition, SIRT7 induces apoptosis *via* miR34a, NF-κB family subunits and the mTOR/insulin like growth factor 2 (IGF2) pathway[105-107]. SIRT7 also influences the metastasis of cancer cells. Yu *et al*[103] showed that cells overexpressing SIRT7 had elevated levels of vimentin and fibronectin, which are markers of mesenchymal lineage, and decreased levels of E-cadherin and β-catenin, which are markers of epithelial lineage indicating enhanced invasion of colon cancer cells.

The role of SIRT7 as a tumor suppressor has been reported to include inhibition of growth and metastasis. Li *et al*[108] demonstrated that SIRT7 inhibited cell proliferation and invasion by deacetylating SMAD4 in oral squamous cell carcinoma. In addition, Tang *et al*[109] also revealed that loss of SIRT7 activated TGF-β signaling and promoted EMT.

Reports concerning the relationship between the SIRT7 expression and the prognosis are conflicting, with some citing a good prognosis while the others describe a poor prognosis[110].

In EC, there are no reports investigating the role of SIRT7, and whether it acts as a tumor-promoting factor or a tumor-suppressing factor remains unclear.

FUTURE PERSPECTIVES

As mentioned above, sirtuins have been investigated in a variety of cancer types and play a dichotomous role depending on the situation. This trend is also true in the field of EC. SIRT1, SIRT2, SIRT3 and SIRT6 have been reported as tumor-promoting factors in ESCC, along with SIRT1 in EAC,

while SIRT4 and SIRT2 have been reported as tumor suppressors in ESCC and EAC, respectively. SIRT5 and SIRT7 are interesting targets of study since their roles in both ESCC and EAC have not yet been reported.

One of the future points to be explored concerning sirtuins in EC is expected to be their utility as biomarkers. In most previous studies, the degree of sirtuin expression was assessed by immunohistochemistry. However, the cut-off values for sirtuin expression differed among studies, and this heterogeneity in assessment methods may have led to conflicting results among cancer types. Therefore, more accurate and less-invasive evaluations are anticipated in the future. Serum SIRT3 Levels have been reported to be a potentially useful biomarker, not only in EC[63] but also in lung cancer[111], suggesting that serum sirtuin levels merit exploration as a minimally invasive biomarker. Furthermore, in recent years, a wide variety of public databases, such as TCGA, have been used for analyses[67]. This is expected to make it possible to obtain more comprehensive and standardizable information in the future.

Since sirtuin enzymes play an important role in the regulation of various cellular events, there is strong interest in pursuing sirtuins as therapeutic targets. Although many reports related to the development of sirtuin inhibitors/activators have been found in electronic searches, only a very limited number of small-molecule compounds, such as reveratol and Ex-527, have been subjected to clinical trials[112]. In the field of EC, the effects of the SIRT1 inhibitors rapamycin and sirtinol have been reported *in vitro* and *in vivo*[35,36]. However, SIRT1, like other sirtuins, has been suggested to promote or inhibit cancer in a context-dependent manner so many comprehensive studies are needed to determine its clinical application. Although not yet presented, other sirtuin-targeted agents still have great therapeutic potential and advances in this area will contribute to the development of EC treatment.

In recent years, the breakthrough of immunotherapy has been considered an important topic in EC [113]. The involvement of sirtuins in immunity has been widely studied since the early discovery that SIRT1 regulates NF-κB, a transcription factor known to control inflammation and immune cell proliferation[114]. There have been no reports on the role of sirtuins in immunotherapy of esophageal cancer, although some reports have appeared in other cancer types. Zhang *et al*[115] showed that pharmacological inhibition of SIRT2 increased natural killer cell infiltration into the tumor and suppressed tumor growth in allograft melanoma. Furthermore, Xiang *et al*[116] demonstrated that SIRT7 suppressed myocyte enhancer factor 2D acetylation and programmed death ligand 1 expression and promoted HCC cell proliferation. Thus, the role of sirtuins in anti-tumor immunity in EC is an issue that deserves further attention and research.

CONCLUSION

In summary, sirtuins may be a key target for EC treatment in the future. However, much research is still needed to determine the clinical application as many aspects remain unresolved. We hope that this review will contribute to the development of this field.

FOOTNOTES

Author contributions: Otsuka R contributed to conception and design; All authors contributed to manuscript writing, figure preparation and review and approval of the article to be published.

Conflict-of-interest statement: The authors declare that they have no conflict of interest.

Country/Territory of origin: Japan

ORCID number: Ryota Otsuka 0000-0001-7360-9069; Koichi Hayano 0000-0003-4733-8220; Hisahiro Matsubara 0000-0002-2335-4704.

S-Editor: Gong ZM
L-Editor: Filipodia
P-Editor: Gong ZM

REFERENCES

1 **Sung H**, Ferlay J, Siegel RL, Laversanne M, Soerjomataram I, Jemal A, Bray F. Global Cancer Statistics 2020: GLOBOCAN Estimates of Incidence and Mortality Worldwide for 36 Cancers in 185 Countries. *CA Cancer J Clin* 2021; **71**: 209-249 [PMID: 33538338 DOI: 10.3322/caac.21660]

2 **Pennathur A**, Gibson MK, Jobe BA, Luketich JD. Oesophageal carcinoma. *Lancet* 2013; **381**: 400-412 [PMID: 23374478 DOI: 10.1016/S0140-6736(12)60643-6]

3 **Michan S**, Sinclair D. Sirtuins in mammals: insights into their biological function. *Biochem J* 2007; **404**: 1-13 [PMID: 17447894 DOI: 10.1042/bj20070140]

4 **Frye RA**. Phylogenetic classification of prokaryotic and eukaryotic Sir2-like proteins. *Biochem Biophys Res Commun* 2000; **273**: 793-798 [PMID: 10873683 DOI: 10.1006/bbrc.2000.3000]

5 **Jaiswal A**, Xudong Z, Zhenyu J, Saretzki G. Mitochondrial sirtuins in stem cells and cancer. *FEBS J* 2021 [PMID: 33866670 DOI: 10.1111/febs.15879]

6 **Zhao E**, Hou J, Ke X, Abbas MN, Kausar S, Zhang L, Cui H. The Roles of Sirtuin Family Proteins in Cancer Progression. *Cancers (Basel)* 2019; **11** [PMID: 31817470 DOI: 10.3390/cancers11121949]

7 **Li K**, Luo J. The role of SIRT1 in tumorigenesis. *N Am J Med Sci (Boston)* 2011; **4**: 104-106 [PMID: 22180829 DOI: 10.7156/v4i2p104]

8 **Sasca D**, Hähnel PS, Szybinski J, Khawaja K, Kriege O, Pante SV, Bullinger L, Strand S, Strand D, Theobald M, Kindler T. SIRT1 prevents genotoxic stress-induced p53 activation in acute myeloid leukemia. *Blood* 2014; **124**: 121-133 [PMID: 24855208 DOI: 10.1182/blood-2013-11-538819]

9 **Motta MC**, Divecha N, Lemieux M, Kamel C, Chen D, Gu W, Bultsma Y, McBurney M, Guarente L. Mammalian SIRT1 represses forkhead transcription factors. *Cell* 2004; **116**: 551-563 [PMID: 14980222 DOI: 10.1016/s0092-8674(04)00126-6]

10 **Wang C**, Chen L, Hou X, Li Z, Kabra N, Ma Y, Nemoto S, Finkel T, Gu W, Cress WD, Chen J. Interactions between E2F1 and SirT1 regulate apoptotic response to DNA damage. *Nat Cell Biol* 2006; **8**: 1025-1031 [PMID: 16892051 DOI: 10.1038/ncb1468]

11 **Dai JM**, Wang ZY, Sun DC, Lin RX, Wang SQ. SIRT1 interacts with p73 and suppresses p73-dependent transcriptional activity. *J Cell Physiol* 2007; **210**: 161-166 [PMID: 16998810 DOI: 10.1002/jcp.20831]

12 **Wong S**, Weber JD. Deacetylation of the retinoblastoma tumour suppressor protein by SIRT1. *Biochem J* 2007; **407**: 451-460 [PMID: 17620057 DOI: 10.1042/bj20070151]

13 **Cohen HY**, Miller C, Bitterman KJ, Wall NR, Hekking B, Kessler B, Howitz KT, Gorospe M, de Cabo R, Sinclair DA. Calorie restriction promotes mammalian cell survival by inducing the SIRT1 deacetylase. *Science* 2004; **305**: 390-392 [PMID: 15205477 DOI: 10.1126/science.1099196]

14 **Pruitt K**, Zinn RL, Ohm JE, McGarvey KM, Kang SH, Watkins DN, Herman JG, Baylin SB. Inhibition of SIRT1 reactivates silenced cancer genes without loss of promoter DNA hypermethylation. *PLoS Genet* 2006; **2**: e40 [PMID: 16596166 DOI: 10.1371/journal.pgen.0020040]

15 **Byles V**, Zhu L, Lovaas JD, Chmilewski LK, Wang J, Faller DV, Dai Y. SIRT1 induces EMT by cooperating with EMT transcription factors and enhances prostate cancer cell migration and metastasis. *Oncogene* 2012; **31**: 4619-4629 [PMID: 22249256 DOI: 10.1038/onc.2011.612]

16 **Noguchi A**, Kikuchi K, Zheng H, Takahashi H, Miyagi Y, Aoki I, Takano Y. SIRT1 expression is associated with a poor prognosis, whereas DBC1 is associated with favorable outcomes in gastric cancer. *Cancer Med* 2014; **3**: 1553-1561 [PMID: 25146318 DOI: 10.1002/cam4.310]

17 **Li C**, Wang L, Zheng L, Zhan X, Xu B, Jiang J, Wu C. SIRT1 expression is associated with poor prognosis of lung adenocarcinoma. *Onco Targets Ther* 2015; **8**: 977-984 [PMID: 25995644 DOI: 10.2147/OTT.S82378]

18 **Zu G**, Ji A, Zhou T, Che N. Clinicopathological significance of SIRT1 expression in colorectal cancer: A systematic review and meta analysis. *Int J Surg* 2016; **26**: 32-37 [PMID: 26763348 DOI: 10.1016/j.ijsu.2016.01.002]

19 **Firestein R**, Blander G, Michan S, Oberdoerffer P, Ogino S, Campbell J, Bhimavarapu A, Luikenhuis S, de Cabo R, Fuchs C, Hahn WC, Guarente LP, Sinclair DA. The SIRT1 deacetylase suppresses intestinal tumorigenesis and colon cancer growth. *PLoS One* 2008; **3**: e2020 [PMID: 18414679 DOI: 10.1371/journal.pone.0002020]

20 **Wang RH**, Zheng Y, Kim HS, Xu X, Cao L, Luhasen T, Lee MH, Xiao C, Vassilopoulos A, Chen W, Gardner K, Man YG, Hung MC, Finkel T, Deng CX. Interplay among BRCA1, SIRT1, and Survivin during BRCA1-associated tumorigenesis. *Mol Cell* 2008; **32**: 11-20 [PMID: 18851829 DOI: 10.1016/j.molcel.2008.09.011]

21 **Simic P**, Williams EO, Bell EL, Gong JJ, Bonkowski M, Guarente L. SIRT1 suppresses the epithelial-to-mesenchymal transition in cancer metastasis and organ fibrosis. *Cell Rep* 2013; **3**: 1175-1186 [PMID: 23583181 DOI: 10.1016/j.celrep.2013.03.019]

22 **Qin T**, Liu W, Huo J, Li L, Zhang X, Shi X, Zhou J, Wang C. SIRT1 expression regulates the transformation of resistant esophageal cancer cells *via* the epithelial-mesenchymal transition. *Biomed Pharmacother* 2018; **103**: 308-316 [PMID: 29656187 DOI: 10.1016/j.biopha.2018.04.032]

23 **Ma MC**, Chiu TJ, Lu HI, Huang WT, Lo CM, Tien WY, Lan YC, Chen YY, Chen CH, Li SH. SIRT1 overexpression is an independent prognosticator for patients with esophageal squamous cell carcinoma. *J Cardiothorac Surg* 2018; **13**: 25 [PMID: 29636061 DOI: 10.1186/s13019-018-0718-5]

24 **Chen GQ**, Tian H, Yue WM, Li L, Li SH, Qi L, Gao C, Si LB, Lu M, Feng F. SIRT1 expression is associated with lymphangiogenesis, lymphovascular invasion and prognosis in pN0 esophageal squamous cell carcinoma. *Cell Biosci* 2014; **4**: 48 [PMID: 25922660 DOI: 10.1186/2045-3701-4-48]

25 **He Z**, Yi J, Jin L, Pan B, Chen L, Song H. Overexpression of Sirtuin-1 is associated with poor clinical outcome in esophageal squamous cell carcinoma. *Tumour Biol* 2016; **37**: 7139-7148 [PMID: 26662958 DOI: 10.1007/s13277-015-4459-y]

26 **Han F**, Zhang S, Liang J, Qiu W. Clinicopathological and predictive significance of SIRT1 and peroxisome proliferator-activated receptor gamma in esophageal squamous cell carcinoma: The correlation with EGFR and Survivin. *Pathol Res*

Pract 2018; **214**: 686-690 [PMID: 29625788 DOI: 10.1016/j.prp.2018.03.018]
27 **Yan L**, Zhao Q, Liu L, Jin N, Wang S, Zhan X. Expression of SIRT1 and survivin correlates with poor prognosis in esophageal squamous cell carcinoma. *Medicine (Baltimore)* 2020; **99**: e21645 [PMID: 32846774 DOI: 10.1097/MD.0000000000021645]
28 **Zhu L**, Dong L, Feng M, Yang F, Jiang W, Huang Z, Liu F, Wang L, Wang G, Li Q. Profiles of autophagy-related genes in esophageal adenocarcinoma. *BMC Cancer* 2020; **20**: 943 [PMID: 32998713 DOI: 10.1186/s12885-020-07416-w]
29 **Cao B**, Shi Q, Wang W. Higher expression of SIRT1 induced resistance of esophageal squamous cell carcinoma cells to cisplatin. *J Thorac Dis* 2015; **7**: 711-719 [PMID: 25973238 DOI: 10.3978/j.issn.2072-1439.2015.04.01]
30 **Chen Y**, Xie T, Ye Z, Wang F, Long D, Jiang M, Fang J, Lin Q, Li K, Wang Z, Fu Z. ADC correlation with Sirtuin1 to assess early chemoradiotherapy response of locally advanced esophageal carcinoma patients. *Radiat Oncol* 2019; **14**: 192 [PMID: 31684999 DOI: 10.1186/s13014-019-1393-y]
31 **Kuo IY**, Huang YL, Lin CY, Lin CH, Chang WL, Lai WW, Wang YC. SOX17 overexpression sensitizes chemoradiation response in esophageal cancer by transcriptional down-regulation of DNA repair and damage response genes. *J Biomed Sci* 2019; **26**: 20 [PMID: 30777052 DOI: 10.1186/s12929-019-0510-4]
32 **Ye Z**, Xie T, Yan F, Wang L, Fang J, Wang Z, Hu F, Wang F, Fu Z. MiR-34a reverses radiation resistance on ECA-109 cells by inhibiting PI3K/AKT/mTOR signal pathway through downregulating the expression of SIRT1. *Int J Radiat Biol* 2021; **97**: 452-463 [PMID: 33507132 DOI: 10.1080/09553002.2021.1866225]
33 **Zhang S**, Wang XI. SIRT1 is a useful biomarker for high-grade dysplasia and carcinoma in Barrett's esophagus. *Ann Clin Lab Sci* 2013; **43**: 373-377 [PMID: 24247792]
34 **Otsuka R**, Sakata H, Murakami K, Kano M, Endo S, Toyozumi T, Matsumoto Y, Suito H, Takahashi M, Sekino N, Hirasawa S, Kinoshita K, Sasaki T, Matsubara H. SIRT1 Expression Is a Promising Prognostic Biomarker in Esophageal Squamous Cell Carcinoma: A Systematic Review and Meta-Analysis. *Canner Diagn Progn* 2022; In press
35 **Liu T**, Liang X, Sun Y, Yang S. Rapamycin suppresses the PI3K/AKT/mTOR signaling pathway by targeting *SIRT1* in esophageal cancer. *Exp Ther Med* 2021; **22**: 1190 [PMID: 34475980 DOI: 10.3892/etm.2021.10624]
36 **Jiang H**, Patil K, Vashi A, Wang Y, Strickland E, Pai SB. Cellular molecular and proteomic profiling deciphers the SIRT1 controlled cell death pathways in esophageal adenocarcinoma cells. *Cancer Treat Res Commun* 2021; **26**: 100271 [PMID: 33341453 DOI: 10.1016/j.ctarc.2020.100271]
37 **Xie HJ**, Jung KH, Nam SW. Overexpression of SIRT2 contributes tumor cell growth in hepatocellular carcinomas. *Mol Cell Toxicol* 2011; **7**: 367-374 [DOI: 10.1007/s13273-011-0046-5]
38 **Liu PY**, Xu N, Malyukova A, Scarlett CJ, Sun YT, Zhang XD, Ling D, Su SP, Nelson C, Chang DK, Koach J, Tee AE, Haber M, Norris MD, Toon C, Rooman I, Xue C, Cheung BB, Kumar S, Marshall GM, Biankin AV, Liu T. The histone deacetylase SIRT2 stabilizes Myc oncoproteins. *Cell Death Differ* 2013; **20**: 503-514 [PMID: 23175188 DOI: 10.1038/cdd.2012.147]
39 **Chen G**, Huang P, Hu C. The role of SIRT2 in cancer: A novel therapeutic target. *Int J Cancer* 2020; **147**: 3297-3304 [PMID: 32449165 DOI: 10.1002/ijc.33118]
40 **Xu L**, Wang L, Zhou L, Dorfman RG, Pan Y, Tang D, Wang Y, Yin Y, Jiang C, Zou X, Wu J, Zhang M. The SIRT2/cMYC Pathway Inhibits Peroxidation-Related Apoptosis In Cholangiocarcinoma Through Metabolic Reprogramming. *Neoplasia* 2019; **21**: 429-441 [PMID: 30933885 DOI: 10.1016/j.neo.2019.03.002]
41 **Chen J**, Chan AW, To KF, Chen W, Zhang Z, Ren J, Song C, Cheung YS, Lai PB, Cheng SH, Ng MH, Huang A, Ko BC. SIRT2 overexpression in hepatocellular carcinoma mediates epithelial to mesenchymal transition by protein kinase B/glycogen synthase kinase-3β/β-catenin signaling. *Hepatology* 2013; **57**: 2287-2298 [PMID: 23348706 DOI: 10.1002/hep.26278]
42 **Huang S**, Zhao Z, Tang D, Zhou Q, Li Y, Zhou L, Yin Y, Wang Y, Pan Y, Dorfman RG, Ling T, Zhang M. Downregulation of SIRT2 Inhibits Invasion of Hepatocellular Carcinoma by Inhibiting Energy Metabolism. *Transl Oncol* 2017; **10**: 917-927 [PMID: 28992545 DOI: 10.1016/j.tranon.2017.09.006]
43 **Nguyen P**, Lee S, Lorang-Leins D, Trepel J, Smart DK. SIRT2 interacts with β-catenin to inhibit Wnt signaling output in response to radiation-induced stress. *Mol Cancer Res* 2014; **12**: 1244-1253 [PMID: 24866770 DOI: 10.1158/1541-7786.MCR-14-0223-T]
44 **Damodaran S**, Damaschke N, Gawdzik J, Yang B, Shi C, Allen GO, Huang W, Denu J, Jarrard D. Dysregulation of Sirtuin 2 (SIRT2) and histone H3K18 acetylation pathways associates with adverse prostate cancer outcomes. *BMC Cancer* 2017; **17**: 874 [PMID: 29262808 DOI: 10.1186/s12885-017-3853-9]
45 **Yang LP**, Feng HQ, Ma JC, Wu H, Liu CR, Hou JD. SIRT2 expression exhibits potential to serve as a biomarker for disease surveillance and prognosis in the management of cervical cancer patients. *Medicine (Baltimore)* 2020; **99**: e18668 [PMID: 32176025 DOI: 10.1097/MD.0000000000018668]
46 **Du F**, Li Z, Zhang G, Shaoyan S, Geng D, Tao Z, Qiu K, Liu S, Zhou Y, Zhang Y, Gu J, Wang G, Li L, Wu W. SIRT2, a direct target of miR-212-5p, suppresses the proliferation and metastasis of colorectal cancer cells. *J Cell Mol Med* 2020; **24**: 9985-9998 [PMID: 32697380 DOI: 10.1111/jcmm.15603]
47 **Yan L**, Zhan X, Jia Z, Liu L, Jin N. Sirtuin 2 (Sirt2) Expression Predicts Lymph Node Metastasis and Poor Overall Survival of Patients with Esophageal Squamous Cell Carcinoma. *Clin Lab* 2018; **64**: 669-675 [PMID: 29739048 DOI: 10.7754/Clin.Lab.2018.170905]
48 **Ong CA**, Shapiro J, Nason KS, Davison JM, Liu X, Ross-Innes C, O'Donovan M, Dinjens WN, Biermann K, Shannon N, Worster S, Schulz LK, Luketich JD, Wijnhoven BP, Hardwick RH, Fitzgerald RC. Three-gene immunohistochemical panel adds to clinical staging algorithms to predict prognosis for patients with esophageal adenocarcinoma. *J Clin Oncol* 2013; **31**: 1576-1582 [PMID: 23509313 DOI: 10.1200/JCO.2012.45.9636]
49 **Peters CJ**, Rees JR, Hardwick RH, Hardwick JS, Vowler SL, Ong CA, Zhang C, Save V, O'Donovan M, Rassl D, Alderson D, Caldas C, Fitzgerald RC; Oesophageal Cancer Clinical and Molecular Stratification (OCCAMS) Study Group. A 4-gene signature predicts survival of patients with resected adenocarcinoma of the esophagus, junction, and gastric cardia. *Gastroenterology* 2010; **139**: 1995-2004.e15 [PMID: 20621683 DOI: 10.1053/j.gastro.2010.05.080]
50 **Li S**, Banck M, Mujtaba S, Zhou MM, Sugrue MM, Walsh MJ. p53-induced growth arrest is regulated by the

mitochondrial SirT3 deacetylase. *PLoS One* 2010; **5**: e10486 [PMID: 20463968 DOI: 10.1371/journal.pone.0010486]
51 **Wei Z**, Song J, Wang G, Cui X, Zheng J, Tang Y, Chen X, Li J, Cui L, Liu CY, Yu W. Deacetylation of serine hydroxymethyl-transferase 2 by SIRT3 promotes colorectal carcinogenesis. *Nat Commun* 2018; **9**: 4468 [PMID: 30367038 DOI: 10.1038/s41467-018-06812-y]
52 **Bergaggio E**, Riganti C, Garaffo G, Vitale N, Mereu E, Bandini C, Pellegrino E, Pullano V, Omedè P, Todoerti K, Cascione L, Audrito V, Riccio A, Rossi A, Bertoni F, Deaglio S, Neri A, Palumbo A, Piva R. IDH2 inhibition enhances proteasome inhibitor responsiveness in hematological malignancies. *Blood* 2019; **133**: 156-167 [PMID: 30455381 DOI: 10.1182/blood-2018-05-850826]
53 **Xu LX**, Hao LJ, Ma JQ, Liu JK, Hasim A. SIRT3 promotes the invasion and metastasis of cervical cancer cells by regulating fatty acid synthase. *Mol Cell Biochem* 2020; **464**: 11-20 [PMID: 31677030 DOI: 10.1007/s11010-019-03644-2]
54 **Allison SJ**, Milner J. SIRT3 is pro-apoptotic and participates in distinct basal apoptotic pathways. *Cell Cycle* 2007; **6**: 2669-2677 [PMID: 17957139 DOI: 10.4161/cc.6.21.4866]
55 **Finley LW**, Carracedo A, Lee J, Souza A, Egia A, Zhang J, Teruya-Feldstein J, Moreira PI, Cardoso SM, Clish CB, Pandolfi PP, Haigis MC. SIRT3 opposes reprogramming of cancer cell metabolism through HIF1α destabilization. *Cancer Cell* 2011; **19**: 416-428 [PMID: 21397863 DOI: 10.1016/j.ccr.2011.02.014]
56 **Xiao K**, Jiang J, Wang W, Cao S, Zhu L, Zeng H, Ouyang R, Zhou R, Chen P. Sirt3 is a tumor suppressor in lung adenocarcinoma cells. *Oncol Rep* 2013; **30**: 1323-1328 [PMID: 23842789 DOI: 10.3892/or.2013.2604]
57 **Fan J**, Shan C, Kang HB, Elf S, Xie J, Tucker M, Gu TL, Aguiar M, Lonning S, Chen H, Mohammadi M, Britton LM, Garcia BA, Alečković M, Kang Y, Kaluz S, Devi N, Van Meir EG, Hitosugi T, Seo JH, Lonial S, Gaddh M, Arellano M, Khoury HJ, Khuri FR, Boggon TJ, Kang S, Chen J. Tyr phosphorylation of PDP1 toggles recruitment between ACAT1 and SIRT3 to regulate the pyruvate dehydrogenase complex. *Mol Cell* 2014; **53**: 534-548 [PMID: 24486017 DOI: 10.1016/j.molcel.2013.12.026]
58 **Yang H**, Zhou L, Shi Q, Zhao Y, Lin H, Zhang M, Zhao S, Yang Y, Ling ZQ, Guan KL, Xiong Y, Ye D. SIRT3-dependent GOT2 acetylation status affects the malate-aspartate NADH shuttle activity and pancreatic tumor growth. *EMBO J* 2015; **34**: 1110-1125 [PMID: 25755250 DOI: 10.15252/embj.201591041]
59 **Yu W**, Denu RA, Krautkramer KA, Grindle KM, Yang DT, Asimakopoulos F, Hematti P, Denu JM. Loss of SIRT3 Provides Growth Advantage for B Cell Malignancies. *J Biol Chem* 2016; **291**: 3268-3279 [PMID: 26631723 DOI: 10.1074/jbc.M115.702076]
60 **Li R**, Quan Y, Xia W. SIRT3 inhibits prostate cancer metastasis through regulation of FOXO3A by suppressing Wnt/β-catenin pathway. *Exp Cell Res* 2018; **364**: 143-151 [PMID: 29421536 DOI: 10.1016/j.yexcr.2018.01.036]
61 **Ozden O**, Park SH, Wagner BA, Song HY, Zhu Y, Vassilopoulos A, Jung B, Buettner GR, Gius D. SIRT3 deacetylates and increases pyruvate dehydrogenase activity in cancer cells. *Free Radic Biol Med* 2014; **76**: 163-172 [PMID: 25152236 DOI: 10.1016/j.freeradbiomed.2014.08.001]
62 **Torrens-Mas M**, Oliver J, Roca P, Sastre-Serra J. SIRT3: Oncogene and Tumor Suppressor in Cancer. *Cancers (Basel)* 2017; **9** [PMID: 28704962 DOI: 10.3390/cancers9070090]
63 **Cobanoğlu U**, Dülger C, Kemik O, Celik S, Sayir F. A novel screening test for esophageal squamous cell carcinoma: sirtuin-3. *Eur Rev Med Pharmacol Sci* 2017; **21**: 5399-5401 [PMID: 29243781 DOI: 10.26355/eurrev_201712_13926]
64 **Yang M**, Yang C, Pei Y. Effects of downregulation of SIRT3 expression on proliferation and apoptosis in esophageal squamous cell carcinoma EC9706 cells and its molecular mechanisms. *Biomed Mater Eng* 2014; **24**: 3883-3890 [PMID: 25227106 DOI: 10.3233/BME-141219]
65 **Zhao Y**, Yang H, Wang X, Zhang R, Wang C, Guo Z. Sirtuin-3 (SIRT3) expression is associated with overall survival in esophageal cancer. *Ann Diagn Pathol* 2013; **17**: 483-485 [PMID: 23871415 DOI: 10.1016/j.anndiagpath.2013.06.001]
66 **Yan SM**, Han X, Han PJ, Chen HM, Huang LY, Li Y. SIRT3 is a novel prognostic biomarker for esophageal squamous cell carcinoma. *Med Oncol* 2014; **31**: 103 [PMID: 25005846 DOI: 10.1007/s12032-014-0103-8]
67 **Wang YS**, Du L, Liang X, Meng P, Bi L, Wang YL, Wang C, Tang B. Sirtuin 4 Depletion Promotes Hepatocellular Carcinoma Tumorigenesis Through Regulating Adenosine-Monophosphate-Activated Protein Kinase Alpha/Mammalian Target of Rapamycin Axis in Mice. *Hepatology* 2019; **69**: 1614-1631 [PMID: 30552782 DOI: 10.1002/hep.30421]
68 **Jeong SM**, Xiao C, Finley LW, Lahusen T, Souza AL, Pierce K, Li YH, Wang X, Laurent G, German NJ, Xu X, Li C, Wang RH, Lee J, Csibi A, Cerione R, Blenis J, Clish CB, Kimmelman A, Deng CX, Haigis MC. SIRT4 has tumor-suppressive activity and regulates the cellular metabolic response to DNA damage by inhibiting mitochondrial glutamine metabolism. *Cancer Cell* 2013; **23**: 450-463 [PMID: 23562301 DOI: 10.1016/j.ccr.2013.02.024]
69 **Csibi A**, Fendt SM, Li C, Poulogiannis G, Choo AY, Chapski DJ, Jeong SM, Dempsey JM, Parkhitko A, Morrison T, Henske EP, Haigis MC, Cantley LC, Stephanopoulos G, Yu J, Blenis J. The mTORC1 pathway stimulates glutamine metabolism and cell proliferation by repressing SIRT4. *Cell* 2021; **184**: 2256 [PMID: 33861966 DOI: 10.1016/j.cell.2021.03.059]
70 **Miyo M**, Yamamoto H, Konno M, Colvin H, Nishida N, Koseki J, Kawamoto K, Ogawa H, Hamabe A, Uemura M, Nishimura J, Hata T, Takemasa I, Mizushima T, Doki Y, Mori M, Ishii H. Tumour-suppressive function of SIRT4 in human colorectal cancer. *Br J Cancer* 2015; **113**: 492-499 [PMID: 26086877 DOI: 10.1038/bjc.2015.226]
71 **Sun H**, Huang D, Liu G, Jian F, Zhu J, Zhang L. SIRT4 acts as a tumor suppressor in gastric cancer by inhibiting cell proliferation, migration, and invasion. *Onco Targets Ther* 2018; **11**: 3959-3968 [PMID: 30022839 DOI: 10.2147/OTT.S156143]
72 **Hu Y**, Lin J, Lin Y, Chen X, Zhu G, Huang G. Overexpression of SIRT4 inhibits the proliferation of gastric cancer cells through cell cycle arrest. *Oncol Lett* 2019; **17**: 2171-2176 [PMID: 30745932 DOI: 10.3892/ol.2018.9877]
73 **Wang C**, Liu Y, Zhu Y, Kong C. Functions of mammalian SIRT4 in cellular metabolism and research progress in human cancer. *Oncol Lett* 2020; **20**: 11 [PMID: 32774484 DOI: 10.3892/ol.2020.11872]
74 **Jeong SM**, Hwang S, Seong RH. SIRT4 regulates cancer cell survival and growth after stress. *Biochem Biophys Res Commun* 2016; **470**: 251-256 [PMID: 26775843 DOI: 10.1016/j.bbrc.2016.01.078]
75 **Liu M**, Wang Z, Ren M, Yang X, Liu B, Qi H, Yu M, Song S, Chen S, Liu L, Zhang Y, Zou J, Zhu WG, Yin Y, Luo J. SIRT4 regulates PTEN stability through IDE in response to cellular stresses. *FASEB J* 2019; **33**: 5535-5547 [PMID:

30649986 DOI: 10.1096/fj.201801987R]
76 **Cui Y**, Yang J, Bai Y, Zhang Y, Yao Y, Zheng T, Liu C, Wu F. miR-424-5p regulates cell proliferation and migration of esophageal squamous cell carcinoma by targeting SIRT4. *J Cancer* 2020; **11**: 6337-6347 [PMID: 33033517 DOI: 10.7150/jca.50587]
77 **Nakahara Y**, Yamasaki M, Sawada G, Miyazaki Y, Makino T, Takahashi T, Kurokawa Y, Nakajima K, Takiguchi S, Mimori K, Mori M, Doki Y. Downregulation of SIRT4 Expression Is Associated with Poor Prognosis in Esophageal Squamous Cell Carcinoma. *Oncology* 2016; **90**: 347-355 [PMID: 27082627 DOI: 10.1159/000445323]
78 **Wang YQ**, Wang HL, Xu J, Tan J, Fu LN, Wang JL, Zou TH, Sun DF, Gao QY, Chen YX, Fang JY. Sirtuin5 contributes to colorectal carcinogenesis by enhancing glutaminolysis in a deglutarylation-dependent manner. *Nat Commun* 2018; **9**: 545 [PMID: 29416026 DOI: 10.1038/s41467-018-02951-4]
79 **Yang X**, Wang Z, Li X, Liu B, Liu M, Liu L, Chen S, Ren M, Wang Y, Yu M, Wang B, Zou J, Zhu WG, Yin Y, Gu W, Luo J. SHMT2 Desuccinylation by SIRT5 Drives Cancer Cell Proliferation. *Cancer Res* 2018; **78**: 372-386 [PMID: 29180469 DOI: 10.1158/0008-5472.CAN-17-1912]
80 **Lu W**, Zuo Y, Feng Y, Zhang M. SIRT5 facilitates cancer cell growth and drug resistance in non-small cell lung cancer. *Tumour Biol* 2014; **35**: 10699-10705 [PMID: 25070488 DOI: 10.1007/s13277-014-2372-4]
81 **Lv XB**, Liu L, Cheng C, Yu B, Xiong L, Hu K, Tang J, Zeng L, Sang Y. SUN2 exerts tumor suppressor functions by suppressing the Warburg effect in lung cancer. *Sci Rep* 2015; **5**: 17940 [PMID: 26658802 DOI: 10.1038/srep17940]
82 **Xiangyun Y**, Xiaomin N, Linping G, Yunhua X, Ziming L, Yongfeng Y, Zhiwei C, Shun L. Desuccinylation of pyruvate kinase M2 by SIRT5 contributes to antioxidant response and tumor growth. *Oncotarget* 2017; **8**: 6984-6993 [PMID: 28036303 DOI: 10.18632/oncotarget.14346]
83 **Zhang R**, Wang C, Tian Y, Yao Y, Mao J, Wang H, Li Z, Xu Y, Ye M, Wang L. SIRT5 Promotes Hepatocellular Carcinoma Progression by Regulating Mitochondrial Apoptosis. *J Cancer* 2019; **10**: 3871-3882 [PMID: 31333804 DOI: 10.7150/jca.31266]
84 **Gu W**, Qian Q, Xu Y, Xu X, Zhang L, He S, Li D. SIRT5 regulates autophagy and apoptosis in gastric cancer cells. *J Int Med Res* 2021; **49**: 300060520986355 [PMID: 33530803 DOI: 10.1177/0300060520986355]
85 **Chang L**, Xi L, Liu Y, Liu R, Wu Z, Jian Z. SIRT5 promotes cell proliferation and invasion in hepatocellular carcinoma by targeting E2F1. *Mol Med Rep* 2018; **17**: 342-349 [PMID: 29115436 DOI: 10.3892/mmr.2017.7875]
86 **Du Z**, Liu X, Chen T, Gao W, Wu Z, Hu Z, Wei D, Gao C, Li Q. Targeting a Sirt5-Positive Subpopulation Overcomes Multidrug Resistance in Wild-Type Kras Colorectal Carcinomas. *Cell Rep* 2018; **22**: 2677-2689 [PMID: 29514096 DOI: 10.1016/j.celrep.2018.02.037]
87 **Chen XF**, Tian MX, Sun RQ, Zhang ML, Zhou LS, Jin L, Chen LL, Zhou WJ, Duan KL, Chen YJ, Gao C, Cheng ZL, Wang F, Zhang JY, Sun YP, Yu HX, Zhao YZ, Yang Y, Liu WR, Shi YH, Xiong Y, Guan KL, Ye D. SIRT5 inhibits peroxisomal ACOX1 to prevent oxidative damage and is downregulated in liver cancer. *EMBO Rep* 2018; **19** [PMID: 29491006 DOI: 10.15252/embr.201745124]
88 **Lin ZF**, Xu HB, Wang JY, Lin Q, Ruan Z, Liu FB, Jin W, Huang HH, Chen X. SIRT5 desuccinylates and activates SOD1 to eliminate ROS. *Biochem Biophys Res Commun* 2013; **441**: 191-195 [PMID: 24140062 DOI: 10.1016/j.bbrc.2013.10.033]
89 **Polletta L**, Vernucci E, Carnevale I, Arcangeli T, Rotili D, Palmerio S, Steegborn C, Nowak T, Schutkowski M, Pellegrini L, Sansone L, Villanova L, Runci A, Pucci B, Morgante E, Fini M, Mai A, Russo MA, Tafani M. SIRT5 regulation of ammonia-induced autophagy and mitophagy. *Autophagy* 2015; **11**: 253-270 [PMID: 25700560 DOI: 10.1080/15548627.2015.1009778]
90 **Chen X**, Xu Z, Zeng S, Wang X, Liu W, Qian L, Wei J, Yang X, Shen Q, Gong Z, Yan Y. SIRT5 downregulation is associated with poor prognosis in glioblastoma. *Cancer Biomark* 2019; **24**: 449-459 [PMID: 30909186 DOI: 10.3233/CBM-182197]
91 **Chen X**, Hao B, Liu Y, Dai D, Han G, Li Y, Wu X, Zhou X, Yue Z, Wang L, Cao Y, Liu J. The histone deacetylase SIRT6 suppresses the expression of the RNA-binding protein PCBP2 in glioma. *Biochem Biophys Res Commun* 2014; **446**: 364-369 [PMID: 24607900 DOI: 10.1016/j.bbrc.2014.02.116]
92 **Zhang ZG**, Qin CY. Sirt6 suppresses hepatocellular carcinoma cell growth *via* inhibiting the extracellular signalregulated kinase signaling pathway. *Mol Med Rep* 2014; **9**: 882-888 [PMID: 24366394 DOI: 10.3892/mmr.2013.1879]
93 **Zhong L**, D'Urso A, Toiber D, Sebastian C, Henry RE, Vadysirisack DD, Guimaraes A, Marinelli B, Wikstrom JD, Nir T, Clish CB, Vaitheesvaran B, Iliopoulos O, Kurland I, Dor Y, Weissleder R, Shirihai OS, Ellisen LW, Espinosa JM, Mostoslavsky R. The histone deacetylase Sirt6 regulates glucose homeostasis *via* Hif1alpha. *Cell* 2010; **140**: 280-293 [PMID: 20141841 DOI: 10.1016/j.cell.2009.12.041]
94 **Fukuda T**, Wada-Hiraike O, Oda K, Tanikawa M, Makii C, Inaba K, Miyasaka A, Miyamoto Y, Yano T, Maeda D, Sasaki T, Kawana K, Fukayama M, Osuga Y, Fujii T. Putative tumor suppression function of SIRT6 in endometrial cancer. *FEBS Lett* 2015; **589**: 2274-2281 [PMID: 26183563 DOI: 10.1016/j.febslet.2015.06.043]
95 **Ouyang L**, Yi L, Li J, Yi S, Li S, Liu P, Yang X. SIRT6 overexpression induces apoptosis of nasopharyngeal carcinoma by inhibiting NF-κB signaling. *Onco Targets Ther* 2018; **11**: 7613-7624 [PMID: 30464510 DOI: 10.2147/OTT.S179866]
96 **Bhardwaj A**, Das S. SIRT6 deacetylates PKM2 to suppress its nuclear localization and oncogenic functions. *Proc Natl Acad Sci U S A* 2016; **113**: E538-E547 [PMID: 26787900 DOI: 10.1073/pnas.1520045113]
97 **Shi L**, Wang Y, Oppong TB, Fu X, Yang H. Prognostic role of SIRT6 in gastrointestinal cancers: a meta-analysis. *Open Med (Wars)* 2020; **15**: 358-365 [PMID: 33335996 DOI: 10.1515/med-2020-0403]
98 **Zhang C**, Yu Y, Huang Q, Tang K. SIRT6 regulates the proliferation and apoptosis of hepatocellular carcinoma *via* the ERK1/2 signaling pathway. *Mol Med Rep* 2019; **20**: 1575-1582 [PMID: 31257493 DOI: 10.3892/mmr.2019.10398]
99 **Zhou HZ**, Zeng HQ, Yuan D, Ren JH, Cheng ST, Yu HB, Ren F, Wang Q, Qin YP, Huang AL, Chen J. NQO1 potentiates apoptosis evasion and upregulates XIAP *via* inhibiting proteasome-mediated degradation SIRT6 in hepatocellular carcinoma. *Cell Commun Signal* 2019; **17**: 168 [PMID: 31842909 DOI: 10.1186/s12964-019-0491-7]
100 **Bai L**, Lin G, Sun L, Liu Y, Huang X, Cao C, Guo Y, Xie C. Upregulation of SIRT6 predicts poor prognosis and promotes metastasis of non-small cell lung cancer *via* the ERK1/2/MMP9 pathway. *Oncotarget* 2016; **7**: 40377-40386

[PMID: 27777384 DOI: 10.18632/oncotarget.9750]

101 **Garcia-Peterson LM**, Ndiaye MA, Singh CK, Chhabra G, Huang W, Ahmad N. SIRT6 histone deacetylase functions as a potential oncogene in human melanoma. *Genes Cancer* 2017; **8**: 701-712 [PMID: 29234488 DOI: 10.18632/genesandcancer.153]

102 **Huang N**, Liu Z, Zhu J, Cui Z, Li Y, Yu Y, Sun F, Pan Q, Yang Q. Sirtuin 6 plays an oncogenic role and induces cell autophagy in esophageal cancer cells. *Tumour Biol* 2017; **39**: 1010428317708532 [PMID: 28653878 DOI: 10.1177/1010428317708532]

103 **Yu H**, Ye W, Wu J, Meng X, Liu RY, Ying X, Zhou Y, Wang H, Pan C, Huang W. Overexpression of sirt7 exhibits oncogenic property and serves as a prognostic factor in colorectal cancer. *Clin Cancer Res* 2014; **20**: 3434-3445 [PMID: 24771643 DOI: 10.1158/1078-0432.CCR-13-2952]

104 **Wei W**, Jing ZX, Ke Z, Yi P. Sirtuin 7 plays an oncogenic role in human osteosarcoma *via* downregulating CDC4 expression. *Am J Cancer Res* 2017; **7**: 1788-1803 [PMID: 28979804]

105 **Wang HL**, Lu RQ, Xie SH, Zheng H, Wen XM, Gao X, Guo L. SIRT7 Exhibits Oncogenic Potential in Human Ovarian Cancer Cells. *Asian Pac J Cancer Prev* 2015; **16**: 3573-3577 [PMID: 25921180 DOI: 10.7314/apjcp.2015.16.8.3573]

106 **Zhang S**, Chen P, Huang Z, Hu X, Chen M, Hu S, Hu Y, Cai T. Sirt7 promotes gastric cancer growth and inhibits apoptosis by epigenetically inhibiting miR-34a. *Sci Rep* 2015; **5**: 9787 [PMID: 25860861 DOI: 10.1038/srep09787]

107 **Yu W**, Cui X, Wan Z, Yu Y, Liu X, Jin L. Silencing forkhead box M1 promotes apoptosis and autophagy through SIRT7/mTOR/IGF2 pathway in gastric cancer cells. *J Cell Biochem* 2018; **119**: 9090-9098 [PMID: 29953672 DOI: 10.1002/jcb.27168]

108 **Li W**, Zhu D, Qin S. SIRT7 suppresses the epithelial-to-mesenchymal transition in oral squamous cell carcinoma metastasis by promoting SMAD4 deacetylation. *J Exp Clin Cancer Res* 2018; **37**: 148 [PMID: 30001742 DOI: 10.1186/s13046-018-0819-y]

109 **Tang X**, Shi L, Xie N, Liu Z, Qian M, Meng F, Xu Q, Zhou M, Cao X, Zhu WG, Liu B. SIRT7 antagonizes TGF-β signaling and inhibits breast cancer metastasis. *Nat Commun* 2017; **8**: 318 [PMID: 28827661 DOI: 10.1038/s41467-017-00396-9]

110 **Wu D**, Li Y, Zhu KS, Wang H, Zhu WG. Advances in Cellular Characterization of the Sirtuin Isoform, SIRT7. *Front Endocrinol (Lausanne)* 2018; **9**: 652 [PMID: 30510540 DOI: 10.3389/fendo.2018.00652]

111 **Tao F**, Gu C, Li N, Ying Y, Feng Y, Ni D, Zhang Q, Xiao Q. SIRT3 acts as a novel biomarker for the diagnosis of lung cancer: A retrospective study. *Medicine (Baltimore)* 2021; **100**: e26580 [PMID: 34232204 DOI: 10.1097/MD.0000000000026580]

112 **Curry AM**, White DS, Donu D, Cen Y. Human Sirtuin Regulators: The "Success" Stories. *Front Physiol* 2021; **12**: 752117 [PMID: 34744791 DOI: 10.3389/fphys.2021.752117]

113 **Puhr HC**, Preusser M, Ilhan-Mutlu A. Immunotherapy for Esophageal Cancers: What Is Practice Changing in 2021? *Cancers (Basel)* 2021; **13** [PMID: 34572859 DOI: 10.3390/cancers13184632]

114 **Warren JL**, MacIver NJ. Regulation of Adaptive Immune Cells by Sirtuins. *Front Endocrinol (Lausanne)* 2019; **10**: 466 [PMID: 31354630 DOI: 10.3389/fendo.2019.00466]

115 **Zhang M**, Acklin S, Gillenwater J, Du W, Patra M, Yu H, Xu B, Yu J, Xia F. SIRT2 promotes murine melanoma progression through natural killer cell inhibition. *Sci Rep* 2021; **11**: 12988 [PMID: 34155309 DOI: 10.1038/s41598-021-92445-z]

116 **Xiang J**, Zhang N, Sun H, Su L, Zhang C, Xu H, Feng J, Wang M, Chen J, Liu L, Shan J, Shen J, Yang Z, Wang G, Zhou H, Prieto J, Ávila MA, Liu C, Qian C. Disruption of SIRT7 Increases the Efficacy of Checkpoint Inhibitor *via* MEF2D Regulation of Programmed Cell Death 1 Ligand 1 in Hepatocellular Carcinoma Cells. *Gastroenterology* 2020; **158**: 664-678.e24 [PMID: 31678303 DOI: 10.1053/j.gastro.2019.10.025]

World Journal of Gastrointestinal Oncology

Submit a Manuscript: https://www.f6publishing.com

World J Gastrointest Oncol 2022 April 15; 14(4): 808-819

DOI: 10.4251/wjgo.v14.i4.808

ISSN 1948-5204 (online)

MINIREVIEWS

Vasoactive intestinal peptide secreting tumour: An overview

Esther Una Cidon

Specialty type: Oncology

Provenance and peer review: Invited article; Externally peer reviewed.

Peer-review model: Single blind

Peer-review report's scientific quality classification

Grade A (Excellent): 0
Grade B (Very good): B
Grade C (Good): 0
Grade D (Fair): 0
Grade E (Poor): 0

P-Reviewer: Xiao Y, China

Received: March 17, 2021
Peer-review started: March 17, 2021
First decision: May 3, 2021
Revised: May 15, 2021
Accepted: March 25, 2022
Article in press: March 25, 2022
Published online: April 15, 2022

Esther Una Cidon, Department of Medical Oncology, University Hospitals Dorset, Bournemouth BH7 7DW, Dorset, United Kingdom

Corresponding author: Esther Una Cidon, MD, MSc, PhD, Doctor, Department of Medical Oncology, University Hospitals Dorset, Medical Oncology Service, Royal Bournemouth Hospital, Castle Lane East, Bournemouth BH7 7DW, Dorset, United Kingdom.
aunacid@hotmail.com

Abstract

Vasoactive intestinal peptide (VIP) secreting tumour (VIPoma) is a rare functional neuroendocrine tumour that typically arises from pancreatic islet cells. These present as sporadic, solitary pancreatic neoplasias with an estimated incidence of one in ten million individuals per year. Only around 5% of VIPomas are associated with multiple endocrine neoplasia type I syndrome. Excessive VIP secretion produces a clinical syndrome characterized by refractory watery diarrhoea, hypokalemia and metabolic acidosis. These coupled with elevated plasma levels of VIP are diagnostic. The majority of VIPomas are malignant and have already metastasized at the time of diagnosis (60%). Metastases occur most frequently in the liver, or regional lymph nodes, lungs, kidneys and bones. Some reports of skin metastases have been documented. Complete surgical resection continues to be the only potentially curative treatment. However, when the neoplasia cannot be excised completely, surgical debulking may provide palliative benefit. Other palliative options have included recently the peptide receptor radionuclide therapy which has shown to be effective and well-tolerated. This article will review all aspects of pancreatic VIPomas highlighting aspects such as clinical presentation, diagnosis and management.

Key Words: VIPoma; Octreotide; Secretory diarrhoea; Multiple endocrine neoplasia; Vasoactive intestinal peptide; Vermer-Morrison syndrome

Core Tip: Vasoactive intestinal peptide (VIP) secreting tumour (VIPoma) is a rare functional neuroendocrine tumour that typically arises from pancreatic islet cells. It is usually sporadic but may present as part of the endocrine neoplasia type I syndrome in 5% of cases. Excessive VIP secretion produces a refractory secretory diarrhoea which left untreated will cause patient's death. The majority of VIPomas are malignant and have already metastasized at the time of diagnosis (60%), being the liver, or regional lymph nodes the most frequent site for metastases. Complete surgical resection is the only potentially curative treatment, however, surgical debulking may provide palliative benefit. Other palliative options include somatostatin analogues and recently the peptide receptor radionuclide therapy which has shown to be effective and well-tolerated.

Citation: Una Cidon E. Vasoactive intestinal peptide secreting tumour: An overview. *World J Gastrointest Oncol* 2022; 14(4): 808-819
URL: https://www.wjgnet.com/1948-5204/full/v14/i4/808.htm
DOI: https://dx.doi.org/10.4251/wjgo.v14.i4.808

INTRODUCTION

Vasoactive intestinal peptide (VIP) secreting tumour (VIPoma) is a rare functional neuroendocrine tumour (NET) secreting VIP in an uncontrolled manner. It is a non-beta pancreatic islet cell tumour that comprises < 10% of all pancreatic NETs[1].

VIPomas were initially reported by Priest and Alexander in 1957. Verner and Morrison in 1958, described a syndrome called WDHA (watery diarrhoea, hypokalemia, achlorhydria) as a consequence of a pancreatic malignancy that caused death due to dehydration and shock[2]. These tumours are also called Verner-Morrison syndrome, pancreatic cholera and WDHA syndrome, in view of the most frequent symptoms[2]. Its estimated incidence is of 1/10000000 individuals per year[3], affecting more women (65%) than men (35%)[4] and it usually appears in the 4th decade[3].

These originate in amine precursor uptake and decarboxylation cells of the gastro-enteropancreatic endocrine system and in adrenal or extra-adrenal neurogenic locations[5]. VIPomas are sporadic in 90% of cases, generally presenting as solitary lesions greater than 3 cm[5], with only in 5% of the cases being multicentric[6]. Pancreatic VIPomas might also be part of multiple endocrine neoplasia (MEN) 1 syndrome[6], which is an autosomal dominant syndrome that combines malignant lesions in the parathyroid glands, pancreatic islet cells, and the pituitary[7]. As well as its participation in familial MEN 1[5] and related disorders, the MEN1 locus has been involved in the development of MEN 1-type sporadic endocrine malignancies.

Pancreatic VIPomas are extremely rare in children, where it has been shown that VIP originates mainly from ganglioneuromas, ganglioneuroblastomas, neurofibromas, or most commonly from other neoplasias in the adrenal area[1,8]. Only a small number of neuroblastomas and ganglioneuroblastomas produce VIP, but this characteristic indicates a more favourable prognosis[8]. Patients with neurogenic neoplasias, usually show normal levels of gastrin, insulin, pancreatic polypeptide and somatostatin, as opposed to those with pancreatic VIPomas[8]. Most VIPomas are intrapancreatic, the majority of them in the body and tail while 25% are located in the head of the pancreas[9]. However, there are cases of extrapancreatic origin, mostly in adrenal glands (35%), followed by paraspinal retroperitoneal ganglia (30-35%), posterior mediastinum (20%), head and neck in 1%-5% and pelvis in 2%-3%; rare locations include the thymus, lung, kidney or anterior mediastinum[10,11].

PATHOPHYSIOLOGY

VIPomas most relevant symptoms are caused by the exaggerated, uncontrolled secretion of VIP. However, other products such as prostaglandin E2, may be secreted as well by this neoplasia[12].

VIP is generated as a precursor substance with a signal peptide of 22 amino acids, then cleaved to the active form of 28 amino acids[12,13]. This product encoding gene is in chromosome 6[14]. It works by attachment to receptors on intestinal epithelial cells and inducing activation of adenylate cyclase and adenosine 3′, 5′- cyclic phosphate (cAMP) production[11]. As such, it will control smooth muscle activity, blood flow in the gastrointestinal tract[15-17] and epithelial cell secretion. This will result in profuse refractory watery diarrhoea leading to water and electrolyte depletion, mainly hypokalemia[18-20]. Some studies have shown that there is a local control of VIP gene expression, suggesting that there is a post transcriptional regulation which may be crucial for normal VIP secretion[21].

VIP also shows a vasodilator effect (with flushing), glucogenolytic effect on the liver (with subsequent hyperglycaemia) and diminish gastric acid secretion[22] leading to hypochlorhydria/achlorhydria[23]. Hyperglycemia and impaired glucose tolerance affect ≤ 50% of patients[24]. The reasons behind these

issues are in relation to direct glycogenolytic activity of the VIP on the liver and the inhibitory effect of hypokalemia on pancreatic islets cells insulin release. Hypercalcemia can also be seen without MEN1 syndrome or raised parathyroid hormone levels. It is believed that elevated bone resorption can be involved, however, it is not clear. In addition, the dehydration, as a consequence of severe diarrhoea, might also aggravate the hypercalcemia. This is seen in 50% of patients[25]. Hypochlorhydria or achlorhydria is described in 75% of patients with VIPoma as a result of the inhibition of histamine and pentagastrin-stimulated gastric acid secretion[26].

DIAGNOSIS

Diagnosis requires demonstration of secretory diarrhoea. Then the laboratory assessment (elevated VIP serum levels are required) and imaging studies will complete the diagnostic tools. Typically, the diagnosis is often delayed and diarrhoea may persist for years before a VIPoma is confirmed[27].

Laboratory

VIPomas are diagnosed when watery diarrhoea, hypokalemia, and achlorhydria are observed in the context of raised serum VIP[1]. Stool volumes of less than 700 mL/d virtually rule out a VIPoma. Generally in this context, stool volumes exceed 3 L/d. Stool osmolality must be compatible with a secretory diarrhoea, that is stool osmotic gap of < 50[8]. VIP levels are determined by radioimmunoassay and these are generally 2-10 times the normal range (20-30 pmol/L) in patients with VIPoma[9]. Figures > 75 pg/mL are consistent with a VIPoma[10], although levels usually reach 160-250 pmol/L or higher.

These levels should be drawn after fasting and a protease inhibitor (such as aprotinin) must be added to the blood sample, otherwise, VIP is degraded rapidly. Moreover, the sample must be kept frozen at -70 °C until it is processed. These levels should be determined when the patient is symptomatic (as VIP release from the tumour fluctuates and it is normal in between the episodes of diarrhoea) and should be repeated to verify the diagnosis. Hence, a normal figure may be a false negative[28].

Hypokalemia and non-anion gap acidosis are also frequently seen in VIPomas[1], same as hypochlorhydria or achlorhydria that may be assessed by checking gastric pH or basal gastric acid output l[1]. Measuring the stool weight and levels of potassium, it could be confirmed the high gastrointestinal potassium losses. Renal function must be assessed by blood urea nitrogen and serum creatinine levels. Magnesium should be determined as well[11]. Stool weight with potassium measurements will confirm the high gastrointestinal potassium losses.

VIPomas may release also other hormones, such as neurotensin, calcitonin or pancreatic polypeptide. Moreover, 66% of the cases with VIPoma will also show raised levels of gastrin and insulin[29]. It has been published one case in the literature, where a patient with VIPoma had increased dopamine levels suggesting that neuroendocrine cells are able to secrete both catecholamines, as well as pancreatic peptides[30].

Imaging

Imaging studies will initially check the pancreas, as it is known that 90% of VIPomas will be found there. These techniques are crucial not only to localize the neoplasia, but also to determine its size and the stage at diagnosis to help establish the treatment pathway[31]. In most cases, finding the VIPoma is easy as most will be larger than 3cm at diagnosis. Computed tomography (CT), magnetic resonance imaging (MRI) and somatostatin receptor scintigraphy (SRS) are three imaging techniques that may be utilised to find the tumour. Some published articles have used 99mTc sestamibi[32] to locate the neoplasia. Unfortunately there are no staging criteria for VIPomas.

CT: Multiphasic CT is crucial in determining the size, location, as well as involvement of adjacent structures, vessels, lymph nodes and presence of calcification[9,15]. CT will search for neck, mediastinal, or retroperitoneal masses and will identify the primary neoplasia in the majority of the cases. It will also help detecting or excluding liver metastases[10]. Peng *et al*[33] examined 31 patients and reported that CT was able to identify correctly all VIPomas in the body and tail of the pancreas. However, only 71% of the tumours in pancreatic head were identified. This neoplasia shows as a hyperattenuating lesion on arterial phase followed by an obscure mass on venous depiction. Calcifications may be detected as well. These are hypervascularized tumours rich in cells and fibrous tissue which is poorly supplied and therefore the contrast agent is held within the lesion[11].

MRI: MRI is useful for assessment of spinal tumours[34] or if CT is contraindicated (*e.g.*, patient is allergic to iodine contrast or in renal failure). VIPomas are best seen on T1-weighted, fat-suppressed images as these are low signal-intensity tumours. MRI has better sensitivity for liver metastases detection. These may be observed as intensive peripheral ring enhancement on immediate post-gadolinium spoiled gradient-echo images[35]. This technique can detect tumours as small as 1 cm[36] and MRI should be performed in those cases with indeterminate lesions.

SRS: 90% of pancreatic NETs have a high number of somatostatin receptors[8]. Therefore, using radionuclide-labelled octreotide or lanreotide may be useful for studying abnormalities found on a CT or for identification of hidden or distant metastases[6]. It might help after surgery as well, if postoperative changes diminish the accuracy of a CT. This technique's sensitivity for all pancreatic NETs is 80-90%; 92% for neoplasias > 1 cm[6].

Endoscopic ultrasound: This will help determine the accurate extent of the disease and it allows a biopsy of the pancreatic lesion.

Single-photon emission CT: Research has suggested that the use of single-photon emission CT (SPECT) might improve the value of somatostatin receptor scintigraphy for the localization of NETs, including VIPomas[37]. Several different radiotracers can be bound to octreotide, and applied together with SPECT or positron emission tomography (PET) imaging to localize areas of enhanced uptake.

PET: 18F-deoxyglucose-PET imaging has also been used to diagnose NETs. However, it may not be as sensitive as somatostatin receptor scintigraphy[38]. The FDA approved the newer functional PET technique with 68-Ga DOTATATE injection as the radioactive diagnostic product for the identification of somatostatin receptor-positive NETs in adult and paediatric patients. PET-CT Gallium-68 dotatate is 97% sensitive for the identification of VIPomas. Contrast enhanced CT and MRI sensitivities are 80 and 85%, respectively[8,11]. Moreover, a recent publication has suggested a role of the high sensitivity Ga-PET/CT not only in the identification of NETs but also in VIPomas prognostication and risk stratification[30].

Immunohistochemically: VIPomas stain positively for VIP, somatostatin, neuronspecific enolase, chromogranin A, synaptophysin and cytokeratin[39,40].

Other techniques: Chest radiography may help with identification/Location of paravertebral masses [41]. Endoscopic retrograde cholangiopancreatography might demonstrate blockage of the major pancreatic duct and perhaps some calcifications in the pancreatic body. Transabdominal ultrasonography help exclude liver metastases, which might show as hepatic calcifications. Electrocardiography can demonstrate QRS widening and T-wave flattening in cases with a very significant hypokalemia. Colonoscopy is another technique that might help with diferential diagnosis, to rule out a villous adenoma as another cause of potassium-losing diarrhoea.

DIFERENTIAL DIAGNOSIS

Other causes of secretory diarrhoea should be checked, mainly the laxative abuse. Patients with VIPomas should show high levels of VIP specially during a bout of diarrhoea. These will confirm the diagnosis. However, mild elevations may occur with short bowel syndrome and inflammatory diseases as well[42].

CLINICAL MANIFESTATIONS

The onset of VIPomas is subtle and its symptoms can bevague. In most case, these neoplasias have already metastasized at diagnosis. A Chinese study with 41 patients showed that the average time from the appearance of symptoms to the final diagnosis was > 15 mo, although patients experience a range of distinguishing signs[43].

The major symptom of VIPomas is long-standing profuse watery diarrhoea of approximately 10 watery stools per day. This diarrhoea persists even after 72 h of fasting[44] as opposed as osmotic diarrhoea[44]. In actual fact, the majority of cases develop diarrhea (89%), weight loss (72%), and hypokalemia (67%)[29], as a consequence of VIP binding to intestinal epithelial cells, upregulating cAMP and leading to secretion of electrolytes into the bowel, causing profuse watery diarrhea[29]. These issues occur as a result of VIP binding to intestinal epithelial cells, thereby upregulating cAMP and leading to secretion of electrolytes into the bowel lumen, causing profuse watery diarrhea[2]. Stool volumes are during fasting at least 20 mL/kg/d but exceed 50 mL/kg/d in most cases. Non-fasting volumes exceed > 3000 mL/d. Faecal osmolality is accounted for by twice the sum of the sodium and potassium levels, evidencing the electrolyte loss. The stools are generally tea coloured and odourless without blood or mucus[1,2]. Initially diarrhoea may evolve in episodes, whereas it becomes constant as the neoplasm progresses. Unfortunately, the diarrhoea may be present for years before the diagnosis is made. As such, in around 33% of patients, the diarrhoea has been present for less than one year before the diagnosis, but 1/4 of patients have diarrhoea for a minimum of 5 years before the diagnosis is established. Faecal excretion of large amounts of potassium and bicarbonate will produce hypokalemia and non–anion gap acidosis. VIPomas will then lead to significant dehydration (45%-95%) and

electrolytes imbalance, most frequently hypokalemia (70%-100%), achlorhydria (35%-76%), hypomagnesemia, hypophosphatemia and metabolic acidosis, all with linked symptoms[45].

Other frequent symptoms include muscular weakness, sickness (nausea, vomiting), lethargy and abdominal painful cramps or bloating. In some cases, skin rash has been shown as well[10] . Flushing similar to that seen with carcinoid syndrome appears in around 33% of patients during the episode of diarrhoea[33]. This flushing is secondary to prostaglandin production by the neoplasm. Patients will be exhausted and suffer from noticeable weight losses and renal failure, unless able to replace the lost fluids and electrolytes and flushing (15%-30%)[24,27]. Finally, ischemic stroke attributed to high haematocrit due to diarrhoea has been mentioned in an extremely rare case report[46].

BIOCHEMICAL FINDINGS

Hypokalemia

This is very a very frequent electrolyte imbalance in patients with VIPoma-induced diarrhoea[27]. Moderate hypokalemia (2.5–3mmol) may produce confusion, disorientation, weakness, constipation, and muscles discomfort or cramps during exercise. Severe hypokalemia (levels under 2.5mmol) may result in extreme weakness and paralysis (flaccid paralysis). Sometimes it may produce respiratory distress and respiratory failure. Changes in ECG (flattened in T waves) can also be found and some cardiac arrythmias may be leading to cardiac arrest.

Bicarbonate alterations

VIPomas can cause a large amount of gasrointestinal loss and bicarbonate wasting through stool. This fact, will lead to metabolic acidosis, contributing as well in hypokalemia[47].

Hypochlorhydria or achlorhydria

This appear as secondary to the direct gastric acid inhibitory effect of VIP, which consequently result in a diminished gastric acid production. Hypochlorhydria appears in 20%-50% of patients with VIPomas [25]. These changes will end up in malabsorption of several electrolytes and vitamins[26].

Other alterations

Hyperglycemia (20%-50%) due to a profound glycogenolytic effects of VIP on the liver that leads to reduced glucose intake by tissues[25]. Hypercalcemia occurs in 25%-50% of cases[25]. It is not clear why hypercalcemia might appear but it may be linked to dehydration, electrolyte disturbances, paraneoplastic syndrome or coincidental MEN-1 syndrome with hyperparathyroidism[15]. Hypomagnesemia may happen as well as a consequence of diarrhoea and lead to tetany in some patients. Other signs of VIPoma may comprise bloating, nausea, vomiting, cutaneous rash, lethargy and weight loss[48].

TREATMENT/MANAGEMENT

General management

The management of VIPomas includes medical and surgical treatment. Its mortality rate is closely linked to uncontrolled WDHA syndrome. This will lead to a sustained dehydration with significant electrolyte and acid-base disturbances, and consequently renal failure, cardiac arrhythmias, neuromuscular deficits, shock, cardiac arrest and eventually death[49]. Therefore, the initial therapy for a VIPoma aims at controlling the symptoms and correcting any volume depletion, electrolytes and acid-base alterations. This entails a rapid replacement of fluids and electrolytes. The ideal fluid replacement should be with an isotonic electrolyte solution with adequate sodium, potassium and base if needed. In many cases, patients will need intravenous replacements and hospital admission[48]. In the absence of finding a neoplasia, symptomatic therapy is advised. This treatment in conjunction with octreotide, will improve preoperative electrolyte balance[30] if surgery is considered (Figure 1).

Somatostatin analogues

Somatostatin analogues (SSAs) inhibit VIP secretion and are used to control symptoms[15]. Somatostatin is a peptide that reduces the secretion of an ample set of hormones[50]. Various studies on functional NETs have shown that controlling hormone levels is crucial to reduce patients' morbidity and mortality[51]. SSAs (octreotide, lanreotide and pasireotide) replicate the effect of somatostatin on G-coupled receptors of cell membrane and will reduce VIP secretion. This will impact positively on diarrhoea control. SSAs will also inhibitit tumour growth[31] in more than 90% of patients[33]. The CLARINET trial (Controlled study of Lanreotide Antiproliferative Response in NETs) reported antiproliferative effects of lanreotide in NETs[52]. SSAs showed rates of tumour stabilization in 50%-60% of the pNETs[22]. Some authors have even suggested that that SSAs may produce a reduction in tumour size.

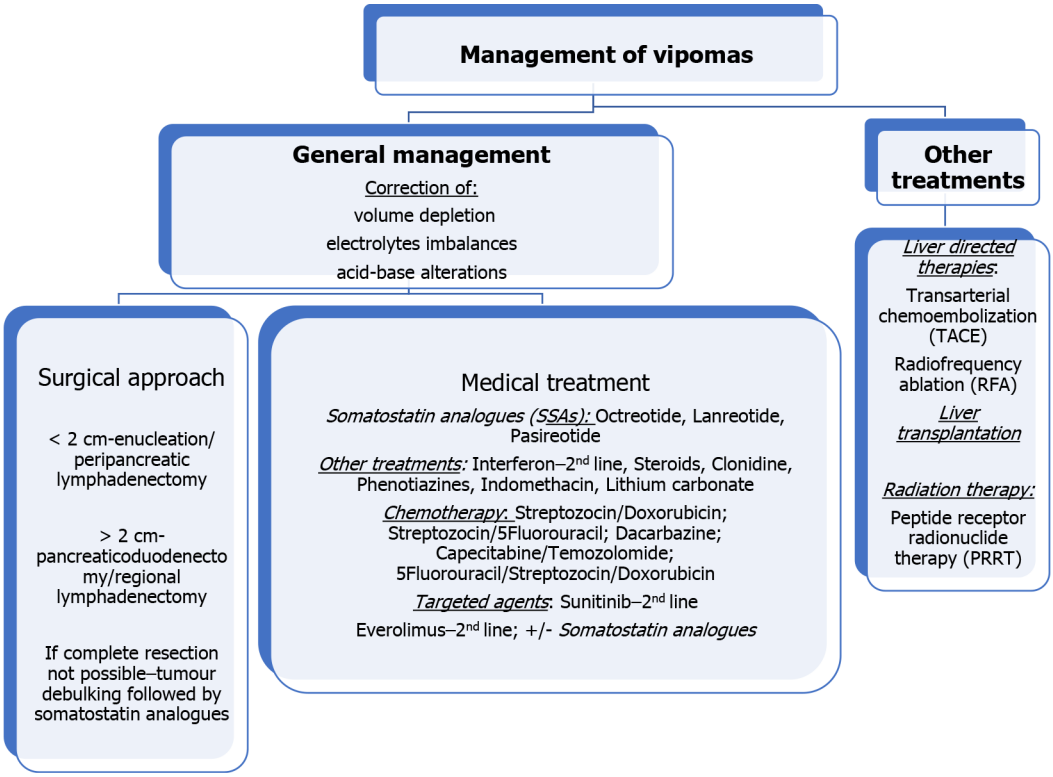

DOI: 10.4251/wjgo.v14.i4.808

Figure 1 Management of vasoactive intestinal peptide secreting tumour.

Although this is still under debate, neoadjuvant therapy with octreotide has been applied in 69.2% of cases[45,53]. Overall, several studies have reported rates of diarrhoea control in more than 50% of the patients, while significant improvements are seen in 25%.

Unfortunately, there are some issues in relation to SSAs. One is the clearly documented resistance with long-term octreotide use, leading to the requirement of significantly high doses to achieve the wanted effect[54]. Another problem is the fact that the diarrhoea reappears when the SSAs is stopped. Thus, octreotide should carry on unless the tumour can be surgically completely removed. Octreotide is a synthetic longacting SSA that stops VIP secretion and is approved for treatment of VIPomas[55]. SSAs are generally well tolerated, although adverse events might occur. Indigestion, bloating, vomiting, bloating, diarrhoea with steatorrhea due to fat malabsorption, and mild glucose intolerance; However, these side effects tend to fade over time[52] (Figure 1).

Interferon

Interferon alfa is added to the treatment management when the highest tolerable dose of octreotide do not control symptoms. It may also cause a modest reduction in tumour size[56]. Interferon alpha (IFN-α) is approved for symptom control (3-5 million IU sc three times weekly) with similar results to SSAs. Due to its less favourable toxicity profile (fatigue, weight loss and, more rarely, depression), this is used in second-line as a supplemental therapy joined to SSA in cases with refractory syndrome[57] (Figure 1).

Steroids

Steroids may diminish symptoms in 50% of patients. This treatment may be used for those patients who did not show a good response to SSAs[58] (Figure 1).

Other agents

Before the availability of octreotide, some patients had shown responses with high dose of prednisone, clonidine, phenotiazine, indomethacin, lithium carbonate, *etc*[58]. Additional loperamide and opiates may be used as well[59] (Figure 1).

Chemotherapy

The activity of cytotoxic chemotherapy in metastatic VIPomas is difficult to assess as many series have published the results for all histologic subtypes of pNETs together. Overall response rate (ORR) is disappointing and as such, chemotherapy is not curative. Moertel *et al*[60] use a combination of streptozotocin and doxorubicin as the standard therapy for progressive or symptomatic unresectable NETs, including VIPomas. This combination reduced diarrhoea and diminished tumour size in 69% (in 14% it

showed a complete regression). Further studies have reported that patients with advanced disease may respond to streptozocin-based chemotherapy, being doxorubicin/streptozotocin combination the gold standard with 5-fluorouracil replacing doxorubicin when the latter is contraindicated[10]. When the standard chemotherapy and SSAs lose effectiveness, 5-FU may be used in combination with interferon alfa.

Other chemotherapy drugs are dacarbazine and more recently capecitabine and temozolomide (CAPTEM). This last combination has shown efficacy from retrospective studies in pancreatic NETs where the number of VIPomas was very small. The study by Strosberg *et al*[61] showed that CAPTEM was able to normalise serum VIP level in one patient with VIPoma. They have only included two patients with thisdisease, the others had different NETs. Kouvaraki *et al*[62] reported that patients with locally advanced or metastatic pancreatic NETs that received 5-fluorouracil, doxorubicin, streptozozin showed a 40% of ORR, and showed longer progression free survival (PFS) and overall survival (OS). The extension of liver metastases seems to be the most important predictor of result. The median time to response was 4 mo. This study included only 2 cases of VIPoma and the authors' data suggest that chromogranin A level after two to four cycles of this combination is a useful surrogate marker for the prediction of response. Temozolomide alone can also be recommended as an alternative chemotherapy in pancreatic NETs. There are no established second-line treatment, but regimens that can be used are 5-FU/Leucovorin/irinotecan (FOLFIRI), 5-FU/Leucovorin/oxaliplatin (FOLFOX), CAPTEM bevacizumab[63].

Chemotherapy may be considered as an alternative to hepatic-directed therapies such as resection, ablation or hepatic artery embolization, but it fails to control the hormonal syndrome[8]. It should be maintained at least for one or two cycles and it may show significant benefits at the end of the first mo. There is little experience with adjuvant chemotherapy after surgical resection in NET G1/G2. However, in aggressive NENs (NEC G3), adjuvant platinum-based chemotherapy can be used, although prospective clinical trials are advised[63]. Schizas *et al*[45] in their systematic review had reported that 6.8% of patients received systemic adjuvant therapy. The number of cases is very small as to be able to draw general conclusions. A multicenter trial evaluated 80 cases with metastatic NETs who were randomised to receive lanreotide, interferon alpha, or both. The authors did not find any significant differences between the arms of the study. Partial response was reported in 4% to 7.1%, stable disease in 17.9%-28% and progressive disease in 50%-56%[56]. Another study of 14 patients with metastatic NETs who received indium in-111 octreotide showed stable disease in 50 % of cases, partial response in 14%, and disease progression in 36%[64]. A quality-of-life study in 13 of these patients found a significant benefit in this[65,66].

European Neuroendocrine Tumour Society (ENETS) have published a position statement on peptide receptor radionuclide therapy (PRRT) for pancreatic neuroendocrine tumours (pNETS)[67]. The early findings with radioembolization with resin 90 Y-microspheres in liver metastases from a variety of NETs have been encouraging. Findings reported complete response in 2.7%, partial response in 60.5%, stabilisation in 22.7% and progressive disease in 4.9%. The median OS documented was 70 mo and no cases of radiation liver failure were reported[68]. Second-line therapy for VIPomas includes IFN-α as mentioned earlier in this article, everolimus and sunitinib[69-72]. ENETS 2016 guidelines approved everolimus and sunitinib as antiproliferative therapies in cases of progressive pNETs, after failure of SSA or chemotherapy.

Sunitinib

A randomized multicentric trial evaluating sunitinib (a tyrosine kinase inhibitor), included 171 advanced well-differentiated NETs, including patients with VIPomas. The results showed an ORR of 9.3% *vs* 0%, PFS 11.4 mo *vs* 5.5 mo in the sunitinib and placebo groups respectively. Nine deaths were reported with sunitinib (10%) *vs* 21 in the placebo group (25%). These results seem to be similar to those obtained with chemotherapy, but with a more favourable toxicity[69,70]. Sunitinib inhibits several receptor tyrosine kinase key to tumour growth, neoangiogenesis and dissemination[73].

Everolimus

mTOR is a serine-threonine kinase involved in cell growth control and cell apoptosis. Its effects are mediated through phosphoinositide 3-kinase/Akt pathway and stimulates downstream protein kinases crucial to cell cycle progression. mTOR inhibitors, alone or combined with octreotide have been studied in patients in pancreatic NETs. Everolimus is a selective mTOR inhibitor with antiangiogenic activity as well.

The RADIANT 1 is a multicentric single arm phase II trial that evaluates everolimus alone or in combination with octreotide in 160 cases of metastatic pNETs after chemotherapy failure[71]. The ORR was 9.6% in those patients not receiving octreotide, with a median PFS of 9.7 mo and OS 24.9 mo. A smaller group of 45 cases received everolimus and continued to receive octreotide. In these cases, the ORR was 4.4% with PFS of 16.7 mo and OS was not reached at the time of data cutoff.

The RADIANT 2 was a phase III trial randomising patients with NETs to everolimus[72] and SSA or to placebo and SSA. 429 patients were included, 6% pNETs. A PFS of 16.4 mo *vs* 11.3 favoured the combination.

RADIANT -3 trial is a phase III study that has been recently reported[74]. It included 410 cases with radiologic disease progression. Patients were randomized to receive everolimus or usual treatment which could include SSA. Findings showed a median PFS of 11 *vs* 4.6 mo and 34% *vs* 9% were reported alive and free of progression at 18 mo with everolimus or usual treatment respectively. 24% of patients in this trial had somatostatinomas, gastrinomas, insulinomas, glucagonomas or VIPomas. This means that everolimus may be used across the spectrum of pNET subtypes. In addition, authors reported that the benefit of everolimus was found in different subgroups of sex, age, geographic regions, race, performance status and previous therapy applied (chemotherapy, radiation or octreotide). As there is a risk of pneumonitis with this therapy, perhaps sunitinib would be a better option in those patients with underlying severe lung disease (Figure 1).

The future

Well-designed randomized clinical trials have significantly improved our treatment options for patients with these tumours. However, we are still far away from an ideal situation and as such, further research is crucial, although difficult, specially taking into account that VIPomas comprise only < 10% of pancreatic NETs.

Several trials have been carried out testing different agents. Some of these trials have finished recruitment and are still awaiting results such as NCT01466036, a phase II study of cabozantinib in advanced pancreatic NETs and carcinoids[73]. It recruited 62 cases and the primary end point is ORR. The final data collection date was expected in March 2021. Another one is NCT02893930, a phase II with sapanisertib[75] in patients with metastatic or refractory pancreatic NETs that cannot be surgically removed. It has been last updated in May 2021 but not results posted yet. NCT00075439 is a phase II study evaluating gefitinib[76] in patients with progressive metastatic NETs which has finished recruitment as well but awaiting results. EPO906 has been assessed in phase II trial in metastatic carcinoids and other NETs, including VIPomas. It has completed recruitment in 2007 but not available results. Other trials have been withdrawn such as the phase 1 trial with Veliparib (ABT-888) in combination with capecitabine and temozolomide in advanced well-differentiated NETs (NCT02831179) [77]. Another study with cabozantinib (a phase III) is still recruiting patients (NCT03375320). It will assess cabozantinib *vs* placebo in cases with advanced NETs or carcinoids[78].

Bevacizumab has also been investigated in a phase II study of everolimus and octreotide with or without bevacizumab in cases with advanced or metastatic pancreatic NETs that are not amenable for surgery. This has finished recruitment. PFS is the primary end point, being secondary end points ORR and OS. One hundred and fifty patients were recruited. At the most recent update (May 2021), the PFS results showed 14 m *vs* 16.7 m without and with bevacizumab respectively. OS is favouring as well the arm with bevacizumab with 34 m *vs* 37.6 m respectively. Although the study is not finished yet, results seem to favour the arm with bevacizumab. What we do not know yet is how many patients with VIPoma were included (NCT01229943)[79].

Data from other two clinical trials, SANET-p (NCT02589821) (NCT02588170)[80,81] have shown PFS benefit with surufatinib, with a tolerable safety[80] and SANET-ep pattern. Surufatinib is a new oral angio-immuno kinase inhibitor. It inhibits selectively the tyrosine kinase activity related to the vascular endothelial and fibroblast growth factor receptors, both inhibiting angiogenesis, and colony stimulating factor-1 receptor, which controls tumour-associated macrophages, stimulating an immune response against tumour cells. The FDA has conceded to surufatinib, an Orphan drug designation for pancreatic NET in 2019 and two Fast Track Designations for development in pancreatic and extra-pancreatic NETs in 2020.

In the SANET-p trial , 172 patients with pNETs were randomised to surufatinib or placebo. At a median follow-up of 19.3 mo in the experimental arm and 11.1 mo in the placebo arm, the investigator-assessed PFS was 10.9 mo (95%CI, 7.5-13.8) *vs* 3.7 mo (95%CI, 2.8-5.6) for surufatinib and placebo respectively (HR, 0.49; 95%CI, 0.32-0.76; P = 0.0011), being the most frequent adverse event of grade 3 or higher with surufatinib *vs* placebo, hypertension (38% *vs* 7%), proteinuria (10% *vs* 2%), and hypertriglyceridemia (7% *vs* 0%). Serious AE occurred in 22% of surufatinib arm *vs* 7% with placebo. Three patients died surufatinib, two of them due to AE and one due to disease progression. One died in the placebo arm due to disease progression.

We should continue to research further to identify actionable mutations or predictive factors for targeted therapy response to better select patients' treatment. Also further efforts are needed to increase knowledge about the optimal sequential therapy that could impact positively in survival and also in quality of life.

CONCLUSION

VIPoma is a rare functional NET that typically presents as sporadic, solitary pancreatic neoplasia with only 5% of cases associated with MEN type I syndrome. It is characterised by a special clinical syndrome of refractory watery diarrhoea, electrolyte and acid-base imbalances related to the excessive VIP secretion.

The only curative option of treatment would be a complete surgical removal. Unfortunately, the majority of VIPomas have have already metastasized at the time of diagnosis leaving only palliative options for these patients. However, surgical debulking for these patients could be considered as it will help control symptoms and prolong survival. Other options include SSA and the newer chemotherapy regimens such as temozolomide, or drugs such as sunitinib or everolimus. Moreover, recent incorporation of treatment with PRRT has shown significant benefits and it is a safe addition to surgery or as a palliative treatment for those cases of widespread metastatic disease or unresectable primary tumour. As a priority, and regardless of the treatment to follow, all patients should have the water depletion, electrolyte imbalance and acid-base profile corrected.

With all these facts in mind, the prognosis may improve but hopefully further multinational clinical trials enrolling more patients with VIPoma can be carried out to get further insight in this rare but challenging disease.

ACKNOWLEDGEMENTS

To my colleagues, current and past, that have always been there.

FOOTNOTES

Author contributions: Una Cidon E designed and performed the research and wrote the paper.

Conflict-of-interest statement: Not applicable.

Country/Territory of origin: United Kingdom

ORCID number: Esther Una Cidon 0000-0002-8650-5821.

S-Editor: Chang KL
L-Editor: A
P-Editor: Chang KL

REFERENCES

1 **VERNER JV**, MORRISON AB. Islet cell tumor and a syndrome of refractory watery diarrhea and hypokalemia. *Am J Med* 1958; **25**: 374-380 [PMID: 13571250 DOI: 10.1016/0002-9343(58)90075-5]
2 **Jensen RT**, Cadiot G, Brandi ML, de Herder WW, Kaltsas G, Komminoth P, Scoazec JY, Salazar R, Sauvanet A, Kianmanesh R; Barcelona Consensus Conference participants. ENETS Consensus Guidelines for the management of patients with digestive neuroendocrine neoplasms: functional pancreatic endocrine tumor syndromes. *Neuroendocrinology* 2012; **95**: 98-119 [PMID: 22261919 DOI: 10.1159/000335591]
3 **Yao JC**, Eisner MP, Leary C, Dagohoy C, Phan A, Rashid A, Hassan M, Evans DB. Population based study of islet cell carcinoma. *Ann Surg Oncol* 2007; **14**: 3492-3500 [PMID: 17896148 DOI: 10.1245/s10434-007-9566-6]
4 **Long RG**, Bryant MG, Mitchell SJ, Adrian TE, Polak JM, Bloom SR. Clinicopathological study of pancreatic and ganglioneuroblastoma tumours secreting vasoactive intestinal polypeptide (vipomas). *Br Med J (Clin Res Ed)* 1981; **282**: 1767-1771 [PMID: 6786616 DOI: 10.1136/bmj.282.6278.1767]
5 **Batcher E**, Madaj P, Gianoukakis AG. Pancreatic neuroendocrine tumors. *Endocr Res* 2011; **36**: 35-43 [PMID: 21226566 DOI: 10.3109/07435800.2010.525085]
6 **Parbhu SK**, Adler DG. Pancreatic neuroendocrine tumors: contemporary diagnosis and management. *Hosp Pract (1995)* 2016; **44**: 109-119 [PMID: 27404266 DOI: 10.1080/21548331.2016.1210474]
7 **Fujiya A**, Kato M, Shibata T, Sobajima H. VIPoma with multiple endocrine neoplasia type 1 identified as an atypical gene mutation. *BMJ Case Rep* 2015; **2015** [PMID: 26564120 DOI: 10.1136/bcr-2015-213016]
8 **Ghaferi AA**, Chojnacki KA, Long WD, Cameron JL, Yeo CJ. Pancreatic VIPomas: subject review and one institutional experience. *J Gastrointest Surg* 2008; **12**: 382-393 [PMID: 17510774 DOI: 10.1007/s11605-007-0177-0]
9 **Chen Y**, Shi D, Dong F, Han SG, Qian ZH, Yang LI, Wang Y, Yu RS, Li QH, Fu YB. Multiple-phase spiral CT findings of pancreatic vasoactive intestinal peptide-secreting tumor: A case report. *Oncol Lett* 2015; **10**: 2351-2354 [PMID: 26622850 DOI: 10.3892/ol.2015.3615]
10 **Krejs GJ**. VIPoma syndrome. *Am J Med* 1987; **82**: 37-48 [PMID: 3035922 DOI: 10.1016/0002-9343(87)90425-6]

11 **Belei OA**, Heredea ER, Boeriu E, Marcovici TM, Cerbu S, Mărginean O, Iacob ER, Iacob D, Motoc AGM, Boia ES. Verner-Morrison syndrome. Literature review. *Rom J Morphol Embryol* 2017; **58**: 371-376 [PMID: 28730220]

12 **Maggi CA**, Giachetti A, Dey RD, Said SI. Neuropeptides as regulators of airway function: vasoactive intestinal peptide and the tachykinins. *Physiol Rev* 1995; **75**: 277-322 [PMID: 7724664 DOI: 10.1152/physrev.1995.75.2.277]

13 **Linder S**, Barkhem T, Norberg A, Persson H, Schalling M, Hökfelt T, Magnusson G. Structure and expression of the gene encoding the vasoactive intestinal peptide precursor. *Proc Natl Acad Sci U S A* 1987; **84**: 605-609 [PMID: 3025882 DOI: 10.1073/pnas.84.2.605]

14 **Gozes I**, Nakai H, Byers M, Avidor R, Weinstein Y, Shani Y, Shows TB. Sequential expression in the nervous system of c-myb and VIP genes, located in human chromosomal region 6q24. *Somat Cell Mol Genet* 1987; **13**: 305-313 [PMID: 2842874 DOI: 10.1007/BF01534924]

15 **Said SI**, Mutt V. Polypeptide with broad biological activity: isolation from small intestine. *Science* 1970; **169**: 1217-1218 [PMID: 5450698 DOI: 10.1126/science.169.3951.1217]

16 **Said SI**, Mutt V. Potent peripheral and splanchnic vasodilator peptide from normal gut. *Nature* 1970; **225**: 863-864 [PMID: 5415118 DOI: 10.1038/225863a0]

17 **Dockray GJ**. Vasoactive intestinal polypeptide and related peptides. In: Walsh JH, Dockray GJ. Gut Hormones: Biochemistry and Physiology, 1st ed. New York: Raven Press, 1994: 447

18 **Meriney DK**. Pathophysiology and management of VIPoma: a case study. *Oncol Nurs Forum* 1996; **23**: 941-8; quiz 949 [PMID: 8829164]

19 **Bloom SR**, Yiangou Y, Polak JM. Vasoactive intestinal peptide secreting tumors. Pathophysiological and clinical correlations. *Ann N Y Acad Sci* 1988; **527**: 518-527 [PMID: 2839088 DOI: 10.1111/j.1749-6632.1988.tb27005.x]

20 **CHARLES B**, COCHRANE WA. Islet cell tumour of the pancreas with chronic diarrhoea and hypokalaemia-a recently recognized syndrome. *Can Med Assoc J* 1960; **82**: 579-586 [PMID: 13809315]

21 **Gozes I**, Shani Y, Rostène WH. Developmental expression of the VIP-gene in brain and intestine. *Brain Res* 1987; **388**: 137-148 [PMID: 2441796 DOI: 10.1016/s0006-8993(87)80007-0]

22 **Friesen SR**. Update on the diagnosis and treatment of rare neuroendocrine tumors. *Surg Clin North Am* 1987; **67**: 379-393 [PMID: 3031836 DOI: 10.1016/s0039-6109(16)44190-3]

23 **Mansour JC**, Chen H. Pancreatic endocrine tumors. *J Surg Res* 2004; **120**: 139-161 [PMID: 15172200 DOI: 10.1016/j.jss.2003.12.007]

24 **Metz DC**, Jensen RT. Gastrointestinal neuroendocrine tumors: pancreatic endocrine tumors. *Gastroenterology* 2008; **135**: 1469-1492 [PMID: 18703061 DOI: 10.1053/j.gastro.2008.05.047]

25 **Piet R**, Dunckley H, Lee K, Herbison AE. Vasoactive Intestinal Peptide Excites GnRH Neurons in Male and Female Mice. *Endocrinology* 2016; **157**: 3621-3630 [PMID: 27501185 DOI: 10.1210/en.2016-1399]

26 **Remme CA**, de Groot GH, Schrijver G. Diagnosis and treatment of VIPoma in a female patient. *Eur J Gastroenterol Hepatol* 2006; **18**: 93-99 [PMID: 16357627 DOI: 10.1097/00042737-200601000-00017]

27 **Brentjens R**, Saltz L. Islet cell tumors of the pancreas: the medical oncologist's perspective. *Surg Clin North Am* 2001; **81**: 527-542 [PMID: 11459269 DOI: 10.1016/s0039-6109(05)70141-9]

28 **de Herder WW**. Biochemistry of neuroendocrine tumours. *Best Pract Res Clin Endocrinol Metab* 2007; **21**: 33-41 [PMID: 17382264 DOI: 10.1016/j.beem.2006.12.002]

29 **Smith SL**, Branton SA, Avino AJ, Martin JK, Klingler PJ, Thompson GB, Grant CS, van Heerden JA. Vasoactive intestinal polypeptide secreting islet cell tumors: a 15-year experience and review of the literature. *Surgery* 1998; **124**: 1050-1055 [PMID: 9854582 DOI: 10.1067/msy.1998.92005]

30 **Nilubol N**, Freedman EM, Quezado MM, Patel D, Kebebew E. Pancreatic Neuroendocrine Tumor Secreting Vasoactive Intestinal Peptide and Dopamine With Pulmonary Emboli: A Case Report. *J Clin Endocrinol Metab* 2016; **101**: 3564-3567 [PMID: 27583474 DOI: 10.1210/jc.2016-2051]

31 **Grozinsky-Glasberg S**, Mazeh H, Gross DJ. Clinical features of pancreatic neuroendocrine tumors. *J Hepatobiliary Pancreat Sci* 2015; **22**: 578-585 [PMID: 25689919 DOI: 10.1002/jhbp.226]

32 **Cesani F**, Ernst R, Walser E, Villanueva-Meyer J. Tc-99m sestamibi imaging of a pancreatic VIPoma and parathyroid adenoma in a patient with multiple type I endocrine neoplasia. *Clin Nucl Med* 1994; **19**: 532-534 [PMID: 7914844 DOI: 10.1097/00003072-199406000-00014]

33 **Peng SY**, Li JT, Liu YB, Fang HQ, Wu YL, Peng CH, Wang XB, Qian HR. Diagnosis and treatment of VIPoma in China: (case report and 31 cases review) diagnosis and treatment of VIPoma. *Pancreas* 2004; **28**: 93-97 [PMID: 14707737 DOI: 10.1097/00006676-200401000-00015]

34 **Semelka RC**, Custodio CM, Cem Balci N, Woosley JT. Neuroendocrine tumors of the pancreas: spectrum of appearances on MRI. *J Magn Reson Imaging* 2000; **11**: 141-148 [PMID: 10713946 DOI: 10.1002/(sici)1522-2586(200002)11:2<141::aid-jmri10>3.0.co;2-u]

35 **Sofka CM**, Semelka RC, Marcos HB, Woosley JT. MR imaging of metastatic pancreatic VIPoma. *Magn Reson Imaging* 1997; **15**: 1205-1208 [PMID: 9408142 DOI: 10.1016/s0730-725x(97)00201-4]

36 **Eldor R**, Glaser B, Fraenkel M, Doviner V, Salmon A, Gross DJ. Glucagonoma and the glucagonoma syndrome - cumulative experience with an elusive endocrine tumour. *Clin Endocrinol (Oxf)* 2011; **74**: 593-598 [PMID: 21470282 DOI: 10.1111/j.1365-2265.2011.03967.x]

37 **Schillaci O**, Corleto VD, Annibale B, Scopinaro F, Delle Fave G. Single photon emission computed tomography procedure improves accuracy of somatostatin receptor scintigraphy in gastro-entero pancreatic tumours. *Ital J Gastroenterol Hepatol* 1999; **31** Suppl 2: S186-S189 [PMID: 10604127]

38 **Virgolini I**, Traub T, Novotny C, Leimer M, Füger B, Li SR, Patri P, Pangerl T, Angelberger P, Raderer M, Andreae F, Kurtaran A, Dudczak R. New trends in peptide receptor radioligands. *Q J Nucl Med* 2001; **45**: 153-159 [PMID: 11476164]

39 **Anderson MA**, Carpenter S, Thompson NW, Nostrant TT, Elta GH, Scheiman JM. Endoscopic ultrasound is highly accurate and directs management in patients with neuroendocrine tumors of the pancreas. *Am J Gastroenterol* 2000; **95**: 2271-2277 [PMID: 11007228 DOI: 10.1111/j.1572-0241.2000.02480.x]

40 **Ram R**, Natanzi N, Saadat P, Eliav D, Vadmal MS. Skin metastasis of pancreatic vasoactive intestinal polypeptide tumor:

case report and review of the literature. *Arch Dermatol* 2006; **142**: 946-947 [PMID: 16847229 DOI: 10.1001/archderm.142.7.946]

41 **Rastogi V**, Singh D, Mazza JJ, Parajuli D, Yale SH. Flushing Disorders Associated with Gastrointestinal Symptoms: Part 1, Neuroendocrine Tumors, Mast Cell Disorders and Hyperbasophila. *Clin Med Res* 2018; **16**: 16-28 [PMID: 29650525 DOI: 10.3121/cmr.2017.1379a]

42 **Zandee WT**, Hofland J, de Herder WW. Vasoactive Intestinal Peptide Tumor (VIPoma). 2021 Aug 28. In: Endotext [Internet]. South Dartmouth (MA): MDText.com, Inc.; 2000– [PMID: 25905195]

43 **Chen C**, Zheng Z, Li B, Zhou L, Pang J, Wu W, Zheng C, Zhao Y. Pancreatic VIPomas from China: Case reports and literature review. *Pancreatology* 2019; **19**: 44-49 [PMID: 30391116 DOI: 10.1016/j.pan.2018.10.007]

44 **Godard-Sebillotte C**, Dramé M, Fagour C, Basileu T, Godaert L. When Symptomatic Treatment Becomes Antitumor Treatment for Vipoma: Opportunity for Frail Elderly Adults. *J Am Geriatr Soc* 2016; **64**: 449-450 [PMID: 26889855 DOI: 10.1111/jgs.13968]

45 **Schizas D**, Mastoraki A, Bagias G, Patras R, Moris D, Lazaridis II, Arkadopoulos N, Felekouras E. Clinicopathological data and treatment modalities for pancreatic vipomas: a systematic review. *J BUON* 2019; **24**: 415-423 [PMID: 31127985]

46 **Anderson CW**, Bennett JJ. Clinical Presentation and Diagnosis of Pancreatic Neuroendocrine Tumors. *Surg Oncol Clin N Am* 2016; **25**: 363-374 [PMID: 27013370 DOI: 10.1016/j.soc.2015.12.003]

47 **Mekhjian HS**, O'Dorisio TM. VIPoma syndrome. *Semin Oncol* 1987; **14**: 282-291 [PMID: 2820063]

48 **Abu-Zaid A**, Azzam A, Abudan Z, Algouhi A, Almana H, Amin T. Sporadic pancreatic vasoactive intestinal peptide-producing tumor (VIPoma) in a 47-year-old male. *Hematol Oncol Stem Cell Ther* 2014; **7**: 109-115 [PMID: 24785507 DOI: 10.1016/j.hemonc.2014.03.002]

49 **Soga J**, Yakuwa Y. Vipoma/diarrheogenic syndrome: a statistical evaluation of 241 reported cases. *J Exp Clin Cancer Res* 1998; **17**: 389-400 [PMID: 10089056]

50 **Zhang X**, Zhou L, Liu Y, Li W, Gao H, Wang Y, Yao B, Jiang D, Hu P. Surgical resection of vasoactive intestinal peptideoma with hepatic metastasis aids symptom palliation: A case report. *Exp Ther Med* 2016; **11**: 783-787 [PMID: 26997993 DOI: 10.3892/etm.2016.3019]

51 **Ito T**, Igarashi H, Uehara H, Jensen RT. Pharmacotherapy of Zollinger-Ellison syndrome. *Expert Opin Pharmacother* 2013; **14**: 307-321 [PMID: 23363383 DOI: 10.1517/14656566.2013.767332]

52 **Caplin ME**, Pavel M, Phan AT, Ćwikła JB, Sedláčková E, Thanh XT, Wolin EM, Ruszniewski P; CLARINET Investigators. Lanreotide autogel/depot in advanced enteropancreatic neuroendocrine tumours: final results of the CLARINET open-label extension study. *Endocrine* 2021; **71**: 502-513 [PMID: 33052555 DOI: 10.1007/s12020-020-02475-2]

53 **Harris AG**, O'Dorisio TM, Woltering EA, Anthony LB, Burton FR, Geller RB, Grendell JH, Levin B, Redfern JS. Consensus statement: octreotide dose titration in secretory diarrhea. Diarrhea Management Consensus Development Panel. *Dig Dis Sci* 1995; **40**: 1464-1473 [PMID: 7628270 DOI: 10.1007/BF02285194]

54 **Nguyen HN**, Backes B, Lammert F, Wildberger J, Winograd R, Busch N, Rieband H, Matern S. Long-term survival after diagnosis of hepatic metastatic VIPoma: report of two cases with disparate courses and review of therapeutic options. *Dig Dis Sci* 1999; **44**: 1148-1155 [PMID: 10389687 DOI: 10.1023/a:1026672022917]

55 **Plouin PF**, Bertherat J, Chatellier G, Billaud E, Azizi M, Grouzmann E, Epelbaum J. Short-term effects of octreotide on blood pressure and plasma catecholamines and neuropeptide Y levels in patients with phaeochromocytoma: a placebo-controlled trial. *Clin Endocrinol (Oxf)* 1995; **42**: 289-294 [PMID: 7758234 DOI: 10.1111/j.1365-2265.1995.tb01877.x]

56 **Faiss S**, Pape UF, Böhmig M, Dörffel Y, Mansmann U, Golder W, Riecken EO, Wiedenmann B; International Lanreotide and Interferon Alfa Study Group. Prospective, randomized, multicenter trial on the antiproliferative effect of lanreotide, interferon alfa, and their combination for therapy of metastatic neuroendocrine gastroenteropancreatic tumors--the International Lanreotide and Interferon Alfa Study Group. *J Clin Oncol* 2003; **21**: 2689-2696 [PMID: 12860945 DOI: 10.1200/JCO.2003.12.142]

57 **Oberg K**. Interferon in the management of neuroendocrine GEP-tumors: a review. *Digestion* 2000; **62** Suppl 1: 92-97 [PMID: 10940694 DOI: 10.1159/000051862]

58 **O'Dorisio TM**, Mekhjian HS, Gaginella TS. Medical therapy of VIPomas. *Endocrinol Metab Clin North Am* 1989; **18**: 545-556 [PMID: 2545444]

59 **Pasricha G**, Padhi P, Daboul N, Monga DK. Management of Well-differentiated Gastroenteropancreatic Neuroendocrine Tumors (GEPNETs): A Review. *Clin Ther* 2017; **39**: 2146-2157 [PMID: 29173655 DOI: 10.1016/j.clinthera.2017.10.010]

60 **Moertel CG**, Lefkopoulo M, Lipsitz S, Hahn RG, Klaassen D. Streptozocin-doxorubicin, streptozocin-fluorouracil or chlorozotocin in the treatment of advanced islet-cell carcinoma. *N Engl J Med* 1992; **326**: 519-523 [PMID: 1310159 DOI: 10.1056/NEJM199202203260804]

61 **Strosberg JR**, Fine RL, Choi J, Nasir A, Coppola D, Chen DT, Helm J, Kvols L. First-line chemotherapy with capecitabine and temozolomide in patients with metastatic pancreatic endocrine carcinomas. *Cancer* 2011; **117**: 268-275 [PMID: 20824724 DOI: 10.1002/cncr.25425]

62 **Kouvaraki MA**, Ajani JA, Hoff P, Wolff R, Evans DB, Lozano R, Yao JC. Fluorouracil, doxorubicin, and streptozocin in the treatment of patients with locally advanced and metastatic pancreatic endocrine carcinomas. *J Clin Oncol* 2004; **22**: 4762-4771 [PMID: 15570077 DOI: 10.1200/JCO.2004.04.024]

63 **Pavel M**, Öberg K, Falconi M, Krenning EP, Sundin A, Perren A, Berruti A; ESMO Guidelines Committee. Electronic address: clinicalguidelines@esmo.org. Gastroenteropancreatic neuroendocrine neoplasms: ESMO Clinical Practice Guidelines for diagnosis, treatment and follow-up. *Ann Oncol* 2020; **31**: 844-860 [PMID: 32272208 DOI: 10.1016/j.annonc.2020.03.304]

64 **Ozkan E**, Tokmak E, Kucuk NO. Efficacy of adding high-dose In-111 octreotide therapy during Sandostatin treatment in patients with disseminated neuroendocrine tumors: clinical results of 14 patients. *Ann Nucl Med* 2011; **25**: 425-431 [PMID: 21476058 DOI: 10.1007/s12149-011-0482-2]

65 **Traub-Weidinger T**, Raderer M, Uffmann M, Angelberger P, Kurtaran A, Leimer M, Preitfellner J, Dudczak R, Virgolini I. Improved quality of life in patients treated with Peptide radionuclides. *World J Nucl Med* 2011; **10**: 115-121 [PMID:

22144870 DOI: 10.4103/1450-1147.89779]
66 **Kwekkeboom DJ**, de Herder WW, Krenning EP. Somatostatin receptor-targeted radionuclide therapy in patients with gastroenteropancreatic neuroendocrine tumors. *Endocrinol Metab Clin North Am* 2011; **40**: 173-185, ix [PMID: 21349418 DOI: 10.1016/j.ecl.2010.12.003]
67 **Kwekkeboom DJ**, Krenning EP, Lebtahi R, Komminoth P, Kos-Kudła B, de Herder WW, Plöckinger U; Mallorca Consensus Conference participants; European Neuroendocrine Tumor Society. ENETS Consensus Guidelines for the Standards of Care in Neuroendocrine Tumors: peptide receptor radionuclide therapy with radiolabeled somatostatin analogs. *Neuroendocrinology* 2009; **90**: 220-226 [PMID: 19713714 DOI: 10.1159/000225951]
68 **Kennedy AS**, Dezarn WA, McNeillie P, Coldwell D, Nutting C, Carter D, Murthy R, Rose S, Warner RR, Liu D, Palmedo H, Overton C, Jones B, Salem R. Radioembolization for unresectable neuroendocrine hepatic metastases using resin 90Y-microspheres: early results in 148 patients. *Am J Clin Oncol* 2008; **31**: 271-279 [PMID: 18525307 DOI: 10.1097/COC.0b013e31815e4557]
69 **Raymond E**, Dahan L, Raoul JL, Bang YJ, Borbath I, Lombard-Bohas C, Valle J, Metrakos P, Smith D, Vinik A, Chen JS, Hörsch D, Hammel P, Wiedenmann B, Van Cutsem E, Patyna S, Lu DR, Blanckmeister C, Chao R, Ruszniewski P. Sunitinib malate for the treatment of pancreatic neuroendocrine tumors. *N Engl J Med* 2011; **364**: 501-513 [PMID: 21306237 DOI: 10.1056/NEJMoa1003825]
70 **Vinik AI**, Raymond E. Pancreatic neuroendocrine tumors: approach to treatment with focus on sunitinib. *Therap Adv Gastroenterol* 2013; **6**: 396-411 [PMID: 24003340 DOI: 10.1177/1756283X13493878]
71 **Yao JC**, Lombard-Bohas C, Baudin E, Kvols LK, Rougier P, Ruszniewski P, Hoosen S, St Peter J, Haas T, Lebwohl D, Van Cutsem E, Kulke MH, Hobday TJ, O'Dorisio TM, Shah MH, Cadiot G, Luppi G, Posey JA, Wiedenmann B. Daily oral everolimus activity in patients with metastatic pancreatic neuroendocrine tumors after failure of cytotoxic chemotherapy: a phase II trial. *J Clin Oncol* 2010; **28**: 69-76 [PMID: 19933912 DOI: 10.1200/JCO.2009.24.2669]
72 **Strosberg JR**, Yao JC, Bajetta E, Aout M, Bakker B, Hainsworth JD, Ruszniewski PB, Van Cutsem E, Öberg K, Pavel ME. Efficacy of octreotide long-acting repeatable in neuroendocrine tumors: RADIANT-2 placebo arm post hoc analysis. *Endocr Relat Cancer* 2015; **22**: 933-940 [PMID: 26373569 DOI: 10.1530/ERC-15-0314]
73 **Chan J**. Cabozantinib in Advanced Pancreatic Neuroendocrine and Carcinoid Tumors. [accessed 2021 July 15]. In: ClinicalTrials.gov [Internet]. Bethesda (MD): U.S. National Library of Medicine. Available from: https://clinicaltrials.gov/ct2/show/NCT01466036
74 **Yao JC**, Shah MH, Ito T, Bohas CL, Wolin EM, Van Cutsem E, Hobday TJ, Okusaka T, Capdevila J, de Vries EG, Tomassetti P, Pavel ME, Hoosen S, Haas T, Lincy J, Lebwohl D, Öberg K; RAD001 in Advanced Neuroendocrine Tumors, Third Trial (RADIANT-3) Study Group. Everolimus for advanced pancreatic neuroendocrine tumors. *N Engl J Med* 2011; **364**: 514-523 [PMID: 21306238 DOI: 10.1056/NEJMoa1009290]
75 **Rajdev L**. Sapanisertib in Treating Patients With Metastatic or Refractory Pancreatic Neuroendocrine Tumor That Cannot Be Removed by Surgery. [accessed 2021 November 23]. In: ClinicalTrials.gov [Internet]. Bethesda (MD): U.S. National Library of Medicine. Available from: https://clinicaltrials.gov/ct2/show/NCT02893930
76 **Hobday T**. Gefitinib in Treating Patients With Progressive Metastatic Neuroendocrine Tumors. [accessed 2022 January 23]. In: ClinicalTrials.gov [Internet]. Bethesda (MD): U.S. National Library of Medicine. Available from: https://clinicaltrials.gov/ct2/show/NCT00075439
77 **Berlin J**. Veliparib, Capecitabine, and Temozolomide in Patients With Advanced, Metastatic, and Recurrent Neuroendocrine Tumor. [accessed 2017 September 28]. In: ClinicalTrials.gov [Internet]. Bethesda (MD): U.S. National Library of Medicine. Available from: https://clinicaltrials.gov/ct2/show/NCT02831179
78 **Chan JA**. Testing Cabozantinib in Patients With Advanced Pancreatic Neuroendocrine and Carcinoid Tumors. [accessed 2022 February 3]. In: ClinicalTrials.gov [Internet]. Bethesda (MD): U.S. National Library of Medicine. Available from: https://clinicaltrials.gov/ct2/show/NCT03375320
79 **Kulke MH**. Everolimus and Octreotide Acetate With or Without Bevacizumab in Treating Patients With Locally Advanced or Metastatic Pancreatic Neuroendocrine Tumors That Cannot Be Removed by Surgery. [accessed 2021 September 9]. In: ClinicalTrials.gov [Internet]. Bethesda (MD): U.S. National Library of Medicine. Available from: https://clinicaltrials.gov/ct2/show/NCT01229943
80 **Fan S**. Phase III Study of Surufatinib in Treating Advanced Pancreatic Neuroendocrine Tumors. [accessed 2021 August 31]. In: ClinicalTrials.gov [Internet]. Bethesda (MD): U.S. National Library of Medicine. Available from: https://clinicaltrials.gov/ct2/show/NCT02589821
81 **Fan S**. Phase III Study of Surufatinib in Treating Advanced Extrapancreatic Neuroendocrine Tumors. [accessed 2021 April 15]. In: ClinicalTrials.gov [Internet]. Bethesda (MD): U.S. National Library of Medicine. Available from: https://clinicaltrials.gov/ct2/show/NCT02588170

World Journal of Gastrointestinal Oncology

Submit a Manuscript: https://www.f6publishing.com

World J Gastrointest Oncol 2022 April 15; 14(4): 820-832

DOI: 10.4251/wjgo.v14.i4.820

ISSN 1948-5204 (online)

MINIREVIEWS

Management of single pulmonary metastases from colorectal cancer: State of the art

Marco Chiappetta, Lisa Salvatore, Maria Teresa Congedo, Maria Bensi, Viola De Luca, Leonardo Petracca Ciavarella, Floriana Camarda, Jessica Evangelista, Vincenzo Valentini, Giampaolo Tortora, Stefano Margaritora, Filippo Lococo

Specialty type: Oncology

Provenance and peer review: Invited article; Externally peer reviewed.

Peer-review model: Single blind

Peer-review report's scientific quality classification

Grade A (Excellent): 0
Grade B (Very good): 0
Grade C (Good): C
Grade D (Fair): 0
Grade E (Poor): 0

P-Reviewer: Kaba E, Turkey

Received: March 26, 2021
Peer-review started: March 26, 2021
First decision: May 3, 2021
Revised: May 26, 2021
Accepted: March 4, 2022
Article in press: March 4, 2022
Published online: April 15, 2022

Marco Chiappetta, Maria Teresa Congedo, Leonardo Petracca Ciavarella, Jessica Evangelista, Stefano Margaritora, Filippo Lococo, Department of Thoracic Surgery, Fondazione Policlinico Universitario Agostino Gemelli IRCCS - Università Cattolica del Sacro Cuore, Rome 00168, Italy

Lisa Salvatore, Maria Bensi, Floriana Camarda, Giampaolo Tortora, Oncologia Medica Comprehensive Cancer Center, Fondazione Policlinico Universitario Agostino Gemelli IRCCS - Università Cattolica del Sacro Cuore, Rome 00168, Italy

Viola De Luca, Vincenzo Valentini, Department of Radiation Therapy, Fondazione Policlinico Universitario Agostino Gemelli IRCCS - Università Cattolica del Sacro Cuore, Rome 00168, Italy

Corresponding author: Filippo Lococo, MD, Assistant Professor, Department of Thoracic Surgery, Fondazione Policlinico Universitario Agostino Gemelli IRCCS - Università Cattolica del Sacro Cuore, Largo Agostino Gemelli 8, Rome 00168, Italy.
filippo.lococo@policlinicogemelli.it

Abstract

Colorectal cancer (CRC) is one of the most common causes of death from cancer. Lung seeding occurs in approximately 10% of patients surgically treated for primary CRC with radical intent: the lung is the most common site of metastases after the liver. While surgical treatment of liver metastases is widely accepted to affect long-term outcomes, more controversial and not standardized is the therapy for CRC patients developing lung metastases. Experience suggests the potential curative role of pulmonary metastasectomy, especially in oligometastatic disease. However, the optimal strategy of care and the definition of prognostic factors after treatment still need to be defined. This review focused on the uncommon scenario of single pulmonary metastases from CRC. We explored pertinent literature and provide an overview of the epidemiology, clinical characteristics and imaging of single pulmonary metastases from CRC. Additionally, we identified the best available evidence for overall management. In particular, we analyzed the role and results of locoregional approaches (surgery, radiotherapy or ablative procedures) and their integration with systemic therapy.

Key Words: Colorectal cancer; Pulmonary metastases; Oligometastases; Chemotherapy; Surgery; Radiotherapy

Core Tip: Single pulmonary metastasis from colorectal cancer is an uncommon scenario in which diagnostic pitfalls should be considered. Locoregional approaches (surgery more than radiotherapy or ablative procedures) might have a potential curative role with rewarding long-term results. However, since recurrences are common, the best long-term results might be expected by integrating loco-regional with systemic treatment. Moreover, despite limited evidence, different factors seem to influence prognosis in this subset of patients and should be considered when planning a tailored care strategy.

Citation: Chiappetta M, Salvatore L, Congedo MT, Bensi M, De Luca V, Petracca Ciavarella L, Camarda F, Evangelista J, Valentini V, Tortora G, Margaritora S, Lococo F. Management of single pulmonary metastases from colorectal cancer: State of the art. *World J Gastrointest Oncol* 2022; 14(4): 820-832
URL: https://www.wjgnet.com/1948-5204/full/v14/i4/820.htm
DOI: https://dx.doi.org/10.4251/wjgo.v14.i4.820

INTRODUCTION

Colorectal cancer (CRC) is one of the three most common cancer types worldwide and is responsible for more than 10% of all cancer deaths in men and women, respectively[1]. Pulmonary metastases occur in 15% of metastatic CRC (mCRC) patients, and the lung is the second site of metastases occurrence after the liver[2]. Many therapeutic options are available, ranging from target therapies to surgical resection. Pulmonary metastases surgery, when feasible, is the best treatment showing a 5-year overall survival (OS) between 25% and 35%[3]. In particular, lung metastasectomy has a long history, and since the 1950s, specific indications were provided with the aim of identifying patient subsets who might benefit from surgical resection[3]. The management of mCRC patients with lung disease requires a multidisciplinary approach and the evaluation of several factors related to patient and tumor characteristics might affect prognosis. The lack of strong scientific evidence makes choosing the most appropriate strategy challenging. National and international guidelines recommend radical resection of lung metastases whenever possible and recommend perioperative or postoperative chemotherapy by evaluating prognostic factors on a case-by-case basis. One of the most considered parameters is the number of lung metastases to predict therapy type, which might be systemic in the case of multiple spreading or ablative in limited or oligo-metastatic disease. However, multiple ablative approaches are currently available and consist of surgical resection, stereotaxic radiotherapy, crio or radiofrequency ablation.

Prognostic factors in single lung metastasis are still undefined, and a better stratification could be fundamental in identifying the most appropriate diagnostic and therapeutic approach.

The aim of this review is to describe possible treatments and survival outcomes in patients with single lung metastases from CRC to support physicians' decision-making on how best to manage these patients.

EPIDEMIOLOGY AND CLINICAL PRESENTATION

Incidence and demographic characteristics

CRC represents the second most common cancer in females and the third in males[4] and almost 700000 people die every year due to CRC, making it the world's fourth most deadly cancer (after lung, liver and stomach cancer)[5]. In 2020, there were approximately 150000 new cases of CRC in the United States[6]. Despite these relevant numbers, the incidence of CRC decreased from 60 per 100000 people in the 1970s to 38 in 2016[7]. This evidence is substantially attributable to screening programs, early CRC detection and better treatment modalities. Although the implementation of screening allows early diagnosis of CRC, approximately 25% of CRC patients have distant metastases at diagnosis[8,9]. Among patients with mCRC, the lung is the most common extra-abdominal site of metastases[10]. In particular, lung metastases occur in about 10%-30% of all patients diagnosed with advanced disease[11], but only 10% are isolated without liver metastasis[12] .

In a 30-year population-based study, synchronous lung metastases were seen in approximately 10% of patients often associated with liver metastases, while synchronous isolated lung metastases were only seen in around 3% of patients and most often in rectal cancer patients[10].

In a systematic analysis performed by Parnaby *et al*[13], the incidence of pulmonary metastases from rectal cancer during initial staging ranged from 10%-18%. For colon cancer patients, the incidence of pulmonary metastases at the time of initial staging ranged from 5%-6%. Tan *et al*[12] analyzed data from a large cohort in Singapore (754 patients over 4 years) and estimated that isolated pulmonary metastases (no other evidence of metastases elsewhere) develop at any point in the follow-up period, not just at initial staging. The incidence of isolated pulmonary metastases in patients with rectal cancer *vs* colon cancer was 12% *vs* 6%.

Radiological presentation and diagnostic approach

Since the introduction of spiral computed tomography (CT) scanners, smaller lesions can be detected at the time of preoperative staging. The significance of indeterminate lung lesions is an open question as the presence of pulmonary metastases during staging CT could change the treatment pathway. Several studies concluded that only a small rate of indeterminate lung lesions are metastases[14]; in approximately 20%-30% of CT scans for CRC staging, indeterminate lesions have been found, but only 10%-20% were malignant[14,15].

Grossmann, in an observational cohort study[16], included preoperative staging CT of the chest and abdomen in 200 patients with CRC, 5 patients had pulmonary metastases and 50 (25%) had indeterminate nodules (8 metastases diagnosed as true at follow-up). Considering the low incidence of pulmonary metastases and the relative minimal impact on treatment plans, the authors concluded that routine staging based on chest CT in CRC patients is not recommended[16], and the presence of indeterminate lung nodules should not delay surgery for CRC[14].

Even if some radiological characteristics can suggest the metastatic nature (well-circumscribed nodules, smooth margins, subpleural or peripheral localization, cavitation or vascular sign), no pathognomonic radiographic features exist that discern metastasis from a primary lung cancer or from benign processes. When multiple nodules are present, the probability of metastatic disease increases significantly. High-resolution helical CT is better than conventional CT as it detects approximately 20%-25% more nodules, as small as 2 to 3 mm[17]. Similarly, an isolated pulmonary nodule presenting as a subsolid lesion (so called ground-glass opacity) are highly suggestive of a primary lung tumor rather than metastatic lesion[18]. In addition, if a single pulmonary nodule is detected during oncological follow-up in a patient with previous CRC history, the probability of malignancy is higher. In a retrospective cohort study including 1104 patients resected at a single institution from 1989 to 1998, 63% of patients with a resected solitary nodule and without previous cancer, 82% with a history of lung cancer, and 79% with a history of extra-pulmonary cancer, had a malignant tumor[19].

In particular, the probability that a solitary pulmonary nodule was cancer ranged from 67% for nodules ≤ 1 cm to 91% for nodules > 3 cm in patients with prior malignancy. Lung cancer was more common than metastasis if the nodule was > 3 cm.

To clarify the significance of indeterminate nodules in patients with CRC discovered by traditional radiological imaging, fluorodeoxyglucose (FDG)-positron emission tomography (PET)-CT has a valuable role as it improves staging accuracy to select the appropriate treatment. A study by Jess *et al*[20] demonstrated that the discovery of an indeterminate lung nodule during staging by means of a CT scan, was identified as a malignant nodule following a PET-CT scan three months after the previous CT scan. However, PET has limited sensitivity for lesions < 1 cm in size, with a sensitivity of 0.405 for metastases of 5-7 mm in diameter to 0.784 for lesions of 8-10 mm and to 0.935 for lesions measuring 11-29 mm in diameter[21]. Moreover, an 18F-FDG PET-CT scan is not particularly effective in distinguishing primary lung tumors from solitary pulmonary metastases and CRC[22], considering that these diseases usually present with an increased metabolic uptake. On the contrary, a negative PET scan result should not be the only determinant when planning the strategy of care. Indeed, if a lung nodule grows, even if the PET scan is negative, surgical resection can be indicated for diagnostic and potentially therapeutic purposes.

The main value of PET is its high level of sensitivity in the detection of extra-thoracic disease. If on the one hand, resection for lung metastasis should not be performed, unless all known disease areas are being treated, on the other hand, positive extra-thoracic or mediastinal uptake is insufficient to exclude a patient from metastasectomy. All suspicious extra-thoracic sites should be investigated, if possible also with a biopsy, before surgery.

Further improvements in radiological differential diagnosis (primary lung tumor *vs* mCRC) could be obtained from radiomics and its application on chest CT-scan or PET-CT scan.

Finally, carcinoembryonic antigen (CEA) could be a useful marker to detect metastasis and recurrence, and current guidelines recommend following up serum CEA regularly to detect recurrent disease. An increased CEA level could be indicative of mCRC when a pulmonary nodule is detected. Moreover, baseline CEA could be a good prognostic factor after recurrence[23].

THERAPY

Surgery

Colorectal neoplasms are the most common epithelial lesions for which pulmonary metastasectomy is indicated and they are the only type of primary metastatic cancer of the lungs in which the survival advantages of pulmonary metastasectomy were demonstrated in a randomized clinical trial, despite being limited by several pitfalls and controversies[24].

In current clinical practice, pulmonary metastasectomy, in the context of controlled primary tumor sites, is performed with curative intent, as favorable survival has been reported in CRC patients with complete resection of pulmonary metastases by several authors[25-28]. This seems to be particularly evident in single pulmonary metastases where complete resections are achievable. The surgeon's approach should be modulated considering various parameters pertaining to safety margins including local growth properties, size, spread and location of lung metastases. It clearly emerges that a strategy of care should be discussed on an individual, interdisciplinary basis to offer the best possible oncological and surgical results and to maximize long-term patient survival rates.

Oncologic principles and indication for surgery: As reported above, a limited subset of CRC patients may benefit from a potentially curative lung metastasectomy[29], provided some strict criteria are met:

Radicality: All pulmonary lesions are technically resectable. In single pulmonary metastases radicality is always achievable, despite the fact that it sometimes requires an anatomical resection instead of the most commonly performed non-anatomical wedge resection.

Feasibility: Patients might tolerate pulmonary resection following evaluation of pulmonary reserve.

Oncological control of disease: The primary CRC site is controlled and extra-thoracic lesions are undetectable (with the exception of resectable liver metastases). General disease control is imperative before performing lung resection and often re-staging imaging (whole body CT-scan or PET-CT scan) is recommended.

Despite that, the presence of solitary pulmonary metastases from CRC ideally represents the best scenario for surgery, and the patient's oncological history needs to be carefully evaluated during a multidisciplinary tumor board encompassing the presence of a thoracic surgeon. In particular, the timing of lung metastases appearance (synchronous with primary CRC, after liver metastasis treatment, recurrence of lung metastases) should always be considered in the treatment plan.

Type of approach, type of resection and other technical aspects: For many decades, radical pulmonary resection *via* thoracotomy has been a standard treatment for metastatic lung tumors[30], even though mini-invasive approaches have been proposed in the last two decades[31,32], resulting in likely similar clinical survival outcomes. However, robust evidence-based data are lacking and no focused analysis has been conducted investigating only CRC patients with solitary pulmonary metastases. A recent meta-analysis performed by Meng *et al*[32] compared the results of 8 studies and showed that no difference between video-assisted thoracic surgery (VATS) *vs* open thoracotomy metastasectomy were detected in terms of the OS rate (HR, 0.72; 95%CI: 0.50-1.04) or the recurrence-free survival rate (HR, 0.79; 95%CI: 0.59-1.08). Nevertheless, as correctly remarked by the authors, further large prospective studies are needed to identify the indications for VATS in patients with pulmonary metastases. In addition, it is logical to assume that in solitary pulmonary lesions VATS procedures are more frequently feasible compared with multiple pulmonary lesions, as completeness of resection it is more easily achieved. Based on these assumptions, we can state that VATS pulmonary resection may be efficacious in most CRC patients with single pulmonary metastases, when two conditions substantially coexist: (1) experience with minimally invasive pulmonary resection; and (2) patient selection (especially anatomical location of the lesion); the interval from chest CT-scan and surgery should be limited to avoid occult pulmonary lesions during VATS procedures.

Concerning the extension of resection, a parenchymal-sparing approach is always recommended for the following reasons: (1) The extent of resection is not related to the survival outcome; (2) Wedge resection seems to be associated with a better short-term outcome compared to segmentectomy/lobectomy[32,33]; and (3) Sparing lung parenchyma is pivotal for eventual re-do surgery. However, segmentectomy seems to be associated with lower relapse rates compared to wedge resection, due to a lower resection-margin recurrence[33]. Therefore, when technically feasible, wedge resection or segmentectomy should be preferred to lobar resection and surgeons should attempt this strategy as much as possible.

With regard to the surgical technique for nodule resection, the standard method consists of stapler use; however, laser-assisted lung resection has emerged as an alternative option. Regardless of the laser type adopted, this technique demonstrated similar early and long-term results after pulmonary metastasectomy[34], and is also associated to a lower local recurrence rate in some studies compared with stapler resection[35]. Moreover, laser resection may avoid the need to perform a lobectomy in selected cases[36] and, owing to recent technological improvements, laser-assisted lung resection may be feasible (especially in single pulmonary metastases) even *via* uniportal VATS (the least invasive approach available today)[37].

Radiotherapy and other loco-regional approaches

Approximately 70% of CRC metastases are unresectable and radiotherapy represents a very promising and rapidly evolving non-invasive treatment modality, particularly stereotactic body radiation therapy (SBRT)[1]. In fact, SBRT can potentially be equally effective and less toxic than surgery, especially in elderly patients and those with important comorbidities[38]. In detail, SBRT is a treatment technique with very sharp radiation dose gradients, which allows the delivery of high doses per fraction in a few days (less than or equal to 8), corresponding to consistently higher biologically equivalent doses in comparison with standard radiotherapy resulting in highly targeted treatment, with good surrounding healthy organ sparing, relative non-invasiveness and good tolerance.

On the other hand, the radiation dose and fractionation schedule are chosen based on several factors, such as tumor size, tumor location and neighboring organs at risk of dose constraints. In most of the clinical trials, SBRT was delivered in a few fractions (3-10), while single fraction SBRT has been less investigated and, in general, the dose administered is between 24 and 65 Gy in total. Moreover, the low number of treatment fractions may also play a role in the activation of an anti-tumor immune response because, in addition to damaging and killing cancer cells, radiation can destroy the adjacent tumor protective stromal microenvironment[39,40].

Four-dimensional (4D)-CT delineates the internal target volume contouring a gross tumor volume, which includes the tumor position in all respiratory cycles and is then expanded with a 3 mm isotropic margin to create the planning treatment volume (PTV); finally, a volumetric modulated arch therapy is planned with a specific treatment planning system. Stereotactic radiotherapy is delivered using a linear accelerator with an energy ranging from 6 to 10 MV photons. During each treatment session, cone-beam CT are performed to verify correct positioning of the patient and the correspondence of the PTV with the target volume identified during the simulation and planning phases[41].

Treatment accuracy can be implemented with respiratory gating techniques, with the benefit of reducing the mean radiation dose received by the lungs to avoid pulmonary acute toxicity, but also pulmonary, cardiac, and esophageal late toxicities[42,43]. In addition, magnetic resonance guidance provides excellent visualization of non-bony structures during radiotherapy.

In terms of results, Filippi *et al*[40] demonstrated similar OS outcomes between SBRT and surgery (89% *vs* 96% at 1 year and 77% *vs* 82% at 2 years, P = 0.134) in 142 patients with lung metastases, including 78 (55%) with single metastases. Moreover, a higher rate of local and distant recurrences occurred in the SBRT cohort, whereas a similar death rate was demonstrated. This retrospective study also showed a worse prognosis in terms of progression-free survival (PFS) in the SBRT cohort, but it cannot be excluded that this was influenced by different follow-up protocols and different sample sizes.

Kobiela *et al*[39] performed a systematic review of oligometastatic patients (average number of lesions per patients = 1.5) and showed that SBRT offers high local control rates (up to 90%) and satisfactory OS rates (up to 70% at 2 years) with a PFS of 9 to 34.4 mo and a relatively low toxicity burden. These data are similar to those obtained by Franzese *et al*[44], who showed a local control rate of 95% at 1 year and 73% at 3 years in 270 patients with a maximum of 5 lung metastases, 59% of the patients had a single disease location. However, disease progression outside the irradiation field still remains the main issue in metastatic CRC patients treated with SBRT. In the oligometastatic setting, SBRT can potentially ablate the whole burden of disease, but more careful selection of patients must be performed[45]. In fact, SBRT is often offered to patients who are usually not eligible for other treatment modalities[1,2,37].

Another retrospective analysis showed excellent promising results in a cohort of 40 patients including 26 with single lung metastases (65%), especially in terms of OS (88% at 1 year, 73% at 2 years), while PFS was 53% at 1 year and 28% at 2 years. Failure at the irradiation site was 7.5% (3 of 56 patients) and the time to progression after SBRT was similar to the surgical series; the typical pattern of failure was intrathoracic progression[41].

Thus, SBRT for CRC oligometastases may be a very good tool for maintaining high local control and good OS rates, especially if the radiation dose is escalated. Previous studies have demonstrated that a higher biologically equivalent dose seems to correlate with higher local control. On the other hand, a higher number of lesions may correlate with lower local control and OS. Comito *et al*[46] demonstrated a correlation between OS and cumulative tumor volume greater than 3 cm.

However, SBRT can result in toxicities. In particular, pulmonary SBRT has a safety profile expressed as moderate acute effects and a characteristic late toxicity pattern, appearing more than 6 mo after the end of treatment, which can be radiologic, secondary to radiation-induced fibrotic changes, and clinical, especially cutaneous erythema and chest wall toxicity (more frequently in terms of chronic neuropathic pain, more rarely as rib fractures). However, various retrospective data have shown that toxicity above grade 3 is extremely rare (mostly G1-G2). In conclusion, stereotactic radiation therapy appears to be a safe and efficient way to treat lung metastases, with very high local control rates, low toxicity and promising PFS in selected oligometastatic patients not suitable for surgical resection.

Systemic therapy

General principles: National and international guidelines (AIOM[47], ESMO[1], and NCCN[48]) agree that radical surgery represents the only potentially curative treatment for lung metastases, and these recommendations are based on retrospective data only. However, guidelines do not clearly define the

role of chemotherapy in this setting. In particular, there is no unanimous consensus on the best timing or on the preferred drug regimen.

Based on the literature and clinical experience, the choice of chemotherapy treatment can be assessed using several variables: patient (performance status, age, comorbidities) and tumor characteristics (RAS/BRAF status, site of the primary tumor right *vs* left, synchronous *vs* metachronous disease), and resectability status of metastases (resectable *vs* potentially resectable *vs* unresectable)[49,50]. In the scenario of single pulmonary metastases from CRC, the multidisciplinary team, composed of oncologists, thoracic surgeons, radiologists, and radiotherapists, plays a crucial role in outlining adequate personalized treatment planning.

In the context of single resectable pulmonary metastases, the "perfect" timing of the surgical approach is debated. "Oncological" prognostic criteria and "technical" surgical criteria should define the adequate strategy (upfront surgery eventually followed by postoperative chemotherapy or perioperative chemotherapy)[51,52]. Based on such results, patients with unfavorable prognostic factors could be considered for perioperative or postoperative chemotherapy to improve their outcome. In contrast, the presence of positive prognostic factors can allow upfront surgery.

The role of perioperative chemotherapy for single resectable pulmonary metastases is controversial due to the absence of prospective randomized trials. Perioperative therapy aims to increase the R0 metastasectomy rate and decrease the possibility of postoperative relapse, with a subsequent improvement in OS. A meta-analysis of eight retrospective studies investigated the role of perioperative chemotherapy in mCRC patients with radically resected lung metastases. Out of 1936 patients with colorectal lung metastases, 926 underwent surgery alone, while 1010 patients also received perioperative chemotherapy. This meta-analysis demonstrated the benefit of perioperative treatment both in terms of OS (HR 0.83, 95%CI: 0.75-0.92, $P < 0.05$) and PFS/recurrence-free survival (RFS)/disease-free survival (DFS) (HR 0.67, 95%CI: 0.53-0.86, $P < 0.05$) compared with surgery alone. Multivariate analysis also confirmed these results (OS: HR 0.56, 95%CI: 0.36–0.86, $P < 0.05$; PFS/RFS/DFS: HR 0.64, 95%CI: 0.46–0.87, $P < 0.05$)[53].

The role of postoperative therapy is also debated as no randomized study has compared postoperative therapy after lung metastasectomy *vs* surgery alone. A meta-analysis of 18 cohort studies involving 3885 patients with colorectal lung metastases evaluated the role of postoperative chemotherapy after radical lung resection compared to surgery alone. Postoperative treatment did not improve OS (HR 0.78; 95%CI: 0.60-1.03, $P = 0.077$) and DFS (HR 0.91; 95%CI: 0.74-1.11, $P = 0.339$) in comparison to surgery alone. However, it is necessary to underline the important limits of this meta-analysis, mainly the retrospective nature of the studies and the high heterogeneity, which may have negatively affected these results[54].

Despite the lack of randomized prospective trials and limited evidence, perioperative or postoperative chemotherapy to treat patients with resectable lung metastases is generally used in clinical practice, particularly for those with unfavorable prognostic factors. The most commonly adopted regimen is monotherapy with fluoropyrimidine or the combination with oxaliplatin (FOLFOX/XELOX). Such recommendations are mainly derived from data on mCRC patients with liver-only disease[55].

In the case of potentially resectable lung metastases, induction chemotherapy has, as the main objective, maximal tumor shrinkage to achieve radical resection. In this setting, the preferred treatment regimen corresponds to the most effective first-line therapy for mCRC, which is established based on patient and tumor characteristics. Patients should be re-evaluated regularly every 8-12 wk during therapy and discussed at multidisciplinary meetings to identify the best response and the most appropriate timing of surgery.

In the setting of oligometastatic disease, mainly involving lung and liver, a surgical approach can be considered, especially when the pulmonary parenchyma is minimally involved. Analysis of the liver in a survey registry evaluated 9619 mCRC patients divided into three groups: group 1 (9185 patients with liver-only disease, radically resected), group 2 (149 patients with liver and lung disease, both radically resected), and group 3 (285 patients with liver and lung disease, only liver resected). The 5-year OS was similar for patients in group 1 and 2 (51.5% and 44.5%, respectively) and worse for patients in group 3 (14.3%) ($P = 0.001$)[56]. Thus, these findings confirm the importance of radical surgery of both liver and lung metastases, when achievable.

Adjuvant therapies in single metastases: As described in the previous paragraph, the role of adjuvant therapies after lung metastasectomy is a debated and interesting issue, but presents discordant data and remarkable bias in patient selection. Indeed, some studies are in favor of adjuvant therapy (AT) administration[57,58], and others report disadvantages after AT administration[59,60].

The focal point is that it is difficult to consider a homogeneous population, considering the primitive tumor site, number of lung or extra-pulmonary surgically treated metastases and previous administered treatments. Moreover, the lack of clear prognostic factors may lead to a case-by-case decision on AT in advanced stage patients, and its role remains debated and requires clarification in appropriate prospective studies.

Regarding its potential use in patients with operated single metastases, very few data are present in the literature. Rapicetta *et al*[61] did not report any survival advantage when AT was administered,

while Guerrera *et al*[62] reported a better outcome when adjuvant chemotherapy was performed in patients with multiple metastases suggesting that no robust data on single metastases are available. The authors confirmed their theories in a recent best evidence topic which showed that AT may improve the prognosis in specific patients with advanced disease or a particular molecular pattern[63].

Based on these reports, clear evidence of AT benefits in patients who underwent lung metastasectomy for single localization is not present, suggesting this therapy especially in patients with multiple metastases. However, further planned research is needed for a better definition of this issue.

OUTCOMES

Prognostic factors and long-term survival

Different prognostic factors have been analyzed in patients with lung metastases from CRC, including factors linked to primitive tumors but also patients' oncological history. The main considered prognostic factors are reported in Table 1, even if detailed analyses in patients with single metastasis are very rare.

The CEA levels are routinely analyzed during follow-up in CRC patients, and it is interesting to note that they may also have a prognostic role in patients with lung metastases, by determining the worse prognosis in patients with CEA levels > 4-5 ng/mL (Table 1). The primitive tumor site does not seem to be associated with prognosis, with only the study by Cavallaro *et al*[64] reporting a better survival rate in the case of right sided tumors *vs* left sided rectal neoplasms. Conversely, the primitive CRC stage resulted in an important prognostic factor, with a poor prognosis in the case of advanced T-stage, presence of neighboring organ invasion or metastases to the loco-regional lymph nodes (Table 1).

It is interesting to note that lymph node spreading seems to be a significant prognostic factor in the case of mediastinal involvement, with various authors reporting that thoracic nodal involvement could be an important prognostic factor for worse long-term outcome[47,65]. Welter and co-workers[66] reported significantly poorer median survival for patients with nodal involvement than for patients without (≈ 30 mo *vs* 86 mo). This may also be a factor in the decision-making process to decide whether a patient is suitable for a surgical intervention or not[67], although the same authors caution that even some patients with intra-thoracic lymph node metastases have a longer OS with surgery than with chemotherapy alone[66].

On the other hand, mediastinal lymphadenectomy during lung metastasectomy is infrequently performed, and is one of the most common missing analyzed variable[68].

Despite no robust evidence being available on this topic to date, hilo/mediastinal lymph node sampling (at least) is advisable during pulmonary metastasectomy from CRC, especially when enlarged lymph nodes (at CT-scan) or uptake (at 18F-FDG PET-CT scan) by lymph nodes are detectable. There are no articles specifically focused on single pulmonary metastases, but oncological principles and indications are also applicable and valid in this scenario.

Tumor dimension, with a cut-off of 2 cm, is another well analyzed parameter in these patients, valid in the presence of single but also multiple metastases[61].

Another interesting argument is the outcome considering the patient's oncological history, which may be extremely various considering the timing of lung metastases appearance, concomitant liver involvement and disease-free intervals after CRC treatment. As we reported in previous paragraphs, multidisciplinary evaluation is fundamental, especially in the case of multi-organ involvement. In particular, patients with a history of extra-thoracic metastases[61,68-70] had a worse prognosis similar to patients with synchronous or bilateral lung involvement[71].

Finally, the DNA fragmentation index (DFI) between CRC treatment and lung metastases appearance is another validated prognostic factor, even if a universal cut-off is not present in the literature. Indeed, a better prognosis stratification is present when the DFI is evaluated at > 6[72], > 12[61,73], or 36 mo[67,74,75] confirming that a long DFI is an important factor when considering treatment for lung metastases from CRC.

A promising factor may be the metabolic activity of the nodule which was found to be a significant prognostic factor in the study by Rapicetta *et al*[61] and Davini *et al*[76]. In detail, Davini *et al*[76] reported that PET negativity was a protective factor for OS (HR 0.46; $P = 0.001$; 95%CI: 0.29–0.72) and for DFI after lung metastasectomy, while Rapicetta *et al*[61] reported that PET positivity in single CRC metastases (RR: 2.702, 95%CI: 1.041-7.013, $P = 0.041$) was a negative independent prognostic factor only for DFI.

With regard to long-term outcome, 5-year OS after single metastasis resection ranged between 32% and 62%[61,71,77], but it is interesting to note that the best survival rates (around 60% at 5 years) were reported in recent studies[61,71] suggesting a progressive improvement in terms of therapeutic strategies, but also regarding more accurate patient selection. The presence of a single metastases was one of the most important prognostic factors in surgically treated patients (Table 1), which was also confirmed in a meta-analysis by Gonzalez *et al*[78], who demonstrated a favorable prognostic role for the number of resected metastases, which was a significant favorable factor associated with CEA levels, DFI, and presence of lymph node involvement. In detail, the authors reported a significantly increased mortality risk in the case of multiple metastases: HR 2.04, 95%CI: 1.72-2.41. On the other hand, very few

Table 1 Main prognostic factors in patients with lung metastases from colorectal cancer

Prognostic factor	Overall survival		Disease-free survival	
	Favorable	Negative	Favorable	Negative
Number of metastases[23,68,71,76-78,86-90]	Single	Multiple		
Preoperative CEA level[61,69,86,87]	< 4-5 ng/mL	> 4-5 ng/mL		
pStage of CRC[71,79,86,87]	Local disease, low Tstage, absence of nodal involvement	Advanced p and T stage, nodal Involvement		
Lung metastases appearance [23,61,69-71,87,91]	Metachronous lung metastases	Bilateral lung synchronous metastasis, past history of extra thoracic metastasis	Long DFI between CRC and first detection of pulmonary metastasis	Synchronous pulmonary metastasis and CRC
Pulmonary metastasis derivation from primary site of CRC[64]	Right colon	Left colon or rectum	Not investigated	Not investigated
Lung metastasis size (cm)[61,69,78,79]	< 2 cm	> 2 cm	Not investigated	Not investigated
Mediastinal lymph node metastasis[23,69,89]	Negative	Positive	Not investigated	Not investigated
Metabolic characteristics[61,79]	Lung metastasis PET negative	Lung metastasis PET positive	Lung metastasis PET negative	Lung metastasis PET positive
Distance between lesion and resection margin (cm)[79]	> 2 cm	< 2 cm	Not investigated	Not Investigated

CRC: Colorectal cancer; CEA: Carcinoembryonic antigen; DFI: DNA fragmentation index; PET: Positron emission tomography.

data are available regarding prognostic factors in this class of patients with single metastases.

Metastasis dimension seems to be significantly related with survival in these patients, with survival improvement in patients with a metastasis dimension less than 2 cm. In particular, Nanji *et al*[79] reported an unadjusted 5-year CSS and OS of 57% and 55%, respectively, for single lesions smaller than 2 cm, and 33% for a single lesion exceeding 2 cm, in agreement with previously published results[61].

Only Rapicetta *et al*[61] performed a more accurate survival analysis in these patients and demonstrated that advanced age and elevated pre-thoracotomy CEA levels were also associated with poor survival. Moreover, the authors analyzed prognostic factors for DFS after metastasectomy and showed that a short DFI between colorectal resection and lung resection (cut-off 12 mo) increased PET uptake and the presence of synchronous lung metastasis were predictive of a short DFS. A long DFS was also found to be a protective factor by Davini *et al*[76], but also included multiple metastases.

The goal of CRC metastasectomy is to obtain a R0 resection[1,2], and there is little evidence regarding the prognostic role of the resection margin distance. Indeed, only Davini *et al*[76] reported a significant difference in survival when comparing a free resection margin > *vs* > 2 cm, while in other studies it was not investigated or did not show statistical significance[61,62]. However, considering the integrated treatments that may follow surgical resection, it is possible that the resection distance did not influence survival when a complete resection was performed.

Finally, Cavallaro *et al*[64] reported a significantly better survival rate when lung metastases were not associated with liver metastases.

Based on these reported studies, CEA pre-thoracotomy levels and short DFI may be evaluated when treating these patients, considering that the prognosis may be poor and a careful advantages/disadvantages analysis should consider the patient's general condition and surgical risks.

Incidence of recurrence and its management

Recurrence after lung metastasectomy is common, ranging between 32.9% and 72%[62,70,73,80] with lung involvement present in about 50% of cases[81] and with a redo surgery rate of about 50%[73].

When technically feasible and in patients able to tolerate a repeated lung resection, the surgical approach seems to ensure interesting results in terms of survival, with 5-year OS ranging between 49% and 76.3%[62,69,78].

In 26 patients with recurrence, Fukada *et al*[69] reported a 5-year OS of 76.9%, while Menna *et al*[82] did not report a survival difference when comparing patients who underwent single or repeated lung metastasectomy. Ogata reported a significantly better survival in patients who underwent repeated resection in the case of single metastases without extra-thoracic disease[80]; however, CEA level, number of pulmonary metastases, mediastinal lymph node metastasis, and DFI also seem to be related

to survival after repeat pulmonary metastasectomy[80,83-85].

However, this excellent survival outcome might be linked to careful patient selection indicating that the surgical approach in patients with limited lung involvement and good performance status may reduce the risks of redo-surgery in these patients. Conversely, repeated surgery may be carefully considered in patients with nodal or extra-thoracic metastases and sub-optimal clinical conditions.

CONCLUSION

Single pulmonary metastasis from CRC is an uncommon scenario with diagnostic pitfalls to be considered. Loco-regional approaches (surgery more than radiotherapy or ablative procedures) may have a potential curative role with rewarding long-term results. However, the absence of randomized prospective trials and limited data availability does not permit definitive conclusions. Chemotherapy, including timing and drug regimen, should be evaluated on a case-by-case basis by the multidisciplinary team by considering both tumor and patient characteristics.

The best long-term results may be expected when integrating loco-regional with systemic treatment. Despite evidence being limited, different factors seem to influence prognosis in this subset of patients and should be considered when planning a tailored care strategy.

ACKNOWLEDGEMENTS

We would like to thank Franziska M Lohmeyer, PhD, Fondazione Policlinico Universitario Agostino Gemelli IRCCS, for her support revising our manuscript language.

FOOTNOTES

Author contributions: Chiappetta M wrote the paper; Congedo MT, Petracca Ciavarella L, Bensi M, De Luca V and Camarda F collected the bibliography and supported manuscript drafting; Evangelista J supported manuscript drafting; Salvatore L and Lococo F revised and edited the manuscript; Margaritora S, Tortorta G and Valentini V supervised the manuscript.

Conflict-of-interest statement: No conflict-of-interest to declare.

Country/Territory of origin: Italy

ORCID number: Marco Chiappetta 0000-0002-3807-6911; Lisa Salvatore 0000-0003-3864-0719; Maria teresa Congedo 0000-0001-5563-0331; Maria Bensi 0000-0002-5647-0525; Viola De Luca 0000-0002-9914-0075; Leonardo Petracca Ciavarella 0000-0002-9659-1014; Floriana Camarda 0000-0002-5206-6867; Jessica Evangelista 0000-0001-6707-6120; Vincenzo Valentini 0000-0003-4637-6487; Giampaolo Tortora 0000-0002-1378-4962; Stefano Margaritora 0000-0002-9796-760X; Filippo Lococo 0000-0002-9383-5554.

S-Editor: Zhang H
L-Editor: Webster JR
P-Editor: Zhang H

REFERENCES

1 **Van Cutsem E**, Cervantes A, Adam R, Sobrero A, Van Krieken JH, Aderka D, Aranda Aguilar E, Bardelli A, Benson A, Bodoky G, Ciardiello F, D'Hoore A, Diaz-Rubio E, Douillard JY, Ducreux M, Falcone A, Grothey A, Gruenberger T, Haustermans K, Heinemann V, Hoff P, Köhne CH, Labianca R, Laurent-Puig P, Ma B, Maughan T, Muro K, Normanno N, Österlund P, Oyen WJ, Papamichael D, Pentheroudakis G, Pfeiffer P, Price TJ, Punt C, Ricke J, Roth A, Salazar R, Scheithauer W, Schmoll HJ, Tabernero J, Taïeb J, Tejpar S, Wasan H, Yoshino T, Zaanan A, Arnold D. ESMO consensus guidelines for the management of patients with metastatic colorectal cancer. *Ann Oncol* 2016; **27**: 1386-1422 [PMID: 27380959 DOI: 10.1093/annonc/mdw235]

2 **Benson AB**, Venook AP, Al-Hawary MM, Cederquist L, Chen YJ, Ciombor KK, Cohen S, Cooper HS, Deming D, Engstrom PF, Garrido-Laguna I, Grem JL, Grothey A, Hochster HS, Hoffe S, Hunt S, Kamel A, Kirilcuk N, Krishnamurthi

S, Messersmith WA, Meyerhardt J, Miller ED, Mulcahy MF, Murphy JD, Nurkin S, Saltz L, Sharma S, Shibata D, Skibber JM, Sofocleous CT, Stoffel EM, Stotsky-Himelfarb E, Willett CG, Wuthrick E, Gregory KM, Freedman-Cass DA. NCCN Guidelines Insights: Colon Cancer, Version 2.2018. *J Natl Compr Canc Netw* 2018; **16**: 359-369 [PMID: 29632055 DOI: 10.6004/jnccn.2018.0021]

3 **Ehrenhaft JL**, Lawrence MS, Sensenig DM. Pulmonary resections for metastatic lesions. *AMA Arch Surg* 1958; **77**: 606-612 [PMID: 13582418 DOI: 10.1001/archsurg.1958.04370010138013]

4 **Bray F**, Ferlay J, Soerjomataram I, Siegel RL, Torre LA, Jemal A. Global cancer statistics 2018: GLOBOCAN estimates of incidence and mortality worldwide for 36 cancers in 185 countries. *CA Cancer J Clin* 2018; **68**: 394-424 [PMID: 30207593 DOI: 10.3322/caac.21492]

5 **Brody H**. Colorectal cancer. *Nature* 2015; **521**: S1 [PMID: 25970450 DOI: 10.1038/521S1a]

6 **Siegel RL**, Miller KD, Jemal A. Cancer statistics, 2020. *CA Cancer J Clin* 2020; **70**: 7-30 [PMID: 31912902 DOI: 10.3322/caac.21590]

7 **Siegel RL**, Miller KD, Goding Sauer A, Fedewa SA, Butterly LF, Anderson JC, Cercek A, Smith RA, Jemal A. Colorectal cancer statistics, 2020. *CA Cancer J Clin* 2020; **70**: 145-164 [PMID: 32133645 DOI: 10.3322/caac.21601]

8 **Amin MB**, Greene FL, Edge SB, Compton CC, Gershenwald JE, Brookland RK, Meyer L, Gress DM, Byrd DR, Winchester DP. The Eighth Edition AJCC Cancer Staging Manual: Continuing to build a bridge from a population-based to a more "personalized" approach to cancer staging. *CA Cancer J Clin* 2017; **67**: 93-99 [PMID: 28094848 DOI: 10.3322/caac.21388]

9 **Kattan MW**, Hess KR, Amin MB, Lu Y, Moons KG, Gershenwald JE, Gimotty PA, Guinney JH, Halabi S, Lazar AJ, Mahar AL, Patel T, Sargent DJ, Weiser MR, Compton C; members of the AJCC Precision Medicine Core. American Joint Committee on Cancer acceptance criteria for inclusion of risk models for individualized prognosis in the practice of precision medicine. *CA Cancer J Clin* 2016; **66**: 370-374 [PMID: 26784705 DOI: 10.3322/caac.21339]

10 **Mitry E**, Guiu B, Cosconea S, Jooste V, Faivre J, Bouvier AM. Epidemiology, management and prognosis of colorectal cancer with lung metastases: a 30-year population-based study. *Gut* 2010; **59**: 1383-1388 [PMID: 20732912 DOI: 10.1136/gut.2010.211557]

11 **Li Y**, Zhou Z, Liu D, Zhou M, Tan F, Liu W, Zhu H. Predictive and Prognostic Factors of Synchronous Colorectal Lung-Limited Metastasis. *Gastroenterol Res Pract* 2020; **2020**: 6131485 [PMID: 33299406 DOI: 10.1155/2020/6131485]

12 **Tan KK**, Lopes Gde L Jr, Sim R. How uncommon are isolated lung metastases in colorectal cancer? *J Gastrointest Surg* 2009; **13**: 642-648 [PMID: 19082673 DOI: 10.1007/s11605-008-0757-7]

13 **Parnaby CN**, Bailey W, Balasingam A, Beckert L, Eglinton T, Fife J, Frizelle FA, Jeffery M, Watson AJ. Pulmonary staging in colorectal cancer: a review. *Colorectal Dis* 2012; **14**: 660-670 [PMID: 21689294 DOI: 10.1111/j.1463-1318.2011.02601.x]

14 **Brent A**, Talbot R, Coyne J, Nash G. Should indeterminate lung lesions reported on staging CT scans influence the management of patients with colorectal cancer? *Colorectal Dis* 2007; **9**: 816-818 [PMID: 17931171 DOI: 10.1111/j.1463-1318.2007.01229.x]

15 **Kronawitter U**, Kemeny NE, Heelan R, Fata F, Fong Y. Evaluation of chest computed tomography in the staging of patients with potentially resectable liver metastases from colorectal carcinoma. *Cancer* 1999; **86**: 229-235 [PMID: 10421258]

16 **Grossmann I**, Avenarius JK, Mastboom WJ, Klaase JM. Preoperative staging with chest CT in patients with colorectal carcinoma: not as a routine procedure. *Ann Surg Oncol* 2010; **17**: 2045-2050 [PMID: 20151212 DOI: 10.1245/s10434-010-0962-y]

17 **Collie DA**, Wright AR, Williams JR, Hashemi-Malayeri B, Stevenson AJ, Turnbull CM. Comparison of spiral-acquisition computed tomography and conventional computed tomography in the assessment of pulmonary metastatic disease. *Br J Radiol* 1994; **67**: 436-444 [PMID: 8193888 DOI: 10.1259/0007-1285-67-797-436]

18 **Ohtaki Y**, Shimizu K, Nagashima T, Nakazawa S, Obayashi K, Azuma Y, Iijima M, Kosaka T, Yajima T, Ogawa H, Tsutsumi S, Arai M, Mogi A, Kuwano H. Clinical and Radiological Discrimination of Solitary Pulmonary Lesions in Colorectal Cancer Patients. *World J Surg* 2018; **42**: 1161-1170 [PMID: 28983707 DOI: 10.1007/s00268-017-4243-9]

19 **Reinhardt MJ**, Wiethoelter N, Matthies A, Joe AY, Strunk H, Jaeger U, Biersack HJ. PET recognition of pulmonary metastases on PET/CT imaging: impact of attenuation-corrected and non-attenuation-corrected PET images. *Eur J Nucl Med Mol Imaging* 2006; **33**: 134-139 [PMID: 16193313 DOI: 10.1007/s00259-005-1901-1]

20 **Jess P**, Seiersen M, Ovesen H, Sandstrøm H, Maltbæk N, Buhl AA, Roikjær O. Has PET/CT a role in the characterization of indeterminate lung lesions on staging CT in colorectal cancer? *Eur J Surg Oncol* 2014; **40**: 719-722 [PMID: 24462549 DOI: 10.1016/j.ejso.2013.11.030]

21 **Benson AB**, Venook AP, Al-Hawary MM, Arain MA, Chen YJ, Ciombor KK, Cohen S, Cooper HS, Deming D, Farkas L, Garrido-Laguna I, Grem JL, Gunn A, Hecht JR, Hoffe S, Hubbard J, Hunt S, Johung KL, Kirilcuk N, Krishnamurthi S, Messersmith WA, Meyerhardt J, Miller ED, Mulcahy MF, Nurkin S, Overman MJ, Parikh A, Patel H, Pedersen K, Saltz L, Schneider C, Shibata D, Skibber JM, Sofocleous CT, Stoffel EM, Stotsky-Himelfarb E, Willett CG, Gregory KM, Gurski LA. Colon Cancer, Version 2.2021, NCCN Clinical Practice Guidelines in Oncology. *J Natl Compr Canc Netw* 2021; **19**: 329-359 [PMID: 33724754 DOI: 10.6004/jnccn.2021.0012]

22 **Yu X**, Song X, Zhu L, Chen W, Dai D, Li X, Xu W. Role of ^{18}F-Fluorodeoxyglucose Positron Emission Tomography/Computed Tomography in the Diagnosis of Newly Found Suspected Malignant Solitary Pulmonary Lesions in Patients Who Have Received Curative Treatment for Colorectal Cancer. *Gastroenterol Res Pract* 2017; **2017**: 3458739 [PMID: 28487728 DOI: 10.1155/2017/3458739]

23 **Cho WK**, Choi DH, Park HC, Park W, Yu JI, Park YS, Park JO, Lim HY, Kang WK, Kim HC, Cho YB, Yun SH, Lee WY. Elevated CEA is associated with worse survival in recurrent rectal cancer. *Oncotarget* 2017; **8**: 105936-105941 [PMID: 29285304 DOI: 10.18632/oncotarget.22511]

24 **Treasure T**, Farewell V, Macbeth F, Monson K, Williams NR, Brew-Graves C, Lees B, Grigg O, Fallowfield L; PulMiCC Trial Group. Pulmonary Metastasectomy versus Continued Active Monitoring in Colorectal Cancer (PulMiCC): a multicentre randomised clinical trial. *Trials* 2019; **20**: 718 [PMID: 31831062 DOI: 10.1186/s13063-019-3837-y]

25 **van Dorp M**, Beck N, Steup WH, Schreurs WH. Surgical treatment of pulmonary metastases in the Netherlands: data from the Dutch Lung Cancer Audit for Surgery. *Eur J Cardiothorac Surg* 2020; **58**: 768-774 [PMID: 32282876 DOI: 10.1093/ejcts/ezaa090]

26 **Rotolo N**, De Monte L, Imperatori A, Dominioni L. Pulmonary resections of single metastases from colorectal cancer. *Surg Oncol* 2007; **16** Suppl 1: S141-S144 [PMID: 18037287 DOI: 10.1016/j.suronc.2007.10.007]

27 **Kim JY**, Park IJ, Kim HR, Kim DK, Lee JL, Yoon YS, Kim CW, Lim SB, Lee JB, Yu CS, Kim JC. Post-pulmonary metastasectomy prognosis after curative resection for colorectal cancer. *Oncotarget* 2017; **8**: 36566-36577 [PMID: 28402263 DOI: 10.18632/oncotarget.16616]

28 **Gonzalez M**, Zellweger M, Nardini M, Migliore M. Precision surgery in lung metastasectomy. *Future Oncol* 2020; **16**: 7-13 [PMID: 31858825 DOI: 10.2217/fon-2018-0713]

29 **Pfannschmidt J**, Dienemann H, Hoffmann H. Surgical resection of pulmonary metastases from colorectal cancer: a systematic review of published series. *Ann Thorac Surg* 2007; **84**: 324-338 [PMID: 17588454 DOI: 10.1016/j.athoracsur.2007.02.093]

30 **Riquet M**, Foucault C, Cazes A, Mitry E, Dujon A, Le Pimpec Barthes F, Médioni J, Rougier P. Pulmonary resection for metastases of colorectal adenocarcinoma. *Ann Thorac Surg* 2010; **89**: 375-380 [PMID: 20103301 DOI: 10.1016/j.athoracsur.2009.10.005]

31 **Greenwood A**, West D. Is a thoracotomy rather than thoracoscopic resection associated with improved survival after pulmonary metastasectomy? *Interact Cardiovasc Thorac Surg* 2013; **17**: 720-724 [PMID: 23832919 DOI: 10.1093/icvts/ivt300]

32 **Meng D**, Fu L, Wang L, Dai Y, Lv W, Zhang J, Hu J. Video-assisted thoracoscopic surgery versus open thoracotomy in pulmonary metastasectomy: a meta-analysis of observational studies. *Interact Cardiovasc Thorac Surg* 2016; **22**: 200-206 [PMID: 26590306 DOI: 10.1093/icvts/ivv309]

33 **Shiono S**, Okumura T, Boku N, Hishida T, Ohde Y, Sakao Y, Yoshiya K, Hyodo I, Mori K, Kondo H. Outcomes of segmentectomy and wedge resection for pulmonary metastases from colorectal cancer. *Eur J Cardiothorac Surg* 2017; **51**: 504-510 [PMID: 27773868 DOI: 10.1093/ejcts/ezw322]

34 **Rolle A**, Pereszlenyi A, Koch R, Richard M, Baier B. Is surgery for multiple lung metastases reasonable? *J Thorac Cardiovasc Surg* 2006; **131**: 1236-1242 [PMID: 16733151 DOI: 10.1016/j.jtcvs.2005.11.053]

35 **Lococo F**, Cesario A, Ricchetti T, Rapicetta C, Paci M, Sgarbi G. Erratum to: Lung Tissue Damage Caused by Heat Accumulation from Adjacent Laser Application: Surgical Implications. *Thorac Cardiovasc Surg* 2014; **62**: e2 [PMID: 25415626 DOI: 10.1055/s-0034-1394168]

36 **Stefani A**, Oricchio F, Cinquepalmi A, Aramini B, Morandi U. Is laser-assisted resection preferable to lobectomy for pulmonary metastasectomy? *Lasers Med Sci* 2020; **35**: 611-620 [PMID: 31410616 DOI: 10.1007/s10103-019-02856-8]

37 **Lococo F**, Iaffaldano A, Zanfrini E, Pogliani L, Tabacco D, Sassorossi C, Mazzarella C, Margaritora S. Thulium cyber laser-assisted uniportal thoracoscopic resection of a pulmonary metastasis from colorectal cancer. *Minerva Chir* 2020; **75**: 475-477 [PMID: 33006450 DOI: 10.23736/S0026-4733.20.08416-3]

38 **Ricardi U**, Badellino S, Filippi AR. Clinical applications of stereotactic radiation therapy for oligometastatic cancer patients: a disease-oriented approach. *J Radiat Res* 2016; **57**: i58-i68 [PMID: 26962198 DOI: 10.1093/jrr/rrw006]

39 **Kobiela J**, Spychalski P, Marvaso G, Ciardo D, Dell'Acqua V, Kraja F, Błażyńska-Spychalska A, Łachiński AJ, Surgo A, Glynne-Jones R, Jereczek-Fossa BA. Ablative stereotactic radiotherapy for oligometastatic colorectal cancer: Systematic review. *Crit Rev Oncol Hematol* 2018; **129**: 91-101 [PMID: 30097241 DOI: 10.1016/j.critrevonc.2018.06.005]

40 **Filippi AR**, Guerrera F, Badellino S, Ceccarelli M, Castiglione A, Guarneri A, Spadi R, Racca P, Ciccone G, Ricardi U, Ruffini E. Exploratory Analysis on Overall Survival after Either Surgery or Stereotactic Radiotherapy for Lung Oligometastases from Colorectal Cancer. *Clin Oncol (R Coll Radiol)* 2016; **28**: 505-512 [PMID: 26899780 DOI: 10.1016/j.clon.2016.02.001]

41 **Filippi AR**, Badellino S, Ceccarelli M, Guarneri A, Franco P, Monagheddu C, Spadi R, Ragona R, Racca P, Ricardi U. Stereotactic ablative radiation therapy as first local therapy for lung oligometastases from colorectal cancer: a single-institution cohort study. *Int J Radiat Oncol Biol Phys* 2015; **91**: 524-529 [PMID: 25542308 DOI: 10.1016/j.ijrobp.2014.10.046]

42 **Kini VR**, Vedam SS, Keall PJ, Patil S, Chen C, Mohan R. Patient training in respiratory-gated radiotherapy. *Med Dosim* 2003; **28**: 7-11 [PMID: 12747612 DOI: 10.1016/S0958-3947(02)00136-X]

43 **Giraud P**, Morvan E, Claude L, Mornex F, Le Pechoux C, Bachaud JM, Boisselier P, Beckendorf V, Morelle M, Carrère MO; STIC Study Centers. Respiratory gating techniques for optimization of lung cancer radiotherapy. *J Thorac Oncol* 2011; **6**: 2058-2068 [PMID: 22052228 DOI: 10.1097/JTO.0b013e3182307ec2]

44 **Franzese C**, Comito T, Toska E, Tozzi A, Clerici E, De Rose F, Franceschini D, Navarria P, Reggiori G, Tomatis S, Scorsetti M. Predictive factors for survival of oligometastatic colorectal cancer treated with Stereotactic body radiation therapy. *Radiother Oncol* 2019; **133**: 220-226 [PMID: 30414754 DOI: 10.1016/j.radonc.2018.10.024]

45 **Franzese C**, Comito T, Franceschini D, Loi M, Clerici E, Navarria P, De Rose F, Di Brina L, Mancosu P, Reggiori G, Tomatis S, Scorsetti M. Recursive partitioning model-based analysis for survival of colorectal cancer patients with lung and liver oligometastases treated with stereotactic body radiation therapy. *J Cancer Res Clin Oncol* 2020; **146**: 1227-1234 [PMID: 32056005 DOI: 10.1007/s00432-020-03148-3]

46 **Comito T**, Cozzi L, Clerici E, Campisi MC, Liardo RL, Navarria P, Ascolese A, Tozzi A, Iftode C, De Rose F, Villa E, Personeni N, Rimassa L, Santoro A, Fogliata A, Mancosu P, Tomatis S, Scorsetti M. Stereotactic Ablative Radiotherapy (SABR) in inoperable oligometastatic disease from colorectal cancer: a safe and effective approach. *BMC Cancer* 2014; **14**: 619 [PMID: 25163798 DOI: 10.1186/1471-2407-14-619]

47 **Salvatore L**, Aprile G, Arnoldi E, Aschele C, Carnaghi C, Cosimelli M, Maiello E, Normanno N, Sciallero S, Valvo F, Beretta GD. Management of metastatic colorectal cancer patients: guidelines of the Italian Medical Oncology Association (AIOM). *ESMO Open* 2017; **2**: e000147 [PMID: 28761730 DOI: 10.1136/esmoopen-2016-000147]

48 **Benson AB 3rd**, Venook AP, Cederquist L, Chan E, Chen YJ, Cooper HS, Deming D, Engstrom PF, Enzinger PC, Fichera A, Grem JL, Grothey A, Hochster HS, Hoffe S, Hunt S, Kamel A, Kirilcuk N, Krishnamurthi S, Messersmith WA,

Mulcahy MF, Murphy JD, Nurkin S, Saltz L, Sharma S, Shibata D, Skibber JM, Sofocleous CT, Stoffel EM, Stotsky-Himelfarb E, Willett CG, Wu CS, Gregory KM, Freedman-Cass D. Colon Cancer, Version 1.2017, NCCN Clinical Practice Guidelines in Oncology. *J Natl Compr Canc Netw* 2017; **15**: 370-398 [PMID: 28275037 DOI: 10.6004/jnccn.2017.0036]

49 **Meimarakis G**, Spelsberg F, Angele M, Preissler G, Fertmann J, Crispin A, Reu S, Kalaitzis N, Stemmler M, Giessen C, Heinemann V, Stintzing S, Hatz R, Winter H. Resection of pulmonary metastases from colon and rectal cancer: factors to predict survival differ regarding to the origin of the primary tumor. *Ann Surg Oncol* 2014; **21**: 2563-2572 [PMID: 24668147 DOI: 10.1245/s10434-014-3646-1]

50 **Suzuki H**, Kiyoshima M, Kitahara M, Asato Y, Amemiya R. Long-term outcomes after surgical resection of pulmonary metastases from colorectal cancer. *Ann Thorac Surg* 2015; **99**: 435-440 [PMID: 25499475 DOI: 10.1016/j.athoracsur.2014.09.027]

51 **Lee WS**, Yun SH, Chun HK, Lee WY, Yun HR, Kim J, Kim K, Shim YM. Pulmonary resection for metastases from colorectal cancer: prognostic factors and survival. *Int J Colorectal Dis* 2007; **22**: 699-704 [PMID: 17109105 DOI: 10.1007/s00384-006-0218-2]

52 **Onaitis MW**, Petersen RP, Haney JC, Saltz L, Park B, Flores R, Rizk N, Bains MS, Dycoco J, D'Amico TA, Harpole DH, Kemeny N, Rusch VW, Downey R. Prognostic factors for recurrence after pulmonary resection of colorectal cancer metastases. *Ann Thorac Surg* 2009; **87**: 1684-1688 [PMID: 19463577 DOI: 10.1016/j.athoracsur.2009.03.034]

53 **Li Y**, Qin Y. Peri-operative chemotherapy for resectable colorectal lung metastasis: a systematic review and meta-analysis. *J Cancer Res Clin Oncol* 2020; **146**: 545-553 [PMID: 32036456 DOI: 10.1007/s00432-020-03142-9]

54 **Zhang C**, Tan Y, Xu H. Does adjuvant chemotherapy improve the prognosis of patients after resection of pulmonary metastasis from colorectal cancer? *Int J Colorectal Dis* 2019; **34**: 1661-1671 [PMID: 31446479 DOI: 10.1007/s00384-019-03362-7]

55 **Nordlinger B**, Sorbye H, Glimelius B, Poston GJ, Schlag PM, Rougier P, Bechstein WO, Primrose JN, Walpole ET, Finch-Jones M, Jaeck D, Mirza D, Parks RW, Mauer M, Tanis E, Van Cutsem E, Scheithauer W, Gruenberger T; EORTC Gastro-Intestinal Tract Cancer Group; Cancer Research UK; Arbeitsgruppe Lebermetastasen und–tumoren in der Chirurgischen Arbeitsgemeinschaft Onkologie (ALM-CAO); Australasian Gastro-Intestinal Trials Group (AGITG); Fédération Francophone de Cancérologie Digestive (FFCD). Perioperative FOLFOX4 chemotherapy and surgery versus surgery alone for resectable liver metastases from colorectal cancer (EORTC 40983): long-term results of a randomised, controlled, phase 3 trial. *Lancet Oncol* 2013; **14**: 1208-1215 [PMID: 24120480 DOI: 10.1016/S1470-2045(13)70447-9]

56 **Andres A**, Mentha G, Adam R, Gerstel E, Skipenko OG, Barroso E, Lopez-Ben S, Hubert C, Majno PE, Toso C. Surgical management of patients with colorectal cancer and simultaneous liver and lung metastases. *Br J Surg* 2015; **102**: 691-699 [PMID: 25789941 DOI: 10.1002/bjs.9783]

57 **Rusch VW**. Pulmonary metastasectomy. Current indications. *Chest* 1995; **107**: 322S-331S [PMID: 7781414 DOI: 10.1378/chest.107.6_supplement.322s]

58 **Higashiyama M**, Kodama K, Takami K, Higaki N, Yokouchi H, Nakayama T, Murata K, Kameyama M, Ashimura J, Naruse Y, Nagumo S. Intraoperative lavage cytologic analysis of surgical margins as a predictor of local recurrence in pulmonary metastasectomy. *Arch Surg* 2002; **137**: 469-474 [PMID: 11926957 DOI: 10.1001/archsurg.137.4.469]

59 **Higashiyama M**, Tokunaga T, Nakagiri T, Ishida D, Kuno H, Okami J. Pulmonary metastasectomy: outcomes and issues according to the type of surgical resection. *Gen Thorac Cardiovasc Surg* 2015; **63**: 320-330 [PMID: 25836329 DOI: 10.1007/s11748-015-0544-9]

60 **Shiono S**, Ishii G, Nagai K, Yoshida J, Nishimura M, Murata Y, Tsuta K, Kim YH, Nishiwaki Y, Kodama T, Iwasaki M, Ochiai A. Predictive factors for local recurrence of resected colorectal lung metastases. *Ann Thorac Surg* 2005; **80**: 1040-1045 [PMID: 16122482 DOI: 10.1016/j.athoracsur.2004.12.033]

61 **Rapicetta C**, Lococo F, Davini F, Carleo F, Kauppi J, Di Stefano TS, Ricciardi S, Di Martino M, Räsänen J, Paci M, Melfi F, Cardillo G. Is Adjuvant Chemotherapy Worthwhile After Radical Resection for Single Lung Metastasis From Colorectal Cancer? *Front Oncol* 2019; **9**: 763 [PMID: 31482063 DOI: 10.3389/fonc.2019.00763]

62 **Guerrera F**, Mossetti C, Ceccarelli M, Bruna MC, Bora G, Olivetti S, Lausi PO, Solidoro P, Ciccone G, Ruffini E, Oliaro A, Filosso PL. Surgery of colorectal cancer lung metastases: analysis of survival, recurrence and re-surgery. *J Thorac Dis* 2016; **8**: 1764-1771 [PMID: 27499967 DOI: 10.21037/jtd.2016.05.98]

63 **Guerrera F**, Falcoz PE, Renaud S, Massard G. Does perioperative chemotherapy improve survival in patients with resectable lung metastases of colorectal cancer? *Interact Cardiovasc Thorac Surg* 2017; **24**: 789-791 [PMID: 28453801 DOI: 10.1093/icvts/ivw389]

64 **Cavallaro P**, Bordeianou L, Stafford C, Clark J, Berger D, Cusack J, Kunitake H, Francone T, Ricciardi R. Impact of Single-organ Metastasis to the Liver or Lung and Genetic Mutation Status on Prognosis in Stage IV Colorectal Cancer. *Clin Colorectal Cancer* 2020; **19**: e8-e17 [PMID: 31899147 DOI: 10.1016/j.clcc.2019.12.001]

65 **Renaud S**, Alifano M, Falcoz PE, Magdeleinat P, Santelmo N, Pagès O, Massard G, Régnard JF. Does nodal status influence survival? *Interact Cardiovasc Thorac Surg* 2014; **18**: 482-487 [PMID: 24442624 DOI: 10.1093/icvts/ivt554]

66 **Welter S**, Jacobs J, Krbek T, Poettgen C, Stamatis G. Prognostic impact of lymph node involvement in pulmonary metastases from colorectal cancer. *Eur J Cardiothorac Surg* 2007; **31**: 167-172 [PMID: 17150367 DOI: 10.1016/j.ejcts.2006.11.004]

67 **Cho JH**, Kim S, Namgung M, Choi YS, Kim HK, Zo JI, Shim YM, Kim J. The prognostic importance of the number of metastases in pulmonary metastasectomy of colorectal cancer. *World J Surg Oncol* 2015; **13**: 222 [PMID: 26205014 DOI: 10.1186/s12957-015-0621-7]

68 **Zabaleta J**, Iida T, Falcoz PE, Salah S, Jarabo JR, Correa AM, Zampino MG, Matsui T, Cho S, Ardissone F, Watanabe K, Gonzalez M, Gervaz P, Emparanza JI, Abraira V. Individual data meta-analysis for the study of survival after pulmonary metastasectomy in colorectal cancer patients: A history of resected liver metastases worsens the prognosis. *Eur J Surg Oncol* 2018; **44**: 1006-1012 [PMID: 29602524 DOI: 10.1016/j.ejso.2018.03.011]

69 **Fukada M**, Matsuhashi N, Takahashi T, Tanaka Y, Okumura N, Yamamoto H, Shirahashi K, Iwata H, Doi K, Yoshida K. Prognostic factors in pulmonary metastasectomy and efficacy of repeat pulmonary metastasectomy from colorectal cancer. *World J Surg Oncol* 2020; **18**: 314 [PMID: 33256771 DOI: 10.1186/s12957-020-02076-3]

70 **Sakamaki Y**, Ishida D, Tanaka R. Prognosis of patients with recurrence after pulmonary metastasectomy for colorectal cancer. *Gen Thorac Cardiovasc Surg* 2020; **68**: 1172-1178 [PMID: 32323124 DOI: 10.1007/s11748-020-01368-5]

71 **Fournel L**, Maria S, Seminel M, Nesci J, Mansuet-Lupo A, Guinet C, Magdeleinat P, Bobbio A, Regnard JF, Alifano M. Prognostic factors after pulmonary metastasectomy of colorectal cancers: a single-center experience. *J Thorac Dis* 2017; **9**: S1259-S1266 [PMID: 29119012 DOI: 10.21037/jtd.2017.04.44]

72 **Hwang MR**, Park JW, Kim DY, Chang HJ, Kim SY, Choi HS, Kim MS, Zo JI, Oh JH. Early intrapulmonary recurrence after pulmonary metastasectomy related to colorectal cancer. *Ann Thorac Surg* 2010; **90**: 398-404 [PMID: 20667318 DOI: 10.1016/j.athoracsur.2010.04.058]

73 **Takakura Y**, Miyata Y, Okajima M, Okada M, Ohdan H. Short disease-free interval is a significant risk factor for intrapulmonary recurrence after resection of pulmonary metastases in colorectal cancer. *Colorectal Dis* 2010; **12**: e68-e75 [PMID: 19843115 DOI: 10.1111/j.1463-1318.2009.02070.x]

74 **Rama N**, Monteiro A, Bernardo JE, Eugénio L, Antunes MJ. Lung metastases from colorectal cancer: surgical resection and prognostic factors. *Eur J Cardiothorac Surg* 2009; **35**: 444-449 [PMID: 19136273 DOI: 10.1016/j.ejcts.2008.10.047]

75 **Yedibela S**, Klein P, Feuchter K, Hoffmann M, Meyer T, Papadopoulos T, Göhl J, Hohenberger W. Surgical management of pulmonary metastases from colorectal cancer in 153 patients. *Ann Surg Oncol* 2006; **13**: 1538-1544 [PMID: 17009154 DOI: 10.1245/s10434-006-9100-2]

76 **Davini F**, Ricciardi S, Zirafa CC, Romano G, Alì G, Fontanini G, Melfi FMA. Correction to: Lung metastasectomy after colorectal cancer: prognostic impact of resection margin on long term survival, a retrospective cohort study. *Int J Colorectal Dis* 2020; **35**: 371-372 [PMID: 31838578 DOI: 10.1007/s00384-019-03485-x]

77 **Pfannschmidt J**, Muley T, Hoffmann H, Dienemann H. Prognostic factors and survival after complete resection of pulmonary metastases from colorectal carcinoma: experiences in 167 patients. *J Thorac Cardiovasc Surg* 2003; **126**: 732-739 [PMID: 14502146 DOI: 10.1016/s0022-5223(03)00587-7]

78 **Gonzalez M**, Gervaz P. Risk factors for survival after lung metastasectomy in colorectal cancer patients: systematic review and meta-analysis. *Future Oncol* 2015; **11**: 31-33 [PMID: 25662325 DOI: 10.2217/fon.14.259]

79 **Nanji S**, Karim S, Tang E, Brennan K, McGuire A, Pramesh CS, Booth CM. Pulmonary Metastasectomy for Colorectal Cancer: Predictors of Survival in Routine Surgical Practice. *Ann Thorac Surg* 2018; **105**: 1605-1612 [PMID: 29518384 DOI: 10.1016/j.athoracsur.2018.02.007]

80 **Ogata Y**, Matono K, Hayashi A, Takamor S, Miwa K, Sasatomi T, Ishibashi N, Shida S, Shirouzu K. Repeat pulmonary resection for isolated recurrent lung metastases yields results comparable to those after first pulmonary resection in colorectal cancer. *World J Surg* 2005; **29**: 363-368 [PMID: 15706447 DOI: 10.1007/s00268-004-7537-7]

81 **Murakawa T**. Past, present, and future perspectives of pulmonary metastasectomy for patients with advanced colorectal cancer. *Surg Today* 2021; **51**: 204-211 [PMID: 32857252 DOI: 10.1007/s00595-020-02119-y]

82 **Menna C**, Berardi G, Tierno SM, Andreetti C, Maurizi G, Ciccone AM, D'Andrilli A, Cassiano F, Poggi C, Diso D, Venuta F, Rendina EA, Ibrahim M. Do Repeated Operations for Recurrent Colorectal Lung Metastases Result in Improved Survival? *Ann Thorac Surg* 2018; **106**: 421-427 [PMID: 29605599 DOI: 10.1016/j.athoracsur.2018.02.065]

83 **Kanzaki R**, Higashiyama M, Oda K, Fujiwara A, Tokunaga T, Maeda J, Okami J, Tanaka K, Shingai T, Noura S, Ohue M, Kodama K. Outcome of surgical resection for recurrent pulmonary metastasis from colorectal carcinoma. *Am J Surg* 2011; **202**: 419-426 [PMID: 21824604 DOI: 10.1016/j.amjsurg.2010.08.016]

84 **Hachimaru A**, Maeda R, Suda T, Takagi Y. Repeat pulmonary resection for recurrent lung metastases from colorectal cancer: an analysis of prognostic factors. *Interact Cardiovasc Thorac Surg* 2016; **22**: 826-830 [PMID: 26920721 DOI: 10.1093/icvts/ivv382]

85 **Chen F**, Sakai H, Miyahara R, Bando T, Okubo K, Date H. Repeat resection of pulmonary metastasis is beneficial for patients with colorectal carcinoma. *World J Surg* 2010; **34**: 2373-2378 [PMID: 20582543 DOI: 10.1007/s00268-010-0695-x]

86 **Shiomi K**, Naito M, Sato T, Nakamura T, Nakashima H, Mikubo M, Matsui Y, Watanabe M, Satoh Y. Effect of adjuvant chemotherapy after pulmonary metastasectomy on the prognosis of colorectal cancer. *Ann Med Surg (Lond)* 2017; **20**: 19-25 [PMID: 28702182 DOI: 10.1016/j.amsu.2017.06.026]

87 **Imanishi M**, Yamamoto Y, Hamano Y, Yamada T, Moriwaki T, Gosho M, Okumura T, Boku N, Kondo H, Hyodo I. Efficacy of adjuvant chemotherapy after resection of pulmonary metastasis from colorectal cancer: a propensity score-matched analysis. *Eur J Cancer* 2019; **106**: 69-77 [PMID: 30471650 DOI: 10.1016/j.ejca.2018.10.003]

88 **Tsitsias T**, Toufektzian L, Routledge T, Pilling J. Are there recognized prognostic factors for patients undergoing pulmonary metastasectomy for colorectal carcinoma? *Interact Cardiovasc Thorac Surg* 2016; **23**: 962-969 [PMID: 27572615 DOI: 10.1093/icvts/ivw273]

89 **Zampino MG**, Maisonneuve P, Ravenda PS, Magni E, Casiraghi M, Solli P, Petrella F, Gasparri R, Galetta D, Borri A, Donghi S, Veronesi G, Spaggiari L. Lung metastases from colorectal cancer: analysis of prognostic factors in a single institution study. *Ann Thorac Surg* 2014; **98**: 1238-1245 [PMID: 25106681 DOI: 10.1016/j.athoracsur.2014.05.048]

90 **Tampellini M**, Ottone A, Bellini E, Alabiso I, Baratelli C, Bitossi R, Brizzi MP, Ferrero A, Sperti E, Leone F, Miraglia S, Forti L, Bertona E, Ardissone F, Berruti A, Alabiso O, Aglietta M, Scagliotti GV. The role of lung metastasis resection in improving outcome of colorectal cancer patients: results from a large retrospective study. *Oncologist* 2012; **17**: 1430-1438 [PMID: 22956535 DOI: 10.1634/theoncologist.2012-0142]

91 **Landes U**, Robert J, Perneger T, Mentha G, Ott V, Morel P, Gervaz P. Predicting survival after pulmonary metastasectomy for colorectal cancer: previous liver metastases matter. *BMC Surg* 2010; **10**: 17 [PMID: 20525275 DOI: 10.1186/1471-2482-10-17]

World Journal of Gastrointestinal Oncology

Submit a Manuscript: https://www.f6publishing.com

World J Gastrointest Oncol 2022 April 15; 14(4): 833-841

DOI: 10.4251/wjgo.v14.i4.833

ISSN 1948-5204 (online)

MINIREVIEWS

Current guidelines in the surgical management of hereditary colorectal cancers

Shantata Kudchadkar, Safia Ahmed, Tanmoy Mukherjee, Jayesh Sagar

Specialty type: Oncology

Provenance and peer review: Invited article; Externally peer reviewed.

Peer-review model: Single blind

Peer-review report's scientific quality classification

Grade A (Excellent): 0
Grade B (Very good): B
Grade C (Good): 0
Grade D (Fair): 0
Grade E (Poor): 0

P-Reviewer: Gao F, United States

Received: July 25, 2021
Peer-review started: July 25, 2021
First decision: October 3, 2021
Revised: October 16, 2021
Accepted: March 4, 2022
Article in press: March 4, 2022
Published online: April 15, 2022

Shantata Kudchadkar, Safia Ahmed, Tanmoy Mukherjee, Jayesh Sagar, Department of Colorectal Surgery, Luton & Dunstable University Hospital NHS Foundation Trust, Luton LU4 0DZ, United Kingdom

Corresponding author: Jayesh Sagar, FRCS (Ed), MBBS, MD, MS, Chief Doctor, Surgeon, Surgical Oncologist, Department of Colorectal Surgery, Luton & Dunstable University Hospital NHS Foundation Trust, Lewsey Road, Luton LU4 0DZ, United Kingdom.
jayesh.sagar@ldh.nhs.uk

Abstract

Incidence of colorectal cancer (CRC) is on rise. While approximately 70% of all CRC cases are sporadic in nature, 20%-25% have familial aggregation and only < 5% is hereditary in origin. Identification of individuals with hereditary predilection for CRC is critical, as it has an impact on their overall surgical management including surgical timing, approach & technique and determines the role of prophylactic surgery and outcome. This review highlights the concept of hereditary CRC, provides insight into its molecular basis, possibility of its application into clinical practice and emphasizes the current treatment strategies with surgical management, based on the available international guidelines.

Key Words: Colorectal cancer; Lynch syndrome; Familial adenomatosis polyposis; Immunohistochemistry; Metachronous colon cancer

Core Tip: Hereditary colorectal cancer, although contributes to only a small number of cases compared to sporadic cases, is significant due to its potential of carriage and also due to complexity in its management, considering possible involvement of cancers of other organs. We aim to look at the available evidence-based guidelines across the globe and attempt to summarize them together for readers to apply with simplicity.

Citation: Kudchadkar S, Ahmed S, Mukherjee T, Sagar J. Current guidelines in the surgical management of hereditary colorectal cancers. *World J Gastrointest Oncol* 2022; 14(4): 833-841
URL: https://www.wjgnet.com/1948-5204/full/v14/i4/833.htm
DOI: https://dx.doi.org/10.4251/wjgo.v14.i4.833

INTRODUCTION

Colorectal cancer (CRC) with a hereditary predisposition includes the most common form Lynch syndrome (LS) or hereditary non-polyposis colorectal cancer (HNPCC) and familial adenomatous polyposis (FAP) with its two phenotypes (classic & attenuated)[1]. For each cancer case in the family, information on age at diagnosis, type of primary cancer, results of any cancer predisposition testing in any relative and family history should be updated periodically[2].

The diagnosis and accurate treatment of individuals with a hereditary component of CRC warrants a detailed knowledge of the primary syndrome and tumor genetics[2]. Immunohistochemistry (IHC) provides more information regarding the disease. The key concept of bowel cancer resection has to be obeyed in all CRC cases, irrespective of the type of mutation. Prime focus is on the oncological and functional outcome. The decision regarding the extended surgery should be based on the mutational status, gene, gender and the estimated individual risk. Minimal invasive surgery is the preferred surgical approach and post-operative quality of life should be the primary surgical outcome[3].

Guidelines from Association of Coloproctology of Great Britain & Ireland (ACPGBI) (2019), European Society for Medical Oncology (ESMO) along with the American Society of Clinical Oncology (ASCO) (2015) & Japanese Society for Cancer of the Colon and Rectum (JSCCR) (2020) for surveillance and management of both LS and FAP are complementary to each other[4-6] and elaborated further in this review.

HEREDITARY NON-POLYPOSIS CRC/LS

LS is characterized by autosomal dominant clustering of CRC and other extra-colonic cancers. It accounts for approximately 3%-5% of all CRC's and in the general population, approximately 1 out of 279 individuals has a pathogenetic mismatch repair (MMR) gene mutation[7].

HNPCC is also the most common predisposing hereditary cause of uterine cancer and is associated with the cancer of the stomach, ovaries and urinary tract (ureter, renal pelvis). The risk of development of LS associated tumors depends on multiple factors such as causative gene, type of mutation, environmental factors *etc*.[6]. HNPCC represents the clinical colorectal manifestation following the familial pattern of inheritance and LS is due to a germline mutation in one of the DNA genes MMR - mutL homolog 1 (MLH1), mutS homolog (MSH)2, MSH6 & PMS2. A change in one of these genes causes an accumulation of multiple errors in DNA repetitive sequences (microsatellites) along the genome[3]. This finding is known as microsatellite instability (MSI), and is frequent but not exclusive in LS. LS is usually associated with a high level of microsatellite instability, which carry a 50% risk of inheritance[8].

In order to identify LS patient, a detailed family history is necessary to confirm the fulfilment of the Amsterdam II and/or the revised Bethesda criteria[9]. Subsequent testing using IHC for MMR proteins, BRAF testing (a gene that encodes a cytoplasmic serine/threonine-protein kinase B-raf) for MLH1 loss of expression and MSI, is used to detect tumors lacking DNA MMR and plan comprehensive sequential testing[4]. Genetic counselling and genetic testing in a DNA sample in a normal tissue is crucial in every individual with a background of considerable family history and/or in those lacking MMR in the tumor specimen obtained during colonoscopy; and must be performed following consent[3].

Colon cancer in LS

Surgical management of LS patients should be individualized. Various factors play an important role when considering a surgical procedure; such as age at diagnosis, pre-existing co-morbidities, stage of the tumor, risks of metachronous colon cancer (MCC), surgical expertise, functional consequences of surgery and patient's wishes. LS patients have a considerable risk for development of metachronous CRC in any residual colorectum left behind, unlike patients with sporadic CRC. In some studies, the risk of metachronous CRC during follow-up is as high as 16% at 10 years[9]. Thus, expert opinion recommends extended resection - total abdominal colectomy (TAC) with ileo-rectal anastomosis (IRA). Life expectancy is increased by 2.3 years, when the procedure is performed in early years of life (before the age of 47), according to de Vos tot Nederveen Cappel *et al*[10]. Following an extended colectomy, decrease in the metachronous cancer risk must be balanced against the bowel functional expectations [11].

For LS patients, CRC risk varies according to the underlying genetic etiology. The lifetime risk is 30%-74% for MLH1, MSH2, and PMS2 mutation carriers, as compared to 10%-22% in MSH6 carriers[12]. In addition, from oncological point of view, there is insufficient evidence for LS patients with MSH6 or PMS2 mutations for advantage of extended colectomy over segmental resection[4]. On the other hand, despite yearly coloscopies, LS patients having MLH1 & MSH2 have a pronounced likelihood for developing metachronous CRC. Hence, in such cases a more extended surgery should be considered at the time of diagnosis.

Retrospective studies have shown the risk of developing a MCC after partial colectomy ranging from 11% to 45% over 8 to 13 years[13-15]. However, no prospective trials have been conducted to demonstrate a true survival benefit of TAC *vs* segmental resection[16]. Total abdominal hysterectomy and

bilateral salpingo-oophorectomy is recommended at the same time in LS patients, who have completed childbearing or are postmenopausal, to prevent the occurrence of endometrial/ovarian cancer[6].

A systematic review and meta-analysis by Malik *et al*[17] evaluated the risk of MCC and mortality in LS following segmental *vs* extensive colectomy. In this study, 1119 patients underwent segmental colectomies with an absolute risk of MCC in this group of 22.4% at the end of follow-up and 270 patients who had extensive colectomies had a MCC absolute risk of 4.7%. Segmental colectomy was significantly associated with an increased relative risk (RR) of MCC. RR after a segmental colectomy was 8.56 [95% confidence interval (CI): 3.37-21.73], as compared to 3.04 (95%CI: 1.46-6.34) in an extended colectomy in patients with a confirmed LS germline mutation and patients with LS diagnosis using the Amsterdam criteria. This study concluded five times greater risk of MCC after a segmental colectomy *vs* extensive colectomy in LS.

Rectal cancer in LS

Roughly 20% to 30% of LS patients will develop rectal cancer, with 15% to 24% of those with rectal cancer as their first presentation. Surgical options include a low anterior resection or abdomino-perineal resection, depending on sphincter involvement; or an extended resection with removal of all at-risk colorectum, *via* either a total proctocolectomy with an end ileostomy (TPC-EI) or more commonly a restorative ileal pouch-anal anastomosis (IPAA)[18,19].

The surgeon must consider various risk factors including possibility of metachronous colon cancer, bowel function, quality of life and co-morbidities of an individual, when determining the extent of bowel resection. A multidisciplinary team discussion including colorectal surgeons, gastroenterologists and pathologists is warranted to decide the best management plan for the patient, at the time of diagnosis of a colorectal primary[20].

International surveillance guidelines for LS

International surveillance guidelines for LS by ACPGBI United Kingdom[4], ESMO with ASCO[5], JSCCR[6] are summarized into pre-operative and post-operative as below.

Pre-operative: Starting age for surveillance colonoscopy should be based on the LS-associated gene[4].

Colonoscopic surveillance is recommended at a 2-yearly interval for all LS patients, starting from 25 years of age for MLH1 & MSH2 mutation carriers and 35 years for MSH6 & PMS2 mutation carriers[4].

Full germline genetic testing for LS should include DNA sequencing and large rearrangement analysis. Analysis of BRAF V600E mutation/ methylation of the MLH1 promoter should be carried out first to rule out a sporadic case, if loss of MLH1/PMS2 protein expression is observed in the tumor[5].

Germline mutation testing is indicated if tumor is MMR deficient and somatic BRAF mutation is not detected or MLH1 promoter methylation is not identified[5].

LS possibility should be individually evaluated in patients with suspicion of LS who have not yet diagnosed by genetic testing[6].

Surveillance of LS-associated tumors (in particular gynaecological, urological & gastrointestinal cancers) should be organized depending on the clinical and biochemical results (MSI/IHC). In LS patients with CRC, screening is suggested prior to elective colectomy[6].

Follow-up recommendations in mutation carriers include gynaecological examination on a yearly basis, in addition to the colonoscopy, starting from 30-35 years of age with 6 mo to 1 year interval. Surveillance methods include endometrial cytology & biopsy, CA 125 level and transvaginal ultrasonography[5,6].

In female LS carriers, risk reducing surgery with prophylactic hysterectomy and bilateral salpingo-oophorectomy can be considered as options, who have completed their childbearing for primary prevention of gynecologic cancer from age 35 onwards[5,6].

Upper gastrointestinal and urinary tract surveillance (urinalysis & cytology) should start at 30-35 years of age, at every 1-2 yearly interval.

Post-operative: Following surgery in LS patients with CRC, life-long surveillance with regular colonoscopy is recommended, due to the risk of possible development of MCC in the remaining colorectum[4,6].

Surveillance for recurrence of CRC following resection should be managed in a similar fashion to sporadic CRC[6].

Colorectal adenomas, when detected should be removed early, as they may progress to CRC in future [6].

Prophylaxis & chemoprevention: Prophylactic colectomy in LS patients (those with MMR mutation, but not developed CRC) is not currently recommended, partly due to the incomplete penetrance of the disease phenotype; as not all patients with a known gene mutation develop CRC[15]. Engel *et al*[21] stated that affected individuals have a 30% to 60% lifetime risk for developing CRC, depending on the underlying gene defect. Møller *et al*[22] conducted a multicentre study in patients with LS associated mutations affecting MLH1, MSH2, MSH6 or PMS2, which showed that collectively incidence of any cancer at 70 years is greater for all MMR gene mutation carriers, with a female predominance at 75% *vs* males at 58%. In MLH1 & MSH2 mutation carriers, malignancy was found from age 25 onwards as

compared to age 40 in MSH6 & PMS2 carriers. CRC cumulative incidence was high in MLH1 & MSH2 mutation carriers at 46% and 35% respectively; and lower in MSH6 & PMS2 mutation carriers at 20% and 10% respectively.

Indigo-carmine chromoendoscopy (CE) is recommended for the screening of LS patients, as compared to the white light endoscopy (WLE) by using optimal preparation, complete examination, and use of CE to reduce the cancer incidence. Various studies by Perrod *et al*[23], Lecomte *et al*[24], Hüneburg *et al*[25] and Hurlstone *et al*[26] reported a WLE adenoma miss-rate ranging between 52%-74%, thus demonstrating superiority of CE over WLE. Patient adherence to endoscopic follow-up programs can be improved by conducting dedicated educational workshops and creating support groups for LS to build motivation to join the program[27].

Recently conducted randomized trials did not characterize any protective effect of aspirin on CRC in a specific population. The CAPP2 trial did not show any aspirin protective effect on colorectal adenoma or cancer incidence after a mean of 29 mo, but a significant reduction in cancer incidence was observed at a mean of 56 mo[28]. Soualy *et al*[29] designed the AAS-Lynch trial to investigate whether the daily use of aspirin, at a dose of 100 or 300 mg, in LS patients under 75 years of age, would decrease the occurrence or recurrence of colorectal adenomas, compared with placebo. This is a prospective, multicentric, double-blind, placebo-controlled, randomized clinical trial and is estimated to be completed by year 2025.

FAP

The main characteristic feature of FAP is the development of hundreds to thousands of adenomas in the colorectum during second decade of life[30,31]. It is an autosomal dominant disease and accounts for less than 1% of all CRCs. It is caused by germline mutations in the tumor suppressor gene - defect in adenomatous polyposis coli (APC) on chromosome 22q21-22[32]. The expression of the disease may vary according to genotype and differ even within patients who share the same mutation due to modifying factors, such as gender[33].

Polyposis syndromes should typically be considered in patients with greater than 20 lifetime adenomas, patients with a personal history of desmoid tumor or other extra-colonic manifestations of FAP, or family members of individuals with known FAP, attenuated FAP (aFAP), or MYH-associated polyposis. Surgical management of FAP is complex and requires both accurate clinical judgment and technical skills. Treatment should include detailed counselling about the nature of the syndrome, its natural history, extra-colonic manifestations and the need for compliance with recommendations for management and surveillance[34].

The cornerstone of the management in FAP is prophylactic colorectal surgery due to 100% risk of CRC by 40 years of age if not treated early. Surgical decision-making, with regards to the timing of prophylactic surgery, extent of bowel resection and types of reconstruction, is influenced by both patient factors and disease characteristics[35].

The three main surgical options for FAP patients include subtotal colectomy with IRA, total proctocolectomy with/without mucosectomy & IPAA and TPC-EI. Table 1 describes indications, benefits and pitfalls of each of the surgical procedure. High ligation of the main blood supply to the bowel with removal of its mesentery form the principal basis of an oncologic bowel resection technique[31,36,37].

The follow-up strategy depends on the surgical procedure performed. Endoscopy should be done every 2-5 years when a pouch is constructed; whereas the interval should be 6 mo with total colectomy. In cases of pouch, a temporary diverting ileostomy may be fashioned to prevent anastomotic leakage[38,39]. Severity of polyposis determines the surgical decision of IRA *vs* IPAA - the more severe the polyposis, the greater the risk of metachronous rectal polyposis and/or rectal neoplasm.

aFAP: It represents a subset of patients who have germline APC mutation, with a diminished or "attenuated" colorectal phenotype. They possess < 100 synchronous colorectal adenomas and are not associated with complete penetrance of CRC. It is characterized by a later onset of colonic polyposis and later development of CRC (after 10-20 years) as compared to classical FAP. Most aFAP patients often undergo colectomy and IRA[42,43].

Minimal invasive surgical approach should be preferred for both forms of FAP. Currently, the standard surgical techniques for treatment of FAP include laparoscopic colectomy and proctocolectomy.

International surveillance guidelines for FAP

International surveillance guidelines for FAP by ACPGBI United Kingdom[4], ESMO with ASCO[5], JSCCR[6] are summarized into pre-operative and post-operative as below.

Pre-operative: Colonoscopic surveillance should usually start from 12-14 years of age in individuals genetically confirmed with a diagnosis of FAP. It is especially in at-risk individuals who have a first-degree relative with a clinical FAP, but absent APC mutation; which should be continued for 5 years, until a clinical diagnosis is reached and they are treated as FAP, or they can enrol in national bowel cancer screening programme when they reach the age[4].

Table 1 Comparing the three main surgical options in familial adenomatosis polyposis[6,30,39-41]

Surgical procedure	Indications	Benefits	Pitfalls
Ileo-rectal anastomosis	< 20 rectal, adenomas; < 1000 colonic, adenomas	Controls colonic polyposis. Better bowel function & good quality of life. Reduced risk of desmoid disease. Avoids stoma. Quicker recovery, especially useful in active teenagers	Risk of rectal cancer. Annual surveillance with proctoscopy & flexible sigmoidoscopy is required
Ileal pouch-anal anastomosis	< 20 rectal, adenomas; < 1000 colonic, adenomas	Removes nearly all polyps in colon & rectum. No need of permanent ileostomy. Quality of life is satisfactory	Increased complications. Unpredictable bowel function. Unpredictable quality of life. Possible need for ileostomy. Pouch complications: (1) Risk of pouch polyposis; and (2) Risk of cancer in anal transition zone. Surveillance is difficult
Proctocolectomy & end ileostomy	Low rectal cancer. When Ileal pouch-anal anastomosis is not indicated. Poor anal sphincter. Function	Complete removal of cancer risk in lower gastrointestinal tract	Permanent ileostomy. Sexual and fertility consequences such as dyspareunia, decrease in fertility, vaginal discharge in females and reduced libido, sexual satisfaction in males

Surveillance colonoscopy intervals may be individualized based on the colonic phenotype every 1-3 years[4]. An interval of 1-2 years is strongly recommended for patients with typical FAP and 2-3 years for patients with aFAP[6].

Germline genetic testing of APC and/or MUTYH should be considered for individuals with multiple colorectal adenomas (> 10). Full germline genetic testing of APC should include DNA sequencing and large rearrangement analysis[5].

The decision on the type of colorectal surgery in FAP patients depends on various factors including severity of rectal polyposis, risk of developing desmoids, mutation site in the APC gene and patient's age & wishes[5].

Search for extracolonic manifestations (gastroduodenal polyposis, thyroid cancer, desmoid tumors) in both variants (FAP and aFAP) is recommended, when colorectal polyposis is diagnosed or at the age of 25-30 years, whichever comes first[5].

Upper GI tract examination and monitoring should start at 25 years of age, every 6 mo to 5 years depending on the polyp burden[4].

Annual neck examination with ultrasound assessment for thyroid gland may be considered, starting at 25-30 years of age[5,6].

Counselling about the risk of formation of post-operative desmoid disease should be done for all FAP patients[4].

Annual abdominal examination and abdominal & pelvic computed tomography or magnetic resonance imaging every 3 yearly is recommended for patients with a family history of desmoid tumors [6].

Ophthalmology opinion and referral is needed in patients with a diagnosis of congenital hypertrophy retinal pigmentation epithelium (CHRPE). FAP screening, genetic testing and colonoscopy is advised in individuals with bilateral and multiple CHRPE lesions[4].

Colonoscopy should be carried out at every 2 yearly intervals, in families with aFAP, starting at the age of 18 to 20 years and continued lifelong in mutation carriers[5].

Post-operative: The cardinal factors influencing the timing of prophylactic proctocolectomy in candidates with FAP are as follows: (1) Total prevalence of colorectal malignancy; (2) Size, morphology & density of the adenomas; (3) Age at cancer occurence & death and presence/absence of desmoid tumors in family members; (4) Germline variant site in the APC gene; (5) Professional factors (educational, work & other environments of the patient); (6) Personal factors (fertility and presence/absence of male sexual dysfunction after IPAA); (7) Presence/absence of gastrointestinal symptoms; and (8) Histopathology of the tumor[6].

The definitive treatment of colorectal adenomas is proctocolectomy (prophylactic proctocolectomy) prior to the development of CRC[6].

Surveillance of the rectum should be carried out every 6 to 12 mo in cases with residual rectum and every 6 mo to 5 years in cases with ileo-anal pouch, depending on the polyp burden[5].

In FAP patients with locally advanced CRC, routine treatment for locally advanced CRC should be performed. The surgical procedure should be selected according to the condition of the FAP patients, if curative resection is possible[6].

Chemotherapy for CRC associated with FAP is similar to that used in sporadic cases[6].

In metastatic disease, treatment similar to that for metastases from sporadic CRC should be used, for curative resection group[6].

In FAP patients undergoing surgery for CRC, post-operative surveillance similar to that in sporadic CRC patients should be planned/performed[6].

Prophylaxis & chemoprevention: The most effective way of cancer prevention is to remove the colon and thus, the timing of prophylactic surgery should be considered, once the diagnosis is established. Severity of the polyposis decides the timing of surgery for patients diagnosed in their teenage years. Correct choice of the surgical procedure is the fundamental factor in reducing cancer risk, overall complications and sustaining a reasonable quality of life.

FAP patients undergoing prophylactic restorative proctocolectomy with IPAA are usually young and active. The frequency of bowel movements and faecal continence is of utmost importance, to have better quality of life. The continent function depends on the stool consistency, quality of sphincter muscles and pelvic nerves[3]. Transanal Total Mesorectal Excision is now a well-recognised surgical procedure in the treatment of mid and low rectal cancer, which involves a "bottom-top dissection" with improved visualization of the pelvic nerves and a rendezvous-approach[44].

Sulindac, a nonsteroidal anti-inflammatory agent, which inhibits cyclooxygenase enzyme (COX)-1 & 2, is the most tested drug in chemoprevention[45]. Lastly, care of FAP patients and their families is best given by centres of experience and excellence[46].

CONCLUSION

5%-10% of CRC cases are due to germline mutations, most of which are autosomal dominant with high penetrance. With accurate treatment, affected patients can benefit greatly when detected early in life. Thorough knowledge of the at-risk genetic mutations forms the cornerstone in formulating a precise treatment plan for patients with hereditary CRC. Syndromes with a 100% penetrance will require prophylactic surgery. In the treatment of every CRC, the basic concept of oncologic surgical procedure needs to be followed. Patient should be actively involved in the surgical decision-making. Lifelong follow-up is the predominant feature of the surgical treatment plan and every patient should be informed of the same well in advance. Improved patient adherence to the screening program is pivotal in surveillance.

FOOTNOTES

Author contributions: Kudchadkar S collected data and prepared the manuscript; Ahmed S and Mukherjee T analysed data; Sagar J reviewed and edited the manuscript.

Conflict-of-interest statement: The authors declare that they have no conflict of interest.

Country/Territory of origin: United Kingdom

ORCID number: Shantata Kudchadkar 0000-0003-2637-5970; Safia Ahmed 0000-0003-2831-5314; Tanmoy Mukherjee 0000-0001-5571-5896; Jayesh Sagar 0000-0002-4242-101X.

Corresponding Author's Membership in Professional Societies: Association of Coloproctology of Great Britain and Ireland, ACP07354.

S-Editor: Wang JJ
L-Editor: A
P-Editor: Wang JJ

REFERENCES

1 **Perea J**, Justo I, Alvaro E, Lomas M, Tasende JD, Marín JC, Franco A, Colina F, Rodríguez Y, Martínez J, Robles L, Urioste M, Hidalgo M. Surgical management of hereditary colorectal cancer: surgery based on molecular analysis and family history. *Rev Esp Enferm Dig* 2009; **101**: 536-540 [PMID: 19785492 DOI: 10.4321/s1130-01082009000800003]

2 **Kennelly RP**, Gryfe R, Winter DC. Familial colorectal cancer: Patient assessment, surveillance and surgical management. *Eur J Surg Oncol* 2017; **43**: 294-302 [PMID: 27546013 DOI: 10.1016/j.ejso.2016.07.008]

3 **Ambe PC**, Möslein G. Surgical management of hereditary colorectal cancer. *Mini-invasive Surg* 2018; **2**: 37 [DOI: 10.20517/2574-1225.2018.45]

4 **Monahan KJ**, Bradshaw N, Dolwani S, Desouza B, Dunlop MG, East JE, Ilyas M, Kaur A, Lalloo F, Latchford A, Rutter MD, Tomlinson I, Thomas HJW, Hill J; Hereditary CRC guidelines eDelphi consensus group. Guidelines for the management of hereditary colorectal cancer from the British Society of Gastroenterology (BSG)/Association of Coloproctology of Great Britain and Ireland (ACPGBI)/United Kingdom Cancer Genetics Group (UKCGG). *Gut* 2020; **69**: 411-444 [PMID: 31780574 DOI: 10.1136/gutjnl-2019-319915]

5 **Stoffel EM**, Mangu PB, Gruber SB, Hamilton SR, Kalady MF, Lau MW, Lu KH, Roach N, Limburg PJ; American Society of Clinical Oncology; European Society of Clinical Oncology. Hereditary colorectal cancer syndromes: American Society of Clinical Oncology Clinical Practice Guideline endorsement of the familial risk-colorectal cancer: European Society for Medical Oncology Clinical Practice Guidelines. *J Clin Oncol* 2015; **33**: 209-217 [PMID: 25452455 DOI: 10.1200/JCO.2014.58.1322]

6 **Tomita N**, Ishida H, Tanakaya K, Yamaguchi T, Kumamoto K, Tanaka T, Hinoi T, Miyakura Y, Hasegawa H, Takayama T, Ishikawa H, Nakajima T, Chino A, Shimodaira H, Hirasawa A, Nakayama Y, Sekine S, Tamura K, Akagi K, Kawasaki Y, Kobayashi H, Arai M, Itabashi M, Hashiguchi Y, Sugihara K; Japanese Society for Cancer of the Colon, Rectum. Japanese Society for Cancer of the Colon and Rectum (JSCCR) guidelines 2020 for the Clinical Practice of Hereditary Colorectal Cancer. *Int J Clin Oncol* 2021; **26**: 1353-1419 [PMID: 34185173 DOI: 10.1007/s10147-021-01881-4]

7 **Win AK**, Jenkins MA, Dowty JG, Antoniou AC, Lee A, Giles GG, Buchanan DD, Clendenning M, Rosty C, Ahnen DJ, Thibodeau SN, Casey G, Gallinger S, Le Marchand L, Haile RW, Potter JD, Zheng Y, Lindor NM, Newcomb PA, Hopper JL, MacInnis RJ. Prevalence and Penetrance of Major Genes and Polygenes for Colorectal Cancer. *Cancer Epidemiol Biomarkers Prev* 2017; **26**: 404-412 [PMID: 27799157 DOI: 10.1158/1055-9965.EPI-16-0693]

8 **Papadopoulos N**, Lindblom A. Molecular basis of HNPCC: mutations of MMR genes. *Hum Mutat* 1997; **10**: 89-99 [PMID: 9259192 DOI: 10.1002/(SICI)1098-1004(1997)10:2<89::AID-HUMU1>3.0.CO;2-H]

9 **Schneider R**, Schneider C, Büttner R, Reinacher-Schick A, Tannapfel A, Fürst A, Rüschoff J, Jakobeit C, Royer-Pokora B, Möslein G. [Colorectal Carcinoma with Suspected Lynch Syndrome: A Multidisciplinary Algorithm]. *Zentralbl Chir* 2015; **140**: 591-599 [PMID: 25372301 DOI: 10.1055/s-0034-1368480]

10 **de Vos tot Nederveen Cappel WH**, Nagengast FM, Griffioen G, Menko FH, Taal BG, Kleibeuker JH, Vasen HF. Surveillance for hereditary nonpolyposis colorectal cancer: a long-term study on 114 families. *Dis Colon Rectum* 2002; **45**: 1588-1594 [PMID: 12473880 DOI: 10.1007/s10350-004-7244-3]

11 **de Vos tot Nederveen Cappel WH**, Buskens E, van Duijvendijk P, Cats A, Menko FH, Griffioen G, Slors JF, Nagengast FM, Kleibeuker JH, Vasen HF. Decision analysis in the surgical treatment of colorectal cancer due to a mismatch repair gene defect. *Gut* 2003; **52**: 1752-1755 [PMID: 14633956 DOI: 10.1136/gut.52.12.1752]

12 **Giardiello FM**, Allen JI, Axilbund JE, Boland CR, Burke CA, Burt RW, Church JM, Dominitz JA, Johnson DA, Kaltenbach T, Levin TR, Lieberman DA, Robertson DJ, Syngal S, Rex DK. Guidelines on genetic evaluation and management of Lynch syndrome: a consensus statement by the US Multi-society Task Force on colorectal cancer. *Am J Gastroenterol* 2014; **109**: 1159-1179 [PMID: 25070057 DOI: 10.1038/ajg.2014.186]

13 **Barrow E**, Hill J, Evans DG. Cancer risk in Lynch Syndrome. *Fam Cancer* 2013; **12**: 229-240 [PMID: 23604856 DOI: 10.1007/s10689-013-9615-1]

14 **Natarajan N**, Watson P, Silva-Lopez E, Lynch HT. Comparison of extended colectomy and limited resection in patients with Lynch syndrome. *Dis Colon Rectum* 2010; **53**: 77-82 [PMID: 20010355 DOI: 10.1007/DCR.0b013e3181c702de]

15 **Parry S**, Win AK, Parry B, Macrae FA, Gurrin LC, Church JM, Baron JA, Giles GG, Leggett BA, Winship I, Lipton L, Young GP, Young JP, Lodge CJ, Southey MC, Newcomb PA, Le Marchand L, Haile RW, Lindor NM, Gallinger S, Hopper JL, Jenkins MA. Metachronous colorectal cancer risk for mismatch repair gene mutation carriers: the advantage of more extensive colon surgery. *Gut* 2011; **60**: 950-957 [PMID: 21193451 DOI: 10.1136/gut.2010.228056]

16 **Baucom RB**, Wise PE. Endoscopic and surgical management of hereditary nonpolyposis colorectal cancer. *Clin Colon Rectal Surg* 2012; **25**: 90-96 [PMID: 23730223 DOI: 10.1055/s-0032-1313779]

17 **Malik SS**, Lythgoe MP, McPhail M, Monahan KJ. Metachronous colorectal cancer following segmental or extended colectomy in Lynch syndrome: a systematic review and meta-analysis. *Fam Cancer* 2018; **17**: 557-564 [PMID: 29189962 DOI: 10.1007/s10689-017-0062-2]

18 **Kalady MF**, Lipman J, McGannon E, Church JM. Risk of colonic neoplasia after proctectomy for rectal cancer in hereditary nonpolyposis colorectal cancer. *Ann Surg* 2012; **255**: 1121-1125 [PMID: 22549751 DOI: 10.1097/SLA.0b013e3182565c0b]

19 **Möslein G**, Nelson H, Thibodeau S, Dozois RR. [Rectal carcinomas in HNPCC]. *Langenbecks Arch Chir Suppl Kongressbd* 1998; **115**: 1467-1469 [PMID: 9931914]

20 **Rodriguez-Bigas MA**, Möeslein G. Surgical treatment of hereditary nonpolyposis colorectal cancer (HNPCC, Lynch syndrome). *Fam Cancer* 2013; **12**: 295-300 [PMID: 23508345 DOI: 10.1007/s10689-013-9626-y]

21 **Engel C**, Vasen HF, Seppälä T, Aretz S, Bigirwamungu-Bargeman M, de Boer SY, Bucksch K, Büttner R, Holinski-Feder E, Holzapfel S, Hüneburg R, Jacobs MAJM, Järvinen H, Kloor M, von Knebel Doeberitz M, Koornstra JJ, van Kouwen M, Langers AM, van de Meeberg PC, Morak M, Möslein G, Nagengast FM, Pylvänäinen K, Rahner N, Renkonen-Sinisalo L, Sanduleanu S, Schackert HK, Schmiegel W, Schulmann K, Steinke-Lange V, Strassburg CP, Vecht J, Verhulst ML, de Vos Tot Nederveen Cappel W, Zachariae S, Mecklin JP, Loeffler M; German HNPCC Consortium, the Dutch Lynch Syndrome Collaborative Group, and the Finnish Lynch Syndrome Registry. No Difference in Colorectal Cancer Incidence or Stage at Detection by Colonoscopy Among 3 Countries With Different Lynch Syndrome Surveillance Policies. *Gastroenterology* 2018; **155**: 1400-1409.e2 [PMID: 30063918 DOI: 10.1053/j.gastro.2018.07.030]

22 **Møller P**, Seppälä T, Bernstein I, Holinski-Feder E, Sala P, Evans DG, Lindblom A, Macrae F, Blanco I, Sijmons R, Jeffries J, Vasen H, Burn J, Nakken S, Hovig E, Rødland EA, Tharmaratnam K, de Vos Tot Nederveen Cappel WH, Hill J, Wijnen J, Green K, Lalloo F, Sunde L, Mints M, Bertario L, Pineda M, Navarro M, Morak M, Renkonen-Sinisalo L, Frayling IM, Plazzer JP, Pylvanainen K, Sampson JR, Capella G, Mecklin JP, Möslein G; Mallorca Group (http://mallorca-group. eu). Cancer incidence and survival in Lynch syndrome patients receiving colonoscopic and gynaecological

surveillance: first report from the prospective Lynch syndrome database. *Gut* 2017; **66**: 464-472 [PMID: 26657901 DOI: 10.1136/gutjnl-2015-309675]

23 **Perrod G**, Samaha E, Rahmi G, Khater S, Abbes L, Savale C, Perkins G, Zaanan A, Chatellier G, Malamut G, Cellier C. Impact of an optimized colonoscopic screening program for patients with Lynch syndrome: 6-year results of a specialized French network. *Therap Adv Gastroenterol* 2018; **11**: 1756284818775058 [PMID: 29872454 DOI: 10.1177/1756284818775058]

24 **Lecomte T**, Cellier C, Meatchi T, Barbier JP, Cugnenc PH, Jian R, Laurent-Puig P, Landi B. Chromoendoscopic colonoscopy for detecting preneoplastic lesions in hereditary nonpolyposis colorectal cancer syndrome. *Clin Gastroenterol Hepatol* 2005; **3**: 897-902 [PMID: 16234028 DOI: 10.1016/s1542-3565(05)00403-9]

25 **Hüneburg R**, Lammert F, Rabe C, Rahner N, Kahl P, Büttner R, Propping P, Sauerbruch T, Lamberti C. Chromocolonoscopy detects more adenomas than white light colonoscopy or narrow band imaging colonoscopy in hereditary nonpolyposis colorectal cancer screening. *Endoscopy* 2009; **41**: 316-322 [PMID: 19340735 DOI: 10.1055/s-0028-1119628]

26 **Hurlstone DP**, Karajeh M, Cross SS, McAlindon ME, Brown S, Hunter MD, Sanders DS. The role of high-magnification-chromoscopic colonoscopy in hereditary nonpolyposis colorectal cancer screening: a prospective "back-to-back" endoscopic study. *Am J Gastroenterol* 2005; **100**: 2167-2173 [PMID: 16181364 DOI: 10.1111/j.1572-0241.2005.41481.x]

27 **Olivier R**, Randrian V, Tougeron D, Saurin JC. Endoscopy to Diagnose and Prevent Digestive Cancers in Lynch Syndrome. *Cancers (Basel)* 2021; **13** [PMID: 34298719 DOI: 10.3390/cancers13143505]

28 **Burn J**, Gerdes AM, Macrae F, Mecklin JP, Moeslein G, Olschwang S, Eccles D, Evans DG, Maher ER, Bertario L, Bisgaard ML, Dunlop MG, Ho JW, Hodgson SV, Lindblom A, Lubinski J, Morrison PJ, Murday V, Ramesar R, Side L, Scott RJ, Thomas HJ, Vasen HF, Barker G, Crawford G, Elliott F, Movahedi M, Pylvanainen K, Wijnen JT, Fodde R, Lynch HT, Mathers JC, Bishop DT; CAPP2 Investigators. Long-term effect of aspirin on cancer risk in carriers of hereditary colorectal cancer: an analysis from the CAPP2 randomised controlled trial. *Lancet* 2011; **378**: 2081-2087 [PMID: 22036019 DOI: 10.1016/S0140-6736(11)61049-0]

29 **Soualy A**, Deutsch D, Benallaoua M, Ait-Omar A, Mary F, Helfen S, Boubaya M, Levy V, Benamouzig R; AAS-Lynch group. Effect of chemoprevention by low-dose aspirin of new or recurrent colorectal adenomas in patients with Lynch syndrome (AAS-Lynch): study protocol for a multicenter, double-blind, placebo-controlled randomized controlled trial. *Trials* 2020; **21**: 764 [PMID: 32887653 DOI: 10.1186/s13063-020-04674-8]

30 **Bülow S**. Diagnosis of familial adenomatous polyposis. *World J Surg* 1991; **15**: 41-46 [PMID: 1847272 DOI: 10.1007/BF01658959]

31 **Half E**, Bercovich D, Rozen P. Familial adenomatous polyposis. *Orphanet J Rare Dis* 2009; **4**: 22 [PMID: 19822006 DOI: 10.1186/1750-1172-4-22]

32 **Aretz S**, Uhlhaas S, Sun Y, Pagenstecher C, Mangold E, Caspari R, Möslein G, Schulmann K, Propping P, Friedl W. Familial adenomatous polyposis: aberrant splicing due to missense or silent mutations in the APC gene. *Hum Mutat* 2004; **24**: 370-380 [PMID: 15459959 DOI: 10.1002/humu.20087]

33 **Lucci-Cordisco E**, Risio M, Venesio T, Genuardi M. The growing complexity of the intestinal polyposis syndromes. *Am J Med Genet A* 2013; **161A**: 2777-2787 [PMID: 24124059 DOI: 10.1002/ajmg.a.36253]

34 **Herzig D**, Hardiman K, Weiser M, You N, Paquette I, Feingold DL, Steele SR. The American Society of Colon and Rectal Surgeons Clinical Practice Guidelines for the Management of Inherited Polyposis Syndromes. *Dis Colon Rectum* 2017; **60**: 881-894 [PMID: 28796726 DOI: 10.1097/DCR.0000000000000912]

35 **Warrier SK**, Kalady MF. Familial adenomatous polyposis: challenges and pitfalls of surgical treatment. *Clin Colon Rectal Surg* 2012; **25**: 83-89 [PMID: 23730222 DOI: 10.1055/s-0032-1313778]

36 **Aziz O**, Athanasiou T, Fazio VW, Nicholls RJ, Darzi AW, Church J, Phillips RK, Tekkis PP. Meta-analysis of observational studies of ileorectal versus ileal pouch-anal anastomosis for familial adenomatous polyposis. *Br J Surg* 2006; **93**: 407-417 [PMID: 16511903 DOI: 10.1002/bjs.5276]

37 **Bülow C**, Vasen H, Järvinen H, Björk J, Bisgaard ML, Bülow S. Ileorectal anastomosis is appropriate for a subset of patients with familial adenomatous polyposis. *Gastroenterology* 2000; **119**: 1454-1460 [PMID: 11113066 DOI: 10.1053/gast.2000.20180]

38 **Al-Sukhni W**, Aronson M, Gallinger S. Hereditary colorectal cancer syndromes: familial adenomatous polyposis and lynch syndrome. *Surg Clin North Am* 2008; **88**: 819-844, vii [PMID: 18672142 DOI: 10.1016/j.suc.2008.04.012]

39 **Kartheuser A**, Stangherlin P, Brandt D, Remue C, Sempoux C. Restorative proctocolectomy and ileal pouch-anal anastomosis for familial adenomatous polyposis revisited. *Fam Cancer* 2006; **5**: 241-60; discussion 261 [PMID: 16998670 DOI: 10.1007/s10689-005-5672-4]

40 **Ziv Y**, Church JM, Oakley JR, McGannon E, Fazio VW. Surgery for the teenager with familial adenomatous polyposis: ileo-rectal anastomosis or restorative proctocolectomy? *Int J Colorectal Dis* 1995; **10**: 6-9 [PMID: 7745328 DOI: 10.1007/BF00337577]

41 **Yeo CJ**. Shackelford's Surgery of the Alimentary Tract, 2 Volume Set (Eighth Edition). In: Kalady MF, Boland CR, Church JM. Inherited Colorectal Cancer and the Genetics of Colorectal Cancer. Amsterdam: Elsevier, 2019: 1959-1980 [DOI: 10.1016/B978-0-323-40232-3.00165-5]

42 **Knudsen AL**, Bülow S, Tomlinson I, Möslein G, Heinimann K, Christensen IJ; AFAP Study Group. Attenuated familial adenomatous polyposis: results from an international collaborative study. *Colorectal Dis* 2010; **12**: e243-e249 [PMID: 20105204 DOI: 10.1111/j.1463-1318.2010.02218.x]

43 **Lynch HT**, Smyrk T, McGinn T, Lanspa S, Cavalieri J, Lynch J, Slominski-Castor S, Cayouette MC, Priluck I, Luce MC. Attenuated familial adenomatous polyposis (AFAP). A phenotypically and genotypically distinctive variant of FAP. *Cancer* 1995; **76**: 2427-2433 [PMID: 8625067 DOI: 10.1002/1097-0142(19951215)76:12<2427::aid-cncr2820761205>3.0.co;2-b]

44 **Monson JRT**, Arsalanizadeh R. Transanal Total Mesorectal Excision (TaTME) and Quality of Rectal Cancer Surgery: Do we Really Know? *Ann Surg* 2017; **266**: e88-e89 [PMID: 27070936 DOI: 10.1097/SLA.0000000000001736]

45 **Cruz-Correa M**, Hylind LM, Romans KE, Booker SV, Giardiello FM. Long-term treatment with sulindac in familial adenomatous polyposis: a prospective cohort study. *Gastroenterology* 2002; **122**: 641-645 [PMID: 11874996 DOI:

10.1053/gast.2002.31890]

46 **Vasen HF**, Velthuizen ME, Kleibeuker JH, Menko FH, Nagengast FM, Cats A, van der Meulen-de Jong AE, Breuning MH, Roukema AJ, van Leeuwen-Cornelisse I, de Vos Tot Nederveen Cappel WH, Wijnen JT. Hereditary cancer registries improve the care of patients with a genetic predisposition to cancer: contributions from the Dutch Lynch syndrome registry. *Fam Cancer* 2016; **15**: 429-435 [PMID: 26973060 DOI: 10.1007/s10689-016-9897-1]

World Journal of Gastrointestinal Oncology

Submit a Manuscript: https://www.f6publishing.com

World J Gastrointest Oncol 2022 April 15; 14(4): 842-857

DOI: 10.4251/wjgo.v14.i4.842

ISSN 1948-5204 (online)

ORIGINAL ARTICLE

Basic Study

Berberine retarded the growth of gastric cancer xenograft tumors by targeting hepatocyte nuclear factor 4α

Ling-Li Li, Ze Peng, Qian Hu, Li-Jun Xu, Xin Zou, Dong-Mei Huang, Ping Yi

Specialty type: Oncology

Provenance and peer review: Unsolicited article; Externally peer reviewed.

Peer-review model: Single blind

Peer-review report's scientific quality classification

Grade A (Excellent): 0
Grade B (Very good): 0
Grade C (Good): C
Grade D (Fair): D
Grade E (Poor): 0

P-Reviewer: Kumarasasmy VM, Mohamed SY

Received: March 1, 2021
Peer-review started: March 2, 2021
First decision: October 3, 2021
Revised: October 15, 2021
Accepted: February 23, 2022
Article in press: February 23, 2022
Published online: April 15, 2022

Ling-Li Li, Ze Peng, Li-Jun Xu, Xin Zou, Dong-Mei Huang, Ping Yi, Department of Integrated Traditional Chinese and Western Medicine, Tongji Hospital, Tongji Medical College, Huazhong University of Science and Technology, Wuhan 430045, Hubei Province, China

Qian Hu, Department of Integrated Traditional Chinese and Western Medicine, West China Hospital of Sichuan University, Chengdu 610041, Sichuan Province, China

Corresponding author: Ping Yi, PhD, MD, Department of Integrated Traditional Chinese and Western Medicine, Tongji Hospital, Tongji Medical College, Huazhong University of Science and Technology, No. 1095 Jiefang Avenue, Wuhan 430045, Hubei Province, China.
pyi219@163.com

Abstract

BACKGROUND

Gastric cancer is the third deadliest cancer in the world and ranks second in incidence and mortality of cancers in China. Despite advances in prevention, diagnosis, and therapy, the absolute number of cases is increasing every year due to aging and the growth of high-risk populations, and gastric cancer is still a leading cause of cancer-related death. Gastric cancer is a consequence of the complex interaction of microbial agents, with environmental and host factors, resulting in the dysregulation of multiple oncogenic and tumor-suppressing signaling pathways. Global efforts have been made to investigate in detail the genomic and epigenomic heterogeneity of this disease, resulting in the identification of new specific and sensitive predictive and prognostic biomarkers. Trastuzumab, a monoclonal antibody against the HER2 receptor, is approved in the first-line treatment of patients with HER2+ tumors, which accounts for 13%-23% of the gastric cancer population. Ramucirumab, a monoclonal antibody against VEGFR2, is currently recommended in patients progressing after first-line treatment. Several clinical trials have also tested novel agents for advanced gastric cancer but mostly with dis-appointing results, such as anti-EGFR and anti-MET monoclonal antibodies. Therefore, it is still of great significance to screen specific molecular targets for gastric cancer and drugs directed against the molecular targets.

AIM

To investigate the effect and mechanism of berberine against tumor growth in gastric cancer xenograft models and to explore the role of hepatocyte nuclear

factor 4α (HNF4α)-WNT5a/β-catenin pathways played in the antitumor effects of berberine.

METHODS

MGC803 and SGC7901 subcutaneous xenograft models were established. The control group was intragastrically administrated with normal saline, and the berberine group was administrated intragastrically with 100 mg/kg/d berberine. The body weight of nude mice during the experiment was measured to assess whether berberine has any adverse reaction. The volume of subcutaneous tumors during this experiment was recorded to evaluate the inhibitory effect of berberine on the growth of MGC803 and SGC7901 subcutaneous transplantation tumors. Polymerase chain reaction assays were conducted to evaluate the alteration of transcriptional expression of HNF4α, WNT5a and β-catenin in tumor tissues and liver tissues from the MGC803 and SGC7901 xenograft models. Western blotting and IHC were performed to assess the protein expression of HNF4α, WNT5a and β-catenin in tumor tissues and liver tissues from the MGC803 and SGC7901 xenograft models.

RESULTS

In the both MGC803 and SGC7901 xenograft tumor models, berberine significantly reduced tumor volume and weight and thus retarded the growth rate of tumors. In the SGC7901 and MGC803 subcutaneously transplanted tumor models, berberine down-regulated the expression of HNF4α, WNT5a and β-catenin in tumor tissues from both transcription and protein levels. Besides, berberine also suppressed the protein expression of HNF4α, WNT5a and β-catenin in liver tissues.

CONCLUSION

Berberine retarded the growth of MGC803 and SGC7901 xenograft model tumors, and the mechanism behind these anti-growth effects might be the downregulation of the expression of HNF4α-WNT5a/β-catenin signaling pathways both in tumor tissues and liver tissues of the xenograft models.

Key Words: Berberine; Gastric cancer; Xenograft models; Hepatocyte nuclear factor 4α; WNT5a

Core Tip: Hepatocyte nuclear factor 4α (HNF4α) is a member of the nuclear receptor transcription factor family, which is at the center of a complex transcriptional regulatory network and regulates the biological effects of different pathways *via* transcriptional regulation of differential target genes. The role of HNF4α in gastric cancer is poorly understood, so the study of the berberine targeting HNF4α in gastric cancer cell xenograft models is of great significance. In this study, we showed that the inhibition of HNF4α genes/proteins by berberine was correlated with the tumor inhibition in gastric cancer xenografts. Further experiments also indicated that berberine downregulated HNF4a to exert its antineoplastic activity *in vivo*.

Citation: Li LL, Peng Z, Hu Q, Xu LJ, Zou X, Huang DM, Yi P. Berberine retarded the growth of gastric cancer xenograft tumors by targeting hepatocyte nuclear factor 4α. *World J Gastrointest Oncol* 2022; 14(4): 842-857
URL: https://www.wjgnet.com/1948-5204/full/v14/i4/842.htm
DOI: https://dx.doi.org/10.4251/wjgo.v14.i4.842

INTRODUCTION

Gastric cancer is the third deadliest cancer in the world and ranks second in the incidence and mortality of cancers in China[1,2]. Despite advances in prevention, diagnosis, and therapy, the absolute number of cases is increasing every year due to aging and the growth of high-risk populations, and gastric cancer is still a leading cause of cancer-related death[1,3]. Gastric cancer is a consequence of the complex interaction of microbial agents, with environmental and host factors, resulting in the dysregulation of multiple oncogenic and tumor-suppressing signaling pathways[1]. Global efforts have been made to investigate in detail the genomic and epigenomic heterogeneity of this disease, resulting in the identification of new specific and sensitive predictive and prognostic biomarkers[4]. Trastuzumab, a monoclonal antibody against the HER2 receptor, is approved in the first-line treatment of patients with HER2+ tumors, which accounts for 13%-23% of the gastric cancer population[5]. Ramucirumab, a monoclonal antibody against VEGFR2, is currently recommended in patients progressing after first-line treatment[6]. Several clinical trials have also tested novel agents, such as anti-EGFR and anti-MET

monoclonal antibodies, to treat advanced gastric cancer but mostly with disappointing results[3]. Therefore, it is still of great significance to screen specific molecular targets for gastric cancer and drugs directed against the molecular targets.

Several epidemiological studies have found that diabetes is linked with an increased risk of gastric cancer and can increase the risk of death in patients with gastric cancer, resulting in a worse prognosis [7,8]. Recently, many studies have focused on diabetes and its causal relation with neoplasms[9]. The emergence of cancer-related properties was likely a change in biological characteristics caused by the hyperglycemic environment created by diabetes, which provides the opportunity to trigger abnormal expression of the healthy genome and promote changes in biological characteristics[10]. It was demonstrated that glucose increased ATP levels to inhibit AMPK and induce the increased expression of hepatocyte nuclear factor 4α (HNF4α)[11]. Hepatocyte nuclear factor 4α is a member of the nuclear receptor transcription factor family, which has a conserved DNA-binding domain and a ligand-binding domain[12]. HNF4α is at the center of a complex transcriptional regulatory network and regulates the biological effects of different pathways *via* transcriptional regulation of differential target genes[13]. HNF4α is involved in a variety of human diseases. HNF4α plays an important role in the development and treatment of diabetes. Neonatal patients with diabetes or young adults with diabetes with mutations in the HNF4α gene usually respond better to oral treatment with sulfonylureas[14]. Furthermore, many studies also suggest that HNF4α might be related to the occurrence and development of tumors. HNF4α was found to be highly expressed in various tumor tissues, such as lung cancers and liver cancers[15,16]. Compared with normal gastric mucosa, the protein and transcript levels of HNF4α in gastric cancer tissues and gastric cancer cell lines are also at higher levels[17]. The role of HNF4α in gastric cancer has gradually received attention. HNF4α can promote the intestinal metaplasia of the gastric mucosa[18]. HNF4α can also be used as a gold standard marker to distinguish gastric metastasis from primary gastric cancer and breast cancer. Studies showed that HNF4α was positively expressed in all patients diagnosed with primary gastric adenocarcinoma and negatively expressed in all cases of primary breast cancer[19,20].

The hyperglycemic environment created by diabetes provides the opportunity to trigger abnormal expression of the healthy genome and promote changes in biological characteristics[10]. The hyperglycemic state observed in the diabetic milieu is predicted to enhance the gastric cancer risk in prediabetic and diabetic individuals[9]. Studies have shown that some diabetes treatment drugs can effectively reduce the risk of cancer and improve prognosis, which is of great significance for understanding the relationship between diabetes and tumorigenesis and provides a new idea for the research of cancer prevention and treatment[21]. Berberine, an extract from the Chinese herbal medicine Coptis, has been widely used in clinical treatment and has shown excellent efficacy in the treatment of intestinal infections. Multiple studies have displayed the potential therapeutic effect of berberine on diabetes[22]. Berberine can target HNF4α to inhibit gluconeogenesis in the treatment of type 2 diabetes and its complications[23]. Berberine improvs insulin resistance associated not only with gut microbiota alteration in branched-chain amino acid biosynthesis, but also with branched-chain amino acid catabolism in liver and adipose tissues[24]. Berberine alleviates tau hyperphosphorylation and axonopathy-associated with diabetic encephalopathy by restoring the PI3K/Akt/GSK3β pathway[25]. Meanwhile, several studies have also showned the potential therapeutic effects of berberine against tumor growth[26-28]. Berberine exerts an inhibitory effect on cell growth and induces apoptosis by inhibiting the activation of EFGR signaling[27]. Berberine can also suppress the growth and induce apoptosis of colorectal cancer cell lines through regulation of the Long Non-Coding RNA (lncRNA) Cancer Susceptibility Candidate 2 (CASC2)/AU-Binding Factor 1 (AUF1)/B-Cell CLL/Lymphoma 2 (Bcl-2) Axis[28]. The structural interaction of berberine with Aldo-keto reductase family 1 member C3 is attributed to the suppression of Aldo-keto reductase family 1 member C3 enzyme activity and the inhibition of 22Rv1 prostate cancer cell growth by decreasing the intracellular androgen synthesis[29]. Berberine could effectively affect both tumor outgrowth and spontaneous metastasis in triple-negative breast cancer, which was associated with the inhibition of NLRP3 inflammasome pathway[30].

Whether HNF4α, which plays an important role in regulating the progression of diabetes and tumors, is just the right target for berberine to exert anti-gastric cancer effects remains to be elucidated. Our previous experiments demonstrated that berberine could induce cycle arrest of gastric cancer cells by targeting AMPK/HNF4α/WNT5a pathways *in vitro*[31]. In this study, berberine was administrated intragastrically to MGC803 and SGC7901 subcutaneous gastric cancer xenograft models. We investigated the effects of berberine against tumor growth and the role of HNF4α-WNT5a/β-catenin pathways involved in the antitumor effects of berberine.

MATERIALS AND METHODS

Chemicals and materials

Berberine chloride with a purity of 98% was purchased from the Sigma-Aldrich, United States. Antibodies against β-catenin were purchased from Cell Signaling Technologies (Boston, MA, United States), WNT5a was purchased from Abgent and HNF4a was purchased from Santa Cruz Biotechnology

(Santa Cruz, CA, United States).

Cell lines and cell culture

The gastric cancer cell lines MGC803 and SGC7901 were supplied by Hubei Biossci Biological Co., Ltd. Both cell lines were routinely cultured in RPMI1640(HyClone, China), supplemented with 10% fetal bovine serum (FBS) (SiJiQing, China), and 1% penicillin-streptomycin solution at 37 ℃ in a 5% CO2 humidified atmosphere. All experiments were performed when cells were in a logarithmic phase.

In vivo tumor xenograft model

Female BALB/c nude mice approximately 4 weeks old (13 g-17 g) were purchased from Hunan Slake Jingda Experimental Co., Ltd. (Hunan, China). Upon arrival, these animals were maintained under specific-pathogen-free conditions (23 ± 2 ℃ and 55 ± 5% humidity) with an automatically controlled 12h light/dark cycle and with a free access to sterilized flood and autoclaved water. After mice were acclimatized for about seven day, MGC803 or SGC7901 gastric cancer cells (10^7 cells per mouse) were subcutaneously injected into the right flank of mice. Animals bearing tumors were randomly divided into two groups, and treatment was initiated after injection for 72 h when a mass of more than 6 mm in maximal diameter was identified in each mouse with daily intragastric administration of normal saline (control group) and 100 mg/kg berberine (BBR group). All animals were sacrificed on Day 18 after treatment and blood as well as tissues from all animals were collected. Tumor xenograft length (L) and width (W) were measured at two-day intervals with Vernier calipers, and tumor volume (V) was calculated using the Formula ($V = W^2 \times L/2$). Mouse body weight was monitored every two d. Animal experiments were performed according to the institutional guidelines and regulations approved by the Huazhong University of Science and Technology Institutional Animal Care and Use Committee.

Immunohistochemistry staining assay

The tumor tissues removed from mice were fixed with 4% formaldehyde and then embedded in paraffin, and then 4μm thick tissue sections were made. After heating in an oven at 60 ℃ for 1 h, the sections was dewaxed in a dewaxing agent and rehydrated by a concentration-gradient of alcohol (100%, 95%, 85%, 75%). Tissue sections were boiled in 10 mmol/L sodium citrate buffer (pH 6.0) at high temperature to recover the antigen and incubated with 3% hydrogen peroxide for 10 minutes to block endogenous peroxidase activity. Sections were incubated with primary antibodies against HNF4a (1: 200), WNT5a (1: 80) and β-catenin (1: 100) at 4 ℃ overnight. Then the tissue was incubated with a secondary antibody and observed under a microscope.

Total RNA Extraction and real-time polymerase chain reaction

Total RNA was extracted using the TRIzol Reagent (Magent, Wuhan) according to the manufacturer's instructions, and then cDNA was synthesized from 2 μg of total RNA using the 5X All-In-One RT MasterMix (ABP) at 25 ℃ for 10 min, 42 ℃ for 15 min and 85 ℃ for 5 min. Real-time polymerase chain reaction (PCR) was used to detect the mRNA expression levels of HNF4α, WNT5a and β-catenin. PCR reactions were performed using LightCycler 480 (Roche Applied Science) in a total volume of 20 μL, including 10 μL of 2X SYBR Green qPCR Master Mix (ABP) at 95 ℃ for 10 min, 95 ℃ for 15 s and 60 ℃ for 60 s, 40 cycles according to the manufacturer's instructions. The relative gene expression was calculated with normalization to an endogenous reference (GAPDH).

The primers were as follows: GENE; Forward Primer (5′-3′); Reverse Primer (5′-3′); HNF4α; ATGCGACTCTCTAAAACCCTTG; ACCTTCAGATGGGGACGTGT; WNT5a; CAACTGGCAG-GACTTTCTCAA; CCTTCTCCAATGTACTGCATGTG; β-catenin; ATGGAGCCGGACAGAAAAGC; TGGGAGGTGTCAACATCTTCTT; GAPDH; TGGCCTTCCGTGTTCCTAC; GAGTTGCTGT-TGAAGTCGCA.

Western blotting

Total protein was extracted from the tumor tissues and liver tissues, and its concentration was determined by the BCA assay. Then, equal amounts of proteins (30ug/Lane) were loaded for electrophoresis, seperated by SDS-polyacrylamide electrophoresis gel (SDS–PAGE) and subsequently transferred to nitrocellulose membranes (NC membrane) (Millipore, United States). After blocking with 5% nonfat milk at room teamperature for 1h, the NC membranes were incubated with the primary antibodies overnight with gentle agitation at 4 ℃. After washing with TBST for three times, the NC membranes were incubated with the secondary antibodies for 1h at room temperature, followed by visualization with a near-infrared double color laser imaging system (Odyssey, Lincoln, NE, United States).

Statistical analysis

All experiments were repeated at least three times. All data are expressed as the mean ± standard deviation. All data were plotted by GraphPad Prism 6 software. Statistical analysis was performed using SPSS (version 20.0) software. A t test was also performed to determine differences between groups. $P < 0.05$ was considered statistically significant.

RESULTS

Berberine inhibited the growth of MGC803 and SGC7901 gastric cancer xenograft tumors

To explore the effect of berberine on gastric cancer xenograft models, we established MGC803 and SGC7901 xenograft tumor models. As shown in Figure 1A, intragastric administration of berberine significantly reduced the tumor weight of MGC803 and SGC7901 subcutaneously transplanted tumors, and the reduction rates were approximately 50.0% and 60.9% of the control group respectively ($P < 0.05$). In addition, as shown in Figure 1B, berberine led to 48.6% inhibition of tumor size in MGC803 xenograft models and 51.3% inhibition of tumor volume in SGC7901 xenograft models when compared to the control group. Berberine significantly inhibited the growth rate of MGC803 and SGC7901 xenograft tumors. Moreover, berberine did not affect the body weight of MGC803 and SGC7901 xenograft models in this experiment (Figure 1C, $P > 0.05$). These results indicated that berberine could significantly retard the growth of MGC803 and SGC7901 xenograft tumors, which was coordinated with the experimental results of Yi *et al*[32].

Berberine inhibited HNF4α expression in tumor and liver tissues in both MGC803 and SGC7901 xenograft tumor models.

HNF4α is at the center of a complex transcriptional regulatory network and is implicated in the initiation and progression of gastric cancer. To investigate the role of HNF4α in the growth of gastric cancer and the underlying mechanism, we examined the effect of berberine on the expression of HNF4α in tumor tissues and liver tissues of MGC803 and SGC7901 xenograft tumor models. Immunohistochemical staining showed that berberine downregulated the expression of HNF4α in tumor tissues from MGC803 and SGC7901 xenograft tumor models. Besides, in the tumor tissues from the MGC803 and SGC7901 xenograft tumor models, berberine significantly reduced both the transcriptional expression and protein expression of HNF4α compared with the control group. Moreover, berberine inhibited the mRNA level of HNF4α in the liver tissues from the MGC803 and SGC7901 xenograft models. Furthermore, berberine also reduced the protein expression of HNF4α in liver tissue from the MGC803 and SGC7901 xenograft models. Therefore, berberine inhibited the expression of HNF4α in MGC803 and SGC7901 xenograft models at both the transcriptional and posttranscriptional levels, and the reduction of HNF4α significantly inhibited the growth of tumor cells (Figure 2).

Berberine inhibited WNT5a expression in tumor and liver tissues in both MGC803 and SGC7901 xenograft tumor models.

WNT5a has been proven to be involved in the development and progression of gastric cancers. WNT5a was the downstream of HNF4α and HNF4α regulated WNT signaling through its target gene WNT5a, a potential prognostic marker of diffuse-type gastric tumours[33]. Therefore, we examined the alteration of the expression levels of WNT5a in tumor tissues and liver tissues from xenograft tumor models. Immunohistochemical staining results showed that compared with the control group, the expression level of WNT5a in tumor tissues from both the MGC803 and SGC7901 xenograft tumor models in the berberine group was significantly down-regulated. Furthermore, berberine also significantly reduced the mRNA and protein levels of WNT5a in the tumor tissues from both the MGC803 and SGC7901 xenograft models compared to the control group. Whereas, in the liver tissues from xenograft models, berberine reduced the mRNA level of WNT5a in MGC803 xenograft models, but did not affect the transcription level of WNT5a in SGC7901 xenograft models. However, berberine reduced the protein expression of WNT5a in the liver tissues from MGC803 as well as SGC7901 xenograft model. Therefore, berberine inhibited WNT5a protein expression in MGC803 and SGC7901 xenograft models, and the downregulation of WNT5a protein expression was associated with the retardation of the tumor growth rate (Figure 3).

Berberine inhibited β-catenin expression in tumor and liver tissues in both MGC803 and SGC7901 xenograft tumor models.

However, as an extracellular ligand, WNT5a activates different intracellular signaling cascades: β-catenin-dependent and β-catenin-independent pathways[34]. In the classical WNT pathway, β-catenin acts as a major mediator and functions as a protein organizer by interacting with numerous partners at the membrane, in the cytosol, and in the nucleus[35,36]. To further illustrate the mechanism of the antitumor effects of berberine, we also detected the expression level of β-catenin in tumor tissues and liver sections upon treatment with berberine. Immunohistochemical staining results showed that in the SGC7901 and MGC803 xenograft models, berberine significantly reduced the expression of β-catenin in tumor tissues. In addition, in both the MGC803 and SGC7901 xenograft tumor models, both the transcriptional and the protein levels of β-catenin in tumor tissue in the berberine group were significantly reduced. Besides, berberine reduced the mRNA level of β-catenin in the liver tissues from SGC7901 xenograft tumor models but did not affect the transcription level of β-catenin in MGC803 xenograft tumor models. Simultaneously, berberine also downregulated the protein expression of β-catenin in the liver tissues of MGC803 xenograft tumor models and SGC7901 xenograft tumor models.

A

Tumor weight (g)		
Xenograft models	**Ctrl**	**BBR**
MGC803	0.32 ± 0.04	0.16 ± 0.02[a]
SGC7901	0.23 ± 0.11	0.09 ± 0.01[a]

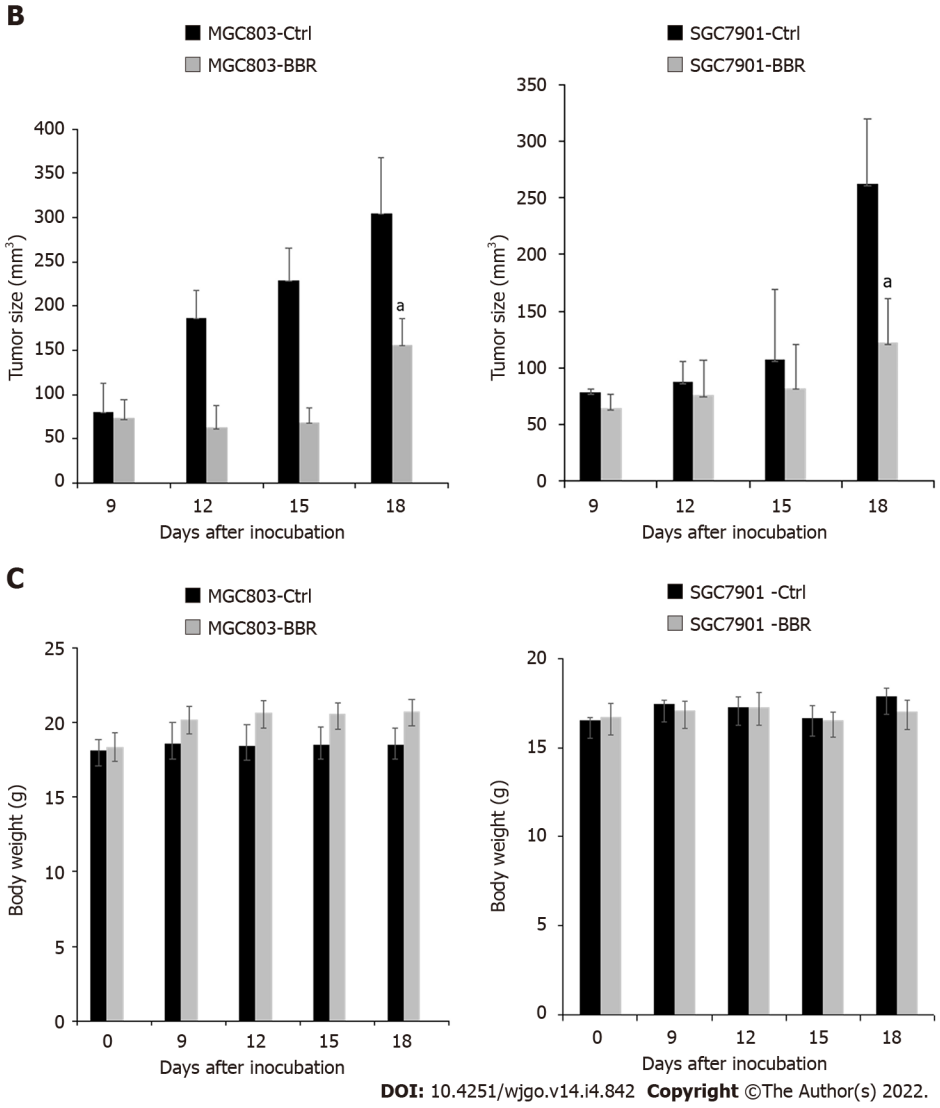

DOI: 10.4251/wjgo.v14.i4.842

Figure 1 Berberine inhibited the growth of MGC803 and SGC7901 xenograft tumors. A: After 18 d of drug treatment, tumors were removed from the mice and weighed; B: Changes in tumor size of mice during the experiment; C: Changes in body weight of mice during the experiment. [a]*P* < 0.05. Ctrl: The control group; BBR: The berberine group.

Therefore, berberine downregulated the protein expression of β-catenin in both MGC803 and SGC7901 xenograft models, and berberine targeted the WNT5a/β-catenin signaling pathways to exert its growth inhibition effects to MGC803 and SGC7901 xenograft model tumors (Figure 4).

DISCUSSION

Berberine is a benzyl tetraisoquinoline alkaloid extracted from Chinese herbal medicines such as Coptis, Phellodendron chinense and Hydrastis canadensis. Berberine has been used clinically for many years and is effective in counteracting numerous diseases such as gastroenteritis, abdominal pain and diarrhea, with antimicrobial and anti-inflammatory properties[37]. Over the past decades, growing evidence clearly indicates that berberine can improve insulin-resistance and the levels of plasma lipids and glucose in type 2 diabetes animal models and humans[38-40]. Berberine could modulate the

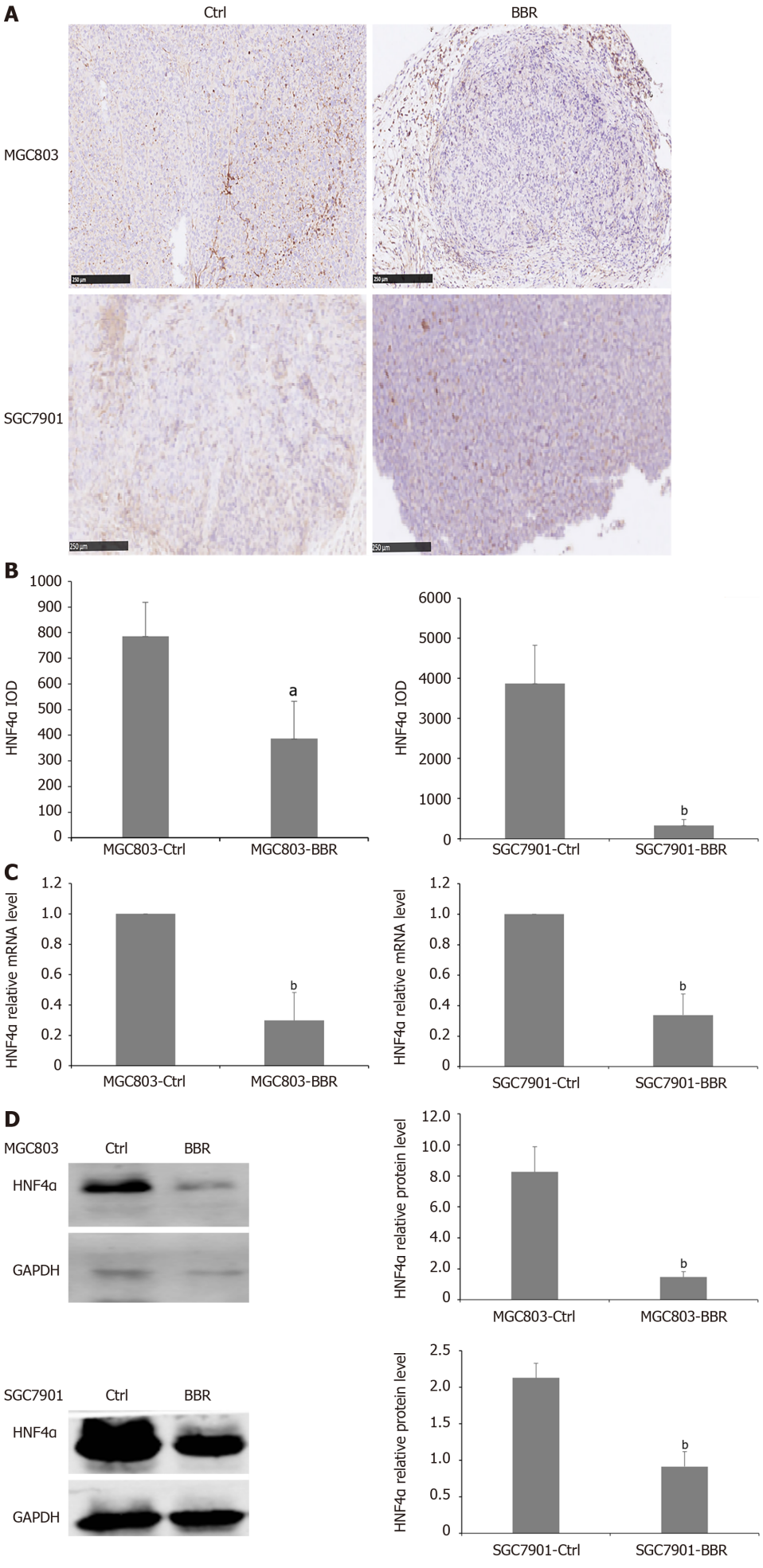
A
Ctrl
BBR
MGC803
SGC7901
B
HNF4α IOD
MGC803-Ctrl
MGC803-BBR
SGC7901-Ctrl
SGC7901-BBR
C
HNF4α relative mRNA level
D
MGC803
HNF4α
GAPDH
SGC7901
HNF4α relative protein level

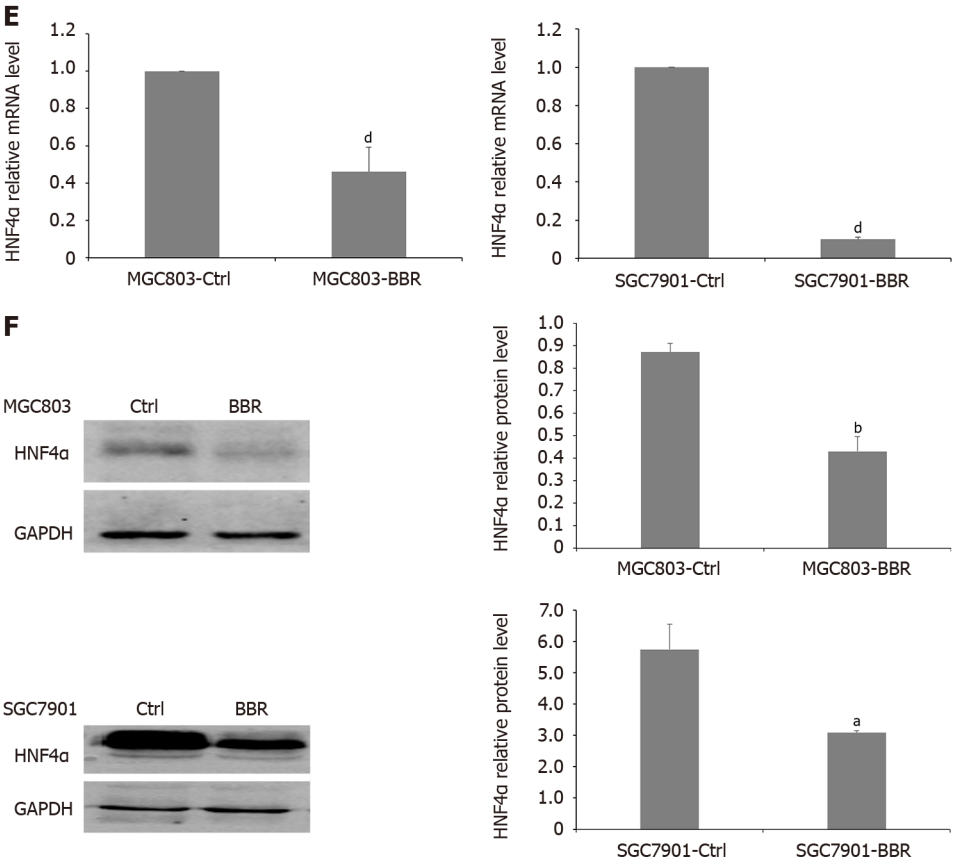

DOI: 10.4251/wjgo.v14.i4.842

Figure 2 Berberine inhibited hepatocyte nuclear factor 4α expression in MGC803 and SGC7901 xenograft tumor models. A: Immunohistochemistry showed that berberine reduced the expression of hepatocyte nuclear factor 4α (HNF4α) in tumor tissues of MGC803 and SGC7901 xenograft tumor models; B: The quantification of immunohistochemistry of the expression of HNF4α in tumor tissues of MGC803 and SGC7901 xenograft tumor models; C: The effect of berberine on HNF4α mRNA expression in tumor tissues of MGC803 and SGC7901 xenograft tumor models; D: The effect of berberine on HNF4α protein expression in tumor tissues of MGC803 and SGC7901 xenograft tumor models; E: The effect of berberine on HNF4α mRNA level in liver tissues of MGC803 and SGC7901 xenografts; F: The effect of berberine on HNF4α protein expression in liver tissues of MGC803 and SGC7901 xenografts. $^{a}P < 0.05$, $^{b}P < 0.01$, $^{d}P < 0.0001$. Ctrl: The control group; BBR: The berberine group.

composition of the gut microbiome and reduce body weight, blood glucose levels, and intestinal inflammation in diabetic mice, which demonstrates its effectiveness in the reduction of diabetic complications in this model[38]. Berberine also attenuated intestinal mucosal barrier dysfunction and immune barrier damage in type 2 diabetic rats[39]. Berberine stimulated insulin secretion in impaired glucose tolerance rats[40]. Recently, berberine has shown potential therapeutic effects in treating cancers[26]. Berberine inhibited the proliferation of SGC-7901 cells and induced apoptosis[41]. Berberine also inhibited EGFR signaling and enhanced the antitumor effects of EGFR inhibitors in gastric cancer[27]. Berberine could also inactivate MAPK signaling pathways to exert growth inhibition effects on MGC803 cells[42]. In this experiment, berberine was discovered to induce a 48.6% inhibition of tumor growth in MGC803 xenograft models and 51.3% retardation of tumor growth in SGC7901 xenograft models without any influence on body weight[42]. Therefore, berberine might be an effective and safe drug candidate for treating gastric cancer. However, whether there exists a shared molecular target which is responsible for the antitumor effects and the antidiabetic effects of berberine remains unclear?

HNF4α is a transcription factor with important roles in liver and gastrointestinal tract development, hepatocyte differentiation, and lipid and glucose metabolism[43]. HNF4α is at the center of a complex transcriptional regulatory network where its disruption is directly linked to glucose metabolism and lipid metabolism[44]. The activation of HNF4α may represent a novel single agent for the treatment of insulin resistance[44]. The activation of HNF4α stimulates glucose metabolism in acute myeloid leukemia cells[45]. What's more, the regulation of HNF4α expression and activity is highly complex, reflecting on the downstream transcriptional networks with diverse functional roles including drug metabolism, lipid homeostasis, gluconeogenesis, cell adhesion, proliferation, and apoptosis[46]. Our previous studies found that HNF4α was involved in the glucose metabolism of DM[47]. Recently, one further study illustrated that inhibition of HNF4α expression could induce cell cycle arrest and apoptosis in gastric cancer cells, thereby exerting antitumor growth effects[31], corresponding to the experiments in which inhibitory RNA and pharmacological inhibition of HNF4α demonstrated antineoplastic activity *in vitro* and *in vivo via* downregulation of cyclins, cell cycle arrest and apoptosis in gastric

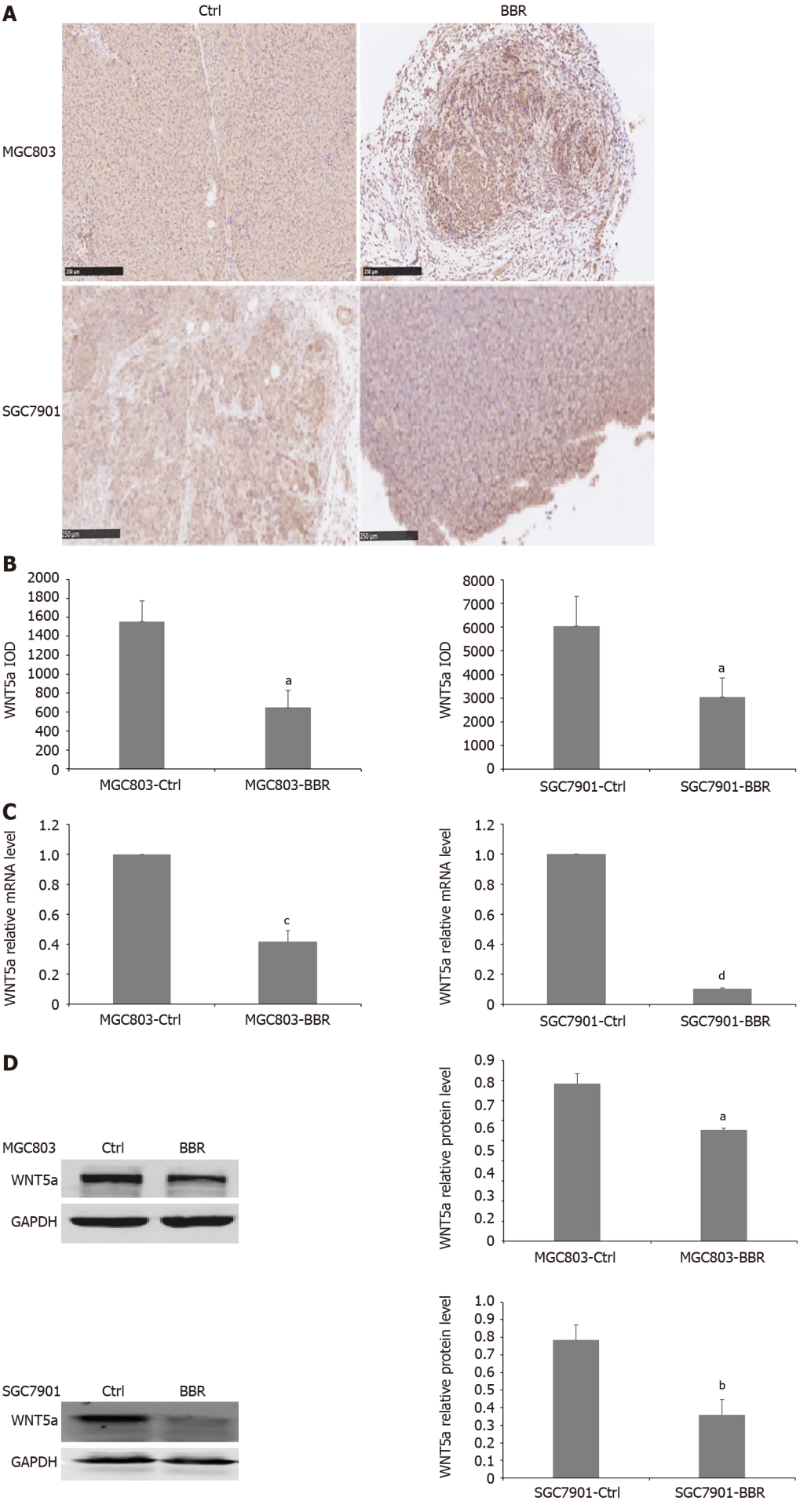
A
Ctrl
BBR
MGC803
SGC7901
B
WNT5a IOD
MGC803-Ctrl
MGC803-BBR
SGC7901-Ctrl
SGC7901-BBR
C
WNT5a relative mRNA level
D
MGC803
Ctrl
BBR
WNT5a
GAPDH
WNT5a relative protein level
SGC7901

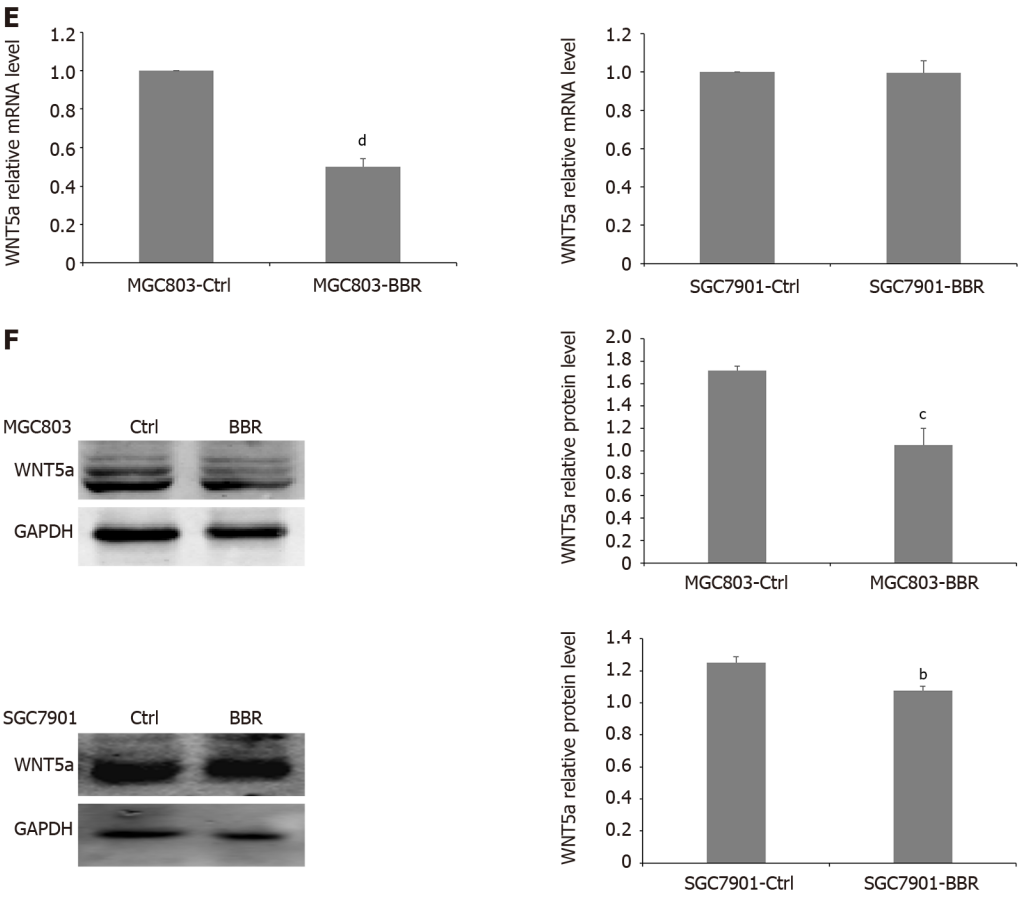

DOI: 10.4251/wjgo.v14.4.842

Figure 3 Berberine inhibited WNT5a expression in MGC803 and SGC7901 xenograft tumor models. A: Immunohistochemistry showed that berberine reduced the expression of WNT5a in tumor tissues of MGC803 and SGC7901 xenograft tumor models; B: The quantification of immunohistochemistry of the expression of WNT5a in tumor tissues of MGC803 and SGC7901 xenograft tumor models; C: The effect of berberine on WNT5a mRNA level in tumor tissues of MGC803 and SGC7901 xenograft tumor models; D: The effect of berberine on WNT5a protein expression in tumor tissues of MGC803 and SGC7901 xenograft tumor models; E: The effect of berberine on WNT5a mRNA expression in liver tissues of MGC803 and SGC7901 xenografts; F: The effect of berberine on WNT5a protein expression in liver tissues of MGC803 and SGC7901 xenografts. $^{a}P < 0.05$, $^{b}P < 0.01$, $^{c}P < 0.001$, $^{d}P < 0.0001$. Ctrl: The control group; BBR: The berberine group.

cancer[33]. HNF4α downregulation could promote tumor migration and invasion in renal cell carcinoma[48]. HNF4α promotes the malignant phenotype of acute myeloid leukemia cells[45]. In this study, berberine could suppressed the expression of HNF4α in tumor tissues and liver tissues from MGC803 and SGC7901 gastric cancer xenograft tumor models. More importantly, the reduced expression of HNF4α might to be associated with the growth retardation of tumors from gastric cancer xenograft models. Therefore, berberine might target HNF4α to inhibit tumor growth in MGC803 and SGC7901 xenograft models.

Studies have shown that WNT5a contains several highly conserved HNF4α binding sites in its promoter region[49]. The expression level of WNT5a decreases after HNF4α gene knockout, which further inhibits cellular glucose uptake and cell proliferation, and also induces apoptosis[33,45]. WNT5a is a member of the WNT family and can activate classical WNT (β-catenin-dependent) signaling pathways[50]. The WNT/β-catenin signaling pathway has been recognized as a potentially therapeutic target for cancers[51]. In the classical WNT pathway, β-catenin acts as a major mediator, facilitates signal transduction, and participates in embryogenesis, cell differentiation, and proliferation processes. When the WNT pathway is on, the cytoplasmic concentration of β-catenin increases, and then it translocates into the nucleus, which activates more than one hundred target genes of the WNT pathway, while when the WNT pathway is off, β-catenin is degraded by the proteasome[52]. In this experiment, we found that the protein expression of WNT5a and β-catenin was both downregulated by berberine, indicating that inactivation of the WNT/β-catenin pathway resulted from berberine. The WNT/β-catenin pathway is involved in the process of tumorigenesis, invasion and metastasis. The role of WNT5a in the occurrence and progression of gastric cancer has gradually been elucidated. It was confirmed that downregulation of WNT5a expression in gastric cancer cells could inhibit EMT onset and increased WNT5a expression could also result in poor differentiation in GC[53,54]. By activating the WNT5a signaling pathway, gastric cancer cell growth was promoted and G1-S cell cycle transition was induced[55]. Overexpression of WNT5a is also associated with enhanced tumor aggressiveness[56,57]. WNT5a was also a potential

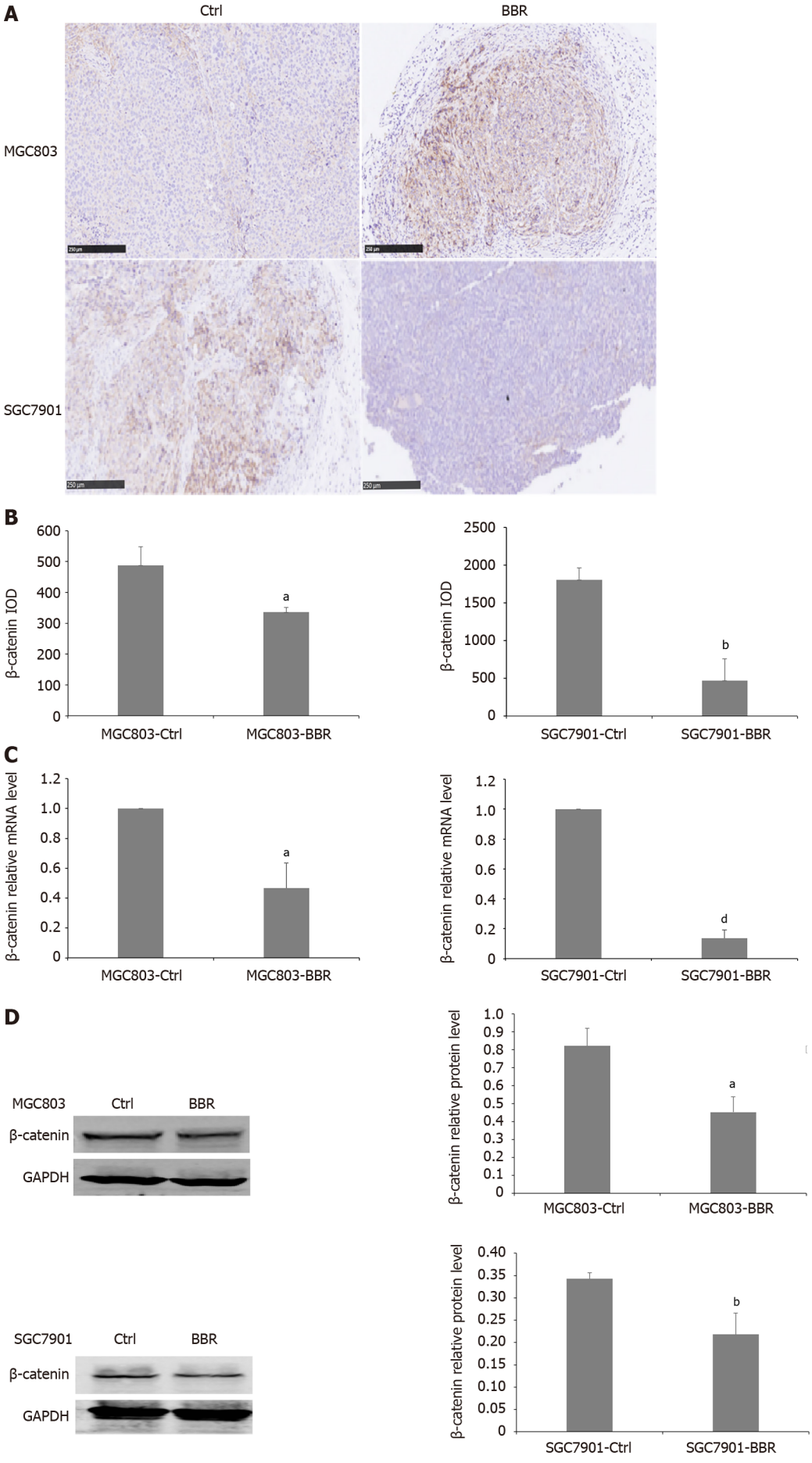
A
Ctrl
BBR
MGC803
SGC7901
B
β-catenin IOD
MGC803-Ctrl
MGC803-BBR
SGC7901-Ctrl
SGC7901-BBR
C
β-catenin relative mRNA level
D
MGC803
Ctrl
BBR
β-catenin
GAPDH
SGC7901
β-catenin relative protein level

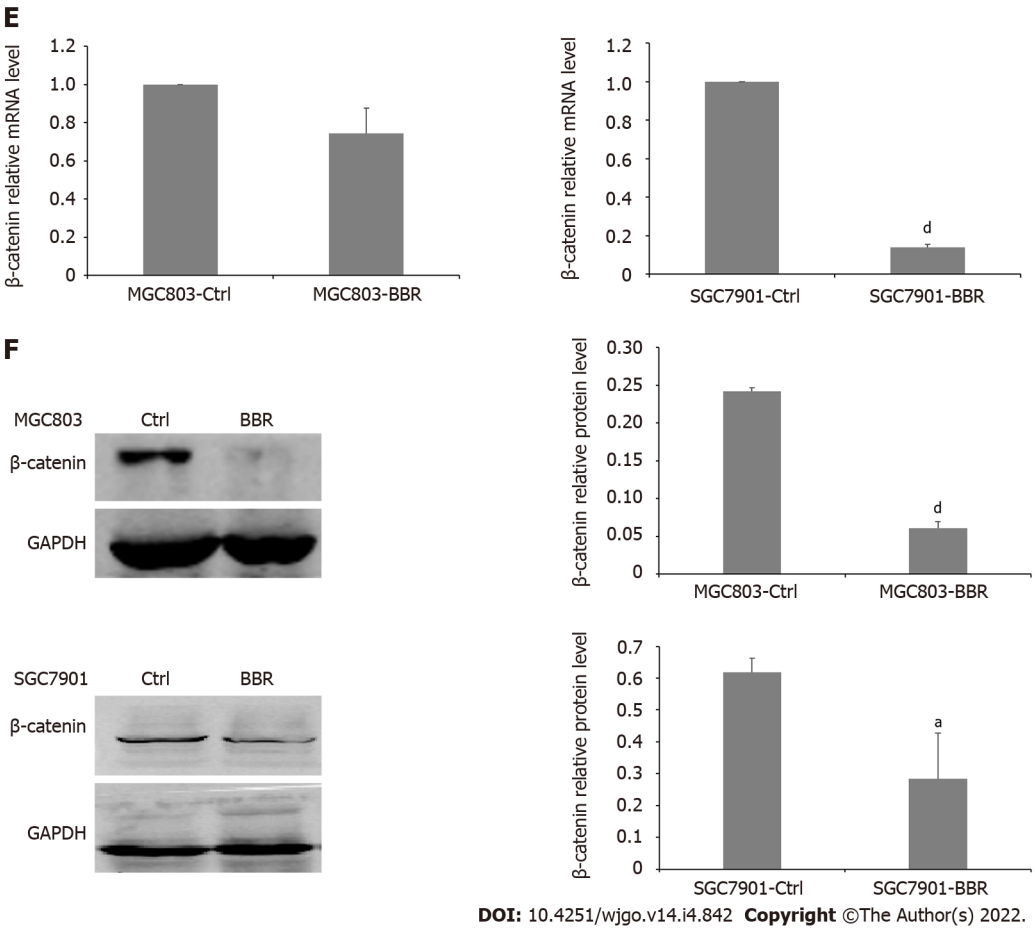

DOI: 10.4251/wjgo.v14.i4.842

Figure 4 Berberine inhibited β-catenin expression in MGC803 and SGC7901 xenograft tumor models. A: Immunohistochemistry showed that berberine reduced the expression of β-catenin in tumor tissues of MGC803 and SGC7901 xenograft tumor models; B: The quantification of immunohistochemistry of the expression of β-catenin in tumor tissues of MGC803 and SGC7901 xenograft tumor models; C: The effect of berberine on β-catenin mRNA alteration in tumor tissues of MGC803 and SGC7901 xenograft tumor models; D: The effect of berberine on β-catenin protein expression in tumor tissues of MGC803 and SGC7901 xenograft tumor models; E: The effect of berberine on β-catenin mRNA in liver tissues of MGC803 and SGC7901 xenografts; F: The effect of berberine on β-catenin protein expression in liver tissues of MGC803 and SGC7901 xenografts. $^{a}P < 0.05$; $^{b}P < 0.01$; $^{c}P < 0.001$; $^{d}P < 0.0001$. Ctrl: The control group; BBR: The berberine group.

suppressor of EMT and downregulation of WNT5a mRNA and protein by EGF is necessary for EGF-induced EMT in gastric cancer SGC-7901 cells[58]. The role of WNT5a in the development of gastric cancer is controversial. Recently the role of β-catenin in promoting the migration and invasion of gastric cancer has also been elucidated. CD44, which interacts with IL-13Rα2, promotes gastric cancer development and metastasis through regulation of the β-catenin signaling pathways[59]. HOXA11-AS not only promotes gastric cancer cell migration and invasion *in vitro*, but also promotes gastric cancer cell metastasis *in vivo*, at least in part, by regulating β-catenin[60]. Studies have also shown that the berberine combined drug HMQ1611 negatively regulates the WNT5a signaling pathway by upregulating axin and inhibiting nuclear transport of β-catenin, thereby inhibiting cancer cell proliferation and metastasis[61]. This experiment demonstrated that the reduction in the expression of WNT5a/β-catenin signaling pathway is associated with tumor growth suppression in MGC803 and SGC7901 xenograft tumor models. This experiment displayed that berberine could downregulate the expression of WNT5a/β-catenin in tumor tissues and liver tissues of MGC803 and SGC7901 gastric cancer xenograft tumor models at the protein level, and thereby inhibiting the growth of MGC803 and SGC7901 gastric cancer xenograft tumors.

CONCLUSION

In conclusion, we found that berberine could exert growth retardation effects on both MGC803 and SGC7901 xenograft tumors, the mechanism behind which might associate with the simultaneous reduction of both the HNF4α and WNT5a/β-catenin from the tumor tissues and liver tissues in the MGC803 and SGC7901 xenograft models. Therefore HNF4α might be a potential target through which berberine exerts the effects of countering against gastric cancers.

ARTICLE HIGHLIGHTS

Research background

Gastric cancer is the third deadliest cancer in the world and ranks second in incidence and mortality of cancers in China. Despite advances in prevention, diagnosis, and therapy, the absolute number of cases is increasing every year due to aging and the growth of high-risk populations, and gastric cancer is still a leading cause of cancer-related death. Gastric cancer is a consequence of the complex interaction of microbial agents with environmental and host factors, resulting in the dysregulation of multiple oncogenic and tumor-suppressing signaling pathways. Global efforts have been undertaken to investigate in detail the genomic and epigenomic heterogeneity of this disease, resulting in the identification of new specific and sensitive predictive and prognostic biomarkers. Trastuzumab, a monoclonal antibody against the HER2 receptor, is approved in the first-line treatment of patients with HER2+ tumors, which accounts for 13%-23% of the gastric cancer population. Ramucirumab, a monoclonal antibody against VEGFR2, is currently recommended in patients progressing after first-line treatment. Several clinical trials have also tested novel agents, such as the anti-EGFR and the anti-MET monoclonal antibodies, for advanced gastric cancer but mostly with disappointing results. Therefore, screening specific molecular targets for gastric cancer and drugs directed against the molecular targets is still urgently needed.

Research motivation

To screen specific molecular targets for gastric cancer and drugs directed against the molecular targets is still urgently needed.

Research objectives

To investigate the effect and mechanism of berberine against tumor growth in gastric cancer xenograft models and to explore the role of hepatocyte nuclear factor 4α (HNF4α)-WNT5a/β-catenin pathway played in the antitumor effects of berberine.

Research methods

MGC803 and SGC7901 subcutaneous xenograft models were established. The control group was intragastrically administrated with normal saline, and the berberine group was administrated intragastrically with 100mg/kg/d berberine. The body weight of nude mice during the experiment was measured to assess whether berberine has any adverse reaction. The volume of subcutaneous tumors during this experiment was recorded to evaluate the inhibitory effect of berberine on the growth of MGC803 and SGC7901 subcutaneous transplantation tumors. Polymerase chain reaction assays were conducted to evaluate the alteration of transcriptional expression of HNF4α, WNT5a and β-catenin in tumor tissues and liver tissues from the MGC803 and SGC7901 xenograft models. Western blotting and IHC were performed to assess the protein expression of HNF4α, WNT5a and β-catenin in tumor tissues and liver tissues from the MGC803 and SGC7901 xenograft models.

Research results

In both MGC803 and SGC7901 xenograft tumor models, berberine significantly reduced tumor volume and weight and retarded the growth rate of tumors. In the SGC7901 and MGC803 subcutaneously transplanted tumor models, berberine downregulated the expression of HNF4α, WNT5a and β-catenin in tumor tissues from both transcription and protein levels. Besides, berberine also suppressed the protein expression of HNF4α, WNT5a and β-catenin in liver tissues.

Research conclusions

Berberine retarded the growth of MGC803 and SGC7901 xenograft model tumors, and the mechanism behind this antigrowth effects might be the downregulation of the expression of HNF4α-WNT5a/β-catenin signaling pathways both in tumor tissues and liver tissues of the xenograft models.

Research perspectives

HNF4α might be a potential target through which berberine exerts effects of both improving diabetes and countering gastric cancers.

FOOTNOTES

Author contributions: Yi P designed the research; Li LL, Peng Z, Xu LJ and Zou X performed the research; Xu LJ, and Zou X contributed analytic tools; Li LL and Peng Z analyzed the data; Li LL wrote the manuscript; Yi P, Hu Q and Huang DM revised the manuscript.

Supported by the National Natural Science Foundation of China, No. 81673757 and No. 81573787.

Institutional review board statement: The study was reviewed and approved by the Huazhong University of Science and Technology Institutional Animal Care and Use Committee.

Conflict-of-interest statement: The authors declare no conflicts of interest regarding the publication of this paper.

Data sharing statement: the data is available from the corresponding author at pyi219@163.com.

Country/Territory of origin: China

ORCID number: Ling-Li Li 0000-0003-4518-1418; Ze Peng 0000-0003-2175-4322; Qian Hu 0000-0002-5783-7085; Li-Jun Xu 0000-0002-2013-9419; Xin Zou 0000-0003-3164-4872; Dong-Mei Huang 0000-0001-7596-7038; Ping Yi 0000-0001-8560-2024.

S-Editor: Wang LL
L-Editor: A
P-Editor: Li X

REFERENCES

1 **Camargo MC**, Figueiredo C, Machado JC. Review: Gastric malignancies: Basic aspects. *Helicobacter* 2019; **24** Suppl 1: e12642 [PMID: 31486241 DOI: 10.1111/hel.12642]
2 **Bray F**, Ferlay J, Soerjomataram I, Siegel RL, Torre LA, Jemal A. Global cancer statistics 2018: GLOBOCAN estimates of incidence and mortality worldwide for 36 cancers in 185 countries. *CA Cancer J Clin* 2018; **68**: 394-424 [PMID: 30207593 DOI: 10.3322/caac.21492]
3 **Serra O**, Galán M, Ginesta MM, Calvo M, Sala N, Salazar R. Comparison and applicability of molecular classifications for gastric cancer. *Cancer Treat Rev* 2019; **77**: 29-34 [PMID: 31195213 DOI: 10.1016/j.ctrv.2019.05.005]
4 **Pellino A**, Riello E, Nappo F, Brignola S, Murgioni S, Djaballah SA, Lonardi S, Zagonel V, Rugge M, Loupakis F, Fassan M. Targeted therapies in metastatic gastric cancer: Current knowledge and future perspectives. *World J Gastroenterol* 2019; **25**: 5773-5788 [PMID: 31636471 DOI: 10.3748/wjg.v25.i38.5773]
5 **Bang YJ**, Van Cutsem E, Feyereislova A, Chung HC, Shen L, Sawaki A, Lordick F, Ohtsu A, Omuro Y, Satoh T, Aprile G, Kulikov E, Hill J, Lehle M, Rüschoff J, Kang YK; ToGA Trial Investigators. Trastuzumab in combination with chemotherapy versus chemotherapy alone for treatment of HER2-positive advanced gastric or gastro-oesophageal junction cancer (ToGA): a phase 3, open-label, randomised controlled trial. *Lancet* 2010; **376**: 687-697 [PMID: 20728210 DOI: 10.1016/s0140-6736(10)61121-x]
6 **Fuchs CS**, Tomasek J, Yong CJ, Dumitru F, Passalacqua R, Goswami C, Safran H, Dos Santos LV, Aprile G, Ferry DR, Melichar B, Tehfe M, Topuzov E, Zalcberg JR, Chau I, Campbell W, Sivanandan C, Pikiel J, Koshiji M, Hsu Y, Liepa AM, Gao L, Schwartz JD, Tabernero J; REGARD Trial Investigators. Ramucirumab monotherapy for previously treated advanced gastric or gastro-oesophageal junction adenocarcinoma (REGARD): an international, randomised, multicentre, placebo-controlled, phase 3 trial. *Lancet* 2014; **383**: 31-39 [PMID: 24094768 DOI: 10.1016/S0140-6736(13)61719-5]
7 **Zheng J**, Xie SH, Santoni G, Lagergren J. Population-based cohort study of diabetes mellitus and mortality in gastric adenocarcinoma. *Br J Surg* 2018; **105**: 1799-1806 [PMID: 30051463 DOI: 10.1002/bjs.10930]
8 **Yang HJ**, Kang D, Chang Y, Ahn J, Ryu S, Cho J, Guallar E, Sohn CI. Diabetes mellitus is associated with an increased risk of gastric cancer: a cohort study. *Gastric Cancer* 2020; **23**: 382-390 [PMID: 31853749 DOI: 10.1007/s10120-019-01033-8]
9 **Abudawood M**. Diabetes and cancer: A comprehensive review. *J Res Med Sci* 2019; **24**: 94 [PMID: 31741666 DOI: 10.4103/jrms.jrms_242_19]
10 **Wu D**, Hu D, Chen H, Shi G, Fetahu IS, Wu F, Rabidou K, Fang R, Tan L, Xu S, Liu H, Argueta C, Zhang L, Mao F, Yan G, Chen J, Dong Z, Lv R, Xu Y, Wang M, Ye Y, Zhang S, Duquette D, Geng S, Yin C, Lian CG, Murphy GF, Adler GK, Garg R, Lynch L, Yang P, Li Y, Lan F, Fan J, Shi Y, Shi YG. Glucose-regulated phosphorylation of TET2 by AMPK reveals a pathway linking diabetes to cancer. *Nature* 2018; **559**: 637-641 [PMID: 30022161 DOI: 10.1038/s41586-018-0350-5]
11 **Li T**, Chanda D, Zhang Y, Choi HS, Chiang JY. Glucose stimulates cholesterol 7alpha-hydroxylase gene transcription in human hepatocytes. *J Lipid Res* 2010; **51**: 832-842 [PMID: 19965590 DOI: 10.1194/jlr.m002782]
12 **Chandra V**, Huang P, Potluri N, Wu D, Kim Y, Rastinejad F. Multidomain integration in the structure of the HNF-4α nuclear receptor complex. *Nature* 2013; **495**: 394-398 [PMID: 23485969 DOI: 10.1038/nature11966]
13 **Jiang S**, Tanaka T, Iwanari H, Hotta H, Yamashita H, Kumakura J, Watanabe Y, Uchiyama Y, Aburatani H, Hamakubo T, Kodama T, Naito M. Expression and localization of P1 promoter-driven hepatocyte nuclear factor-4α (HNF4α) isoforms in human and rats. *Nucl Recept* 2003; **1**: 5 [PMID: 12952540 DOI: 10.1186/1478-1336-1-5]
14 **Barbetti F**, D'Annunzio G. Genetic causes and treatment of neonatal diabetes and early childhood diabetes. *Best Pract Res Clin Endocrinol Metab* 2018; **32**: 575-591 [PMID: 30086875 DOI: 10.1016/j.beem.2018.06.008]

15 **Nakajima N**, Yoshizawa A, Nakajima T, Hirata M, Furuhata A, Sumiyoshi S, Rokutan-Kurata M, Sonobe M, Menju T, Miyamoto E, Chen-Yoshikawa TF, Date H, Haga H. GATA6-positive lung adenocarcinomas are associated with invasive mucinous adenocarcinoma morphology, hepatocyte nuclear factor 4α expression, and KRAS mutations. *Histopathology* 2018; **73**: 38-48 [PMID: 29469192 DOI: 10.1111/his.13500]

16 **Zhang X**, Xu Y, Qian Z, Zheng W, Wu Q, Chen Y, Zhu G, Liu Y, Bian Z, Xu W, Zhang Y, Sun F, Pan Q, Wang J, Du L, Yu Y. circRNA_104075 stimulates YAP-dependent tumorigenesis through the regulation of HNF4a and may serve as a diagnostic marker in hepatocellular carcinoma. *Cell Death Dis* 2018; **9**: 1091 [PMID: 30361504 DOI: 10.1038/s41419-018-1132-6]

17 **Orsolini L**, Papanti GD, Francesconi G, Schifano F. Mind navigators of chemicals' experimenters? *Cyberpsychol Behav Soc Netw* 2015; **18**: 296-300 [PMID: 25965863 DOI: 10.18632/oncotarget.3753]

18 **Kojima K**, Kishimoto T, Nagai Y, Tanizawa T, Nakatani Y, Miyazaki M, Ishikura H. The expression of hepatocyte nuclear factor-4alpha, a developmental regulator of visceral endoderm, correlates with the intestinal phenotype of gastric adenocarcinomas. *Pathology* 2006; **38**: 548-554 [PMID: 17393984 DOI: 10.1080/00313020601024011]

19 **Koyama T**, Sekine S, Taniguchi H, Tsuda H, Ikegami M, Hano H, Kushima R. Hepatocyte nuclear factor 4A expression discriminates gastric involvement by metastatic breast carcinomas from primary gastric adenocarcinomas. *Hum Pathol* 2011; **42**: 1777-1784 [PMID: 21733563 DOI: 10.1016/j.humpath.2011.04.002]

20 **Jucá PCFC**, Corrêa S, Vignal GM, Accioly MTS, Lustosa SAS, Abdelhay E, Matos D. HNF4A expression as a potential diagnostic tool to discriminate primary gastric cancer from breast cancer metastasis in a Brazilian cohort. *Diagn Pathol* 2017; **12**: 43 [PMID: 28583188 DOI: 10.1186/s13000-017-0635-2]

21 **Ranc K**, Jørgensen ME, Friis S, Carstensen B. Mortality after cancer among patients with diabetes mellitus: effect of diabetes duration and treatment. *Diabetologia* 2014; **57**: 927-934 [PMID: 24633676 DOI: 10.1007/s00125-014-3186-z]

22 **Kumar A**, Ekavali, Chopra K, Mukherjee M, Pottabathini R, Dhull DK. Current knowledge and pharmacological profile of berberine: An update. *Eur J Pharmacol* 2015; **761**: 288-297 [PMID: 26092760 DOI: 10.1016/j.ejphar.2015.05.068]

23 **Wei S**, Zhang M, Yu Y, Lan X, Yao F, Yan X, Chen L, Hatch GM. Berberine Attenuates Development of the Hepatic Gluconeogenesis and Lipid Metabolism Disorder in Type 2 Diabetic Mice and in Palmitate-Incubated HepG2 Cells through Suppression of the HNF-4α miR122 Pathway. *PLoS One* 2016; **11**: e0152097 [PMID: 27011261 DOI: 10.1371/journal.pone.0152097]

24 **Yue SJ**, Liu J, Wang AT, Meng XT, Yang ZR, Peng C, Guan HS, Wang CY, Yan D. Berberine alleviates insulin resistance by reducing peripheral branched-chain amino acids. *Am J Physiol Endocrinol Metab* 2019; **316**: E73-E85 [PMID: 30422704 DOI: 10.1152/ajpendo.00256.2018]

25 **Wang S**, He B, Hang W, Wu N, Xia L, Wang X, Zhang Q, Zhou X, Feng Z, Chen Q, Chen J. Berberine Alleviates Tau Hyperphosphorylation and Axonopathy-Associated with Diabetic Encephalopathy *via* Restoring PI3K/Akt/GSK3β Pathway. *J Alzheimers Dis* 2018; **65**: 1385-1400 [PMID: 30175975 DOI: 10.3233/JAD-180497]

26 **Wang N**, Tan HY, Li L, Yuen MF, Feng Y. Berberine and Coptidis Rhizoma as potential anticancer agents: Recent updates and future perspectives. *J Ethnopharmacol* 2015; **176**: 35-48 [PMID: 26494507 DOI: 10.1016/j.jep.2015.10.028]

27 **Wang J**, Yang S, Cai X, Dong J, Chen Z, Wang R, Zhang S, Cao H, Lu D, Jin T, Nie Y, Hao J, Fan D. Berberine inhibits EGFR signaling and enhances the antitumor effects of EGFR inhibitors in gastric cancer. *Oncotarget* 2016; **7**: 76076-76086 [PMID: 27738318 DOI: 10.18632/oncotarget.12589]

28 **Dai W**, Mu L, Cui Y, Li Y, Chen P, Xie H, Wang X. Berberine Promotes Apoptosis of Colorectal Cancer *via* Regulation of the Long Non-Coding RNA (lncRNA) Cancer Susceptibility Candidate 2 (CASC2)/AU-Binding Factor 1 (AUF1)/B-Cell CLL/Lymphoma 2 (Bcl-2) Axis. *Med Sci Monit* 2019; **25**: 730-738 [PMID: 30681073 DOI: 10.12659/msm.912082]

29 **Tian Y**, Zhao L, Wang Y, Zhang H, Xu D, Zhao X, Li Y, Li J. Berberine inhibits androgen synthesis by interaction with aldo-keto reductase 1C3 in 22Rv1 prostate cancer cells. *Asian J Androl* 2016; **18**: 607-612 [PMID: 26698234 DOI: 10.4103/1008-682x.169997]

30 **Yao M**, Fan X, Yuan B, Takagi N, Liu S, Han X, Ren J, Liu J. Berberine inhibits NLRP3 Inflammasome pathway in human triple-negative breast cancer MDA-MB-231 cell. *BMC Complement Altern Med* 2019; **19**: 216 [PMID: 31412862 DOI: 10.1186/s12906-019-2615-4]

31 **Hu Q**, Li L, Zou X, Xu L, Yi P. Berberine Attenuated Proliferation, Invasion and Migration by Targeting the AMPK/HNF4α/WNT5A Pathway in Gastric Carcinoma. *Front Pharmacol* 2018; **9**: 1150 [PMID: 30405404 DOI: 10.3389/fphar.2018.01150]

32 **Yi T**, Zhuang L, Song G, Zhang B, Li G, Hu T. Akt signaling is associated with the berberine-induced apoptosis of human gastric cancer cells. *Nutr Cancer* 2015; **67**: 523-531 [PMID: 25837881 DOI: 10.1080/01635581.2015.1004733]

33 **Chang HR**, Nam S, Kook MC, Kim KT, Liu X, Yao H, Jung HR, Lemos R Jr, Seo HH, Park HS, Gim Y, Hong D, Huh I, Kim YW, Tan D, Liu CG, Powis G, Park T, Liang H, Kim YH. HNF4α is a therapeutic target that links AMPK to WNT signalling in early-stage gastric cancer. *Gut* 2016; **65**: 19-32 [PMID: 25410163 DOI: 10.1136/gutjnl-2014-307918]

34 **Kikuchi A**, Yamamoto H, Sato A, Matsumoto S. Wnt5a: its signalling, functions and implication in diseases. *Acta Physiol (Oxf)* 2012; **204**: 17-33 [PMID: 21518267 DOI: 10.1111/j.1748-1716.2011.02294.x]

35 **Xu W**, Kimelman D. Mechanistic insights from structural studies of beta-catenin and its binding partners. *J Cell Sci* 2007; **120**: 3337-3344 [PMID: 17881495 DOI: 10.1242/jcs.013771]

36 **Kim W**, Kim M, Jho EH. Wnt/β-catenin signalling: from plasma membrane to nucleus. *Biochem J* 2013; **450**: 9-21 [PMID: 23343194 DOI: 10.1042/bj20121284]

37 **Tillhon M**, Guamán Ortiz LM, Lombardi P, Scovassi AI. Berberine: new perspectives for old remedies. *Biochem Pharmacol* 2012; **84**: 1260-1267 [PMID: 22842630 DOI: 10.1016/j.bcp.2012.07.018]

38 **Zhang W**, Xu JH, Yu T, Chen QK. Effects of berberine and metformin on intestinal inflammation and gut microbiome composition in db/db mice. *Biomed Pharmacother* 2019; **118**: 109131 [PMID: 31545226 DOI: 10.1016/j.biopha.2019.109131]

39 **Gong J**, Hu M, Huang Z, Fang K, Wang D, Chen Q, Li J, Yang D, Zou X, Xu L, Wang K, Dong H, Lu F. Berberine Attenuates Intestinal Mucosal Barrier Dysfunction in Type 2 Diabetic Rats. *Front Pharmacol* 2017; **8**: 42 [PMID: 28217099 DOI: 10.3389/fphar.2017.00042]

40 **Leng SH**, Lu FE, Xu LJ. Therapeutic effects of berberine in impaired glucose tolerance rats and its influence on insulin secretion. *Acta Pharmacol Sin* 2004; **25**: 496-502 [PMID: 15066220]

41 **Yang Y**, Zhang N, Li K, Chen J, Qiu L, Zhang J. Integration of microRNA-mRNA profiles and pathway analysis of plant isoquinoline alkaloid berberine in SGC-7901 gastric cancers cells. *Drug Des Devel Ther* 2018; **12**: 393-408 [PMID: 29535501 DOI: 10.2147/DDDT.S155993]

42 **Li HL**, Wu H, Zhang BB, Shi HL, Wu XJ. MAPK pathways are involved in the inhibitory effect of berberine hydrochloride on gastric cancer MGC 803 cell proliferation and IL-8 secretion *in vitro* and *in vivo*. *Mol Med Rep* 2016; **14**: 1430-1438 [PMID: 27278862 DOI: 10.3892/mmr.2016.5361]

43 **Babeu JP**, Boudreau F. Hepatocyte nuclear factor 4-alpha involvement in liver and intestinal inflammatory networks. *World J Gastroenterol* 2014; **20**: 22-30 [PMID: 24415854 DOI: 10.3748/wjg.v20.i1.22]

44 **Huang KW**, Reebye V, Czysz K, Ciriello S, Dorman S, Reccia I, Lai HS, Peng L, Kostomitsopoulos N, Nicholls J, Habib RS, Tomalia DA, Sætrom P, Wilkes E, Cutillas P, Rossi JJ, Habib NA. Liver Activation of Hepatocellular Nuclear Factor-4 α by Small Activating RNA Rescues Dyslipidemia and Improves Metabolic Profile. *Mol Ther Nucleic Acids* 2020; **19**: 361-370 [PMID: 31877412 DOI: 10.1016/j.omtn.2019.10.044]

45 **Shi J**, Dai R, Chen Y, Guo H, Han Y, Zhang Y. LncRNA LINP1 regulates acute myeloid leukemia progression *via* HNF4α /AMPK/WNT5A signaling pathway. *Hematol Oncol* 2019; **37**: 474-482 [PMID: 31325181 DOI: 10.1002/hon.2651]

46 **Lu H**. Crosstalk of HNF4*α* with extracellular and intracellular signaling pathways in the regulation of hepatic metabolism of drugs and lipids. *Acta Pharm Sin B* 2016; **6**: 393-408 [PMID: 27709008 DOI: 10.1016/j.apsb.2016.07.003]

47 **Yan ZQ**, Leng SH, Lu FE, Lu XH, Dong H, Gao ZQ. [Effects of berberine on expression of hepatocyte nuclear factor 4alpha and glucokinase activity in mouse primary hepatocytes]. *Zhongguo Zhong Yao Za Zhi* 2008; **33**: 2105-2109 [PMID: 19160796 DOI: 10.11569/wcjd.v15.i36.3842]

48 **Gao Y**, Yan Y, Guo J, Zhang Q, Bi D, Wang F, Chang Z, Lu L, Yao X, Wei Q. HNF4α downregulation promotes tumor migration and invasion by regulating Ecadherin in renal cell carcinoma. *Oncol Rep* 2019; **42**: 1066-1074 [PMID: 31322246 DOI: 10.3892/or.2019.7214]

49 **Nam S**, Chang HR, Kim KT, Kook MC, Hong D, Kwon CH, Jung HR, Park HS, Powis G, Liang H, Park T, Kim YH. PATHOME: an algorithm for accurately detecting differentially expressed subpathways. *Oncogene* 2014; **33**: 4941-4951 [PMID: 24681952 DOI: 10.1038/onc.2014.80]

50 **Endo M**, Nishita M, Fujii M, Minami Y. Insight into the role of Wnt5a-induced signaling in normal and cancer cells. *Int Rev Cell Mol Biol* 2015; **314**: 117-148 [PMID: 25619716 DOI: 10.1016/bs.ircmb.2014.10.003]

51 **Pai SG**, Carneiro BA, Mota JM, Costa R, Leite CA, Barroso-Sousa R, Kaplan JB, Chae YK, Giles FJ. Wnt/beta-catenin pathway: modulating anticancer immune response. *J Hematol Oncol* 2017; **10**: 101 [PMID: 28476164 DOI: 10.1186/s13045-017-0471-6]

52 **Kleszcz R**. The canonical Wnt pathway. *Postepy Biochem* 2019; **65**: 183-192 [PMID: 31643165 DOI: 10.18388/pb.2019_268]

53 **Xue Y**, Zhang L, Zhu Y, Ke X, Wang Q, Min H. Regulation of Proliferation and Epithelial-to-Mesenchymal Transition (EMT) of Gastric Cancer by ZEB1 *via* Modulating Wnt5a and Related Mechanisms. *Med Sci Monit* 2019; **25**: 1663-1670 [PMID: 30829316 DOI: 10.12659/MSM.912338]

54 **Zhang C**, Wang T, Wu H, Zhang L, Li K, Wang F, Chen Y, Jin J, Hua D. HEF1 regulates differentiation through the Wnt5a/β-catenin signaling pathway in human gastric cancer. *Biochem Biophys Res Commun* 2019; **509**: 201-208 [PMID: 30579603 DOI: 10.1016/j.bbrc.2018.12.104]

55 **Zhao L**, Liu Y, Tong D, Qin Y, Yang J, Xue M, Du N, Liu L, Guo B, Hou N, Han J, Liu S, Liu N, Zhao X, Wang L, Chen Y, Huang C. MeCP2 Promotes Gastric Cancer Progression Through Regulating FOXF1/Wnt5a/β-Catenin and MYOD1/Caspase-3 Signaling Pathways. *EBioMedicine* 2017; **16**: 87-100 [PMID: 28131747 DOI: 10.1016/j.ebiom.2017.01.021]

56 **Shojima K**, Sato A, Hanaki H, Tsujimoto I, Nakamura M, Hattori K, Sato Y, Dohi K, Hirata M, Yamamoto H, Kikuchi A. Wnt5a promotes cancer cell invasion and proliferation by receptor-mediated endocytosis-dependent and -independent mechanisms, respectively. *Sci Rep* 2015; **5**: 8042 [PMID: 25622531 DOI: 10.1038/srep08042]

57 **Ara H**, Takagishi M, Enomoto A, Asai M, Ushida K, Asai N, Shimoyama Y, Kaibuchi K, Kodera Y, Takahashi M. Role for Daple in non-canonical Wnt signaling during gastric cancer invasion and metastasis. *Cancer Sci* 2016; **107**: 133-139 [PMID: 26577606 DOI: 10.1111/cas.12848]

58 **Zhang Y**, Du J, Zheng J, Liu J, Xu R, Shen T, Zhu Y, Chang J, Wang H, Zhang Z, Meng F, Wang Y, Chen Y, Xu Y, Gu L. EGF-reduced Wnt5a transcription induces epithelial-mesenchymal transition *via* Arf6-ERK signaling in gastric cancer cells. *Oncotarget* 2015; **6**: 7244-7261 [PMID: 25779663 DOI: 10.18632/oncotarget.3133]

59 **Geng B**, Pan J, Zhao T, Ji J, Zhang C, Che Y, Yang J, Shi H, Li J, Zhou H, Mu X, Xu C, Wang C, Xu Y, Liu Z, Wen H, You Q. Chitinase 3-like 1-CD44 interaction promotes metastasis and epithelial-to-mesenchymal transition through β-catenin/Erk/Akt signaling in gastric cancer. *J Exp Clin Cancer Res* 2018; **37**: 208 [PMID: 30165890 DOI: 10.1186/s13046-018-0876-2]

60 **Liu Z**, Chen Z, Fan R, Jiang B, Chen X, Chen Q, Nie F, Lu K, Sun M. Over-expressed long noncoding RNA HOXA11-AS promotes cell cycle progression and metastasis in gastric cancer. *Mol Cancer* 2017; **16**: 82 [PMID: 28441948 DOI: 10.1186/s12943-017-0651-6]

61 **Dai B**, Ma Y, Yang T, Fan M, Yu R, Su Q, Wang H, Liu F, Yang C, Zhang Y. Synergistic effect of berberine and HMQ1611 impairs cell proliferation and migration by regulating Wnt signaling pathway in hepatocellular carcinoma. *Phytother Res* 2019; **33**: 745-755 [PMID: 30565332 DOI: 10.1002/ptr.6267]

World Journal of Gastrointestinal Oncology

Submit a Manuscript: https://www.f6publishing.com

World J Gastrointest Oncol 2022 April 15; 14(4): 858-871

DOI: 10.4251/wjgo.v14.i4.858

ISSN 1948-5204 (online)

ORIGINAL ARTICLE

Basic Study

Bi-specific T1 positive-contrast-enhanced magnetic resonance imaging molecular probe for hepatocellular carcinoma in an orthotopic mouse model

Xiao-Hong Ma, Kun Chen, Shuang Wang, Si-Yun Liu, Deng-Feng Li, Yong-Tao Mi, Zhi-Yuan Wu, Chun-Feng Qu, Xin-Ming Zhao

Specialty type: Oncology

Provenance and peer review: Invited article; Externally peer reviewed.

Peer-review model: Single blind

Peer-review report's scientific quality classification

Grade A (Excellent): 0
Grade B (Very good): 0
Grade C (Good): C
Grade D (Fair): 0
Grade E (Poor): 0

P-Reviewer: Muguruma N, Japan

Received: April 28, 2021
Peer-review started: April 28, 2021
First decision: July 14, 2021
Revised: August 31, 2021
Accepted: March 14, 2022
Article in press: March 14, 2022
Published online: April 15, 2022

Xiao-Hong Ma, Shuang Wang, Deng-Feng Li, Yong-Tao Mi, Xin-Ming Zhao, Diagnostic Radiology, National Cancer Center/National Clinical Research Center for Cancer/Cancer Hospital, Chinese Academy of Medical Sciences and Peking Union Medical College, Beijing 100021, China

Kun Chen, Zhi-Yuan Wu, Chun-Feng Qu, State Key Laboratory of Molecular Oncology, National Cancer Center/Cancer Hospital, Chinese Academy of Medical Sciences & Peking Union Medical College, Beijing 100021, China

Si-Yun Liu, GE Healthcare (China), Beijing 100176, China

Corresponding author: Xin-Ming Zhao, MD, Chairman, Professor, Diagnostic Radiology, National Cancer Center/National Clinical Research Center for Cancer/Cancer Hospital, Chinese Academy of Medical Sciences and Peking Union Medical College, No. 17 Panjiayuan Nanli, Chaoyang District, Beijing 100021, China. zhaoxinming@cicams.ac.cn

Abstract

BACKGROUND

Hepatocellular carcinoma (HCC) is the second leading cause of cancer-related mortality. HCC-targeted magnetic resonance imaging (MRI) is an effective noninvasive diagnostic method that involves targeting clinically-related HCC biomarkers, such as alpha-fetoprotein (AFP) or glypican-3 (GPC3), with iron oxide nanoparticles. However, *in vivo* studies of HCC-targeted MRI utilize single-target iron oxide nanoprobes as negative (T2) contrast agents, which might weaken their future clinical applications due to tumor heterogeneity and negative MRI contrast. Ultra-small superparamagnetic iron oxide (USPIO) nanoparticles (approximately 5 nm) are potential optimal positive (T1) contrast agents. We previously verified the efficiency of AFP/GPC3-double-antibody-labeled iron oxide MR molecular probe *in vitro*.

AIM

To validate the effectiveness of a bi-specific probe *in vivo* for enhancing T1-weighted positive contrast to diagnose the early-stage HCC.

METHODS

The single- and double-antibody-conjugated 5-nm USPIO probes, including anti-

AFP-USPIO (UA), anti-GPC3-USPIO (UG), and anti-AFP-USPIO-anti-GPC3 (UAG), were synthesized. T1- and T2-weighted MRI were performed on day 10 after establishment of the orthotopic HCC mouse model. Following intravenous injection of U, UA, UG, and UAG probes, T1- and T2-weighted images were obtained at 12, 12, and 32 h post-injection. At the end of scanning, mice were euthanized, and a histologic analysis was performed on tumor samples.

RESULTS

T1- and T2-weighted MRI showed that absolute tumor-to-background ratios in UAG-treated HCC mice peaked at 24 h post-injection, with the T1- and T2-weighted signals increasing by 46.7% and decreasing by 11.1%, respectively, relative to pre-injection levels. Additionally, T1-weighted contrast in the UAG-treated group at 24 h post-injection was enhanced 1.52-, 2.64-, and 4.38-fold compared to those observed for single-targeted anti-GPC3-USPIO, anti-AFP-USPIO, and non-targeted USPIO probes, respectively. Comparison of U-, UA-, UG-, and UAG-treated tumor sections revealed that UAG-treated mice exhibited increased stained regions compared to those observed in UG- or UA-treated mice.

CONCLUSION

The bi-specific T1-positive contrast-enhanced MRI probe (UAG) for HCC demonstrated increased specificity and sensitivity to diagnose early-stage HCC irrespective of tumor size and/or heterogeneity.

Key Words: Hepatocellular carcinoma; Molecular imaging; Magnetic resonance imaging; Positive contrast agent; Alpha-fetoprotein; Glypican-3

Core Tip: Use of single biomarkers might hinder the detection efficiency of existing hepatocellular carcinoma (HCC) molecular probes due to tumor heterogeneity, while negative (T2) contrast agents could result in inaccurate diagnoses. Therefore, we developed double-antigen-targeting magnetic resonance imaging (MRI) probes for hepatic tumors by conjugating alpha-fetoprotein or glypican-3 antibodies simultaneously to a 5-nm ultra-small superparamagnetic iron oxide (USPIO) and investigated its performance in orthotopic HCC mouse model. The bi-specific T1-positive contrast-enhanced MRI probe for HCC demonstrated increased specificity and sensitivity to diagnose early-stage HCC irrespective of tumor size and/or heterogeneity. Moreover, the *in vivo* enhancement of imaging by the USPIO probes appeared dose-dependent and requires further investigation.

Citation: Ma XH, Chen K, Wang S, Liu SY, Li DF, Mi YT, Wu ZY, Qu CF, Zhao XM. Bi-specific T1 positive-contrast-enhanced magnetic resonance imaging molecular probe for hepatocellular carcinoma in an orthotopic mouse model. *World J Gastrointest Oncol* 2022; 14(4): 858-871
URL: https://www.wjgnet.com/1948-5204/full/v14/i4/858.htm
DOI: https://dx.doi.org/10.4251/wjgo.v14.i4.858

INTRODUCTION

Hepatocellular carcinoma (HCC) is a human malignancy with a high incidence rate, affecting populations worldwide[1,2]. Non-invasive magnetic resonance imaging (MRI) is one of the most accessible and effective methods for clinical HCC screening, diagnosis, and prognosis. Additionally, MRI represents a comprehensive imaging technique which is uninfluenced by ionized radiation and is capable of both morphological and functional imaging. Multiple MRI techniques have been developed including diffusion-weighted imaging[3], perfusion-weighted imaging[4], iron quantification[5], and contrast-agent-based imaging, which use gadolinium hepatobiliary contrast agents or superparamagnetic iron oxide nanoparticles[6,7] for early-stage HCC identification. Functional MRI is of adequate sensitivity and accuracy to diagnose typical HCC with a tumor diameter > 1 cm; however, it remains challenging to identify benign and malignant tumors < 1 cm or micro-hepatocellular carcinoma (MHCC) due to undetectable changes in blood supply or a lack of specificity from imaging contrast agents[8,9].

Molecular MRI has led to the development of new strategies to enhance specificity and contrast for early detection of small cancerous tumors[10-12]. The latter has been used by binding early-stage cancer biomarkers with superparamagnetic iron nanoparticles in order to enable active cancer-cell targeting

[13]. The sensitivity and specificity of this technique is dependent on the expression levels of the target molecules, the magnetic relaxivity of the nanoparticles, and the imaging scheme is unlimited by changes in blood supply. Additionally, the active targeting strategy and use of nanoparticles allow for increased specificity and sensitivity than hepatobiliary contrast agents, which are based on hypointense signals associated with cancer foci against normal hepatic parenchyma and solid benign lesions that uptake the agents differently[14,15].

HCC-targeted MRI systems have demonstrated their preclinical effectiveness *in vitro* and *in vivo*. These methods involve binding HCC biomarkers (antibodies, aptamers, or peptide ligands) to iron oxide nanoparticles in order to target clinical HCC-related overexpressed antigens, such as alpha-fetoprotein (AFP) or glypican-3 (GPC3)[16-20]. AFP is a widely used HCC serum biomarker with a specificity and sensitivity of up to 96% and 65%, respectively, and false-positive and false-negative detection rates of approximately 40%[21]. GPC3 is a promising early HCC tissue biomarker expressed on the cell membrane. The biomarker is highly specific for HCC tumors (84.6%) but rare in normal liver parenchyma or benign lesions[22-24]. There are certain limitations of HCC MRI molecular probes. First, single biomarkers might hinder detection efficiency of existing HCC molecular probes due to tumor heterogeneity. Additionally, iron oxide nanoparticles used in the majority of current HCC imaging studies are utilized as negative (T2) contrast agents, which could result in inaccurate diagnosis[25,26]. However, opportunities to improve these probes also exist.

Nanoparticles exhibit size-dependent magnetic properties. Ultra-small superparamagnetic iron oxide (USPIO) nanoparticles of a small core size (approximately 5 nm) are suggested as optimal positive (T1) contrast agents that enhance T1 and suppress T2 signals induced by reductions in volume of magnetic anisotropy, surface spin disorder, and exposure of iron ions with unpaired electrons[26-30]. Additionally, slow phagocytosis of USPIO nanoparticles by macrophages makes them ideal for liver-tumor MRI[31-33]. However, there have been controversial results concerning the T1-specific effects of targeted USPIO probes *in vivo*, mainly concerning whether probe clustering suppresses T1-related effects[26].

Therefore, in this study, we developed double-antigen-targeting MRI probes for HCC tumors by conjugating the AFP and GPC3 antibodies simultaneously to a 5-nm USPIO probe. Our previous study demonstrated that compared with single-target probes, bi-specific probes enhanced the T2-weighted contrast in Hepa1-6 cells expressing AFP and GPC3[34]. The aim of the present study was to provide an *in vivo* validation of the effectiveness of a bi-specific probe for enhancing T1-weighted positive contrast to overcome tumor-heterogeneity limitations in early-stage HCC diagnosis. To this end, we established an orthotopic HCC mouse model and injected double-antigen-targeting MRI probes to investigate probe specificity, sensitivity, and T1/T2 MRI properties using a 3.0 Tesla clinical MR scanner and histologic analysis, relative to observations using single-antibody-labeled and unlabeled USPIO probes.

MATERIALS AND METHODS

Reagents, antibodies, and animals

N-succinimidyl ester-functionalized 5-nm USPIO probes were purchased from Sigma-Aldrich (747440; St. Louis, MO, United States). The alpha fetoprotein antibodies were obtained from Abcam (rabbit monoclonal, ab213328; mouse monoclonal, ab212325; Cambridge, United Kingdom). GPC3 antibodies were obtained from Abcam (rabbit polyclonal, ab66596) and R&D Systems (mouse monoclonal, MAB2119; Minneapolis, MN, United States). Other chemical agents were purchased from Sigma-Aldrich and of analytical grade.

Male C57BL/6J (C57) mice (8–12 weeks old) were purchased from Vital River Laboratory Animal Technology (Beijing, China). The study protocols (NCC2015A011) were approved by the Animal Care and Use Committee of Cancer Hospital, Chinese Academy of Medical Sciences (CH-CAMS). All the mice were maintained under specific pathogen-free conditions at the Laboratory Animal Services Center of CH-CAMS. The animal protocol was designed to minimize pain or discomfort to the animals. The animals were acclimatized to laboratory conditions (23 °C, 12 h/12 h light/dark, 50% humidity, ad libitumaccess to food and water) for 2 wk prior to establishment of HCC model.

Preparation and physical characterization of antibody conjugated USPIO probes

The synthesis of single- and double-antibody-conjugated USPIO probes, including anti-AFP-USPIO (UA), anti-GPC3-USPIO (UG), and anti-AFP-USPIO-anti-GPC3 (UAG), was performed according to our previously described protocol[34]. Briefly, 18 mg/mL N-succinimidyl ester-functionalized 5-nm USPIO (abbreviated as U) were reacted separately or simultaneously with AFP (ab212325) and GPC3 (MAB2119) antibodies (400 μg/mL each) in phosphate-buffered solution (pH 7.4) at a final volume of 1 mL with gentle stirring for 3 h at room temperature approximately 23 °C to form the final probes.

The morphology and size distribution of the USPIO core were characterized by transmission electron microscopy (TEM; FEI Tecnai G² F30; FEI, Hillsboro, OR, United States) using an acceleration voltage of 300 kV. The hydrodynamic diameters of the U, UA, UG, and UAG probes were measured by dynamic light scattering (DLS; Zetasizer Nano ZS90, Malvern Instruments, Malvern, United Kingdom) using a

non-invasive back scatter mode with a detected scattering angle of 173° at 25 °C.

USPIO phantom imaging and quantitative analysis

To investigate the MRI characteristics of USPIO, the phantom was constructed using USPIO water solutions with gradient concentrations, which were transferred to individual wells (300 μL) of a 96-well plate (iron concentrations of each USPIO solution: 5, 2, 1.5, 1, 0.75, 0.5, 0.25, 0.1 0.05, and 0.01 mM).

Phantom MRI was performed using a 3.0 Tesla clinical MR scanner (750W; GE Healthcare, Pittsburgh, PA, United States) with an 8-channel head coil. The T1-relaxation times were measured by IR sequence with a fixed echo time (TE) of 7 ms, repetition time (TR) of 2000 ms, and multiple inversion times (TI; 1800, 1500, 1100, 800, 500, 300, 200, and 100 ms). T2 images were acquired using spin echo (SE) sequence with different TE (10–170 ms). The parameters were set as follows: TR (2000 ms), TE (10, 20, 30, 40, 50, 70, 90, 110, 130, 150, and 170 ms), matrix (256 × 256), field of view (FOV; 20 × 20 mm), slice thickness/separation (3 mm/3.3 mm), and number of excitations (NEX; 2.0).

$$SI = A \times [1 - 2 \times \exp(-TI/T1) + \exp(-TR/T1)] \quad \text{Eq. (1)}$$

$$SI = A \times \exp(-TE/T2) + C \quad \text{Eq. (2)}$$

$$(1/T_i)_w = (1/T_i)_{wo} + r_i[\text{Fe}],\ i = 1,2 \quad \text{Eq. (3)}$$

During data analysis, the two slices in the center at axial view of MRI images for cylinder samples in the 96-well plate were chosen for further analysis. T1- and T2-relaxation times were analyzed in a voxel-based manner by fitting measured T1-signal intensity versus TI according to Eq. (1) and T2-signal intensity versus TE according to Eq. (2), respectively. The proton relaxivities (r_1: Longitudinal relaxivity; and r_2: Transverse relaxivity) were obtained from linear regression according to Eq. (3)[35,36]. $(1/T_i)_w$ and $(1/T_i)_{wo}$ represent water-proton relaxation rates (the inverse values of the T1- and T2-relaxation times) in the presence and absence of USPIO.

In vivo experimental procedure

In vivo experiments were performed as illustrated in Figure 1. First, orthotopic HCC models were established using C57 mice. The tumors were allowed to develop for 9 d after inoculation, and mice were prepared for *in vivo* MRI on day ten. Before each USPIO probe injection, the HCC mice were scanned for pre-injection (0 h; baseline) T1- and T2-weighted image collection. Following intravenous probe injection of U, UA, UG, and UAG, T1- and T2-weighted images were collected at 12, 12, and 32 h post-injection. At the end of scanning, mice were euthanized, and histological analyses were performed on tumor samples.

Orthotopic HCC mouse model

Hepa1-6 murine hepatoma cells were purchased from ATCC (CRL-1830; Manassas, VA, United States). GPC3-expressing Hepa1-6 cells (Hepa1-6/GPC3) were established in our laboratory, as previously reported[37], and maintained using standard protocols on media supplemented with 1 mg/mL G418 (Invitrogen, Carlsbad, CA, United States). Hepa1-6/GPC3 cells at the proliferation phase were then cultured in the absence of G418 overnight to generate orthotopic HCC in 8-week-old C57BL/6J mice with weight of 18-20 g. The mice were anesthetized with tribromoethanol (Avertin) at a dosage of 400 mg/kg body weight *via* intraperitoneal injection. The abdominal cavity below the sternum was opened, and the liver was exposed under sterile conditions. A total of 10^6 Hepa1-6/GPC3 cells in 20 μL RPMI-1640 were injected under the liver capsule using a precise micro-syringe (Becton, Dickinson and Company, New Jersey, United States). The tumors were developed after inoculation and were suitable for *in vivo* MRI on day 10.

In vivo MRI assessment

In vivo MRI studies were performed on the 3.0 Tesla MR device (GE Healthcare) with a 4-channel animal coil. During scanning, the abdominal region of the mouse was placed at the center of the coil, with the liver as the target.

Mice were anesthetized using tribromoethanol (Avertin) at a dosage of 400 mg/kg body weight *via* intraperitoneal injection. The anesthesia normally took effect at 3- to 5-min post-injection and was sustained for approximately 30 to 45 min. The anesthetic was kept on ice during the experiment. Solutions of the U, UA, UG, and UAG probes were transferred into medical-grade physiological saline (0.9% sodium chloride; pH = 7.5) with a final usage volume of 200 μL.

Prior to the USPIO probe injection, 12 HCC model mice were anaesthetized. T1- and T2-weighted imaging was conducted successively on all mice in order to select a minimum of eight with observable or obvious tumors. The eight mice were then divided into four groups, each of which was treated with either of the U, UA, UG, or UAG probes, respectively, prior to further MRI experiments. Pre-injection images were recorded as 0 h data, followed by administration of the U, UA, UG and UAG probe solution *via* tail-vein injection at a dose of 0.8 mg Fe/kg (or 1.6 mg Fe/kg) over 5 s when the mice were awake. Mice underwent *in vivo* MRI at 12, 12, and 32 h post-injection. The U-treated animal group was used as the control for comparison with the UA-, UG-, and UAG-treated groups.

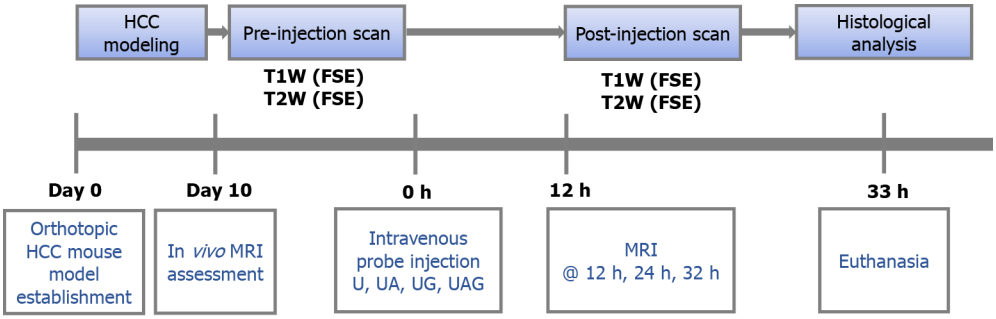

DOI: 10.4251/wjgo.v14.i4.858

Figure 1 Experiment workflow. Probe treatment and T1- and T2-weighted magnetic resonance imaging were performed on day 10 after establishment of the orthotopic hepatocellular carcinoma mouse model. MRI: Magnetic resonance imaging; HCC: hepatocellular carcinoma; UA: Anti-AFP-USPIO; UG: Anti-GPC3-USPIO; UAG: Anti-AFP-USPIO-anti-GPC3.

Anesthesia was administered at each time point (12, 24, and 32 h) post-injection; however, the subsequent dosage was reduced by 50% compared to the first dosage at 0 h in order to protect the mice and reduce drug resistance.

T1- and T2-weighted images for each USPIO probe were acquired after administering anesthesia using the same MRI sequence used for pre-injection scanning: (1) Axial T1-weighted image/FSE with TR/TE = 475/10 ms, FOV = 60 mm × 60 mm, matrix = 512 × 512, resolution = 0.1172 mm × 0.1172 mm, slice thickness/slice separation = 0.8 mm/1.6 mm, and NEX = 4.0; and (2) Axial T2-weighted image/fast SE with TR/TE = 1500/92 ms, FOV = 60 mm × 60 mm, matrix = 512 × 512, resolution = 0.1172 mm × 0.1172 mm, and slice thickness/slice separation = 0.8 mm/1.6 mm.

T1- and T2-signal enhancement in the tumor respective to the background was analyzed by manually drawing a region of interest (ROI) around the tumor and normal liver parenchyma. To assess tumor intensity, the largest cross section of the tumor was delineated along the outer margin on the T1-weighted or T2-weighted images and the mean intensities were recorded. Considering that the tumor might not be recognized on the T1-weighted images at the pre-injection time point, the tumor was delineated on the pre-injection T2-weighted images and copied to the T1-weighted images for intensity calculation. For liver parenchyma intensity, a ROI with an approximately 3 mm^2 area on the liver lobes next to the tumor was drawn 2-3 times at different positions. The average of the mean intensity in these ROIs were then taken as the final background liver intensity. Next, the mean intensity of the tumor was divided by the averaged liver background intensity to obtain the tumor-to-background (T/B) ratio. The T/B ratio of mean intensity for the two ROIs was calculated to describe the signal enhancement resulting from each USPIO probe, and the ratio values were averaged for two mice from UAG-, UG-, UA-, and U-treated groups (0.8 mg Fe/kg dosage) respectively if the image quality was acceptable at each time point. The increase of T/B ratios at 12, 12, and 32 h post-injection relative to that at 0 h (pre-injection) were used to describe the binding effect of the probe to the tumor site.

Histologic analysis

Mice were euthanized after MR scanning, and the livers were harvested for histological analysis. Fresh tissues were fixed with 10% paraformaldehyde and embedded in paraffin, after which they were cut into 5-μm thick serial sections. The sections were immunochemically stained according to manufacturer instructions with monoclonal rabbit anti-mouse anti-AFP (ab213328; Abcam) or polyclonal rabbit anti-mouse anti-GPC3 (ab66596; Abcam). Adjacent slices were used for hematoxylin and eosin (H&E) and Prussian Blue staining, respectively. All stained sections were examined under a light microscope at 4 ×, 10 ×, and 20 × magnification. The expression level of AFP or GPC3 and concentrated USPIO were further analyzed by quantifying the ratio of three 3′-diaminobenzidine (DAB-) or Prussian-blue-stained pixels from the tumor region using Image J (Wayne Rasband and contributors, National Institutes of Health, United States. http://imagej.nih.gov/ij).

RESULTS

Physical characterization of antibody conjugated USPIO probes

As previously reported[34], the USPIO probes were uniformly dispersed and exhibited a core diameter of 4.88 ± 0.16 nm and an average hydrodynamic diameter of 40.46 ± 0.53 nm. After antibody binding to the USPIO surface, the average hydrodynamic size of UA, UG, and UAG increased to 56.48 ± 0.52 nm, 54.76 ± 1.02 nm, and 59.60 ± 1.87 nm, respectively. The zeta potentials of UA, UG, and UAG were -12.74 mV, -11.22 mV, and -10.23 mV, respectively, varying from the zeta potential of unlabeled USPIO (-26.13 mV).

USPIO phantom MRI and quantitative analysis

The core diameter (4.88 ± 0.16 nm) of USPIO suggests that it has a good potential as a positive contrast agent[26,28,38]. In the present study, we collected the T1- and T2-weighted images of the phantom (Figure 2A and B) and observed positive enhancement (brighter images at higher USPIO concentrations) of the T1-weighted signal and negative enhancement (darker images at higher USPIO concentrations) of the T2-weighted signal according to USPIO concentration. However, the enhancement of the T1-weighted signal was reversed and began decreasing in the absence of iron at a concentration of 0.75 mM.

The T1 and T2 maps calculated for each USPIO concentration were illustrated in Figure 2C. The longitudinal and transversal relaxation times for the T1 and T2 signals, respectively, were calculated from mean values from the T1 and T2 maps for each USPIO concentration. By using the linear fitting, the proton-relaxation rates ($R_1 = 1/T_1$; and $R_2 = 1/T_2$) with respect to the iron ion concentrations according to Eq. (3), we obtained molar relaxivities (r_1 and r_2) of 0.698 ± 0.017 $mM^{-1} \cdot s^{-1}$ and 41.017 ± 1.484 $mM^{-1} \cdot s^{-1}$, respectively (Figure 2D and E).

In vivo MRI

T1- and T2-weighted MRIs were performed before and after intravenous injection of the U, UA, UG, and UAG probes into HCC models, respectively (Figures 3 and 4). The T/B ratios of the enhanced T1- and T2-weighted signal intensity enhancement (or increasing rates relative to pre-injection signals) at each time point were calculated and plotted (Figure 5).

We found that the T1- and T2-weighted images showed the tumor site in both dark and bright contrast prior to the administration of each USPIO probe, respectively, which agreed with clinical HCC-diagnosis guidance. For the T1-weighted MRI, we observed a non-homogeneous, brightened signal at HCC foci in mice receiving UAG or UG probes at 24 h post-injection. The T1-weighted T/B signal ratio (TBSR) for UAG-treated mice increased by 46.7% relative to baseline (0 h) and was higher than that of the other probes at approximately 24 h post-injection, which decreased over time. This indicated that the UAG exhibited a higher binding efficiency with the tumor site. UG-treated and UA-treated livers showed a similar trend in signal intensity as those treated with UAG probes, with a 30.7% and 17.7% increase in T1-weighted TBSR at 24 h post-injection relative to baseline, respectively, which was higher than the intensities observed in mice injected with the U probes. However, the intensity contrast trend over time for mice receiving U probes was unclear. It showed a weak signal peak at approximately 12 h post-injection, with a 12.1% increase in intensity relative to pre-injection levels, while some fluctuations also existed after 12 h time point.

For the T2-weighted MRI, the tumor site showed an initially bright image that darkened after the administration of the targeted USPIO probes. Compared to the pre-injection levels, the TBSR for UAG-treated mice decreased by 11.1% at 24 h post-injection and then increased again over time. Additionally, the ratios in UG- and UA-treated mice increased until 12 h, which subsequently decreased. The ratio in UG-treated mice decreased to its minimum level at 24 h post-injection, with an approximately 1.3% increase in ratio compared with pre-injection. The ratio in UA-treated mice decreased at 24 h post-injection and subsequently decreased by 32.8% at 32 h post-injection with an unknown trend due to measurement suspension. Moreover, the ratio in U-treated mice showed a weak decreasing trend after probe injection until reaching a 9.4% decrease at 24 h compared with pre-injection, which subsequently increased.

Figure 6 illustrated the T1- and T2-weighted images of HCC-mouse livers treated with higher dosages of the UAG probe (1.6 mg Fe/kg body weight), revealing T1-hyperintense and T2-hypointense shrinkage of the tumor at 24 h post-injection of the probes.

Histological analysis

Histological analysis and Prussian Blue staining were used to detect iron uptake and were analyzed qualitatively to evaluate the establishment of the HCC model and *in vivo* MRI results (Figure 7). H&E staining results for U-, UA-, UG-, and UAG-treated livers showed that the tumor cells in the HCC tissues were irregular, with imbalanced nucleus: Cytoplasm ratios and were mostly distributed in lumps. Immunochemical staining verified that the AFP and GPC3 antigens were primarily expressed in the HCC tissue, whereas few were observed in hepatic parenchyma of the same liver.

Uptake of different USPIO probes by the HCC tissue was evaluated by iron Prussian Blue staining (Figure 7). We observed an increase of stained areas distributed in HCC tissues relative to normal liver tissues. A comparison of the U-, UA-, UG-, and UAG-treated tumor sections revealed that UAG-treated mice exhibited a higher accumulation of stained regions relative to those observed in UG- or UA-treated mice. The semi-quantitative results summarized in Supplementary Table 1 might also indicate that UAG-treated mice had higher iron concentrations and targeting specificity in the tumor under similar expression levels for AFP or GPC3. Additionally, all of the targeted USPIO probes exhibited a higher uptake rate for the HCC tissues when compared to the non-targeted USPIO probes. These results indicated that the double-antigen-targeted UAG probe targeted the HCC tissues more effectively than the single-targeted or non-targeted USPIO probes.

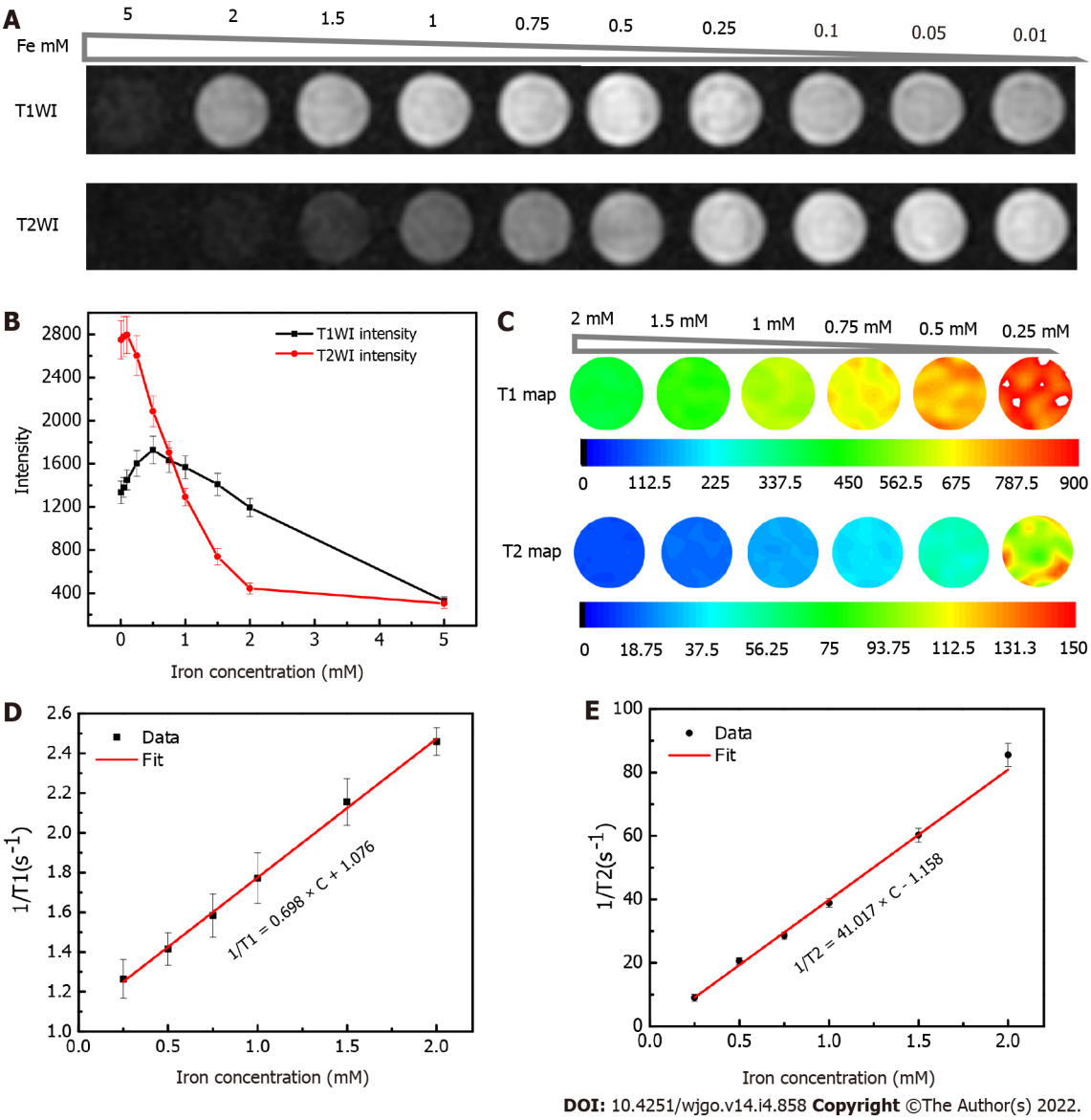

DOI: 10.4251/wjgo.v14.i4.858 **Copyright** ©The Author(s) 2022.

Figure 2 Magnetic resonance imaging properties of ultra-small superparamagnetic iron oxide phantoms. A: T1- and T2-weighted images of a series of 0.9% saline water solutions containing different concentrations of the ultra-small superparamagnetic iron oxide probes as indicated by iron concentration; B: Changes in the T1- and T2-weighted signal intensities according to iron concentration, with standard deviation also illustrated; C: T1 and T2 map illustrated in pseudo color under different iron concentration; D: Linear regression fitting of the longitudinal relaxation-rate (1/T1); E: transversal relaxation-rate (1/T2) data *vs* different iron concentrations (with standard deviation also illustrated) for extracting the longitudinal relaxivity (r_1) and transverse relaxivity (r_2), respectively.

DISCUSSION

The diagnosis of early-stage HCC is crucial for the establishment of a treatment strategy and for improving prognosis. To this end, molecular probes with high specificity and sensitivity are highly efficacious for HCC imaging. The present study has provided preliminary data supporting the *in vivo* efficacy of USPIO (5-nm core size)-conjugated AFP and GPC3 antibodies for use as a double-antigen-targeted MR molecular probe for HCC. Thereby supporting our hypothesis that it would demonstrate improved targeting efficiency relative to USPIO labeled with a single-antibody or non-targeted USPIOs and functions as a positive contrast agent. We propose that the double-antibody strategy might increase cancer-cell selection and enable tumor-specific diagnosis, regardless of tumor heterogeneity.

We chose the AFP and GPC3 antibodies as biomarkers for HCC targeting. Although several studies demonstrated the feasibility of peptide ligands as biomarkers for binding GPC3[20], we used monoclonal antibodies in the present study to ensure their homogeneity, purity, and avidity.

The histological results demonstrated the preference of the GPC3- and AFP-conjugated USPIO probes (UA, UG, and UAG) for antigen-expressing tumor sites, without any pronounced deposition of the probes in the liver parenchyma. *In vivo* MRI (Figures 3 and 4) provided evidence of the increased tumor-targeting efficiency of the UAG, compared to that observed in single-antibody UG or UA probes, with all of the targeted probes displaying improved specificity than the non-targeted USPIO probe.

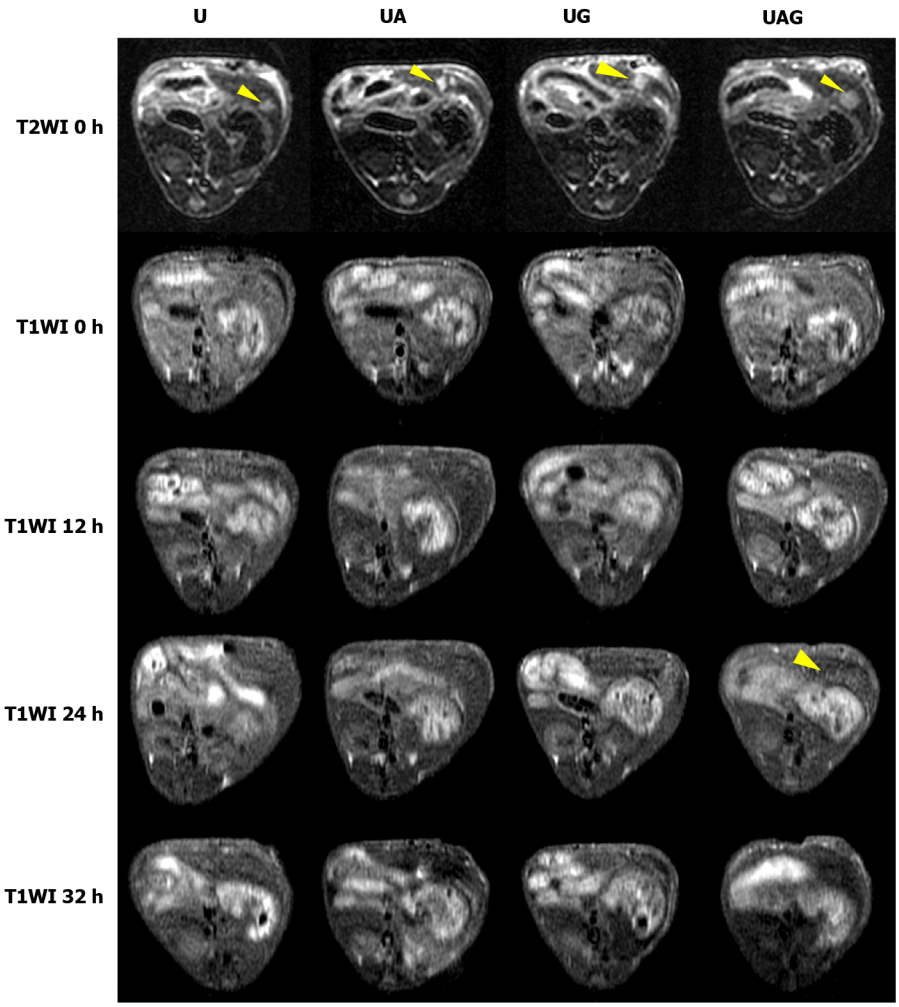

DOI: 10.4251/wjgo.v14.i4.858

Figure 3 T1-weighted images of hepatocellular carcinoma-model mice administered with ultra-small superparamagnetic iron oxide probes at various time points. Columns represent livers treated with different probes, and the first row shows pre-injection (0 h) T2-weighted images as references for the tumor location indicated by yellow arrowhead. UA: Anti-AFP-USPIO; UG: Anti-GPC3-USPIO; UAG: Anti-AFP-USPIO-anti-GPC3.

Additionally, T1- and T2- weighted MRIs showed that the absolute TBSRs in UAG-treated mice were higher than those in UG-, UA-, and U-treated mice at 24 h post-injection. These results were congruent with those of *in vitro* MRI experiments, showing that UAG-treated Hepa1-6 cells displayed the best T2-weighted contrast[37]. Based on these results, the higher degree of specificity in the binding of UAG to HCC tumors *in vivo* at 24 h post-injection represented the optimal imaging time point for HCC tumors.

Moreover, UG-treated livers showed a similar signal trend to that of UAG-treated livers, with maximal enhancement of the T1-weighted TBSR at 24 h post-injection and higher ratios than that of UA and U probes. This might imply a predominant targeting function by the GPC3 antibody on the part of the UAG probes. Furthermore, the maximum T1-weighted TBSR in UAG-treated mice at 24 h and the 1.24-fold enhancement in the ratio for UA-treated livers compared with U-treated livers at 12 h post-injection might suggest that the AFP antibody was involved in enhancing probe targeting efficiency. However, the signal trend for UA-treated livers was not as significantly distinguishable as those treated with UAG- or UG-, when they were compared with livers signal treated with non-targeted USPIO probes. GPC3 expressed on the cell membrane differed from AFP, which is an antigen secreted into the cytoplasm. We chose AFP as a target based on the tumor site to likely be harboring concentrated amounts of AFP antigens that could be secreted into the serum. Although adding biomarkers for cytoplasmic targeting might help enhance the specificity of double-marker-labeled probes, the optimization of single-target probes specific for cytoplasmic sites might require further consideration.

Iron oxide nanoparticles are widely used for molecular MRI imaging because of their relevant advantages including superparamagnetism, chemical modification, and biosafety[39,40]. The surface modification and hydrodynamic size of iron oxide nanoparticles are essential for optimizing delivery efficiency to their cellular targets[41,42]. Additionally, the core size of the iron oxide nanoparticles significantly influenced their magnetic properties and the MRI effect[27,29,38]. In the present study, N-succinimidyl ester-functionalized USPIO with a core size < 5 nm was purchased and conjugated with AFP and GPC3 antibodies for evaluation as double-antigen-targeting molecular MRI probes for HCC.

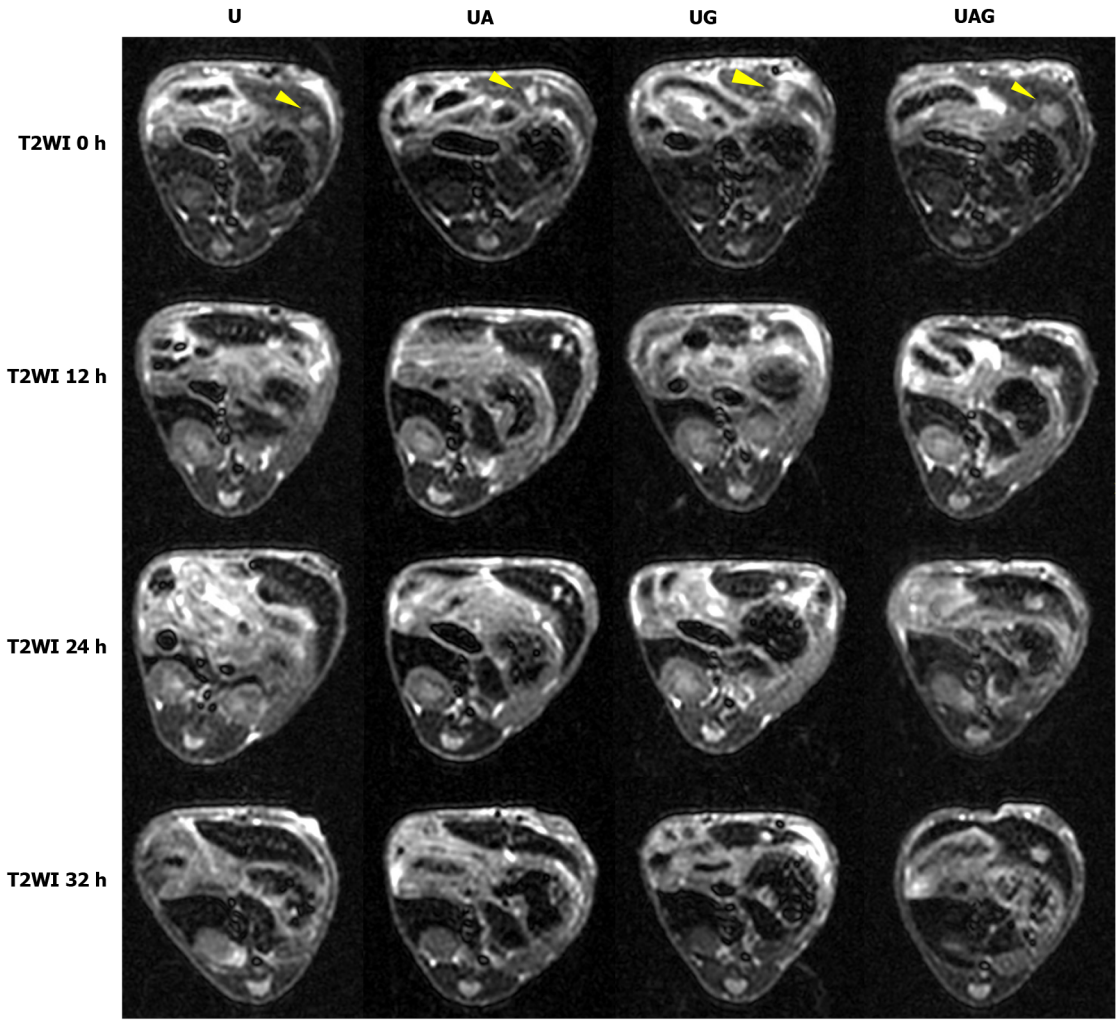

DOI: 10.4251/wjgo.v14.i4.858

Figure 4 T2-weighted images of hepatocellular carcinoma-model mice administered ultra-small superparamagnetic iron oxide probes at various time points. Columns represent livers treated with different probes. (Yellow arrowhead: tumor location). UA: Anti-AFP-USPIO; UG: Anti-GPC3-USPIO; UAG: Anti-AFP-USPIO-anti-GPC3.

DLS measurements of the U, UA, UG, and UAG probes showed that the hydrodynamic sizes of both double- and single-antibody labeled USPIO probes remained within a range of 50–60 nm. This has the potential to promote applications to determine tumor-vessel permeability and retention effects while avoiding phagocytosis by macrophages rich in normal liver tissue or quick renal clearance[31,41-44]. Moreover, the negative zeta potentials of each of the probes allowed for deeper penetration into tissues [43].

To evaluate the MRI-specific properties of the USPIO probes, we performed both phantom and *in vivo* studies. Phantom results showed that the USPIO probes either positively or negatively enhanced the T1- and T2-weighted signal and shortened the T1- and T2-relaxation times (r_1 = 0.698 $mM^{-1}·s^{-1}$; r_2 = 41.017 $mM^{-1}·s^{-1}$). However, the shortening of r_1 was dose-dependent, and the overdose effect that weakened enhancement of the T1 signal was attributed to the increased T2-relaxation rate observed at higher iron concentrations, which was consistent with previous studies[26]. Therefore, we found that a moderate dosage of 0.8 mg Fe/kg body weight was adequate for the *in vivo* experiments and allowed the determination of T1- and T2-weighted TBSRs for UAG-treated mice at different time points before and after probe injection, up to 24 h post-injection. This differed from a previous report as the aggregation of USPIO probes at the target might have diminished their T1 performance[26]. It is possible that the feasibility of targeted USPIO probes as positive contrast agents is dosage-dependent, as reflected in the T1-hyperintense signal observed at an increased UAG dosage of 1.6 mg Fe/kg body weight (Figure 6). For T2-weighted MRI, only the TBSR in UAG-treated mice showed the best negative enhancement, with an 11.1% decrease until 24 h post-injection relative to the pre-injection TBSR, which was similar to that observed from T1-weighted imaging. The other probes, (UA, UG, and U) did not show significant T2 enhancement or showed a relatively weaker enhancement compared with UAG-treated samples during the first 24 h after probe injection. This might suggest that the double-conjugated antibodies on the UAG probe helped accelerate target recognition during circulation and competed with signal decreases

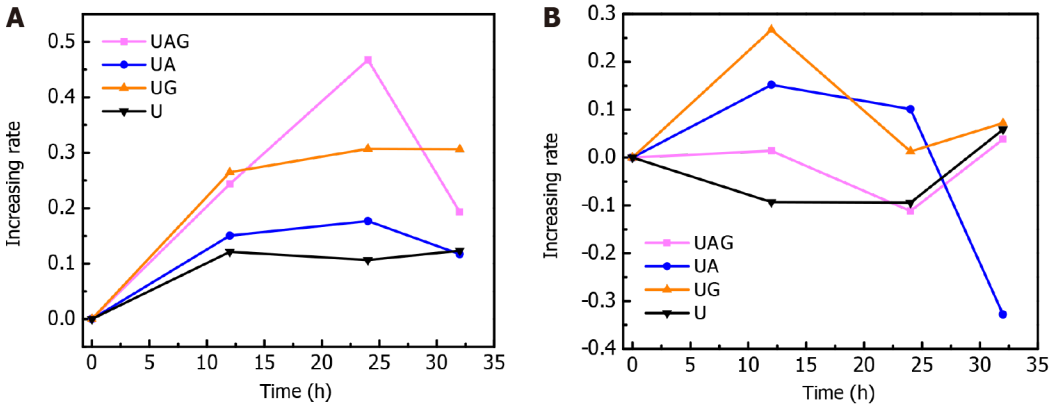

DOI: 10.4251/wjgo.v14.i4.858 **Copyright** ©The Author(s) 2022.

Figure 5 Time-dependent increasing rates of T1- and T2-weighted T/B signal ratios. Increasing rates of T1- and T2-weighted T/B signal ratio at different time points (12, 24, and 32 h) post-injection as compared with pre-injection (0 h) of the U, anti-alpha-fetoprotein (AFP)-ultra-small superparamagnetic iron oxide (USPIO), anti-glypican-3 (GPC3)-USPIO, and anti-AFP-USPIO-anti-GPC3 probes. Data points represent averaged rates from two mice if the image quality was acceptable. A: T1-weighted T/B signal ratios; B: T2-weighted T/B signal ratios. UA: Anti-AFP-USPIO; UG: Anti-GPC3-USPIO; UAG: Anti-AFP-USPIO-anti-GPC3.

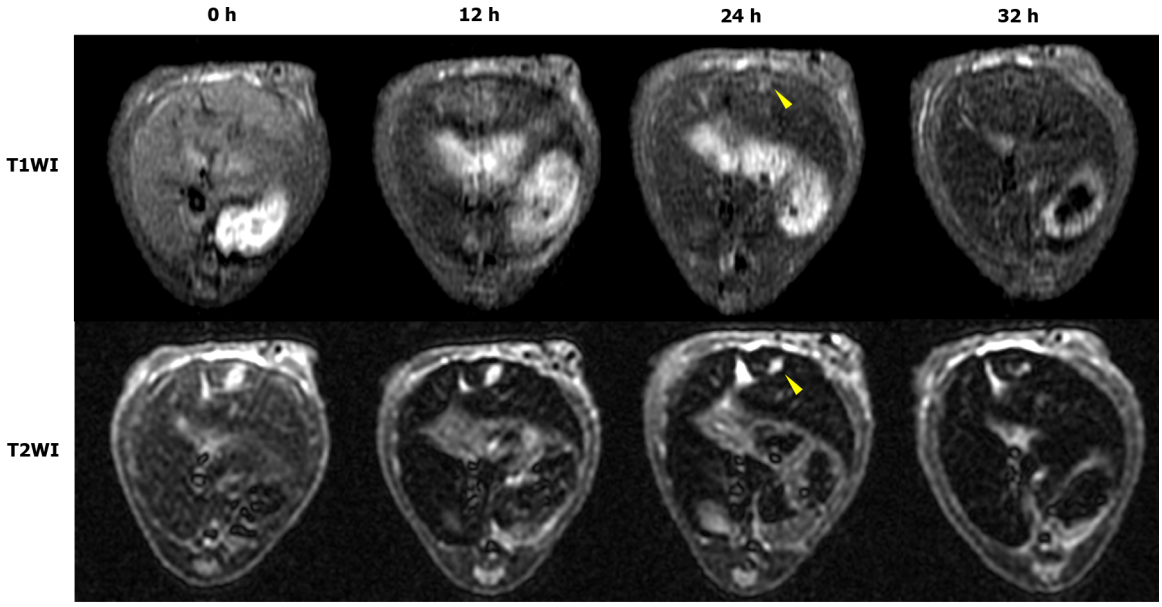

DOI: 10.4251/wjgo.v14.i4.858 **Copyright** ©The Author(s) 2022.

Figure 6 T1- and T2-weighted images of hepatocellular carcinoma-model mice treated with the anti-alpha-fetoprotein-ultra-small superparamagnetic iron oxide-anti-glypican-3 probe (1.6 mg Fe/kg body weight). Top (T1WI) and bottom (T2WI) rows, from left to right: T1- and T2-weighted images, respectively, at 0 h (pre-injection) and 12-, 24-, and 32-h (post-injection). (Yellow arrowhead: Tumor location).

resulting from normal liver uptake.

Clinical hepatobiliary contrast agents primarily bind to organic anion-transporting polypeptides (OATPs) expressed in normal hepatocytes in order to distinguish HCC lesions exhibiting low-level OATP expression. The success of OATP-based agents is highly dependent upon liver function and might lead to confusion for other diseases also exhibiting low-level OATP expression, such as liver metastasis without knowledge of the primary tumor[20,45]. Additionally, the advantages of OATP-based probes are fewer for MHCC exhibiting tumor sizes of < 1 cm[8,20,46]. The double-antibody labeled MRI probes used in the present study allowed for the direct recognition of multiple tumor biomarkers to enhance detection specificity and sensitivity, and has the potential to improve the diagnostic performance for HCC. Specifically, the positive contrast enhancement renders such targeted probes as efficacious for clinical study, although the optimal dosage and imaging time points require further investigation.

This study had several limitations. Firstly, the conjugation of two antibodies might increase the effective molecular weight of the probe and influence its circulation or infiltration rate. We found that the optimal imaging time was approximately 24 h post-injection of the probe, which might be clinically taxing. However, based on the double-labeling strategy described here, it might be possible to utilize

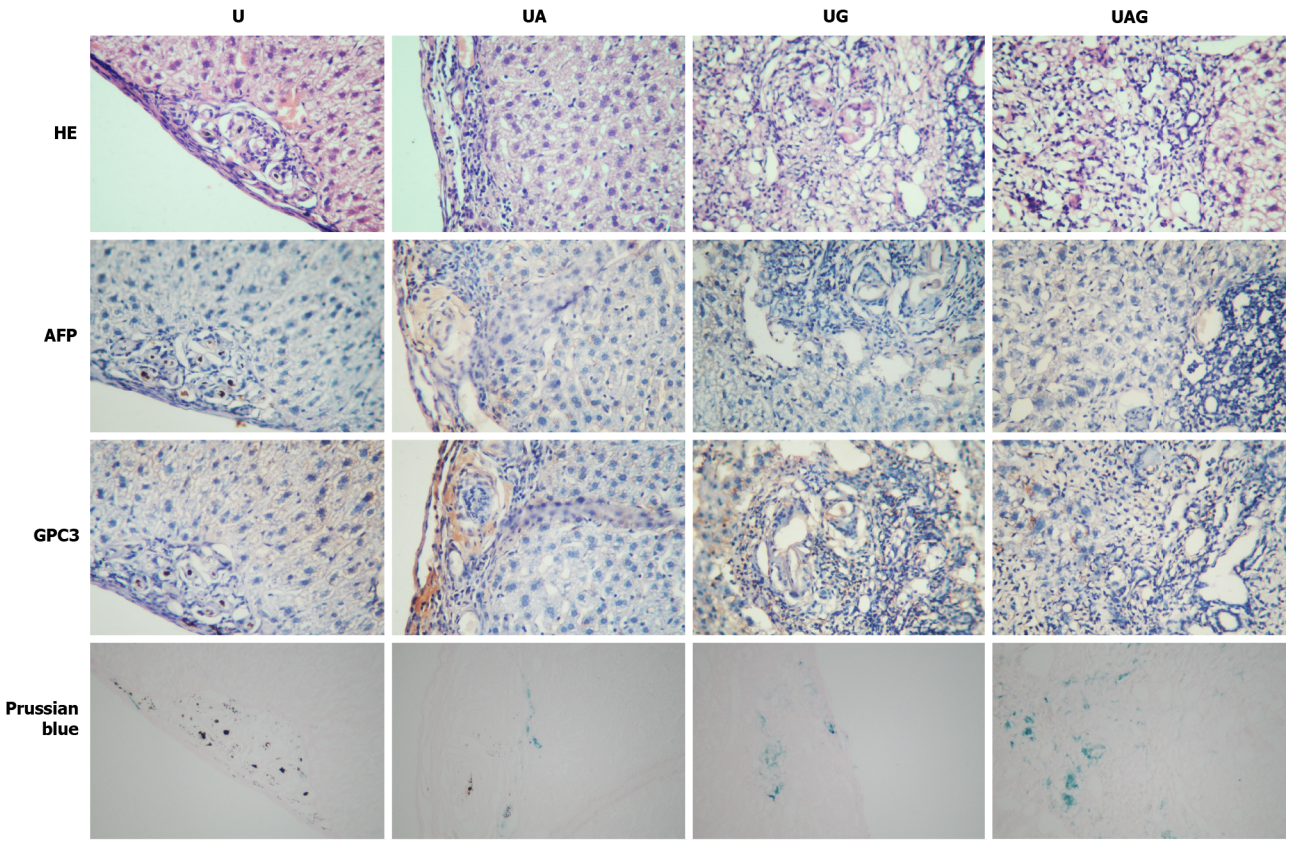

DOI: 10.4251/wjgo.v14.i4.858

Figure 7 Histological results of hepatocellular carcinoma tumors treated with U, anti-alpha-fetoprotein-ultra-small superparamagnetic iron oxide, anti-glypican-3-ultra-small superparamagnetic iron oxide, and anti-alpha-fetoprotein-ultra-small superparamagnetic iron oxide-anti-glypican-3 probes. UA: Anti-AFP-USPIO; UG: Anti-GPC3-USPIO; UAG: Anti-AFP-USPIO-anti-GPC3; USPIO: Ultra-small superparamagnetic iron oxide; AFP: Alpha-fetoprotein; GPC3: Glypican-3.

peptides or other ligands with small molecular weights for lesion targeting. Secondly, this study lacked detailed experiments to determine changes in imaging properties according to changes in probe dosage. This preliminary study mainly validated the feasibility of targeted USPIO probes as positive contrast agents; therefore, further dose-related studies are required to explore the unusual T2 effects we observed and to optimize the dosage for improved positive contrast enhancement. Thirdly, the N-succinimidyl ester-functionalized USPIO probe might promote cross-linking with other N-containing molecules, as we observed non-specific binding of the non-targeting USPIO probe with the tumor site. Therefore, a more specific surface modification might be considered in order to optimize the probe design. Lastly, as limited by the experimental conditions, the mice were anesthetized by tribromoethanol (Avertin) *via* intraperitoneal injection, which might increase the difficulty of dosage control among multiple time-point scanning and might limit extended observations with high-imaging quality. In the future studies, gas anesthesia should be adopted to improve the accuracy of dosage control and alleviate potential animal suffering.

CONCLUSION

In this study, we prepared double-antigen-targeting MRI probes for HCC tumors by conjugating AFP and GPC3 antibodies to a USPIO probe < 5 nm in size. *In vitro* phantom experiments revealed that USPIO probes of this size could shorten the longitudinal relaxation time, T1, and transversal relaxation time, T2, making them candidate positive and negative MRI contrast agents. Our *in vivo* MRI results using an orthotopic HCC mouse model demonstrated the efficacy of the UAG probe and its potential for use as a targeted positive contrast agent for HCC based on its increased specificity and sensitivity relative to single-antibody and non-targeted USPIO probes. Moreover, we found that the *in vivo* enhancement of imaging by the USPIO probes was likely dose-dependent and requires further investigation. These findings represent preliminary experimental data to promote the development of optimized molecular MRI systems capable of diagnosing early-stage HCC, regardless of tumor heterogeneity and size.

ARTICLE HIGHLIGHTS

Research background

Hepatocellular carcinoma (HCC) threated the human heavily. It is urgent to find an effective method to detect and diagnose the HCC early. Our previous study has already verified the efficiency of alpha-fetoprotein (AFP)/glypican-3 (GPC3)-double-antibody-labeled iron oxide magnetic resonance imaging (MRI) molecular probe *in vitro*.

Research motivation

We validated the effectiveness of a bi-specific probe for enhancing T1-weighted positive contrast to detect and diagnose the early-stage HCC in an orthotopic mouse model. It will provide the evidence for the human application.

Research objectives

To *in vivo* validate the effectiveness of a bi-specific probe for early detection and diagnosis of the early-stage HCC.

Research methods

We synthesized the single- and double-antibody-conjugated 5-nm ultra-small superparamagnetic iron oxide (USPIO) probes respectively. T1- and T2-weighted MRI were performed on the mouse model injection of the different probes at 12-, 24-, and 32-h. All the tumor samples were histologically analyzed.

Research results

The bi-specific probe was the most effective kind of the probes in our experiment.

Research conclusions

The bi-specific T1-positive contrast-enhanced MRI probe for HCC demonstrated increased specificity and sensitivity to diagnose early-stage HCC.

Research perspectives

The *in vivo* enhancement in imaging by the USPIO probes was likely dose-dependent and requires further investigation.

FOOTNOTES

Author contributions: Ma XH, Qu CF, and Zhao XM designed the research; Ma XH, Liu SY, Chen K, Wu ZY, Li DF and Mi YT performed the research; Ma XH, Wang S and Liu SY contributed new reagents or analytic tools; Ma XH, Liu SY, and Chen K analyzed the data and wrote the paper.

Supported by PUMC Youth Fund, No. 2017320010; Chinese Academy of Medical Sciences (CAMS) Research Fund, No. ZZ2016B01; and Beijing HopeRun Special Fund of Cancer Foundation of China, No. LC2016B15.

Institutional animal care and use committee statement: This study was approved by the ethics committee of National Cancer Center/Cancer Hospital, Chinese Academy of Medical Sciences and Peking Union Medical College.

Conflict-of-interest statement: The authors declare that there are no conflicts of interest regarding the publication of the paper.

Data sharing statement: No additional data is available.

ARRIVE guidelines statement: The authors have read the ARRIVE guidelines, and the manuscript was prepared and revised according to the ARRIVE guidelines.

Country/Territory of origin: China

ORCID number: Xiao-Hong Ma 0000-0002-9048-8374; Kun Chen 0000-0003-3146-2577; Shuang Wang 0000-0001-9241-

2018; Si-Yun Liu 0000-0001-5611-382X; Deng-Feng Li 0000-0001-5754-3442; Yong-Tao Mi 0000-0002-8071-0621; Zhi-Yuan Wu 0000-0002-8814-0280; Chun-Feng Qu 0000-0001-9973-0887; Xin-Ming Zhao 0000-0001-7286-771X.

S-Editor: Fan JR
L-Editor: A
P-Editor: Yuan YY

REFERENCES

1 **Ferlay J**, Soerjomataram I, Dikshit R, Eser S, Mathers C, Rebelo M, Parkin DM, Forman D, Bray F. Cancer incidence and mortality worldwide: sources, methods and major patterns in GLOBOCAN 2012. *Int J Cancer* 2015; **136**: E359-E386 [PMID: 25220842 DOI: 10.1002/ijc.29210]
2 **Chen W**, Zheng R, Baade PD, Zhang S, Zeng H, Bray F, Jemal A, Yu XQ, He J. Cancer statistics in China, 2015. *CA Cancer J Clin* 2016; **66**: 115-132 [PMID: 26808342 DOI: 10.3322/caac.21338]
3 **Yang D**, She H, Wang X, Yang Z, Wang Z. Diagnostic accuracy of quantitative diffusion parameters in the pathological grading of hepatocellular carcinoma: A meta-analysis. *J Magn Reson Imaging* 2020; **51**: 1581-1593 [PMID: 31654537 DOI: 10.1002/jmri.26963]
4 **Semaan S**, Vietti Violi N, Lewis S, Chatterji M, Song C, Besa C, Babb JS, Fiel MI, Schwartz M, Thung S, Sirlin CB, Taouli B. Hepatocellular carcinoma detection in liver cirrhosis: diagnostic performance of contrast-enhanced CT vs. MRI with extracellular contrast vs. gadoxetic acid. *Eur Radiol* 2020; **30**: 1020-1030 [PMID: 31673837 DOI: 10.1007/s00330-019-06458-4]
5 **Horvat N**, Monti S, Oliveira BC, Rocha CCT, Giancipoli RG, Mannelli L. State of the art in magnetic resonance imaging of hepatocellular carcinoma. *Radiol Oncol* 2018; **52**: 353-364 [PMID: 30511939 DOI: 10.2478/raon-2018-0044]
6 **Vilgrain V**, Van Beers BE, Pastor CM. Insights into the diagnosis of hepatocellular carcinomas with hepatobiliary MRI. *J Hepatol* 2016; **64**: 708-716 [PMID: 26632635 DOI: 10.1016/j.jhep.2015.11.016]
7 **Yang S**, Lin J, Lu F, Han Z, Fu C, Gu H. Use of Ultrasmall Superparamagnetic Iron Oxide Enhanced Susceptibility Weighted Imaging and Mean Vessel Density Imaging to Monitor Antiangiogenic Effects of Sorafenib on Experimental Hepatocellular Carcinoma. *Contrast Media Mol Imaging* 2017; **2017**: 9265098 [PMID: 29097941 DOI: 10.1155/2017/9265098]
8 **Choi MH**, Choi JI, Lee YJ, Park MY, Rha SE, Lall C. MRI of Small Hepatocellular Carcinoma: Typical Features Are Less Frequent Below a Size Cutoff of 1.5 cm. *AJR Am J Roentgenol* 2017; **208**: 544-551 [PMID: 28026208 DOI: 10.2214/AJR.16.16414]
9 **Elsayes KM**, Hooker JC, Agrons MM, Kielar AZ, Tang A, Fowler KJ, Chernyak V, Bashir MR, Kono Y, Do RK, Mitchell DG, Kamaya A, Hecht EM, Sirlin CB. 2017 Version of LI-RADS for CT and MR Imaging: An Update. *Radiographics* 2017; **37**: 1994-2017 [PMID: 29131761 DOI: 10.1148/rg.2017170098]
10 **Zhang C**, Liu H, Cui Y, Li X, Zhang Z, Zhang Y, Wang D. Molecular magnetic resonance imaging of activated hepatic stellate cells with ultrasmall superparamagnetic iron oxide targeting integrin $\alpha v\beta_3$ for staging liver fibrosis in rat model. *Int J Nanomedicine* 2016; **11**: 1097-1108 [PMID: 27051285 DOI: 10.2147/IJN.S101366]
11 **Chen Q**, Shang W, Zeng C, Wang K, Liang X, Chi C, Yang J, Fang C, Tian J. Theranostic imaging of liver cancer using targeted optical/MRI dual-modal probes. *Oncotarget* 2017; **8**: 32741-32751 [PMID: 28416757 DOI: 10.18632/oncotarget.15642]
12 **Mu K**, Zhang S, Ai T, Jiang J, Yao Y, Jiang L, Zhou Q, Xiang H, Zhu Y, Yang X, Zhu W. Monoclonal antibody-conjugated superparamagnetic iron oxide nanoparticles for imaging of epidermal growth factor receptor-targeted cells and gliomas. *Mol Imaging* 2015; **14** [PMID: 26044549 DOI: 10.2310/7290.2015.00002]
13 **Dulińska-Litewka J**, Łazarczyk A, Hałubiec P, Szafrański O, Karnas K, Karewicz A. Superparamagnetic Iron Oxide Nanoparticles-Current and Prospective Medical Applications. *Materials (Basel)* 2019; **12** [PMID: 30791358 DOI: 10.3390/ma12040617]
14 **Huppertz A**. Modern liver MR imaging contrast agents. *Imag Dec MRI* 2010; **11**: 33-37 [DOI: 10.1111/j.1617-0830.2007.00106.x]
15 **Leonhardt M**, Keiser M, Oswald S, Kühn J, Jia J, Grube M, Kroemer HK, Siegmund W, Weitschies W. Hepatic uptake of the magnetic resonance imaging contrast agent Gd-EOB-DTPA: role of human organic anion transporters. *Drug Metab Dispos* 2010; **38**: 1024-1028 [PMID: 20406852 DOI: 10.1124/dmd.110.032862]
16 **Li Y**, Chen Z, Li F, Wang J, Zhang Z. Preparation and *in vitro* studies of MRI-specific superparamagnetic iron oxide antiGPC3 probe for hepatocellular carcinoma. *Int J Nanomedicine* 2012; **7**: 4593-4611 [PMID: 22956868 DOI: 10.2147/IJN.S32196]
17 **Li YW**, Chen ZG, Zhao ZS, Li HL, Wang JC, Zhang ZM. Preparation of magnetic resonance probes using one-pot method for detection of hepatocellular carcinoma. *World J Gastroenterol* 2015; **21**: 4275-4283 [PMID: 25892879 DOI: 10.3748/wjg.v21.i14.4275]
18 **Huang KW**, Chieh JJ, Horng HE, Hong CY, Yang HC. Characteristics of magnetic labeling on liver tumors with anti-alpha-fetoprotein-mediated Fe3O4 magnetic nanoparticles. *Int J Nanomedicine* 2012; **7**: 2987-2996 [PMID: 22787394 DOI: 10.2147/IJN.S30061]
19 **Zhao M**, Liu Z, Dong L, Zhou H, Yang S, Wu W, Lin J. A GPC3-specific aptamer-mediated magnetic resonance probe for hepatocellular carcinoma. *Int J Nanomedicine* 2018; **13**: 4433-4443 [DOI: 10.2147/IJN.S168268]
20 **Li W**, Xiao X, Li X, Xu Y, Ma L, Guo L, Yan C, Wu Y. Detecting GPC3-Expressing Hepatocellular Carcinoma with L5 Peptide-Guided Pretargeting Approach: In Vitro and In Vivo MR Imaging Experiments. *Contrast Media Mol Imaging* 2018; **2018**: 9169072 [PMID: 30275801 DOI: 10.1155/2018/9169072]

21 **Tsuchiya N**, Sawada Y, Endo I, Saito K, Uemura Y, Nakatsura T. Biomarkers for the early diagnosis of hepatocellular carcinoma. *World J Gastroenterol* 2015; **21**: 10573-10583 [PMID: 26457017 DOI: 10.3748/wjg.v21.i37.10573]

22 **Chauhan R**, Lahiri N. Tissue- and Serum-Associated Biomarkers of Hepatocellular Carcinoma. *Biomark Cancer* 2016; **8**: 37-55 [PMID: 27398029 DOI: 10.4137/BIC.S34413]

23 **Wu Y**, Liu H, Ding H. GPC-3 in hepatocellular carcinoma: current perspectives. *J Hepatocell Carcinoma* 2016; **3**: 63-67 [PMID: 27878117 DOI: 10.2147/JHC.S116513]

24 **Filmus J**, Capurro M. Glypican-3: a marker and a therapeutic target in hepatocellular carcinoma. *FEBS J* 2013; **280**: 2471-2476 [PMID: 23305321 DOI: 10.1111/febs.12126]

25 **Na HB**, Lee JH, An K, Park YI, Park M, Lee IS, Nam DH, Kim ST, Kim SH, Kim SW, Lim KH, Kim KS, Kim SO, Hyeon T. Development of a T1 contrast agent for magnetic resonance imaging using MnO nanoparticles. *Angew Chem Int Ed Engl* 2007; **46**: 5397-5401 [PMID: 17357103 DOI: 10.1002/anie.200604775]

26 **Liu ZT**, Cai JL, Su H, Yang J, Sun W, Ma Y, Liu S, Zhang C. Feasibility of USPIOs for T1-weighted MR molecular imaging of tumor receptors. *RSC Advances* 2017; **7**: 31671-31681 [DOI: 10.1039/C7RA04903J]

27 **Wang G**, Zhang X, Skallberg A, Liu Y, Hu Z, Mei X, Uvdal K. One-step synthesis of water-dispersible ultra-small Fe3O4 nanoparticles as contrast agents for T1 and T2 magnetic resonance imaging. *Nanoscale* 2014; **6**: 2953-2963 [PMID: 24480995 DOI: 10.1039/c3nr05550g]

28 **Kim BH**, Lee N, Kim H, An K, Park YI, Choi Y, Shin K, Lee Y, Kwon SG, Na HB, Park JG, Ahn TY, Kim YW, Moon WK, Choi SH, Hyeon T. Large-scale synthesis of uniform and extremely small-sized iron oxide nanoparticles for high-resolution T1 magnetic resonance imaging contrast agents. *J Am Chem Soc* 2011; **133**: 12624-12631 [PMID: 21744804 DOI: 10.1021/ja203340u]

29 **Huang J**, Wang L, Zhong X, Li Y, Yang L, Mao H. Facile non-hydrothermal synthesis of oligosaccharides coated sub-5 nm magnetic iron oxide nanoparticles with dual MRI contrast enhancement effect. *J Mater Chem B* 2014 [PMID: 25181490 DOI: 10.1039/C4TB00811A]

30 **Bao Y**, Sherwood J A, Sun Z. Magnetic iron oxide nanoparticles as T 1 contrast agents for magnetic resonance imaging. *J Mater Chem C* 2018; **6**: 1280-1290 [DOI: 10.1039/C7TC05854C]

31 **Daldrup-Link HE**. Ten Things You Might Not Know about Iron Oxide Nanoparticles. *Radiology* 2017; **284**: 616-629 [PMID: 28825888 DOI: 10.1148/radiol.2017162759]

32 **Cortajarena AL**, Ortega D, Ocampo SM, Gonzalez-García A, Couleaud P, Miranda R, Belda-Iniesta C, Ayuso-Sacido A. Engineering Iron Oxide Nanoparticles for Clinical Settings. *Nanobiomedicine (Rij)* 2014; **1**: 2 [PMID: 30023013 DOI: 10.5772/58841]

33 **Xiao YD**, Paudel R, Liu J, Ma C, Zhang ZS, Zhou SK. MRI contrast agents: Classification and application (Review). *Int J Mol Med* 2016; **38**: 1319-1326 [PMID: 27666161 DOI: 10.3892/ijmm.2016.2744]

34 **Ma XH**, Wang S, Liu SY, Chen K, Wu ZY, Li DF, Mi YT, Hu LB, Chen ZW, Zhao XM. Development and *in vitro* study of a bi-specific magnetic resonance imaging molecular probe for hepatocellular carcinoma. *World J Gastroenterol* 2019; **25**: 3030-3043 [PMID: 31293339 DOI: 10.3748/wjg.v25.i24.3030]

35 **Song Y**, Kang YJ, Jung H, Kim H, Kang S, Cho H. Lumazine Synthase Protein Nanoparticle-Gd(III)-DOTA Conjugate as a T1 contrast agent for high-field MRI. *Sci Rep* 2015; **5**: 15656 [PMID: 26493381 DOI: 10.1038/srep15656]

36 **Zhou Z**, Lu ZR. Gadolinium-based contrast agents for magnetic resonance cancer imaging. *Wiley Interdiscip Rev Nanomed Nanobiotechnol* 2013; **5**: 1-18 [PMID: 23047730 DOI: 10.1002/wnan.1198]

37 **Chen K**, Wu Z, Zang M, Wang C, Wang Y, Wang D, Ma Y, Qu C. Immunization with glypican-3 nanovaccine containing TLR7 agonist prevents the development of carcinogen-induced precancerous hepatic lesions to cancer in a murine model. *Am J Transl Res* 2018; **10**: 1736-1749 [PMID: 30018715]

38 **Smolensky ED**, Park HY, Zhou Y, Rolla GA, Marjańska M, Botta M, Pierre VC. Scaling Laws at the Nano Size: The Effect of Particle Size and Shape on the Magnetism and Relaxivity of Iron Oxide Nanoparticle Contrast Agents. *J Mater Chem B* 2013; **1**: 2818-2828 [PMID: 23819021 DOI: 10.1039/C3TB00369H]

39 **Kandasamy G**, Maity D. Recent advances in superparamagnetic iron oxide nanoparticles (SPIONs) for *in vitro* and *in vivo* cancer nanotheranostics. *Int J Pharm* 2015; **496**: 191-218 [PMID: 26520409 DOI: 10.1016/j.ijpharm.2015.10.058]

40 **Gao Z**, Ma T, Zhao E, Docter D, Yang W, Stauber RH, Gao M. Small is Smarter: Nano MRI Contrast Agents - Advantages and Recent Achievements. *Small* 2016; **12**: 556-576 [PMID: 26680328 DOI: 10.1002/smll.201502309]

41 **Kievit FM**, Zhang M. Cancer nanotheranostics: improving imaging and therapy by targeted delivery across biological barriers. *Adv Mater* 2011; **23**: H217-H247 [PMID: 21842473 DOI: 10.1002/adma.201102313]

42 **Veiseh O**, Gunn JW, Zhang M. Design and fabrication of magnetic nanoparticles for targeted drug delivery and imaging. *Adv Drug Deliv Rev* 2010; **62**: 284-304 [PMID: 19909778 DOI: 10.1016/j.addr.2009.11.002]

43 **Feng Q**, Liu Y, Huang J, Chen K, Xiao K. Uptake, distribution, clearance, and toxicity of iron oxide nanoparticles with different sizes and coatings. *Sci Rep* 2018; **8**: 2082 [PMID: 29391477 DOI: 10.1038/s41598-018-19628-z]

44 **Longmire M**, Choyke PL, Kobayashi H. Clearance properties of nano-sized particles and molecules as imaging agents: considerations and caveats. *Nanomedicine (Lond)* 2008; **3**: 703-717 [PMID: 18817471 DOI: 10.2217/17435889.3.5.703]

45 **Vavricka SR**, Jung D, Fried M, Grützner U, Meier PJ, Kullak-Ublick GA. The human organic anion transporting polypeptide 8 (SLCO1B3) gene is transcriptionally repressed by hepatocyte nuclear factor 3beta in hepatocellular carcinoma. *J Hepatol* 2004; **40**: 212-218 [PMID: 14739090 DOI: 10.1016/j.jhep.2003.10.008]

46 **Tang Q**, Ma C. Performance of Gd-EOB-DTPA-enhanced MRI for the diagnosis of LI-RADS 4 category hepatocellular carcinoma nodules with different diameters. *Oncol Lett* 2018; **16**: 2725-2731 [PMID: 30008946 DOI: 10.3892/ol.2018.8884]

World Journal of Gastrointestinal Oncology

Submit a Manuscript: https://www.f6publishing.com

World J Gastrointest Oncol 2022 April 15; 14(4): 872-886

DOI: 10.4251/wjgo.v14.i4.872

ISSN 1948-5204 (online)

ORIGINAL ARTICLE

Basic Study

Xihuang pills induce apoptosis in hepatocellular carcinoma by suppressing phosphoinositide 3-kinase/protein kinase-B/mechanistic target of rapamycin pathway

Yong-Jie Teng, Zhe Deng, Zhao-Guang Ouyang, Qing Zhou, Si Mei, Xing-Xing Fan, Yong-Rong Wu, Hong-Ping Long, Le-Yao Fang, Dong-Liang Yin, Bo-Yu Zhang, Yin-Mei Guo, Wen-Hao Zhu, Zhen Huang, Piao Zheng, Di-Min Ning, Xue-Fei Tian

Specialty type: Oncology

Provenance and peer review: Unsolicited article; Externally peer reviewed.

Peer-review model: Single blind

Peer-review report's scientific quality classification

Grade A (Excellent): 0
Grade B (Very good): B, B
Grade C (Good): 0
Grade D (Fair): 0
Grade E (Poor): 0

P-Reviewer: Hassaan NA, Egypt; Prasetyo EP, Indonesia

Received: September 7, 2021
Peer-review started: September 7, 2021
First decision: December 4, 2021
Revised: December 30, 2021
Accepted: March 14, 2022
Article in press: March 14, 2022
Published online: April 15, 2022

Yong-Jie Teng, Qing Zhou, Hong-Ping Long, Le-Yao Fang, The First Hospital of Hunan University of Chinese Medicine, Hunan University of Chinese Medicine, Changsha 410208, Hunan Province, China

Zhe Deng, Yong-Rong Wu, Yin-Mei Guo, Wen-Hao Zhu, Zhen Huang, Piao Zheng, Di-Min Ning, Xue-Fei Tian, College of Integrated Chinese and Western Medicine, Hunan Key Laboratory of Translational Research in Formulas and Zheng of Traditional Chinese Medicine, Hunan University of Chinese Medicine, Changsha 410208, Hunan Province, China

Zhao-Guang Ouyang, Department of Preventive Dentistry, Guangzhou Key Laboratory of Basic and Applied Research of Oral Regenerative Medicine, Guangzhou Medical University, Guangzhou 510132, Guangdong Province, China

Si Mei, Department of Physiology, Hunan University of Chinese Medicine, Changsha 410208, Hunan Province, China

Xing-Xing Fan, State Key Laboratory of Quality Research in Chinese Medicine, Macau Institute For Applied Research in Medicine and Health, Macau University of Science and Technology, Macau, China

Dong-Liang Yin, School of Pharmacy, Hunan University of Chinese Medicine, Changsha 410208, Hunan Province, China

Bo-Yu Zhang, College of Acupuncture and Massage, Hunan University of Chinese Medicine, Changsha 410208, Hunan Province, China

Corresponding author: Xue-Fei Tian, PhD, Professor, College of Integrated Chinese and Western Medicine, Hunan Key Laboratory of Translational Research in Formulas and Zheng of Traditional Chinese Medicine, Hunan University of Chinese Medicine, No. 300 Xueshi Road, Yuelu District, Changsha 410208, Hunan Province, China. 003640@hnucm.edu.cn

Abstract

BACKGROUND

The phosphoinositide 3-kinase/protein kinase-B/mechanistic target of rapamycin

(PI3K/Akt/mTOR) signalling pathway is crucial for cell survival, differentiation, apoptosis and metabolism. Xihuang pills (XHP) are a traditional Chinese preparation with antitumour properties. They inhibit the growth of breast cancer, glioma, and other tumours by regulating the PI3K/Akt/mTOR signalling pathway. However, the effects and mechanisms of action of XHP in hepatocellular carcinoma (HCC) remain unclear. Regulation of the PI3K/Akt/mTOR signalling pathway effectively inhibits the progression of HCC. However, no study has focused on the XHP-associated PI3K/Akt/mTOR signalling pathway. Therefore, we hypothesized that XHP might play a role in inhibiting HCC through the PI3K/Akt/mTOR signalling pathway.

AIM

To confirm the effect of XHP on HCC and the possible mechanisms involved.

METHODS

The chemical constituents and active components of XHP were analysed using ultra-performance liquid chromatography-quadrupole time of flight mass spectrometry (UPLC-Q-TOF-MS). Cell-based experiments and *in vivo* xenograft tumour experiments were utilized to evaluate the effect of XHP on HCC tumorigenesis. First, SMMC-7721 cells were incubated with different concentrations of XHP (0, 0.3125, 0.625, 1.25, and 2.5 mg/mL) for 12 h, 24 h and 48 h. Cell viability was assessed using the CCK-8 assay, followed by an assessment of cell migration using a wound healing assay. Second, the effect of XHP on the apoptosis of SMMC-7721 cells was evaluated. SMMC-7721 cells were stained with fluorescein isothiocyanate and annexin V/propidium iodide. The number of apoptotic cells and cell cycle distribution were measured using flow cytometry. The cleaved protein and mRNA expression levels of caspase-3 and caspase-9 were detected using Western blotting and quantitative reverse-transcription polymerase chain reaction (RT-qPCR), respectively. Third, Western blotting and RT–qPCR were performed to confirm the effects of XHP on the protein and mRNA expression of components of the PI3K/Akt/mTOR signalling pathway. Finally, the effects of XHP on the tumorigenesis of subcutaneous hepatocellular tumours in nude mice were assessed.

RESULTS

The following 12 compounds were identified in XHP using high-resolution mass spectrometry: Valine, 4-gingerol, myrrhone, ricinoleic acid, glycocholic acid, curzerenone, 11-keto-β-boswellic acid, oleic acid, germacrone, 3-acetyl-9,11-dehydro-β-boswellic acid, 5β-androstane-3,17-dione, and 3-acetyl-11-keto-β-boswellic acid. The cell viability assay results showed that treatment with 0.625 mg/mL XHP extract decreased HCC cell viability after 12 h, and the effects were dose- and time-dependent. The results of the cell scratch assay showed that the migration of HCC cells was significantly inhibited in a time-dependent manner by the administration of XHP extract (0.625 mg/mL). Moreover, XHP significantly inhibited cell migration and resulted in cell cycle arrest and apoptosis. Furthermore, XHP downregulated the PI3K/Akt/mTOR signalling pathway, which activated apoptosis executioner proteins (*e.g.*, caspase-9 and caspase-3). The inhibitory effects of XHP on HCC cell growth were determined *in vivo* by analysing the tumour xenograft volumes and weights.

CONCLUSION

XHP inhibited HCC cell growth and migration by stimulating apoptosis *via* the downregulation of the PI3K/Akt/mTOR signalling pathway, followed by the activation of caspase-9 and caspase-3. Our findings clarified that the antitumour effects of XHP on HCC cells are mediated by the PI3K/Akt/mTOR signalling pathway, revealing that XHP may be a potential complementary therapy for HCC.

Key Words: Hepatocellular carcinoma; Xihuang pills; Apoptosis; Antitumour; Phosphoinositide 3-kinase/protein kinase-B/mechanistic target of rapamycin pathway

Core Tip: The study revealed that Xihuang pills (XHP) increases caspase-9 and caspase-3 activities by inhibiting the phosphoinositide 3-kinase/protein kinase-B/mechanistic target of rapamycin signalling pathway and induces apoptosis and cell cycle arrest. Consequently, our study indicated that XHP inhibits the growth, migration, and proliferation of hepatocellular carcinoma (HCC) cells. Our study provides a better understanding of the antitumour effects of XHP and reveals the underlying mechanism. The findings of this study suggest that XHP might serve as a supplementary medicine in HCC treatment.

Citation: Teng YJ, Deng Z, Ouyang ZG, Zhou Q, Mei S, Fan XX, Wu YR, Long HP, Fang LY, Yin DL, Zhang BY, Guo YM, Zhu WH, Huang Z, Zheng P, Ning DM, Tian XF. Xihuang pills induce apoptosis in hepatocellular carcinoma by suppressing phosphoinositide 3-kinase/protein kinase-B/mechanistic target of rapamycin pathway. *World J Gastrointest Oncol* 2022; 14(4): 872-886
URL: https://www.wjgnet.com/1948-5204/full/v14/i4/872.htm
DOI: https://dx.doi.org/10.4251/wjgo.v14.i4.872

INTRODUCTION

Hepatocellular carcinoma (HCC) is a primary liver cancer with a poor prognosis, and limited treatments are available for patients with advanced HCC[1]. The absence of specific clinical signs and symptoms makes the early diagnosis of HCC even more difficult[2]. Although diagnostic and therapeutic methods have improved in recent years, the efficacy of HCC treatments is only 30%–40%[3]. In addition, the toxicity and side effects associated with conventional treatments remain a clinical challenge that demands a prompt solution. Therefore, the development of effective antitumour drugs with reduced toxicity is needed. The carcinogenesis of HCC is regulated by several signalling pathways, and the phosphoinositide 3-kinase/protein kinase-B/mechanistic target of rapamycin (PI3K/Akt/mTOR) pathway is one of the most important pathways[4].

The PI3K/Akt/mTOR signalling pathway is crucial for cell survival, differentiation, apoptosis and metabolism[5-7]. PI3K is a member of the lipid kinase family[8], and its activation initiates the expression of the second messenger phosphatidylinositol 3,4,5-triphosphate (PIP3). PIP3 induces the activation of multiple protein kinases, such as Akt. Activated Akt then facilitates cell differentiation, proliferation, metabolism, apoptosis and angiogenesis *via* the upregulation of several downstream effectors, including mTOR, B-cell lymphoma 2 (Bcl-2) family proteins, glycogen synthase kinase 3, S6 protein kinase, and caspase-9[3]. Activated caspase-9 induces the function of caspase-3 zymogen and induces apoptosis through proteolysis[9]. As a highly conserved mechanism of programmed cell death, apoptosis maintains tissue homeostasis. A reduction in apoptosis can induce the occurrence of tumours and promote their development[10]. PI3K/Akt/mTOR signalling, an apoptosis-related pathway[11], is often abnormally activated in HCC[4]. Therefore, apoptosis may be induced by suppressing the PI3K/Akt/mTOR pathway, which inhibits the proliferation of HCC cells.

Xihuang pills (XHP), a traditional Chinese antitumour prescription, are composed of four Chinese herbs, namely, *Bos taurus domesticus Gmelin*, *Boswellia carteri Birdwood*, *Moschus berezovskii Flerov* and *Commiphora myrrha (Nees) Engl*[12]. XHP exerts antitumour effects, reduces side effects, and improves the quality of life and survival rate of patients receiving tumour therapy[12]. Clinical studies have shown that XHP combined with chemotherapy effectively enhances the tumour response in patients with breast cancer, and reduces the toxicity and side effects of chemotherapy[13]. Several studies have confirmed that the antitumour activity of XHP depends on the PI3K-Akt-mTOR signalling pathway. Li *et al*[14] reported that XHP promotes apoptosis of Treg cells through the PI3K/Akt/AP-1 signalling pathway, improves the immunosuppressive state of the tumour microenvironment, and inhibits tumour growth. Fu *et al*[15] reported that XHP enhances the antitumour effect of temozolomide on glioblastoma-transplanted tumours through the Akt/mTOR pathway. According to Shao *et al*[16], XHP regulates the apoptosis of U-8MG glioblastoma cells through the ROS-mediated Akt/mTOR/FOXO1 pathway.

Collectively, the antitumour effect of XHP is associated with suppression of the PI3K/Akt/mTOR signalling pathway. Regulation of the PI3K/Akt/mTOR signalling pathway effectively inhibits the progression of HCC[4]. A growing number of studies have documented the antitumour effects of XHP on breast cancer, lung cancer, colon cancer, glioma, *etc*. However, few studies have been performed on HCC. No research has focused on the XHP-associated PI3K/Akt/mTOR signalling pathway. Therefore, we hypothesized that XHP might play a role in inhibiting HCC through the PI3K/Akt/mTOR signalling pathway. Our results confirm that XHP induces apoptosis and inhibits proliferation, both *in vivo* and *in vitro*. Moreover, this inhibitory effect depends on the PI3K/Akt/mTOR signalling pathway. Thus, this research revealed a potential antitumour effect of XHP on HCC cells.

MATERIALS AND METHODS

Chemicals

XHP was purchased from Tong Ren Tang Technologies Co., Ltd. (Beijing, China, Lot number: 17043278). All study parameters fulfilled the requirements of standard quality. For extraction, XHP was soaked in 6 mL of double distilled water for 24 h, followed by ultrasonic dissolution. The precipitates were collected *via* centrifugation at 3000 rpm for 5 min and resuspended in 6 mL of dimethyl sulfoxide (DMSO; Sigma–Aldrich, Shanghai, China) using an ultrasonic dissolver. Another centrifugation step was performed, and the precipitates were collected. An XHP extract was then prepared using the obtained precipitates and stored at 4 °C for future use. According to the pharmacological dosage regulations of XHP, the daily dose of XHP for adults is 6 g/d, and the body weight of each mice is about 20 g. The dose of XHP was determined by dose extrapolation based on dose-body surface area normalization, this dosage was converted to 78 mg/kg[17].

The study of XHP using high resolution mass spectrometry

The compounds present in XHP were analysed using high-resolution mass spectrometry (MS). XHP (3 g) was ground into a powder and extracted with 10 mL of 100% methanol, followed by ultrasonic extraction for 45 min. The supernatant was collected by centrifugation at 8000 rpm for 5 min and then filtered with a 0.22 μm microporous filter membrane. The filtrate was collected and measured using a UPLC-Q-TOF-MS (1290 UPLC-6540, Agilent Technologies Inc., United States) system. An Agilent ZORBAX Eclipse Plus C18 column (100 mm × 3.0 mm, 1.8 μm) was utilized for chromatographic separation. The mobile phase consisted of acetonitrile (A) and 0.1% formic acid, which were prepared as solutions with different gradients: 0–10 min containing 5%–15% A; 10–15 min containing 15%–20% A; 15–25 min containing 25%–45% A; and 25–40 min containing 45%–80% A. The flow rate of the mobile phase was 0.4 mL/min, and the injection volume was 1 μL/sample. Parameters for the MS system were fixed according to the manufacturer's recommendation. In detail, the ionization mode, electrospray ionization and accurate mass data correction were performed using electrospray ionization-L Low Concentration Tuning Mix (G1969-85000). Positive and negative ion switching and the MRE scan model were used, and the mass range was set from 100 m/z to 1700 m/z. The electrospray capillary voltage was 4.0 kV. The sheath gas temperature and drying gas temperature were set to 350 °C. The drying gas (nitrogen) flow rate was 6.8 L/min. After the first mass analysis in full scan mode, a secondary MS scan was conducted in data-dependent mode, and collision-induced dissociation (CID) was used to fragment the first three strong peaks. Subsequently, the secondary scan data were obtained from 50 to 1000 m/z with fragmentation voltages of 10, 20, and 30 kV.

Cell culture and treatment

The SMMC-7721 HCC cell line was purchased from the Beinac Biotechnology Research Institute (Beijing, China) and was not contaminated, as determined by short tandem repeat (STR) identification. SMMC-7721 cells were cultured in Dulbecco's modified Eagle's medium (Gibco, New York, United States) supplemented with 10% heat-inactivated foetal bovine serum (Gibco, New York, United States) and 1% (v/v) penicillin–streptomycin (Gibco, New York, United States). Cells were cultured in a humidified atmosphere containing 5% CO_2 at 37 °C. When cells reached 80% confluence, they were treated with different concentrations of the XHP extract (0, 0.3125, 0.625, 1.25, and 2.5 mg/mL) for various durations (0 h, 6 h, 12 h, 24 h, and 48 h).

Cell viability assay

Cell Counting Kit-8 (CCK-8, Gibco, New York, United States) was used to measure cell viability. Briefly, 100 μL of suspended SMMC-7721 cells (1×10^5 cells/mL) in logarithmic growth phase were inoculated in 96-well plates. Subsequently, cells were treated with different concentrations of XHP extract (0, 0.625, 1.25, and 2.5 mg/mL) for different durations. Cells treated with the same volume of 0.1% DMSO and cultured for the same time were considered the control group. After an incubation for 0 h, 6 h, 12 h, 24 h, or 48 h, the absorbance was measured using a microplate reader (Awareness Stat Fax ®2600, Qingdao, China) at 450 nm. Cell viability was determined by comparing treated cells to controls. All assays were repeated at least three times.

Wound healing assay

SMMC-7721 cells were inoculated into 12-well plates after digestion. After spreading cells over the bottom of the plate, a pipette tip (1 mL) was used to create scratch wounds in the cell layer, ensuring that all wounds had a consistent width. The cell culture media were then aspirated, and cell debris created by the scratch were removed by rinsing the plate three times with phosphate-buffered saline (PBS). Then, serum-free culture medium was added to the plate, and an inverted fluorescence microscope (Olympus, type IX71) was used for imaging. The culture plate was placed in a cell incubator (Thermo) for 48 h to allow cell migration. The plate was removed from the incubator every 12 h for imaging. The assay results were analysed according to the collected imaging data.

Apoptosis analysis

Apoptosis was detected using the Annexin V-APC Apoptosis Detection Kit (KeyGEN, Nanjing, Jiangsu, China) according to the manufacturer's instructions. Briefly, cells were digested with 0.25% trypsin (Beyotime Biotechnology Co., Ltd., Shanghai, China) after washes with PBS, followed by centrifugation at 3000 rpm for 5 min. The collected cells were washed with PBS twice and suspended in 500 μL of binding buffer. Then, 5 μL of fluorescein isothiocyanate-labelled annexin V-APC were added and evenly mixed with 5 μL of propidium iodide (PI) at room temperature for 15 min in the dark. Subsequently, a flow cytometer (Beckman Coulter, Brea, CA, United States) was used to quantify the apoptotic cells.

Analysis of cell cycle arrest

The DNA content and cell cycle distribution were measured using a FACSCalibur flow cytometer (Beckman Coulter, Brea, CA, United States). SMMC-7721 cells were inoculated in 6-well plates at a density of 5×10^5 cells/well. After a 24 h incubation, cells were treated with or without XHP extract for 48 h. Subsequently, the cells were fixed with 75% ethanol at 4 °C overnight, followed by washes with PBS. The cells were incubated at room temperature for 15–30 min in the dark and then analysed using flow cytometry.

Western blotting

Mouse tumour tissue specimens were obtained and lysed in RIPA lysis buffer (20 mmol/L HEPES, 1 mmol/L EDTA, 1% Triton X-100, 2 mmol/L EGTA, 150 mmol/L NaCl, 20 mmol/L phosphoglycerol, and 10% protease glycerol). The suspension was then homogenized and subsequently centrifuged at 12000 rpm for 15 min at 4 °C. A BCA detection kit (Beyotime, Shanghai, China) was used to determine the protein concentration. Polyacrylamide gel electrophoresis was used for protein separation Then, the proteins were transferred to a polyvinylidene fluoride membrane with a transfer device in cold buffer. A freshly prepared 5% skim milk solution was utilized for blocking at room temperature for 2 h. Afterwards, specific primary antibodies were incubated with the membrane at 4 °C overnight. The membrane was then washed with Tris-buffered saline supplemented with 0.1% Tween-20 (TBST) and incubated with peroxidase-conjugated secondary antibodies. Visualization was performed using the Super Sight West Pico Blotting kit (Pierce, Massachusetts, United States). The following primary antibodies were used: Cleaved caspase-3 (1:4000), cleaved caspase-9 (1:2000), Akt (1:2000), mTOR (1:2000), P-PI3K (1:1000), P-AKT (1:2000), and P-mTOR (1:2000), which were obtained from Abcam plc. (Cambridge, England). Antibodies against PI3K (1:5000) and β-actin (1:5000) were obtained from Proteintech Group, Inc. (Chicago, United States). Trypsin and PBS were purchased from HyClone Company (Logan, Utah, United States), and DMSO was obtained from Sigma (Germany).

Quantitative reverse-transcription polymerase chain reaction

Total RNA was extracted from SMMC7721 cells using TRIzol reagent (Takara) according to the manufacturer's instructions. Reverse transcription was then performed using reverse transcriptase to produce cDNA templates. The quantitative reverse-transcription polymerase chain reaction (RT–qPCR) conditions were set up as follows: 95 °C for 3 min, followed by 40 cycles of 95 °C for 15 s and 60 °C for 30 s. The following primers were used: F-TGGCAACAGAATTTGAGTCCT and R-ACCATCTTCT-CACTTGGCAT for caspase 3, F-AAGCCAACCCTAGAAAACCTTACCC and R-AGCACCGACAT-CACCAAATCCTC for caspase-9, F-TGCGTCTACTAAAATGCATGG and R-AACTGAAGGTTAAT-GGGTCA for PI3K, F-AGCCCTGGACTACCTGCACTCG, R-CTGTGATCTTAATGTGCCCGTCCT for AKT, and F-CCAAAGGCAACAAGCGATCCCGAA and R-CTCCAAGTTCCACACCGTCCA for mTOR.

Animal and tumour xenograft experiments

All laboratory animals were carefully monitored, and the animal experiments were reviewed and approved by the Ethical Review Committee of Experimental Animal Welfare at Central South University. Additionally, experiments were performed according to the European Community guidelines for laboratory animal use and care. All animals were housed under specific pathogen-free conditions. Subcutaneous xenograft tumours were established by subcutaneously injecting SMMC7721 cells (1×10^7 cells/mouse) (Shanghai SLAC Laboratory Animal Co., Ltd., Shanghai, China) into 5-week-old male BALB/c nude mice. Mouse weights and tumour volumes were measured every other day using the formula for an ellipsoid (length × width^2 × 0.5). When the tumour volume reached approximately 100 mm^3, mice were randomly classified into two groups (n = 5 mice per group). Mice in the control group received oral administration of distilled water daily, whereas mice in the XHP group received XHP extract (78 mg/kg body weight/day) by oral gavage. After 2 wk, mice were sacrificed to investigate the effect of XHP on subcutaneous xenograft tumours.

Statistical analysis

All statistical calculations were performed using GraphPad Prism 7 software (GraphPad Software Company, United States). Data are presented as the means ± SD. One-way analysis of variance (ANOVA) followed by the least significant difference test were conducted to analyse the differences

Table 1 Analysis information of 12 compounds in Xihuang pills

Number	RT (min)	Mass	Molecular formula	Name
1	1.088	117.0778	C5H11NO2	Valine
2	16.110	267.1588	C15H22O4	4-Gingerol
3	19.579	228.1131	C15H16O2	Myrrhone
4	20.357	321.2403	C18H34O3	Ricinoleic acid
5	23.486	465.3060	C26H43NO6	Glycocholic acid
6	32.635	231.1366	C15H18O2	Curzerenone
7	33.057	470.3377	C30H46O4	11-keto-β-boswellic acid
8	33.977	282.4610	C18H34O2	Oleic acid
9	35.078	218.1674	C15H22O	Germacrone
10	36.543	496.3517	C32H48O4	3-Acetyl-9,11-dehydro-β-boswellic Acid
11	38.816	288.2084	C19H28O2	5β-androstane-3,17-dione
12	39.500	512.3485	C32H48O5	3-Acetyl-11-keto-β-boswellic acid

between two groups. A $P < 0.05$ was considered statistically significant.

RESULTS

Components of XHP

The main components of XHP responsible for its inhibitory effects on HCC were analysed using high-resolution MS. Ion flow diagrams were extracted, and the molecular formulas of the compounds were compared with the information in the literature and database for identification (Figure 1). The following 12 compounds were identified: Valine, 4-gingerol, myrrhone, ricinoleic acid, glycocholic acid, curzerenone, 11-keto-β-boswellic acid, oleic acid, germacrone, 3-acetyl-9,11-dehydro-β-boswellic acid, 5β -androstane-3,17-dione, and 3-acetyl-11-keto-β-boswellic acid (Table 1).

The inhibitory effects of XHP extract on HCC cell viability and migration

The effects of XHP extract on HCC cell viability were investigated. Cells were separated into five groups and treated with different concentrations of the XHP extract according to their human equivalent doses (0, 0.3125, 0.625, 1.25, and 2.5 mg/mL), and cell viability was determined using the CCK-8 assay at 12, 24, and 48 h posttreatment. The lowest concentration at which the XHP extract exerted an antitumour effect was 0.625 mg/mL (Figure 2A) at 12 h post-treatment (Figure 2B). The XHP extract inhibited SMMC-7721 cell viability in a dose- and time-dependent manner (Figure 2A and B). Treatment with the effective XHP extract dose, *i.e.*, 0.625 mg/mL, significantly inhibited the migration of SMMC-7721 cells in a time-dependent manner (Figure 2C), as determined using a cell scratch assay.

XHP extract promotes HCC cell apoptosis in a dose-dependent manner

Apoptosis plays an important role in anti-tumour therapy. Therefore, annexin V and PI staining were performed to confirm the apoptosis-inducing effect of the XHP extract on SMMC-7721 cells. As shown in Figure 3A, the proportion of apoptotic cells among XHP-treated SMMC-7721 cells was significantly increased, ranging from 11.87% to 82.42%. Moreover, flow cytometry showed that the proportion of SMMC-7721 cells in G2/M phase was substantially increased, from 18.83% to 42.66% (Figure 3B), indicating cell cycle arrest in SMMC-7721 cells after XHP extract treatment. Subsequently, the expression levels of apoptosis-related proteins caspase-3 and caspase-9 were determined. Similar to the results of the flow cytometry analysis, *in vivo* experiments revealed that the protein expression levels of cleaved caspase-3 and cleaved caspase-9 were significantly increased in the subcutaneous xenograft tumours from nude mice. The mRNA expression levels of caspase-3 and caspase-9 also showed similar trends. (Figure 3C). These results were confirmed by *in vitro* experiments. After treatment with different concentrations of the XHP extract, mRNA expression, as well as protein levels of caspase-3 and caspase-9, were increased in SMMC-7721 cells in a dose-dependent manner (Figure 3D). These results were consistent with the data obtained from the cell viability and migration assays. Collectively, our results indicated that XHP extract promotes HCC cell apoptosis in a dose-dependent manner.

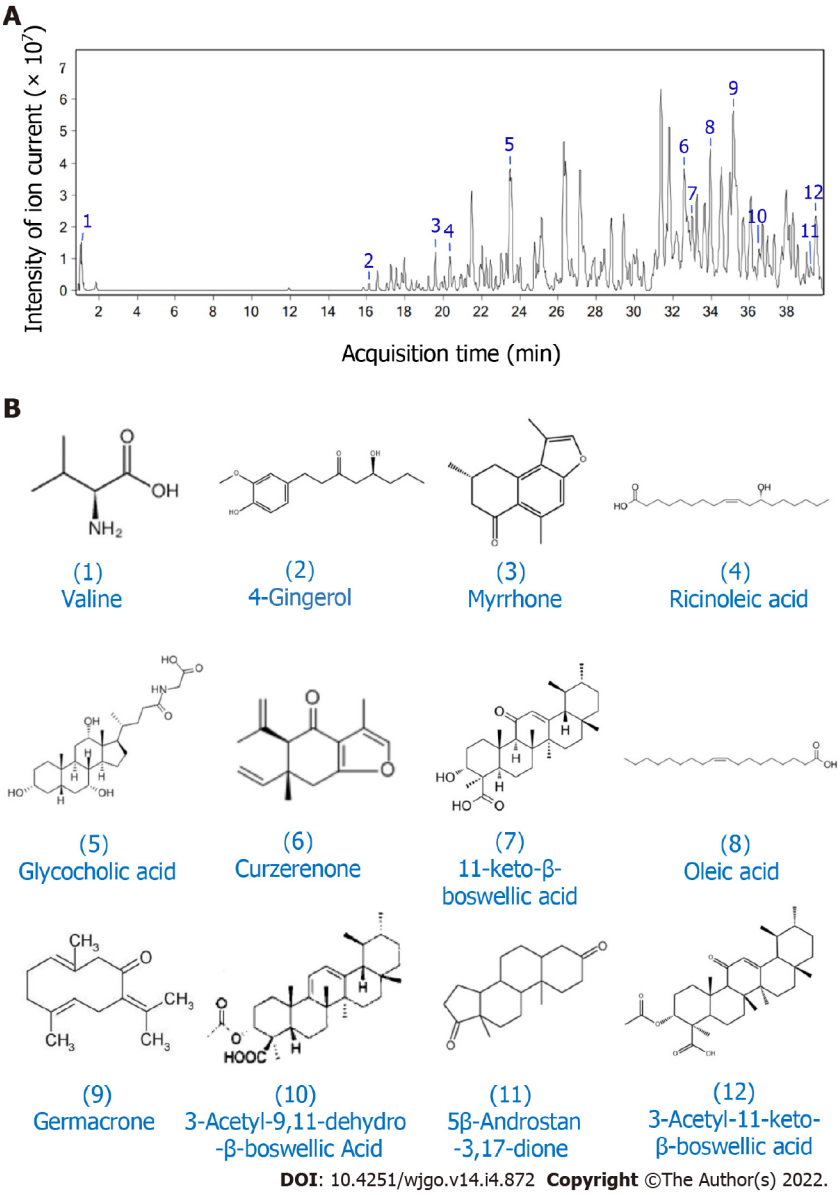

DOI: 10.4251/wjgo.v14.i4.872

Figure 1 Components of Xihuang Pills. The fingerprint of the Xihuang pill was determined using high-resolution mass spectrometry. A: The 12 compounds were labelled according to chromatographic retention times, and their molecular structures were analysed; B: The chemical formulae of 12 compounds. The chemical structures of 12 compounds and chemical formulae obtained from chemsrc (https://m.chemsrc.com/mip/), according to the compound numbering scheme in Table 1.

The inhibitory effects of XHP extract on the expression of components of the PI3K/Akt/mTOR signalling pathway in HCC cells

The PI3K/Akt/mTOR signalling pathway plays significant roles in regulating the cell cycle, apoptosis, and proliferation of HCC. The protein and mRNA expression levels of PI3K, Akt and mTOR were detected to clarify the mechanism involving the PI3K/Akt/mTOR signalling pathway in XHP-induced apoptosis and migration. *In vivo* experiments showed that the ratios of phosphorylated PI3K, Akt, and mTOR to the total protein were noticeably reduced after treatment with the proper concentration of XHP (*i.e.*, 78 mg/kg) (Figure 4A) in the subcutaneous xenograft HCC mouse model. RT–qPCR analysis further confirmed the inhibitory effects of XHP on PI3K, Akt, and mTOR mRNA expression levels (Figure 4B). Moreover, *in vitro* cell experiments showed that XHP extract inhibited the phosphorylation and mRNA expression levels of components of the PI3K/Akt/mTOR signalling pathway in a dose-dependent manner (Figure 4C and D). The data described above indicate that XHP extract inhibits the PI3K/Akt/mTOR signalling pathway in a dose-dependent manner.

Inhibitory effects of XHP on the growth of subcutaneous xenograft tumours in HCC mice

A xenograft tumour model was established using male BALB/c nude mice to confirm the antitumour effect of XHP *in vivo*. As shown in Figure 5A, the subcutaneous xenograft tumours were significantly reduced after XHP treatment compared to the control group. This result was further confirmed by calculating the volume (Figure 5B) and weight (Figure 5C). However, the overall body weight of the

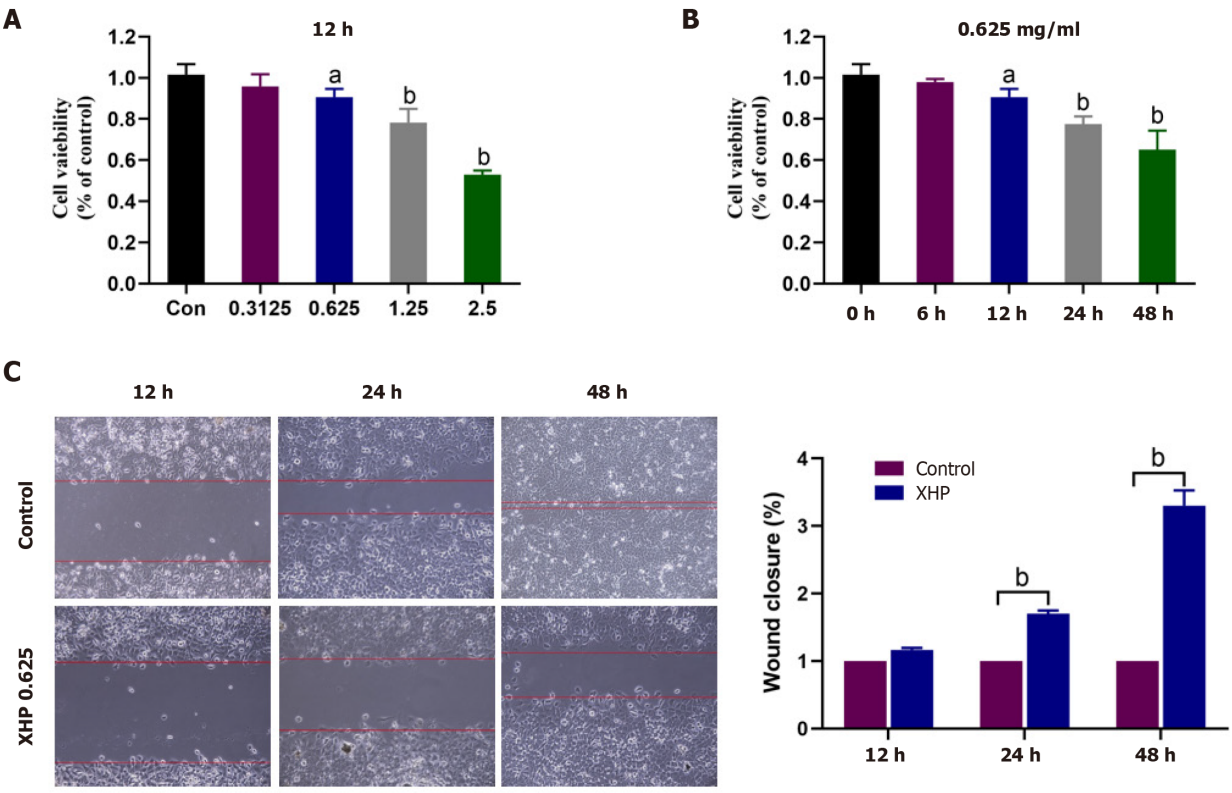

DOI: 10.4251/wjgo.v14.i4.872

Figure 2 Xihuang pills extract inhibits the growth and migration of SMMC7721 cells. Cells were treated with different concentrations of the Xihuang pills (XHP) extract (0, 0.3125, 0.625, 1.25, and 2.5 mg/mL) for 12 h, 24 h, and 48 h. Cell viability was measured using Cell Counting Kit-8. A: A representative graph showing the effects of treatment with various concentrations of the XHP extract for 12 h; B: A representative graph showing that treatment with 0.625 mg/mL XHP extract induces a decrease in cell viability after 12 h; C: The migration of SMMC-7721 cells was measured using a cell scratch assay with or without the administration of 0.625 mg/mL XHP for 48 h. Data are presented as the means ± SD. $^{a}P < 0.05$ and $^{b}P < 0.01$ compared with the control group.

nude mice did not decrease. A significant difference in body weight was not observed between the two groups (Figure 5D). The *in vivo* experiment revealed the protective effect of XHP on preventing the progression of HCC tumorigenesis in the established mouse model.

DISCUSSION

HCC is an aggressive tumour characterized by a high degree of proliferation and invasion. Considering the limitations of current treatment methods, more effective treatments with reduced toxicity must be established. Notably, traditional Chinese medicine and its prepared compounds may serve as supplementary treatments for HCC[16]. XHP is an effective antitumour drug included in the traditional Chinese medicine system. Studies have shown that XHP inhibits the proliferation and metastasis of tumour cells[12]. However, the specific effects and mechanisms of XHP in HCC progression have not been discussed. In this study, we showed that XHP exerts an inhibitory effect on HCC cells by *in vivo* and *in vitro* experiments. Moreover, we identified that XHP reduces the viability and migration of tumour cells *via* the PI3K/Akt/mTOR signalling pathway. This pathway is involved in tumour cell apoptosis of HCC. Thus, the results of our study confirmed the antitumour properties of XHP in HCC, as well as the potential mechanism.

Abnormal activation of the PI3K/Akt/mTOR signalling pathway is a crucial factor promoting HCC development. It induces HCC cell proliferation and cell cycle arrest by inhibiting apoptosis[18-20]. The combination of growth factors and receptors in tumour cells activates PI3K, increasing cell viability, proliferation, and migration[21,22]. PI3K increases the viability of tumour cells in HCC by regulating apoptosis[23-25]. Moreover, Akt serves as a downstream target and mediates the antiapoptotic effects of PI3K, with Akt regulating the sequential steps of apoptotic signalling[26]. Akt activates many downstream proteins, including mTOR, Bcl-2-associated agonist of cell death (Bad), and GSK3[27,28]. In terms of cell cycle regulation, Akt expression suppresses the activity of GSK3β, reduces the expression of cyclin D1 and promotes the expression of Rb, thereby promoting cell cycle progression[29]. Caspase-3 is the primary executioner of apoptosis. It specifically lyses poly (ADP-ribose) polymerase and other substrates, leading to DNA fragmentation and eventual apoptosis[30]. Thus, this mechanism plays an

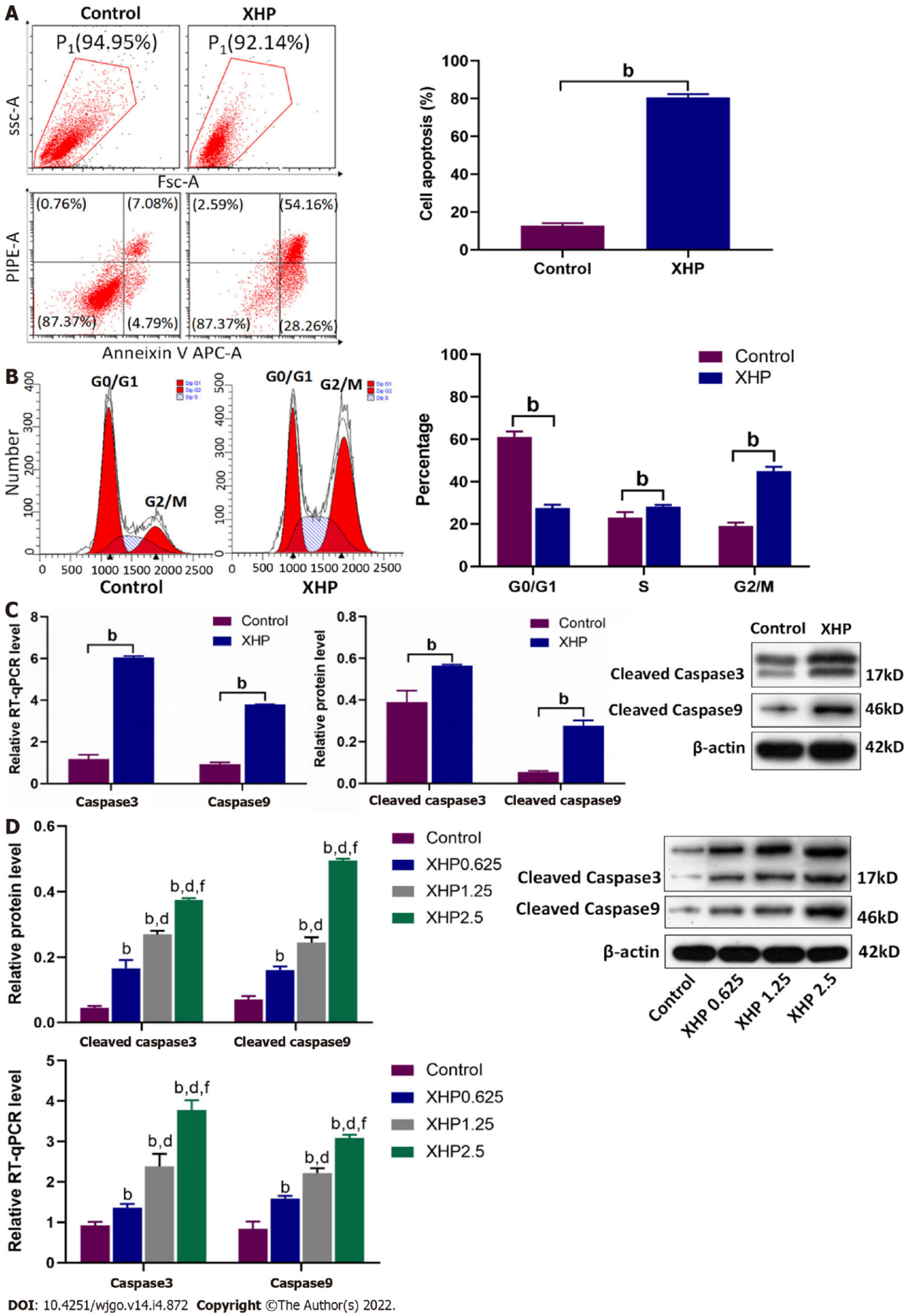

DOI: 10.4251/wjgo.v14.i4.872

Figure 3 SMMC-7721 cell apoptosis is induced by Xihuang pills extract. SMMC-7721 cells were stained with annexin V/propidium iodide and fluorescein isothiocyanate after treatment with or without 0.625 mg/mL Xihuang pills (XHP) extract for 12 h. A and B: Flow cytometry was used to detect the number

of apoptotic cells (A) and the cell cycle distribution (B); C: Cleaved caspase-3 and cleaved caspase-9 protein expression levels were detected by Western blotting, and caspase-3 and caspase-9 mRNA expression levels were detected by reverse-transcription polymerase chain reaction (RT–qPCR); D: After treating SMMC-7721 cells with different concentrations of the XHP extract, cleaved caspase-3 and cleaved caspase-9 protein expression levels were determined using Western blotting, whereas caspase-3 and caspase-9 mRNA expression levels were determined using RT–qPCR. The experiment was repeated three times, and the data are presented as the means ± SD. [a]*P* < 0.05 and [b]*P* < 0.01 compared with the control group; [c]*P* < 0.05 and [d]*P* < 0.01 compared with the XHP 0.625 group; [e]*P* < 0.05 and [f]*P* < 0.01 compared with the XHP 1.25 group.

important role in the inhibition of cancer cell invasion and metastasis[31]. The caspase-3 zymogen is regulated by caspase-9[19]. Activation of PI3K may inhibit caspase 3 activity and DNA fragmentation in several cell types. Therefore, PI3K is essential for maintaining cell viability. Furthermore, Bcl-2 has an important role in caspase-3-mediated apoptosis[32]. mTOR, a downstream target of Akt, phosphorylates Bad (an apoptotic molecule) and induces the expression of antiapoptotic Bcl-2 family proteins. Moreover, it inhibits the release of cytochrome c from the mitochondria, thereby inhibiting the activation of caspase-9 and caspase-3 and increasing cell viability[19,23,33]. Thus, the PI3K/Akt/mTOR signalling pathway regulates apoptosis by modulating caspase-9 and caspase-3 activity.

In this study, the high resolution MS was used to analyze the compound composition of XHP. Twelve compounds in XHP were identified, which were valine, 4-gingerol, myrrhone, ricinoleic acid, glycocholic acid, curzerenone, 11-keto-β-boswellic acid, oleic acid, germacrone, 3-acetyl-9,11-dehydro-β-boswellic acid, 5β-androstane-3,17-dione, and 3-acetyl-11-keto-β-boswellic acid. Among them, Curcuzederone, 11-keto-α-Boswellic Acid, Oleic Acid and 3-acetyl-11-keto-beta-Boswellic Acid have been reported to have good anticancer activity. They inhibit tumor growth by promoting apoptosis of cancer cells[34-38]. We speculate that the anti-tumor effect of XHP may be through these active ingredients, and we will further clarify the role of the active ingredients in future studies.

Activation of apoptosis is one of the crucial strategies for anti-tumour therapy[10,39-41]. The results of this study revealed that XHP effectively suppressed the growth of HCC cells at a concentration of 0.625 mg/mL in a dose- and time-dependent manner. The scratch assay revealed that XHP treatment also inhibited HCC cell migration in a time-dependent manner. Apoptosis experiments further confirmed that XHP treatment arrested the cell cycle in G2/M phase, facilitating the apoptosis of HCC cells. Based on these results, XHP exerts an inhibitory effect on the growth and migration of tumour cells by inducing apoptosis.

We further investigated the effects of XHP on the PI3K/Akt/mTOR pathway. XHP treatment inhibited the PI3K/Akt/mTOR pathway both *in vivo* and *in vitro* in a dose-dependent manner. Moreover, the activities of cleaved caspase-9 and cleaved caspase-3 were increased in response to XHP treatment. Therefore, we hypothesized that XHP may cause cell cycle arrest *via* the PI3K/Akt/mTOR signalling pathway and regulates the expression of the apoptosis executioner proteins cleaved caspase-9 and cleaved caspase-3, thereby promoting apoptosis in HCC and inhibiting the growth and migration of tumour cells. In addition, an *in vivo* experiment in nude mice further confirmed the inhibitory effects of XHP on HCC cells, as evidenced by decreases in tumour volume and weight. However, the effect of XHP on the mitochondrial apoptotic pathway, such as autophagy, was not detected in this study. The exact step that XHP modulated in the PI3K/Akt/mTOR pathway is unclear. Therefore, further research is needed to obtain a comprehensive interpretation of the XHP-regulated antitumour effect.

CONCLUSION

In conclusion, XHP increases cleaved caspase-9 and cleaved caspase-3 activities by inhibiting the PI3K/Akt/mTOR signalling pathway and induces apoptosis and cell cycle arrest. Consequently, XHP inhibits the growth, migration, and proliferation of HCC cells. Our study provides a better understanding of the antitumour effects of XHP and reveals the underlying mechanism. The findings of this study suggest that XHP may serve as a supplementary medicine in HCC treatment.

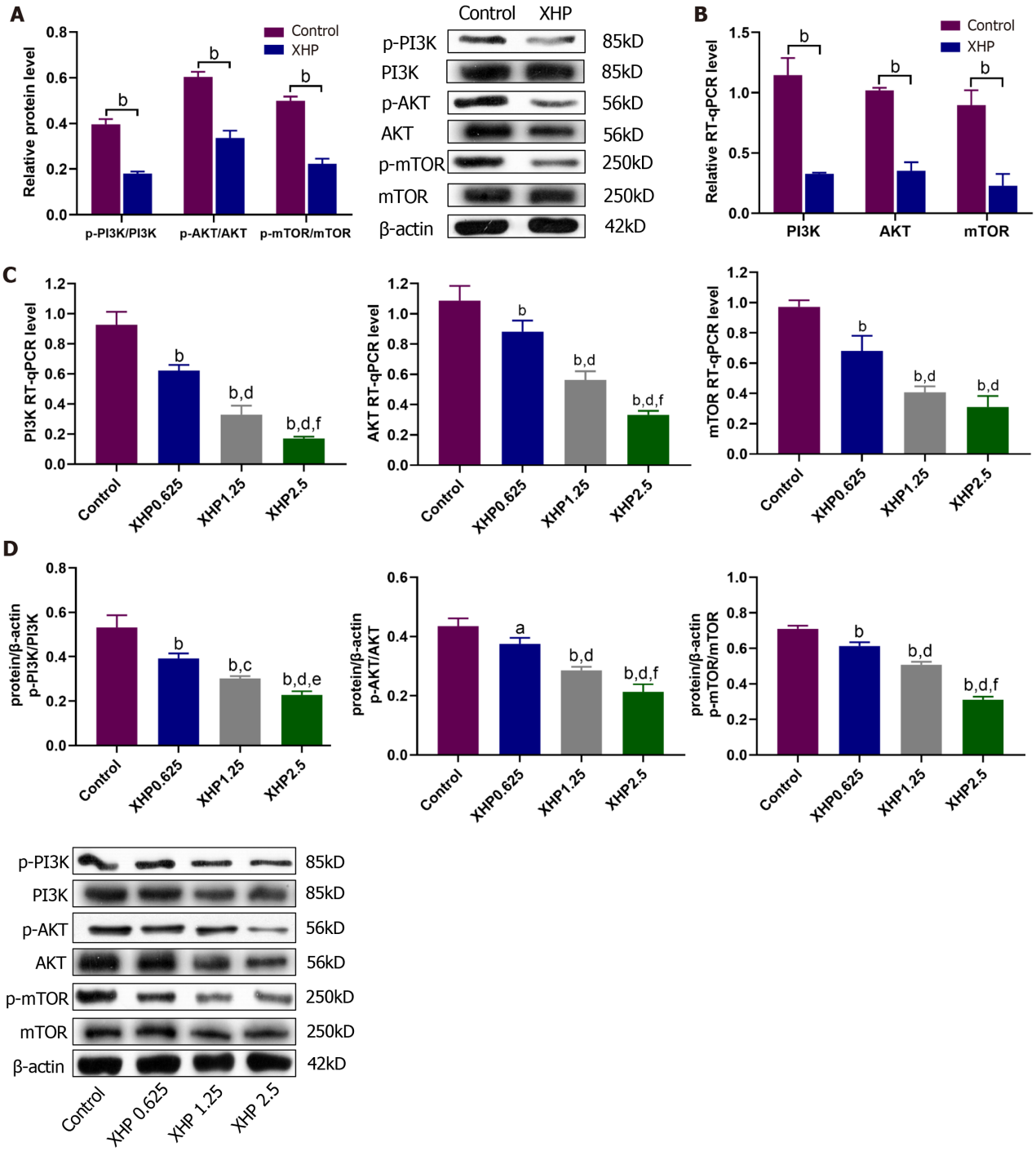

DOI: 10.4251/wjgo.v14.i4.872

Figure 4 Inhibitory effects of Xihuang pills extract on the expression of components of the phosphoinositide 3-kinase/protein kinase-B/mechanistic target of rapamycin signalling pathway both *in vivo* and *in vitro*. A: The protein expression levels and ratios of phosphoinositide 3-kinase/protein kinase-B/mechanistic target of rapamycin (PI3K/Akt/mTOR) and p-PI3K/p-Akt/p-mTOR in SMMC-7721 cells were detected using Western blotting; B: PI3K/Akt/mTOR mRNA expression levels in SMMC-7721 cells, as determined using reverse-transcription polymerase chain reaction (RT-qPCR); C: PI3K/Akt/mTOR mRNA expression levels in SMMC-7721 cells after treatment with different concentrations of Xihuang pills (XHP), as measured using RT–qPCR; D: Levels of the PI3K/Akt/mTOR and p-PI3K/p-Akt/p-mTOR proteins in SMMC-7721 cells treated with different concentrations of the XHP extract were detected using Western blotting. Relative protein and mRNA expression levels are shown in representative histograms. The experiment was repeated three times, and the data are presented as the means ± SD. $^{a}P < 0.05$ and $^{b}P < 0.01$ compared with the control group; $^{c}P < 0.05$ and $^{d}P < 0.01$ compared with the XHP 0.625 group; $^{e}P < 0.05$ and $^{f}P < 0.01$ compared with the XHP 1.25 group.

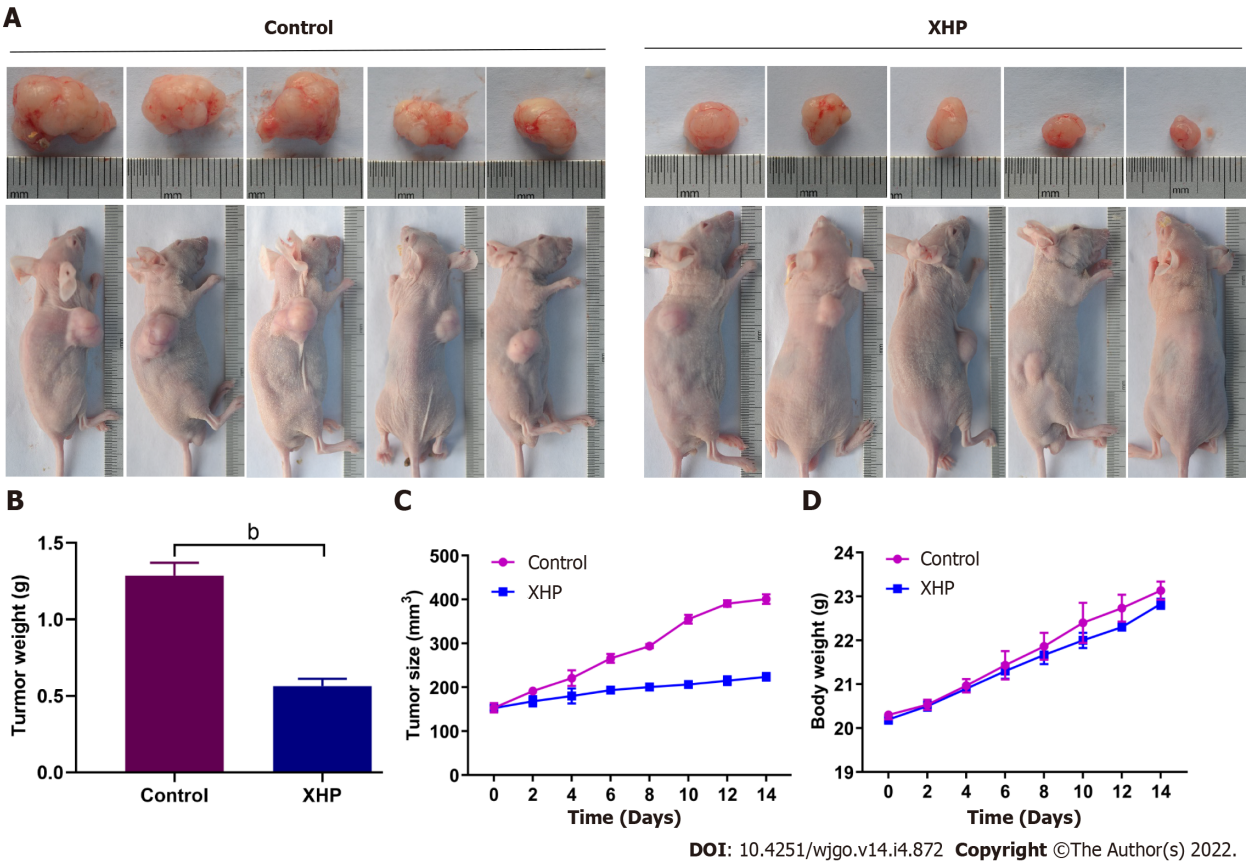

DOI: 10.4251/wjgo.v14.i4.872

Figure 5 Xihuang pills treatment inhibits tumour growth *in vivo*. SMMC7721 cells were injected subcutaneously into the lower right side of 5-week-old BALB/c male nude mice. After a model of subcutaneous xenograft tumours was successfully established in nude mice, animals were randomly divided into two groups. Each group was then treated with either 0.2 mL of distilled water (control) or 78 mg/kg of body weight Xihuang pills. A: Representative images of subcutaneous xenograft tumours at the end of treatment; B: Subcutaneous tumour weights measured at the end of the treatment; C: Average subcutaneous tumour volume measured every 2 d; D: Average mouse body weight measured every 2 d. The experiment was repeated three times, and the data are presented as the means ± SD. The results were analysed using one-way analysis of variance, followed by the least significant difference test. $^{a}P < 0.05$ and $^{b}P < 0.01$ compared with the control group. XHP: Xihuang pills.

ARTICLE HIGHLIGHTS

Research background

Xihuang pills (XHP) are a traditional Chinese preparation with antitumour properties. They inhibit the growth of breast cancer, glioma, and other tumours by regulating the phosphoinositide 3-kinase/protein kinase-B/mechanistic target of rapamycin (PI3K/Akt/mTOR) signalling pathway. However, the effects and mechanisms of action of XHP in hepatocellular carcinoma (HCC) remain unclear. Regulation of the PI3K/Akt/mTOR signalling pathway effectively inhibits the progression of HCC.

Research motivation

We hypothesized that XHP might play a role in inhibiting HCC through the PI3K/Akt/mTOR signalling pathway.

Research objectives

To confirm the effect of XHP on HCC and the possible mechanisms involved.

Research methods

The chemical constituents and active components of XHP were analysed using ultra-performance liquid chromatography-quadrupole time of flight mass spectrometry (MS) (UPLC-Q-TOF-MS). First, cell-based experiments and *in vivo* xenograft tumour experiments were utilized to evaluate the effect of XHP on HCC tumorigenesis. Cell viability was assessed using the CCK-8 assay, followed by an assessment of cell migration using a wound healing assay. Second, the effect of XHP on the apoptosis of SMMC-7721 cells was evaluated. Third, Western blotting and reverse-transcription polymerase chain reaction were performed to confirm the effects of XHP on the protein and mRNA expression of components of the

PI3K/Akt/mTOR signalling pathway. Finally, the effects of XHP on the tumorigenesis of subcutaneous hepatocellular tumours in nude mice were assessed.

Research results

The 12 compounds were identified in XHP by high-resolution MS. The cell viability assay results showed that treatment with 0.625 mg/mL XHP extract decreased HCC cell viability after 12 h. Moreover, XHP significantly inhibited cell migration and resulted in cell cycle arrest and apoptosis. Furthermore, XHP downregulated the PI3K/Akt/mTOR signalling pathway, which activated apoptosis executioner proteins (*e.g.*, caspase-9 and caspase-3). The inhibitory effects of XHP on HCC cell growth were determined *in vivo* by analysing the tumour xenograft volumes and weights.

Research conclusions

XHP inhibited HCC cell growth and migration by stimulating apoptosis *via* the downregulation of the PI3K/Akt/mTOR signalling pathway, followed by the activation of caspase-9 and caspase-3. Our findings clarified that the antitumour effects of XHP on HCC cells are mediated by the PI3K/Akt/mTOR signalling pathway.

Research perspectives

Our findings revealed that XHP may be a potential complementary therapy for HCC.

FOOTNOTES

Author contributions: Teng YJ, Deng Z, and Wu YR completed the experiment and wrote the paper; Teng YJ, Deng Z, and Ouyang ZG reviewed the manuscript; Tian XF and Zhou Q provided research ideas; Long HP and Fang LY performed HPLC analysis; Zhang BY has processed the figures of the article; Fan XX, Yin DL, Guo YM, Zheng P, Huang Z and Ning DM conducted statistical analysis; all authors have read and approved the manuscript to ensure its accuracy and completeness.

Supported by National Natural Science Foundation of China, No. U20A20408 and No. 82074450; Natural Science Foundation of Hunan Province, No. 2020JJ4066; Hunan Province "Domestic First-class Cultivation Discipline" Integrated Traditional Chinese and Western Medicine Open Fund Project, No. 2020ZXYJH34 and No. 2020ZXYJH35; Hunan Graduate Scientific Research Innovation Project, No. QL20210173 and No. CX20210730; Hunan Province Science and Technology Innovation Talents Plan College Students Science and Technology Innovation and Entrepreneurship Project, No. 2020RC1004; Guangzhou Health Science and Technology Project, No. 20221A011102; and Hunan Traditional Chinese Medicine Scientific Research Project, No. 202101.

Institutional animal care and use committee statement: This study was reviewed and approved by the Ethics Review Committee of Experimental Animal Welfare at the Central South University in Changsha, China.

Conflict-of-interest statement: The authors declare that they have no competing interests.

Data sharing statement: Dataset available from the corresponding author at 003640@hnucm.edu.cn. Participants gave informed consent for data sharing.

ARRIVE guidelines statement: The authors have read the ARRIVE guidelines, and the manuscript was prepared and revised according to the ARRIVE guidelines.

Country/Territory of origin: China

ORCID number: Yong-Jie Teng 0000-0001-8354-8829; Zhe Deng 0000-0002-3283-6289; Zhao-Guang Ouyang 0000-0002-8119-485X; Qing Zhou 0000-0002-9633-7542; Si Mei 0000-0002-4263-1121; Xing-Xing Fan 0000-0002-7751-7193; Yong-Rong Wu 0000-0002-3265-600X; Hong-Ping Long 0000-0001-8891-5851; Le-Yao Fang 0000-0002-8226-2017; Dong-Liang Yin 0000-0002-2367-1419; Bo-Yu Zhang 0000-0002-5940-7265; Yin-Mei Guo 0000-0003-0635-1218; Wen-Hao Zhu 0000-0002-2326-7475; Zhen Huang 0000-0002-8437-7141; Piao Zheng 0000-0003-3649-8181; Di-Min Ning 0000-0003-4335-7141; Xue-Fei Tian 0000-0003-4786-0844.

S-Editor: Fan JR
L-Editor: A
P-Editor: Guo X

REFERENCES

1 **Dasgupta P**, Henshaw C, Youlden DR, Clark PJ, Aitken JF, Baade PD. Global Trends in Incidence Rates of Primary Adult Liver Cancers: A Systematic Review and Meta-Analysis. *Front Oncol* 2020; **10**: 171 [PMID: 32185125 DOI: 10.3389/fonc.2020.00171]

2 **Ko KL**, Mak LY, Cheung KS, Yuen MF. Hepatocellular carcinoma: recent advances and emerging medical therapies. *F1000Res* 2020; **9** [PMID: 32595940 DOI: 10.12688/f1000research.24543.1]

3 **Rahmani F**, Ziaeemehr A, Shahidsales S, Gharib M, Khazaei M, Ferns GA, Ryzhikov M, Avan A, Hassanian SM. Role of regulatory miRNAs of the PI3K/AKT/mTOR signaling in the pathogenesis of hepatocellular carcinoma. *J Cell Physiol* 2020; **235**: 4146-4152 [PMID: 31663122 DOI: 10.1002/jcp.29333]

4 **Zhou Q**, Lui VW, Yeo W. Targeting the PI3K/Akt/mTOR pathway in hepatocellular carcinoma. *Future Oncol* 2011; **7**: 1149-1167 [PMID: 21992728 DOI: 10.2217/fon.11.95]

5 **Brotelle T**, Bay JO. [PI3K-AKT-mTOR pathway: Description, therapeutic development, resistance, predictive/prognostic biomarkers and therapeutic applications for cancer]. *Bull Cancer* 2016; **103**: 18-29 [PMID: 26582734 DOI: 10.1016/j.bulcan.2015.09.011]

6 **Fresno Vara JA**, Casado E, de Castro J, Cejas P, Belda-Iniesta C, González-Barón M. PI3K/Akt signalling pathway and cancer. *Cancer Treat Rev* 2004; **30**: 193-204 [PMID: 15023437 DOI: 10.1016/j.ctrv.2003.07.007]

7 **Polivka J Jr**, Janku F. Molecular targets for cancer therapy in the PI3K/AKT/mTOR pathway. *Pharmacol Ther* 2014; **142**: 164-175 [PMID: 24333502 DOI: 10.1016/j.pharmthera.2013.12.004]

8 **Janku F**. Phosphoinositide 3-kinase (PI3K) pathway inhibitors in solid tumors: From laboratory to patients. *Cancer Treat Rev* 2017; **59**: 93-101 [PMID: 28779636 DOI: 10.1016/j.ctrv.2017.07.005]

9 **Zhang Y**, Xie C, Li A, Liu X, Xing Y, Shen J, Huo Z, Zhou S, Xie Y, Cao W, Ma Y, Xu R, Cai S, Tang X, Ma D. PKI-587 enhances chemosensitivity of oxaliplatin in hepatocellular carcinoma through suppressing DNA damage repair pathway (NHEJ and HR) and PI3K/AKT/mTOR pathway. *Am J Transl Res* 2019; **11**: 5134-5149 [PMID: 31497229]

10 **Pistritto G**, Trisciuoglio D, Ceci C, Garufi A, D'Orazi G. Apoptosis as anticancer mechanism: function and dysfunction of its modulators and targeted therapeutic strategies. *Aging (Albany NY)* 2016; **8**: 603-619 [PMID: 27019364 DOI: 10.18632/aging.100934]

11 **Hong SW**, Jung KH, Lee HS, Choi MJ, Son MK, Zheng HM, Hong SS. SB365 inhibits angiogenesis and induces apoptosis of hepatocellular carcinoma through modulation of PI3K/Akt/mTOR signaling pathway. *Cancer Sci* 2012; **103**: 1929-1937 [PMID: 22909393 DOI: 10.1111/j.1349-7006.2012.02409.x]

12 **Guo Q**, Xu X, He S, Yuan Y, Chen S, Hua B. Xi huang pills enhance the tumor treatment efficacy when combined with chemotherapy: A meta-analysis and systematic review. *J Cancer Res Ther* 2018; **14**: S1012-S1018 [PMID: 30539838 DOI: 10.4103/0973-1482.192795]

13 **Mao D**, Feng L, Huang S, Zhang S, Peng W. Meta-Analysis of Xihuang Pill Efficacy When Combined with Chemotherapy for Treatment of Breast Cancer. *Evid Based Complement Alternat Med* 2019; **2019**: 3502460 [PMID: 30992708 DOI: 10.1155/2019/3502460]

14 **Li XY**, Su L, Jiang YM, Gao WB, Xu CW, Zeng CQ, Song J, Xu Y, Weng WC, Liang WB. The Antitumor Effect of Xihuang Pill on Treg Cells Decreased in Tumor Microenvironment of 4T1 Breast Tumor-Bearing Mice by PI3K/AKT~AP-1 Signaling Pathway. *Evid Based Complement Alternat Med* 2018; **2018**: 6714829 [PMID: 29849718 DOI: 10.1155/2018/6714829]

15 **Fu J**, Zhu SH, Xu HB, Xu YQ, Wang X, Wang J, Kong PS. Xihuang pill potentiates the anti-tumor effects of temozolomide in glioblastoma xenografts through the Akt/mTOR-dependent pathway. *J Ethnopharmacol* 2020; **261**: 113071 [PMID: 32603676 DOI: 10.1016/j.jep.2020.113071]

16 **Shao M**, He Z, Yin Z, Ma P, Xiao Q, Song Y, Huang Z, Ma Y, Qiu Y, Zhao A, Zhou T, Wang Q. Xihuang Pill Induces Apoptosis of Human Glioblastoma U-87 MG Cells *via* Targeting ROS-Mediated Akt/mTOR/FOXO1 Pathway. *Evid Based Complement Alternat Med* 2018; **2018**: 6049498 [PMID: 30046342 DOI: 10.1155/2018/6049498]

17 **Nair A**, Morsy MA, Jacob S. Dose translation between laboratory animals and human in preclinical and clinical phases of drug development. *Drug Dev Res* 2018; **79**: 373-382 [PMID: 30343496 DOI: 10.1002/ddr.21461]

18 **Golob-Schwarzl N**, Krassnig S, Toeglhofer AM, Park YN, Gogg-Kamerer M, Vierlinger K, Schröder F, Rhee H, Schicho R, Fickert P, Haybaeck J. New liver cancer biomarkers: PI3K/AKT/mTOR pathway members and eukaryotic translation initiation factors. *Eur J Cancer* 2017; **83**: 56-70 [PMID: 28715695 DOI: 10.1016/j.ejca.2017.06.003]

19 **Wu T**, Dong X, Yu D, Shen Z, Yu J, Yan S. Natural product pectolinarigenin inhibits proliferation, induces apoptosis, and causes G2/M phase arrest of HCC *via* PI3K/AKT/mTOR/ERK signaling pathway. *Onco Targets Ther* 2018; **11**: 8633-8642 [PMID: 30584322 DOI: 10.2147/OTT.S186186]

20 **Wu Y**, Zhang Y, Qin X, Geng H, Zuo D, Zhao Q. PI3K/AKT/mTOR pathway-related long non-coding RNAs: roles and mechanisms in hepatocellular carcinoma. *Pharmacol Res* 2020; **160**: 105195 [PMID: 32916254 DOI: 10.1016/j.phrs.2020.105195]

21 **Goncalves MD**, Hopkins BD, Cantley LC. Phosphatidylinositol 3-Kinase, Growth Disorders, and Cancer. *N Engl J Med* 2018; **379**: 2052-2062 [PMID: 30462943 DOI: 10.1056/NEJMra1704560]

22 **Jiang S**, Wang Q, Feng M, Li J, Guan Z, An D, Dong M, Peng Y, Kuerban K, Ye L. C2-ceramide enhances sorafenib-induced caspase-dependent apoptosis *via* PI3K/AKT/mTOR and Erk signaling pathways in HCC cells. *Appl Microbiol Biotechnol* 2017; **101**: 1535-1546 [PMID: 27807662 DOI: 10.1007/s00253-016-7930-9]

23 **Khemlina G**, Ikeda S, Kurzrock R. The biology of Hepatocellular carcinoma: implications for genomic and immune therapies. *Mol Cancer* 2017; **16**: 149 [PMID: 28854942 DOI: 10.1186/s12943-017-0712-x]

24 **Song L**, Luo Y, Li S, Hong M, Wang Q, Chi X, Yang C. ISL Induces Apoptosis and Autophagy in Hepatocellular Carcinoma *via* Downregulation of PI3K/AKT/mTOR Pathway *in vivo* and in vitro. *Drug Des Devel Ther* 2020; **14**: 4363-4376 [PMID: 33116421 DOI: 10.2147/DDDT.S270124]

25 **Xue S**, Zhou Y, Zhang J, Xiang Z, Liu Y, Miao T, Liu G, Liu B, Liu X, Shen L, Zhang Z, Li M, Miao Q. Anemoside B4 exerts anti-cancer effect by inducing apoptosis and autophagy through inhibiton of PI3K/Akt/mTOR pathway in

hepatocellular carcinoma. *Am J Transl Res* 2019; **11**: 2580-2589 [PMID: 31105864]
26 **Lee YI**, Kang-Park S, Do SI, Lee YI. The hepatitis B virus-X protein activates a phosphatidylinositol 3-kinase-dependent survival signaling cascade. *J Biol Chem* 2001; **276**: 16969-16977 [PMID: 11278872 DOI: 10.1074/jbc.M011263200]
27 **Aoki M**, Fujishita T. Oncogenic Roles of the PI3K/AKT/mTOR Axis. *Curr Top Microbiol Immunol* 2017; **407**: 153-189 [PMID: 28550454 DOI: 10.1007/82_2017_6]
28 **Coutte L**, Dreyer C, Sablin MP, Faivre S, Raymond E. [PI3K-AKT-mTOR pathway and cancer]. *Bull Cancer* 2012; **99**: 173-180 [PMID: 21742593 DOI: 10.1684/bdc.2011.1384]
29 **Li A**, Zhang R, Zhang Y, Liu X, Wang R, Liu J, Xie Y, Cao W, Xu R, Ma Y, Cai W, Wu B, Cai S, Tang X. BEZ235 increases sorafenib inhibition of hepatocellular carcinoma cells by suppressing the PI3K/AKT/mTOR pathway. *Am J Transl Res* 2019; **11**: 5573-5585 [PMID: 31632530]
30 **Crowley LC**, Waterhouse NJ. Detecting Cleaved Caspase-3 in Apoptotic Cells by Flow Cytometry. *Cold Spring Harb Protoc* 2016; **2016** [PMID: 27803251 DOI: 10.1101/pdb.prot087312]
31 **Zhou M**, Liu X, Li Z, Huang Q, Li F, Li CY. Caspase-3 regulates the migration, invasion and metastasis of colon cancer cells. *Int J Cancer* 2018; **143**: 921-930 [PMID: 29524226 DOI: 10.1002/ijc.31374]
32 **Tsujimoto Y**. Role of Bcl-2 family proteins in apoptosis: apoptosomes or mitochondria? *Genes Cells* 1998; **3**: 697-707 [PMID: 9990505 DOI: 10.1046/j.1365-2443.1998.00223.x]
33 **Li TT**, Zhu D, Mou T, Guo Z, Pu JL, Chen QS, Wei XF, Wu ZJ. IL-37 induces autophagy in hepatocellular carcinoma cells by inhibiting the PI3K/AKT/mTOR pathway. *Mol Immunol* 2017; **87**: 132-140 [PMID: 28433890 DOI: 10.1016/j.molimm.2017.04.010]
34 **Al-Amin M**, Eltayeb NM, Khairuddean M, Salhimi SM. Bioactive chemical constituents from *Curcuma caesia* Roxb. rhizomes and inhibitory effect of curcuzederone on the migration of triple-negative breast cancer cell line MDA-MB-231. *Nat Prod Res* 2021; **35**: 3166-3170 [PMID: 31726856 DOI: 10.1080/14786419.2019.1690489]
35 **Schmiech M**, Ulrich J, Lang SJ, Büchele B, Paetz C, St-Gelais A, Syrovets T, Simmet T. 11-Keto-α-Boswellic Acid, a Novel Triterpenoid from *Boswellia* spp. with Chemotaxonomic Potential and Antitumor Activity against Triple-Negative Breast Cancer Cells. *Molecules* 2021; **26** [PMID: 33445710 DOI: 10.3390/molecules26020366]
36 **Jung S**, Lee S, Lee H, Yoon J, Lee EK. Oleic acid-embedded nanoliposome as a selective tumoricidal agent. *Colloids Surf B Biointerfaces* 2016; **146**: 585-589 [PMID: 27424089 DOI: 10.1016/j.colsurfb.2016.06.058]
37 **Mizushina Y**, Takeuchi T, Sugawara F, Yoshida H. Anti-cancer targeting telomerase inhibitors: β-rubromycin and oleic acid. *Mini Rev Med Chem* 2012; **12**: 1135-1143 [PMID: 22876944 DOI: 10.2174/138955712802762220]
38 **Riaz A**, Rasul A, Kanwal N, Hussain G, Shah MA, Sarfraz I, Ishfaq R, Batool R, Rukhsar F, Adem Ş. Germacrone: A Potent Secondary Metabolite with Therapeutic Potential in Metabolic Diseases, Cancer and Viral Infections. *Curr Drug Metab* 2020; **21**: 1079-1090 [PMID: 32723267 DOI: 10.2174/1389200221999200728144801]
39 **Goldar S**, Khaniani MS, Derakhshan SM, Baradaran B. Molecular mechanisms of apoptosis and roles in cancer development and treatment. *Asian Pac J Cancer Prev* 2015; **16**: 2129-2144 [PMID: 25824729 DOI: 10.7314/apjcp.2015.16.6.2129]
40 **Lin Y**, Chen Y, Wang S, Ma J, Peng Y, Yuan X, Lv B, Chen W, Wei Y. Plumbagin induces autophagy and apoptosis of SMMC-7721 cells *in vitro* and in vivo. *J Cell Biochem* 2019; **120**: 9820-9830 [PMID: 30536473 DOI: 10.1002/jcb.28262]
41 **Wang K**. Autophagy and apoptosis in liver injury. *Cell Cycle* 2015; **14**: 1631-1642 [PMID: 25927598 DOI: 10.1080/15384101.2015.1038685]

World Journal of Gastrointestinal Oncology

Submit a Manuscript: https://www.f6publishing.com

World J Gastrointest Oncol 2022 April 15; 14(4): 887-896

DOI: 10.4251/wjgo.v14.i4.887

ISSN 1948-5204 (online)

ORIGINAL ARTICLE

Retrospective Study

Effect of hepatic artery resection and reconstruction on the prognosis of patients with advanced hilar cholangiocarcinoma

Yuan-Ming Li, Zhi-Xin Bie, Run-Qi Guo, Bin Li, Cheng-En Wang, Fei Yan

Specialty type: Oncology

Provenance and peer review: Unsolicited article; Externally peer reviewed.

Peer-review model: Single blind

Peer-review report's scientific quality classification

Grade A (Excellent): 0
Grade B (Very good): B, B, B
Grade C (Good): 0
Grade D (Fair): 0
Grade E (Poor): 0

P-Reviewer: Ahn KS, South Korea; Kim R, United States; Nathan H, United States

Received: November 3, 2021
Peer-review started: November 3, 2021
First decision: December 2, 2021
Revised: December 16, 2021
Accepted: March 5, 2022
Article in press: March 5, 2022
Published online: April 15, 2022

Yuan-Ming Li, Zhi-Xin Bie, Run-Qi Guo, Bin Li, Cheng-En Wang, Fei Yan, Minimally Invasive Tumor Therapies Center, Beijing Hospital, National Center of Gerontology, Institute of Geriatric Medicine, Chinese Academy of Medical Sciences, Beijing 100730, China

Corresponding author: Yuan-Ming Li, PhD, Associate Chief Physician, Minimally Invasive Tumor Therapies Center, Beijing Hospital, National Center of Gerontology, Institute of Geriatric Medicine, Chinese Academy of Medical Sciences, No. 1 Dongdan Dahua Street, Dongcheng District, Beijing 100730, China. liym@vip.126.com

Abstract

BACKGROUND

Hilar cholangiocarcinoma (HC) is a good adaptation certificate of hepatic arterectomy, and hepatic arterectomy is conductive to the radical resection of cholangiocarcinoma, which simplifies the operation and helps with a combined resection of the peripheral portal tissue. With continuous development of surgical techniques, especially microsurgical technique, vascular invasion is no longer a contraindication to surgery in the past 10 years. However, hepatic artery reconstruction after hepatic arterectomy has been performed to treat liver tumor in many centers with better results, but it is rarely applied in advanced HC.

AIM

To determine the prognosis of patients with advanced HC after hepatic artery resection and reconstruction.

METHODS

A total of 98 patients with HC who underwent radical operation in our hospital were selected for this retrospective analysis. According to whether the patients underwent hepatic artery resection and reconstruction or not, they were divided into reconstruction (n = 40) and control (n = 58) groups. The traumatic indices, surgical resection margin, liver function tests before and after the operation, and surgical complications were compared between the two groups.

RESULTS

Operation time, blood loss, hospital stay, and gastrointestinal function recovery time were higher in the reconstruction group than in the control group ($P < 0.05$); The R0 resection rates were 90.00% and 72.41% in the reconstruction and control groups, respectively ($P < 0.05$). Serum alanine aminotransferase was lower in the reconstruction group on day one and three postoperatively, whereas serum

aspartate aminotransferase was lower on the third day ($P < 0.05$). Preoperatively, the Karnofsky performance status scores were similar between the groups ($P > 0.05$), but was higher in the reconstruction group ($P < 0.05$) two weeks postoperatively. There was no difference in the complication rate between the two groups (27.50% *vs* 32.67%, $P > 0.05$). Two-year survival rate (42.50% *vs* 39.66%) and two-year survival time (22.0 mo *vs* 23.0 mo) were similar between the groups ($P > 0.05$).

CONCLUSION

Radical surgery combined with reconstruction after hepatic artery resection improves R0 resection rate and reduces postoperative liver injury in advanced HC. However, the operation is difficult and the effect on survival time is not clear.

Key Words: Advanced stage; Hilar cholangiocarcinoma; Hepatic artery resection; Reconstruction; Radical surgery

Core Tip: Through retrospective analysis of 98 patients with hilar cholangiocarcinoma, we confirmed that radical surgery combined with reconstruction after hepatic artery resection can increase the R0 resection rate of advanced hilar cholangiocarcinoma and reduce postoperative liver injury. However, this operation is more difficult, and the impact on survival time is still unclear, and further follow-up studies are still needed.

Citation: Li YM, Bie ZX, Guo RQ, Li B, Wang CE, Yan F. Effect of hepatic artery resection and reconstruction on the prognosis of patients with advanced hilar cholangiocarcinoma. *World J Gastrointest Oncol* 2022; 14(4): 887-896

URL: https://www.wjgnet.com/1948-5204/full/v14/i4/887.htm

DOI: https://dx.doi.org/10.4251/wjgo.v14.i4.887

INTRODUCTION

Hilar cholangiocarcinoma (HC) is the most common type of cholangiocarcinoma, arising from the epithelium of the bile duct mucosa above the cystic duct opening[1-4]. Operation is the only measure to improve prognosis[5]. However, the procedure can be extremely challenging due to the anatomic parts involved and important adjacent structures[6,7]. Invasion of the hepatic artery corresponds to advanced disease, limiting radical resection and increasing the incidence of postoperative complications, such as abdominal bleeding, infection, and liver failure[8]. In some cases, compromise of the hepatic artery may not be due to true invasion, but due to compression of the artery by the enlarging tumor. Combined vascular resection in advanced HC is proposed by many authors, with notable rates of successful surgical outcomes[9]. How to effectively reduce the incidence of postoperative complications and improve radical cure has become a topic of intense clinical interest. Currently, there is a paucity of research about the impact of hepatic artery resection and reconstruction for advanced HC. If the hepatic artery is invaded, radical excision cannot be performed, and only palliative surgery is offered with the goal of symptom relief and definitive treatment[10,11]. Resection and reconstruction of the affected hepatic artery and portal vein can be combined with resection of the affected lateral liver, to improve surgical outcomes. Our study aimed to determine the effect of hepatic artery resection and reconstruction in patients with advanced HC, and to provide some clinical guidance.

MATERIALS AND METHODS

Data

A total of 98 patients with HC who underwent radical operation in our hospital from February 2015 to June 2018 were selected for this retrospective analysis. According to whether the patients underwent hepatic artery resection and reconstruction or not, they were divided into reconstruction ($n = 40$) and control ($n = 58$) groups. Inclusion criteria were as follows: (1) Age: 19-75 years; (2) American Society of Anesthesiologists Classification grade I-III; (3) HC diagnosed through abdominal computed tomography, magnetic resonance imaging, or endoscopic retrograde cholangiopancreatography; (4) Bismuth-Corlette type I-IV; (5) Follow up data for at least two years; and (6) Study plan that does not

violate the requirements of relevant medical ethics. Exclusion criteria include: (1) Presence of concurrent extrahepatic malignancy; (2) Previous history of hepatobiliary surgery due to other reasons; (3) Serious comorbidities (cerebrovascular accident, acute myocardial infarction, *etc.*); and (4) Lack of data. The two groups were comparable in their baseline characteristics as shown in Table 1.

Surgical method

The control group underwent routine radical surgery. After general anesthesia, a reverse "L"-shaped incision was made below the right costal margin to explore the tumor, then the hepatic artery and portal vein under the duodenal ligament were separated. The common bile duct was cut open, and the gallbladder was dissociated and pulled upward together with the common bile duct. Nerves and lymph nodes were removed from top down to expose and skeletonize the hepatic artery and portal vein. The location and state of the tumor were evaluated, and invasion of the confluence of the hepatic and bile ducts was carefully determined. Liver lobectomy was performed, the contralateral bile duct was cut open at 0.5 cm of the tumor margin, and the hepatic artery and portal vein on the affected side were resected together with the lesion. Prophylactic antibiotics and hydration were administered as per postoperative protocol.

The reconstruction group underwent combined hepatectomy and hepatic artery reconstruction under general anesthesia. A reverse "L"-shaped incision was made below the right costal margin to explore the tumor, then the hepatic artery and portal vein under the duodenal ligament were separated. Sixteen groups of lymph nodes were examined after the abdominal resection, in order to determine whether there was metastasis to the peritoneum and liver. The bile duct was cut off behind the duodenum, the tumor was dissociated toward the head direction, and the lymph nodes and connective tissue of the hepatic duodenal ligament were completely removed. If the bile duct margin was negative, the dissected portal vein was resected and ligated. The liver was then cut through by a phacoemulsification suction knife. The opposite lateral bile duct was resected and biliary drainage tubes were inserted and fixed. The tumor and affected artery were resected together, and 70 Prolene sutures were used to reconstruct the hepatic artery through interrupted anastomosis. The reconstruction method was based on arterial invasion length, and included reconstruction using a great saphenous vein graft and in situ reconstruction after resection of the involved artery. If there was no evidence of bleeding within 24 h, 4000 IU of low-molecular-weight heparin sodium was administered subcutaneously once daily for 3-5 d. Antiplatelet therapy with clopidogrel was initiated after initiation of oral intake.

Monitoring parameters

The operation time, operation blood loss, length of hospital stay, postoperative gastrointestinal function recovery time, R0 resection rate, serum alanine aminotransferase (ALT), aspartate aminotransferase (AST), total bilirubin (TBIL), Karnofsky performance status (KPS) score, surgical complications, two-year survival rate and survival time between the two groups were statistically analyzed.

Morning fasting venous blood samples (3 mL) were collected from all the participants and centrifuged at 3000 r/min at room temperature for 5 min to separate the serum. Hitachi 7170 automatic biochemical analyzer was used to measure the serum ALT, AST, and TBIL levels. Alanine aminotransferase was > 40 U/L, AST > 35 U/L, and TBIL > 22 μmol/L, which were considered abnormal[12,13].

The incidence of postoperative complications (including biliary fistula, liver failure, incision infection, urinary tract infection, pulmonary infection, *etc.*) was recorded in both groups.

Statistical analysis

Statistical analysis was carried out using SPSS 21.0. Measurement of data, such as operation time, operation blood loss, and length of hospital stay in the two groups were expressed as mean ± SD; *t* test was used for comparison between the two groups; χ^2 test was used to compare categorical variables between the groups. The Kaplan-Meier method was used for survival analysis. $P < 0.05$ was considered statistically significant.

RESULTS

Comparison of surgical trauma indices between the two groups

The operation time, operation blood loss, length of hospital stay, and postoperative gastrointestinal function recovery time in the reconstruction group were higher than those of the control group ($P < 0.05$, Table 2).

Comparison of operational resection margin between the two groups

The R0 resection was achieved in 90.00% of the reconstruction group and 72.41% of the control group, with a statistically significant difference ($P < 0.05$, Table 3).

Table 1 Comparison of baseline data between the two groups, *n* (%)

Normal information	Reconstruction group (*n* = 40)	Regular group (*n* = 58)	*t*/χ^2 value	*P* value
Age (yr)	58.6 ± 7.0	59.0 ± 6.6	-0.2877	0.77422
Body mass index (kg/m^2)	22.6 ± 1.9	22.8 ± 2.3	-0.4533	0.65132
Sex			1.319	0.251
Male	28 (70)	34 (58.62)		
Female	12 (30)	24 (41.38)		
Surgical approach			1.227	0.746
Cholangiocarcinoma resection	11 (27.5)	22 (37.93)		
Left liver + Caudate lobe	13 (32.5)	15 (25.86)		
Right liver + Caudate lobe	12 (30)	16 (27.59)		
Other types	4 (10)	5 (8.62)		
Bismuth-Corlette type			1.179	0.758
I type	14 (35)	25 (43.1)		
II type	16 (40)	21 (36.21)		
III type	8 (20)	8 (13.79)		
IV type	2 (5)	4 (6.9)		
Regional lymph node metastasis			0.764	0.382
Yes	18 (45)	21 (36.21)		
No	22 (55)	37 (63.79)		
Adjuvant chemotherapy			1.696	0.193
Yes	35 (87.5)	55 (94.83)		
No	5 (12.5)	3 (5.17)		

Table 2 Comparison of surgical trauma indexes between the two groups (mean ± SD)

Group	*n*	Operation time (min)	Surgical bleeding (mL)	Gastrointestinal function recovery time (h)	Hospital stay (d)
Reconstruction group	40	11.36 ± 1.03	906.8 ± 155.3	73.6 ± 13.0	21.61 ± 3.9
Regular group	58	9.71 ± 0.81	720.3 ± 160.1	64.8 ± 11.0	19.3 ± 3.2
t value		8.863	5.737	3.612	3.210
P value		0.000	0.000	0.000	0.002

Table 3 Comparison of the effect of operational resection between the two groups, *n* (%)

Group	*n*	R0 excision	Non-R0 resection
Reconstruction group	40	36 (90.00)	4 (10.00)
Regular group	58	42 (72.41)	16 (27.59)
χ^2		4.507	
P value		0.034	

Comparison of the KPS scores between the two groups before and after operation

Before the operation, there was no significant difference in the KPS scores between groups ($P > 0.05$). Two weeks after the surgery, the KPS score of the reconstruction group was significantly higher than that of the control group ($P < 0.05$), as shown in Table 4 and Figure 1.

Table 4 Comparison of Karnofsky performance status scores between the two groups of patients before and after operation (mean ± SD, scores)

Group	*n*	Preoperative	2 wk after surgery	8 wk after surgery
Reconstruction group	40	75.1 ± 4.2	66.9 ± 5.0	76.7 ± 4.8
Regular group	58	73.7 ± 3.5	64.0 ± 5.7	75.4 ± 5.0
χ^2		1.793	2.600	1.286
P value		0.076	0.011	0.202

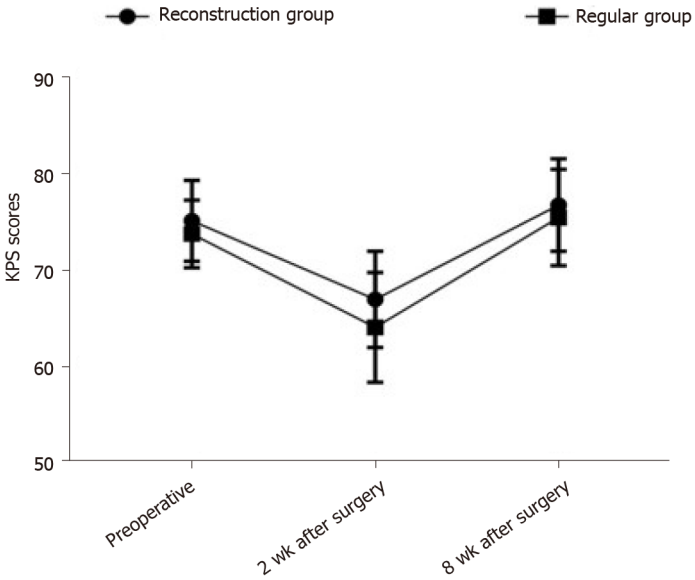

DOI: 10.4251/wjgo.v14.i4.887

Figure 1 Line chart of changes in Karnofsky performance status scores before and after surgery in the two groups. The mean ± SD are depicted for each time point. KPS: Karnofsky performance status.

Comparison of liver function indices between the two groups

The liver function indices of the two groups were compared before and after the operation. The results showed that the serum ALT on day one and three postoperatively, was lower in the reconstruction group than in the control group. The same was true for the serum AST three days postoperatively. The differences were statistically significant ($P < 0.05$), as shown in Table 5.

Complication rate in the two groups

There was no significant difference in the rate of surgical complications between the reconstruction (27.50%) and control (32.67%) groups ($P > 0.05$, Table 6).

Survival analysis

There was no significant difference between the two-year survival rate of 42.50% in the reconstruction group and 39.66% in the control group ($P > 0.05$), as shown in Table 7.

There was no significant difference in the two-year survival time between the reconstruction group (22.0 mo) and the control group (23.0 mo) ($P > 0.05$), as shown in Figure 2.

DISCUSSION

According to our study, the R0 resection rate in the reconstruction group was higher than in the control group. Hilar cholangiocarcinoma has a higher vascular invasion rate, especially involving the hepatic artery. However, reconstruction after hepatic artery resection can improve the operational resection rate and achieve R0 resection. The combination of portal vein resection and remodeling does not increase the incidence of postoperative complications in HC. The compromise of hepatic artery patency due to tumor invasion, leads to progressive and chronic arterial hypoperfusion of the liver, causing a shift from the normal dual portal vein- and hepatic artery-dependent blood and oxygen supply to single portal

Table 5 Comparison of liver function indexes between two groups of patients (mean ± SD)

Index	Preoperative	1 d after operation	3 d after operation
ALT (U/L)			
Reconstruction group	78.9 ± 19.6	451.2 ± 88.1	357.1 ± 93.0
Regular group	83.0 ± 20.1	489.8 ± 94.7	401.2 ± 85.0
t value	-1.003	-2.040	-2.429
P value	0.319	0.044	0.017
AST (U/L)			
Reconstruction group	83.5 ± 28.0	438.1 ± 93.0	395.8 ± 81.7
Regular group	80.0 ± 24.6	470.7 ± 87.2	441.5 ± 96.1
t value	0.654	-1.770	-2.456
P value	0.515	0.080	0.016
TBIL (μmol/L)			
Reconstruction group	144.3 ± 35.1	122.2 ± 28.0	44.1 ± 13.0
Regular group	138.5 ± 37.3	118.0 ± 26.9	40.0 ± 12.5
t value	0.775	0.747	1.570
P value	0.440	0.457	0.120

ALT: alanine aminotransferase; AST: aspartate aminotransferase; TBIL: total bilirubin.

Table 6 Observation of complication rate

Group	*n*	Biliary fistula	Liver failure	Incision infection	Urinary tract infection	Lung infection	Complication rate, *n* (%)
Reconstruction group	40	1	1	2	4	3	11 (27.50)
Regular group	58	3	2	3	5	6	19 (32.76)
χ^2							0.308
P value							0.579

Table 7 Two-year survival rate observation, *n* (%)

Group	*n*	Survive	Death
Reconstruction group	40	17 (42.50)	23 (57.50)
Regular group	58	23 (39.66)	35 (60.34)
χ^2		0.079	
P value		0.778	

vein-dependent supply. After the hepatic artery reconstruction, hepatic arterial blood supply can be fully restored; thus, preventing complications and possibly improving prognosis. Therefore, R0 resection of the tumor is key to a successful negative operational margin.

At present, the hilar vascular structure is relatively complicated, and the biological characteristic of HC is invasive growth. There are still controversies within the academic circles about radical operation of HC combined with hepatic artery resection and reconstruction. By the time HC patients are diagnosed, the liver tissues around the vascular and bile ducts are often invaded. Radical tumor resection is a common method for the treatment of HC. However, the invasion of the hilar blood vessels is a contraindication to surgical resection, making the rate of radical HC resection lower. In recent years, as the vascular anastomosis technology has matured, hilar vascular resection and reconstruction has been applied in the treatment of HC, which has expanded the surgical indications. In this type of surgery, studies have found [11-13] that the degree of tumor differentiation, whether there is lymph node metastasis, and whether there is peripheral nerve invasion are factors that affect the prognosis of

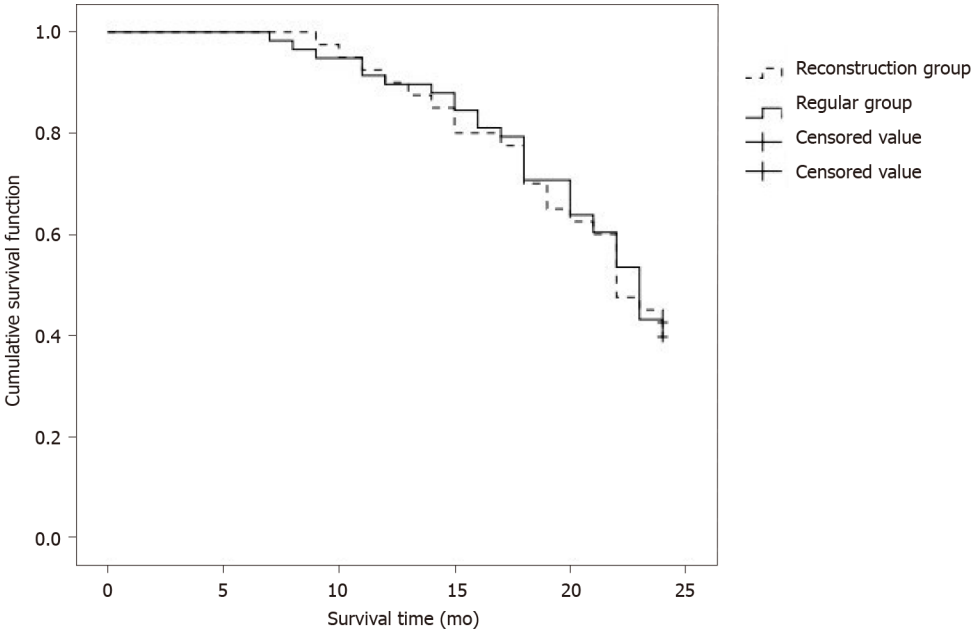

DOI: 10.4251/wjgo.v14.i4.887

Figure 2 Kaplan-Meier survival curves for the two groups of patients.

HC patients. In addition to the above factors, this study also gives supplementary discussion. Our research results showed that the perioperative indicators of the reconstruction group are better than those of the conventional group, and the recovery of gastrointestinal function after surgery is also better. After the hepatic artery reconstruction, the blood and oxygen supply of the liver cells can be significantly improved. At the same time, it can effectively ensure the normal blood supply of the gastrointestinal tract, and play an important role in the recovery and regeneration of hepatocyte function after surgery, and the prevention and treatment of abnormal gastrointestinal function. Hepatic artery reconstruction is increasingly showing a trend of "precision". In this study, 70 prolene sutures were used to reconstruct the hepatic artery with intermittent anastomosis. The reconstruction method depends on the length of the patient's arterial invasion. Combined with perfect surgical management, surgical safety is well guaranteed. Postoperative complications are mainly related to operation time and surgical trauma. This study found that the reconstruction group's plan was safe and feasible. Two weeks after the operation, the KPS score in the reconstruction group was higher than in the control group. A higher operational complication rate in the reconstruction group may be due to the advanced stage of the portal cholangiocarcinoma, as indicated by the involvement of the hepatic artery, which limits long-term efficacy of any treatment. The operational treatment of HC is very challenging, especially in advanced cases of vascular invasion[17]. Removal of the portal vein and hepatic artery requires higher surgical skill, relatively longer operation time, and increased blood loss. However, the hepatic artery is a large diameter muscular artery, which provides a good substrate for anastomosis, especially after the branches around the hepatic aorta have already been severed. Anatomic and physiologic variants of the artery need to be taken under consideration prior to determining anastomosis capability. In the right candidates, radical HC resection, combined with hepatic artery resection and reconstruction, can restore the dual blood supply to the liver, as early as possible, can reduce residual cancer tissue, improve resection and cure rate of advanced HC, as well as improve patients' self-care ability.

Alanine amino transferase and AST can be used to evaluate the extent of hepatocellular injury, with the elevation of ALT being roughly parallel to the degree of cellular injury[18,19]. The vast majority of TBIL in the human body comes from aging red blood cells, which are metabolized by the liver. The TBIL is excreted by the bile ducts and enters the bile ducts at all levels, so it can be elevated upon hepatic or biliary tract injury[10,20]. This study found that postoperatively, the levels of ALT and AST in the reconstruction group were improved compared with those in the control group, and the liver damage in the reconstruction group was less. When patients with hilar cholangiocarcinoma undergo combined hepatic arterial resection, the blood supply of the liver will be affected because most patients with advanced HC have severe jaundice, and the jaundice further affects the blood supply of the Liver's portal vein. The restoration of liver function is meaningful. The reasons for analyzing the results of this study include liver damage caused by advanced HC patients is different from liver cirrhosis. After the biliary obstruction is relieved, the liver function of advanced HC patients can gradually recover because in the radical operation of HC, the hepatic hilum is used as the cleaning target. Most of the branch connections between the arteries have also been severed. Free hepatoduodenal ligament can affect the

hepatic artery collateral circulation in the hilar of the liver. After cutting off, the establishment of collateral circulation becomes difficult, and the hepatic artery becomes ischemic. Prolonged severe liver damage, postoperative liver function indicators (such as ALT and AST) increase, and hepatic artery blood supply are of great significance to the recovery of liver function in patients after radical surgery. The hepatic artery reconstruction implemented in the reconstruction group can increase the blood and oxygen supply of the hepatocytes, while ensuring the blood supply of the bile duct, which has less impact on liver function. Additionally, the reconstruction group first completed arterial resection and reconstruction, opened the blood flow of the hepatic artery, then blocked the portal vein, and completed the portal vein resection and reconstruction to reduce liver ischemic damage.

The application of hepatic artery resection in HC is still controversial. Studies have reported that unfavorable clinicopathological factors in patients with combined hepatic artery resection and reconstruction lead to a higher five-year mortality rate in patients after surgery. Whether reconstruction is necessary is also a dispute. Based on the results of this study, we believe that postoperative reconstruction should be a routine. The following points should be addressed upon reconstruction after hepatic artery resection: (1) The reserved hepatic blood vessels tend to adhere to the tumor. If the tumor cannot be completely removed, vascular reconstruction is required; (2) After resection of the two ends of the blood vessels, the reconstruction tension should be moderate; (3) Portal vein wedge resection and reconstruction can be tried, or alternatively, plastic reconstruction using other vascular branches near the hepatic artery can be attempted; and (4) If blood vessel invasion is detected, but the blood vessel cannot be removed successfully during the operation, it is recommended that the blood vessel be reserved. Because of our short follow up period, the long-term survival after radical operation combined with reconstruction after the hepatic arterectomy was not determined; therefore, more extended follow up is needed in future studies.

CONCLUSION

In conclusion, radical resection combined with hepatic artery reconstruction for advanced HC can lead to improved R0 resection rate and decrease liver injury, postoperatively. However, the procedure is more difficult, and the effect on survival time remains unclear. Further studies with larger sample sizes and prolonged observation times are needed.

ARTICLE HIGHLIGHTS

Research background

Hilar cholangiocarcinoma (HC) is a good indication for hepatic artery resection, and hepatic artery resection is conducive to radical resection of cholangiocarcinoma. With the continuous development of surgical techniques, especially microsurgery techniques, vascular invasion is no longer a contraindication to surgery. Hepatic artery reconstruction after hepatic artery resection has been used in many centers to treat liver tumors, but it is rarely used in advanced HC.

Research motivation

This study provided treatment strategies for patients with advanced HC.

Research objectives

This study aimed to determine the prognosis of patients with advanced HC after hepatic artery resection and reconstruction.

Research methods

A total of 98 patients with HC who underwent radical operation in our hospital were selected for retrospective analysis.

Research results

The operation time, blood loss, hospitalization time and gastrointestinal function recovery time of the reconstruction group were higher than those of the control group. The R0 resection rates of the reconstruction group and the control group were 90.00% and 72.41%, respectively. In the reconstruction group, serum alanine aminotransferase was lower on the 1st and 3rd day after operation, and serum aspartate aminotransferase was lower on the 3rd day. Although the preoperative Karnovsky performance status score was similar between the groups, it was higher in the reconstruction group 2 wk after the operation. There was no difference in the incidence of complications between the two groups. The 2-year survival rate and 2-year survival time were similar between the groups.

Research conclusions

Radical surgery combined with reconstruction after hepatic artery resection improves R0 resection rate and reduces postoperative liver injury in advanced HC. However, the operation is difficult and the effect on survival time is not clear.

Research perspectives

Hepatic artery resection may be more widely used in advanced HC.

FOOTNOTES

Author contributions: Li YM and Bie ZX design the study; Guo RQ drafted the work, Li B and Wang CE collected the data; Yan F analysed and interpreted data; Li YM wrote the manuscript; and all the authors reviewed and approved the final version to be published.

Institutional review board statement: This study was approved by the Ethics Committee of Beijing Hospital.

Informed consent statement: All study participants, or their legal guardian, provided informed written consent prior to study enrollment.

Conflict-of-interest statement: The authors declared that there is no conflict of interest between them.

Data sharing statement: No additional data are available.

Country/Territory of origin: China

ORCID number: Yuan-Ming Li 0000-0003-4680-1711; Zhi-Xin Bie 0000-0003-3365-0694; Run-Qi Guo 0000-0001-7026-6937; Bin Li 0000-0003-0045-8639; Cheng-En Wang 0000-0002-8728-4995; Fei Yan 0000-0001-5735-9645.

S-Editor: Wang JL
L-Editor: A
P-Editor: Wang JL

REFERENCES

1 **Giuliante F**, Ardito F, Vellone M, Nuzzo G. Liver resections for hilar cholangiocarcinoma. *Eur Rev Med Pharmacol Sci* 2010; **14**: 368-370 [PMID: 20496550]
2 **Nagino M**, Nimura Y, Kamiya J, Kanai M, Uesaka K, Hayakawa N, Yamamoto H, Kondo S, Nishio H. Segmental liver resections for hilar cholangiocarcinoma. *Hepatogastroenterology* 1998; **45**: 7-13 [PMID: 9496478]
3 **Shimizu H**, Kimura F, Yoshidome H, Ohtsuka M, Kato A, Yoshitomi H, Furukawa K, Miyazaki M. Aggressive surgical resection for hilar cholangiocarcinoma of the left-side predominance: radicality and safety of left-sided hepatectomy. *Ann Surg* 2010; **251**: 281-286 [PMID: 20054275 DOI: 10.1097/SLA.0b013e3181be0085]
4 **Li B**, Xiong XZ, Zhou Y, Wu SJ, You Z, Lu J, Cheng NS. Prognostic value of lymphovascular invasion in Bismuth-Corlette type IV hilar cholangiocarcinoma. *World J Gastroenterol* 2017; **23**: 6685-6693 [PMID: 29085213 DOI: 10.3748/wjg.v23.i36.6685]
5 **Rassam F**, Roos E, van Lienden KP, van Hooft JE, Klümpen HJ, van Tienhoven G, Bennink RJ, Engelbrecht MR, Schoorlemmer A, Beuers UHW, Verheij J, Besselink MG, Busch OR, van Gulik TM. Modern work-up and extended resection in perihilar cholangiocarcinoma: the AMC experience. *Langenbecks Arch Surg* 2018; **403**: 289-307 [PMID: 29350267 DOI: 10.1007/s00423-018-1649-2]
6 **Obulkasim H**, Shi X, Wang J, Li J, Dai B, Wu P, Wang S, Wang X, Ding Y. Podoplanin is an important stromal prognostic marker in perihilar cholangiocarcinoma. *Oncol Lett* 2018; **15**: 137-146 [PMID: 29391878 DOI: 10.3892/ol.2017.7335]
7 **Bird NTE**, McKenna A, Dodd J, Poston G, Jones R, Malik H. Meta-analysis of prognostic factors for overall survival in patients with resected hilar cholangiocarcinoma. *Br J Surg* 2018; **105**: 1408-1416 [PMID: 29999515 DOI: 10.1002/bjs.10921]
8 **Komaya K**, Ebata T, Yokoyama Y, Igami T, Sugawara G, Mizuno T, Yamaguchi J, Nagino M. Recurrence after curative-intent resection of perihilar cholangiocarcinoma: analysis of a large cohort with a close postoperative follow-up approach. *Surgery* 2018; **163**: 732-738 [PMID: 29336813 DOI: 10.1016/j.surg.2017.08.011]
9 **Matsumoto T**, Kubota K, Aoki T, Shimizu T, Mori S, Kato M, Asato H. A Novel Approach for Hepatic Arterial

Reconstruction after Total Pancreatectomy with Common Hepatic Artery Resection Using Inferior Phrenic Artery. *Dig Surg* 2019; **36**: 99-103 [PMID: 29414805 DOI: 10.1159/000486630]

10 **Sugiura T**, Okamura Y, Ito T, Yamamoto Y, Ashida R, Ohgi K, Nakagawa M, Uesaka K. Left Hepatectomy with Combined Resection and Reconstruction of Right Hepatic Artery for Bismuth Type I and II Perihilar Cholangiocarcinoma. *World J Surg* 2019; **43**: 894-901 [PMID: 30377720 DOI: 10.1007/s00268-018-4833-1]

11 **Harada N**, Yoshizumi T, Uchiyama H, Ikegami T, Itoh S, Takeishi K, Toshima T, Nagao Y, Yoshiya S, Mori M. Impact of middle hepatic artery reconstruction after living donor liver transplantation using the left lobe. *Clin Transplant* 2020; **34**: e13850 [PMID: 32150767 DOI: 10.1111/ctr.13850]

12 **Tsai CY**, Watanabe N, Ebata T, Mizuno T, Kamei Y, Nagino M. Right hepatectomy for a detoured left hepatic artery in hilar cholangiocarcinoma-report of a rare but rational resection. *World J Surg Oncol* 2016; **14**: 288 [PMID: 27852277 DOI: 10.1186/s12957-016-1045-8]

13 **Dai HS**, Bie P, Wang SG, He Y, Li DJ, Tian F, Zhao X, Chen ZY. [Clinical application of combined hepatic artery resection and reconstruction in surgical treatment for hilar cholangiocarcinoma]. *Zhonghua Wai Ke Za Zhi* 2018; **56**: 41-46 [PMID: 29325352 DOI: 10.3760/cma.j.issn.0529-5815.2018.01.010]

14 **De Lu C**, Huang J, Wu SD, Hua YF, Javed AA, Fang JZ, Wang CN, Ye S. Total Hilar En Bloc Resection with Left Hemihepatectomy and Caudate Lobectomy: a Novel Approach for Treatment of Left-Sided Perihilar Cholangiocarcinoma (with Video). *J Gastrointest Surg* 2017; **21**: 1906-1914 [PMID: 28875398 DOI: 10.1007/s11605-017-3561-4]

15 **Rhu J**, Kim JM, Choi GS, David Kwon CH, Joh JW. Impact of Extra-anatomical Hepatic Artery Reconstruction During Living Donor Liver Transplantation on Biliary Complications and Graft and Patient Survival. *Transplantation* 2019; **103**: 1893-1902 [PMID: 30747851 DOI: 10.1097/TP.0000000000002601]

16 **Pitt HA**, Nakeeb A, Abrams RA, Coleman J, Piantadosi S, Yeo CJ, Lillemore KD, Cameron JL. Perihilar cholangiocarcinoma. Postoperative radiotherapy does not improve survival. *Ann Surg* 1995; **221**: 788-97; discussion 797 [PMID: 7794082 DOI: 10.1097/00000658-199506000-00017]

17 **Mizuno T**, Ebata T, Yokoyama Y, Igami T, Yamaguchi J, Onoe S, Watanabe N, Kamei Y, Nagino M. Combined Vascular Resection for Locally Advanced Perihilar Cholangiocarcinoma. *Ann Surg* 2022; **275**: 382-390 [PMID: 32976284 DOI: 10.1097/SLA.0000000000004322]

18 **Nanashima A**, Imamura N, Hiyoshi M, Yano K, Hamada T, Chiyotanda T, Nagatomo K, Hamada R, Ito H. A successfully resected case of left trisectionectomy with arterio-portal combined resection for advanced cholangiocarcinoma. *Int J Surg Case Rep* 2018; **53**: 90-95 [PMID: 30390491 DOI: 10.1016/j.ijscr.2018.10.036]

19 **Li O**, Yi W, Yang P, Guo C, Peng C. Relationship between serum MMP-9 level and prognosis after radical resection for Hilar cholangiocarcinoma patients. *Acta Cir Bras* 2019; **34**: e201900409 [PMID: 31038586 DOI: 10.1590/s0102-865020190040000009]

20 **Yoshikawa J**, Kato Y, Shirakata Y, Sugioka A, Uyama I. Transpositional celiac artery graft: Novel graft selection for huge right hepatic artery reconstruction in left-sided hepatectomy for perihilar cholangiocarcinoma. *Asian J Surg* 2021; **44**: 562 [PMID: 33349553 DOI: 10.1016/j.asjsur.2020.12.007]

World Journal of Gastrointestinal Oncology

Submit a Manuscript: https://www.f6publishing.com

World J Gastrointest Oncol 2022 April 15; 14(4): 897-919

DOI: 10.4251/wjgo.v14.i4.897

ISSN 1948-5204 (online)

ORIGINAL ARTICLE

Retrospective Study

Prognostic significance of serum inflammation indices for different tumor infiltrative pattern types of gastric cancer

Yu-Fei Wang, Xin Yin, Tian-Yi Fang, Yi-Min Wang, Lei Zhang, Xing-Hai Zhang, Dao-Xu Zhang, Yao Zhang, Xi-Bo Wang, Hao Wang, Ying-Wei Xue

Specialty type: Oncology

Provenance and peer review: Unsolicited article; Externally peer reviewed.

Peer-review model: Single blind

Peer-review report's scientific quality classification

Grade A (Excellent): 0
Grade B (Very good): B
Grade C (Good): 0
Grade D (Fair): 0
Grade E (Poor): 0

P-Reviewer: Nakai Y

Received: August 7, 2021
Peer-review started: August 7, 2021
First decision: October 3, 2021
Revised: October 8, 2021
Accepted: February 22, 2022
Article in press: February 22, 2022
Published online: April 15, 2022

Yu-Fei Wang, Xin Yin, Tian-Yi Fang, Yi-Min Wang, Dao-Xu Zhang, Yao Zhang, Xi-Bo Wang, Hao Wang, Ying-Wei Xue, Department of Gastroenterological Surgery, Harbin Medical University Cancer Hospital, Harbin 150081, Heilongjiang Province, China

Lei Zhang, Xing-Hai Zhang, Department of Pathology, Harbin Medical University Cancer Hospital, Harbin 150081, Heilongjiang Province, China

Corresponding author: Ying-Wei Xue, PhD, Chief Doctor, Professor, Department of Gastroenterological Surgery, Harbin Medical University Cancer Hospital, No. 150 Haping Road, Harbin 150081, Heilongjiang Province, China. xueyingwei@hrbmu.edu.cn

Abstract

BACKGROUND

Inflammatory indices are considered to be potential prognostic biomarkers for patients with gastric cancer (GC). However, there is no evidence defining the prognostic significance of inflammatory indices for GC with different tumor infiltrative pattern (INF) types.

AIM

To evaluate the significance of inflammatory indices and INF types in predicting the prognosis of patients with GC.

METHODS

A total of 962 patients who underwent radical gastrectomy were retrospectively selected for this study. Patients were categorized into the expansive growth type (INFa), the intermediate type (INFb), and the infiltrative growth type (INFc) groups. The cutoff values of inflammatory indices were analyzed by receiver operating characteristic curves. The Kaplan–Meier method and log-rank test were used to analyze overall survival (OS). The chi-square test was used to analyze the association between inflammatory indices and clinical characteristics. The independent risk factors for prognosis in each group were analyzed by univariate and multivariate analyses based on logistic regression. Nomogram models were constructed by R studio.

RESULTS

The INFc group had the worst OS ($P < 0.001$). The systemic immune-inflammation index ($P = 0.039$) and metastatic lymph node ratio (mLNR) ($P = 0.003$) were

independent risk factors for prognosis in the INFa group. The platelet-lymphocyte ratio (PLR) (P = 0.018), age (P = 0.026), body mass index (P = 0.003), and postsurgical tumor node metastasis (pTNM) stage (P < 0.001) were independent risk factors for prognosis in the INFb group. The PLR (P = 0.021), pTNM stage (P = 0.028), age (P = 0.021), and mLNR (P = 0.002) were independent risk factors for prognosis in the INFc group. The area under the curve of the nomogram model for predicting 5-year survival in the INFa group, INFb group, and INFc group was 0.787, 0.823, and 0.781, respectively.

CONCLUSION

The outcome of different INF types GC patients could be assessed by nomograms based on different inflammatory indices and clinicopathologic features.

Key Words: Gastric cancer; Tumor infiltrative pattern; Systemic immune-inflammation index; Platelet-lymphocyte ratio; Prognosis; Nomogram

Core Tip: This is a retrospective study to analyze the relationship between peripheral circulating immune cells, inflammatory indices and the tumor infiltrative pattern (INF) types and to verify their ability to evaluate the outcome of gastric cancer (GC) patients. Our results showed that the systemic immune-inflammation index and platelet–lymphocyte ratio were independent prognostic factors for the expansive growth type, the intermediate type, and the infiltrative growth type groups. Based on different inflammatory indicators and clinicopathologic features, the nomogram models can predict the prognosis of different INF types GC patients, which deserve further testing and extension in clinical practice.

Citation: Wang YF, Yin X, Fang TY, Wang YM, Zhang L, Zhang XH, Zhang DX, Zhang Y, Wang XB, Wang H, Xue YW. Prognostic significance of serum inflammation indices for different tumor infiltrative pattern types of gastric cancer. *World J Gastrointest Oncol* 2022; 14(4): 897-919
URL: https://www.wjgnet.com/1948-5204/full/v14/i4/897.htm
DOI: https://dx.doi.org/10.4251/wjgo.v14.i4.897

INTRODUCTION

Gastric cancer (GC) is the sixth most common cancer and the third leading cause of cancer-related death, with more than 865000 deaths every year[1]. To better predict the individual prognosis of GC patients according to tumor biological characteristics, physicians had proposed a variety of classifications[2,3], including the tumor infiltrative pattern (INF) proposed in 1977[4]. The INF types are defined in the Japanese Classification of Gastric Carcinoma[5], which categorizes GC as the expansive growth type (INFa), the intermediate type (INFb), and the infiltrative growth type (INFc). Previous studies have shown that different INF types differ in clinicopathological features and prognosis and can be used as predictors of postoperative recurrence and prognosis in GC patients[6-9]. However, GC is a highly heterogeneous malignant tumor, and the prognosis of patients with the same INF may also show significant differences. Therefore, it is worth further exploring the prognosis of GC patients with different INF types to guide clinical treatment.

With the popularization and development of immunotherapy, the significant role of tumor immunity in malignant tumors has gradually attracted the attention of clinical experts[10]. From 2014 to 2018, the postsurgical tumor node metastasis-immunology (pTNM-I) stage proposed by Galon *et al*[11] and Pagès *et al*[12] was well applied in colon cancer patients. It suggests that the traditional pTNM staging combined with tumor immunity can give more serviceable prognostic and treatment information. Nevertheless, tumor heterogeneity will lead to the restriction of immunohistochemical detection of GC by site selection. As a part of tumor immunity, the peripheral blood immune system also has a significant effect on tumor progression. Our previous studies have confirmed that the inflammatory index plays an important role in the early diagnosis of GC and the evaluation of the outcome of GC patients with different Lauren classification[13,14]. In addition, in liver metastases, different tumor growth pattern subtypes have different levels of lymphocyte infiltration, indicating that they have different immune states in the tumor microenvironment[15]. However, no study has analyzed the relationship between INF and the peripheral blood immune inflammatory response in GC. Therefore, whether the immune difference and prognosis of GC patients with different INF types can be evaluated by peripheral blood inflammatory indices deserves further exploration.

Table 1 Baseline characteristics of the patients

Characteristics	INFa (*n* = 183)	INFb (*n* = 331)	INFc (*n* = 448)
Sex			
Male	133 (72.7)	248 (74.9)	308 (68.8)
Female	50 (27.3)	83 (25.1)	140 (31.2)
Age (yr)	58.81 ± 9.59	59.30 ± 9.73	57.06 ± 10.55
Borrmann type			
0-1	31 (16.9)	51 (15.4)	21 (4.7)
2	62 (33.9)	105 (31.7)	104 (23.2)
3	74 (40.4)	138 (41.7)	242 (54.0)
4-5	16 (8.8)	37 (11.2)	81 (18.1)
Tumor location			
Lower third	156 (85.2)	227 (68.6)	329 (73.4)
Middle third	21 (11.5)	64 (19.3)	75 (16.8)
Upper third	4 (2.2)	33 (10.0)	31 (6.9)
Entire stomach	2 (1.1)	7 (2.1)	13 (2.9)
Tumor size (mm)	44.40 ± 24.85	53.06 ± 25.78	56.31 ± 27.38
pTNM stage			
I	72 (39.3)	70 (21.1)	36 (8.0)
II	60 (32.8)	127 (38.4)	137 (30.6)
III	51 (27.9)	134 (40.5)	275 (61.4)
Histological type			
Well and medium differentiation	112 (61.2)	149 (45.0)	126 (28.1)
Poor differentiation	46 (25.1)	88 (26.6)	207 (46.2)
Others	25 (13.7)	94 (28.4)	115 (25.7)
mLNR	0.09 ± 0.16	0.12 ± 0.17	0.19 ± 0.22
Vascular infiltration			
No	137 (74.9)	231 (69.8)	317 (70.8)
Yes	46 (25.1)	100 (30.2)	131 (29.2)
Nerve infiltration			
No	123 (67.2)	198 (59.8)	251 (56.0)
Yes	60 (32.8)	133 (40.2)	197 (44.0)
Postoperative chemotherapy			
Yes	58 (31.7)	90 (27.2)	167 (37.3)
No	125 (68.3)	241 (72.8)	281 (62.7)

Tumor infiltrative pattern, tumor location, postsurgical tumor node metastasis stage, histological type, mLNR, vascular infiltration and nerve infiltration were according to the postoperative pathology report. INF: Tumor infiltrative pattern; INFa: Expansive growth type; INFb: Intermediate type; INFc: Infiltrative growth type; mLNR: Metastatic lymph node ratio; pTNM: Postsurgical tumor node metastasis.

From September 2012 and July 2015, 962 patients at Harbin Medical University Cancer Hospital were included in the study. The clinical applicability of different inflammatory indices, including the neutrophil-lymphocyte ratio (NLR), platelet-lymphocyte ratio (PLR), and systemic immune-inflammation index (SII), was evaluated. At the same time, the difference of peripheral blood immune cells in different INF types was further analyzed. Finally, we constructed predictive models by combining inflammatory indices with the clinicopathological features of patients based on INF types.

Table 2 Chi-square test analysis of the associations between the inflammation index and clinicopathological features

Characteristics	INFa			INFb			INFc		
	SII ≤ 523.01 (119)	SII > 523.01 (64)	*P* value	PLR ≤ 134.02 (195)	PLR > 134.02 (136)	*P* value	PLR ≤ 134.02 (273)	PLR > 134.02 (175)	*P* value
Sex			0.443			0.979			0.489
Male	84 (70.6)	49 (76.6)		146 (74.9)	102 (75.0)		191 (70.0)	117 (66.9)	
Female	35 (29.4)	15 (23.4)		49 (25.1)	34 (25.0)		82 (30.0)	58 (33.1)	
Age (yr)			0.126			0.878			**< 0.001**
≤ 60	68 (57.1)	29 (45.3)		103 (52.8)	73 (53.7)		191 (70.0)	86 (49.1)	
> 60	51 (42.9)	35 (54.7)		92 (47.2)	63 (46.3)		82 (30.0)	89 (50.9)	
BMI			0.105			**0.038**			0.592
≤ 22.49	52 (43.7)	36 (56.3)		85 (43.6)	75 (55.1)		138 (50.5)	93 (53.1)	
> 22.49	67 (56.3)	28 (43.7)		110 (56.4)	61 (44.9)		135 (49.5)	82 (46.9)	
CEA			0.064			0.608			0.782
≤ 5 ng/mL	108 (90.8)	52 (81.2)		162 (83.1)	110 (80.9)		235 (86.1)	149 (85.1)	
> 5 ng/mL	11 (9.2)	12 (18.8)		33 (16.9)	26 (19.1)		38 (13.9)	26 (14.9)	
CA19-9			**0.014**			0.198			0.156
≤ 37 U/mL	112 (94.1)	53 (82.8)		168 (86.2)	110 (83.7)		246 (90.1)	150 (85.7)	
> 37 U/mL	7 (5.9)	11 (17.2)		27 (13.8)	26 (16.3)		27 (9.9)	25 (14.3)	
Borrmann type			**0.005**			0.051			0.454
0-2	71 (59.7)	22 (34.4)		84 (43.1)	72 (53.0)		80 (29.3)	45 (25.7)	
3	40 (33.6)	34 (53.1)		92 (47.2)	46 (33.8)		141 (51.6)	101 (57.7)	
4	8 (6.7)	8 (12.5)		19 (9.7)	18 (13.2)		52 (19.1)	29 (16.6)	
Tumor diameter (mm)			**< 0.001**			**< 0.001**			**< 0.001**
≤ 50	95 (79.8)	31 (48.4)		131 (67.2)	63 (46.3)		172 (63.0)	75 (42.9)	
> 50	24 (20.2)	33 (51.6)		64 (32.8)	73 (53.7)		101 (37.0)	100 (57.1)	
Tumor location			0.992			0.051			0.423
Middle and upper third	16 (13.4)	9 (14.0)		57 (29.2)	40 (29.4)		62 (22.7)	44 (25.1)	
Lower third	102 (85.7)	54 (84.4)		137 (70.3)	90 (66.2)		205 (75.1)	124 (70.9)	
Entire stomach	1 (0.9)	1 (1.6)		1 (0.5)	6 (4.4)		6 (2.2)	7 (4.0)	
Histological type			**< 0.001**			**0.041**			**< 0.001**
Well and medium differentiation	74 (62.2)	38 (59.4)		99 (50.8)	50 (36.8)		78 (28.6)	48 (27.4)	
Poor differentiation	2 (1.7)	19 (30.0)		47 (24.1)	41 (30.1)		120 (43.9)	87 (49.7)	
Others	18 (15.1)	7 (10.9)		49 (25.1)	45 (33.1)		75 (27.5)	40 (22.9)	
pTNM stage			**< 0.001**			**0.022**			**< 0.001**
I	61 (51.3)	11 (17.2)		51 (26.2)	19 (14.0)		29 (10.6)	7 (4.0)	
II	36 (30.2)	24 (37.5)		73 (37.4)	54 (39.7)		96 (35.2)	41 (23.4)	
III	22 (18.5)	29 (45.3)		71 (36.4)	63 (46.3)		148 (54.2)	127 (72.6)	
mLNR			**0.019**			0.290			**0.001**
≤ 0.07	84 (70.6)	34 (53.1)		109 (55.9)	68 (50.0)		131 (48.0)	56 (32.0)	
> 0.07	35 (29.4)	30 (46.9)		86 (44.1)	68 (50.0)		142 (52.0)	119 (68.0)	

Vascular infiltration			0.494			**0.030**		0.146
No	91 (76.5)	46 (71.9)		145 (74.4)	86 (63.2)		200 (73.3)	117 (66.9)	
Yes	28 (23.5)	18 (28.1)		50 (25.6)	50 (36.8)		73 (26.7)	58 (33.1)	
Nerve infiltration			0.098			0.592		0.238
No	85 (71.4)	38 (59.4)		119 (61.0)	79 (58.1)		159 (58.2)	92 (52.6)	
Yes	34 (28.6)	26 (40.6)		76 (39.0)	57 (41.9)		114 (41.8)	83 (47.4)	

Carcino-embryonic antigen and carbohydrate antigen 19-9 were according to the tumor marker examination. Tumor infiltrative pattern, tumor location, postsurgical tumor node metastasis stage, histological type, mLNR, vascular infiltration and nerve infiltration were according to the postoperative pathology report. Statistically significant *P* values are in bold ($P < 0.05$). INF: Tumor infiltrative pattern; INFa: Expansive growth type; INFb: Intermediate type; INFc: Infiltrative growth type; BMI: body mass index; CEA: Carcino-embryonic antigen; CA19-9: Carbohydrate antigen 19-9; mLNR: Metastatic lymph node ratio; pTNM: Postsurgical tumor node metastasis.

MATERIALS AND METHODS

Patients

All GC patients underwent radical gastrectomy according to their respective conditions[16]. GC was diagnosed by tissue specimens obtained during gastroscopy and confirmed by pathologists examining tissue samples after surgery. The patients underwent routine pre-operative auxiliary examinations, including abdominal ultrasound, gastric computed tomography (CT)/magnetic resonance imaging, chest X-ray, tumor markers examination, hematology examination, and electrocardiogram during hospitalization. If necessary, patients underwent positron emission tomography (PET)/CT. Patients were followed up until the date of death or for 5 years, whichever came first.

The exclusion criteria were as follows: (1) preoperative neoadjuvant therapy; (2) platelet therapy was performed within 3 mo before surgery; (3) severe heart disease; (4) active hemorrhage; (5) intravascular coagulation; (6) severe infection; (7) hematological malignancies; and (8) steroid drug treatment.

Formulation of postoperative chemotherapy regimens were according to the National Comprehensive Cancer Network Clinical Practice Guidelines in Oncology[17]. For GC patients with stage II or III, oxaliplatin + capecitabine and oxaliplatin + S-1 were the main treatment options. A total of 315 patients who underwent complete postoperative chemotherapy were included in our study.

Clinicopathological data

Clinicopathological data of patients were saved in the Gastric Cancer Information Management System v1.2 of Harbin Medical University Cancer Hospital (Copyright No. 2013SR087424, http://www.sgihmu.com), including age, gender, body mass index (BMI), Borrmann type, tumor location, tumor diameter, histological type, metastatic lymph node ratio (mLNR), nerve infiltration, vascular infiltration, resection, pTNM stage, postoperative chemotherapy and laboratory examination. pTNM stage is consistent with the eighth edition of the American Joint Commission on Cancer. Other auxiliary examinations (CT, ultrasound, and gastroscopy) or tumor markers were performed on all patients every 3-6 mo postoperatively. In addition, PET/CT examinations are performed as needed.

Definition of INF types

The pathological INF types were diagnosed by two institutional pathologists, which using paraffin sections stained with hematoxylin and eosin. GC tissue specimens were classified as INFa (tumor grows expansively and has an obvious boundary with the surrounding tissue), INFb (tumor shows an intermediate type between the expansive growth type and the infiltrative growth type), and INFc (tumor grows infiltratively and has no obvious boundary with the surrounding tissue), according to the Japanese Classification of Gastric Carcinoma[5] (Figure 1).

Blood sample

Blood samples were taken on an empty stomach the day after admission. Venous blood was collected from the cubital vein. Then, it was sent to the blood laboratory to separate the serum and calculate the corresponding inflammatory index. NLR = neutrophil count (N)/lymphocyte count (L), PLR = platelet count (P)/L, SII = N × P/L.

Statistical analysis

Overall survival (OS) was defined as the time from surgery to death or the last surviving follow-up visit. OS is shown as the mean and 95%CI. Receiver operating characteristic curve (ROC) analysis and the area under the curve (AUC) were used to compare the diagnostic significance of each inflammatory index. The Youden index was used to analyzed the optimal cutoff value of each inflammatory index, which was calculated by the equation: sensitivity-(1-specificity). The optimal cutoff value of each

Table 3 Prognostic factors of patients with gastric cancer by univariate and multivariate analyses based on logistic regression analysis in the expansive growth type group

Characteristics	INFa			
	Univariate analysis		Multivariate analysis	
	HR (95%CI)	*P* value	HR (95%CI)	*P* value
Sex		0.584		
Male	1			
Female	1.261 (0.550-2.894)			
Age (yr)	1.019 (0.979-1.061)	0.349		
BMI	0.880 (0.772-1.003)	0.055		
SII	1.002 (1.001-1.003)	**0.001**	1.001 (1.000-1.003)	**0.039**
ALT	0.988 (0.954-1.023)	0.491		
Total protein	0.968 (0.916-1.023)	0.251		
CEA	1.030 (0.996-1.065)	0.087		
CA19-9	1.002 (0.998-1.006)	0.278		
Borrmann type		**0.007**		0.272
0-1	1		1	
2	3.818 (0.448-32.517)	0.220	5.312 (0.450-62.711)	0.185
3	8.947 (1.135-70.530)	**0.038**	5.450 (0.496-59.870)	0.166
4-5	23.333 (2.525-215.647)	**0.005**	14.134 (0.944-211.701)	0.055
Tumor location		0.691		
Lower third	1			
Middle third	1.176 (0.366-3.782)	0.785		
Upper third	1.667 (0.167-16.657)	0.664		
Entire stomach	5.000 (0.303-82.520)	0.261		
Tumor size (mm)	1.032 (1.016-1.049)	**< 0.001**	1.012 (0.989-1.034)	0.310
pTNM stage		**< 0.001**		0.796
I	1		1	
II	2.615 (0.747-9.159)	0.133	0.660 (0.154-2.830)	0.576
III	10.968 (3.457-34.794)	**< 0.001**	0.532 (0.080-3.525)	0.513
Histological type		0.160		
Well and medium differentiation	1			
Poor differentiation	2.282 (0.972-5.360)	0.058		
Others	1.617 (0.527-4.959)	0.401		
mLNR	438.799 (38.101-5053.535)	**< 0.001**	471.355 (8.218-27035.275)	**0.003**
Vascular infiltration		0.080		
No	1			
Yes	2.065 (0.917-4.647)			
Nerve infiltration		**0.025**		0.621
No	1		1	
Yes	2.432 (1.118-5.288)		1.286 (0.474-3.490)	
Postoperative chemotherapy		0.720		
Yes	1			

No	1.159 (0.517-2.597)

Carcinoembryonic antigen and carbohydrate antigen 19-9 were according to the tumor marker examination. Tumor infiltrative pattern, tumor location, postsurgical tumor node metastasis stage, histological type, metastatic lymph node ratio, vascular infiltration and nerve infiltration were according to the postoperative pathology report. Statistically significant *P* values are in bold ($P < 0.05$). INF: Tumor infiltrative pattern; INFa: Expansive growth type; INFb: Intermediate type; INFc: Infiltrative growth type; HR: Hazard ratio; BMI: Body mass index; SII: Systemic immune-inflammation index; ALT: Alanine transaminase; CEA: Carcinoembryonic antigen; CA19-9: Carbohydrate antigen 19-9; mLNR: Metastatic lymph node ratio; pTNM: Postsurgical tumor node metastasis.

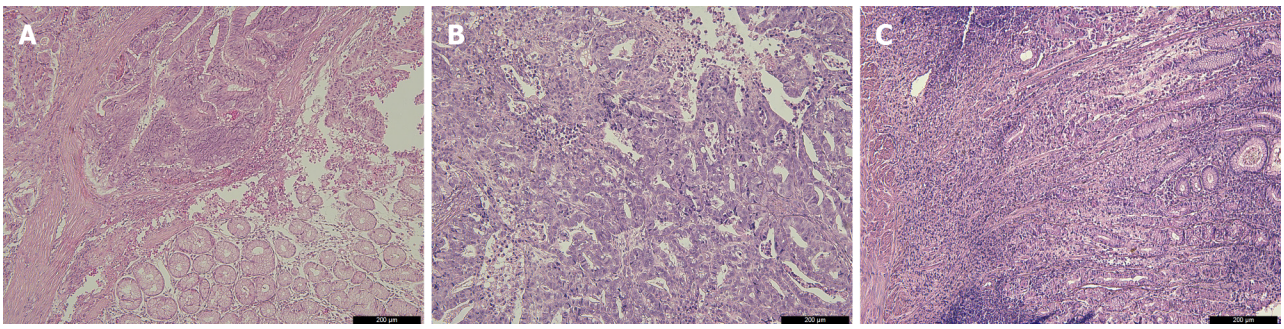

Figure 1 Representative hematoxylin and eosin staining patterns of samples of each tumor infiltrative pattern type. A: The expansive growth type; B: The intermediate type; C: The infiltrative growth type. INFa: The expansive growth type; INFb: The intermediate type; INFc: The infiltrative growth type.

inflammatory index was determined by the maximum value of the Youden index. The chi-square test was used to analyze the association between the inflammatory indices and clinicopathological factors. Survival curves for different INF types were analyzed by the log-rank test and Kaplan–Meier method. Based on logistic regression, univariate and multivariate analyses were used to analyze the independent prognostic factors for different INF types. Hazard ratios (HRs) and 95%CIs of each factor were shown. Boxplots and scatterplots were drawn by GraphPad Prism 8. The nomogram models were drawn through R studio by the "SvyNom" and "rms" packages. SPSS version 25.0 (SPSS Inc., Chicago, IL, United States) was used for analysis, and $P < 0.05$ was considered statistically significant.

RESULTS

Clinicopathological characteristics and survival based on INF

In the INFa group, the age range was 33-87 years (median 55 years), and the ratio of male to female was 133:50. In the INFb group, the age range was 30-79 years (median 60 years), and the ratio of male to female was 248:83. In the INFc group, the age range was 24-85 years (median 57 years), and the ratio of male to female was 308:140. Table 1 shows the clinicopathological features of the three groups.

There were statistically significant differences in OS among the INFa, INFb and INFc groups ($P < 0.001$). The OS of patients with INFc was worse than the OS of patients with INFa and INFb (Figure 2A). In the three groups, the OS of patients with stage I, II, and III GC was significantly different (all $P < 0.001$) (Figure 2B-D). These results are shown in the supplementary materials (Supplementary Table 1).

NLR, PLR and SII scores

The NLR, PLR, and SII scores of 1.99, 126.90, and 529.24, respectively, were calculated as the most appropriate cutoff thresholds by the Youden index of the ROC for all patients based on preoperative hematology. The AUCs were 0.591 (95%CI: 0.553-0.630), 0.620 (95%CI: 0.583-0.658), and 0.594 (95%CI: 0.555-0.632), respectively (Figure 2E). The AUCs of NLR, PLR, and SII for the INFa, INFb and INFc groups are shown in the Supplementary Table 2 (Figure 2F-H).

Inflammatory indices and patient survival

In patients with INFa, a significant difference in OS was found between patients with SII > 523.01 and those with SII ≤ 523.01 (OS: 56.55 mo *vs* 44.98 mo, $P < 0.001$; HR: 4.502, 95%CI: 2.166-9.355). According to the pTNM stage, for stages I and II, the difference in OS between patients with SII > 523.01 and those with SII ≤ 523.01 was not significant ($P = 0.450$ and $P = 0.146$). For stage III, patients with SII ≤ 523.01 had better survival ($P = 0.003$) (Figure 3A-D). The SII score was significantly associated with carbohydrate antigen 19-9 (CA19-9), Borrmann type, tumor diameter, histological type, pTNM stage, and mLNR, as determined by the chi-square test of clinicopathologic features (all $P < 0.05$) (Table 2).

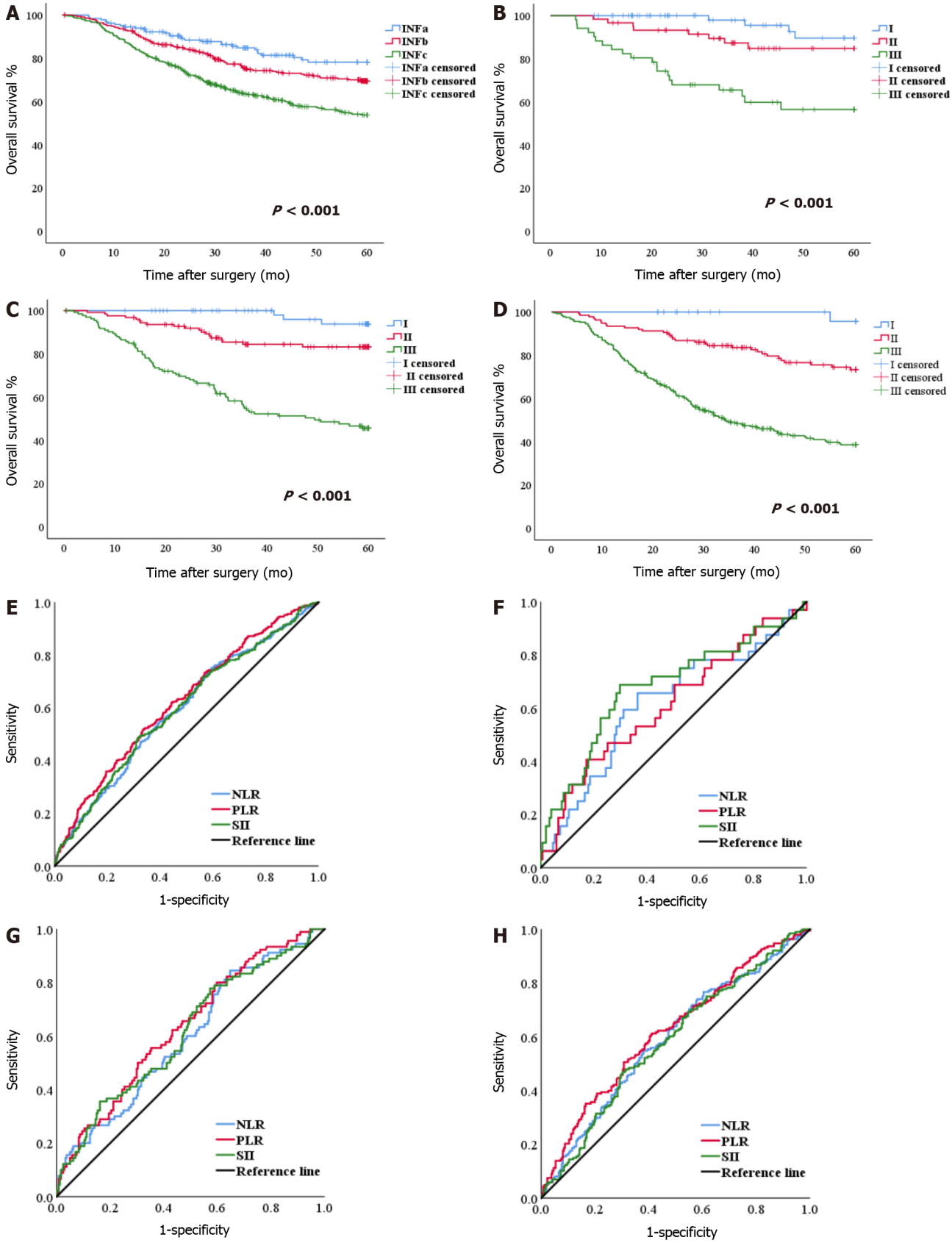

Figure 2 Survival curve analyses for patients and receiver operating characteristic curves of inflammatory indices. A: Survival curves of all patients; B-D: Survival curves of patients with the expansive growth type (INFa), the intermediate type (INFb), and the infiltrative growth type (INFc); E-H: Receiver operating characteristic curve of neutrophil-lymphocyte ratio, platelet-lymphocyte ratio, and systemic immune-inflammation index in all patients, INFa group, INFb group, and INFc group. INFa: The expansive growth type; INFb: The intermediate type; INFc: The infiltrative growth type; ROC: Receiver operating characteristic; NLR: Neutrophil-lymphocyte ratio; PLR: Platelet-lymphocyte ratio; SII: Systemic immune-inflammation index.

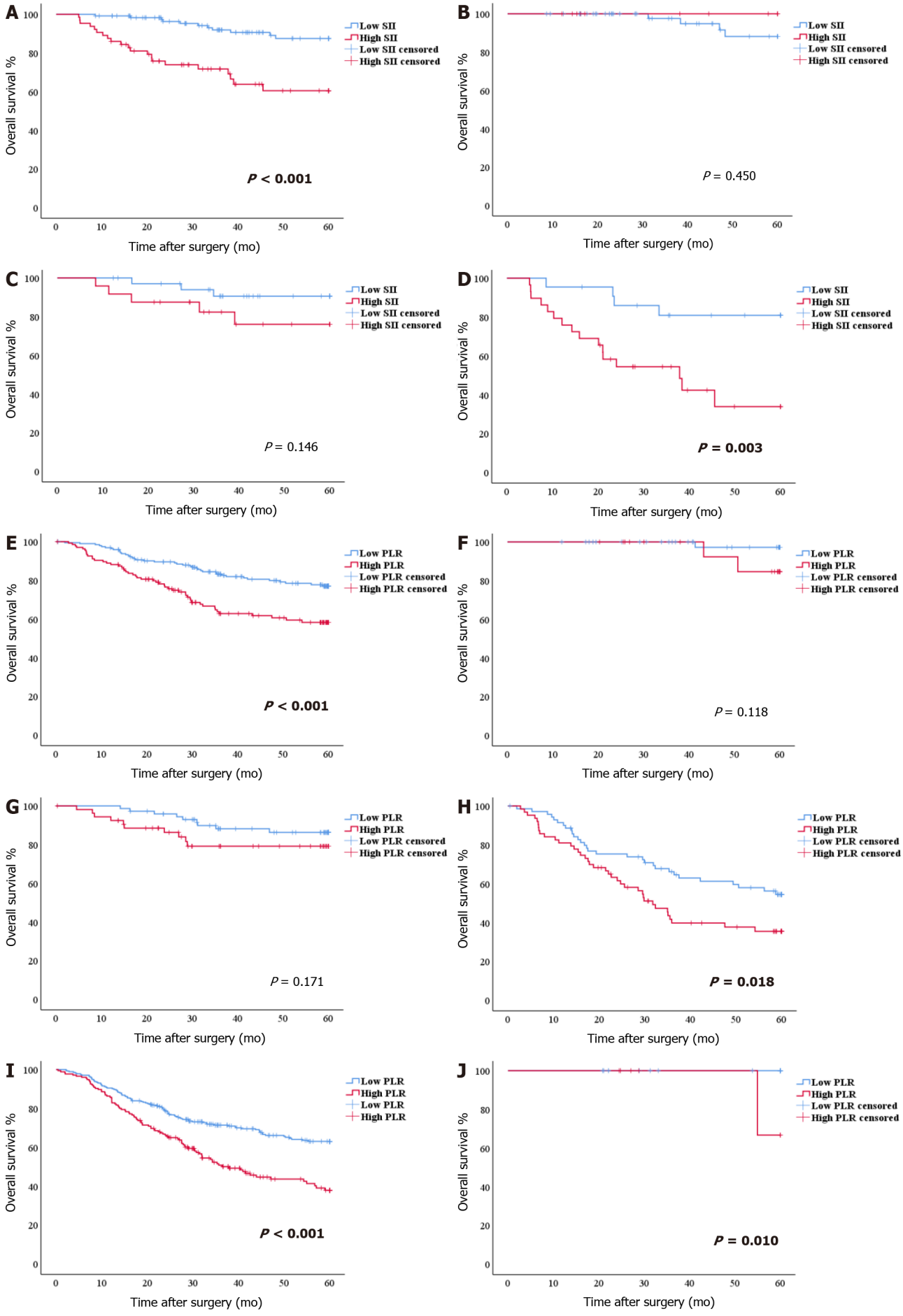
A
Overall survival %
Time after surgery (mo)
Low SII
High SII
Low SII censored
High SII censored
P < 0.001
B
P = 0.450
C
P = 0.146
D
P = 0.003
E
Low PLR
High PLR
Low PLR censored
High PLR censored
P < 0.001
F
P = 0.118
G
P = 0.171
H
P = 0.018
I
P < 0.001
J
P = 0.010

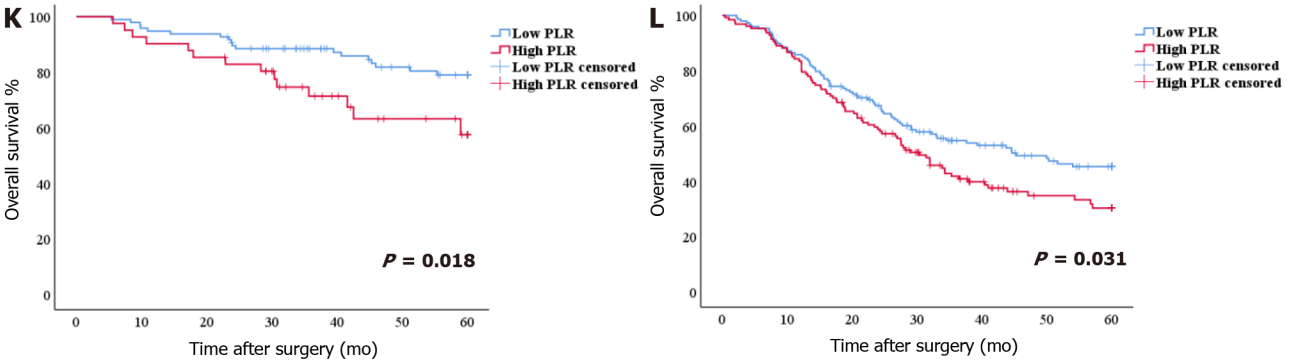

Figure 3 Survival curve analyses based on the systemic immune-inflammation index and platelet-lymphocyte ratio. A-D: Survival curves of patients with the expansive growth type based on the systemic immune-inflammation index in all stages, stage I, stage II, and stage III; E–H: Survival curves of patients with the intermediate type based on the platelet-lymphocyte ratio (PLR) in all stages, stage I, stage II, and stage III; I–L: Survival curves of patients with the infiltrative growth type based on the PLR in all stages, stage I, stage II, and stage III. INFa: The expansive growth type; INFb: The intermediate type; INFc: The infiltrative growth type; PLR: Platelet-lymphocyte ratio; SII: Systemic immune-inflammation index.

In patients with INFb, a significant difference in OS was found between patients with PLR > 134.02 and those with PLR ≤ 134.02 (OS: 52.47 mo *vs* 44.37 mo, $P < 0.001$; HR: 2.191, 95%CI: 1.444-3.323). According to the pTNM stage, for stages I and II, the difference in OS between patients with PLR > 134.02 and those with PLR ≤ 134.02 was not significant ($P = 0.118$ and $P = 0.171$). For stage III, the OS of patients with PLR ≤ 134.02 was better ($P = 0.018$) (Figure 3E-H). The PLR score was significantly associated with BMI, tumor diameter, histological type, pTNM stage, and mLNR, as determined by the chi-square test of clinicopathologic features (all $P < 0.05$) (Table 2).

In patients with INFc, a significant difference in OS was found between patients with PLR > 134.02 and those with PLR > 134.02 (OS: 46.53 mo *vs* 37.97 mo, $P < 0.001$; HR: 1.956, 95%CI: 1.467-2.307). According to the pTNM stage, for stages I, II, and III, patients with PLR ≤ 134.02 had better survival ($P = 0.010$, $P = 0.018$ and $P = 0.031$) (Figure 3I-L). The PLR score was significantly associated with age, tumor diameter, histological type, pTNM stage, and mLNR, as determined by the chi-square test of clinicopathologic features (all $P < 0.05$) (Table 2).

Inflammatory indices and postoperative chemotherapy

For INFa and INFb GC, there were no statistically significant differences in OS between patients with and without postoperative chemotherapy (all $P > 0.05$) (Figure 4A-F). For INFc GC, in the PLR ≤ 134.02 group, the OS of patients with postoperative chemotherapy was significantly better than that of patients without postoperative chemotherapy (OS: 50.22 mo *vs* 43.90 mo, $P = 0.030$) (Figure 4H). However, in the overall group and the PLR > 134.02 group, there were no statistically significant differences in OS between patients with and without postoperative chemotherapy ($P = 0.057$ and $P = 0.770$) (Figure 4G and I).

Immune cells and INF

According to pTNM stage, peripheral circulating immune cell parameters, including neutrophil percentage, lymphocyte percentage and platelet count were analyzed. For I-III stage GC patients, the percentages of neutrophils and lymphocytes were not significantly different among the three groups ($P > 0.05$) (Figure 5A-F). For patients with stage I GC, the platelet count of INFc group was significantly higher than that of INFa group ($P < 0.05$) (Figure 5G). For patients with stage II GC, the platelet count of INFc group was significantly lower than that of INFb group ($P < 0.05$) (Figure 5H). For patients with stage III GC, the platelet count of INFc group was significantly lower than that of INFa and INFb group ($P < 0.05$) (Figure 5I).

Univariate and multivariate regression analyses in the three groups

To identify the independent risk factors for prognosis in the three groups, univariate and multivariate analyses based on the logistic risk regression model were implemented. In the INFa group, univariate analysis and multivariate analysis showed that SII ($P = 0.039$) and mLNR ($P = 0.003$) were independent prognostic factors for INFa GC (Table 3). In the INFb group, univariate analysis and multivariate analysis showed that age ($P = 0.026$), BMI ($P = 0.003$), PLR ($P = 0.018$) and pTNM stage ($P < 0.001$) were independent risk factors for the prognosis of INFb GC (Table 4). In the INFc group, univariate analysis and multivariate analysis showed that age ($P = 0.021$), PLR ($P = 0.021$), pTNM stage ($P = 0.028$) and mLNR ($P = 0.002$) were independent prognostic factors for INFc GC (Table 5).

Table 4 Prognostic factors of patients with gastric cancer by univariate and multivariate analyses based on logistic regression analysis in the intermediate type group

Characteristics	INFb			
	Univariate analysis		Multivariate analysis	
	HR (95%CI)	*P* value	HR (95%CI)	*P* value
Sex		0.115		
Male	1			
Female	0.617 (0.339-1.124)			
Age (yr)	1.033 (1.007-1.061)	**0.014**	1.036 (1.004-1.069)	**0.026**
BMI	0.814 (0.746-0.888)	**< 0.001**	0.861 (0.781-0.950)	**0.003**
PLR	1.008 (1.003-1.012)	**< 0.001**	1.006 (1.001-1.012)	**0.018**
ALT	0.976 (0.949-1.004)	0.094		
Total protein	0.975 (0.946-1.004)	0.092		
CEA	1.004 (0.995-1.014)	0.338		
CA19-9	1.003 (1.001-1.006)	**0.012**	1.000 (0.998-1.003)	0.650
Borrmann type		**0.005**		0.226
0-1	1		1	
2	1.031 (0.430-2.473)	0.945	0.715 (0.246-2.079)	0.538
3	2.410 (1.081-5.372)	**0.031**	1.530 (0.554-4.223)	0.412
4-5	3.182 (1.201-8.429)	**0.020**	1.339 (0.374-4.797)	0.654
Tumor location		0.088	-	-
Lower third	1			
Middle third	1.195 (0.641-2.228)	0.575		
Upper third	1.527 (0.697-3.345)	0.290		
Entire stomach	7.634 (1.441-40.446)	**0.017**		
Tumor size (mm)	1.021 (1.012-1.032)	**< 0.001**	1.007 (0.994-1.021)	0.302
pTNM stage		**< 0.001**		**< 0.001**
I	1		1	
II	3.929 (1.120-13.785)	**0.033**	2.036 (0.528-7.856)	0.302
III	23.010 (6.895-76.795)	**< 0.001**	8.306 (2.053-33.597)	**0.003**
Histological types		0.739		
Well and medium differentiation	1			
Poor differentiation	1.105 (0.617-1.977)	0.738		
Others	0.853 (0.472-1.542)	0.599		
mLNR	87.343 (18.612-409.881)	**< 0.001**	2.267 (0.291-17.641)	0.434
Vascular infiltration		**< 0.001**		0.149
No	1		1	
Yes	3.160 (1.897-5.263)		1.585 (0.848-2.963)	
Nerve infiltration		**0.003**		0.859
No	1		1	
Yes	2.097 (1.283-3.428)		1.057 (0.573-1.951)	
Postoperative chemotherapy		0.493		
Yes	1			

No	0.823 (0.472-1.436)

Carcinoembryonic antigen and carbohydrate antigen 19-9 were according to the tumor marker examination. Tumor infiltrative pattern, tumor location, postsurgical tumor node metastasis stage, histological type, metastatic lymph node ratio, vascular infiltration and nerve infiltration were according to the postoperative pathology report. Statistically significant *P* values are in bold ($P < 0.05$). INF: Tumor infiltrative pattern; INFa: Expansive growth type; INFb: Intermediate type; INFc: Infiltrative growth type; HR: Hazard ratio; BMI: Body mass index; PLR: Platelet–lymphocyte ratio; ALT: Alanine transaminase; CEA: Carcinoembryonic antigen; CA19-9: Carbohydrate antigen 19-9; mLNR: Metastatic lymph node ratio; pTNM: Postsurgical tumor node metastasis.

Nomogram

We combined independent prognostic risk factors to construct nomogram models to evaluate the prognosis of patients in different INF groups (Figure 6A, D and G). For predicting the survival of patients with INFa, INFb and INFc GC within 3 and 5 years after radical resection, ROC analysis showed that the AUCs of the nomogram models were both greater than those of pTNM stage alone (Figure 6B, C, E, F, H and I). The results of the nomogram models are shown in the Supplementary Table 3.

DISCUSSION

In East Asia, INF has gradually become a clinicopathological feature for routine evaluation in surgical specimens[7]. Hematoxylin eosin staining is easy to determine it, which is convenient for clinical application. Recent retrospective studies have further demonstrated that INF can be an ideal predictor of recurrence and metastasis patterns after radical gastrectomy. INFc is an independent risk factor for peritoneal metastasis and is more prone to lymph node metastasis, while the liver metastasis rate of INFa/b is significantly higher than that of INFc[6,8,9]. Our study also confirmed that the prognosis of patients with INFa and INFb GC was better than that of patients with INFc GC. This evidence shows that INF can effectively help clinical experts predict the recurrence pattern and prognosis of GC patients. In addition, with the great achievements of tumor immunotherapy, it has been found that the tumor microenvironment and immune inflammatory response in peripheral blood can effectively reduce the impact of GC heterogeneity, providing more comprehensive information for the personalized treatment of patients[14,18]. This study was aimed at investigating the peripheral blood immune response is great value to different INF types GC patients in evaluating prognosis and individualized chemotherapy.

As the significant role of the systemic immune inflammatory response in gastrointestinal tumors has gradually become widely recognized by clinical experts, inflammatory indices, such as NLR, PLR and LMR, have been indicated to be prognostic markers of GC, esophageal cancer or colorectal cancer[19,20]. These indices can also evaluate the possible benefits and prospects of immunotherapy according to their baseline levels to support personalized immunotherapy[21]. As a part of systemic immunity, peripheral blood immunity also plays a significant role in the process of tumor metastasis. The proliferation of tumor cells causes them to break through mechanical pressure, escape immune monitoring, enter peripheral veins and form circulating tumor cells (CTCs)[22]. In this process, the close relationship between neutrophils and CTCs promotes the cell cycle process of CTCs and expands the metastatic potential of CTCs[23]. In addition, cytokines, such as tumor necrosis factor α released by CTC-associated neutrophils, play a key role in promoting tumor cell proliferation[23]. Lymphocytes can restrain the migration and proliferation of CTCs by secreting cytokines such as perforin/granzyme[24]. In addition, platelets can form aggregates with CTCs to escape host immune monitoring and release transforming growth factor β (TGF-β), inducing epithelial-mesenchymal transformation to promote distant metastasis [25]. The current research results showed that the higher the levels of the inflammatory indices SII and PLR are, the greater the possibility of early distant metastasis and the worse the prognosis. The AUC of the SII was higher in patients with INFa GC in ROC analysis, and the SII was an independent prognostic factor. This finding also showed that the pivotal role of neutrophils, lymphocytes and platelets for patients with INFa GC in the external circulation immunity. Besides, PLR also was a key predictor of the prognosis of patients with INFb and INFc GC. This finding further suggests that in peripheral circulating immunity of different INF types, the subsets of immune cells that play a major part are different.

In this study, we found that there was no significant difference in the percentages of neutrophils and lymphocytes among the three groups. In patients with stage II and III GC, the platelet count of INFc group was significantly lower than that of INFa and INFb group, which seems to contradict the conclusion that the prognosis of patients with INFc GC was poor. The reason for this may be that different INF groups differ greatly in their sensitivity to peripheral immune cells. Due to the influence of GC heterogeneity, the immune microenvironment of different subtypes of GC patients is greatly different[26]. Because of the unique biological characteristics of infiltrative growth with no distinct border with the surrounding tissue, tumor cells in patients with INFc GC may be more likely to enter

Table 5 Prognostic factors of patients with gastric cancer by univariate and multivariate analyses based on logistic regression analysis in the infiltrative growth type group

Characteristics	INFc			
	Univariate analysis		Multivariate analysis	
	HR (95%CI)	*P* value	HR (95%CI)	*P* value
Sex		0.570		
Male	1			
Female	0.889 (0.592-1.335)			
Age (yr)	1.028 (1.009-1.047)	**0.003**	1.026 (1.004-1.049)	**0.021**
BMI	0.965 (0.915-1.017)	0.184		
PLR	1.007 (1.004-1.010)	**< 0.001**	1.004 (1.001-1.008)	**0.021**
ALT	0.984 (0.966-1.003)	0.096		
Total protein	0.995 (0.973-1.018)	0.683		
CEA	1.006 (0.998-1.014)	0.161		
CA19-9	1.000 (1.000-1.006)	**0.020**	1.001 (0.999-1.004)	0.387
Borrmann type		**< 0.001**		0.055
0-1	1		1	
2	2.104 (0.574-7.708)	0.262	1.193 (0.290-4.903)	0.807
3	4.298 (1.233-14.981)	**0.022**	1.781 (0.460-6.891)	0.403
4-5	14.250 (3.837-52.919)	**< 0.001**	3.735 (0.835-16.696)	0.085
Tumor location		**< 0.001**		0.059
Lower third	1		1	
Middle third	2.791 (1.669-4.670)	**< 0.001**	1.952 (1.052-3.622)	**0.034**
Upper third	1.985 (0.947-4.160)	0.069	1.955 (0.820-4.658)	0.130
Entire stomach	22.330 (2.867-173.902)	**0.003**	4.687 (0.523-41.965)	0.167
Tumor size (mm)	1.028 (1.020-1.037)	**< 0.001**	1.004 (0.993-1.016)	0.433
pTNM stage		**< 0.001**		**0.028**
I	1		1	
II	10.667 (1.405-80.956)	**0.022**	8.549 (1.073-68.125)	**0.043**
III	45.208 (6.106-334.716)	**< 0.001**	13.795 (1.693-112.382)	**0.014**
Histological types		0.643		
Well and medium differentiation	1			
Poor differentiation	1.026 (0.656-1.604)	0.912		
Others	0.826 (0.493-1.384)	0.468		
mLNR	93.645 (30.921-283.603)	**< 0.001**	11.042 (2.407-50.664)	**0.002**
Vascular infiltration		**< 0.001**		0.783
No	1		1	
Yes	2.899 (1.905-4.411)		1.080 (0.623-1.874)	
Nerve infiltration		**0.029**		0.471
No	1		1	
Yes	1.524 (1.044-2.226)		1.187 (0.745-1.892)	
Postoperative chemotherapy		0.315		
Yes	1			

No	0.891 (0.554-1.209)

Carcinoembryonic antigen and carbohydrate antigen 19-9 were according to the tumor marker examination. Tumor infiltrative pattern, tumor location, postsurgical tumor node metastasis stage, histological type, metastatic lymph node ratio, vascular infiltration and nerve infiltration were according to the postoperative pathology report. Statistically significant *P* values are in bold ($P < 0.05$). INF: Tumor infiltrative pattern; INFa: Expansive growth type; INFb: Intermediate type; INFc: Infiltrative growth type; HR: Hazard ratio; BMI: Body mass index; PLR: Platelet–lymphocyte ratio; ALT: Alanine transaminase; CEA: Carcinoembryonic antigen; CA19-9: Carbohydrate antigen 19-9; mLNR: Metastatic lymph node ratio; pTNM: Postsurgical tumor node metastasis.

the peripheral circulation to form CTCs. This results in that even if the platelets of patients with INFc GC being lower than those of patients with INFa and INFb GC in the same period, their peripheral circulating platelets are more likely to form aggregates with CTCs in patients with INFc GC, thus avoiding host immune monitoring and causing distant metastasis. In addition, we found that the platelet count of patients with INFc GC did not increase with increasing pTNM stage. The platelet count of patients with stage I disease was higher than that of patients with stage II and III disease. This may be related to the small number of INFc patients with stage I disease included in our study. Therefore, our next research direction is to explore the distribution and function of immune cell subsets according to INF.

We found that for the INFc group, patients with a low PLR were more sensitive to postoperative chemotherapy. The therapeutic effect of chemotherapy on different individuals depends not only on the sensitivity of cancer cells to chemotherapeutic drugs, but also on the immune status of tumor microenvironment. Ohe *et al*[27] also found that GC patients with a low PLR were more sensitive to chemotherapy. Platelets in peripheral blood are released from damaged endothelial cells by cisplatin-based chemotherapy, adhere to and accumulate on the vascular wall through von Willebrand factor [28]. Coalescented and activated platelets secrete multifarious cytokines, such as TGF-β and vascular endothelial growth factor A (VEGF-A). They induce the up regulation of cancer cell metastasis and drug resistance by acting on epithelial-mesenchymal transformation[29,30]. In addition, peripheral blood lymphocytes continually enter and exit lymph nodes, which leads to the initiation and activation of antigen-presenting dendritic cells (DCs). DCs can recognize the neoantigens of tumor cells induced by chemotherapy immunogenicity and make tumor cells sensitive to T cell-mediated killing[31]. This evidence suggests that patients with a low PLR GC are more sensitive to chemotherapy than other patients due to fewer platelets and more lymphocytes in their peripheral circulation. Our study also found that chemotherapy had better efficacy in the INFc group than in the other two groups. Wang *et al* [32] found that the survival rate of patients with early neutropenia after postoperative chemotherapy was higher. In addition, neutrophils and platelets in peripheral blood can inhibit natural killer cells by releasing chemical mediators, such as interleukin-1 and VEGF-A, and advance the immune resistance and escape of CTCs to chemotherapy drugs[33-36]. Our results showed that the percentages of neutrophils and platelets in INFc were lower than those in INFa and INFb in stage II and III GC patients, which may be why INFc is more sensitive to chemotherapy. Therefore, it is necessary to further investigate whether targeted therapy can improve postoperative survival in patients with INFa and INFb GC.

Clinically, some clinicians have realized that pTNM stage depends on postoperative pathology can provide efficacious but imperfect information for individual treatment. The same stage patients show significant individual differences in prognosis. Many studies have suggested that tumor immunity can bring into play an efficacious supplementary role[37,38]. Analyzing the proportion of immune cells in body fluids can effectively evaluate the prognosis of metastatic GC patients and provide them with more personalized treatment[39]. Li *et al*[20] constructed a nomogram based on inflammation and nutritional markers to predict the prognosis of GC patients receiving neoadjuvant chemotherapy and D2 Lymph node dissection. As a result, this type of prediction model constructed by combining inflammatory markers with clinicopathological features has the advantages of more accurate and individualized evaluation of patient prognosis and reducing the differences caused by heterogeneity. Based on the logistic risk regression model, our study found that the SII and mLNR were independent risk factors related to the prognosis of INFa GC patients. PLR, age, BMI and pTNM stage are independent risk factors related to the prognosis of INFb GC patients. PLR, age, pTNM stage and mLNR are independent risk factors related to the prognosis of INFc GC patients. Then, the nomogram models were constructed to predict the prognosis of patients with different INF types. We found that the nomogram models were better than the conventional pTNM stage alone in predicting the prognosis of patients with different INF types of GC within 3 years and 5 years after radical resection. The prediction models for evaluating the prognosis of different INF types patients combining inflammatory biomarkers and clinicopathological features were effective, which deserve further testing and extension in clinical practice.

There were some limitations in this study. First, the existence of internal bias and heterogeneity were inevitable as it was a retrospective study. Second, this was a single-center study, focusing only on Asian populations. Whether these results are widely applicable to other populations needs to be further studied by enlarging the sample size and source.

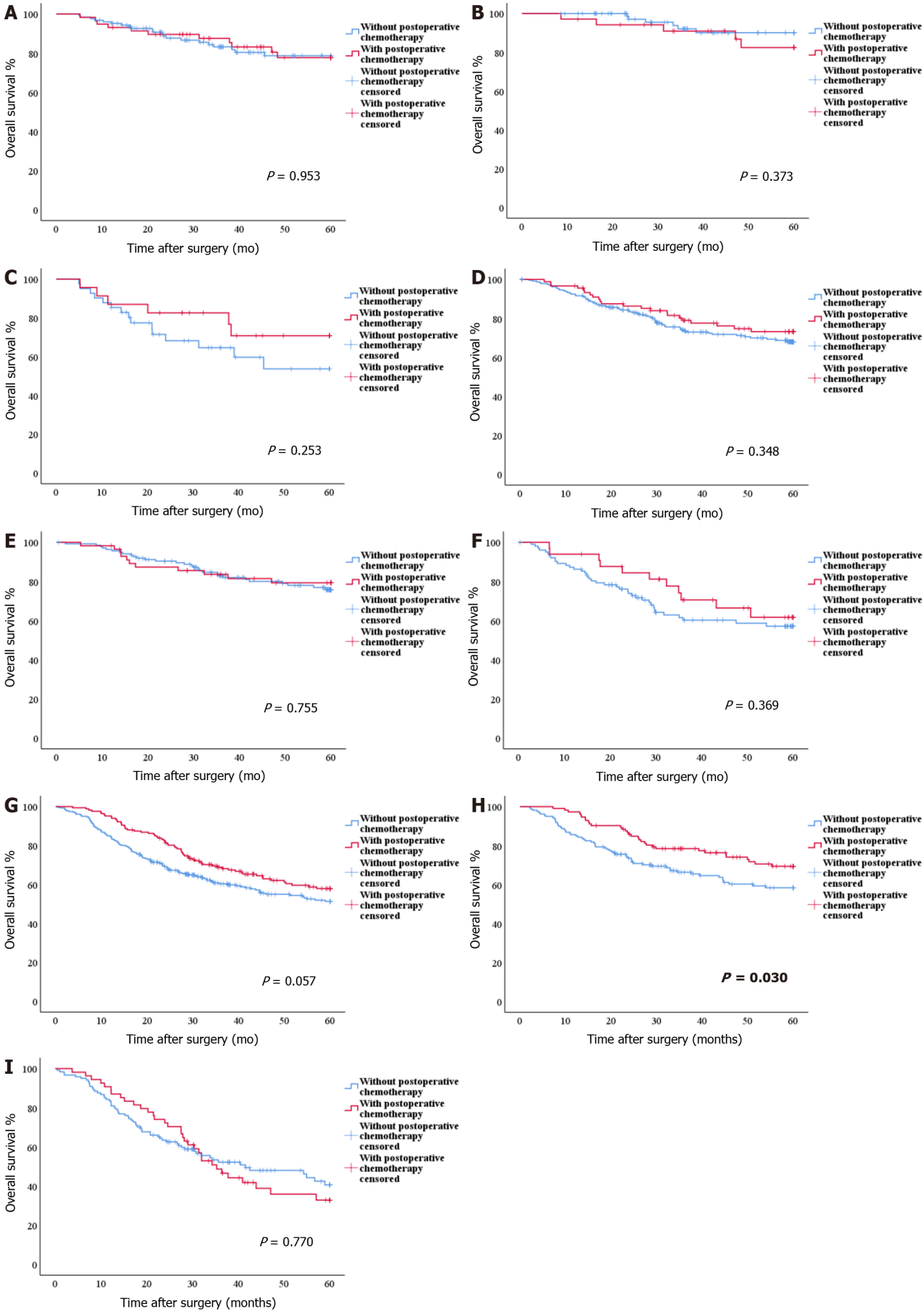

Figure 4 Survival curve analyses based on postoperative chemotherapy. A-C: Survival curves with and without postoperative chemotherapy in all the

expansive growth type (INFa) gastric cancer (GC) patients, INFa GC patients with systemic immune-inflammation index (SII) ≤ 523.01, and INFa GC patients with SII > 523.01; D-F: Survival curves with and without postoperative chemotherapy in all the intermediate type (INFb), GC patients, INFb GC patients with platelet-lymphocyte ratio (PLR) ≤ 134.02, and INFb GC patients with PLR > 134.02; G–I: Survival curves with and without postoperative chemotherapy in all the infiltrative growth type (INFc) GC patients, INFc GC patients with PLR ≤ 134.02, and INFc GC patients with PLR > 134.02. INFa: The expansive growth type; INFb: The intermediate type; INFc: The infiltrative growth type; PLR: Platelet-lymphocyte ratio; SII: Systemic immune-inflammation index.

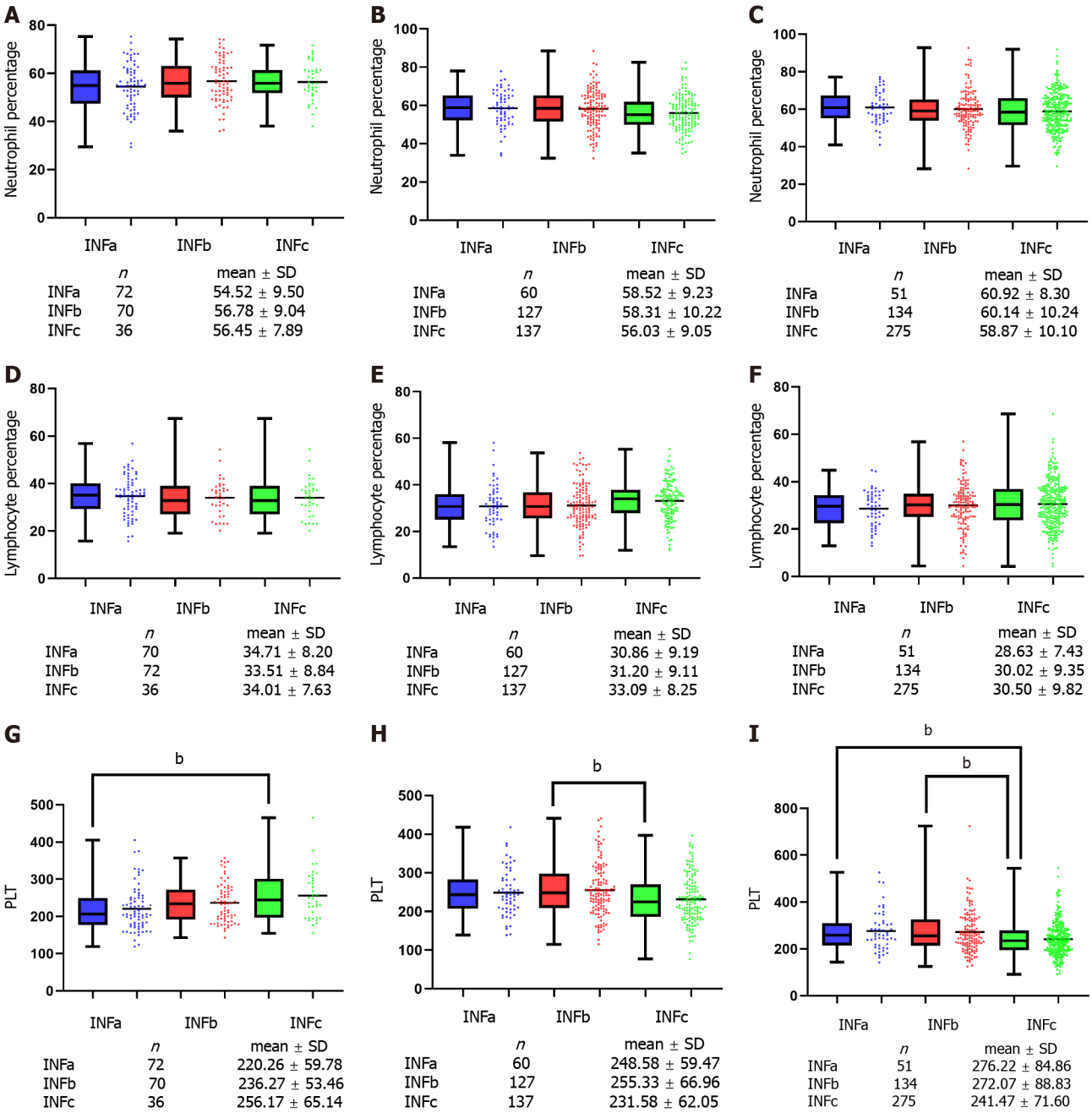

Figure 5 The relationship between peripheral circulating immune cells and different tumor infiltrative pattern types. A-C: Boxplot combined with scatterplot of neutrophil percentage based on tumor infiltrative pattern (INF) types in stage I, stage II, and stage III; D-F: Boxplot combined with scatterplot of lymphocyte percentage based on INF types in stage I, stage II, and stage III; G–I: Boxplot combined with scatterplot of platelet count based on INF types in stage I, stage II, and stage III. INFa: The expansive growth type; INFb: The intermediate type; INFc: The infiltrative growth type; PLT: Platelet.

CONCLUSION

The SII and PLR were independent risk factors for the prognosis of patients with GC in the INFa, INFb and INFc groups. The nomogram based on these two inflammatory biomarkers combined with clinicopathologic features can evaluate the prognosis of GC patients with different INF types, and its predictive ability is better than that of the traditional pTNM stage alone.

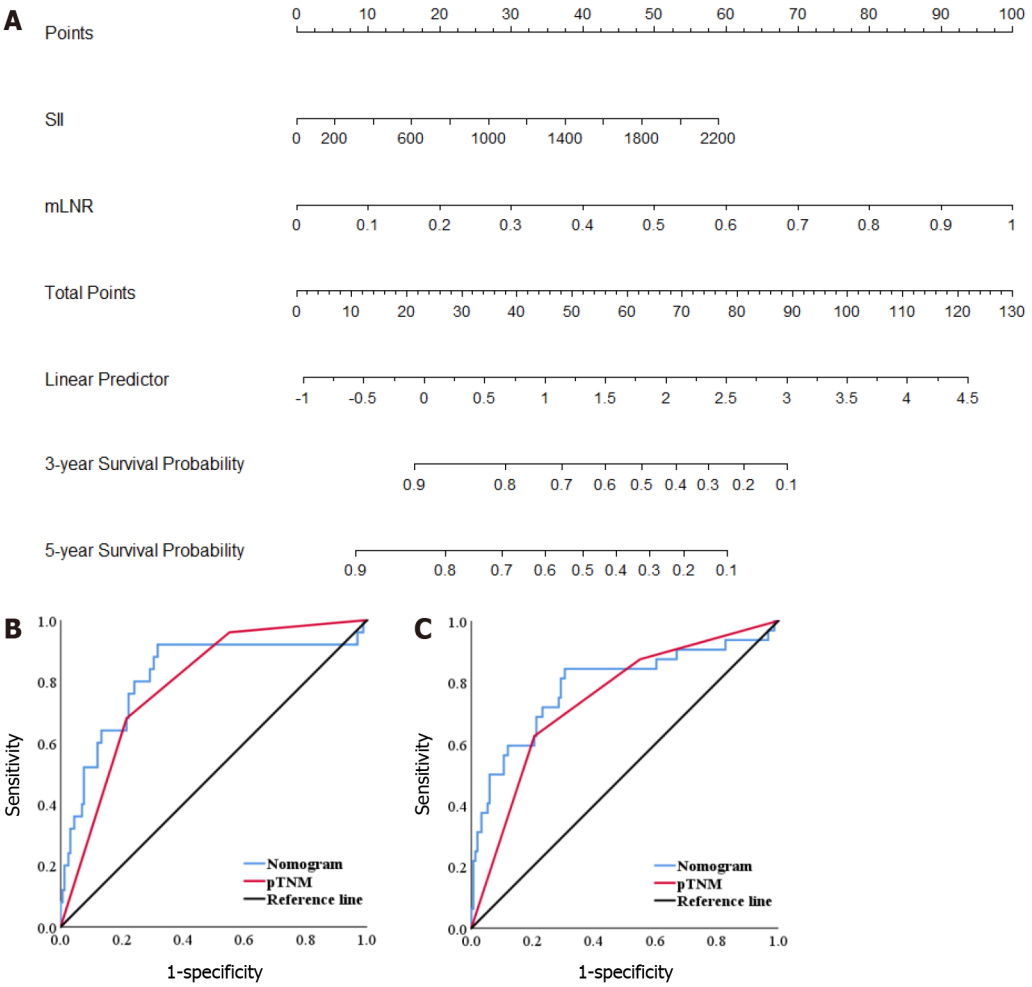
A
Points
0 10 20 30 40 50 60 70 80 90 100
SII
0 200 600 1000 1400 1800 2200
mLNR
0 0.1 0.2 0.3 0.4 0.5 0.6 0.7 0.8 0.9 1
Total Points
0 10 20 30 40 50 60 70 80 90 100 110 120 130
Linear Predictor
-1 -0.5 0 0.5 1 1.5 2 2.5 3 3.5 4 4.5
3-year Survival Probability
0.9 0.8 0.7 0.6 0.5 0.4 0.3 0.2 0.1
5-year Survival Probability
0.9 0.8 0.7 0.6 0.5 0.4 0.3 0.2 0.1
B
Sensitivity
1-specificity
Nomogram
pTNM
Reference line
C
Sensitivity
1-specificity
Nomogram
pTNM
Reference line
D
Points
0 10 20 30 40 50 60 70 80 90 100
Age
30 40 50 60 70 80
BMI
36 34 32 30 28 26 24 22 20 18 16 14
PLR
0 50 100 150 200 250 300 350 400 450 500
pTNM
2
1 3
Total Points
0 20 40 60 80 100 120 140 160 180 200 220 240 260
Linear Predictor
-3 -2.5 -2 -1.5 -1 -0.5 0 0.5 1 1.5 2 2.5 3 3.5
3-year Survival Probability
0.9 0.8 0.7 0.6 0.5 0.4 0.3 0.2 0.1
5-year Survival Probability
0.9 0.8 0.7 0.6 0.5 0.4 0.3 0.2 0.1

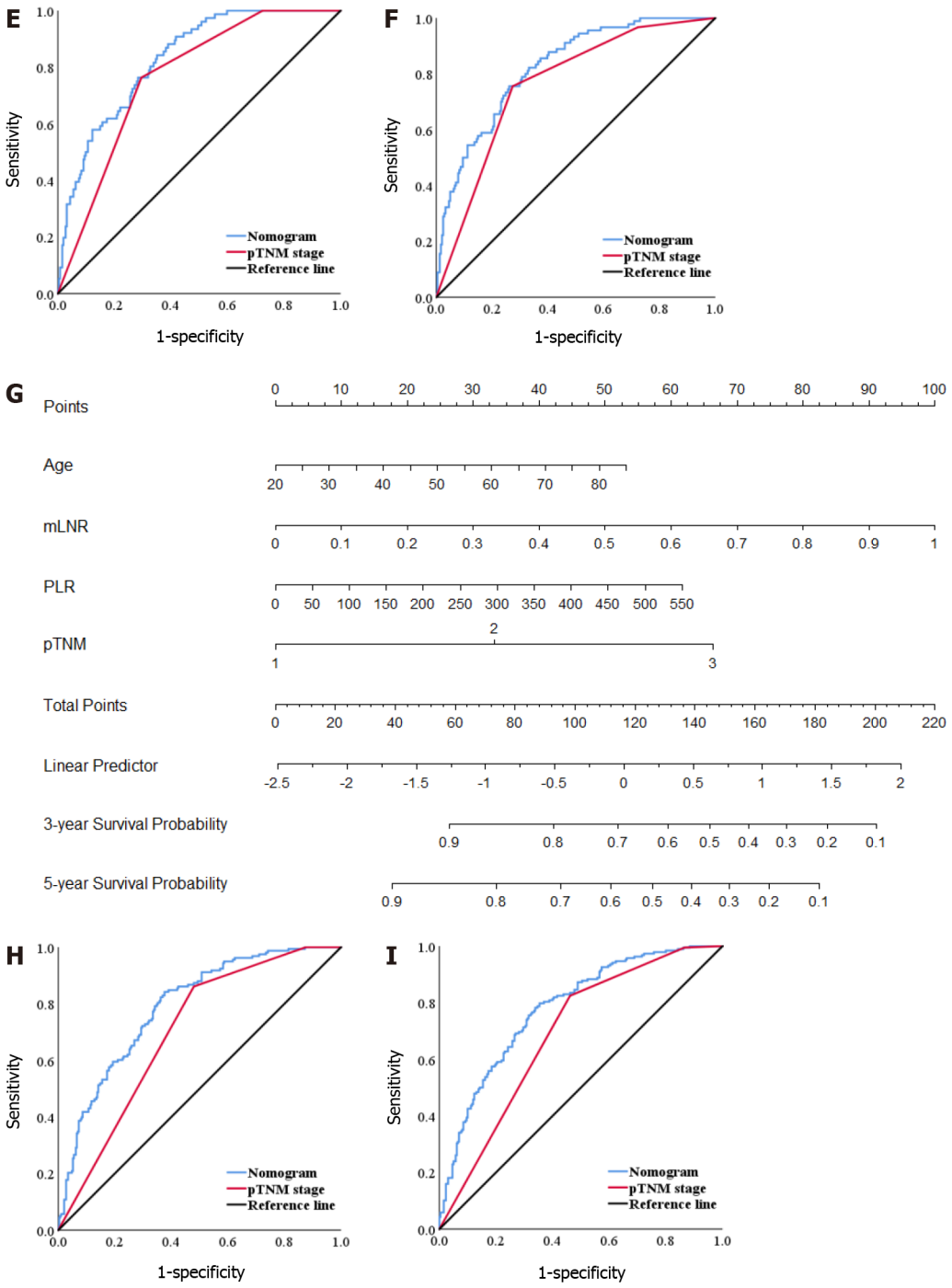

Figure 6 Nomogram models predicting the survival of patients with different tumor infiltrative pattern types. A, D and G: Nomogram models predicting the 3-year and 5-year survival of patients with the expansive growth type (INFa), the intermediate type (INFb), and the infiltrative growth type (INFc) gastric cancer (GC); B and C: Receiver operating characteristic (ROC) of the nomogram model and postsurgical tumor node metastasis (pTNM) stage predicting the 3-year and 5-year survival of patients with INFa GC; E and F: ROC of the nomogram model and pTNM stage predicting the 3-year and 5-year survival of patients with INFb GC; H and I: ROC curve of the nomogram model and pTNM stage predicting the 3-year and 5-year survival of patients with INFc GC. INFa: The expansive growth type; INFb: The intermediate type; INFc: The infiltrative growth type; ROC: Receiver operating characteristic curve; mLNR: Metastatic lymph node ratio; BMI: Body mass index; PLR: Platelet-lymphocyte ratio; SII: Systemic immune-inflammation index.

ARTICLE HIGHLIGHTS

Research background

Gastric cancer (GC) is an important public health burden worldwide. In East Asia, the tumor infiltrative pattern (INF) has gradually become a clinicopathologic feature routinely evaluated in surgically resected specimens. The INF type categorizes GC as the expansive growth type (INFa), the intermediate type (INFb), and the infiltrative growth type (INFc). Different INF types differ in clinicopathological features and prognosis and can be used as predictors of postoperative recurrence and prognosis in GC

patients. Many studies have shown that inflammatory indices are potential prognostic indices for GC patients. However, there is no evidence defining the prognostic significance of immune inflammatory indices for GC with different INF types.

Research motivation

Evaluating whether inflammatory indices have prognostic significance for GC with different INF types will provide a basis for clinicians to treat and predict the prognosis of these patients in the future.

Research objectives

To analyze the relationships among peripheral circulating immune cells, inflammatory indices and INF types and to evaluate their ability to evaluate the outcome of patients with GC.

Research methods

This retrospective study analyzed the clinicopathological characteristics and long-term survival data of 962 patients who underwent radical gastrectomy. Patients were categorized into the INFa, INFb, and INFc groups. The differences of clinicopathological features between the three groups were analyzed by chi-square test. The cutoff values of inflammatory indices were analyzed by receiver operating characteristic curves. The Kaplan–Meier and log-rank tests were used to analyze overall survival (OS). The independent risk factors for patients prognosis were analyzed by univariate and multivariate analyses based on the logistic regression. The nomogram models were constructed by R studio.

Research results

Based on the postoperative pathology report, there were 183, 331 and 448 patients in the INFa, INFb, and INFc groups, respectively. The OS of the INFc group was significantly lower than that of the other two groups ($P < 0.001$). The systemic immune-inflammation index ($P = 0.039$) and metastatic lymph node ratio (mLNR) ($P = 0.003$) were independent risk factors for prognosis in the INFa group. The platelet–lymphocyte ratio (PLR) ($P = 0.018$), age ($P = 0.026$), body mass index ($P = 0.003$), and postsurgical tumor node metastasis (pTNM) stage ($P < 0.001$) were independent risk factors for prognosis in the INFb group. The PLR ($P = 0.021$), age ($P = 0.021$), pTNM stage ($P = 0.028$), and mLNR ($P = 0.002$) were independent risk factors for prognosis in the INFc group. The area under the curve of the nomogram model for predicting 5-year survival in the INFa group, INFb group, and INFc group was 0.787, 0.823, and 0.781, respectively.

Research conclusions

The nomogram model based on different inflammatory indices and clinicopathological features can be used to evaluate the prognosis of different INF types GC patients.

Research perspectives

Further multicentric studies are needed to expansion of the sample size and external validation of nomogram model was performed to determine its predictive ability.

FOOTNOTES

Author contributions: Wang YF and Yin X designed and conceived this project, and they contributed equally to this work; Wang YF, Yin X, Fang TY and Wang YM, Zhang L, Zhang XH interpreted and analyzed the data; Xue YW revised the manuscript for important intellectual content; Wang YF, Yin X, Fang TY, Wang YM, Zhang L, Zhang XH, Zhang DX, Zhang Y, Wang XB, Wang H participated in the patient information collection; all authors read and approved the final manuscript.

Supported by the Harbin Science and Technology Bureau Research and Development Project of Applied Technology, No. 2017RAXXJ054; and Nn 10 Program of Harbin Medical University Cancer Hospital, No. Nn 10 PY 2017-03.

Institutional review board statement: The study was approved by the Ethics Committee of the Affiliated Tumor Hospital of Harbin Medical University.

Informed consent statement: All study participants or their legal guardian provided informed written consent about personal and medical data collection prior to study enrolment.

Conflict-of-interest statement: All the authors have no conflict of interest related to the manuscript.

Data sharing statement: Patients' data were saved in the Gastric Cancer Information Management System v1.2 of Harbin Medical University Cancer Hospital (Copyright No. 2013SR087424, http://www.sgihmu.com).

Country/Territory of origin: China

ORCID number: Yu-Fei Wang 0000-0002-1410-2716; Xin Yin 0000-0003-3587-371X; Tian-Yi Fang 0000-0002-5015-4898; Yi-Min Wang 0000-0002-9824-4097; Lei Zhang 0000-0002-0280-7081; Xing-Hai Zhang 0000-0003-0667-2126; Dao-Xu Zhang 0000-0002-2202-7437; Yao Zhang 0000-0002-3405-570X; Xi-Bo Wang 0000-0002-4141-8134; Hao Wang 0000-0003-4909-8937; Ying-Wei Xue 0000-0002-8427-9736.

S-Editor: Zhang H
L-Editor: A
P-Editor: Yuan YY

REFERENCES

1 **Global Burden of Disease Cancer Collaboration**, Fitzmaurice C, Abate D, Abbasi N, Abbastabar H, Abd-Allah F, Abdel-Rahman O, Abdelalim A, Abdoli A, Abdollahpour I, Abdulle ASM, Abebe ND, Abraha HN, Abu-Raddad LJ, Abualhasan A, Adedeji IA, Advani SM, Afarideh M, Afshari M, Aghaali M, Agius D, Agrawal S, Ahmadi A, Ahmadian E, Ahmadpour E, Ahmed MB, Akbari ME, Akinyemiju T, Al-Aly Z, AlAbdulKader AM, Alahdab F, Alam T, Alamene GM, Alemnew BTT, Alene KA, Alinia C, Alipour V, Aljunid SM, Bakeshei FA, Almadi MAH, Almasi-Hashiani A, Alsharif U, Alsowaidi S, Alvis-Guzman N, Amini E, Amini S, Amoako YA, Anbari Z, Anber NH, Andrei CL, Anjomshoa M, Ansari F, Ansariadi A, Appiah SCY, Arab-Zozani M, Arabloo J, Arefi Z, Aremu O, Areri HA, Artaman A, Asayesh H, Asfaw ET, Ashagre AF, Assadi R, Ataeinia B, Atalay HT, Ataro Z, Atique S, Ausloos M, Avila-Burgos L, Avokpaho EFGA, Awasthi A, Awoke N, Ayala Quintanilla BP, Ayanore MA, Ayele HT, Babaee E, Bacha U, Badawi A, Bagherzadeh M, Bagli E, Balakrishnan S, Balouchi A, Bärnighausen TW, Battista RJ, Behzadifar M, Bekele BB, Belay YB, Belayneh YM, Berfield KKS, Berhane A, Bernabe E, Beuran M, Bhakta N, Bhattacharyya K, Biadgo B, Bijani A, Bin Sayeed MS, Birungi C, Bisignano C, Bitew H, Bjørge T, Bleyer A, Bogale KA, Bojia HA, Borzì AM, Bosetti C, Bou-Orm IR, Brenner H, Brewer JD, Briko AN, Briko NI, Bustamante-Teixeira MT, Butt ZA, Carreras G, Carrero JJ, Carvalho F, Castro C, Castro F, Catalá-López F, Cerin E, Chaiah Y, Chanie WF, Chattu VK, Chaturvedi P, Chauhan NS, Chehrazi M, Chiang PP, Chichiabellu TY, Chido-Amajuoyi OG, Chimed-Ochir O, Choi JJ, Christopher DJ, Chu DT, Constantin MM, Costa VM, Crocetti E, Crowe CS, Curado MP, Dahlawi SMA, Damiani G, Darwish AH, Daryani A, das Neves J, Demeke FM, Demis AB, Demissie BW, Demoz GT, Denova-Gutiérrez E, Derakhshani A, Deribe KS, Desai R, Desalegn BB, Desta M, Dey S, Dharmaratne SD, Dhimal M, Diaz D, Dinberu MTT, Djalalinia S, Doku DT, Drake TM, Dubey M, Dubljanin E, Duken EE, Ebrahimi H, Effiong A, Eftekhari A, El Sayed I, Zaki MES, El-Jaafary SI, El-Khatib Z, Elemineh DA, Elkout H, Ellenbogen RG, Elsharkawy A, Emamian MH, Endalew DA, Endries AY, Eshrati B, Fadhil I, Fallah Omrani V, Faramarzi M, Farhangi MA, Farioli A, Farzadfar F, Fentahun N, Fernandes E, Feyissa GT, Filip I, Fischer F, Fisher JL, Force LM, Foroutan M, Freitas M, Fukumoto T, Futran ND, Gallus S, Gankpe FG, Gayesa RT, Gebrehiwot TT, Gebremeskel GG, Gedefaw GA, Gelaw BK, Geta B, Getachew S, Gezae KE, Ghafourifard M, Ghajar A, Ghashghaee A, Gholamian A, Gill PS, Ginindza TTG, Girmay A, Gizaw M, Gomez RS, Gopalani SV, Gorini G, Goulart BNG, Grada A, Ribeiro Guerra M, Guimaraes ALS, Gupta PC, Gupta R, Hadkhale K, Haj-Mirzaian A, Hamadeh RR, Hamidi S, Hanfore LK, Haro JM, Hasankhani M, Hasanzadeh A, Hassen HY, Hay RJ, Hay SI, Henok A, Henry NJ, Herteliu C, Hidru HD, Hoang CL, Hole MK, Hoogar P, Horita N, Hosgood HD, Hosseini M, Hosseinzadeh M, Hostiuc M, Hostiuc S, Househ M, Hussen MM, Ileanu B, Ilic MD, Innos K, Irvani SSN, Iseh KR, Islam SMS, Islami F, Jafari Balalami N, Jafarinia M, Jahangiry L, Jahani MA, Jahanmehr N, Jakovljevic M, James SL, Javanbakht M, Jayaraman S, Jee SH, Jenabi E, Jha RP, Jonas JB, Jonnagaddala J, Joo T, Jungari SB, Jürisson M, Kabir A, Kamangar F, Karch A, Karimi N, Karimian A, Kasaeian A, Kasahun GG, Kassa B, Kassa TD, Kassaw MW, Kaul A, Keiyoro PN, Kelbore AG, Kerbo AA, Khader YS, Khalilarjmandi M, Khan EA, Khan G, Khang YH, Khatab K, Khater A, Khayamzadeh M, Khazaee-Pool M, Khazaei S, Khoja AT, Khosravi MH, Khubchandani J, Kianipour N, Kim D, Kim YJ, Kisa A, Kisa S, Kissimova-Skarbek K, Komaki H, Koyanagi A, Krohn KJ, Bicer BK, Kugbey N, Kumar V, Kuupiel D, La Vecchia C, Lad DP, Lake EA, Lakew AM, Lal DK, Lami FH, Lan Q, Lasrado S, Lauriola P, Lazarus JV, Leigh J, Leshargie CT, Liao Y, Limenih MA, Listl S, Lopez AD, Lopukhov PD, Lunevicius R, Madadin M, Magdeldin S, El Razek HMA, Majeed A, Maleki A, Malekzadeh R, Manafi A, Manafi N, Manamo WA, Mansourian M, Mansournia MA, Mantovani LG, Maroufizadeh S, Martini SMS, Mashamba-Thompson TP, Massenburg BB, Maswabi MT, Mathur MR, McAlinden C, McKee M, Meheretu HAA, Mehrotra R, Mehta V, Meier T, Melaku YA, Meles GG, Meles HG, Melese A, Melku M, Memiah PTN, Mendoza W, Menezes RG, Merat S, Meretoja TJ, Mestrovic T, Miazgowski B, Miazgowski T, Mihretie KMM, Miller TR, Mills EJ, Mir SM, Mirzaei H, Mirzaei HR, Mishra R, Moazen B, Mohammad DK, Mohammad KA, Mohammad Y, Darwesh AM, Mohammadbeigi A, Mohammadi H, Mohammadi M, Mohammadian M, Mohammadian-Hafshejani A, Mohammadoo-Khorasani M, Mohammadpourhodki R, Mohammed AS, Mohammed JA, Mohammed S, Mohebi F, Mokdad AH, Monasta L, Moodley Y, Moosazadeh M, Moossavi M, Moradi G, Moradi-Joo M, Moradi-Lakeh M, Moradpour F, Morawska L, Morgado-da-Costa J, Morisaki N, Morrison SD, Mosapour A, Mousavi SM, Muche AA, Muhammed OSS, Musa J, Nabhan AF, Naderi M, Nagarajan AJ, Nagel G, Nahvijou A, Naik G, Najafi F, Naldi L, Nam HS, Nasiri N, Nazari J, Negoi I, Neupane S, Newcomb PA, Nggada HA, Ngunjiri JW, Nguyen CT, Nikniaz L, Ningrum DNA, Nirayo YL, Nixon MR, Nnaji CA, Nojomi M, Nosratnejad S, Shiadeh MN, Obsa MS, Ofori-Asenso R, Ogbo FA, Oh IH, Olagunju AT, Olagunju TO, Oluwasanu MM, Omonisi AE, Onwujekwe OE, Oommen

AM, Oren E, Ortega-Altamirano DDV, Ota E, Otstavnov SS, Owolabi MO, P A M, Padubidri JR, Pakhale S, Pakpour AH, Pana A, Park EK, Parsian H, Pashaei T, Patel S, Patil ST, Pennini A, Pereira DM, Piccinelli C, Pillay JD, Pirestani M, Pishgar F, Postma MJ, Pourjafar H, Pourmalek F, Pourshams A, Prakash S, Prasad N, Qorbani M, Rabiee M, Rabiee N, Radfar A, Rafiei A, Rahim F, Rahimi M, Rahman MA, Rajati F, Rana SM, Raoofi S, Rath GK, Rawaf DL, Rawaf S, Reiner RC, Renzaho AMN, Rezaei N, Rezapour A, Ribeiro AI, Ribeiro D, Ronfani L, Roro EM, Roshandel G, Rostami A, Saad RS, Sabbagh P, Sabour S, Saddik B, Safiri S, Sahebkar A, Salahshoor MR, Salehi F, Salem H, Salem MR, Salimzadeh H, Salomon JA, Samy AM, Sanabria J, Santric Milicevic MM, Sartorius B, Sarveazad A, Sathian B, Satpathy M, Savic M, Sawhney M, Sayyah M, Schneider IJC, Schöttker B, Sekerija M, Sepanlou SG, Sepehrimanesh M, Seyedmousavi S, Shaahmadi F, Shabaninejad H, Shahbaz M, Shaikh MA, Shamshirian A, Shamsizadeh M, Sharafi H, Sharafi Z, Sharif M, Sharifi A, Sharifi H, Sharma R, Sheikh A, Shirkoohi R, Shukla SR, Si S, Siabani S, Silva DAS, Silveira DGA, Singh A, Singh JA, Sisay S, Sitas F, Sobngwi E, Soofi M, Soriano JB, Stathopoulou V, Sufiyan MB, Tabarés-Seisdedos R, Tabuchi T, Takahashi K, Tamtaji OR, Tarawneh MR, Tassew SG, Taymoori P, Tehrani-Banihashemi A, Temsah MH, Temsah O, Tesfay BE, Tesfay FH, Teshale MY, Tessema GA, Thapa S, Tlaye KG, Topor-Madry R, Tovani-Palone MR, Traini E, Tran BX, Tran KB, Tsadik AG, Ullah I, Uthman OA, Vacante M, Vaezi M, Varona Pérez P, Veisani Y, Vidale S, Violante FS, Vlassov V, Vollset SE, Vos T, Vosoughi K, Vu GT, Vujcic IS, Wabinga H, Wachamo TM, Wagnew FS, Waheed Y, Weldegebreal F, Weldesamuel GT, Wijeratne T, Wondafrash DZ, Wonde TE, Wondmieneh AB, Workie HM, Yadav R, Yadegar A, Yadollahpour A, Yaseri M, Yazdi-Feyzabadi V, Yeshaneh A, Yimam MA, Yimer EM, Yisma E, Yonemoto N, Younis MZ, Yousefi B, Yousefifard M, Yu C, Zabeh E, Zadnik V, Moghadam TZ, Zaidi Z, Zamani M, Zandian H, Zangeneh A, Zaki L, Zendehdel K, Zenebe ZM, Zewale TA, Ziapour A, Zodpey S, Murray CJL. Global, Regional, and National Cancer Incidence, Mortality, Years of Life Lost, Years Lived With Disability, and Disability-Adjusted Life-Years for 29 Cancer Groups, 1990 to 2017: A Systematic Analysis for the Global Burden of Disease Study. *JAMA Oncol* 2019; **5**: 1749-1768 [PMID: 31560378 DOI: 10.1001/jamaoncol.2019.2996]

2 **Lauren P**. The two histological main types of gastric carcinoma: diffuse and so-called intestinal-type carcinoma. An attempt at a histo-clinical classification. *Acta Pathol Microbiol Scand* 1965; **64**: 31-49 [PMID: 14320675 DOI: 10.1111/apm.1965.64.1.31]

3 **Song XH**, Zhang WH, Kai-Liu, Chen XL, Zhao LY, Chen XZ, Kun-Yang, Zhou ZG, Hu JK. Prognostic impact of Borrmann classification on advanced gastric cancer: a retrospective cohort from a single institution in western China. *World J Surg Oncol* 2020; **18**: 204 [PMID: 32792016 DOI: 10.1186/s12957-020-01987-5]

4 **Ming SC**. Gastric carcinoma. A pathobiological classification. *Cancer* 1977; **39**: 2475-2485 [PMID: 872047 DOI: 10.1002/1097-0142(197706)39:6<2475::aid-cncr2820390626>3.0.co;2-l]

5 **Japanese Gastric Cancer Association**. Japanese classification of gastric carcinoma: 3rd English edition. *Gastric Cancer* 2011; **14**: 101-112 [PMID: 21573743 DOI: 10.1007/s10120-011-0041-5]

6 **Saito H**, Miyatani K, Takaya S, Kuroda H, Matsunaga T, Fukumoto Y, Osaki T, Ikeguchi M. Tumor infiltration pattern into the surrounding tissue has prognostic significance in advanced gastric cancer. *Virchows Arch* 2015; **467**: 519-523 [PMID: 26277483 DOI: 10.1007/s00428-015-1811-y]

7 **Maehara Y**, Oshiro T, Adachi Y, Ohno S, Akazawa K, Sugimachi K. Growth pattern and prognosis of gastric cancer invading the subserosa. *J Surg Oncol* 1994; **55**: 203-208 [PMID: 8159002 DOI: 10.1002/jso.2930550402]

8 **Kanda M**, Mizuno A, Fujii T, Shimoyama Y, Yamada S, Tanaka C, Kobayashi D, Koike M, Iwata N, Niwa Y, Hayashi M, Takami H, Nakayama G, Sugimoto H, Fujiwara M, Kodera Y. Tumor Infiltrative Pattern Predicts Sites of Recurrence After Curative Gastrectomy for Stages 2 and 3 Gastric Cancer. *Ann Surg Oncol* 2016; **23**: 1934-1940 [PMID: 26847679 DOI: 10.1245/s10434-016-5102-x]

9 **Nakagawa N**, Kanda M, Ito S, Mochizuki Y, Teramoto H, Ishigure K, Murai T, Asada T, Ishiyama A, Matsushita H, Tanaka C, Kobayashi D, Fujiwara M, Murotani K, Kodera Y. Pathological tumor infiltrative pattern and sites of initial recurrence in stage II/III gastric cancer: Propensity score matching analysis of a multi-institutional dataset. *Cancer Med* 2018; **7**: 6020-6029 [PMID: 30411544 DOI: 10.1002/cam4.1868]

10 **Topalian SL**, Taube JM, Anders RA, Pardoll DM. Mechanism-driven biomarkers to guide immune checkpoint blockade in cancer therapy. *Nat Rev Cancer* 2016; **16**: 275-287 [PMID: 27079802 DOI: 10.1038/nrc.2016.36]

11 **Galon J**, Costes A, Sanchez-Cabo F, Kirilovsky A, Mlecnik B, Lagorce-Pagès C, Tosolini M, Camus M, Berger A, Wind P, Zinzindohoué F, Bruneval P, Cugnenc PH, Trajanoski Z, Fridman WH, Pagès F. Type, density, and location of immune cells within human colorectal tumors predict clinical outcome. *Science* 2006; **313**: 1960-1964 [PMID: 17008531 DOI: 10.1126/science.1129139]

12 **Pagès F**, Mlecnik B, Marliot F, Bindea G, Ou FS, Bifulco C, Lugli A, Zlobec I, Rau TT, Berger MD, Nagtegaal ID, Vink-Börger E, Hartmann A, Geppert C, Kolwelter J, Merkel S, Grützmann R, Van den Eynde M, Jouret-Mourin A, Kartheuser A, Léonard D, Remue C, Wang JY, Bavi P, Roehrl MHA, Ohashi PS, Nguyen LT, Han S, MacGregor HL, Hafezi-Bakhtiari S, Wouters BG, Masucci GV, Andersson EK, Zavadova E, Vocka M, Spacek J, Petruzelka L, Konopasek B, Dundr P, Skalova H, Nemejcova K, Botti G, Tatangelo F, Delrio P, Ciliberto G, Maio M, Laghi L, Grizzi F, Fredriksen T, Buttard B, Angelova M, Vasaturo A, Maby P, Church SE, Angell HK, Lafontaine L, Bruni D, El Sissy C, Haicheur N, Kirilovsky A, Berger A, Lagorce C, Meyers JP, Paustian C, Feng Z, Ballesteros-Merino C, Dijkstra J, van de Water C, van Lent-van Vliet S, Knijn N, Mușină AM, Scripcariu DV, Popivanova B, Xu M, Fujita T, Hazama S, Suzuki N, Nagano H, Okuno K, Torigoe T, Sato N, Furuhata T, Takemasa I, Itoh K, Patel PS, Vora HH, Shah B, Patel JB, Rajvik KN, Pandya SJ, Shukla SN, Wang Y, Zhang G, Kawakami Y, Marincola FM, Ascierto PA, Sargent DJ, Fox BA, Galon J. International validation of the consensus Immunoscore for the classification of colon cancer: a prognostic and accuracy study. *Lancet* 2018; **391**: 2128-2139 [PMID: 29754777 DOI: 10.1016/S0140-6736(18)30789-X]

13 **Fang T**, Wang Y, Yin X, Zhai Z, Zhang Y, Yang Y, You Q, Li Z, Ma Y, Li C, Song H, Shi H, Yu X, Gao H, Sun Y, Xie R, Xue Y. Diagnostic Sensitivity of NLR and PLR in Early Diagnosis of Gastric Cancer. *J Immunol Res* 2020; **2020**: 9146042 [PMID: 32211444 DOI: 10.1155/2020/9146042]

14 **Yin X**, Fang T, Wang Y, Zhang D, Li C, Xue Y. Prognostic significance of serum inflammation indexes in different Lauren classification of gastric cancer. *Cancer Med* 2021; **10**: 1103-1119 [PMID: 33410261 DOI: 10.1002/cam4.3706]

15 **van Dam PJ**, Daelemans S, Ross E, Waumans Y, Van Laere S, Latacz E, Van Steen R, De Pooter C, Kockx M, Dirix L,

Vermeulen PB. Histopathological growth patterns as a candidate biomarker for immunomodulatory therapy. *Semin Cancer Biol* 2018; **52**: 86-93 [PMID: 29355613 DOI: 10.1016/j.semcancer.2018.01.009]

16 **Japanese Gastric Cancer Association**. Japanese gastric cancer treatment guidelines 2018 (5th edition). *Gastric Cancer* 2021; **24**: 1-21 [PMID: 32060757 DOI: 10.1007/s10120-020-01042-y]

17 **Ajani JA**, D'Amico TA, Almhanna K, Bentrem DJ, Chao J, Das P, Denlinger CS, Fanta P, Farjah F, Fuchs CS, Gerdes H, Gibson M, Glasgow RE, Hayman JA, Hochwald S, Hofstetter WL, Ilson DH, Jaroszewski D, Johung KL, Keswani RN, Kleinberg LR, Korn WM, Leong S, Linn C, Lockhart AC, Ly QP, Mulcahy MF, Orringer MB, Perry KA, Poultsides GA, Scott WJ, Strong VE, Washington MK, Weksler B, Willett CG, Wright CD, Zelman D, McMillian N, Sundar H. Gastric Cancer, Version 3.2016, NCCN Clinical Practice Guidelines in Oncology. *J Natl Compr Canc Netw* 2016; **14**: 1286-1312 [PMID: 27697982 DOI: 10.6004/jnccn.2016.0137]

18 **Jiang Y**, Xie J, Huang W, Chen H, Xi S, Han Z, Huang L, Lin T, Zhao LY, Hu YF, Yu J, Cai SR, Li T, Li G. Tumor Immune Microenvironment and Chemosensitivity Signature for Predicting Response to Chemotherapy in Gastric Cancer. *Cancer Immunol Res* 2019; **7**: 2065-2073 [PMID: 31615816 DOI: 10.1158/2326-6066.CIR-19-0311]

19 **Zhang X**, Hu D, Lin X, Zhang H, Xia Y, Lin J, Zheng X, Peng F, Jie J, Niu W. Prognostic Value of an Inflammation-Related Index in 6,865 Chinese Patients With Postoperative Digestive Tract Cancers: The FIESTA Study. *Front Oncol* 2019; **9**: 427 [PMID: 31192131 DOI: 10.3389/fonc.2019.00427]

20 **Li Z**, Li S, Ying X, Zhang L, Shan F, Jia Y, Ji J. The clinical value and usage of inflammatory and nutritional markers in survival prediction for gastric cancer patients with neoadjuvant chemotherapy and D2 Lymphadenectomy. *Gastric Cancer* 2020; **23**: 540-549 [PMID: 32072387 DOI: 10.1007/s10120-019-01027-6]

21 **Bilen MA**, Martini DJ, Liu Y, Lewis C, Collins HH, Shabto JM, Akce M, Kissick HT, Carthon BC, Shaib WL, Alese OB, Pillai RN, Steuer CE, Wu CS, Lawson DH, Kudchadkar RR, El-Rayes BF, Master VA, Ramalingam SS, Owonikoko TK, Harvey RD. The prognostic and predictive impact of inflammatory biomarkers in patients who have advanced-stage cancer treated with immunotherapy. *Cancer* 2019; **125**: 127-134 [PMID: 30329148 DOI: 10.1002/cncr.31778]

22 **Mohme M**, Riethdorf S, Pantel K. Circulating and disseminated tumour cells - mechanisms of immune surveillance and escape. *Nat Rev Clin Oncol* 2017; **14**: 155-167 [PMID: 27644321 DOI: 10.1038/nrclinonc.2016.144]

23 **Szczerba BM**, Castro-Giner F, Vetter M, Krol I, Gkountela S, Landin J, Scheidmann MC, Donato C, Scherrer R, Singer J, Beisel C, Kurzeder C, Heinzelmann-Schwarz V, Rochlitz C, Weber WP, Beerenwinkel N, Aceto N. Neutrophils escort circulating tumour cells to enable cell cycle progression. *Nature* 2019; **566**: 553-557 [PMID: 30728496 DOI: 10.1038/s41586-019-0915-y]

24 **Ferrone C**, Dranoff G. Dual roles for immunity in gastrointestinal cancers. *J Clin Oncol* 2010; **28**: 4045-4051 [PMID: 20644090 DOI: 10.1200/JCO.2010.27.9992]

25 **Kanikarla-Marie P**, Lam M, Menter DG, Kopetz S. Platelets, circulating tumor cells, and the circulome. *Cancer Metastasis Rev* 2017; **36**: 235-248 [PMID: 28667367 DOI: 10.1007/s10555-017-9681-1]

26 **Derks S**, de Klerk LK, Xu X, Fleitas T, Liu KX, Liu Y, Dietlein F, Margolis C, Chiaravalli AM, Da Silva AC, Ogino S, Akarca FG, Freeman GJ, Rodig SJ, Hornick JL, van Allen E, Li B, Liu SX, Thorsson V, Bass AJ. Characterizing diversity in the tumor-immune microenvironment of distinct subclasses of gastroesophageal adenocarcinomas. *Ann Oncol* 2020; **31**: 1011-1020 [PMID: 32387455 DOI: 10.1016/j.annonc.2020.04.011]

27 **Ohe Y**, Fushida S, Yamaguchi T, Kinoshita J, Saito H, Okamoto K, Nakamura K, Tajima H, Ninomiya I, Ohta T. Peripheral Blood Platelet-Lymphocyte Ratio Is Good Predictor of Chemosensitivity and Prognosis in Gastric Cancer Patients. *Cancer Manag Res* 2020; **12**: 1303-1311 [PMID: 32110104 DOI: 10.2147/CMAR.S241069]

28 **Dieckmann KP**, Struss WJ, Budde U. Evidence for acute vascular toxicity of cisplatin-based chemotherapy in patients with germ cell tumour. *Anticancer Res* 2011; **31**: 4501-4505 [PMID: 22199322]

29 **Labelle M**, Begum S, Hynes RO. Direct signaling between platelets and cancer cells induces an epithelial-mesenchymal-like transition and promotes metastasis. *Cancer Cell* 2011; **20**: 576-590 [PMID: 22094253 DOI: 10.1016/j.ccr.2011.09.009]

30 **Xu J**, Lamouille S, Derynck R. TGF-beta-induced epithelial to mesenchymal transition. *Cell Res* 2009; **19**: 156-172 [PMID: 19153598 DOI: 10.1038/cr.2009.5]

31 **Kroemer G**, Galluzzi L, Kepp O, Zitvogel L. Immunogenic cell death in cancer therapy. *Annu Rev Immunol* 2013; **31**: 51-72 [PMID: 23157435 DOI: 10.1146/annurev-immunol-032712-100008]

32 **Wang Y**, Chen Y, Yin H, Gu X, Shi Y, Dai G. Timing of chemotherapy-induced neutropenia is a prognostic factor in patients with advanced gastric cancer undergoing first-line chemotherapy with oxaliplatin and capecitabine: a retrospective study. *Cancer Med* 2018; **7**: 997-1005 [PMID: 29532995 DOI: 10.1002/cam4.1308]

33 **Proctor MJ**, Morrison DS, Talwar D, Balmer SM, O'Reilly DS, Foulis AK, Horgan PG, McMillan DC. An inflammation-based prognostic score (mGPS) predicts cancer survival independent of tumour site: a Glasgow Inflammation Outcome Study. *Br J Cancer* 2011; **104**: 726-734 [PMID: 21266974 DOI: 10.1038/sj.bjc.6606087]

34 **Wang TT**, Zhao YL, Peng LS, Chen N, Chen W, Lv YP, Mao FY, Zhang JY, Cheng P, Teng YS, Fu XL, Yu PW, Guo G, Luo P, Zhuang Y, Zou QM. Tumour-activated neutrophils in gastric cancer foster immune suppression and disease progression through GM-CSF-PD-L1 pathway. *Gut* 2017; **66**: 1900-1911 [PMID: 28274999 DOI: 10.1136/gutjnl-2016-313075]

35 **Zhang D**, Zhou J, Tang D, Zhou L, Chou L, Chou KY, Tao L, Lu LM. Neutrophil infiltration mediated by CXCL5 accumulation in the laryngeal squamous cell carcinoma microenvironment: A mechanism by which tumour cells escape immune surveillance. *Clin Immunol* 2017; **175**: 34-40 [PMID: 27876461 DOI: 10.1016/j.clim.2016.11.009]

36 **Nagtegaal ID**, Marijnen CA, Kranenbarg EK, Mulder-Stapel A, Hermans J, van de Velde CJ, van Krieken JH. Local and distant recurrences in rectal cancer patients are predicted by the nonspecific immune response; specific immune response has only a systemic effect--a histopathological and immunohistochemical study. *BMC Cancer* 2001; **1**: 7 [PMID: 11481031 DOI: 10.1186/1471-2407-1-7]

37 **Kirkwood JM**, Butterfield LH, Tarhini AA, Zarour H, Kalinski P, Ferrone S. Immunotherapy of cancer in 2012. *CA Cancer J Clin* 2012; **62**: 309-335 [PMID: 22576456 DOI: 10.3322/caac.20132]

38 **Cheung KS**, Leung WK, Seto WK. Application of Big Data analysis in gastrointestinal research. *World J Gastroenterol*

2019; **25**: 2990-3008 [PMID: 31293336 DOI: 10.3748/wjg.v25.i24.2990]

39 **Park HS**, Kwon WS, Park S, Jo E, Lim SJ, Lee CK, Lee JB, Jung M, Kim HS, Beom SH, Park JY, Kim TS, Chung HC, Rha SY. Comprehensive immune profiling and immune-monitoring using body fluid of patients with metastatic gastric cancer. *J Immunother Cancer* 2019; **7**: 268 [PMID: 31639056 DOI: 10.1186/s40425-019-0708-8]

World Journal of Gastrointestinal Oncology

Submit a Manuscript: https://www.f6publishing.com

World J Gastrointest Oncol 2022 April 15; 14(4): 920-934

DOI: 10.4251/wjgo.v14.i4.920

ISSN 1948-5204 (online)

ORIGINAL ARTICLE

Retrospective Study

Regorafenib combined with programmed cell death-1 inhibitor against refractory colorectal cancer and the platelet-to-lymphocyte ratio's prediction on effectiveness

Yu-Jie Xu, Peng Zhang, Jin-Long Hu, Hong Liang, Yan-Yan Zhu, Yao Cui, Po Niu, Min Xu, Ming-Yue Liu

Specialty type: Oncology

Provenance and peer review: Unsolicited article; Externally peer reviewed.

Peer-review model: Single blind

Peer-review report's scientific quality classification

Grade A (Excellent): 0
Grade B (Very good): B
Grade C (Good): C
Grade D (Fair): 0
Grade E (Poor): 0

P-Reviewer: Cho YS, South Korea; Shomura M, Japan

Received: October 9, 2021
Peer-review started: October 9, 2021
First decision: December 12, 2021
Revised: January 4, 2022
Accepted: March 25, 2022
Article in press: March 25, 2022
Published online: April 15, 2022

Yu-Jie Xu, Jin-Long Hu, Yan-Yan Zhu, Yao Cui, Po Niu, Ming-Yue Liu, Department of Oncology, Henan Provincial People's Hospital, People's Hospital of Zhengzhou University, Zhengzhou 450003, Henan Province, China

Peng Zhang, Hong Liang, Department of Gastrointestinal Surgery, Henan Provincial People's Hospital, People's Hospital of Zhengzhou University, Zhengzhou 450003, Henan Province, China

Min Xu, Department of Hepatology, The Third People's Hospital of Zhengzhou, Zhengzhou 450003, Henan Province, China

Corresponding author: Ming-Yue Liu, Doctor, MD, PhD, Chief Doctor, Department of Oncology, Henan Provincial People's Hospital, People's Hospital of Zhengzhou University, No. 7 Weiwu Road, Zhengzhou 450003, Henan Province, China. 1816160187@e.gzhu.edu.cn

Abstract

BACKGROUND

The effectiveness of regorafenib plus programmed cell death-1 (PD-1) inhibitor in treating microsatellite stable (MSS) metastatic colorectal cancer (mCRC) remains controversial.

AIM

To investigate the benefits of regorafenib combined with PD-1 inhibitor in treating MSS mCRC and explore indicators predicting response.

METHODS

This retrospective study included a total of 30 patients with microsatellite stable metastatic colorectal cancer treated with regorafenib combined with programmed cell death-1 inhibitor at Henan Provincial People's Hospital between December 2018 and December 2020. During a 4-wk treatment cycle, regorafenib was performed for 3 continuous weeks. PD-1 inhibitor was intravenously injected starting on the first day of the oral intake of regorafenib. We reviewed tumor response, progression-free survival (PFS), overall survival, and treatment-related adverse events (TRAEs) and evaluated association between platelet-to-lymphocyte ratio (PLR) and outcomes in this retrospective study.

RESULTS

Stable disease and progressive disease were found in 18 (60.0%) and 12 (40.0%) patients, respectively. The disease control rate was 60.0%. The median follow-up time was 12.0 mo, and median PFS was 3.4 mo [95% confidence interval (CI): 2.2-4.6 mo]. Of the 12 patients with progressive disease, 10 (83.3%) had liver metastasis before starting the combined treatment. Among the 18 patients with SD, 10 (55.6%) did not have liver metastases. One patient without liver metastases at baseline was found with a substantially prolonged PFS of 11.2 mo. The liver metastasis, the choice of programmed cell death-1 inhibitor other than nivolumab or pembrolizumab and previous exposure to regorafenib was't associated with treatment outcome. The median PFS in the low-PLR group was 4.2 mo (95%CI: 3.5-4.9 mo), compared with 2.8 mo (95%CI: 1.4-4.2 mo) in the high-PLR group (P = 0.005). The major TRAEs included hand-foot syndrome (33.3%), hypertension (23.3%), malaise (20.0%), and gastrointestinal reaction (16.7%). The incidence of grade 3 TRAEs was 13.3% (4/30), which comprised abnormal capillary proliferation (n = 1), transaminase elevation (n = 1), and hand-foot syndrome (n = 2). No grade 4 or higher toxicity was observed.

CONCLUSION

Regorafenib combined with PD-1 inhibitor could lead to a longer PFS in some patients with MSS mCRC. The PLR might be a prediction of the patient response to this therapy.

Key Words: Colorectal neoplasms; Microsatellite stable; Programmed cell death-1 inhibitor; Platelet-to-lymphocyte ratio; Regorafenib; Progression-free survival

Core Tip: The use of regorafenib combined with programmed cell death-1 inhibitor in the treatment of refractory microsatellite stable colorectal cancer has contradictory results in some small-scale studies. The purpose of this paper is to analyze the real-world data of our center in the past 2 years so as to provide more treatment experience and reference for treatment selection. The progression-free survival and overall survival of patients with refractory microsatellite stable colorectal cancer treated with regorafenib combined with programmed cell death-1 inhibitor were analyzed retrospectively, and the safety and adverse reactions under different doses were reviewed. The platelet-to-lymphocyte ratio was found as a potential screening index for patients with prolonged progression-free survival.

Citation: Xu YJ, Zhang P, Hu JL, Liang H, Zhu YY, Cui Y, Niu P, Xu M, Liu MY. Regorafenib combined with programmed cell death-1 inhibitor against refractory colorectal cancer and the platelet-to-lymphocyte ratio's prediction on effectiveness. *World J Gastrointest Oncol* 2022; 14(4): 920-934
URL: https://www.wjgnet.com/1948-5204/full/v14/i4/920.htm
DOI: https://dx.doi.org/10.4251/wjgo.v14.i4.920

INTRODUCTION

Colorectal cancer (CRC) is one of the most common malignant tumors worldwide. More than 1.8 million new patients with CRC were reported in 2018, of which 881000 died of CRC[1,2]. In China, CRC is the fifth leading cause of cancer-related death. The number of CRC-related deaths was about 191000 in 2015 [3]. A variety of patients are diagnosed with advanced CRC, accompanied by distant metastases in addition to the primary tumor[4]. Despite multidisciplinary management based on surgery, systemic therapy, and radiotherapy[5-7], the prognosis of patients with advanced CRC is still poor, with 5-year survival rates of 71% and 14% for regional and distant disease, respectively[8].

The Guidelines of the Chinese Society of Clinical Oncology (CSCO) recommend chemotherapy with or without targeted therapy (such as cetuximab and bevacizumab) for the first- and second-line therapies of advanced CRC[9]. Although the CSCO guidelines also recommended later-line therapy for CRC after progression, the treatment efficacy is generally limited[9]. Regorafenib is an oral, small-molecular multi-target kinase inhibitor that can exert anti-tumor effects through inhibiting several key processes, such as tumor cell proliferation, metastasis, angiogenesis, and immune escape[10,11]. The international CORRECT trial promoted regorafenib as the standard drug for treating metastatic CRC (mCRC)[12].

The emergence of immunotherapy in recent years has brought long-term survival benefits for many patients. Still, to date, only patients with microsatellite instablility-high mCRC could benefit from immunotherapy using a single drug[13]. Considering that the efficacy of single targeted drug was suboptimal, combination therapy could bring new hopes for patients. The preliminary findings from the REGONIVO study reported the efficacy of regorafenib combined with nivolumab. The objective response rate (ORR) was 33% in 24 Asian patients with proficient mismatch repair (MMR)/microsatellite stable (MSS) refractory mCRC, and the median progression-free survival (PFS) was prolonged by more than 6 mo. Therefore, the findings possibly provided new chances for patients with repeated failures after third- or further-line therapies to prolong the survival time and improve the quality of life[14]. The combination of regorafenib with programmed cell death-1 (PD-1) for patients with refractory CRC after multi-line standard therapies is now used by many medical centers worldwide. A retrospective study in 18 patients with refractory MSS mCRC, including five Asian patients, performed by the National Cancer Institute in the United States recently failed to show the effectiveness of regorafenib combined with nivolumab or pembrolizumab but suggested that patients without liver metastases could benefit from the treatment[15]. A study conducted in 23 Chinese patients with MSS advanced CRC also did not demonstrate the effectiveness of this combination[16]. These two studies[15,16] were inconsistent with the REGONIVO study[14]. Hence, additional clinical studies are needed to investigate the benefits and adverse events of regorafenib combined with PD-1 inhibitors.

The effects of specific treatments among different patients and different studies vary greatly. Thus, identifying factors that could predict the prognosis of patients treated with regorafenib combined with PD-1 inhibitors is clinically relevant. Carcinoembryonic antigen (CEA) is commonly used in clinical practice to monitor treatment efficacy in patients with CRC[17,18]. Other indicators are also related to the prognosis of patients with cancer[19-23], such as neutrophil-to-lymphocyte ratio (NLR) and platelet-to-lymphocyte ratio (PLR).

Despite the emergence of new drugs and the changes in the combination of targeted therapy, the effectiveness of mCRC treatment is still suboptimal, especially the treatments after third-line therapy, with a 5-year survival rate of only 11%[24]. Therefore, this retrospective study investigated patients with MSS mCRC treated with regorafenib combined with a PD-1 inhibitor in the last 2 years. This study may suggest a novel therapeutic approach that could be tried in a clinical trial.

MATERIALS AND METHODS

Study design and patients

This retrospective study included patients with MSS mCRC treated with regorafenib combined with PD-1 inhibitor at Henan Provincial People's Hospital between December 2018 and December 2020. This study was approved by the ethics committee of People's Hospital of Zhengzhou University (Henan Province, China) and performed in accordance with the Declaration of Helsinki. The requirement for informed consent was waived by the committee because of the retrospective nature of the study.

The inclusion criteria were: (1) Histologically or cytologically proven with MSS mCRC; (2) Treated with more than two lines of standard chemotherapy regimens (including fluorouracil, oxaliplatin, and irinotecan, with or without biological agents such as bevacizumab and cetuximab); (3) Treated with regorafenib combined with PD-1 inhibitor (due to the accessibility of drugs and financial burden of patients, other low-cost PD-1 inhibitors approved in China, such as camrelizumab, sintilimab, toripalimab, and tislelizumab, could also be used in addition to nivolumab and pembrolizumab); (4) With evaluable lesions and with detailed clinical data and follow-up results; and (5) Downregulation of the expression of four MMR enzymes (MutL homolog 1/MutS homolog 2/MutS homolog 6/PMS1 homolog 2) assessed by immunohistochemistry, or the MMR/MSI status was evaluated by the 2B3D method.

Treatment regimen

During a 4 wk treatment cycle, oral drug administration was performed for 3 continuous weeks. Regorafenib was orally administered at 80, 120, or 160 mg once per day. Dose reduction or temporary discontinuation of regorafenib was performed for the patients with treatment-related toxicities. PD-1 inhibitor was intravenously injected starting on the 1st day of the oral intake of regorafenib, including 240 mg every 3 wk for toripalimab, 200 mg every 2 or 3 wk for camrelizumab, 240 mg every 2 wk for nivolumab, 200 mg every 3 wk for pembrolizumab and sintilimab, or 200 mg every 3 wk for tislelizumab.

Data collection

Collected data included age, sex, Eastern Cooperative Oncology Group (ECOG) performance status (PS), site of the primary tumor, site of the metastases, MSI/MMR, gene status, lines of treatment, and previous treatments. The blood routine examination and CEA results before treatment and after three and five cycles of combination therapy were longitudinally analyzed. CEA was detected by microarray chemiluminescence immunoassay (Sunlant Biological SLXP-001, Wuxi, Jiangsu Province, China). The

platelet and lymphocyte counts were measured using a Hessian-Meikang XN-9000 automatic modular blood and body fluid analyzer. The PLR was calculated as the absolute platelet count divided by the absolute lymphocyte count in full blood.

According to the Response Evaluation Criteria in Solid Tumors (RECIST) version 1.1, tumor responses were evaluated every two or three cycles of immunotherapy. If signs of rapid disease progression were noted, the evaluation was performed at earlier time points. ORR included complete response (CR) and partial response (PR). Disease control rate (DCR) was defined as the sum of the ORR and stable disease (SD) rate. PFS was defined as the time from the start of treatment to disease progression or death. Overall survival (OS) referred to the time from the start of treatment to death. Toxicity was evaluated according to the Common Toxicity Criteria for Adverse Events Version 5.0 (CTCAE 5.0) and the 2019 CSCO immune checkpoint inhibitor-related toxicity management guideline [25]. Follow-up was censored on April 15, 2021.

Statistical analysis

SPSS 26.0 (IBM, Armonk, NY, United States) was used for statistical analysis. Continuous data with a normal distribution (according to the Shapiro-Wilk test) were described using means ± SD, while continuous data without a normal distribution were described as medians and interquartile range (Q1, Q3). The t-test was used for comparing continuous data with a normal distribution, and the rank-sum test was used for comparing continuous data without a normal distribution. Categorical data were presented as n (%) and tested using the χ^2 test. The receiver operating characteristic (ROC) curve was used to estimate the best cutoff value of NLR and PLR before treatment. The patients were divided into the low-NLR, high-NLR, low-PLR, and high-PLR groups according to the cut-off value of ROC curve. The Kaplan-Meier method was used for univariable survival analysis. The log-rank test was used to analyze the differences in PFS and OS among different influencing factors. Two-sided P values < 0.05 were considered statistically significant.

RESULTS

Characteristics of the patients

Between December 2018 and December 2020, a total of 30 patients with MSS mCRC were included. Table 1 and Supplementary Table 1 present the characteristics of the patients. The patients were treated with regorafenib combined with PD-1 inhibitor as the third- (46.7%) or further-line therapy (53.3%). Of these patients, 12 (40.0%) were ≥ 60 years and 18 (60.0%) < 60 years. Fourteen (46.7%) and sixteen (53.3%) were males and females, respectively. Twenty-one (70.0%) and 9 (30.0%) patients had an ECOG PS of 0-1 and ≥ 2, respectively. The primary lesion was on the left side (including the left colon, sigmoid colon, and rectum) in 24 patients (80.0%) and on the right side (including the ascending colon and liver curvature of the transverse colon) in 6 patients (20.0%). Eighteen (60.0%) patients had liver metastases, 11 (36.7%) had lung metastases, 6 (20.0%) had peritoneal metastases, and 18 patients (60.0%) had multiple metastases in ≥ two sites (Table 1). All patients were proven with MSS (proficient MMR) type CRC using immunohistochemistry or polymerase chain reaction, and 1 (3.3%) patient had been treated with PD-1 inhibitor before. The genetic test showed that 7 (36.7%) and 12 (60.0%) patients had RAS mutation and wild-type RAS, respectively, while 11 patients did not have a genetic mutation test. No patient had BRAF mutation.

Characteristics of the treatments

Nineteen (63.3%) patients were treated with regorafenib for a median treatment duration of 4.3 mo [95% confidence interval (CI): 2.0-6.7 mo] before the combination therapy in this study. During the combination therapy, the initial dose of regorafenib was 80, 120, and 160 mg in 18, 8, and 4 patients, respectively. Of the 30 patients receiving combination therapy, 9 were treated with sintilimab, 8 with toripalimab, 5 with camrelizumab, 4 with tislelizumab, 3 with nivolumab, and 1 with pembrolizumab (Table 1 and Supplementary Table 1).

Clinical response

According to RECIST 1.1, 18 (60.0%) of the 30 patients who received combination therapy achieved SD, and 12 (40.0%) had progressive disease (PD); no PR or CR was found. The DCR was 60.0% (Table 2 and Supplementary Table 1). Of the 12 patients with PD, 10 (83.3%) had liver metastases at baseline. Among the 18 patients with SD, 10 (55.6%) had no liver metastases.

Survival

Up to April 15, 2021, the median follow-up time was 12.0 mo. The median PFS of the patients was 3.4 mo (95%CI: 2.2-4.6 mo) (Figure 1A and B). One patient without liver metastases at baseline was found with a substantially prolonged PFS of 11.2 mo. Still, of the patients with liver metastases at baseline, no prolonged PFS was observed in 2 patients even after the combination therapy using local hepatectomy

Table 1 Characteristics of the individual patients

No.	Age (yr)	Sex	ECOG PS	Primary tumor	Site of metastases	Liver metastases	RAS and BRAF mutation	Lines of treatment	Prior 5-Fu	Prior platinum	Prior irinotecan	Prior bevacizumab	Prior cetuximab	Prior regorafenib	Prior PD-1
1	56	Female	1	Sigmoid colon	Abdominal metastases	No	Wild-type	3	Yes	Yes	Yes	Yes	Yes	No	No
2	62	Female	3	Ascending colon	Multiple metastases	Yes	Not tested	4	Yes	Yes	Yes	Yes	No	Yes	No
3	51	Female	0	Rectum	Multiple metastases	Yes	Not tested	3	Yes	Yes	Yes	Yes	No	No	No
4	52	Female	1	Sigmoid colon	Multiple metastases	No	KRAS mutation	3	Yes	Yes	Yes	Yes	No	No	No
5	66	Female	1	Ascending colon	Multiple metastases	Yes	Not tested	4	Yes	Yes	Yes	Yes	No	Yes	No
6	57	Female	2	Sigmoid colon	Multiple metastases	No	Wild-type	3	Yes	Yes	Yes	Yes	Yes	No	No
7	48	Female	3	Liver curvature of the transverse colon	Multiple metastases	Yes	Not tested	3	Yes	Yes	Yes	Yes	No	No	No
8	61	Female	2	Rectum	Pelvic metastases	No	KRAS mutation	3	Yes	Yes	Yes	Yes	No	No	No
9	65	Female	1	Rectum	Ovary metastases	No	Wild-type	4	Yes	Yes	Yes	Yes	Yes	Yes	No
10	65	Female	0	Ascending colon	Lung metastases	No	Not tested	3	Yes	Yes	Yes	Yes	No	No	No
11	56	Female	2	Left half of the colon	Ovary metastases	No	Wild-type	3	Yes	Yes	Yes	Yes	Yes	No	No
12	27	Male	0	Sigmoid colon	Pelvic metastases	No	Wild-type	4	Yes	Yes	Yes	Yes	Yes	Yes	Yes
13	58	Male	1	Sigmoid colon	Liver metastases	Yes	Not tested	3	Yes	Yes	Yes	Yes	No	No	No
14	70	Female	1	Rectum	Lung metastases	No	Not tested	4	Yes	Yes	Yes	Yes	No	No	No
15	54	Male	1	Ascending colon	Multiple metastases	Yes	KRAS mutation	3	Yes	Yes	Yes	Yes	No	No	No
16	55	Male	1	Rectum	Multiple metastases	Yes	NRAS mutation	4	Yes	Yes	Yes	Yes	No	Yes	No
17	48	Female	0	Rectum	Multiple metastases	Yes	Wild-type	3	Yes	Yes	Yes	Yes	Yes	No	No
18	55	Male	1	Rectum	Multiple	Yes	Wild-type	3	Yes	Yes	Yes	Yes	Yes	No	No

					metastases									
19	64	Male	2	Rectum	Multiple metastases	Yes	KRAS mutation	3	Yes	Yes	Yes	Yes	No	No	No
20	58	Female	0	Ascending colon	Multiple metastases	Yes	Wild-type	3	Yes	Yes	Yes	Yes	Yes	No	No
21	44	Female	2	Sigmoid colon	Multiple metastases	Yes	Wild-type	3	Yes	Yes	Yes	Yes	Yes	No	No
22	51	Male	1	Rectum	Multiple metastases	Yes	Not tested	4	Yes	Yes	Yes	Yes	No	Yes	No
23	56	Male	1	Rectum	Lung metastases	No	Not tested	4	Yes	Yes	Yes	Yes	No	No	No
24	61	Male	2	Rectum	Multiple metastases	Yes	Not tested	4	Yes	Yes	Yes	Yes	No	No	No
25	73	Male	0	Rectum	Multiple metastases	Yes (radiofrequency)	Wild-type	3	Yes	Yes	Yes	Yes	Yes	No	No
26	61	Male	1	Rectum	Multiple metastases	Yes	Wild-type	4	Yes	Yes	Yes	Yes	Yes	Yes	No
27	58	Male	2	Sigmoid colon	Multiple metastases	No	KRAS mutation	3	Yes	Yes	Yes	Yes	No	No	No
28	57	Female	1	Sigmoid colon	Liver metastases	Yes (hepatectomy)	KRAS mutation	3	Yes	Yes	Yes	Yes	No	No	No
29	67	Male	2	Rectum	Liver metastases	Yes	Not tested	3	Yes	Yes	Yes	Yes	No	No	No
30	61	Male	1	Sigmoid colon	Peritoneal metastasis	No	Wide-type	3	Yes	Yes	Yes	Yes	Yes	No	No

ECOG PS: Eastern Cooperative Oncology Group performance status.

and radiofrequency ablation. The median PFS was 2.8 mo (95%CI: 0.8-4.7 mo) for the 18 patients with liver metastases and 3.5 mo (95%CI: 3.0-4.0 mo) for the 12 patients without liver metastases, with no significant difference (P = 0.17) (Figure 1C). The median PFS of the 19 patients treated with previous regorafenib treatment was 2.8 mo (95%CI: 1.0-4.6 mo), while the median PFS of the 11 patients naïve to regorafenib was 3.4 mo (95%CI: 2.8-4.0 mo); the difference was not statistically significant (P = 0.55) (Figure 1D). The median PFS was not significantly different between the patients with or without RAS mutation (P = 0.37). The 4 patients with imported PD-1 inhibitor (nivolumab or pembrolizumab) and 26 patients with domestic PD-1 inhibitor (sintilimab, toripalimab, camrelizumab, or tislelizumab) did not differ in median PFS (P = 0.31). At the time of April 15, 2021, the data for OS were still not mature. Detailed PFS and OS data can be found in Table 2.

Table 2 Treatments and outcomes

No.	Initial dose of regorafenib (mg)	Dose adjustment (mg)	PD-1 inhibitor used in combination	Number of treatment cycles	Best response	PFS (mo)	OS (mo)
1	120		Camrelizumab	16	SD	11.2	12.0
2	80		Tislelizumab	7	SD	5.0	7.0
3	160	160→80	Nivolumab	4	PD	3.4	Not reached
4	80		Camrelizumab	4	PD	3.4	4.0
5	80		Tislelizumab	3	SD	2.0	5.0
6	80		Toripalimab	5	SD	3.5	Not reached
7	80		Tislelizumab	7	SD	5.0	9.0
8	80		Pembrolizumab	5	PD	3.5	Not reached
9	120		Sintilimab	4	SD	2.8	Not reached
10	160	160→80	Toripalimab	8	SD	5.6	Not reached
11	80		Tislelizumab	2	SD	1.4	Not reached
12	160		Toripalimab	4	SD	2.8	Not reached
13	120		Nivolumab	6	SD	4.2	Not reached
14	80		Toripalimab	5	SD	3.5	Not reached
15	120		Sintilimab	6	SD	3.5	Not reached
16	80		Nivolumab	15	SD	10.5	Not reached
17	160	160→80	Sintilimab	4	PD	2.8	Not reached
18	80		Camrelizumab	5	PD	3.5	Not reached
19	80		Toripalimab	2	SD	1.4	Not reached
20	120		Camrelizumab	4	PD	3.4	7.0
21	80		Toripalimab	2	PD	1.4	Not reached
22	120		Camrelizumab	1	SD	0.7	12.0
23	80		Sintilimab	2	PD	1.4	10.0
24	80		Toripalimab	9	SD	6.3	11.0
25	120	120→80	Sintilimab	2	PD	1.4	Not reached
26	80		Sintilimab	3	SD	2.1	10.0
27	80		Toripalimab	6	SD	4.2	Not reached
28	120		Sintilimab	2	PD	1.4	Not reached
29	80		Sintilimab	1	PD	0.7	not reached
30	80		Sintilimab	2	PD	1.4	Not

reached

OS: Overall survival; PD: Progressive disease; PFS: Progression-free survival; SD: Stable disease; PD-1: Programmed cell death-1.

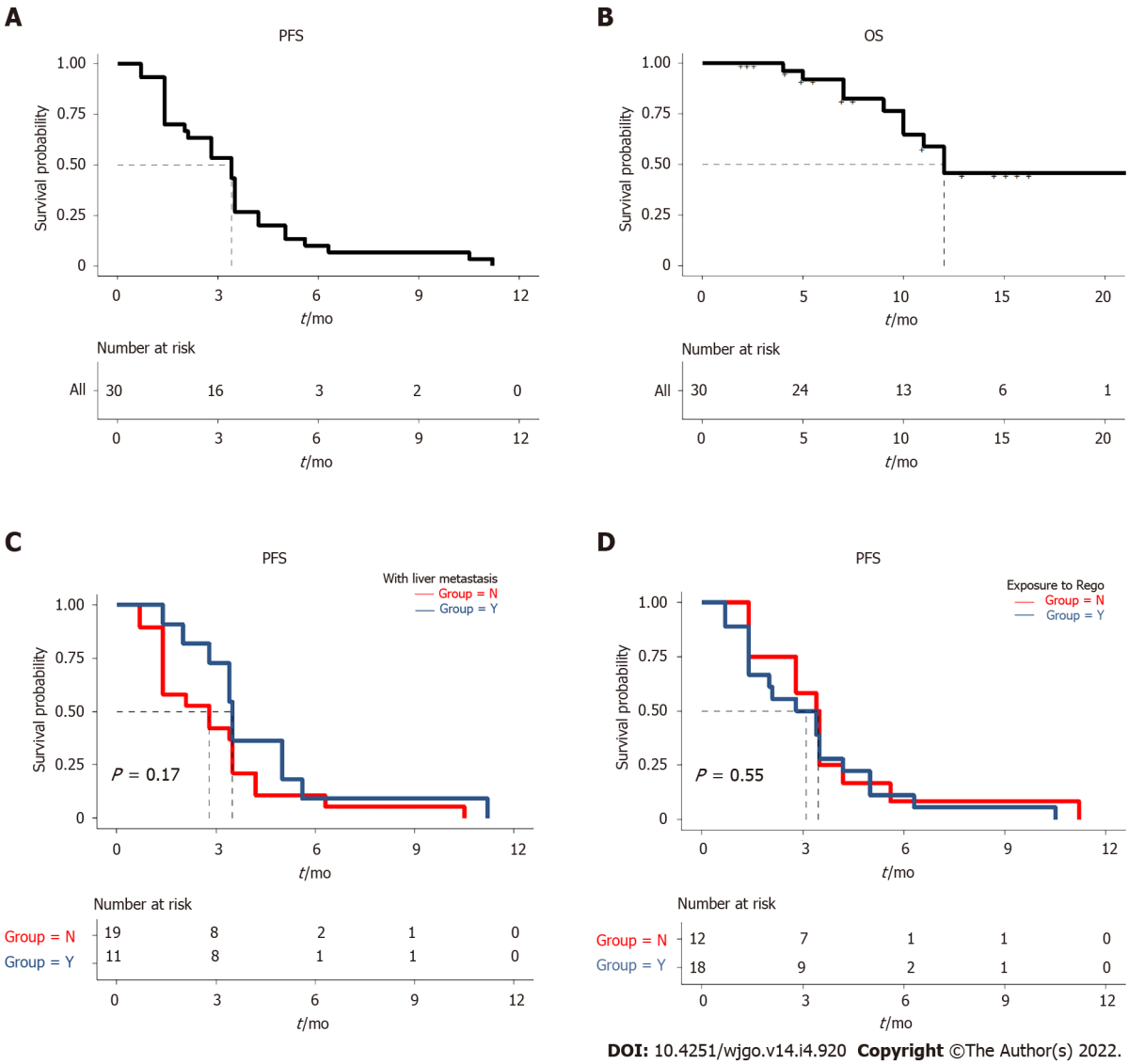

DOI: 10.4251/wjgo.v14.i4.920

Figure 1 Kaplan-Meier survival curves. A: Progression-free survival (PFS) of 30 patients; B: Overall survival of the whole cohort; C: PFS according to the patients with or without liver metastasis ($P > 0.05$); D: PFS according to previous exposure to regorafenib or not ($P > 0.05$). PFS: Progression-free survival; OS: Overall survival.

Safety profile

Of the 30 patients, treatment-related adverse events (TRAEs) occurred in 17 patients (56.7%). The major TRAEs included hand-foot syndrome (33.3%), hypertension (23.3%), malaise (20.0%), and gastrointestinal reaction (16.7%). The other TRAEs included transaminase elevation (13.3%), diarrhea (10.0%), abnormal capillary proliferation (6.7%), thrombocytopenia (6.7%), hypothyroidism (6.7%), proteinuria (6.7%), rash (6.7%), anemia (3.3%), myocardial enzyme elevation (3.3%), and oral mucositis (3.3%). The incidence of grade 3 TRAEs was 13.3% (4/30), which comprised abnormal capillary proliferation ($n = 1$), transaminase elevation ($n = 1$), and hand-foot syndrome ($n = 2$). No grade 4 or higher toxicity was observed. For patients treated with different initial doses of regorafenib, more grade 3 TRAEs were observed in the 160 mg group. Specifically, 3 of the 4 patients treated with an initial dose of regorafenib of 160 mg had grade 3 TRAEs, including grade 3 hand-foot syndrome in 2 patients and grade 3 abnormal capillary proliferation in 1 patient. For all 3 patients, the dose of regorafenib was reduced to 80 mg. In the 8 patients treated with an initial dose of regorafenib of 120 mg, 1 patient had grade 3 transaminase elevation. For this patient, regorafenib and PD-1 inhibitor were discontinued until the transaminase levels returned to normal. Subsequently, the regorafenib dose was reduced to 80 mg to

treat the patient combined with a PD-1 inhibitor. All 18 patients in the 80 mg group had good tolerance; they could tolerate the therapy after symptomatic treatment until PD. Table 3 lists the details of the TRAEs.

Relationship between PLR and treatment response

The NLR and PLR of the 30 patients were calculated, and the ROC curves were plotted. The area under the ROC curve (AUC) of NLR was 0.533, which could not effectively predict the treatment efficacy (Figure 2A). The AUC of PLR was 0.774, the maximum Youden index was 0.549, the corresponding cutoff value of PLR was 118, and the sensitivity and specificity were 85.7% and 69.2%, respectively (Figure 2B).

The median PLR was 151.1 (96.0-211.8). The PLR values differed significantly between the SD and PD groups (P = 0.047) (Figure 3A). Subsequently, the patients were divided into the PLR < 118 group (low-PLR group, n = 11) and PLR ≥ 118 group (high-PLR group, n = 19) according to the cutoff value. The median PFS in the low-PLR group was 4.2 mo (95%CI: 3.5-4.9 mo), compared with 2.8 mo (95%CI: 1.4-4.2 mo) in the high-PLR group (P = 0.005) (Figure 3B). The PLR may be an indicator to predict patient response and selected those who with longer PFS to regorafenib combined with PD-1 inhibitor. For the 12 patients with PD, the CEA increased after one and two cycles of treatment (Figure 4A). For the 18 patients in the SD group, the CEA in 1 patient increased transiently with a low amplitude after the first treatment cycle (higher than the normal range). In contrast, after the second treatment cycle, the CEA in all the patients was stable or decreased compared with before treatment (Figure 4B). The PLR in 3 patients decreased slightly after the first treatment cycle, while the PLR in 11 patients increased after two treatment cycles (Figure 4C). Still, the PLR level in 5 patients increased slightly after the first treatment cycle (higher than the cutoff value). The PLR in 1 patient still increased after the second treatment cycle (Figure 4D). The sensitivity of PLR was slightly lower than that of CEA for predicting treatment response.

DISCUSSION

This study aimed to investigate the benefits of regorafenib combined with a PD-1 inhibitor in treating MSS mCRC and explore indicators predicting treatment response and prognosis. Treatment using regorafenib combined with PD-1 inhibitor could lead to a longer PFS in some patients with MSS mCRC with failure to standard treatment. Our study also analyzed and compared the PLR of the patients in different treatment cycles with the corresponding CEA levels and explored the possible predictive value of PLR for predicting the response to treatment.

Recently, many studies on combination therapy with immunotherapy were performed to improve the immune responses and clinical efficacies on malignant tumors[26,27]. Still, studies on immunotherapy combined with vascular endothelial growth factor (VEGF) inhibitors have not shown significant improvements in PFS or OS[28,29]. Combination therapy using regorafenib and PD-1 inhibitors has already shown synergistic effects in mouse models[15,30]. In addition, the REGONIVO trial in Japan reported that the response rate was 36%, and the median PFS was 7.9 mo in 25 patients with mCRC (including one with microsatellite instablility-high mCRC) treated with regorafenib plus nivolumab [14]. On the other hand, a retrospective study in the United States did not replicate the findings of the REGONIVO study[15]. Specifically, the clinical responses of the patients were relatively poor; the rate of disease progression was as high as 69%, and the rate of SD was only 31%, without PR or CR[15]. A retrospective study in Shandong, China analyzed the data of 23 patients; SD was found in 18 patients, and the DCR was 78.3%; PD was found in 5 patients, and the PD rate was 21.7%[16]. In the present study, the data of 30 patients were retrospectively analyzed, making it the largest study to date. Of these patients, 18 had SD during the treatment, and the DCR was 60.0%, which was substantially higher than the 31% reported by the American study[15]. The median PFS was 3.4 mo in this study, which was not as outstanding as in the REGONIVO study (7.9 mo) but was longer than the 2.0 mo reported by the American study and comparable with the 3.1 mo reported by the Shandong study. The PFS in 2 patients was longer than 10 mo and was 11.2 mo for the patient with the longest PFS.

The differences between the findings of this study and those of the American study could be due to the following reasons. First, 77.8% of the patients included in the American study had baseline liver metastases. Second, only 4 Asian patients were included in the American study, and patients of different ethnicities could respond differently to the treatment. Liver metastasis was considered an important factor influencing the study results. As an immune-tolerant organ, the liver is related to high percentages of immune suppressor cells[31]. The immune tolerance of the liver is used by primary hepatocellular carcinoma and liver metastases to inhibit the anti-tumor immune responses and decrease the efficacy of treatments using immune checkpoint inhibitors[32]. In addition, several studies demonstrated that liver metastases could also exert systemic immunosuppression effects in patients with cancer, which consequently inhibited the intra- and extrahepatic immune responses[33,34]. A promising method to overcome the inherent immune escape of liver tumors is the combination therapy of liver cancer using anti-VEGF drugs and immune checkpoint inhibitors, as the anti-VEGF drugs could

Table 3 Treatment-related adverse event

Adverse event	Number of patients (n = 30), n (%)		
	Any grade	Grade 1-2	Grade 3
Any event	17 (56.7)	13 (43.3)	4 (13.3)
Hand-foot syndrome	10 (33.3)	8 (26.7)	2 (6.7)
Hypertension	7 (23.3)	7 (23.3)	0
Malaise	6 (20.0)	6 (20.0)	0
Gastrointestinal reaction	5 (16.7)	5 (16.7)	0
Transaminase elevation	4 (13.3)	3 (10.0)	1 (3.3)
Diarrhea	3 (10.0)	3 (10.0)	0
Abnormal capillary proliferation	2 (6.7)	1 (3.3)	1 (3.3)
Hypothyroidism	2 (6.7)	2 (6.7)	0
Proteinuria	2 (6.7)	2 (6.7)	0
Rash	2 (6.7)	2 (6.7)	0
Thrombocytopenia	2 (6.7)	2 (6.7)	0
Anemia	1 (3.3)	1 (3.3)	0
Myocardial enzyme elevation	1 (3.3)	1 (3.3)	0
Oral mucositis	1 (3.3)	1 (3.3)	0
Leukopenia/neutropenia	0	0	0

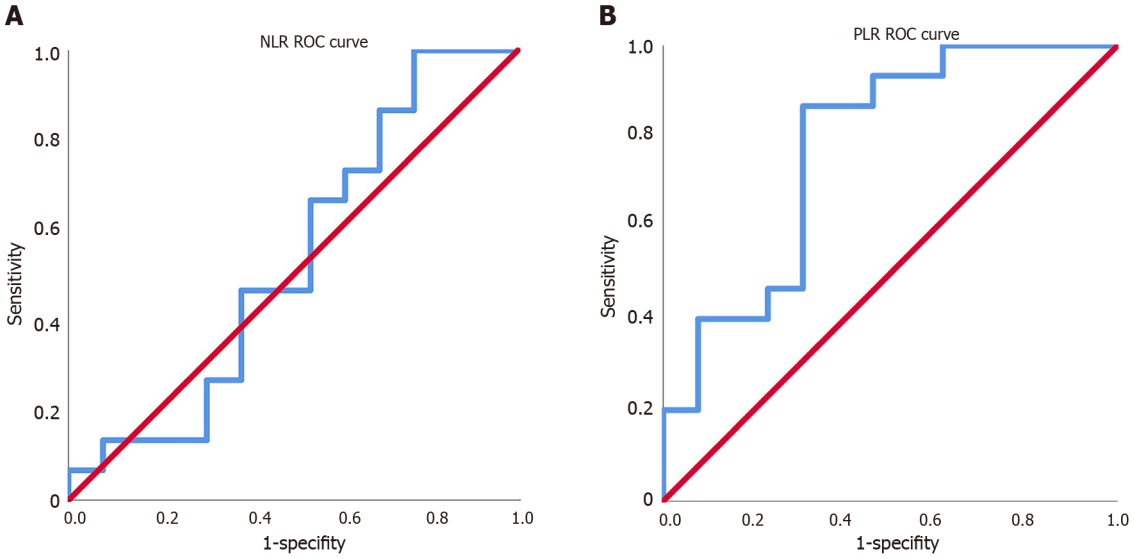

DOI: 10.4251/wjgo.v14.i4.920

Figure 2 Receiver operating characteristics curves. A: The receiver operating characteristics curves of neutrophil-to-lymphocyte ratio; B: The receiver operating characteristics curves of platelet-to-lymphocyte ratio. NLR: Platelet -to-lymphocyte ratio; PLR: Neutrophil-to-lymphocyte ratio; ROC: Receiver operating characteristics.

reverse the VEGF-mediated immune suppression, promote T-cell infiltration of tumor microenvironment, and consequently enhance the treatment effects of ICIs[35]. The multicenter study in Shandong [25] and the REGONIVO study[14] included 56.5% and 52.0% of patients with liver metastases, respectively, while this frequency was 77.8% in the American study. The present study included 60% of patients with liver metastases. The relatively encouraging findings of the REGONIVO study could be related to the good ECOG PS of the patients, while the failure of the American study could be directly related to the high percentage of patients with liver metastases. In the present study, the ECOG PS and the percentage of liver metastases were more evenly distributed. Moreover, the number of patients with each domestic PD-1 inhibitor was limited in our study. Due to the national conditions and patients'

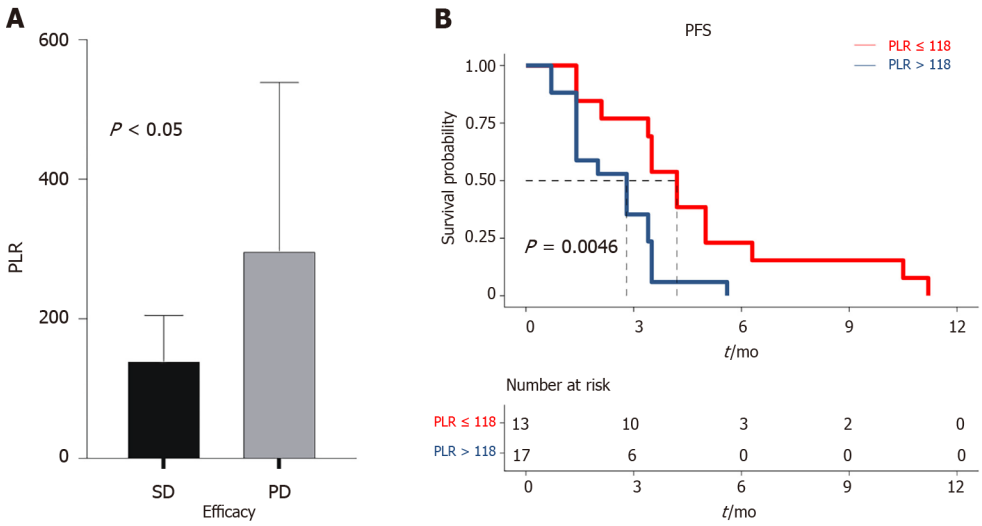

DOI: 10.4251/wjgo.v14.i4.920

Figure 3 Relationship between platelet-to-lymphocyte ratio and treatment response. A: Difference in platelet-to-lymphocyte ratio according to stable disease and progressive disease; B: Progression-free survival according to the platelet-to-lymphocyte ratio ($P < 0.05$). PLR: Platelet-to-lymphocyte ratio; PFS: Progression-free survival; SD: Stable disease; PD: Progressive disease.

financial burden, the number of patients who received nivolumab ($n = 3$) or pembrolizumab ($n = 1$) was also very low. Thus, we analyzed the difference in PFS between patients with imported PD-1 inhibitor (nivolumab or pembrolizumab) and those with domestic anti-PD-1 inhibitor (sintilimab, toripalimab, camrelizumab, or tislelizumab), which showed no statistical significance. This comforting result was also supported by previous clinical trials of domestic PD-1 inhibitors. Thus, the study could provide more objective evidence for evaluating the clinical efficacy of this treatment regimen.

In the present study, the doses of regorafenib included 160, 120, and 80 mg. The dose of regorafenib in all 4 patients treated with 160 mg was reduced to 80 mg due to grade 3 TRAE, and the regorafenib dose in some patients treated with 120 mg was also reduced to 80 mg due to abnormal transaminase levels. Regorafenib treatment could be continued at this dose for all patients, suggesting that 80 mg could be used as the best dose in the combination therapy for further investigation. Besides nivolumab and pembrolizumab used worldwide, four other PD-1 inhibitors common in China were included in this study because many patients cannot afford nivolumab and pembrolizumab.

Since the cost of the combination treatment is relatively high, discovering predictive markers for treatment efficacy is important to identify the patients who could best benefit from the treatment. The findings showed that the specificity of PLR was slightly lower than that of CEA (the PLR of one patient with SD still increased slightly after two treatment cycles), while the sensitivity was comparable (the trend of changes in most patients conformed to the treatment efficacy after the first treatment cycle). The PFS was significantly different between the PLR-low and -high groups, indicating that the PLR was negatively correlated to PFS. The findings suggested that the PLR could be used as a reference to predict the treatment efficacy and PFS of patients when selecting the combination therapy. An Italian study demonstrated that PLR was an independent factor influencing the outcomes of CRC[36]. Moreover, patients with high PLR also showed a high expression level of programmed cell death-ligand 1 in circulating tumor cells, suggesting that PLR may also be a predictive marker of change in tumor immune microenvironment[36]. This may explain why PLR can predict the effectiveness of PD-1 inhibitor combination therapy but NLR cannot.

This study has limitations. Although we retrospectively included all the patients, only 30 were included in this study. The treatment responses of this treatment regimen need to be verified through prospective studies with large sample sizes. No multivariable Cox regression model could be established due to the relatively small sample size of this study, and the predict value of PLR should be further validated.

CONCLUSION

In conclusion, treatment using regorafenib combined with PD-1 inhibitor could lead to a longer PFS in some patients with MSS mCRC with failure to standard treatment. The PLR should be examined further for its ability to predict response to regorafenib combined with a PD-1 inhibitor. These results could help the design of a prospective trial in patients with refractory MSS mCRC.

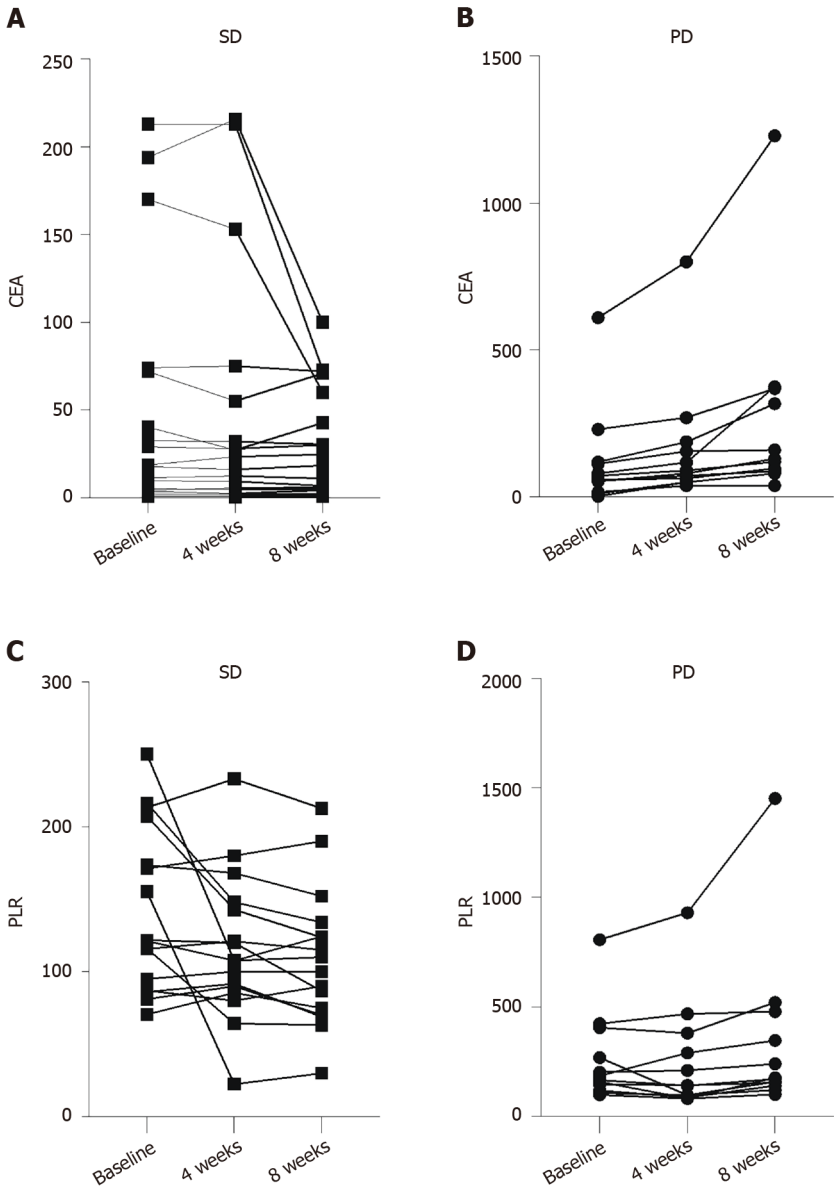

DOI: 10.4251/wjgo.v14.i4.920

Figure 4 Dynamic changes in carcinoembryonic antigen (μg/mL) and platelet-to-lymphocyte ratio after one and two treatment cycles. A: Carcinoembryonic antigen (μg/mL) in time in patients with stable disease; B: Carcinoembryonic antigen (μg/mL) in time in patients with progressive disease; C: Platelet-to-lymphocyte in time in patients with stable disease; D: Platelet-to-lymphocyte in time in patients with progressive disease. PLR: Platelet-to-lymphocyte ratio; SD: Stable disease; PD: Progressive disease.

ARTICLE HIGHLIGHTS

Research background

The effectiveness of the combination therapy using regorafenib and programmed cell death-1 (PD-1) inhibitors in treating metastatic colorectal cancer (mCRC) in the REGONIVO trial in Japan and a retrospective study in the United States are inconsistent.

Research motivation

As the effectiveness of the combination therapy remains controversial, we evaluated the situation and data of the combination therapy including the efficacy and safety in our medical centre in order to provide more clinical evidence for this treatment.

Research objectives

The objectives of this study were to investigate the tumor response, progression-free survival, overall survival, and treatment-related adverse events of the treatment and explore a potential indicators predicting response and prognosis.

Research methods

We identified patients with microsatellite stable (MSS) mCRC treated with regorafenib combined with PD-1 inhibitor at Henan Provincial People's Hospital between December 2018 and December 2020. Collected data included age, sex, Eastern Cooperative Oncology Group (ECOG) performance status (PS), site of the primary tumor, site of the metastases, MSI/MMR, gene status, lines of treatment, and previous treatments. The blood routine examination and CEA results before treatment and after three and five cycles of combination therapy were longitudinally analyzed.

Research results

We included 30 patients with MSS mCRC treated with regorafenib combined with PD-1 inhibitor. The disease control rate was 60.0%. The median follow-up time was 12.0 mo, and median PFS was 3.4 mo [95% confidence interval (CI): 2.2-4.6 mo]. The median PFS in the low-PLR group was 4.2 mo (95%CI: 3.5-4.9 mo), compared with 2.8 mo (95%CI: 1.4-4.2 mo) in the high-PLR group (P = 0.005). Four (13.3%) patients experienced grade 3 TRAE.

Research conclusions

We find that some patients can benefit from the combination therapy even after multi-line therapy and adverse events are generally tolerable. The PLR might be a potential indicator to predict patient response to this combination therapy.

Research perspectives

This study provides experiences and could help to design a prospective trial for patients with MSS mCRC those who failure to standard therapy.

FOOTNOTES

Author contributions: Liu MY and Xu YJ designed the research; Xu YJ, Zhang P, and Hu JL performed the research; Liang H, Zhu YY, and Cui Y contributed new reagents/analytic tools; Xu YJ, Zhang P, Niu P, and Xu M analyzed the data; Liu MY, Xu YJ, and Zhang P wrote the paper.

Supported by the Henan Provincial Department of Science and Technology, No. 212102310047.

Institutional review board statement: This study was approved by the ethics committee of People's Hospital of Zhengzhou University (Henan Province, China) and performed in accordance with the Declaration of Helsinki.

Informed consent statement: The requirement for informed consent was waived by the committee because of the retrospective nature of the study.

Conflict-of-interest statement: The authors declare no conflict of interest.

Data sharing statement: No additional data are available.

Country/Territory of origin: China

ORCID number: Yu-Jie Xu 0000-0003-1833-6541; Peng Zhang 0000-0002-1359-8035; Jin-Long Hu 0000-0002-0032-0202; Hong Liang 0000-0003-4686-9791; Yan-Yan Zhu 0000-0003-2395-0351; Yao Cui 0000-0003-0273-9178; Po Niu 0000-0001-9369-6980; Min Xu 0000-0002-2949-0133; Ming-Yue Liu 0000-0001-6090-0295.

S-Editor: Wang LL
L-Editor: Filipodia
P-Editor: Li X

REFERENCES

1 **Ferlay J**, Colombet M, Soerjomataram I, Mathers C, Parkin DM, Piñeros M, Znaor A, Bray F. Estimating the global cancer incidence and mortality in 2018: GLOBOCAN sources and methods. *Int J Cancer* 2019; **144**: 1941-1953 [PMID: 30350310 DOI: 10.1002/ijc.31937]

2 **Bray F**, Ferlay J, Soerjomataram I, Siegel RL, Torre LA, Jemal A. Global cancer statistics 2018: GLOBOCAN estimates of incidence and mortality worldwide for 36 cancers in 185 countries. *CA Cancer J Clin* 2018; **68**: 394-424 [PMID: 30207593 DOI: 10.3322/caac.21492]

3 **Chen W**, Zheng R, Baade PD, Zhang S, Zeng H, Bray F, Jemal A, Yu XQ, He J. Cancer statistics in China, 2015. *CA Cancer J Clin* 2016; **66**: 115-132 [PMID: 26808342 DOI: 10.3322/caac.21338]

4 **Fu Q**, Zhang Q, Lou Y, Yang J, Nie G, Chen Q, Chen Y, Zhang J, Wang J, Wei T, Qin H, Dang X, Bai X, Liang T. Correction: Primary tumor-derived exosomes facilitate metastasis by regulating adhesion of circulating tumor cells *via* SMAD3 in liver cancer. *Oncogene* 2019; **38**: 5740-5741 [PMID: 31068668 DOI: 10.1038/s41388-019-0830-6]

5 **Van Cutsem E**, Cervantes A, Adam R, Sobrero A, Van Krieken JH, Aderka D, Aranda Aguilar E, Bardelli A, Benson A, Bodoky G, Ciardiello F, D'Hoore A, Diaz-Rubio E, Douillard JY, Ducreux M, Falcone A, Grothey A, Gruenberger T, Haustermans K, Heinemann V, Hoff P, Köhne CH, Labianca R, Laurent-Puig P, Ma B, Maughan T, Muro K, Normanno N, Österlund P, Oyen WJ, Papamichael D, Pentheroudakis G, Pfeiffer P, Price TJ, Punt C, Ricke J, Roth A, Salazar R, Scheithauer W, Schmoll HJ, Tabernero J, Taïeb J, Tejpar S, Wasan H, Yoshino T, Zaanan A, Arnold D. ESMO consensus guidelines for the management of patients with metastatic colorectal cancer. *Ann Oncol* 2016; **27**: 1386-1422 [PMID: 27380959 DOI: 10.1093/annonc/mdw235]

6 **NCCN Clinical Practice Guidelines in Oncology (NCCN Guidelines)**. Colon Cancer. Version 2.2021. Fort Washington: National Comprehensive Cancer Network, 2021

7 **NCCN Clinical Practice Guidelines in Oncology (NCCN Guidelines)**. Rectal Cancer. Version 1.2021. Fort Washington: National Comprehensive Cancer Network, 2021

8 **Siegel RL**, Miller KD, Jemal A. Cancer statistics, 2019. *CA Cancer J Clin* 2019; **69**: 7-34 [PMID: 30620402 DOI: 10.3322/caac.21551]

9 **Diagnosis And Treatment Guidelines For Colorectal Cancer Working Group CSOCOC**. Chinese Society of Clinical Oncology (CSCO) diagnosis and treatment guidelines for colorectal cancer 2018 (English version). *Chin J Cancer Res* 2019; **31**: 117-134 [PMID: 30996570 DOI: 10.21147/j.issn.1000-9604.2019.01.07]

10 **Dhillon S**. Regorafenib: A Review in Metastatic Colorectal Cancer. *Drugs* 2018; **78**: 1133-1144 [PMID: 29943375 DOI: 10.1007/s40265-018-0938-y]

11 **Grothey A**, Blay JY, Pavlakis N, Yoshino T, Bruix J. Evolving role of regorafenib for the treatment of advanced cancers. *Cancer Treat Rev* 2020; **86**: 101993 [PMID: 32199197 DOI: 10.1016/j.ctrv.2020.101993]

12 **Yamaguchi K**, Komatsu Y, Satoh T, Uetake H, Yoshino T, Nishida T, Yamazaki N, Takikawa H, Morimoto T, Chosa M, Sunaya T, Hamada Y, Muro K, Sugihara K. Large-Scale, Prospective Observational Study of Regorafenib in Japanese Patients with Metastatic Colorectal Cancer in a Real-World Clinical Setting. *Oncologist* 2019; **24**: e450-e457 [PMID: 30606885 DOI: 10.1634/theoncologist.2018-0377]

13 **Le DT**, Uram JN, Wang H, Bartlett BR, Kemberling H, Eyring AD, Skora AD, Luber BS, Azad NS, Laheru D, Biedrzycki B, Donehower RC, Zaheer A, Fisher GA, Crocenzi TS, Lee JJ, Duffy SM, Goldberg RM, de la Chapelle A, Koshiji M, Bhaijee F, Huebner T, Hruban RH, Wood LD, Cuka N, Pardoll DM, Papadopoulos N, Kinzler KW, Zhou S, Cornish TC, Taube JM, Anders RA, Eshleman JR, Vogelstein B, Diaz LA Jr. PD-1 Blockade in Tumors with Mismatch-Repair Deficiency. *N Engl J Med* 2015; **372**: 2509-2520 [PMID: 26028255 DOI: 10.1056/NEJMoa1500596]

14 **Fukuoka S**, Hara H, Takahashi N, Kojima T, Kawazoe A, Asayama M, Yoshii T, Kotani D, Tamura H, Mikamoto Y, Hirano N, Wakabayashi M, Nomura S, Sato A, Kuwata T, Togashi Y, Nishikawa H, Shitara K. Regorafenib Plus Nivolumab in Patients With Advanced Gastric or Colorectal Cancer: An Open-Label, Dose-Escalation, and Dose-Expansion Phase Ib Trial (REGONIVO, EPOC1603). *J Clin Oncol* 2020; **38**: 2053-2061 [PMID: 32343640 DOI: 10.1200/JCO.19.03296]

15 **Wang C**, Chevalier D, Saluja J, Sandhu J, Lau C, Fakih M. Regorafenib and Nivolumab or Pembrolizumab Combination and Circulating Tumor DNA Response Assessment in Refractory Microsatellite Stable Colorectal Cancer. *Oncologist* 2020; **25**: e1188-e1194 [PMID: 32406541 DOI: 10.1634/theoncologist.2020-0161]

16 **Li J**, Cong L, Liu J, Peng L, Wang J, Feng A, Yue J, Li L, Wang X. The Efficacy and Safety of Regorafenib in Combination With Anti-PD-1 Antibody in Refractory Microsatellite Stable Metastatic Colorectal Cancer: A Retrospective Study. *Front Oncol* 2020; **10**: 594125 [PMID: 33282742 DOI: 10.3389/fonc.2020.594125]

17 **Cho WK**, Choi DH, Park HC, Park W, Yu JI, Park YS, Park JO, Lim HY, Kang WK, Kim HC, Cho YB, Yun SH, Lee WY. Elevated CEA is associated with worse survival in recurrent rectal cancer. *Oncotarget* 2017; **8**: 105936-105941 [PMID: 29285304 DOI: 10.18632/oncotarget.22511]

18 **Auclin E**, Taieb J, Lepage C, Aparicio T, Faroux R, Mini E, Folprecht G, Salazar R, Benetkiewicz M, Banzi M, Louvet C, Van Laethem JL, Tabernero J, Hickish T, de Gramont A, André T, Vernerey D. Carcinoembryonic Antigen Levels and Survival in Stage III Colon Cancer: *Post hoc* Analysis of the MOSAIC and PETACC-8 Trials. *Cancer Epidemiol Biomarkers Prev* 2019; **28**: 1153-1161 [PMID: 31263053 DOI: 10.1158/1055-9965.EPI-18-0867]

19 **Tanoglu A**, Karagoz E. Neutrophil and platelet-to-lymphocyte ratio: new predictors of dropout and recurrence after liver transplantation for hepatocellular cancer? *Transpl Int* 2014; **27**: e80-e81 [PMID: 24612189 DOI: 10.1111/tri.12291]

20 **Huang S**, Li D, Zhuang L, Sun L, Wu J. A meta-analysis of the efficacy and safety of adjuvant sorafenib for hepatocellular carcinoma after resection. *World J Surg Oncol* 2021; **19**: 168 [PMID: 34112190 DOI: 10.1186/s12957-021-02280-9]

21 **Miao Y**, Yan Q, Li S, Li B, Feng Y. Neutrophil to lymphocyte ratio and platelet to lymphocyte ratio are predictive of chemotherapeutic response and prognosis in epithelial ovarian cancer patients treated with platinum-based chemotherapy. *Cancer Biomark* 2016; **17**: 33-40 [PMID: 27314290 DOI: 10.3233/CBM-160614]

22 **Zhang Y**, Lu JJ, Du YP, Feng CX, Wang LQ, Chen MB. Prognostic value of neutrophil-to-lymphocyte ratio and platelet-to-lymphocyte ratio in gastric cancer. *Medicine (Baltimore)* 2018; **97**: e0144 [PMID: 29561419 DOI: 10.1097/MD.0000000000010144]

23 **Kim JY**, Jung EJ, Kim JM, Lee HS, Kwag SJ, Park JH, Park T, Jeong SH, Jeong CY, Ju YT. Dynamic changes of neutrophil-to-lymphocyte ratio and platelet-to-lymphocyte ratio predicts breast cancer prognosis. *BMC Cancer* 2020; **20**: 1206 [PMID: 33287745 DOI: 10.1186/s12885-020-07700-9]

24 **Messersmith WA**. NCCN Guidelines Updates: Management of Metastatic Colorectal Cancer. *J Natl Compr Canc Netw*

2019; **17**: 599-601 [PMID: 31117039 DOI: 10.6004/jnccn.2019.5014]

25 **Zhang L**, Wang J, Zhang B, Chu Q, Su C, Wu H, Chen X, Wang B, Yin Y, Zhu B, Sun J. Attitudes and Practices of Immune Checkpoint Inhibitors in Chinese Patients With Cancer: A National Cross-Sectional Survey. *Front Pharmacol* 2021; **12**: 583126 [PMID: 33841138 DOI: 10.3389/fphar.2021.583126]

26 **Golshani G**, Zhang Y. Advances in immunotherapy for colorectal cancer: a review. *Therap Adv Gastroenterol* 2020; **13**: 1756284820917527 [PMID: 32536977 DOI: 10.1177/1756284820917527]

27 **Johdi NA**, Sukor NF. Colorectal Cancer Immunotherapy: Options and Strategies. *Front Immunol* 2020; **11**: 1624 [PMID: 33042104 DOI: 10.3389/fimmu.2020.01624]

28 **Mettu NB**, Twohy E, Ou FS, Halfdanarson TR, Lenz HJ, Breakstone R, Boland PM, Crysler O, Wu C, Grothey A, Nixon AB, Bolch E, Niedzwiecki D, Fruth B, Schweitzer B, Elsing A, Hurwitz H, Fakih MG, Bekaii-Saab T. BACCI: A phase II randomized, double-blind, multicenter, placebo-controlled study of capecitabine (C) bevacizumab (B) plus atezolizumab (A) or placebo (P) in refractory metastatic colorectal cancer (mCRC): An ACCRU network study. *Anna Oncol* 2019; **30** [DOI: 10.1093/annonc/mdz246.011]

29 **Grothey A**, Tabernero J, Arnold D, De Gramont A, Ducreux MP, O'Dwyer PJ, Van Cutsem E, Bosanac I, Srock S, Mancao C, Gilberg F, Winter J, Schmoll HJ. Fluoropyrimidine (FP) + bevacizumab (BEV) + atezolizumab *vs* FP/BEV in BRAFwt metastatic colorectal cancer (mCRC): Findings from Cohort 2 of MODUL – a multicentre, randomized trial of biomarker-driven maintenance treatment following first-line induction therapy. *Ann Oncol* 2018; **29**: 714-715 [DOI: 10.1093/annonc/mdy424.020]

30 **Shigeta K**, Matsui A, Kikuchi H, Klein S, Mamessier E, Chen IX, Aoki S, Kitahara S, Inoue K, Shigeta A, Hato T, Ramjiawan RR, Staiculescu D, Zopf D, Fiebig L, Hobbs GS, Quaas A, Dima S, Popescu I, Huang P, Munn LL, Cobbold M, Goyal L, Zhu AX, Jain RK, Duda DG. Regorafenib combined with PD1 blockade increases CD8 T-cell infiltration by inducing CXCL10 expression in hepatocellular carcinoma. *J Immunother Cancer* 2020; **8** [PMID: 33234602 DOI: 10.1136/jitc-2020-001435]

31 **Zheng M**, Tian Z. Liver-Mediated Adaptive Immune Tolerance. *Front Immunol* 2019; **10**: 2525 [PMID: 31787967 DOI: 10.3389/fimmu.2019.02525]

32 **Yu J**, Green MD, Li S, Sun Y, Journey SN, Choi JE, Rizvi SM, Qin A, Waninger JJ, Lang X, Chopra Z, El Naqa I, Zhou J, Bian Y, Jiang L, Tezel A, Skvarce J, Achar RK, Sitto M, Rosen BS, Su F, Narayanan SP, Cao X, Wei S, Szeliga W, Vatan L, Mayo C, Morgan MA, Schonewolf CA, Cuneo K, Kryczek I, Ma VT, Lao CD, Lawrence TS, Ramnath N, Wen F, Chinnaiyan AM, Cieslik M, Alva A, Zou W. Liver metastasis restrains immunotherapy efficacy *via* macrophage-mediated T cell elimination. *Nat Med* 2021; **27**: 152-164 [PMID: 33398162 DOI: 10.1038/s41591-020-1131-x]

33 **Lee JC**, Mehdizadeh S, Smith J, Young A, Mufazalov IA, Mowery CT, Daud A, Bluestone JA. Regulatory T cell control of systemic immunity and immunotherapy response in liver metastasis. *Sci Immunol* 2020; **5** [PMID: 33008914 DOI: 10.1126/sciimmunol.aba0759]

34 **Tumeh PC**, Hellmann MD, Hamid O, Tsai KK, Loo KL, Gubens MA, Rosenblum M, Harview CL, Taube JM, Handley N, Khurana N, Nosrati A, Krummel MF, Tucker A, Sosa EV, Sanchez PJ, Banayan N, Osorio JC, Nguyen-Kim DL, Chang J, Shintaku IP, Boasberg PD, Taylor EJ, Munster PN, Algazi AP, Chmielowski B, Dummer R, Grogan TR, Elashoff D, Hwang J, Goldinger SM, Garon EB, Pierce RH, Daud A. Liver Metastasis and Treatment Outcome with Anti-PD-1 Monoclonal Antibody in Patients with Melanoma and NSCLC. *Cancer Immunol Res* 2017; **5**: 417-424 [PMID: 28411193 DOI: 10.1158/2326-6066.CIR-16-0325]

35 **Voron T**, Colussi O, Marcheteau E, Pernot S, Nizard M, Pointet AL, Latreche S, Bergaya S, Benhamouda N, Tanchot C, Stockmann C, Combe P, Berger A, Zinzindohoue F, Yagita H, Tartour E, Taieb J, Terme M. VEGF-A modulates expression of inhibitory checkpoints on CD8+ T cells in tumors. *J Exp Med* 2015; **212**: 139-148 [PMID: 25601652 DOI: 10.1084/jem.20140559]

36 **Raimondi L**, Raimondi FM, Di Benedetto L, Cimino G, Spinelli GP. PD-L1 Expression on Circulating Tumour Cells May Be Predictive of Response to Regorafenib in Patients Diagnosed with Chemorefractory Metastatic Colorectal Cancer. *Int J Mol Sci* 2020; **21** [PMID: 32962309 DOI: 10.3390/ijms21186907]

World Journal of Gastrointestinal Oncology

Submit a Manuscript: https://www.f6publishing.com

World J Gastrointest Oncol 2022 April 15; 14(4): 935-946

DOI: 10.4251/wjgo.v14.i4.935

ISSN 1948-5204 (online)

ORIGINAL ARTICLE

Clinical Trials Study

Genome-wide methylation profiling of early colorectal cancer using an Illumina Infinium Methylation EPIC BeadChip

Yu-Ling Wu, Tao Jiang, Wei Huang, Xing-Yu Wu, Peng-Jun Zhang, Ya-Ping Tian

Specialty type: Oncology

Provenance and peer review: Unsolicited article; Externally peer reviewed.

Peer-review model: Single blind

Peer-review report's scientific quality classification

Grade A (Excellent): A
Grade B (Very good): 0
Grade C (Good): C
Grade D (Fair): 0
Grade E (Poor): 0

P-Reviewer: Kołat D, Poland; Osera S, Japan

Received: December 19, 2021
Peer-review started: December 19, 2021
First decision: February 21, 2022
Revised: February 21, 2022
Accepted: April 3, 2022
Article in press: April 3, 2022
Published online: April 15, 2022

Yu-Ling Wu, Wei Huang, Medical School of Chinese PLA, Beijing 100853, China

Tao Jiang, Ya-Ping Tian, Medical Innovation Research Division, Chinese PLA General Hospital, Beijing 100853, China

Xing-Yu Wu, Nankai University School of Medicine, Tianjin 300071, China

Peng-Jun Zhang, Key Laboratory of Carcinogenesis and Translational Research (Ministry of Education/Beijing), Interventional Therapy Department, Peking University Cancer Hospital and Institute, Beijing 100142, China

Corresponding author: Ya-Ping Tian, MD, Professor, Medical Innovation Research Division, Chinese PLA General Hospital, No. 28 Fuxing Road, Haidian District, Beijing 100853, China. tianyp@301hospital.com.cn

Abstract

BACKGROUND

DNA methylation is a part of epigenetic modification, that is closely related to the growth and development of colorectal cancer (CRC). Specific methylated genes and methylated diagnostic models of tumors have become current research focuses. The methylation status of circulating DNA in plasma might serve as a potential biomarker for CRC.

AIM

To investigate genome-wide methylation pattern in early CRC using the Illumina Infinium Human Methylation 850K BeadChip.

METHODS

The 850K Methylation BeadChip was used to analyze the genome-wide methylation status of early CRC patients (n = 5) and colorectal adenoma patients (n = 5). Gene ontology (GO) and Kyoto Encyclopedia of Genes and Genomes (KEGG) pathways enrichment analyses were performed on the selected differentially methylated sites to further discover candidate methylation biomarkers in plasma.

RESULTS

A total of 1865 methylated CpG sites with significant differences were detected, including 676 hypermethylated sites and 1189 hypomethylated sites. The distri-

bution of these sites covered from the 1st to 22nd chromosomes and are mainly distributed on the gene body and gene promoter region. GO and KEGG enrichment analysis showed that the functions of these genes were related to biological regulation, molecular binding, transcription factor activity and signal transduction pathway.

CONCLUSION

The study demonstrated that the Illumina Infinium Human Methylation 850K BeadChip can be used to investigate genome-wide methylation status of plasma DNA in early CRC and colorectal adenoma patients.

Key Words: Colorectal cancer; DNA methylation; 850K Methylation BeadChip; Plasma; colorectal adenoma

Core Tip: DNA methylation is associated with the growth and development of colorectal cancer (CRC). CRC usually develops from its precancerous lesion, colorectal adenoma. The study demonstrated that the Illumina Infinium Human Methylation 850K BeadChip can be used to investigate genome-wide methylation status of plasma DNA in early CRC and colorectal adenoma patients.

Citation: Wu YL, Jiang T, Huang W, Wu XY, Zhang PJ, Tian YP. Genome-wide methylation profiling of early colorectal cancer using an Illumina Infinium Methylation EPIC BeadChip. *World J Gastrointest Oncol* 2022; 14(4): 935-946

URL: https://www.wjgnet.com/1948-5204/full/v14/i4/935.htm

DOI: https://dx.doi.org/10.4251/wjgo.v14.i4.935

INTRODUCTION

Colorectal cancer (CRC) is a common malignancy with high morbidity and mortality. Tumors are highly associated with aberrant DNA methylation alterations, which are involved in the regulation of genomic function[1]. DNA methylation in promoter regions leads to gene silencing, which plays an important role in the development and progression of CRC. The incidence of CRC is insidious, and its early manifestation is not obvious, thus, early effective screening is of great significance to reduce morbidity and mortality[2]. CRC usually develops from its precancerous lesion, colorectal adenoma. The evolution from colorectal adenoma to CRC is associated with hypermethylation of tumor-related genes and genome-wide hypomethylation of CpG sites[3,4]. Various histological subtypes of colorectal adenoma also have different methylation patterns[5]. Genome-wide methylation profiling of early CRC and colorectal adenoma will contribute to the discovery of tumor biomarkers, thus improving the early screening rate of CRC.

Circulating tumor DNA (ctDNA), a free DNA released by tumor cells, was found in plasma. The genetic alterations between ctDNA and tumor cell DNA were consistent. A variety of tumor-specific alterations could be detected through ctDNA, including abnormal methylation[6]. Therefore, the detection of ctDNA methylation in plasma can facilitate the cancer diagnosis. Some research had studied genomic methylation of CRC in plasma or serum[7-10], but few focused on the ctDNA methylation differences between early CRC and colorectal adenoma. The Illumina Infinium Human Methylation 850K BeadChip has technical superiority in high-throughput detection for genomic methylation status. The 850K chip contains 91% of the 450K chip and 413745 additional sites (a total of 866895 CpG sites), covering gene promoter regions, gene coding regions, CpG islands and enhancers in the ENCODE and FANTOM5 programs[11-13]. The research efficiency has been greatly improved.

In the present study, an Illumina Infinium Human Methylation 850K BeadChip was used to detect methylation differences of plasma DNA between CRC patients and colorectal adenoma patients, gene ontology (GO) and Kyoto Encyclopedia of Genes and Genomes (KEGG) pathway enrichment analyses was also performed to investigate the biological functions of differentially methylated sites (DMSs). This study aimed to investigate the different methylation pattern in plasma DNA between early CRC and colorectal adenoma using the Human Methylation 850K BeadChip.

Table 1 Patient characteristics

	Gender	Age	Group	TNM stage
C1	Male	52	CRC (I)	I
C2	Male	62	CRC (I)	I
C3	Female	62	CRC (I)	I
C4	Male	64	CRC (I)	I
C5	Female	79	CRC (I)	I
A1	Female	69	Adenoma	
A2	Male	69	Adenoma	
A3	Male	69	Adenoma	
A4	Male	49	Adenoma	
A5	Male	74	Adenoma	

CRC: Colorectal cancer; TNM: Tumor-node-metastasis.

MATERIALS AND METHODS

Patients

In this study, the Human Methylation 850K BeadChip assay included early CRC patients (n = 5) and colorectal adenoma patients (n = 5) hospitalized in the Chinese PLA General Hospital from January 2018 to January 2020 (Table 1). Their ages ranged from 52 to 79 years old, with an average age of 63 years old. Inclusion criteria: None of the patients had received any treatment when their peripheral blood samples were taken, including surgical resection, radiotherapy, chemotherapy, and targeted therapy; all patients who underwent colonoscopy and endoscopic biopsy, which were confirmed as colorectal adenoma (without cancerization) by pathology, were included in the adenoma group, which were confirmed as CRC by pathology and at stage I according to the American Joint Committee on Cancer tumor-node-metastasis staging system for CRC, were included in the tumor group; all patients had no other malignant tumors or serious diseases. Later clinical follow-up was required for all patients. If the postoperative pathological results of the tumor tissue were inconsistent with those of endoscopic biopsy, postoperative histopathology prevailed, and cases that did not meet the inclusion criteria were excluded. All participants signed written informed consent for the collection of samples and subsequent analyses before inclusion.

DNA isolation and bisulfite conversion

Peripheral blood was collected from the veins of patients and centrifuged within 30 min (4°C, 3000 rpm, 10 min). The plasma was collected and stored at 4°C for DNA extraction within 3 days, according to the instructions of the QIAamp MinElute ccfDNA Mini Kit (QIAGEN, Germany, 55204). The DNA was treated with bisulfite to convert cytosine to uracil according to the instructions of the EZ DNA Methylation-Gold Kit (Zymo Research, USA, D5001/D5003). Subsequently Qubit ssDNA HS Assay Kit (Invitrogen, USA, Q32854) as well as Qubit 3.0 fluorescence quantizer (Thermo Fisher, USA) were used for DNA quantitative analysis after bisulfite conversion. The bisulfite-converted DNA was stored at -20 °C until use.

850K methylation assay and bioinformatic analysis

Genome-wide methylation profiling was perfrormed by Illumina Infinium Human Methylation 850K BeadChip (Sinotech Genomics, China), in accordance with Illumina's standard protocol. Bisulfite-converted DNA was used for alkali denaturation and genomic amplification. Then, the amplified DNA was used for hybridization, washing, fluorescent staining, single-base extension and scanning on an 850K BeadChip. An IScan software analysis system (Illumina, USA) was used for signal acquisition and analysis. The data (IDAT files) were mainly analyzed using the ChAMP package in R. We used β values (range, 0-1) to represent the DNA methylation level, wAhich were calculated from the intensity ratio of the methylated signals to the total (methylated and unmethylated) signals for each site. Then we compared the β values of each probe site in the samples between the CRC group and adenoma group, calculating the average β value of each site and the difference in β values between groups ($\Delta\beta$). For plasma samples, a CpG site with $|\Delta\beta| > 0.1$ and a P value < 0.01 was considered as a DMS ($\Delta\beta > 0.1$ was considered a hypermethylated site, and $\Delta\beta < -0.1$ was considered a hypomethylated site). The Benjamini and Hochberg method was applied to reduce the false-positive rate[14].

Table 2 The distribution of differentially methylated sites, (*n*)

Chromosome	DMSs	Hypermethylated	Hypomethylated
chr1	162	62	100
chr2	158	53	105
chr3	104	35	69
chr4	83	22	61
chr5	112	35	77
chr6	112	25	87
chr7	115	55	60
chr8	89	27	62
chr9	79	33	46
chr10	91	29	62
chr11	104	42	62
chr12	105	41	64
chr13	53	18	35
chr14	50	22	28
chr15	58	22	36
chr16	72	34	38
chr17	76	35	41
chr18	38	13	25
chr19	88	33	55
chr20	60	22	38
chr21	25	7	18
chr22	31	11	20

DMSs: Differentially methylated sites.

We also conducted GO and KEGG enrichment analyses for DMSs using the R package. In the functional enrichment analysis, the *P* values represented the likelihood that the gene associated with the GO term would be enriched in the input gene list, and a *P* value less than 0.05 was considered significant.

RESULTS

Genome-wide detection of methylation in CRC plasma by the 850K methylation BeadChip

The 850K methylation BeadChip included a total of 866895 CpG sites, screening out 1865 differentially methylated CpG sites between CRC and adenoma plasma samples ($|\Delta\beta| > 0.1$, $P < 0.01$), including 676 hypermethylation sites and 1189 hypomethylation sites (Figure 1). These DMSs were widely distributed on all chromosomes, among which, chromosomes 1 and 2 had the most sites and chromosomes 21 and 22 had the least sites (Table 2). Figure 2A and B shows the distribution of DMSs on the chromosomes of the genome. There were also differences in the distribution of the gene structure elements, mainly in the gene body (64.1%) and gene promoter region (32.7%, including TSS1500, TSS200, 5'UTR, and 1stExon). The distribution of DMSs in and around CpG islands was also different, mainly in the CpG Shore (53.7%) and CpG Island regions (20.3%) (Figure 3A and B).

GO enrichment analysis

GO enrichment analysis including the biological process, cellular component, and molecular function categories, was performed. A *P* value of < 0.05 was considered statistically significant. After GO enrichment analysis of the selected DMSs, 783 GO functional annotations were obtained, including 571 terms of biological processes, 107 terms of cell components and 105 terms of molecular functions. These

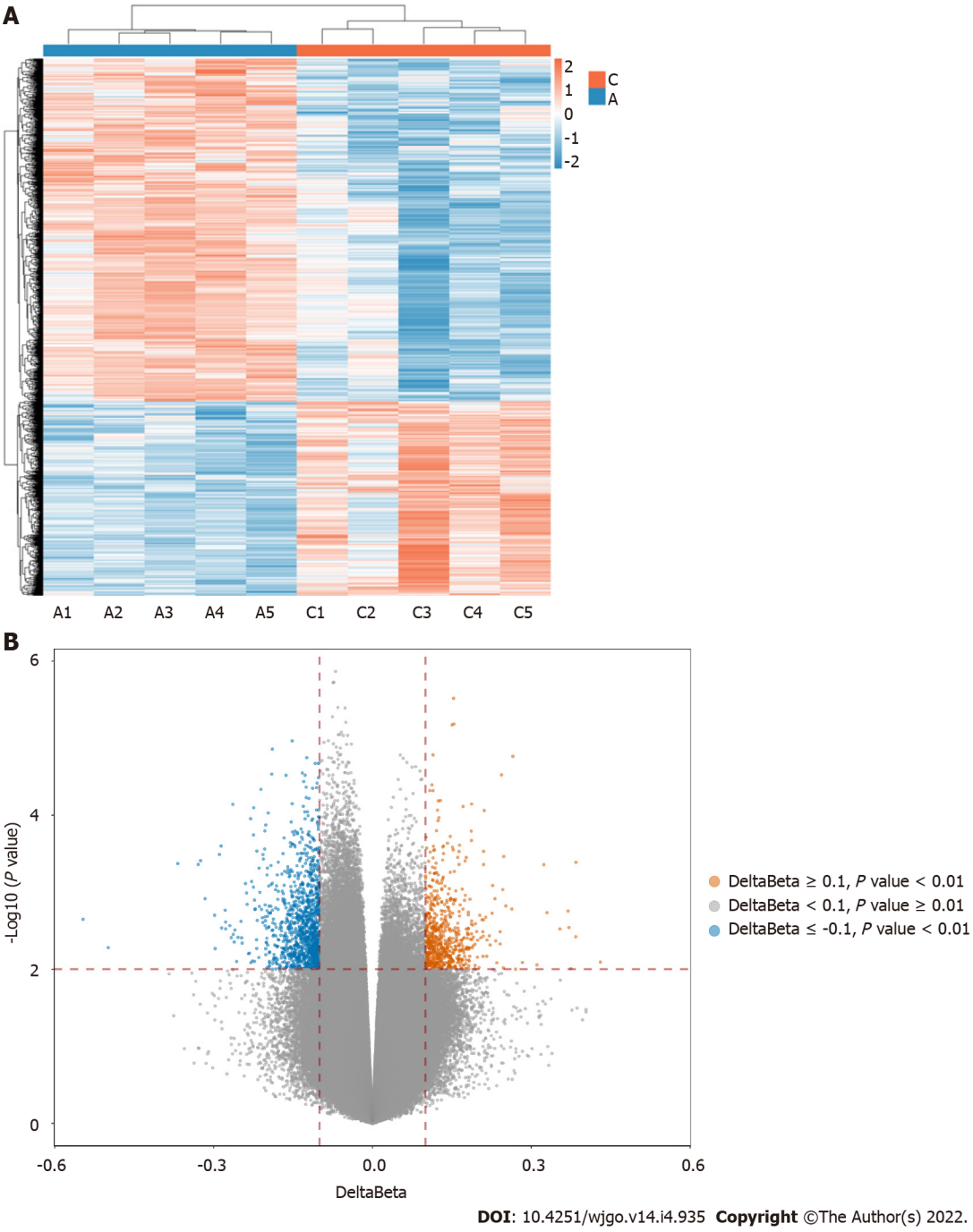

DOI: 10.4251/wjgo.v14.i4.935

Figure 1 The heatmap and volcano of the differentially methylated sites. A: Adenoma group; B: Delta β data. Ca: Cancer group.

GO functional terms indicated that DMSs in CRC cover a variety of functional communities. In terms of biological process, differentially expressed genes were mainly enriched in biological regulation, cellular process, metabolic process, regulation of biological process, and single organism process. The cell component analysis showed that molecules distributed in the extracellular region, cell membrane, organelle and synapse were significantly enriched. At the molecular level, functional enrichment annotation showed that the highly enriched genes were associated with molecular binding, catalytic activity and signaling pathways (Figure 4A). The bubble diagram in Figure 4B shows the top 30 GO terms with the most significant enrichment effect. Significantly enriched biological processes included gamma−aminobutyric acid depletion and transport and cerebellar Purkinje cell layer development. Significantly enriched cellular components included the filopodium tip and apical cortex. Significantly enriched molecular functions included microfilament motor activity, ephrin receptor activity and phosphatidylinositol phospholipase C and sphingolipid binding (Figure 4B).

KEGG pathway enrichment analysis

KEGG pathways were divided into cellular processes, environmental information processing, genetic

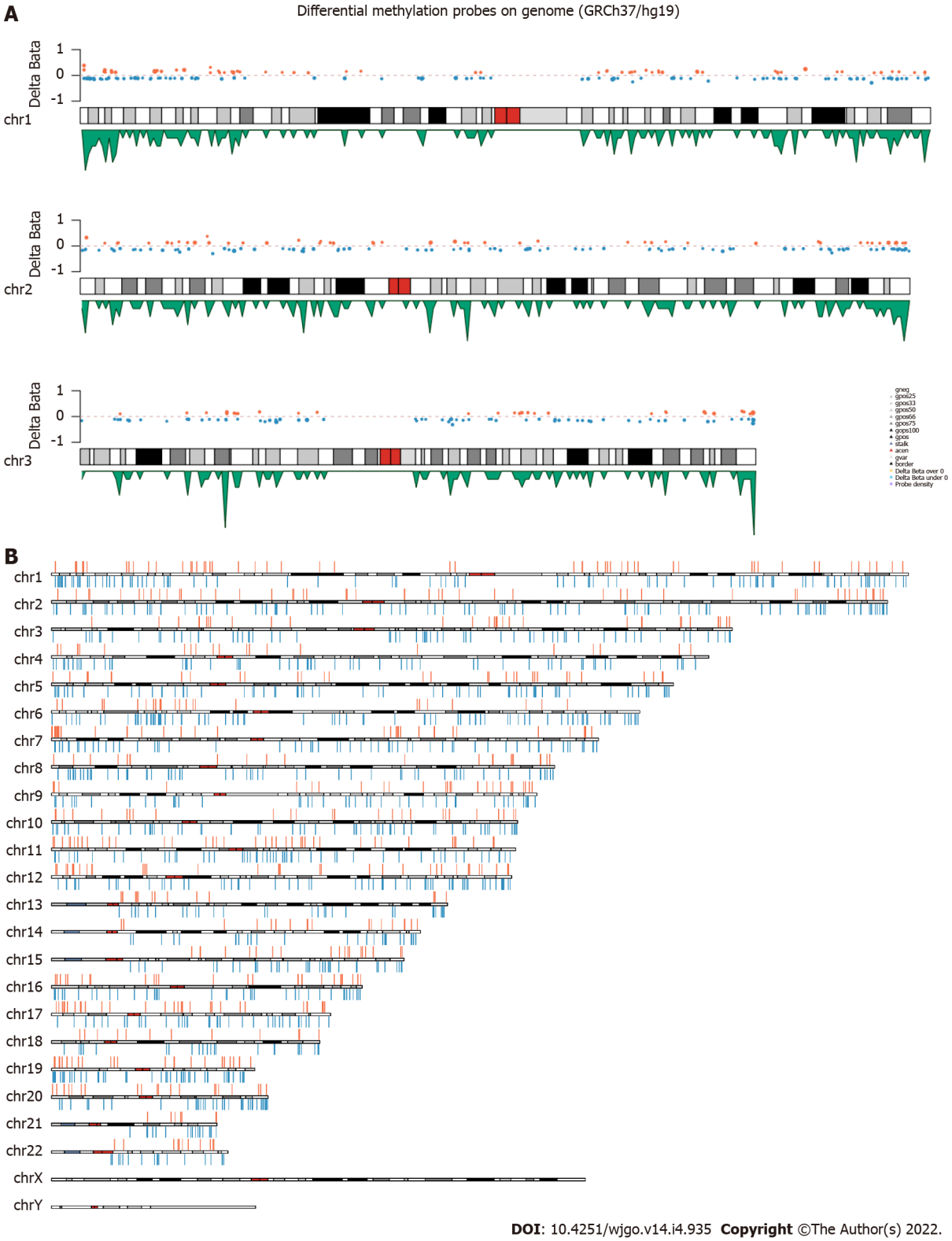

DOI: 10.4251/wjgo.v14.i4.935

Figure 2 The distribution of differentially methylated sites. A: Examples of the distribution of differentially methylated sites (DMSs) on chromosome 1, 2, and 3. The orange and blue dots represent the CpGs which are $\Delta\beta > 0$ and $\Delta\beta < 0$ respectively, the green peak represents the density of probes; B: Schematic map of the genomic DMSs, where red and blue represent the CpGs which are $\Delta\beta > 0$ and $\Delta\beta < 0$ respectively.

information processing, human disease metabolism, metabolism, and organismal systems. KEGG annotation results of DMSs were classified according to the above six pathways (Figure 5A). A total of 26 KEGG signaling pathways were significantly enriched, which are shown in the bubble diagram (Figure 5B). KEGG analysis showed that DMSs were involved in various cellular pathways in CRC. Significantly enriched pathways included long-term depression, calcium signaling pathway, synapse related pathway, Rap1 signaling pathway, PI3K-Akt signaling pathway and MAPK signaling pathway.

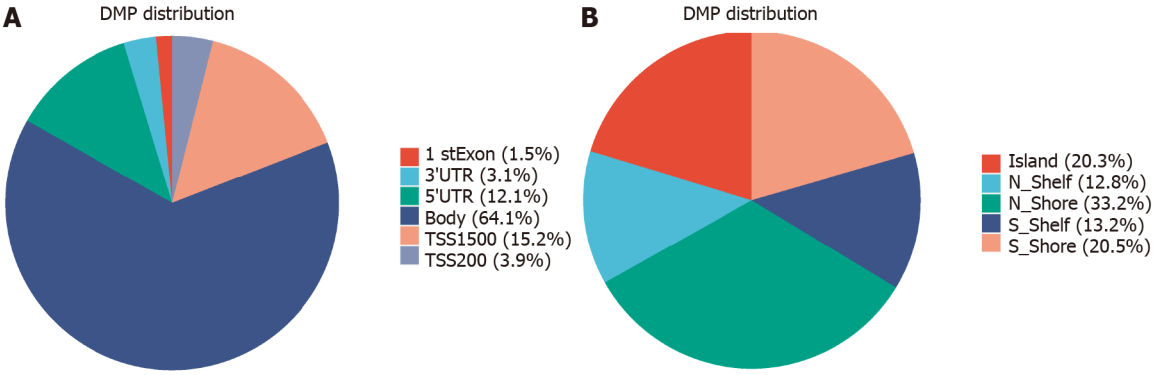

DOI: 10.4251/wjgo.v14.i4.935

Figure 3 Distribution of differentially methylated sites. A: Distribution of differentially methylated sites (DMSs) in gene structural elements; B: Distribution of DMSs in and around CpG island.

DISCUSSION

Cancer is associated with a series of abnormal alterations in genetics and epigenetics. Mutations or epigenetic alterations in key pathways involved in cell growth and division may induce the occurrence of tumors[15]. Aberrant methylation modifications in the colon can be observed in early premalignant lesions such as adenoma and normal mucosa of para-carcinoma tissue[16]. And DNA methylation is an important epigenetic alteration that leads to silencing of the expression of tumor-related genes, and many abnormal methylations have been found in the genomic DNA of tumor cells, which are also reflected in plasma ctDNA. Therefore, the detection of ctDNA in plasma is becoming a new method of cancer diagnosis and monitoring[9]. Current ctDNA detection techniques based on gene mutations mainly rely on the number of tumor-derived DNA molecules in the sample, the number of mutated cancer cells, the concentration fraction of ctDNA and the sensitivity of analysis[17]. Using methylation patterns to detect ctDNA in plasma has advantages over mutation-based tests. Epigenetic modifications are more consistent in tumor cells than genetic mutations[18]. Therefore, early CRC can be diagnosed by detecting the methylation pattern of ctDNA.

The detecting DNA for 850K Methylation BeadChip is first treated with bisulfite to convert methylation differences into differences in bases. The Illumina Infinium Human Methylation 850K BeadChip has two detection methods (Infinium I and Infinium II). Infinium I has two specific probes for the bisulfite-converted DNA sequence. The M-type magnetic beads match the methylated sites, and the U-type magnetic beads match the unmethylated sites. Infinium II had only one probe, and only one base is added for single nucleotide extension after pairing. Different bases are added for methylated and unmethylated sequences, producing different fluorescence signals, and the level of methylation is calculated according to the signal ratio[11,19].

This study used an Illumina Infinium Human Methylation 850K BeadChip to detect and analyze the genome-wide methylation status of 5 early CRC patients and 5 cases of adenoma. According to the research findings, there were 1865 DMSs, including 676 hypermethylated sites and 1189 hypomethylated sites. The distribution of these methylated sites in the chromosomes, gene structural elements, CpG islands and their surrounding regions were all different. Then GO and KEGG enrichment analyses were performed on the differentially methylated genes. GO and KEGG functional annotation indicated that differentially methylated genes in CRC cover a variety of different functional aspects and participate in multiple biological pathways. Examples are Calcium signaling pathway, Rap1 signaling pathway, PI3K-Akt signaling pathway, MAPK signaling pathway, cell adhesion pathway and metabolic pathway, are all important biological pathways in tumor research[20-23]. These results indicated that multiple signaling pathways might be simultaneously regulated by DNA methylation in the progression of colorectal adenoma to early CRC. The limitation of this study is the small sample size due to the high cost. Due to the low content of plasma DNA, there was basically no residual after the chip detection, so we had not conducted other studies for verification. This project used an 850K Methylation chip to detect more than 850000 sites with low initial detecting DNA content, suitable for the methylation screening of trace DNA. Compared with other methylation chips, its detection flux had a qualitative improvement. And compared with the next generation whole-genome methylation sequencing technology, it solved the contradiction that the initial DNA content of sequencing technology is high (3-5 μg) while the plasma DNA content is very low[24]. Previously, the 850K methylation chip detection for CRC mostly used tissue or mucosal samples[25], so the sampling method is invasive and might cause tumor heterogeneity due to sampling deviation. In this study, plasma samples from patients with CRC and adenoma were used for genome-wide methylation analysis to screen for differentially methylated sites. Non-invasive samples were obtained from peripheral blood of patients. Therefore, this novel technology can be used as an effective tool for screening plasma DNA

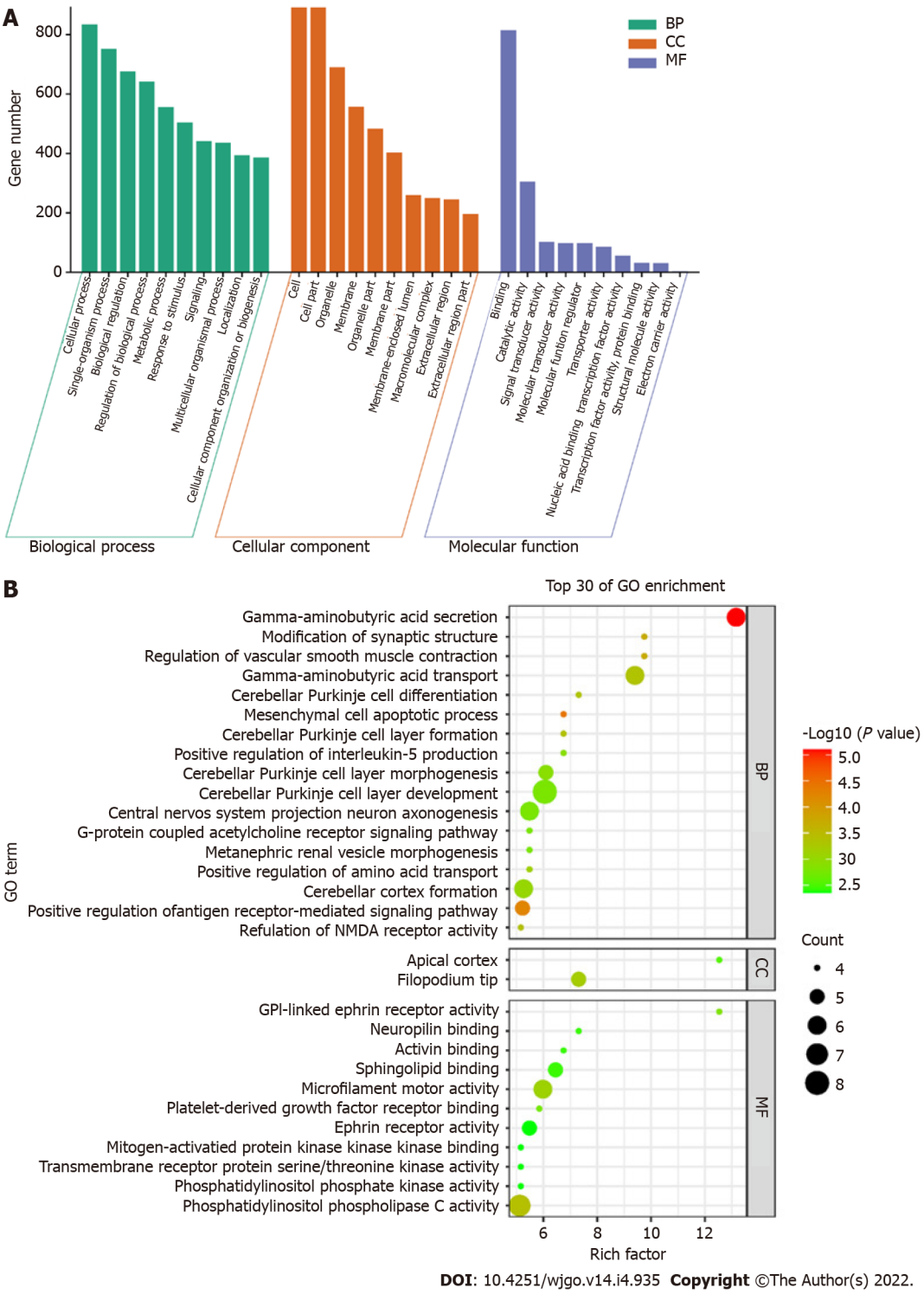

DOI: 10.4251/wjgo.v14.i4.935

Figure 4 Gene ontology analysis. A: Gene ontology (GO) function distribution of differentially methylated sites; B: Bubble diagram of GO enrichment results. GO: Gene ontology; BP: Biological process; CC: Cellular component; MF: Molecular function.

methylation sites.

CONCLUSION

This study showed that the Illumina Infinium Human Methylation 850K BeadChip can be used to investigate genome-wide methylation pattern of plasma DNA in tumors for the discovery of biomarkers. The limitations of this study are the sample size and the deficiency of verification. Further researches are needed on how to reduce the amount of initial DNA for the chip, and how to apply the selected biomarkers to cancer diagnosis.

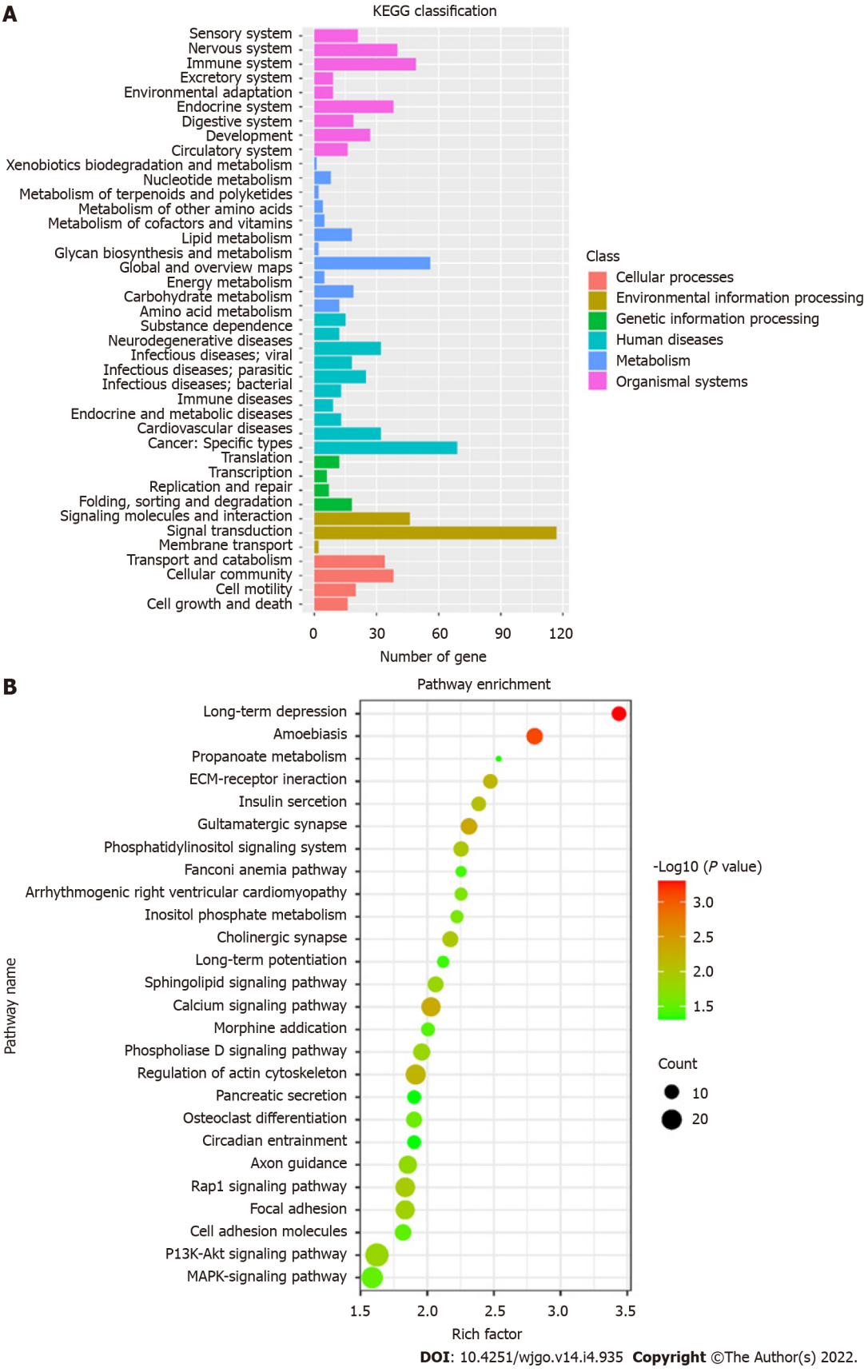

DOI: 10.4251/wjgo.v14.i4.935

Figure 5 Kyoto Encyclopedia of Genes and Genomes analysis. A: Kyoto Encyclopedia of Genes and Genomes (KEGG) pathway classification map; B: Bubble diagram of KEGG enrichment pathways. KEGG: Kyoto Encyclopedia of Genes and Genomes.

ARTICLE HIGHLIGHTS

Research background

DNA methylation is closely related to the growth and development of colorectal cancer (CRC). Circulating tumor DNA (ctDNA) in plasma also has tumor-specific methylation patterns, the methylation status of ctDNA might serve as a potential biomarker.

Research motivation

In this study, we investigated the different methylation pattern between early CRC and colorectal adenoma.

Research objectives

This study aimed to analyze the genomic methylation status of CRC and discover potential methylated biomarkers for CRC diagnosis by Illumina Infinium Human Methylation 850K BeadChip.

Research methods

We used 850K Methylation BeadChip and enrichment analysis to select the differentially methylated sites of early CRC patients (n = 5) and colorectal adenoma patients (n = 5). Then, the gene ontology (GO) and Kyoto Encyclopedia of Genes and Genomes (KEGG) pathway analysis was performed.

Research results

We found 1865 methylated sites with significant differences (676 hypermethylated sites and 1189 hypomethylated sites). The distribution of these sites covered from the 1st to 22nd chromosomes and are mainly distributed on the gene body and gene promoter region. GO and KEGG enrichment analysis identified that the functions of these genes were related to biological regulation, molecular binding, transcription factor activity and signal transduction pathway.

Research conclusions

The Illumina Infinium Human Methylation 850K BeadChip can be used to investigate genome-wide methylation status of plasma DNA to select potential methylated biomarkers for CRC diagnosis.

Research perspectives

Genome-wide methylation analysis of early CRC and screening of biomarkers by 850K Methylation BeadChip provided a new possibility for early diagnosis of CRC.

FOOTNOTES

Author contributions: Wu YL, Jiang T, Zhang PJ and Tian YP designed the study; Wu YL performed the research, wrote the paper; Wu YL and Jiang T analyzed the data, and revised the manuscript for final submission; Huang W, Wu XY participated in the processing of bioinformatic analysis; Wu YL and Jiang T contributed equally to this study; Zhang PJ and Tian YP are the co-corresponding authors; and all authors have read and approve the final manuscript.

Supported by National Natural Science Foundation of China, No. 81972010; the National Key Research and Development Program of China, No. 2020YFC2002700, and No. 2020YFC2004604.

Institutional review board statement: The study was reviewed and approved by the Medical Ethics Committee of PLA General Hospital.

Clinical trial registration statement: We declared that this study has been reviewed and approved by the Medical Ethics Committee of PLA General Hospital. The number was S2022-003-01.

Informed consent statement: All study participants, or their legal guardian, provided informed written consent prior to study enrollment.

Conflict-of-interest statement: We declare that we have no financial or personal relationships with other individuals or organizations that can inappropriately influence our work and that there is no professional or other personal interest of any nature in any product, service and/or company that could be construed as influencing the position presented in or the review of the manuscript.

Data sharing statement: No additional data are available.

CONSORT 2010 statement: The authors have read the CONSORT 2010 statement, and the manuscript was prepared and revised according to the CONSORT 2010 statement.

Country/Territory of origin: China

ORCID number: Yu-Ling Wu 0000-0002-4138-2215; Tao Jiang 0000-0002-2127-9085; Wei Huang 0000-0001-8431-1831; Xing-Yu Wu 0000-0002-6268-1126; Peng-Jun Zhang 0000-0002-7391-2495; Ya-Ping Tian 0000-0002-8245-3745.

S-Editor: Wang JL
L-Editor: A
P-Editor: Wang JL

REFERENCES

1 **Edwards JR**, Yarychkivska O, Boulard M, Bestor TH. DNA methylation and DNA methyltransferases. *Epigenetics Chromatin* 2017; **10**: 23 [PMID: 28503201 DOI: 10.1186/s13072-017-0130-8]
2 **Brenner H**, Stock C, Hoffmeister M. Effect of screening sigmoidoscopy and screening colonoscopy on colorectal cancer incidence and mortality: systematic review and meta-analysis of randomised controlled trials and observational studies. *BMJ* 2014; **348**: g2467 [PMID: 24922745 DOI: 10.1136/bmj.g2467]
3 **Jones PA**, Baylin SB. The epigenomics of cancer. *Cell* 2007; **128**: 683-692 [PMID: 17320506 DOI: 10.1016/j.cell.2007.01.029]
4 **García-Solano J**, Turpin MC, Torres-Moreno D, Huertas-López F, Tuomisto A, Mäkinen MJ, Conesa A, Conesa-Zamora P. Two histologically colorectal carcinomas subsets from the serrated pathway show different methylome signatures and diagnostic biomarkers. *Clin Epigenetics* 2018; **10**: 141 [PMID: 30413173 DOI: 10.1186/s13148-018-0571-3]
5 **Fiedler D**, Hirsch D, El Hajj N, Yang HH, Hu Y, Sticht C, Nanda I, Belle S, Rueschoff J, Lee MP, Ried T, Haaf T, Gaiser T. Genome-wide DNA methylation analysis of colorectal adenomas with and without recurrence reveals an association between cytosine-phosphate-guanine methylation and histological subtypes. *Genes Chromosomes Cancer* 2019; **58**: 783-797 [PMID: 31334584 DOI: 10.1002/gcc.22787]
6 **Luo H**, Zhao Q, Wei W, Zheng L, Yi S, Li G, Wang W, Sheng H, Pu H, Mo H, Zuo Z, Liu Z, Li C, Xie C, Zeng Z, Li W, Hao X, Liu Y, Cao S, Liu W, Gibson S, Zhang K, Xu G, Xu RH. Circulating tumor DNA methylation profiles enable early diagnosis, prognosis prediction, and screening for colorectal cancer. *Sci Transl Med* 2020; **12** [PMID: 31894106 DOI: 10.1126/scitranslmed.aax7533]
7 **Rahier JF**, Druez A, Faugeras L, Martinet JP, Géhénot M, Josseaux E, Herzog M, Micallef J, George F, Delos M, De Ronde T, Badaoui A, D'Hondt L. Circulating nucleosomes as new blood-based biomarkers for detection of colorectal cancer. *Clin Epigenetics* 2017; **9**: 53 [PMID: 28515797 DOI: 10.1186/s13148-017-0351-5]
8 **Barault L**, Amatu A, Siravegna G, Ponzetti A, Moran S, Cassingena A, Mussolin B, Falcomatà C, Binder AM, Cristiano C, Oddo D, Guarrera S, Cancelliere C, Bustreo S, Bencardino K, Maden S, Vanzati A, Zavattari P, Matullo G, Truini M, Grady WM, Racca P, Michels KB, Siena S, Esteller M, Bardelli A, Sartore-Bianchi A, Di Nicolantonio F. Discovery of methylated circulating DNA biomarkers for comprehensive non-invasive monitoring of treatment response in metastatic colorectal cancer. *Gut* 2018; **67**: 1995-2005 [PMID: 28982739 DOI: 10.1136/gutjnl-2016-313372]
9 **Symonds EL**, Pedersen SK, Murray D, Byrne SE, Roy A, Karapetis C, Hollington P, Rabbitt P, Jones FS, LaPointe L, Segelov E, Young GP. Circulating epigenetic biomarkers for detection of recurrent colorectal cancer. *Cancer* 2020; **126**: 1460-1469 [PMID: 31909823 DOI: 10.1002/cncr.32695]
10 **Molnár B**, Galamb O, Kalmár A, Barták BK, Nagy ZB, Tóth K, Tulassay Z, Igaz P, Dank M. Circulating cell-free nucleic acids as biomarkers in colorectal cancer screening and diagnosis - an update. *Expert Rev Mol Diagn* 2019; **19**: 477-498 [PMID: 31046485 DOI: 10.1080/14737159.2019.1613891]
11 **Moran S**, Arribas C, Esteller M. Validation of a DNA methylation microarray for 850,000 CpG sites of the human genome enriched in enhancer sequences. *Epigenomics* 2016; **8**: 389-399 [PMID: 26673039 DOI: 10.2217/epi.15.114]
12 **Naumov VA**, Generozov EV, Zaharjevskaya NB, Matushkina DS, Larin AK, Chernyshov SV, Alekseev MV, Shelygin YA, Govorun VM. Genome-scale analysis of DNA methylation in colorectal cancer using Infinium HumanMethylation450 BeadChips. *Epigenetics* 2013; **8**: 921-934 [PMID: 23867710 DOI: 10.4161/epi.25577]
13 **Sandoval J**, Heyn H, Moran S, Serra-Musach J, Pujana MA, Bibikova M, Esteller M. Validation of a DNA methylation microarray for 450,000 CpG sites in the human genome. *Epigenetics* 2011; **6**: 692-702 [PMID: 21593595 DOI: 10.4161/epi.6.6.16196]
14 **Hochberg Y**, Benjamini Y. More powerful procedures for multiple significance testing. *Stat Med* 1990; **9**: 811-818 [PMID: 2218183 DOI: 10.1002/sim.4780090710]
15 **Vrba L**, Futscher BW. A suite of DNA methylation markers that can detect most common human cancers. *Epigenetics* 2018; **13**: 61-72 [PMID: 29212414 DOI: 10.1080/15592294.2017.1412907]
16 **Takane K**, Fukuyo M, Matsusaka K, Ota S, Rahmutulla B, Matsushita K, Miyauchi H, Nakatani Y, Matsubara H, Kaneda A. The frequency of promoter DNA hypermethylation is decreased in colorectal neoplasms of familial adenomatous polyposis. *Oncotarget* 2018; **9**: 32653-32666 [PMID: 30220972 DOI: 10.18632/oncotarget.25987]
17 **Wong FC**, Sun K, Jiang P, Cheng YK, Chan KC, Leung TY, Chiu RW, Lo YM. Cell-free DNA in maternal plasma and

serum: A comparison of quantity, quality and tissue origin using genomic and epigenomic approaches. *Clin Biochem* 2016; **49**: 1379-1386 [PMID: 27620950 DOI: 10.1016/j.clinbiochem.2016.09.009]

18 **Sun K**, Jiang P, Chan KC, Wong J, Cheng YK, Liang RH, Chan WK, Ma ES, Chan SL, Cheng SH, Chan RW, Tong YK, Ng SS, Wong RS, Hui DS, Leung TN, Leung TY, Lai PB, Chiu RW, Lo YM. Plasma DNA tissue mapping by genome-wide methylation sequencing for noninvasive prenatal, cancer, and transplantation assessments. *Proc Natl Acad Sci U S A* 2015; **112**: E5503-E5512 [PMID: 26392541 DOI: 10.1073/pnas.1508736112]

19 **Solomon O**, MacIsaac J, Quach H, Tindula G, Kobor MS, Huen K, Meaney MJ, Eskenazi B, Barcellos LF, Holland N. Comparison of DNA methylation measured by Illumina 450K and EPIC BeadChips in blood of newborns and 14-year-old children. *Epigenetics* 2018; **13**: 655-664 [PMID: 30044683 DOI: 10.1080/15592294.2018.1497386]

20 **Zhu L**, Yan F, Wang Z, Dong H, Bian C, Wang T, Yu E, Li J. Genome-wide DNA methylation profiling of primary colorectal laterally spreading tumors identifies disease-specific epimutations on common pathways. *Int J Cancer* 2018; **143**: 2488-2498 [PMID: 30183087 DOI: 10.1002/ijc.31765]

21 **Wong CC**, Xu J, Bian X, Wu JL, Kang W, Qian Y, Li W, Chen H, Gou H, Liu D, Yat Luk ST, Zhou Q, Ji F, Chan LS, Shirasawa S, Sung JJ, Yu J. In Colorectal Cancer Cells With Mutant KRAS, SLC25A22-Mediated Glutaminolysis Reduces DNA Demethylation to Increase WNT Signaling, Stemness, and Drug Resistance. *Gastroenterology* 2020; **159**: 2163-2180.e6 [PMID: 32814111 DOI: 10.1053/j.gastro.2020.08.016]

22 **Kel A**, Boyarskikh U, Stegmaier P, Leskov LS, Sokolov AV, Yevshin I, Mandrik N, Stelmashenko D, Koschmann J, Kel-Margoulis O, Krull M, Martínez-Cardús A, Moran S, Esteller M, Kolpakov F, Filipenko M, Wingender E. Walking pathways with positive feedback loops reveal DNA methylation biomarkers of colorectal cancer. *BMC Bioinformatics* 2019; **20**: 119 [PMID: 30999858 DOI: 10.1186/s12859-019-2687-7]

23 **Nguyen LH**, Goel A, Chung DC. Pathways of Colorectal Carcinogenesis. *Gastroenterology* 2020; **158**: 291-302 [PMID: 31622622 DOI: 10.1053/j.gastro.2019.08.059]

24 **Warton K**, Lin V, Navin T, Armstrong NJ, Kaplan W, Ying K, Gloss B, Mangs H, Nair SS, Hacker NF, Sutherland RL, Clark SJ, Samimi G. Methylation-capture and Next-Generation Sequencing of free circulating DNA from human plasma. *BMC Genomics* 2014; **15**: 476 [PMID: 24929644 DOI: 10.1186/1471-2164-15-476]

25 **Liu L**, Chen Y, Liu T, Yu J, Ma L, Wu H. Genome-wide DNA methylation profiling and gut flora analysis in intestinal polyps patients. *Eur J Gastroenterol Hepatol* 2021; **33**: 1071-1081 [PMID: 34213504 DOI: 10.1097/MEG.0000000000002181]

Published by **Baishideng Publishing Group Inc**
7041 Koll Center Parkway, Suite 160, Pleasanton, CA 94566, USA
Telephone: +1-925-3991568
E-mail: bpgoffice@wjgnet.com
Help Desk: https://www.f6publishing.com/helpdesk
https://www.wjgnet.com